UNIVERSITY OF SOUTHAMPTON

"Ground-truthing the Boron-based Proxies"

by

Michael J. Henehan

A thesis submitted in partial fulfillment for the degree of Doctor of Philosophy

in the

Faculty of Natural and Environmental Sciences

Ocean and Earth Sciences

October 2015

Declaration of Authorship

I, Michael James Henehan, declare that this thesis titled, 'Ground-truthing the Boron-based Proxies' and the work presented in it are my own. I confirm that:

- This work was done wholly or mainly while in candidature for a research degree at this University.
- Where any part of this thesis has previously been submitted for a degree or any other qualification at this University or any other institution, this has been clearly stated.
- Where I have consulted the published work of others, this is always clearly attributed.
- Where I have quoted from the work of others, the source is always given. With the exception of such quotations, this thesis is entirely my own work.
- I have acknowledged all main sources of help.
- Where the thesis is based on work done by myself jointly with others, I have made clear exactly what was done by others and what I have contributed myself.

Signed: _____

Date: _____

"Nothing ever succeeds which exuberant spirits have not helped to produce."

Friedrich Nietzsche

FIGURE 1: Youthful exuberance, February 2011. Modified after Allie Brosh.

FIGURE 2: New-found realism, February 2012. Modified after Allie Brosh.

UNIVERSITY OF SOUTHAMPTON

Abstract

Faculty of Natural and Environmental Sciences
Ocean and Earth Sciences

Doctor of Philosophy

by Michael J. Henehan

Boron-based proxies (δ^{11}B and B/Ca ratios), as applied to foraminiferal shells, have attracted increasing attention in recent years, because of their propensity to record past carbonate system conditions (and hence past levels of atmospheric CO_2). However, questions still surround the central tenets upon which these proxies are based. For instance, why do all published calibration studies (bar one) describe pH-δ^{11}B relationships in foraminifera that are counter to what aqueous theory would predict? Why do different organisms record different patterns in δ^{11}B? How applicable are sparse observations from culture experiments to the open ocean, and indeed, the oceans of the past? Finally, how and why is boron actually incorporated into foraminiferal shells?

This PhD project goes some way to answering these questions. It extends the applicability of the boron isotope-pH proxy, by contributing to our understanding of the inorganic basis of the proxy, the causes behind (and variability in) foraminiferal 'vital effects', and the mechanisms of boron incorporation in foraminiferal calcite. Specifically, three new species-specific calibrations (measured by MC-ICPMS) are presented, along with new insights into intraspecies δ^{11}B variability, and new approaches for the propagation of uncertainty in palaeo-pH estimates. As a consequence, this project will permit greater confidence in future reconstructions of palaeo-CO_2. These observations lend further support to foraminiferal microenvironment alteration's being the main driver of deviations from the aqueous basis of the proxy.

Conversely, however, this PhD project casts doubt on the utility of B/Ca ratios as a palaeo-proxy. Measurements of B/Ca in open-ocean *Globigerinoides ruber* bear little relation to *in situ* carbonate system parameters, but instead highlight a previously unnoticed driver of boron incorporation (alongside salinity): PO_4^{3-} concentrations. While further study is required, this finding appears to imply that boron incorporation in foraminifera is dictated by inorganic crystal growth kinetics, rather than the carbonate system.

Acknowledgements

This PhD research would not have happened without the help and support of a large number of people, whose contributions are acknowledged here.

I have been immensely lucky to have had superb supervisors here at the NOC. I thank Gavin Foster firstly for giving me the opportunity to come to work with him (in spite of a somewhat chaotic showing, or lack thereof, at interview). Aside from having a huge positive impact on my academic development, his support, encouragement, reassurance, patience and sense of humour have been limitless, and always very much appreciated. I thank Paul Wilson, too, for the friendly ear, valuable advice and enjoyable discussion that he has always afforded to me when called upon (even if the relatively distal nature of his office meant he managed to escape much of my pestering!).

Secondly, I thank the other members of the B-Team here at the NOC: Miguel Martínez-Botí, Tom Chalk, Rosanna Greenop, Marcus Gutjahr (now at GEOMAR, but once B-Team, always B-Team), Eleni Anagnostou, Joe Stewart and Sara Fowell. The world of boron isotope analysis may, at times, be a dark and unforgiving place, but the good humour, camaraderie, and conscientious and tireless mutual assistance of the team here can be always be relied upon. It is not an exaggeration to say that without the other B-Team members, much of the data presented in this thesis could not have been produced.

Also at the NOC, I thank Andy Milton for his tireless efforts in maintaining the mass spectrometers, and his invaluable troubleshooting expertise (even at rather unsociable hours). Matt Cooper and Agnes Michalik are also thanked for their hard work in supplying and managing a busy boron lab, and fixing things when they inevitably go wrong. I thank Clive Trueman for helping me to brush up on my statistics, for his patience in communicating statistics to me, and his training in the use of *R*. I thank Jennifer Rutter for teaching me how to use LaTeX, and Sunil Patel for the provision of an excellent thesis LaTeX template.

I have also been very lucky to work with some all-round brilliant people from other institutes around the world. James Rae (Caltech) is thanked for the huge part he has played in my academic development from my early days at the University of Bristol, his enormously insightful ideas and comments in drafting manuscripts and chapters, his hard work in culturing and analysing foraminifera, and his part in teaching me how to analyse boron isotopes. Jonathan Erez (Hebrew University, Jerusalem) is thanked for imparting priceless knowledge on the subjects of foraminiferal culturing, foraminiferal ecology, biomineralisation and good falafel. Helen Bostock (NIWA, Wellington) is thanked for giving me the opportunity to experience a research cruise first hand, taking a keen interest in my academic development, and providing priceless core-top sample material.

Michal Kucera (now MARUM) is thanked for valuable tutorship in planktic foraminiferal taxonomy, insights and wealth of core-top sample material. Brittney Marshall (University of South Carolina) is thanked for insightful conversation, ongoing collaboration and provision of sample material. I also give special thanks to Katy Prentice (now Imperial College, London) for her unending dedication, selflessness, grit and determination in pulling through three months' hard slog at the IUI, Eilat.

The staff and students at the IUI, in particular Asaph and Tanya Rivlin and Itay Cohen, are thanked for their invaluable assistance and companionship during culturing experiments at the IUI. I thank also the other research scientists and crew on board the RVV Tangaroa (most notably Pete Gerring and Kevin McGill) for sharing their experience and skills during the Solander Trough voyage.

Oscar Branson (now Cambridge) is thanked for getting me involved with his coccolithophores, providing valuable sample material, and offering helpful discussion. Heather Stoll and her team at the University of Oviedo (most notably Luz Maria Mejia, Lorena Abrevaya, Clara Bolton, and Maité Hernandez-Sanchez) are thanked for the useful lab skills that they taught me in cleaning coccolithophores and diatoms, and for ongoing collaborations.

Basak Kısakürek (Kiel) and Barbara Donner (MARUM) are thanked for the provision of valuable sample material. David Aldridge and Sari Giering are also thanked for the provision of towed sample material, which sadly never made it into this thesis.

Bärbel Hönisch (LDEO), Kat Allen (LDEO), Oscar Branson (Cambridge), Emmanuel Gloor (Leeds), Howie Spero (UC Davis), Richard Zeebe (University of Hawaii), Ralf Aurahs (University of Tübingen), Kateryna Klochko (Carnegie Institute) and Julene Marr (Victoria University, Wellington) are all thanked for useful scientific discussions. I thank Sang-Tae Kim and Christa Klein Gebbinck (McMaster University) for their involvement in ongoing collaborations. Tim Elliott (University of Bristol) is thanked for his good humour and valuable input during the drafting of Henehan et al. (2013). Rachael James (NOCS) is thanked for her input during the drafting of Henehan et al. (2013), and her guidance as my panel chair. I thank Daniela Schmidt (University of Bristol) for her encouragement and support in the early days of my academic career, and for getting me involved with Gavin and James in the first place.

I thank Mark Stinchcombe (NOCS) for nutrient data from culture solutions, Cynthia Dumousseaud (NOCS) for DIC and Alkalinity analysis of Eilat culture solutions, and Neil Jenkins (NOCS) for the provision of heat guns for column-making.

I am grateful for the funding from the Natural Environmental Research Council (NERC) that facilitated this PhD Studentship. I have been lucky enough to attend a lot of

valuable conferences, workshops and summer schools, that have helped my academic development considerably. I am grateful to NERC for subsidising my attendance at the Life and the Planet Spring School, and to UK-IODP for subsidising my attendance at the Urbino Summer School in Palaeoclimatology.

I thank my family for their unwavering support and encouragement, and for letting me get on with it these past few years. I thank Gary Bilotta for his past support, and the large part he has played in my development up till now.

Finally, but by no means least, I thank the many many friends I have made at NOCS for making it a great place to be- while I cannot thank them all by name this by no means detracts from the goodwill and gratitude I express to them. Special thanks in particular, though, go to my wonderful blue-housemates (especially Jennifer Rutter, Gemma Smith, Grant Duffy [the stalwarts!], but also Anya Crocker, Mike Cassidy, Alex Beaton, Yasmin Labibi, and more transient residents and couchsurfers) who have made the Blue House a wonderfully happy home for these past three years, and have variously provided (in no particular order): welcome distraction, scientific advice, relationship counselling, free food, career guidance, lifts, wine, GIS assistance, amusement, statistics training and tea. Jennifer in particular is also thanked for her constructive criticisms in the drafting of this acknowledgment section.

Contents

List of Figures

List of Tables

Abbreviations

AIC	**A**ikaike **I**nformation **C**riterion
COC	**C**entre **o**f **C**alcification
CV	**C**alcifying **V**acuole
DIC	**D**issolved **I**norganic **C**arbon
DOC	**D**issolved **O**rganic **C**arbon
GAM	**GAM**etogenic (usually pertaining to calcite layers)
MAS NMR	**M**agic **A**ngle **S**pinning **N**uclear **M**agnetic **R**esonance **A**nalysis
MC-ICPMS	**M**ulti-**C**ollector **I**nductively **C**oupled **P**lasma **M**ass **S**pectrometry
NIST SRM 951	**N**ational **I**nstitute of **St**andards **S**tandard **R**eference **M**aterial 951
N-TIMS	**N**egative **T**hermal **I**onisation **M**ass **S**pectrometry
PIC	**P**articulate **I**norganic **C**arbon
POC	**P**articulate **O**rganic **C**arbon
SEM	**S**canning **E**lectron **M**icroscop(e/y)
TAlk	**T**otal **Alk**alinity
TE	**T**race **E**lement
TE-NTIMS	**T**otal **E**vaporation **N**egative **T**hermal **I**onisation **M**ass **S**pectrometry

Symbols

Symbol	*Description*	*Unit*
Ω	the saturation state of the ocean with regards to a given calcium carbonate mineral (either $\Omega_{calcite}$ or $\Omega_{aragonite}$).	*n/a*
${}^{11-10}K_B$	Equilibrium constant for the isotopic fractionation between $B(OH)_3$ and $B(OH)_4{}^-$, assuming in the context of this thesis (unless otherwise stated) a seawater medium.	*n/a*
$pK^*{}_B$	disassociation constant for boric acid in seawater, i.e. the pH at which the abundances of $B(OH)_3$ and $B(OH)_4{}^-$ are equal. Its value is dependent on temperature, salinity and pressure.	*n/a*
α	Alternative symbol often used elsewhere to express ${}^{11-10}K_B$, although often in the literature it may refer to $\frac{1}{{}^{11-10}K_B}$. Sometimes written α_{3-4}, α_{4-3} or α_B.	*n/a*
η	The 'Kolmogorov scale' describing, in essence, the size of the smallest eddie possible for a given viscosity of a fluid.	mm
P_{max}	The light level at which maximum rate of photosynthesis for a given organism or symbiotic association occurs.	μmol photons $m^{-2}s^{-1}$

Chapter 1

Background to the Project: The Boron Isotope Proxy

1.1 Atmospheric CO_2 levels and their effect on Earth's climate.

The absorption and reflectance of infrared radiation by CO_2 is a phenomenon that has been understood since the pioneering works of the Irishman John Tyndall in the 1860s (Tyndall, 1862). Later, Arrhenius (1896) linked this effect to the earth's climate system, and speculated that changes in the Earth's climate may have been linked to changes in the concentrations of CO_2 in the atmosphere. Today, it is now clear that the release of greenhouse gases (principally CO_2) from fossil fuels has been responsible for temperature changes of $\sim$0.6 - 0.8 °C since the industrial revolution, and a drop in ocean pH of 0.11 units (Caldeira and Wickett, 2003, Jacobson, 2005). Given that atmospheric CO_2 levels continue to rise (crossing the 400 ppm threshold earlier this year), much research has focussed on predicting the long-term temperature response to this increase in CO_2, i.e. the determining the sensitivity of the climate to CO_2 change. Most estimates range from 2 - 4.5 °C per doubling of atmospheric CO_2 (IPCC, 2007), but some models suggest it may be as high as 11 °C per doubling of CO_2 (Stainforth et al., 2005). Given its importance in planning mitigation strategies, it is crucial that the uncertainty on this figure is reduced. One way of doing this is to look at climate events and transitions in the past, from the geological record, and quantify the temperature change observed for

a given CO_2 fluctuation. However, to do this, accurate and reliable proxies for both temperature and pCO_2 are required.

1.2 Reconstructing CO_2 levels: Proxies used

A number of proxies have been used to reconstruct CO_2 levels in the past, including (i) the $\delta^{13}C$ of pedogenic carbonates, (ii) stomatal density on fossil leaves, (iii) the $\delta^{13}C$ of alkenone biomarkers, and (iv) boron-based proxies in corals and foraminiferal carbonates.

The $\delta^{13}C$ of pedogenic carbonates (i.e. $CaCO_3$ precipitated within palaeosols) is one approach that has produced important estimates of past CO_2 levels (e.g. Nordt et al., 2002, 2003, Robinson et al., 2002, Breecker et al., 2010). Carbonate $\delta^{13}C$, in this case, is a function of the amount of biologically-respired CO_2 present in the soil (which may be partially inferred from the sedimentology of the section) and the CO_2 levels in the atmosphere (Cerling, 1984, 1991). The main advantage of this method is its applicability to early Mesozoic and Palaeozoic sediments, stretching back as far as the Silurian period (Mora et al., 1991), where non-lithified, unaltered marine sediments are unavailable. However, there are limitations to the technique. There is some chance of diagenetic alteration (Royer et al., 2001), although the extent to which this may affect readings is not entirely clear (Cerling, 1991, **?**). Numerous assumptions must be made regarding conditions within the palaeosol (e.g. depth of soil profile, diffusivity of CO_2, time of year when carbonates were formed, the $\delta^{13}C$ of soil organic matter; Bowen and Beerling, 2004, and references within). In addition, these carbonates may take thousands of years to form, and are often hard to date beyond geological formation level, which precludes high resolution studies of transient carbon system perturbations. Uncertainty is also very high during periods where atmospheric CO_2 levels are low relative to soil-respired CO_2 (Ekart et al., 1999, reconstruct Holocene CO_2 values at 430 $\pm$ 770 ppm at 2σ uncertainty), which effectively limits their application to greenhouse periods. During rapid carbon isotope excursion (CIE) events such as the PETM, moreover, there might be some disequilibrium between different carbon reservoirs, hindering interpretation of results (Ekart et al., 1999). Furthermore, measurements may often be subject to a positive bias, as a result of the decay of ^{13}C-enriched organic matter deep within the soil (Bowen and Beerling, 2004).

Another terrestrial proxy used to generate CO_2 records is the stomatal index, i.e. the density of stomata on fossil leaves. Stomata control gaseous exchange in plants, but they are also the main site of water loss (via transpiration). Thus as the partial pressure of atmospheric CO_2 rises, plants may reduce the density of stomata to minimise water loss, but take in the same amount of C (Woodward and Bazzaz, 1988). In this way, the density of stomata on fossil leaves may reflect levels of CO_2 in the atmosphere. As with palaeosols, however, there are limitations and complications. Firstly, responses are species-specific (Woodward and Kelly, 1995), and thus this limits the applicability of the proxy to well-preserved specimens of still extant, calibrated species. Secondly, substantial variability in stomatal density is seen in the leaves of a single plant, and thus the propensity for error is enhanced (Poole et al., 1996). Thirdly, because there is a physiological limit to the possible density of stomata on a leaf, stomatal density-CO_2 curves are sigmoidal: this means that at CO_2 levels above 350 ppm, sensitivity to pCO_2 changes may be dampened (Royer, 2001). CO_2 levels may also change within a forest canopy (Bazzaz and Williams, 1991), and may deviate from atmospheric CO_2 to a degree greater than the typical quoted uncertainty of the technique. In addition, because stomatal density responds to the partial pressure of CO_2 (which varies with altitude) rather than its concentration (Woodward and Bazzaz, 1988), assumptions must be made about the altitude at time of deposition (Körner et al., 1986). Finally, as with pedogenic carbonates, accurate dating can in some cases prove difficult, meaning that high-resolution CO_2 records are often difficult to construct. Some settings, however (for example, cyclic lacustrine sediments) do allow for fine temporal resolution (for example, accurate reconstruction of last deglacial CO_2 rise; Rundgren and Beerling, 1999).

Another CO_2 proxy, this time marine based, that is widely used in pCO_2 reconstruction (e.g. Jasper and Hayes, 1990, Freeman and Hayes, 1992, Pagani et al., 2005b, 2011, Seki et al., 2010, Pagani et al., 1999) is the alkenone $\delta^{13}C$ proxy (Popp et al., 1989, 1998). Alkenones are long-chained, unsaturated ethyl and methyl ketone biomarker compounds produced by coccolithophores. Carbon isotope signatures of these compounds (or more specifically the isotopic offset between these compounds and ambient $\delta^{13}C_{sw}$, ϵ_p) is dependent on ambient $[CO_{2(aq)}]$ (Degens et al., 1968, Freeman and Hayes, 1992), but also to a number of physiological interferences, such as cell size (Popp et al., 1998, Henderiks and Pagani, 2007), growth rates (as may be dictated by nutrient availability; Bidigare et al., 1997), the effect of irradiance (Rost et al., 2002), temperature (Degens

et al., 1968), the extent to which CO_2 is actively transported into the cell (Keller and Morel, 1999) and membrane permeability (Rau et al., 1996). These physiological factors are typically summarised as one single term, '*b*', (Bidigare et al., 1997, Pagani et al., 2005b), which has been shown in the modern ocean to correlate well with $[PO_4^{3-}]$ (e.g. Pagani et al., 2011). Using these correlations precise and accurate CO_2 reconstructions can be made (e.g. Jasper and Hayes, 1990, Pagani et al., 2002). However, deep-time applications require a great many assumptions to be made. Critically, term '*b*' has a very large effect on reconstructed CO_2, and in some cases the assumptions made regarding this factor drive the proxy signal, rather than the measured $\delta^{13}C$ itself (see, for example, Seki et al., 2010).

Given these issues, boron-based CO_2 proxies in carbonates (based on the inorganic pH-dependent speciation of boron in seawater Hemming and Hanson, 1992) could well constitute a valuable addition to the arsenal of CO_2 proxies. Boron isotope-based reconstructions have been shown to faithfully reproduce atmospheric CO_2 levels from ice cores (Hönisch and Hemming, 2005a, Foster, 2008, Henehan et al., 2013), and have already provided valuable insights into the carbon cycles of the past (Palmer et al., 1998, Sanyal et al., 1997, Foster et al., 2012, Seki et al., 2010, Pearson and Palmer, 1999, 2000, Pearson et al., 2009, Yu et al., 2013). However, boron-based proxies, like the others already discussed, are not without their numerous caveats and complications. It is these caveats that form the main focus of this PhD project, with the ultimate aim of improving our understanding of the Earth's climate system and its sensitivity to carbon cycle perturbations (both in the past and in the immediate future).

1.3 The Boron-based carbonate system proxies

1.3.1 The aqueous basis behind the Boron Isotope and B/Ca Proxies

The boron isotope and B/Ca proxies have a well-understood foundation in inorganic aqueous chemistry that has played a major part in establishing them as reliable carbonate system proxies. Boron is almost exclusively present in seawater in one of two forms: the tetrahedrally-coordinated borate molecule, $B(OH)_4^-$, and the trigonally-coordinated boric acid, or $B(OH)_3$. Some boron does exist in polynuclear forms at typical seawater pH, but this amount is negligible under normal seawater boron concentrations (Su and

Suarez, 1995). The relative proportions of the two species is dependent on pH, such that at low pH boron is entirely in the form of $B(OH)_3$, and at high pH it is found as $B(OH)_4^-$ (see Fig 1.1, Panel A).

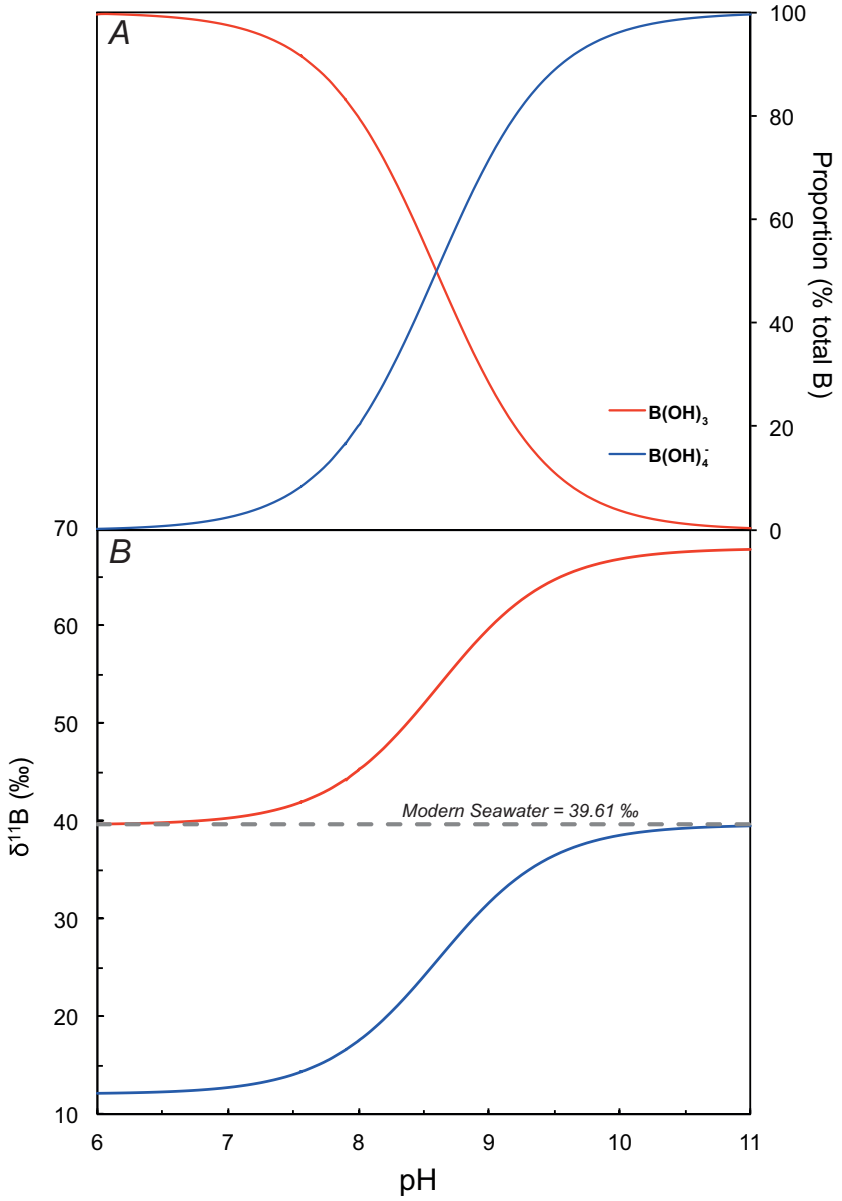

FIGURE 1.1: The relative abundances (Panel A) and isotopic compositions (Panel B) of the two most abundant boron species in seawater, at 25 °C and S = 35 psu. Boric acid, $B(OH)_3$, is marked in red, while borate ion, $B(OH)_4^-$, is marked in blue.

Equilibration of the two boron species is rapid (125 μs, Zeebe et al., 2001), and is described by the disassociation equation 1.1 below.

$$B(OH)_3 + H_2O \Leftrightarrow B(OH)_4^- + H^+ \tag{1.1}$$

In addition to pH, the equilibration and thus relative abundance of $B(OH)_3$ and $B(OH)_4{}^-$ is also dependent on temperature, salinity and pressure. The effects of these conditions on the equilibration of boron are parameterised as pK_B^*, otherwise known as the boron disassociation constant. Put simply, pK_B^* is the pH at which the proportions of $B(OH)_3$ and $B(OH)_4{}^-$ in a given solution are equal. Provided estimates of *in situ* temperature, salinity and pressure are known, this constant may be calculated relatively simply, using the equations of Dickson (1990) and programs such as CO2sys.exe (Lewis and Wallace, 1998), CO2calc (Robbins et al., 2010) or CO2sys.m van Heuven et al. (2011).

Boron has two stable isotopes, ^{11}B and ^{10}B (80 % and 20 % of total B respectively), with the ratio of these two stable isotopes most commonly expressed in delta notation such that

$$\delta^{11}B \text{ (in ‰)} = [\frac{^{11}B/^{10}B_{sample}}{^{11}B/^{10}B_{standard}} - 1] \times 1000 \tag{1.2}$$

The 'standard' in question is NIST SRM 951 boric acid (Catanzaro et al., 1970). Associated with the equilibration of the two aqueous boron species is an isotopic fractionation, as a result of differences in molecular geometries (Urey, 1947). Specifically, $B(OH)_3$ is isotopically heavier than $B(OH)_4{}^-$, with the isotope exchange reaction described by Equation 1.3 below.

$$^{10}B(OH)_3 + {}^{11}B(OH)_4^- \Leftrightarrow {}^{11}B(OH)_3 + {}^{10}B(OH)_4^- \tag{1.3}$$

The equilibrium constant, $^{11-10}K_B$, is described as

$$^{11-10}K_B = \frac{^{11}B(OH)_3 \times {}^{10}B(OH)_4^-}{^{10}B(OH)_3 \times {}^{11}B(OH)_4^-} \quad . \tag{1.4}$$

Thus, driven by the equilibration of boron species, the isotopic composition of both boron species also varies with pH, as shown in Figure 1.1, Panel B. The $\delta^{11}B_{sw}$, as indicated by the dashed grey line in Figure 1.1B, or the $\delta^{11}B$ of either aqueous species,

can thus be calculated by rearrangement of equation 1.5 below.

$$\delta^{11}B_{(B_T)} \times [B_T] = (\delta^{11}B_{B(OH)_4^-} \times [B(OH)_4^-]) + (\delta^{11}B_{B(OH)_3} \times [B(OH)_3]) \quad (1.5)$$

Furthermore, providing the value of ${}^{11-10}K_B$ is known (see Section 1.3.3.3), pK_B^* can be calculated from salinity, temperature and pressure, and the δ^{11}B of total aqueous Boron ($\delta^{11}B_{sw}$) is known, then for a given pH the isotopic composition of either aqueous boron species can be calculated, for example for $B(OH)_4^-$ using Equation 1.6 below (Hemming and Hanson, 1992).

$$pH = pK_B^* - log\left(\frac{\delta^{11}B_{B(OH)_4^-} - \delta^{11}B_{sw}}{\delta^{11}B_{sw} - {}^{11-10}K_B * \delta^{11}B_{B(OH)_4^-} - 1000 * ({}^{11-10}K_B - 1)}\right) \quad (1.6)$$

1.3.2 Extension to Marine Carbonates: The B/Ca proxy

The B/Ca proxy is based on known speciation of boron in seawater discussed above. Since $B(OH)_4^-$, the charged ion, is thought to be only species of boron incorporated into $CaCO_3$, it was proposed that B/Ca ratios in $CaCO_3$ should increase with increased $[B(OH)_4^-]$ (Hemming and Hanson, 1992). Given that the relative abundance of $B(OH)_4^-$ is pH dependent (see Fig. 1.1), B/Ca ratios in $CaCO_3$ should then respond to changes in the marine carbonate system. A central assumption, therefore, is that only $B(OH)_4^-$ is incorporated into $CaCO_3$. This issue has in the past been the subject of some considerable debate, and is still sometimes cited as contentious (Xiao et al., 2013), despite the proximity of all published measurements of carbonate δ^{11}B to the theoretical δ^{11}B of $B(OH)_4^-$ ion (e.g. Hemming and Hanson, 1992, Sanyal et al., 1996, 2000, 2001, Foster, 2008, this study). For example, Klochko et al. (2009) cite small offsets in almost all measured $\delta^{11}B_{CaCO_3}$ values from the new aqueous $\delta^{11}B_{B(OH)_4^-}$-pH curve (after Klochko et al., 2006) as evidence for incorporation of both boron species. They support this with reference to magic angle spinning nuclear magnetic resonance analysis (MAS NMR) showing 46% of boron in calcium carbonate is trigonally co-ordinated (and thus, they suggest, boric acid) and 54% is tetrahedral (read borate ion). However, even accounting for small offsets from $\delta^{11}B_{B(OH)_4^-}$that are observed, no δ^{11}B measurements in $CaCO_3$ could permit such large scale incorporation of $B(OH)_3$. Ultimately, such assertions are unnecessary: the incidence of

trigonally-coordinated boron in $CaCO_3$ is not in itself proof of the incorporation of boric acid. The incidence of trigonally-coordinated boron in the $CaCO_3$ lattice merely requires that tetrahedral borate is recoordinated upon incorporation (as suggested by Sen et al., 1994, Hemming et al., 1998, Ruiz-Agudo et al., 2012). As such the possible incorporation of $B(OH)_3$ acid is not discussed further in this thesis.

However, the speciation of boron in seawater is not the only control on boron incorporation in $CaCO_3$: the site at which boron substitutes into the crystal lattice also has a part to play. Hemming and Hanson (1992) suggest that boron substitutes at the CO_3^{2-} site in $CaCO_3$, given the similarity of B-O and C-O bond lengths (0.137 and 0.128 nm respectively; Kakihana et al., 1977), although they also note the possibility that B resides in defect sites. Based on this assertion, Hemming and Hanson (1992) proposed the formula for boron substitution into $CaCO_3$ described in equation 5.1 below.

$$CaCO_{3_{solid}} + B(OH)^-_{4_{aqueous}} \Rightarrow Ca(HBO_3)_{solid} + HCO^-_{3_{aqueous}} + H_2O \tag{1.7}$$

By extension, they defined the exchange distribution coefficient (K_D) for this reaction as

$$K_{D^B_{calcite}} = \frac{[HBO_3^{2-}/CO_3^{2-}]_{solid}}{[B(OH)_4^-/HCO_3^-]_{fluid}} \tag{1.8}$$

which was later shortened (Yu et al., 2007b, Zeebe and Wolf-Gladrow, 2001) to

$$K_{D^B_{calcite}} = \frac{[B/Ca]_{solid}}{[B(OH)_4^-/HCO_3^-]_{fluid}} \quad . \tag{1.9}$$

Consequently, if this mechanism for incorporation is correct, B/Ca ratios in foraminifera should be dependent not only on the pH-driven speciation of boron species, described above, but on the speciation of aqueous dissolved inorganic carbon (DIC) compounds that compete for incorporation sites (also dependent on pH, temperature, pressure and salinity; Zeebe and Wolf-Gladrow, 2001). Both inorganic precipitation experiments (Hemming et al., 1995, Sanyal et al., 2000, He et al., 2013) and culture experiments of planktic foraminifera (Sanyal et al., 1996, 2001, Allen et al., 2011, 2012, and this study, Chapter 5) do demonstrate that the carbonate system is indeed a strong control on B/Ca ratios in $CaCO_3$. However, this observation is not consistently reproduced in field studies, and it seems there may be other controls on

planktic foraminiferal B/Ca ratios (Allen et al., 2011, 2012, Allen and Hönisch, 2012), that are discussed later in section 1.4.4.

1.3.3 Extension to Marine Carbonates: The δ^{11}B-pH proxy

Unlike foraminiferal B/Ca ratios (see 1.4.4), the δ^{11}B-pH proxy appears to adhere closely to inorganic theory. Based on the reasonable assumption that $B(OH)_4^-$ is the only boron species incorporated into $CaCO_3$ (discussed above), then in situ pH may be reconstructed from the measured $\delta^{11}B$ of $CaCO_3$ by substituting $\delta^{11}B_{CaCO_3}$ into Equation 1.6, as in Equation 1.10 below (Hemming and Hanson, 1992).

$$pH = pK_B^* - log\left(\frac{\delta^{11}B_{CaCO_3} - \delta^{11}B_{sw}}{\delta^{11}B_{sw} - {}^{11-10}K_B * \delta^{11}B_{CaCO_3} - 1000 * ({}^{11-10}K_B - 1)}\right) \quad (1.10)$$

As discussed previously, all published measurements of carbonate $\delta^{11}B$ lie close to (but not on) the theoretical $\delta^{11}B$ of $B(OH)_4^-$ ion, and show a pH dependence similar (but not equal) to aqueous $B(OH)_4^-$ (for example Hemming and Hanson, 1992, Sanyal et al., 1996, 2000, 2001, Foster, 2008, Hönisch et al., 2009, this study). While this general agreement with aqueous theory has rightly led to considerable optimism regarding the potential of the δ^{11}B-pH proxy, there remain some inconsistencies with theory that are yet to be explained. It is these inconsistencies that form the central focus of much of this PhD project, and consequently they will be discussed in due course. Firstly, as is clear from this equation, and as mentioned in section 1.3.1, three other parameters must also be characterised before pH can be calculated from $\delta^{11}B_{CaCO_3}$: pK_B^*, $\delta^{11}B_{sw}$, and ${}^{11-10}K_B$. Following considerable advances in the past thirty years, however, these variables are now increasingly well understood, and do not hinder application of the δ^{11}B-pH proxy.

1.3.3.1 pK_B^*

As discussed in section 1.3.1, pK_B^* is easily calculable according to Dickson (1990) from *in situ* temperature, salinity and pressure. That said, it should be noted that older derivations of pK_B^* do exist, and so caution should be taken when comparing pH reconstructions from some early studies (e.g. Vengosh et al., 1991, Hemming and Hanson, 1992, Sanyal et al., 1995, Palmer et al., 1987) that use alternative values of

pK_B^* (e.g. Hershey et al., 1986). These definitions of pK_B^* may be derived from different solution chemistries and with reference to different pH scales (e.g. NBS vs. total hydrogen scale Dickson, 1990), and consequently resultant reconstructions of pH are not strictly comparable. That said, uncertainty in the the estimation of pK_B^* typically introduces relatively little additional uncertainty in pCO_2 reconstruction (relative to analytical reproducibility, for example; see section 3.2.5.3). Where it does become more crucial is in discussions of the shape and inflection of δ^{11}B-pH calibration curves, where pH has been manipulated beyond typical seawater values, as discussed by Klochko et al. (2009), Henehan et al. (2013) and later in this thesis in Chapter 3.

1.3.3.2 $\delta^{11}B_{sw}$

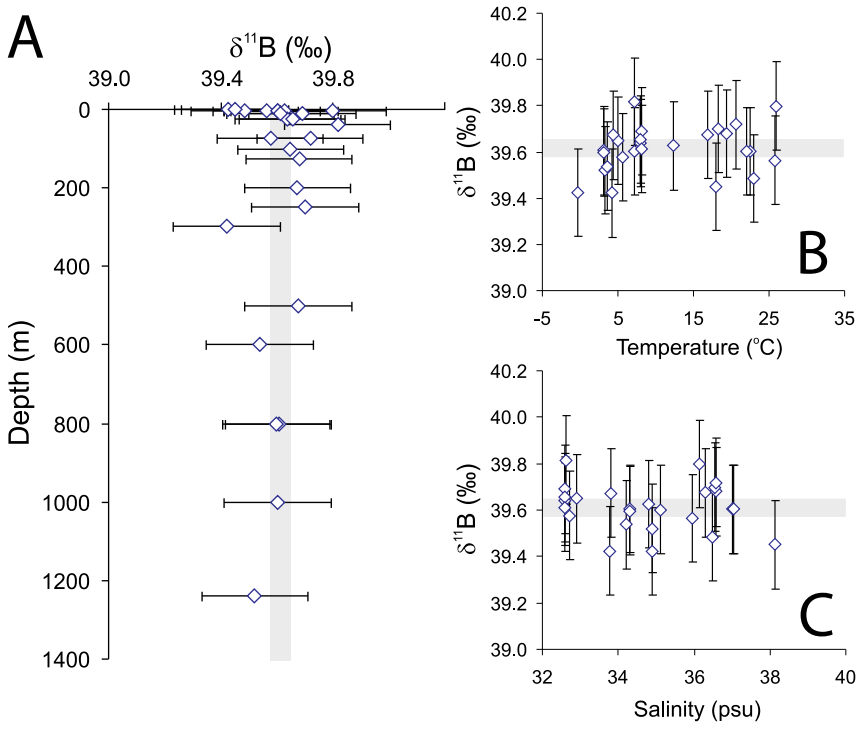

FIGURE 1.2: In the modern ocean, multiple analyses (n = 28) of boron isotope ratios in seawater from different depths (Panel A), temperatures (Panel B) and salinities (Panel C) give uniformly consistent values of δ^{11}B. Redrawn from Foster et al. (2010). Grey bands indicate ±0.4 ‰ uncertainty (2se) on the mean value of 39.61 ‰. Individual error bars reflect long term analytical reproducibility at Bristol Isotope Group, University of Bristol, determined by repeat analysis of an in-house seawater standard.

$\delta^{11}B_{sw}$ is an important variable, in that it strongly effects calculated values of pH calculable from $\delta^{11}B_{CaCO_3}$. While very early works reported inconsistent values of

$\delta^{11}B_{sw}$(Shima, 1963, Agyei, 1968, Nomura et al., 1982), since Spivack and Edmond (1987), analyses from all around the global oceans fall consistently at or around 39.5‰. The latest published estimate of $\delta^{11}B_{sw}$, measured using MC-ICMPS, is 39.61 ± 0.04 ‰ (Foster et al., 2010), with no discernible difference between waters from different hydrographic regimes (see Fig. 1.2). Whilst there remains little controversy regarding the boron isotopic composition of modern seawater, some uncertainty does arise when applying the δ^{11}B-pH proxy to the geological record beyond the residence time of boron in the oceans (10-20 Ma; Taylor and McLennan, 1985, Lemarchand et al., 2002b, Simon et al., 2006), due to an incomplete understanding of the evolution of $\delta^{11}B_{sw}$ through time. Various modelled trajectories have been proposed (see Lemarchand et al., 2002b, Simon et al., 2006), but crucially, without means of empirical validation. Furthermore, given that even the level and isotopic composition of boron flux to the modern oceans is poorly constrained and based on large scale extrapolations (see Lemarchand et al., 2002b), much work remains to be done before modelled estimates of past $\delta^{11}B_{sw}$ can be relied upon. Consequently, attempts have been made to infer the $\delta^{11}B_{sw}$ from other parameters, such as the surface-thermocline pH gradient (Pearson and Palmer, 1999), coupled $\delta^{13}C$ and $\delta^{11}B$ measurements from mixed-layer planktic and epibenthic foraminifera (Foster et al., 2012), or trends in an imbricated multispecies benthic foraminiferal $\delta^{11}B$ record through the Cænozoic (Raitzsch and Hönisch, 2013). While there are uncertainties associated with each individual approach (for example the assumptions that must be made regarding species-specific vital effects), combining these multiple approaches (ideally converging on similar estimates of $\delta^{11}B_{sw}$) has good potential in constraining Phanerozoic $\delta^{11}B_{sw}$, and in turn pCO_2, beyond the residence time of oceanic boron.

1.3.3.3 $^{11-10}K_B$ and pH-sensitivity

The fractionation factor, $^{11-10}K_B$, put simply, expresses the offset in boron isotopic composition between boric acid and borate (as previously defined in Eq. 1.4). Crucially, it describes the degree of change in $\delta^{11}B_{B(OH)_4^-}$ expected with a given change in pH (i.e. the pH-sensitivity of $\delta^{11}B_{B(OH)_4^-}$). $^{11-10}K_B$, also often referred to as α, was first estimated by Kakihana et al. (1977) at 1.0194, with a slight temperature dependence. This value (being for a long time the only available estimate) was widely adopted and applied in palaeo-pH reconstructions (e.g., Pearson and Palmer, 1999,

Sanyal et al., 1995, Hönisch and Hemming, 2005a). However, by 2005 several groups had begun to re-estimate $^{11-10}K_B$ using a variety of methods, (as summarised in Table 1.1), and it had become apparent that persistence in the use of Kakihana et al. (1977)'s value was not well-founded (Zeebe, 2005, Pagani et al., 2005a, Pagani and Spivack, 2007).

A major advance was made in 2006, when Klochko et al. (2006) determined the fractionation factor empirically for the first time, from the difference in the dissociation constants of $^{11}B(OH)_3$ and $^{10}B(OH)_3$ in a number of media (including artificial seawater) using precise spectophotometry. Their observed value of $^{11-10}K_B$= 1.0272 ± 0.0006 was substantially higher than the conventional Kakihana value, and agreed with more recent theoretical derivations (see Oi, 2000, Liu and Tossell, 2005, Table 1.1). In addition, Rustad and Bylaska (2007) revealed errors in calculation that had led Kakihana et al. (1977) and Sanchez-Valle et al. (2005) to underestimate the value of $^{11-10}K_B$. These authors went on to independently calculate $^{11-10}K_B$ as between 1.026 and 1.028 (Rustad et al., 2010), in agreement with the empirical value of Klochko et al. (2006). Given this convergence between calculated and observed $^{11-10}K_B$, throughout this thesis $^{11-10}K_B$ is taken as 1.0272 ± 0.0006 (Klochko et al., 2006).

1.3.3.4 Converting palaeo-pH to palaeo-CO_2

As already shown, given approximations for pK_B^*, $^{11-10}K_B$ and $\delta^{11}B_{sw}$, it is possible to derive ocean pH from foraminiferal $\delta^{11}B$. However, in order to estimate aqueous pCO_2 from ocean pH, an approximation of one other carbonate system parameter is required. Given two carbonate system parameters out of six (HCO_3^-, CO_3^{2-}, $CO_{2(aq.)}$, pH, Total Alkalinity and Dissolved Inorganic Carbon; Zeebe and Wolf-Gladrow, 2001) it is possible to resolve the whole carbonate system and calculate aqueous pCO_2 via Henry's law. The most common second carbonate system parameter used in aqueous pCO_2 reconstruction is Total Alkalinity (or TAlk), largely because a) the reconstructed carbonate system is relatively insensitive to changes in TAlk, b) because TAlk in the modern ocean is strongly correlated to salinity, which may be more easily estimated from sea-level or foraminiferal $\delta^{18}O$ and Mg/Ca (see for example Hönisch and Hemming, 2005b) and c) because TAlk may also be approximated from CCD depth and other hydrographic properties (e.g. Foster et al., 2012).

Study	**°C**	$^{11-10}K_B$	α	β (‰)	**Methods Used**
Kakihana et al. (1977)	24.95	1.0194	0.981	19.4	Empirical spectra and force field modelling
Hemming et al. (1995)	20	1.0162	0.984	16.2	Precipitation of calcite at known pH
Oi (2000)	25	1.0207-1.0360	0.965 - 0.98	20.7	Ab-initio molecular orbital theory
Zeebe (2005)	25	1.02 - 1.05, probably $\geq$ 1.03	0.95 - 0.98, probably $\leq$ 0.97	20-50, probably $\geq$ 30	Evaluation of all approaches
Pagani et al. (2005a)	25	1.0267	0.974	26.7	Curve-fitting to published observations
Sanchez-Valle et al. (2005)	26.85	1.0176	0.983	17.6	Empirical spectra and force field modelling
Liu and Tossell (2005)	25	1.027	0.974	27	Ab-initio molecular orbital theory
Klochko et al. (2006)	25	1.0272 $\pm$ 0.0006	0.974 $\pm$ 0.001	27.2 $\pm$ 0.6	Spectrophotometry in isotopically pure buffer solutions
Rustad et al. (2010)	n/s	1.026 - 1.028	0.973-0.975	26-28	Ab-initio molecular orbital theory

TABLE 1.1: Published estimates for the value of $^{11-10}K_B$, or as sometimes expressed, α_{4-3} (i.e. the inverse of $^{11-10}K_B$, e.g. Pagani et al., 2005a, Rollion-Bard and Erez, 2010) or β (i.e. the difference in ‰ between $B(OH)_3$ and $B(OH)_4^-$). Where possible, the temperature for each calculated value is given, as well as the method through which the value was derived.

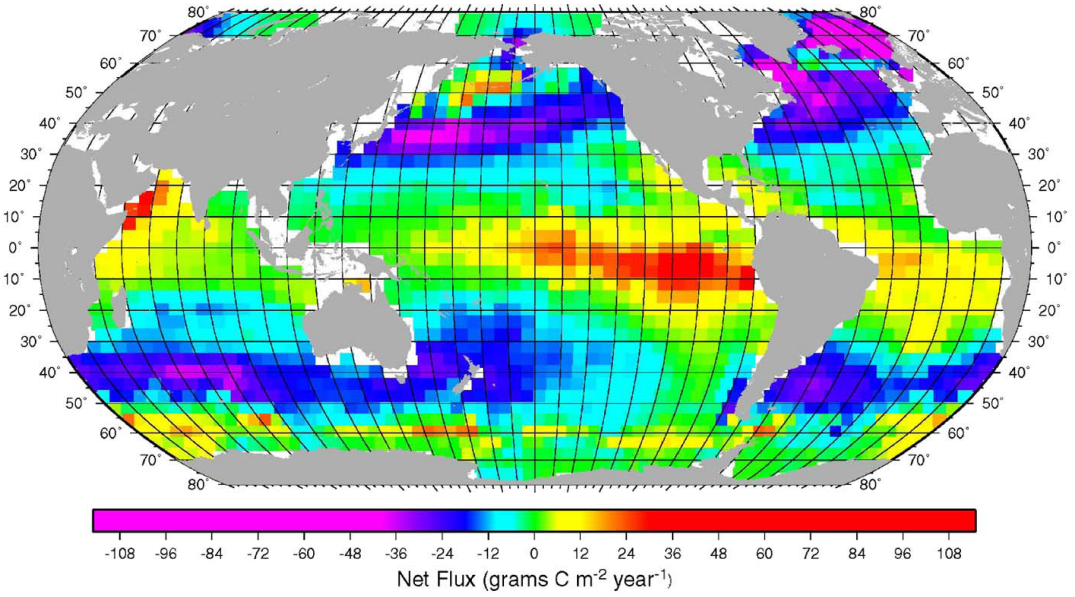

FIGURE 1.3: In the modern ocean, air-sea disequilibrium (with regards pCO_2) is widespread, with upwelling areas such as the Gulf of Oman or the Eastern Equatorial Pacific being higher in pCO_2 than the atmosphere, and other high latitude regions being relatively depleted. As such, air-sea disequilibrium should be considered when interpreting aqueous pCO_2reconstructed from $\delta^{11}B$ and its relation to atmospheric pCO_2. Modified from Takahashi et al. (2009).

Finally, for reconstructed mixed-layer aqueous pCO_2 to be interpreted as atmospheric pCO_2, one must either assume equilibrium with the atmosphere (as in Foster, 2008) or, where possible, correct for disequilibrium (as in Henehan et al., 2013). Air-sea disequilibrium with regards CO_2 (or ΔpCO_2) can be large, for example in areas of upwelling (see Fig. 1.3). As such, downcore atmospheric CO_2 reconstructions should ideally be sited in stable, oligotrophic ocean settings, where ΔpCO_2 is minimal. That said, $\delta^{11}B$ measurements in regions of disequilibrium can also be useful, for example to reconstruct past intensities of upwelling or deep mixing (e.g. Palmer et al., 2010, Martìnez-Botì et al., in prep.).

Although there are clearly numerous constants and secondary parameters that need to be defined to generate pCO_2 data from boron isotopes, as we will show in Chapter 3, these issues are not restrictive. Neither second carbonate system (e.g. TAlk), nor estimates of the disassociation constant (pK^*_B) have a major control on pCO_2 estimates produced via the boron isotope-pH proxy. Furthermore, the long residence time of boron in the ocean means that within the past 10 - 20 Myr (Simon et al., 2006, Lemarchand et al., 2002b) the question of $\delta^{11}B_{sw}$ is not a significant source of

uncertainty. As it stands, boron isotope-derived CO_2 estimates (providing they are properly calibrated) are second in accuracy and precision only to ice-cores in the modern era (see Chapter 3, Fig. 3.10) and have the potential to greatly improve our understanding of the Earth's climate system. That said, the proxy is still not without its controversies, and it is these outstanding issues (detailed below) that this PhD thesis attempts to address.

1.4 Boron-based proxies: controversies and quandaries

1.4.1 Analytical issues

One issue that clouds comparisons of boron isotope datasets produced by different laboratories, and may also result in artificial offsets from the $\delta^{11}B$ of $B(OH)_4^-$, is that of analytical artefacts resulting from different analytical protocols. Precise measurement of $\delta^{11}B$ is difficult for a number of reasons. Firstly, the large mass difference between ^{10}B and ^{11}B relative to absolute mass results in large machine-induced fractionations that can be difficult to correct for. Secondly, since boron has only two naturally-occurring isotopes and synthetic isotopes of boron are short lived, double-spike approaches (such as have proved successful in other systems, e.g., Zn Bermin et al., 2006) cannot be used to correct machine induced isotope fractionation. It is perhaps not altogether surprising, then, that early interlaboratory comparisons (Gonfiantini et al., 2003, Aggarwal et al., 2009) revealed ranges in $\delta^{11}B$ measured in the same sample material of up to 11 ‰; levels of inconsistency that are wholly incompatible with palaeo-pH reconstruction (where precisions of < 0.5 ‰ are required).

Various methods have been used to measure boron isotopes, each with strengths and weaknesses. Negative thermal ionization mass spectrometry (N-TIMS) has produced by far the bulk of published boron isotope measurements in carbonates, not least because of its high ionisation efficiency and thus propensity for measurement of relatively small sample sizes (Aggarwal and Palmer, 1995). Sample B is loaded onto filaments (typically Re) in known matrices (typically artificial seawater or dissolved $CaCO_3$) and heated to produce BO^{2-} ions. However, instrumental mass fractionation of the dominant $^{10}B^{16}O^{2-}$ and $^{11}B^{16}O^{2-}$ species is considerable and varies within runs

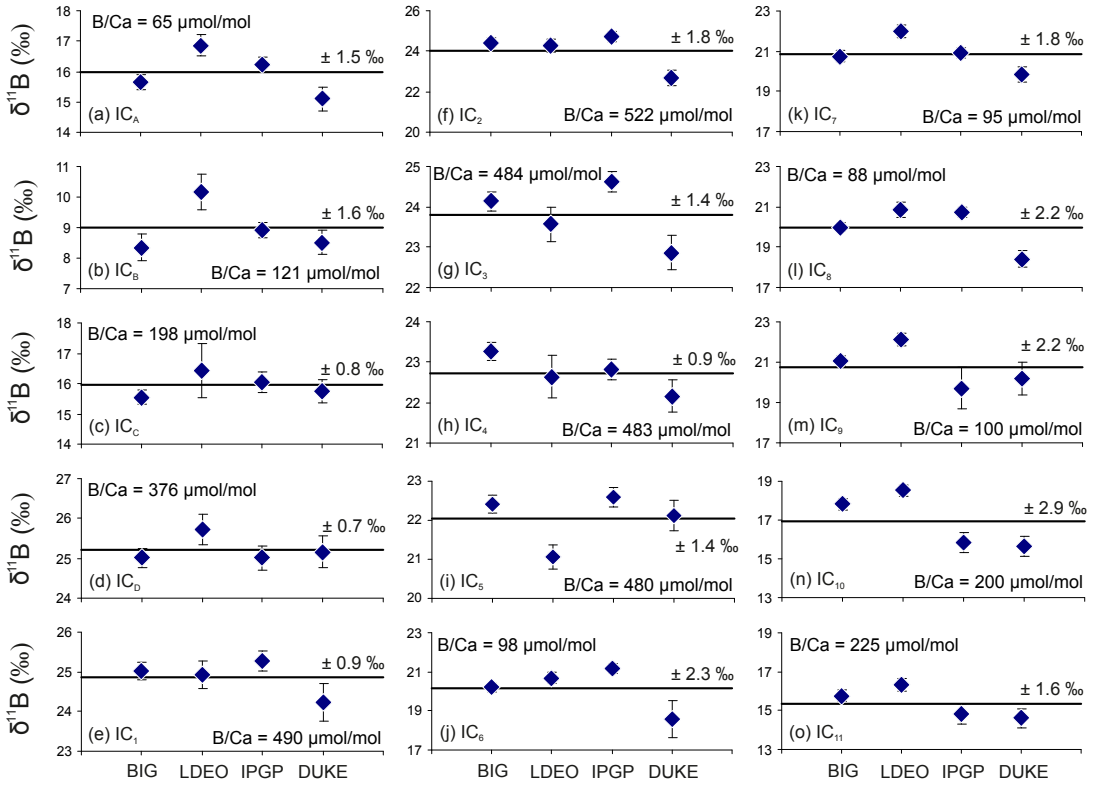

FIGURE 1.4: Analyses of 15 different $CaCO_3$ samples at four different laboratories reveals large-scale variation in measured $\delta^{11}B$. Variability of results are greater at lower B/Ca ratios (see panels j - m) although this pattern is by no means uniformly consistent (e.g. panels a and n). Laboratory abbreviations are as follows: BIG = Bristol Isotope Group, LDEO = Lamont-Doherty Earth Observatory, IPGP = Institut de Physique du Globe de Paris, DUKE = Duke University. Figure modified from Foster et al. (2013).

(Zeininger and Heumann, 1983). Furthermore, samples are often analysed in dissolved $CaCO_3$ matrix (following Hemming and Hanson, 1994), while standards (seawater and NIST SRM 951 boric acid) are measured in seawater matrix, which fractionates differently. As a consequence, it is not possible to accurately quantify the amount of in-run fractionation taking place, making absolutely accurate measurements difficult (Sanyal et al., 1995, Foster et al., 2006). Workers have attempted to mitigate this by running within a controlled temperature range of (900 - 1050 °C), by integrating signals over a set time (typically 20 - 30 minutes) once a set ionisation threshold has been reached, and by discounting data if there is in-run drift of > 1 ‰ (Hemming and Hönisch, 2007). In addition, samples are typically analysed 3-10 times (Hemming and Hanson, 1994, Sanyal et al., 1996, Hemming and Hönisch, 2007), and a subset of these analyses that meet certain criteria for acceptability are averaged to give a mean and standard error (Hemming and Hönisch, 2007). One final issue sometimes faced with

analyses by NTIMS is isobaric interference from $^{12}C^{14}N^{16}O$ ions at mass 42, originating from organic impurities in the carbonate matrix. To counter this, signals at mass 26 ($^{12}C^{14}N$) are monitored, and $\delta^{11}B$ measurements may be rejected if a signal is observed above baseline values. However, as Foster et al. (2006) point out, even with strict 'quality control' measures such as these (as outlined by Hemming and Hönisch, 2007), between laboratories, measurements for similar carbonates often disagree. Measurements of $\delta^{11}B$ in modern *Porites* coral carbonates via NTIMS (Vengosh et al., 1991, Hemming and Hanson, 1992, Gaillardet and Allègre, 1995) varied by up to 3 ‰ between laboratories (Hemming et al., 1998). In foraminifera, measurements of Holocene *G. sacculifer*/*G. trilobus* analysed via NTIMS span a range of up to ∼10 ‰, from 14.7 ‰ (Vengosh et al., 1991) to 25 ‰ (Pearson and Palmer, 2000). More recently, Hönisch et al. (2003) report systematic offsets of ∼ 2 ‰ between NTIMS measurements from Southampton and NTIMS measurements from GEOMAR, Kiel. In addition, differences of ∼1.1 ‰ are observed between analyses of foraminifera at Lamont-Doherty Earth Observatory (LDEO) and State University New York (SUNY) Stony Brook (Hönisch et al., 2009).

With these issues in mind, a new interlaboratory comparison study was undertaken (Foster et al., 2013) to investigate and quantify the degree of interlaboratory bias between four of the leading laboratories carrying out routine $\delta^{11}B$ measurement in biogenic carbonates. While this study found good agreement between analytical techniques when measuring boric acid solutions (±0.31 to ±0.61 ‰) and seawater (39.65 ±0.41 ‰), it reveals significant and non-systematic variation in measurements of samples with a $CaCO_3$ matrix (±0.65 to ±2.86 ‰, see Fig. 1.4). Moreover, interlaboratory inconsistencies appear to be related to both the B:matrix ratio of the sample material and the amount of B available for analysis: lower B/Ca $CaCO_3$ samples (similar in B/Ca to foraminifera) and samples of <200 ng B more often result in larger analytical discrepancies. Given that a change of 1 ‰ might equate to a seawater pH change of ∼0.15, this is clearly pressing issue facing palaeo-pH reconstruction, and highlights the need for laboratories to fully demonstrate analytical accuracy *a priori*, as has been done for MC-ICPMS analyses via standard addition experiments (Ni, 2010). That said, the intercomparison study of Foster et al. (2013) does suggest that relative differences between samples measured in the same laboratory may be, for the most part, consistent, even if data may be offset in terms of

absolute δ^{11}B (e.g. see Fig. 1.4, panels *n* - *o*). In this way, palaeo-pH reconstructions can still be undertaken, providing species-specific calibrations are re-calculated such that they intercept laboratory-specific core-top measurements (as in Foster et al., 2012). Nonetheless, inconsistencies in absolute δ^{11}B render thorough and quantitative investigations of such issues as foraminiferal vital effects (see section 1.4.2) very difficult. At present, more in-depth interlaboratory comparisons (comprising $\sim$ 15 laboratories worldwide, including the University of Southampton and co-ordinated by Drs. Ed Hathorne and Marcus Gutjahr [GEOMAR, Kiel], Dr. Gavin Foster [NOC, Southampton] and Dr. Bärbel Hönisch [LDEO, New York]) are being undertaken to explore this issue still further.

1.4.2 'Vital Effects' in foraminiferal carbonate δ^{11}B

As discussed in section 1.3.3, δ^{11}B measurements from biogenic carbonates typically sit close to the $\delta^{11}B_{B(OH)_4^-}$. However, barring the data of Rae et al. (2011), all measured carbonates still show some offset. Analytical difficulties (as discussed above) aside, it is likely that some of this variation in recorded $\delta^{11}B_{CaCO_3}$ compared to ambient $\delta^{11}B_{B(OH)_4^-}$ is due to 'vital effects'. The term 'vital effect' is used in a palaeoceanographic context to describe an interference of the life processes of a proxy recorder upon the proxy signal itself. Vital effects in corals, for example, are most likely due to the segregation and pH alteration of the calcifying fluids from ambient seawater (see for example Reynaud et al., 2004, Trotter et al., 2011, McCulloch et al., 2012, Anagnostou et al., 2012, Venn et al., 2013). However, this PhD project focusses mainly on foraminiferal proxy records, and as such hereon the term 'vital effects' is used mainly to refer to changes in the recorded δ^{11}B of a foraminiferan shell caused by its life habits and biology. These foraminiferal vital effects have the potential to cloud palaeo-CO_2 reconstructions if not fully understood, or failing that, characterised through species-specific calibrations. Not only this, but since any deviation from idealised δ^{11}B could imply a pH alteration (either of the microenvironment or the calcifying fluid, as discussed in sections 1.4.2.2 and 1.4.2.3), vital effects in boron isotopes carry large implications for our understanding of other proxy systems that have been shown to be affected by pH, for example δ^{18}O (Spero et al., 1997), δ^{13}C (Zeebe et al., 1999a), and Mg/Ca (Russell et al., 2004).

Within the planktic foraminifera, all measured species show considerable offsets, either towards values of $\delta^{11}B$ that are heavier than aqueous $B(OH)_4^-$ (*O. universa*, Sanyal et al. 1996; *G. sacculifer*, Sanyal et al. 2001; *G. ruber*, Foster 2008, Henehan et al. 2013) or lighter (*N. dutertrei*, Foster 2008; *G. bulloides*, Hönisch et al. 2003; *N. pachyderma*, Yu et al. 2013). What's more, the magnitude of these offsets may also vary with foraminiferal size (Hönisch and Hemming, 2004, Ni et al., 2007, Henehan et al., 2013). In this section, some of the various hypotheses advocated to explain these observed patterns of $\delta^{11}B$ in foraminifera are discussed. These themes will be revisited and developed further during the course of this thesis.

1.4.2.1 Life habits

Some vital effects in foraminifera may not stem from any intrinsic biochemical process, but are instead a product of the habitat in which they live. In the case of some benthic foraminifera, for example, observed vital effects may be linked to an infaunal life habit (Rae et al., 2011). Because infaunal species precipitate their tests within sea-floor sediments, their boron isotopic composition not only reflect a lower pH due to bacterial respiration, but a drop in the $\delta^{11}B$ of pore-waters (due to processes such as desorption from clay and the dissolution of opals and carbonates). This change in $\delta^{11}B_{CaCO_3}$ along the pore-water pH and $\delta^{11}B_{\text{porewater}}$ gradient has been well documented both in MC-ICPMS analysis (Rae et al., 2011) and N-TIMS analysis (Hönisch et al., 2008) of various benthic species, including (to name but a few) *Oridorsalis umbonatus*, *Gyroidina soldanii* and *Uvigerina peregrina*.

Depth preference in planktic foraminifera, this time in the water column, may also have an influence on recorded $\delta^{11}B$, due to typical variations in pH, pK_B^* (itself a function of salinity, temperature and pressure) and light with depth in the water column (see Fig. 1.5). While this in itself cannot be considered a vital effect, and indeed allows past pH profiles to be reconstructed (e.g. Palmer et al., 1998), it becomes an issue when planktic foraminifera migrate in the water column throughout their life cycle (e.g. Erez and Honjo, 1981), resulting in different chambers/layers recording conditions from different depths. Since planktic foraminifera are typically analysed in bulk samples, this can see depth-integrated signals in $\delta^{11}B$ recorded, potentially hindering interpretation of $\delta^{11}B$ data. Furthermore, intratest heterogeneity may also

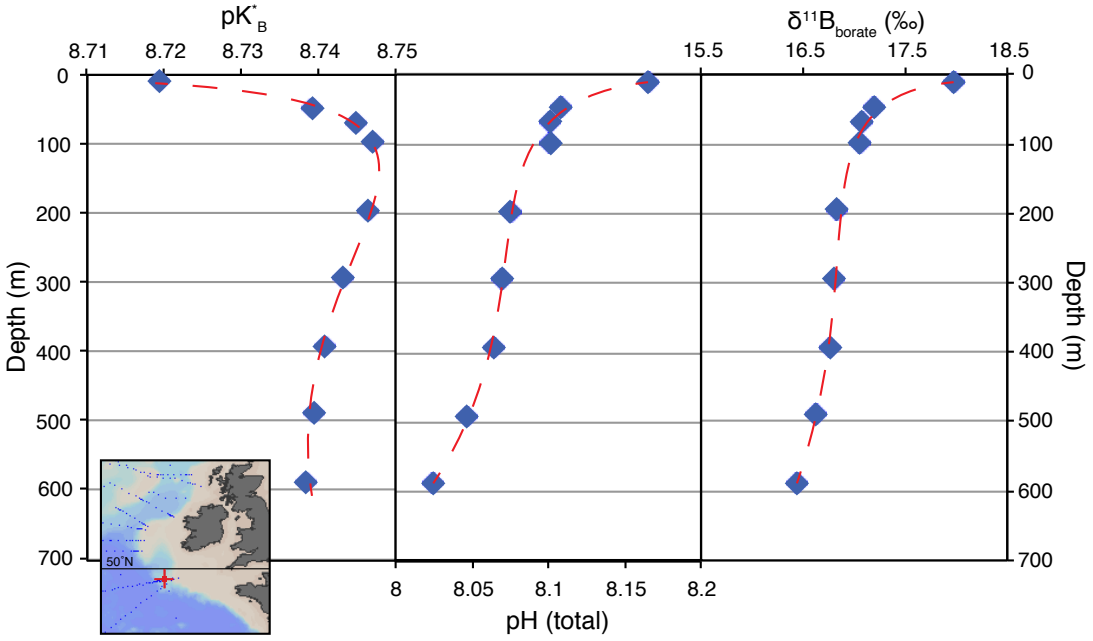

FIGURE 1.5: An example of pK^*_B, pH and $\delta^{11}B_{B(OH)_4^-}$ changes along a verticle depth profile. Example taken from 49 °N, 12 °W in the Northeast Atlantic (map inset), from GLODAP (Key et al., 2004). pH (on the total scale) and pK^*_B were calculated using CO2sys.m (van Heuven et al., 2011), and $\delta^{11}B_{B(OH)_4^-}$ assumes a $\delta^{11}B_{sw}$= 39.61 ‰ (Foster et al., 2010). Note light attenuation might also affect the intensity of vital effects (see section 1.4.2.3).

result in modification of δ^{11}B signals with dissolution (see section 1.4.2.4 below). Thus for reconstruction of mixed-layer pH (and by proxy atmospheric CO_2), it is preferable to use mixed-layer species of foraminifera whose migration in the water column is minimal (e.g. *G. ruber*). Where this is not possible, an understanding of a species habitat preference is necessary. The magnitude of vital effects associated with depth migrations will vary with different species depth preferences, as well as the strength of physicochemical gradients in the local water mass (and how these gradients change through time), but should be considered in palaeo-reconstructions.

1.4.2.2 Biomineralisation and alteration of vacuolised seawater

It has been suggested that some vital effects in foraminifera may be intrinsically linked to the processes of biomineralisation (e.g. Rollion-Bard and Erez, 2010). *In vivo* observations of calcification fluids in vacuoles within symbiont-bearing benthic foraminifera (Bentov and Erez, 2005, Bentov et al., 2009, de Nooijer et al., 2008)

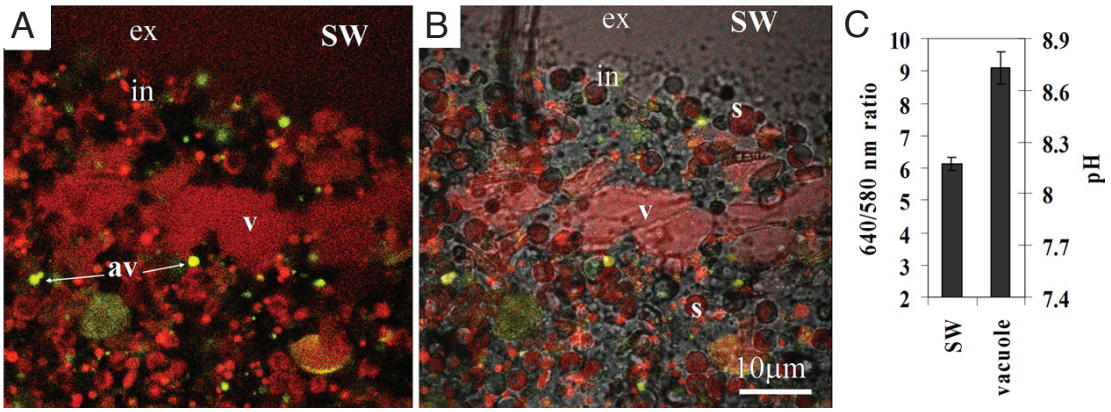

FIGURE 1.6: Modified from Bentov et al. (2009), these images illustrate the pH of seawater vacuoles in *Amphistegina lobifera*, as visualised using with SNARF-1 dextran. Panel A shows the alkaline seawater vacuoles in red (representing 640 nm wavelength flourescence), and low-pH vesicles in yellow-green (denoting relatively stronger 580 nm flourescence). Panel B is the same image overlain with transmitted light imaging, while Panel C illustrates the emission ratio 640/580 nm, and the corresponding pH, of the large seawater vacuole (marked 'v' in Panels A and B) and the ambient seawater. The small vesicles with bright yellow color (marked 'av') were thought to be, according to their low 640/580 fluorescence ratio, acidic (pH <6). However, more recent investigations suggest these may in fact be internal symbionts (J. Erez, pers. comm.). Other symbols denote: intracellular space ('in'), extracellular space ('ex') and algal symbionts ('s').

suggest that forams vacuolise seawater via endocytosis, and then raise the pH in these vacuoles to 8.5 - 9 in order to increase the $CaCO_3$ saturation state (Ω_{CaCO_3}) and thus aid calcification (see Fig. 1.6).

Microelectrodes have also revealed high pH at the calcification site in *Amphistegina lobifera*, a symbiont-bearing benthic foram (Grinstein et al., 2004). While no calcifying vacuoles have been observed unequivocally in planktic foraminifera (mysterious 'cryptosomes' Lee et al., 1965, might however be analogous), it seems unlikely that the mode of calcification would be greatly different within the low-Mg calcite foraminifera. It might seem likely, then, that recorded $\delta^{11}B$ should in fact reflect the pH of these biologically altered fluids, and not ambient pH. Spot analyses of *A. lobifera* using secondary ionisation mass spectrometry (SIMS, Rollion-Bard and Erez, 2010) found a range of $\delta^{11}B$ values within an individual shell, with the lowest $\delta^{11}B$ values reflecting ambient pH and the highest reflecting the pH of altered seawater vacuoles (see Fig. 1.7). If this was to be true of planktics, it could explain some of the observed elevated $\delta^{11}B$ and lowered pH sensitivities apparent from whole test analyses (e.g. Sanyal et al., 1996, 2001). That said, a $\sim$ 0.8 ‰ offset from the theoretical $B(OH)_4^-$ curve in *G.*

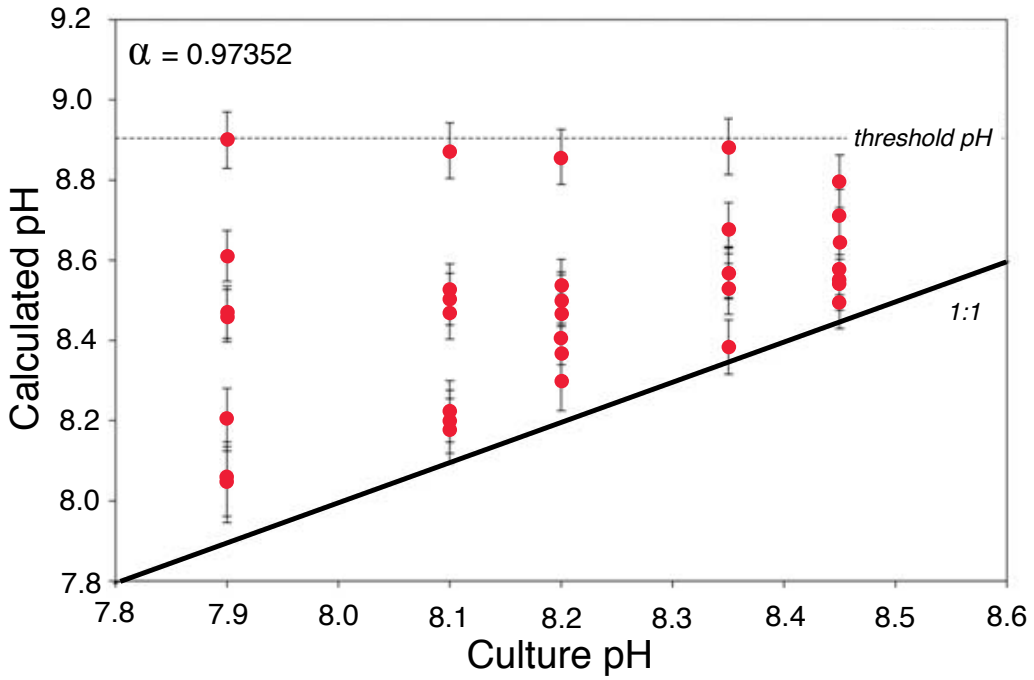

FIGURE 1.7: Results of spot analyses of *Amphistegina lobifera* using SIMS (Rollion-Bard and Erez, 2010), showing a range of δ^{11}B values within the shell. Since the lowest δ^{11}B values translate to ambient pH values (calculated using the $^{11-10}K_B$ of (Klochko et al., 2006)) and the highest do not exceed a threshold value reflecting the pH of altered seawater vacuoles (Bentov et al., 2009, de Nooijer et al., 2008), the authors interpret this as evidence of biomineralisation-induced vital effects. Figure is redrawn from Rollion-Bard and Erez (2010).

ruber (Foster, 2008) only equates to a pH elevated by ~ 0.07, which seems incompatibly low given a vacuole pH of 8.8-9. Furthermore, core top symbiont-barren benthic forams appear to reflect ambient pH without any stemming offset from internal pH upregulation (Rae et al., 2011).

In order to explain this lack of vital effect in epifaunal benthic foraminifera, Rae et al. (2011) propose a hypothetical mechanism for boron incorporation. These authors hypothesise that as seawater vacuoles are formed, $B(OH)_3$ is rapidly removed, leaving only $B(OH)_4^-$. Through this method as long as all boron remaining in the vacuole is incorporated into $CaCO_3$, no matter what re-equilibration of boron occurs within the vacuolised seawater, $\delta^{11}B_{CaCO_3}$ will reflect the δ^{11}B of ambient $B(OH)_4^-$ ion. While this would disagree with Rollion-Bard and Erez (2010), it should be noted that the large reported error values associated with SIMS ($\pm$ 0.9 ‰, 1σ, thus 1.8 ‰ at 95% confidence) may mean at least some internal variation in their study is

analytically-derived. In addition, the presence of internal photosymbionts in the benthic species studied by Rollion-Bard and Erez (2010) may contribute to the observed low pH sensitivity, as will be discussed in section 1.4.2.3 (given that this has been shown to raise the pH in the microenvironment of the foraminifera; Köhler-Rink and Kühl, 2000, Glas et al., 2012a). That said, there remain considerable hurdles to the mechanism for boron incorporation proposed by Rae et al. (2011). Firstly, $B(OH)_3$ would need to be removed from the vacuole faster than the equilibration time of boric acid (125 μs, Zeebe et al., 2001), which seems challenging. In addition, it would require both charged $B(OH)_4^-$ and uncharged $B(OH)_3$ (albeit in the low quantities likely to be present at elevated vacuole pH) to be incorporated into the growing $CaCO_3$ lattice, which seems chemically hard to explain.

Another proposed mechanism for a vital effect linked to biomineralisation is that there is an effect of precipitation rate upon recorded $\delta^{11}B$. The basis of any such vital effect is the idea that as precipitation rate increases, there may be a kinetic effect, seeing the lighter ^{10}B isotope preferentially incorporated, in a similar manner to carbon isotopes (Turner, 1982). However, Zeebe et al. (2001) argue that any kinetic effect due to changes in calcification rate is unlikely: even with large changes in calcification rate, precipitation is typically 3 to 8 orders of magnitude slower than boron isotope equilibration in aqueous boron species. Consequently, it is assumed surface-adsorbed boron would re-equilibrate too quickly with aqueous boron for any preferential take-up of isotopically lighter $B(OH)_4^-$ to be preserved in the $CaCO_3$ lattice. Another hypothesis is that at rapid precipitation rates the isotopically-heavy boric acid may be incorporated into the $CaCO_3$ lattice as an impurity. However, this has not been demonstrable experimentally, and would still require a mechanism and a site for uncharged $B(OH)_3$ to adsorb onto the growing crystal face. One difficulty in testing kinetic issues experimentally is that precipitation experiments tend to control precipitation rate by altering $pH/[CO_3^{2-}]/\Omega$, meaning any effect of precipitation rate cannot be studied in isolation. To this end, decoupling growth rate and carbonate saturation would certainly be desirable.

1.4.2.3 Microenvironment alteration

Because of the viscosity of seawater, the immediate vicinity (specifically, the region below the Kolmogorov scale, η, where viscosity predominates turbulent flow; Kolmogorov, 1991) around a foraminiferal test sees little turbulent mixing (Lazier and Mann, 1989). This region is known as the diffusive boundary layer, since transport of nutrients, dissolved carbon species, etc. is dictated not by any advection, but by diffusion only. Because of the relatively slow equilibration and diffusion rates (see Zeebe et al., 1999b) of dissolved carbon species, the carbonate system within this diffusive boundary layer around a foraminifera may be perturbed relative to the surrounding waters (Zeebe et al., 1999a), and, it is thought, may consequently produce vital effects in recorded $\delta^{11}B_{CaCO_3}$.

The microenvironment of the foraminifera is influenced by a number of processes, schematically represented in Fig. 1.8. The host foraminifera takes in O_2 and releases CO_2 through metabolism and respiration, thereby lowering pH. In addition, the process of calcification involves the takeup of Ca^{2+} and DIC, and the release of H^+ ions, reducing alkalinity and DIC in a 2:1 ratio and lowering aqueous pH. As such, in the absence of photosynthesising symbionts, the foraminiferal microenvironments should be lower in pH than the ambient seawater.

In contrast, in symbiont-bearing foraminifera (during the day), carbonate system perturbation is thought to be dominated by the takeup of DIC (probably mainly CO_{2aq} Colman et al., 2002, Zeebe et al., 1999a) and release of O_2 by photosynthetic symbionts. This raises pH and lowers DIC, to the extent that the acidifying effects of host respiration and calcification are predominated (Zeebe et al., 1999a, 2003). It should also be noted that in the absence of light, symbionts cease to take up DIC but continue to release CO_2 through respiration of stored sugars, thus accentuating microenvironment acidification.

There is considerable empirical evidence for these microenvironment perturbations in foraminifera. Jørgensen et al. (1985) profiled the pH and O_2 of the microenvironment around *Globigerina sacculifer* using microelectrodes, and found that in the absence of light the pH around the foram dropped to ca. 8.15 from an ambient seawater pH of 8.23 (due to respiration and calcification). However, with increasing light intensity and increasing photosynthetic activity the pH in the microenvironment of the foram

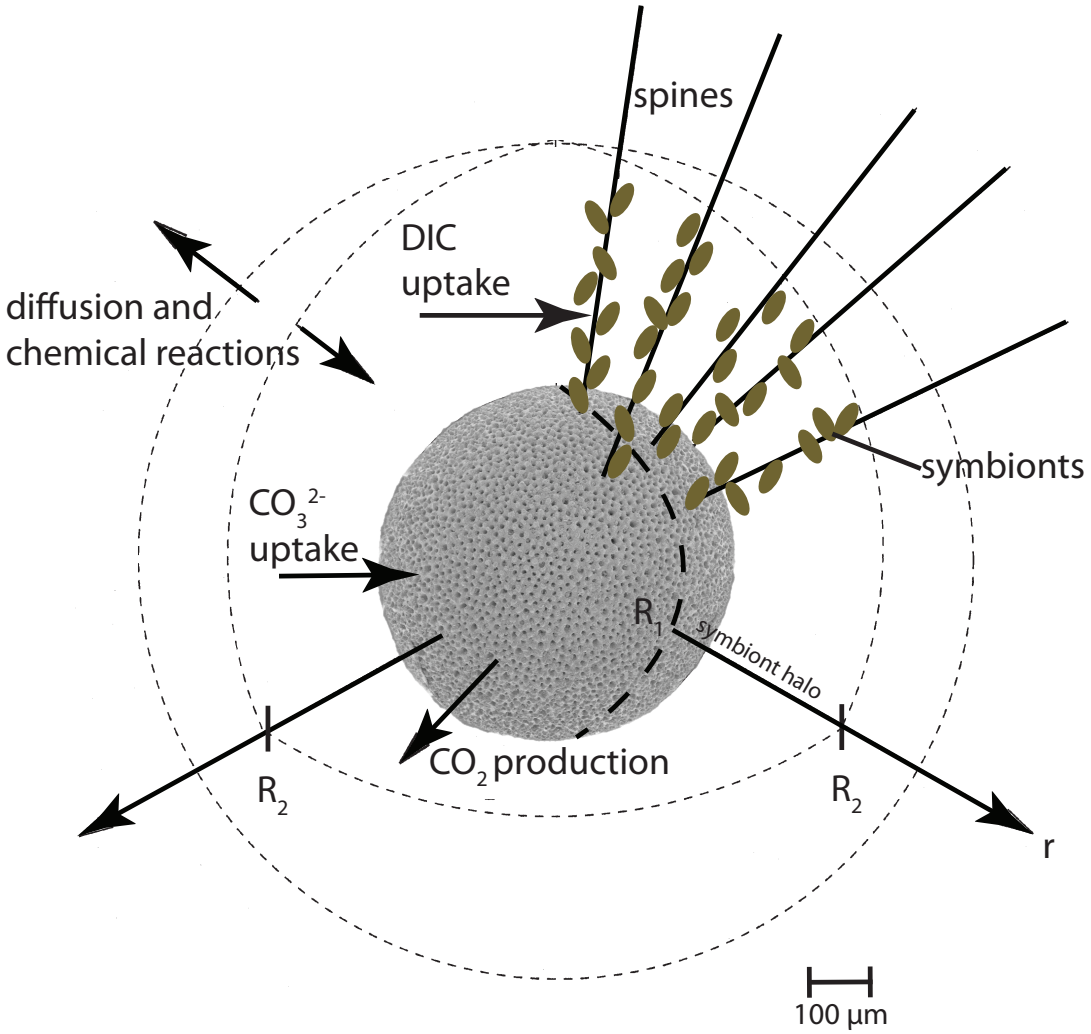

FIGURE 1.8: Microenvironments around foraminifera see carbonate system perturbation from numerous forcings. This schematic, redrawn from Zeebe et al. (1999a), illustrates some of these forcings. Within the symbiont halo (between R_1, the test edge, and R_2), DIC is taken up by photosynthesising symbionts, and by calcification in the host foraminifera. CO_2 is also released by respiration in the host foraminifera and the symbionts. Calcification also takes in Ca^{2+} and releases H^+ ions at R_1. From R_1 to r, the edge of diffusive boundary layer, DIC and $B(OH)_3/B(OH)_4^-$ equilibration relies on diffusion and chemical speciation and reaction.

increased, peaking at about 8.6 at P_{max} (photosynthetic saturation). Subsequently, Rink et al. (1998) and Köhler-Rink and Kühl (2005) expanded these experiments using multiple individuals of *O. universa*, and demonstrated that microenvironment pH alteration can be even greater, with pH at the test boundary (R_1, Fig. 1.8) peaking at >8.8 at 717 μmol photons m^{-2} s^{-1} irradiance, and dropping to <8.0 in the absence of light. Similarly, among benthic foraminifera, large symbiont-bearing benthic foraminifera show similar patterns of microenvironment pH elevation (Köhler-Rink and Kühl, 2000, Glas et al., 2012a) and slow-growing, symbiont-barren species show little or no pH perturbation (Glas et al., 2012a). That said, Glas et al. (2012b) observed substantial (ΔpH up to -1.75) and often prolonged (up to 7 h) acidification close to the site of calcification in *Ammonia tepida* during calcification.

Given, then, that these phenomena are readily observable, it is perhaps unsurprising that microenvironment effects are most commonly invoked as the source of boron isotope vital effects. Furthermore, diffusion-reaction modelling of foraminiferal microenvironment effects (Wolf-Gladrow et al., 1999, Zeebe et al., 1999a, 2003) agrees permissively not only with published the microelectrode observations of Jørgensen et al. (1985) and Rink et al. (1998), but with δ^{11}B measurements of *O. universa* from Hönisch et al. (2003). These authors attempted to empirically quantify the effect of symbiont photosynthesis upon shell δ^{11}B by culturing *O. universa* under high (315-326 μmol photons m^2 s^{-1}) and low (18-20 μmol photons m^2 s^{-1}) light levels, and observed a 1.5 $\pm$ 0.9 ‰ ($\sim$ 0.2 pH unit) offset between the two treatments, which is perhaps lower than expected. However, once the increased alkalinity of the high [B] culture solutions is accounted for, these observations agree with modelled values (Zeebe et al., 2003). Averaged microenvironment pH alteration from micro-electrode observations of *G. sacculifer* (i.e. mean of light and dark conditions, accounting for typical ratios of day:night calcification Jørgensen et al., 1985, Lea et al., 1995) is permissively compatible with the + $\sim$ 0.8 ‰ offset in $\delta^{11}B_{CaCO_3}$ from $\delta^{11}B_{B(OH)_4^-}$ observed in *G. sacculifer* and *G. ruber* (Foster, 2008), if it is assumed 'light' conditions seen by open ocean, lower mixed-layer *G. sacculifer* are lower than P_{max}[1](400 μEinst $m^{-2}s^{-1}$ Jørgensen et al., 1985). Furthermore, MC-ICPMS analysis of *Neogloboquadrina dutertrei* (Foster, 2008) and *N. pachyderma* (Yu et al., 2013) - non-symbiont-bearing planktic foraminifera - produced values of δ^{11}B below that of $\delta^{11}B_{B(OH)_4^-}$, consistent with the imprint of a microenvironment altered by respiration and calcification only.

Finally, microelectrode measurements from the microenvironments of low metabolic rate, symbiont-barren benthic foraminifera suggest pH perturbation is minimal (Glas et al., 2012a), which would corroborate the lack of vital effect in δ^{11}B observed by Rae et al. (2011).

As such, microenvironment-driven vital effects in δ^{11}B would appear to be well-founded, and have the potential to explain many observed geochemical phenomena in foraminiferal tests, in terms of boron isotopes (Zeebe et al., 2003, Hönisch et al., 2003), δ^{18}O (Bemis et al., 1998), δ^{13}C (Zeebe et al., 1999a), and Mg/Ca (Eggins et al., 2004). Notwithstanding this apparent convergence of modelled understanding and empirical data, a number of issues remain:

1. The offset in δ^{11}B between *G. sacculifer* and *O. universa* culture calibrations seems too large to be explained by microenvironment effects alone, as noted by Zeebe et al. (2003). They would either imply unfeasibly high microenvironment pH values in *G. sacculifer*, or pH values in *O. universa* that are lower than those predicted by microenvironment models. That these calibrations were analysed in the same laboratory suggests this offset is unlikely to be the result of some interlaboratory bias.

2. Furthermore, the *O. universa* calibration of Sanyal et al. (1996) produced values of δ^{11}B below those of inorganic precipitates (Sanyal et al., 2000, see Fig. 1.9 above), which, analytical issues aside, would also seem at odds with the modelled values for *O. universa*.

3. Hönisch et al. (2003) report that open ocean specimens of *O. universa*, when analysed via NTIMS, matched more closely not their high-light experiments, but low-light experiments, which suggests culture experiments may not be accurately reproducing the vital effects produced in nature.

4. Model results from Zeebe et al. (2003) suggest that microenvironment pH perturbation, and therefore any offset between $\delta^{11}B_{CaCO_3}$ and $\delta^{11}B_{B(OH)_4^-}$, should be constant regardless of ambient pH. Thus either a) the lowered pH sensitivity in planktic foraminifera δ^{11}B relative to $B(OH)_4^-$ (discussed later in

[1] P_{max} is the light level at which maximum rates of photosynthesis occur, determined to be 300-400 μEinst $m^{-2}s^{-1}$ for *G. sacculifer* (Jørgensen et al., 1985) and 386 μEinst $m^{-2}s^{-1}$ for *O. universa* (Spero and Parker, 1985).

section 1.4.3) implies the existence of some other underlying fractionation, with the microenvironment effect superimposed onto the top (which seems unlikely; see section 1.4.3), or b) microenvironment models may omit some crucial detail that would see pH-sensitivity change with microenvironment alteration.

5. Central to the issue of foraminiferal biomineralisation, it remains unclear how foraminifera apparently record microenvironment effects when calcifying fluids are so extensively modified (de Nooijer et al., 2008, 2009a,b, Bentov et al., 2009).

1.4.2.4 Size Fraction effects

Not entirely unrelated to the vital effects mentioned earlier (given that the mechanisms often proposed as explanations often involve habitat, kinetic or microenvironment changes), is that of the effect of foraminiferal size on recorded δ^{11}B. While commonly seen in δ^{18}O and δ^{13}C (e.g. Norris, 1996, Kroon and Darling, 1995, Bemis et al., 1998), and in other trace element proxies (Ni et al., 2007, Friedrich et al., 2012), there is not yet a wealth of data on size fraction effects on boron isotope ratios in foraminifera. Rae et al. (2011) analysed size fractions of a number of epifaunal benthic foraminifera and found no discernible effect of size upon recorded δ^{11}B signals. However, Hönisch and Hemming (2004) noted a strong size fraction effect in core-top *G. sacculifer* from both the Ontong-Java Plateau and Indian Ocean; a finding which was later corroborated by Ni et al. (2007) in Pacific, but not Atlantic, core-tops. While the observed trends in δ^{11}B with size are comparable, the authors reach somewhat different conclusions about their causality. Hönisch and Hemming (2004), suggest that relatively heavier δ^{11}B in larger specimens may be linked to a shallower depth habit during ontogeny in larger specimens, and as such a greater symbiont-derived vital effect stemming from increased light. This, they argue, is supported by increasing δ^{13}C with size, as commonly observed in symbiont-bearing foraminifera (e.g. Oppo and Fairbanks, 1989, Hemleben and Bijma, 1994). While they observe a correlation between shell weight and δ^{11}B, they suggest this may be due to increased calcification under high light conditions Spero and Lea (1993).

In contrast, Ni et al. (2007) favour a dissolution-based explanation for decreasing δ^{11}B with size, due in part to the variability in patterns they observe between Pacific and Atlantic core-top sites. In this scenario, isotopically lighter gametogenic calcite

(because of its precipitation at lower light levels, colder temperatures and after the digestion of symbionts) is less subject to post depositional dissolution, and since smaller foraminiferal shells have a proportionally larger surface area, they suffer a greater relative loss of ontogenetic calcite relative to gametogenic (and thus are left lighter in δ^{11}B). Their argument is lent further support by later findings from Seki et al. (2010), who see a drop in δ^{11}B and B/Ca in *G. sacculifer* along a transect in bottom water Ω_{CaCO_3} along the Ceara Rise (consistent with a dissolution effect). Meanwhile neither set of authors see a comparable dissolution effect in *G. ruber*, as one might expect from a species that precipitates no significant gametogenic calcite layer. One cautionary note regarding this preferential dissolution hypothesis, however, is that SEM images from Hönisch and Hemming (2004) and Bé (1980) appear to indicate dissolution of the gametogenic calcite veneer in at least equal measure. Furthermore, Hönisch and Hemming (2004) highlight that dissolution in the sediment may depend not only on bottom water Ω_{CaCO_3}, but on the extent to which organic matter is being respired within the sediment; something which is not discussed in Seki et al. (2010). Clearly, then, more data is required to more thoroughly investigate the causes of size-fraction effects on δ^{11}B.

1.4.3 Is pH sensitivity in $\delta^{11}B_{CaCO_3}$ equivalent to that of $\delta^{11}B_{B(OH)_4^-}$?

Despite the increasing convergence of theoretical and empirical studies around the Klochko et al. (2006) value of $^{11-10}K_B$ for boron species in seawater, as discussed previously, some authors advocate the retention of the Kakihana et al. (1977) fractionation factor as an empirical calibration to apply to marine $CaCO_3$ (Hemming and Hönisch, 2007, Hönisch et al., 2007, 2008, Katz et al., 2010). For instance, Hönisch et al. (2007) state that 1.0194 is 'statistically the factor that best describes the shape and inflection of all empirical carbonate calibrated to date'. However, while it is true that all planktic foram, coral and inorganic carbonate calibrations to date do show a weaker-than-predicted sensitivity to pH, or in other words they would support a value of $^{11-10}K_B < 1.0272$ (see Fig. 3.1), it is incorrect to imply that there is any definitive universality in these calibrations. Although large margins of uncertainty in planktic foraminiferal calibrations mean that they are statistically indistinguishable (see Fig. 3.1), when one also considers the considerable disparity in the shapes of coral calibrations (e.g. Hönisch et al., 2004, Krief et al., 2010, Trotter et al., 2011,

McCulloch et al., 2012, Anagnostou et al., 2012), universality seems currently far from assured. Moreover, most calibrations would in fact advocate a $^{11-10}K_B$ that is lower than that of Kakihana et al. (1977). As such, its use even as a universal empirical fractionation factor seems unfounded.

One line of evidence that is often cited as support for a value of $^{11-10}K_B$ for carbonates < 1.0272 is the observed pH dependency of the δ^{11}B of the inorganic carbonate precipitates of (Sanyal et al., 2000, see Fig. 1.9). These authors precipitated calcium carbonate (calcite polymorph) at three different pH values, and observed a pH sensitivity in the $\delta^{11}B_{CaCO_3}$ that is lower than that of aqueous borate observed by Klochko et al. (2006). Since existing (Sanyal et al., 1996, 2001, Henehan et al., 2013, see Chapter 4) planktonic foraminiferal calibrations show pH sensitivities that are within uncertainty of this inorganic calibration (see section 3.2.3.2), it is perhaps on the face of it reasonable to infer that the lowered-than-aqueous pH sensitivities observed in foraminifera are due to some inorganic fractionation inherent in calcification of marine biogenic $CaCO_3$. However, as discussed by Henehan et al. (2013), no such inorganic fractionation is evident in epifaunal benthic foraminifera (Rae et al., 2011) and, as we show in Chapter 4, neither is it likely in symbiont-barren planktic foraminifera. It seems probable therefore that the lowered pH sensitivity in planktic foraminiferal calibrations may be explained by some vital effect (for example, the action of photosynthetic symbionts, see section 1.4.2.3), but clearly the inorganic precipitation experiments of Sanyal et al. (2000) would still require some explanation. The apparently lowered sensitivity observed may be an artefact of inadequate characterisation of pH or pK_B^* in these experiments: the authors use NBS-buffer calibrated electrodes, and do not explicitly characterise the pK_B^* of the experimental solutions. Alternatively, it may be an artefact of inconsistent and rapid precipitation rates in these experiments (100 mg in between 3 and 24 hours) that are not representative of foraminiferal calcification rates and may conceivably cause kinetic fractionation. Finally, as discussed in section 1.4.1, although most evidence suggests that relative differences measured via NTIMS are reliable (even if absolute measurements may not be), it is conceivable that the highly variable B/Ca ratios in these calcite precipitates may mean the NTIMS matrix effect was not consistent between analyses (see Foster et al., 2013).

With these issues in mind, in a collaboration with Asst. Prof. Sang-Tae Kim and Miss

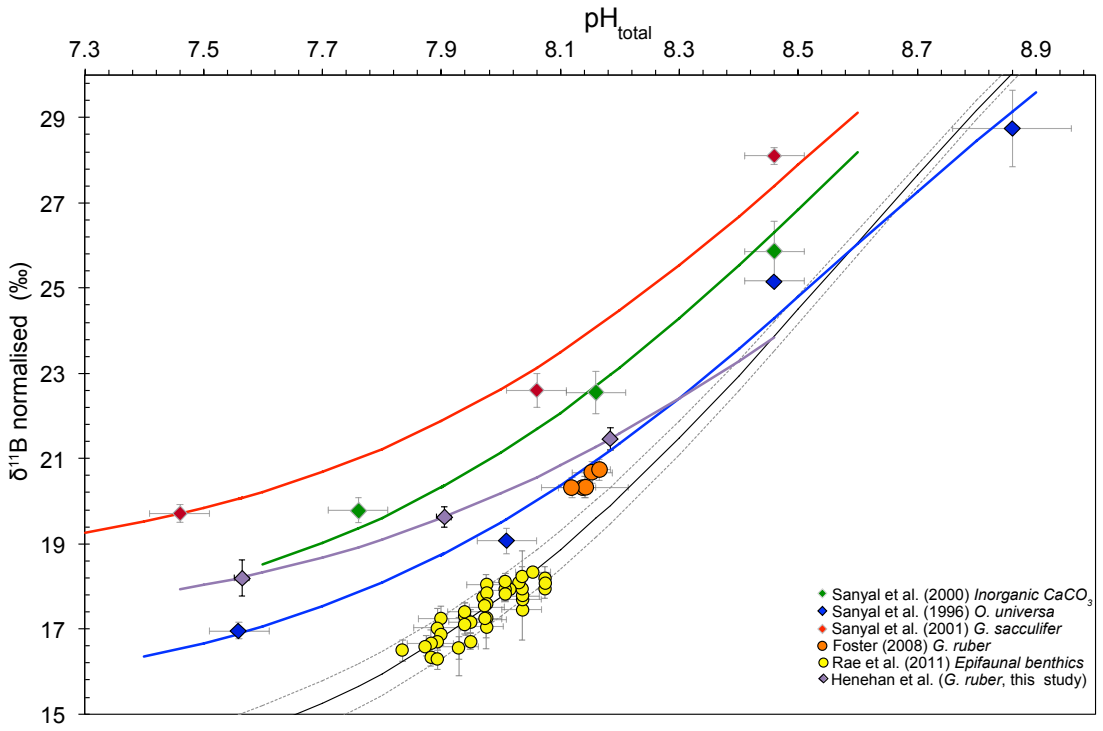

FIGURE 1.9: Published bulk planktic foraminiferal culture and inorganic precipitate experiments, plotted in δ^{11}B-pH space. For the purposes of graphical representation, the data were normalised to a $\delta^{11}B_{sw}$= 39.61 ‰ (both panels), and to a temperature of 26 °C and a salinity of 37.2 psu. The black line depicts the value of aqueous $\delta^{11}B_{B(OH)_4^-}$ at these environmental conditions, with the dotted lines representing the error value on the value of $^{11-10}K_B$ (± 0.0006) in seawater at 25 °C reported by Klochko et al. (2006). Coloured calibration lines are best fits through calibration data, varying $^{11-10}K_B$ and a from Equation 3.4; see section 3.2.3 for more details.

Christa Klein Gebbinck at McMaster University, the systematics of boron incorporation into carbonates have been re-examined. Aragonite was precipitated at across a range of pH (at 25 °C), at rates representative of natural biomineralisation processes (< 10 mg/day; an order of magnitude lower than previous experiments), and slow enough to ensure equilibrium for O and C isotopes (and by inference, B, since equilibration times for B are shorter Zeebe et al., 1999b). The approach used to precipitate $CaCO_3$ was an adapted constant addition method (Kim et al., 2006, 2007, as previously used to examine oxygen and carbon isotope fractionations). In these experiments, ionic strength was similar to natural seawater (I = 0.7 mol kg^{-1}), and as such pK_B^* could be calculated via Dickson (1990). Boron isotope measurements were taken from mother solutions, as well as from the precipitates themselves. While more data at low pH values is still being collected, preliminary results are shown in Fig. 1.10. These data illustrate that when precipitated at rates comparable to those seen in

biology, when pK_B^* is well characterised, and when samples are analysed via MC-ICPMS, the δ^{11}B of inorganic precipitates reflect ambient $\delta^{11}B_{B(OH)_4^-}$ without any fractionation.

While these preliminary data were not gathered in time to be incorporated into discussions within Henehan et al. (2013), when coupled with findings from symbiont-barren species (Chapter 4) and epifaunal benthic foraminifera (Rae et al., 2011), they constitute a strong body of evidence that suggests there is no underlying inorganic fractionation of δ^{11}B inherent in the calcification process, and that the value of ${}^{11-10}K_B$ reported by Klochko et al. (2006) is reliable and representative of fractionation between species in $CaCO_3$. Therefore it seems preferable to look to vital effects to explain reduced pH-sensitivities in published planktic foraminiferal calibrations.

One further controversy relating to the pH sensitivity of $\delta^{11}B_{CaCO_3}$ is the suggestion that it may change with temperature. This is based on the assertion that the fractionation factor (${}^{11-10}K_B$) between boron species in seawater is temperature dependant. Given that the fractionation factor is a function of parameters such as molecular vibrational frequency, which varies with temperature, most theoretical investigations into the value of ${}^{11-10}K_B$ advocate variation with temperature (e.g. Kakihana et al., 1977, Rustad et al., 2010, Zeebe, 2005). However, as Zeebe (2005) discusses, the sensitivity of theoretically-derived values of ${}^{11-10}K_B$ to temperature depends largely on the derivations of molecular forces, and hence vibrational frequencies, used in the calculation (see Fig. 1.11). Since no single method of calculation can be considered definitive, it is as yet impossible to reliably characterise the temperature dependence of ${}^{11-10}K_B$ via theoretical calculations.

Given these complications, then, it is preferable to look to empirical measurements. In their experimental derivation of ${}^{11-10}K_B$, Klochko et al. (2006) did not observe any clear temperature effect on the value of ${}^{11-10}K_B$. That said, they cannot conclusively discount the possibility: their analyses were carried out at only two temperatures, and the high margin of uncertainty for the published 40 °C estimate could permissively accommodate a variation of ${}^{11-10}K_B$ with temperature. As a result of this uncertainty, some reconstructions have opted to incorporate a (somewhat arbitrarily assigned) temperature-dependence for ${}^{11-10}K_B$ (e.g. Hönisch et al., 2008, Raitzsch and Hönisch,

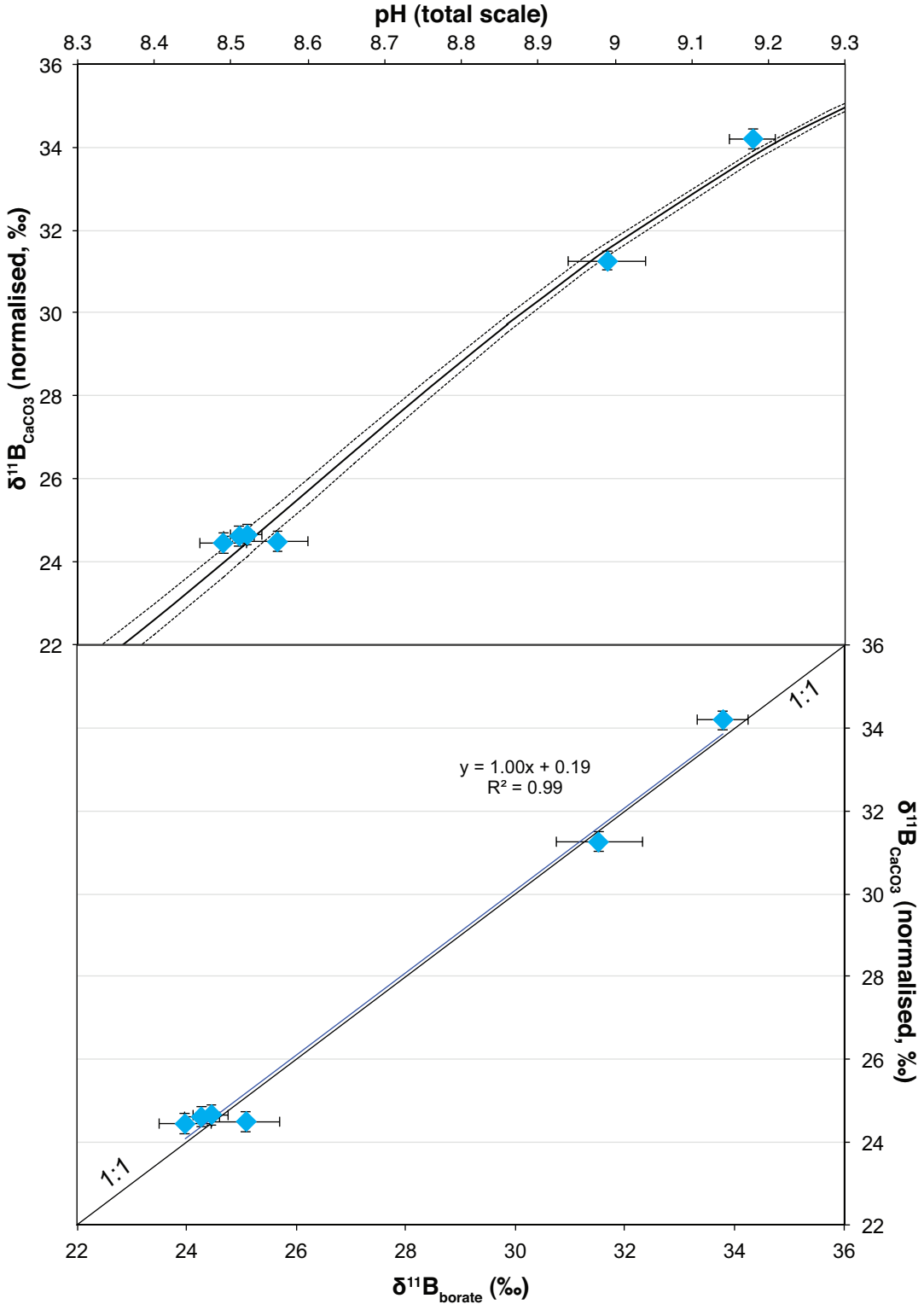

FIGURE 1.10: A new calibration, in preparation, for inorganic aragonite precipitates. Although as yet we have no data at low pH, it would appear that these new precipitates show little or no fractionation of $\delta^{11}B_{B(OH)_4^-}$ upon incorporation into $CaCO_3$. The data are shown in both δ^{11}B-pH space (Panel A) and $\delta^{11}B_{CaCO_3}$-$\delta^{11}B_{B(OH)_4^-}$space (Panel B, see section 3.2.3.2 for further explanation). Note also that these data are normalised to $\delta^{11}B_{sw}$=39.61‰, for greater ease of comparison with measurements from natural systems.

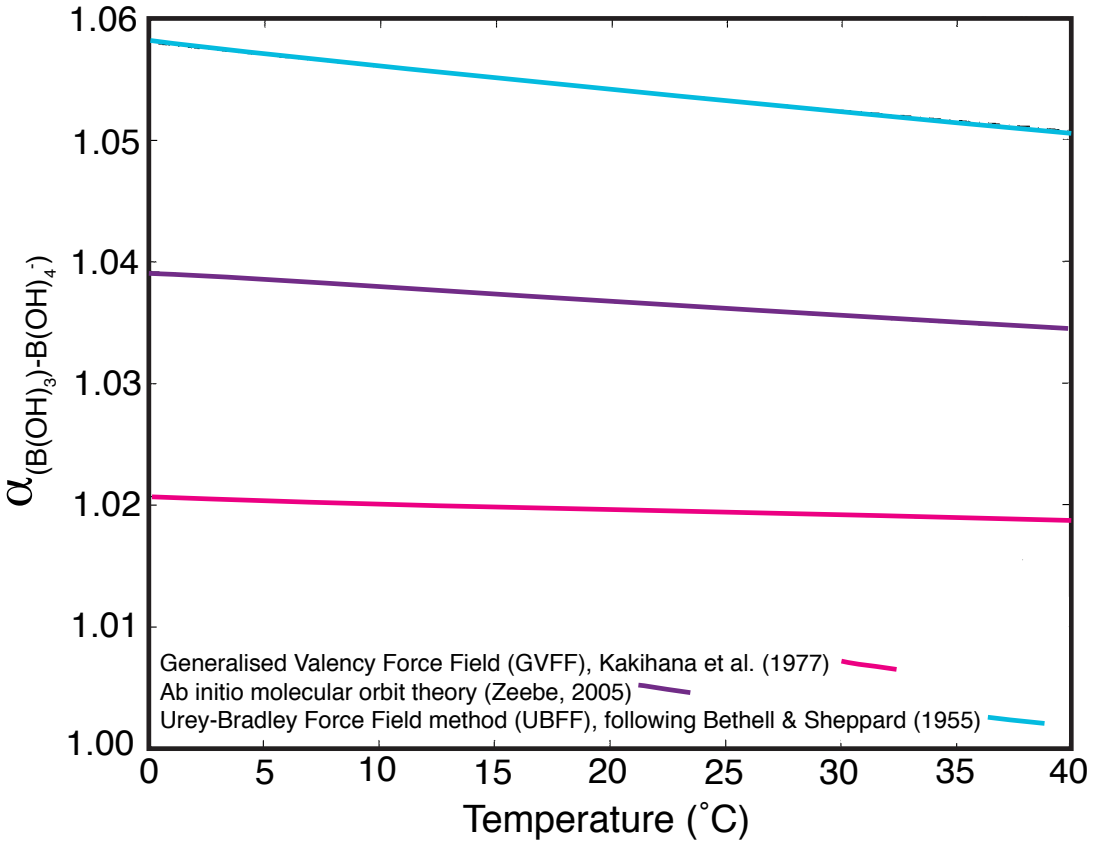

FIGURE 1.11: Depending on the method used to derive $^{11-10}K_B$ mathematically, both absolute values and their variation with temperature will differ. Modified after Zeebe (2005), this plot illustrates the varying temperature dependence of three contrasting derivations of $^{11-10}K_B$.

2013). However, as yet there are no published data that unequivocally show a temperature dependence in foraminiferal δ^{11}B (although suggested by Wara et al. 2003, their argument is based on potentially circumstantial correlations). Furthermore, measurements of benthic forams (Rae et al., 2011, Supp. Fig. 3) do not support a discernible temperature-dependence of $^{11-10}K_B$ (see Fig. 1.12). Extending the Klochko et al. (2006) experiments at a greater range of temperatures and with more replicates per treatment might serve to solve the matter more definitively, but at this point it seems wiser to defer to empirical observations, all of which suggest no discernible effect of temperature upon $^{11-10}K_B$ within the typical range of ocean temperature.

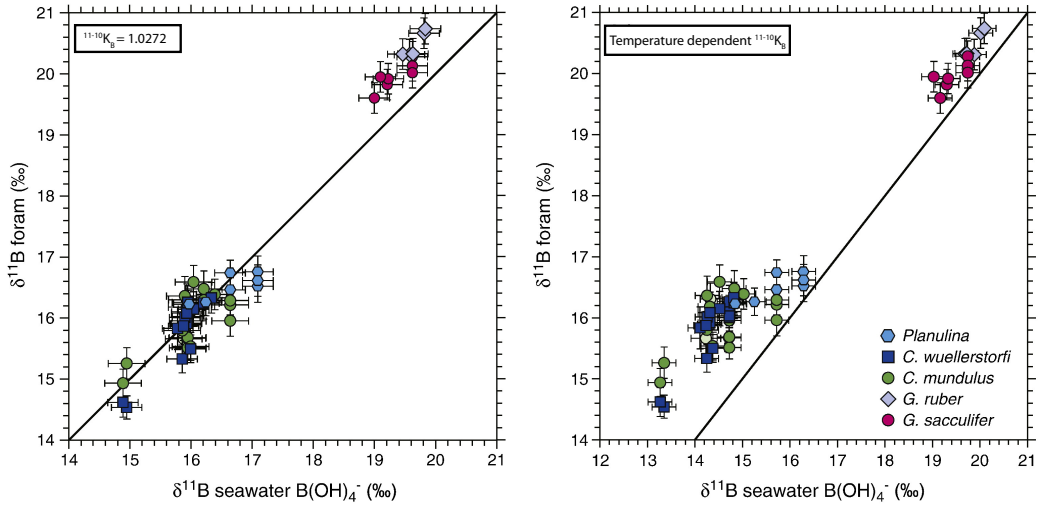

FIGURE 1.12: Modified from Rae et al. (2011), this plot shows that without any temperature effect on $^{11-10}K_B$ (left panel), observed δ^{11}B in epifaunal benthic foraminifera agrees with that of ambient $\delta^{11}B_{B(OH)_4^-}$. Incorporation of the temperature dependence of $^{11-10}K_B$ inferred by Hönisch et al. (2008) results in substantial deterioration in fit.

1.4.4 The B/Ca proxy: Drivers of boron incorporation in planktic foraminifera

Like the δ^{11}B-pH proxy, B/Ca ratios in foraminifera are thought to be driven by pH and carbonate system changes in the ocean, as a result of well understood aqueous chemistry (summarised in sections 1.3.1 and 1.3.2). However, it is clear that pH is unlikely to be the only control on boron incorporation (see Allen and Hönisch, 2012, for a review). Instead, temperature (Wara et al., 2003, Yu et al., 2007b, Tripati et al., 2009, 2011), salinity (Allen et al., 2011, 2012), foraminiferal physiology and ontogeny (Ni et al., 2007, Allen et al., 2011, 2012), crystal surface processes (Hemming et al., 1995, Hobbs and Reardon, 1999) and post-depositional dissolution (Seki et al., 2010, Coadic et al., 2013) have all variously been suggested as dominant controls. In contrast, in benthic foraminifera, existing field calibrations do seem to favour a strong carbonate system control on B/Ca ratios (Yu and Elderfield, 2007, Yu et al., 2010, Rae et al., 2011), albeit only through the parameterisation $\Delta[CO_3^{2-}]$, for reasons that are not entirely clear (Yu and Elderfield, 2007). Given species-specific differences, the apparent disagreement between controls on planktic and benthic foraminiferal B/Ca, the range of alternative drivers for boron incorporation suggested for planktic foraminifera and the lack of basis in aqueous boron chemistry for any correlation with $\Delta[CO_3^{2-}]$, it is

clear that B/Ca ratios in foraminiferal calcite are not simply dictated by the inorganic speciation of boron and DIC in seawater. Thus there remain fundamental gaps in our understanding of the controls on boron incorporation into foraminiferal $CaCO_3$.

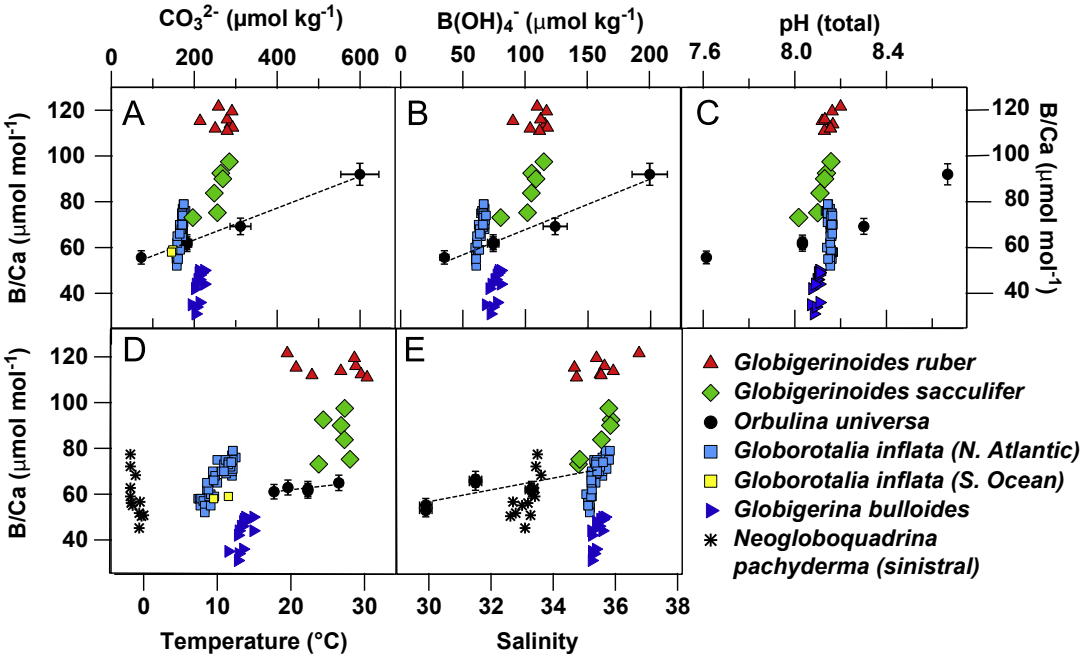

FIGURE 1.13: While cultured *O. universa* show a strong relationship with carbonate system/pH related parameters (Panels A-C), there are strong species offsets (all panels), suggesting perhaps some biological control and/or unidentified controls on B/Ca. In addition, some datasets (*G. inflata* and *G. bulloides*, Panel D) hint at a temperature effect on B/Ca, and others (e.g., cultured *O. universa*, Panel E) demonstrate a salinity dependence. Data shown are from (Foster, 2008, *G. ruber*, *G. sacculifer*, core-top), (Yu et al., 2007b, *G. inflata*, *G. bulloides*, core-top), (Hendry et al., 2009, *N. pachyderma*, sediment trap) and (Allen et al., 2011, *O. universa*, cultures). Modified from Allen and Hönisch (2012)

The first of these suggested drivers, temperature, should influence boron incorporation through its influence on K_1, K_2 and K_B constants (Zeebe and Wolf-Gladrow, 2001), which in turn alter $\frac{B(OH)_4^-}{HCO_3^-}$ ratios in seawater. However, this effect is small, and likely beyond the limits of analytical detectability. Despite this, numerous studies (Wara et al., 2003, Yu et al., 2007b, Tripati et al., 2009, 2011) still point to temperature as a major driver of B/Ca ratios in planktic foraminifera. Given that neither cultures of *O. universa* between 18 - 26 °C by Allen et al. (2011), nor cultures of *G. ruber* and *G. sacculifer* from 24 - 30 °C by Allen et al. (2012) show a significant relationship between B/Ca and temperature, however, this seems unlikely. Instead observed temperature dependencies are likely either an artefact of describing B/Ca ratios in

terms of K_D ($K_D = \frac{B/Ca}{B(OH)_4^-/HCO_3^-}$, as in Yu et al., 2007b, Tripati et al., 2009), which may produce artificial relationships (due to the effect of temperature on the denominator, or the incorporation of an inherent SST-pCO_2 relationship; see Allen and Hönisch, 2012), or alternatively a product of the correlation of temperature with other parameters, such as $[CO_3^{2-}]$, as may be the case in Yu et al. (2007b). Furthermore, down-core correlations of B/Ca with Mg/Ca-derived SST (as in Wara et al., 2003, Yu et al., 2007b) could arise coincidentally, as a result of some unknown inorganic process such as paired substitution, or as a result of diagenetic loss of trace elements (Coadic et al., 2013, Dekens et al., 2002), and should not be taken as proof of a temperature effect on B/Ca in the face of evidence from cultures that disagrees.

As with temperature, salinity will alter the equilibrium constants of seawater, and in turn should affect $\frac{B(OH)_4^-}{HCO_3^-}$, and hence B/Ca. However, Allen et al. (2011, 2012) found salinity to have a much larger effect on B/Ca ratios in planktic foraminifera than that expected from the alteration of equilibrium constants alone. This salinity effect might be partially explained by an increase in $[B]_{sw}$ at high salinities: Allen et al. (2011) note that increasing $[B(OH)_4^-]$ by raising total $[B]_{sw}$ at a constant pH resulted in a disproportionately large response in B/Ca compared to experiments where $[B(OH)_4^-]$ was increased through pH-dependent speciation. This disproportionate effect of $[B]_{sw}$ may be a product of competition between B and other ions (e.g. CO_3^{2-}, or alternatively, other impurities- see below) for incorporation sites. However, it is also possible that increasing salinity may significantly raise B/Ca without any elevation of $[B]_{sw}$. For example, Kitano et al. (1978a) found that boron incorporation into inorganically precipitated $CaCO_3$ rose with the addition of pure NaCl (i.e. with no concurrent rise in $[B]_{sw}$), which suggests that there is some other effect, perhaps linked to ionic strength affecting crystal surface processes (e.g. by raising the activities of the reactants), or ion pairing in solution.

Indeed, crystal surface processes have been shown to have a strong effect on boron incorporation into inorganic precipitates. Hemming et al. (1995) highlight that increased boron incorporation in inorganically-precipitated aragonite (where, they argue, B is incorporated in tetrahedral form without need of re-coordination, following Sen et al., 1994) relative to calcite is evidence for the kinetic requirements of boron re-coordination being an incorporation-limiting factor. Boron doping in inorganic precipitation experiments (e.g. Ruiz-Agudo et al., 2012) disrupts orderly crystal

growth patterns (see Fig. 1.14), illustrating that incorporation of boron necessitates reorganisation of lattice and growth face structures. These studies suggest that slower rates of calcite crystal precipitation are key to the levels of B incorporated, as they permit more complete re-coordination of tetrahedral boron into trigonal form. In addition, Hemming et al. (1995) and Hemming et al. (1998) also suggest that boron incorporation may be dictated by the availability of defect or anion sites, which in turn is dependent on both the structure of the growing crystal face, and the degree to which these sites may be occupied by other competing impurities. In this way crystallographic processes or other chemical substitutions that might drive an increase in the number of defects sites should produce elevated B/Ca ratios. Later studies reaffirm the importance of crystal growth processes in boron incorporation, including Hobbs and Reardon (1999) and Ruiz-Agudo et al. (2012). It is perhaps surprising, then, that these sorts of influences have been largely overlooked by the palaeoceanographic community.

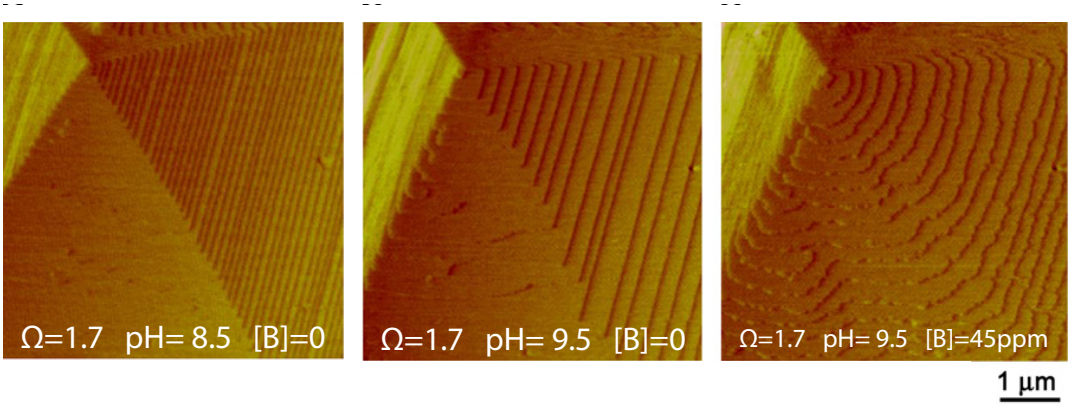

FIGURE 1.14: Atomic force microscopy (AFM) imagery illustrates the effect of aqueous boron on growing hillocks of calcite. Elevated pH without the addition of boron causes elongation of obtuse growth steps due to the dehydration of Ca^{2+} ions (centre). The presence of boron (right) retards obtuse step growth (the step at which boron is more readily incorporated). Images modified from Ruiz-Agudo et al. (2012).

A final inorganic factor which may affect the recorded B/Ca of foraminifera is that of post-depositional alteration: dissolution and recrystallisation. Ni et al. (2007) note decreasing TE/Ca ratios in smaller size fractions of *G. sacculifer* and *G. ruber*, which they interpret as loss of impurities with dissolution (because smaller tests have a large surface:volume ratio and are more susceptible to dissolution). More conclusive, however, are the data of Seki et al. (2010) and Coadic et al. (2013), that show that B/Ca decreases systematically long depth transects, as waters at the sediment

interface become more corrosive. Any such dissolution effect could constitute a significant barrier to the successful application of the B/Ca proxy, particularly over large events such as the PETM, where the lysocline may have fluctuated and the intensity of deep-sea carbonate dissolution may have varied.

In addition to these multiple inorganic processes, the life processes of the foraminifera must also introduce vital effects in B/Ca ratios. The large interspecific differences in B/Ca between planktic foraminifera (see for example Allen et al., 2012), and between planktic and benthic foraminifera (see for example Foster, 2008), show that boron incorporation must be (by some unknown means) biologically mediated. The difference in B/Ca between various species of planktic foraminifera could be consistent with existing theories of microenvironment alteration (see Section 1.4.2.3). Firstly, increasing B/Ca from *O. universa*<*G. sacculifer*<*G. ruber* is similar to the increase in δ^{11}B between these species (see Chapter 4), and indeed the shallowing depth habitats (and increasing illumination and symbiont photosynthesis) of these species (Hemleben et al., 1989). Secondly, symbiont bearing foraminifera record higher B/Ca ratios than symbiont barren foraminifera, which would be consistent with a lower microenvironment pH (and thus $\frac{B(OH)_4^-}{DIC}$) in those foraminifera that do not possess photosynthetic symbionts. Thirdly, increasing B/Ca with size fraction, as seen by Ni et al. (2007) and Hönisch and Hemming (2004), if not caused by post-depositional dissolution, might be caused by intensification of vital effects with growth, as suggested by Henehan et al. (2013). Finally, observed patterns of intratest variability are permissively consistent with day:night microenvironment pH fluctuations (*O. universa* LA-ICPMS profiles; Allen et al., 2011) or pre-gametogenic expulsion of symbionts (*G. sacculifer* final chambers; Allen et al., 2012). That said, the scale of disparity in B/Ca between some benthics and planktics (a 2× to 4× increase in benthics) might imply some difference in biomineralisation mechanisms, since the microenvironment of symbiont barren benthic foraminifera experiences no pH elevation (Glas et al., 2012a).

Clearly the controls on boron incorporation are complex and potentially numerous. For B/Ca to prove valuable as a proxy, there is considerable work to be undertaken. Allen and Hönisch (2012) make some very useful suggestions with regards research priorities, namely: 1) determining environmental controls, 2) investigating size-fraction effects, 3) establishing species specific calibrations, 4) determining biological processes that affect B uptake, and 5) constraining past seawater [B]. As these authors state, "in Pleistocene

down-core records, planktic foraminiferal B/Ca exhibits species- and site-specific offsets but no consistent temporal pattern", illustrating that B/Ca ratios are some way off being a reliable proxy for the past carbonate system, and remain enigmatic.

1.5 Aims and Objectives

1.5.1 Aim 1: Examining the sources of vital effects, and lowered pH-sensitivity, in foraminiferal δ^{11}B

As discussed in section 1.4.2, there are a number of possible explanations to explain the incongruity between planktic foraminiferal δ^{11}B and that of ambient aqueous $B(OH)_4^-$. Of these, perhaps the most well supported is the concept of microenvironmental carbonate system perturbation, as it is consistent with microelectrode observations (Jørgensen et al., 1985, Rink et al., 1998, Köhler-Rink and Kühl, 2000, 2005, Glas et al., 2012b), offsets between symbiont-bearing and symbiont-barren species (e.g. Hönisch et al., 2003, Foster, 2008), the effect of light intensity (Hönisch et al., 2003), diffusion-reaction models (Wolf-Gladrow et al., 1999, Zeebe et al., 1999a, 2003) and indeed vital effects in other proxy systems (Bemis et al., 1998, Zeebe et al., 1999a, Eggins et al., 2004). Despite this strong empirical basis, a number of issues relating to vital effects remain unexplained (see section 1.4.2.3). The *main* overarching aim of this PhD project, therefore, is to ascertain the cause(s) for foraminiferal vital effects in δ^{11}B. Under the umbrella of this main goal are a number of more specific issues that this PhD project aims to address:

- Firstly, this project aims to test how much existing NTIMS species calibrations be relied upon as characterisations of vital effects, given analytical issues discussed in section 1.4.1. This seems particularly pertinent given a) a large offset between *O. universa* and *G. sacculifer* calibrations (Sanyal et al., 1996, 2001) that is difficult to explain via existing microenvironment models and b) *O. universa*'s calibration (Sanyal et al., 1996) being lighter in δ^{11}B than inorganic carbonate (which again is counter to microenvironment models; Zeebe et al. 2003). In order for models of vital effects to be well-grounded, we must be sure of absolute values of δ^{11}B, not only relative differences.

- Secondly, this project aims to explore just how applicable laboratory culture conditions (and thus *in vitro* calibrations) are to open ocean conditions. For example, Hönisch et al. (2003) showed that towed *O. universa* from Hönisch et al. (2003) did not agree with high-light culture samples (i.e. typical conditions in calibration studies), but with low-light treatments. Considering also the possibility of geographical variations in foraminiferal morphospecies (e.g. Morard et al., 2009) and even proxy calibrations (e.g. Marr et al., 2011), this project aims to combine insights from cultures with data from globally distributed core-tops, tows and sediment traps to permit greater confidence in conclusions drawn.

- Thirdly, this project aims to investigate what processes lie behind the lowered pH-sensitivity seen in planktic foraminiferal calibrations (Sanyal et al., 1996, 2001). Are they the result of some fractionation inherent in the incorporation of boron into $CaCO_3$, or might they instead be a product of either analytical problems or microenvironmental alteration? The new inorganic calibration discussed above (Fig. 1.10) already goes some way towards this goal, but comparison of pH-sensitivities in symbiont-barren and symbiont-bearing foraminifera (measured via MC-ICPMS) are also important since boron incorporation processes in foraminiferal calcite and inorganic aragonite precipitates may be different.

1.5.2 Aim 2: Extending the applicability of the δ^{11}B-pH proxy through species-specific calibrations

As pointed out by Hönisch et al. (2007), even if the drivers of deviation from aqueous theory are not fully understood, provided reliable species-specific calibrations are employed, this does not preclude successful application of the boron isotope-pH proxy. Prior to the commencement of this PhD project, however, only two species of foraminifera had been calibrated, and even these calibrations carried problems (for example the ill-defined interlaboratory biases discussed in section 1.4.1).

One of the main objectives of this study, therefore, was to expand the number of planktic foraminiferal species for whom δ^{11}B-pH relationships have been reliably calibrated, thereby expanding the possibilities for down-core palaeo-pH and CO_2 reconstruction.

Given that it is consistently seen to be the shallowest-dwelling of all tropical planktic foraminifera, and as such better records mixed layer (and, assuming air-sea equilibrium, atmospheric) CO_2 levels, *Globigerinoides ruber* is an ideal subject for palaeo-pH reconstruction. However, due to the challenges inherent in culturing this species in large numbers (Spindler et al., 1984, Hemleben et al., 1987), no calibration for this species was available. As such, the first aim of this project was to calibrate the δ^{11}B-pH relationship in *G. ruber* (Chapter 3), to permit more confidence in pH reconstructions, and test the assertion by Foster (2008) that this species shows a sensitivity similar to aqueous $\delta^{11}B_{B(OH)_4^-}$.

O. universa was the first species of foraminifera to be calibrated (Sanyal et al., 1996). However, there are a number of issues with this calibration, including being lighter in δ^{11}B than inorganic carbonates (Sanyal et al., 2000), which is seemingly counter to modelled and observed microenvironment alteration (Zeebe et al., 2003, Rink et al., 1998). Thus one aim of this project was to calibrate this species via MC-ICPMS, verifying the existing NTIMS calibration and therefore extending the applicability of the δ^{11}B-pH proxy to this ubiquitous and easily picked species.

Finally, in higher latitude oceans and some periods of geological time (e.g. the Eocene-Oligocene, Norris, 1996, Wade, 2004), symbiont-bearing species are not found. Thus it was imperative during the course of this PhD to calibrate a symbiont-barren species, not only to extend the applicability of the δ^{11}B-pH proxy to the calibrated species, but to provide a basis for extension to other extinct symbiont-barren species. Given it is normally interpreted as a shallow-dwelling symbiont-barren species (Hemleben et al., 1989), *Globigerina bulloides* was the preferred candidate. Together these three calibrations would more than double the number of species available for use in palaeo-pH reconstructions.

One final consideration in extending the δ^{11}B-pH proxy to more species and more sites is whether there is a need to tightly constrain size fractions for boron isotope analysis. Since sample size limitations may often prove restrictive in downcore applications of the δ^{11}B-pH proxy, this project set out to understand the mechanisms behind size-fraction changes, or at the very least characterise them for individual species. In doing so, this PhD project aims to extend pH reconstructions to sites where sample availability is limited (in species where δ^{11}B is found not to vary with size), and

produce more accurate pH reconstructions elsewhere (in species where too broad a sampled size range may otherwise introduce error).

1.5.3 Aim 3: Testing the applicability of the B/Ca proxy

Since the analysis of boron isotope ratios is not straightforward (see section 1.4.1), and since both the δ^{11}B and B/Ca ratio proxies should be driven by the same basis in aqueous chemistry (see Section 1.3.1 above, and Hemming and Hanson, 1992), it is unsurprising that the B/Ca proxy has garnered some considerable attention amongst the palaeo-proxy community (e.g. Yu and Elderfield, 2007, Brown et al., 2011, Tripati et al., 2009, 2011). However, unlike the δ^{11}B-pH proxy, that agrees reasonably well with its theoretical basis (Fig. 1.10), the B/Ca proxy appears to show a somewhat less clear picture. While in epifaunal benthic foraminifera, the carbonate system does appear to control B/Ca ratios (Yu and Elderfield, 2007, Brown et al., 2011, Rae et al., 2011) the best correlate is $\Delta[CO_3^{2-}]$, with $\frac{B(OH)_4^-}{DIC}$ and $\frac{B(OH)_4^-}{HCO_3^-}$ relatively poorer correlates. In planktic foraminifera, meanwhile, a number of other factors have been proposed as controls, including temperature and salinity (see Allen and Hönisch, 2012, for review). Clearly then, the controls on boron incorporation in foraminifera are not fully understood. One of the main aims of this PhD project, therefore, was to test the controls on foraminiferal B/Ca ratios, in culture and (crucially) in *in situ* conditions (using core-tops, tows and sediment traps), to determine the viability of B/Ca ratios as a palaeo-carbonate system proxy. In addition, by determining the drivers of boron incorporation in foraminifera, this PhD project aims to shed further light on the processes of biomineralisation and trace element incorporation. This is important since it is unclear at present how microenvironment effects discussed above (that seem to be well supported by empirical evidence) can be compatible with known internal pH modifications (section 1.4.2.2).

1.6 Thesis plan

- Chapter 2 documents the methods used to measure boron isotopes via MC-ICPMS at the University of Southampton, typical reproducibility and comparability to other laboratories.

- Chapter 3 describes the calibration of δ^{11}B-pH relationships in the shallow-dwelling planktic foraminifera *G. ruber*, incorporating culture experiments from Eilat and measurements from core-tops, tow and sediment trap samples. Much of this chapter was published as part of Henehan et al. (2013), which is attached in Appendix C.

- In Chapter 4, calibrations are presented for both the deep-dwelling symbiont-bearing species *O. universa* and the symbiont-barren species *G. bulloides*, greatly extending the geographical reach of the δ^{11}B-pH proxy. Insights on vital effects from these two calibrations are discussed.

- Chapter 5 details an investigation into the controls on B/Ca ratios in *G. ruber*, applying multivariate statistical approaches to discern which environmental parameters control boron incorporation in this planktic foraminifera.

- in Chapter 6, the findings of chapters 3-5 are discussed, with reference to the aims set out at the beginning of this PhD project. In addition, some future avenues of research, and preliminary data from these areas, are presented.

Chapter 2

Methods: Analysis of Boron Isotopes via MC-ICPMS

2.1 Introduction

Analysis of boron isotopes in $CaCO_3$ is not a trivial matter, and it is perhaps for this reason that this isotope system has not been more widely studied and applied. The first measurements of boron isotopes were largely focussed on the requirements of the nuclear industry (because of the large cross section of ^{10}B; Bartholomew and Campion, 1957, it is an important resource for neutron capture). Early measurements of boron isotope composition (barring initial attempts with Gas Source Mass Spectrometry, e.g. Parwel et al., 1956) used Positive Thermal Ionisation Mass Spectrometry (PTIMS), measuring the $Na_2BO_2^+$ ion (e.g., Shima, 1963, Catanzaro et al., 1970). Sample sizes used in these early analyses were typically ~ 5 μg B. While adequate for the analysis of nuclear materials and some natural minerals, these requirements would have rendered analysis of foraminiferal carbonate unfeasible (typical sample sizes analysed at NOCS are 5 - 20 ng B). While PTIMS has been refined somewhat since these early analyses (for example with the use of $Cs_2BO_2^+$ ions, multicollector TIMS instruments, and the use of different filament materials), and has produced some of the highest precision boron isotope measurements to date (e.g. $\pm$ 0.11 ‰ 2σ external reproducibility for >50 ng B; Deyhle, 2001), sample size requirements for this method are still somewhat prohibitive and have limited the applicability of the technique with regards

foraminiferal carbonates. That said, recent advances, for example a mannitol 'pre-bake' step (Ishikawa and Nagaishi, 2011), may yet serve to alleviate this issue somewhat.

The principle advance in the measurement of boron isotopes, with regards to its palaeoceanographic application, was the development of Negative Thermal Ionisation Mass Spectrometry, or NTIMS. This method achieves greater ionisation efficiencies, and thus allows for the analysis of sample sizes ($\sim$ 1 ng; Hemming and Hanson, 1994). With the development of this technique the application of the boron isotope system to marine carbonates became more feasible: while early measurements suggested highly variable values of δ^{11}B in marine carbonates (Vengosh et al., 1991), with improved accuracy δ^{11}B measurements in marine carbonates converged on values close to the δ^{11}B of aqueous $B(OH)_4^-$ ion (Hemming and Hanson, 1992). This observation led Hemming and Hanson (1992) to propose that $\delta^{11}B_{CaCO_3}$ may be a tracer of past ocean pH. Building on this observation, throughout the 1990s and early 2000s several influential works utilised NTIMS measurements of δ^{11}B in foraminiferal carbonates to reconstruct atmospheric CO_2 changes through the Phanerozoic (e.g. Sanyal et al., 1995, Palmer et al., 1998, Pearson and Palmer, 1999, 2000, Hönisch and Hemming, 2005b). However, problems with boron isotope analysis via NTIMS are numerous (including large in-run fractionation, mass interferences, and matrix-specific differential ionisation behaviour between standards and samples; Aggarwal and Palmer, 1995, Sanyal et al., 1995, Foster et al., 2006) and have resulted in considerable inconsistencies in measured δ^{11}B values between laboratories (see Gonfiantini et al., 2003, Foster et al., 2006, Hemming and Hönisch, 2007, Foster et al., 2008, Foster, 2008, Ni et al., 2010, Rae et al., 2011, Foster et al., 2013). While some authors have taken steps to improve the NTIMS technique, for example by oxidative treatment prior to loading (Vinson et al., 2011), we instead take a different approach, using the Multicollector Inductively-Coupled Mass Spectrometry (MC-ICPMS) method of Foster (2008).

2.2 Analysis of Boron Isotopes via MC-ICPMS at the National Oceanography Centre, Southampton

2.2.1 Blank reduction strategies

Given that boron is a ubiquitous contaminant, prior measures to reduce analytical blank are critical to the production of accurate δ^{11}B data. Such measures must include a) reduction in airborne particulate B blank, b) purification of all reagents involved in sample preparation, c) effective cleaning protocols for sample vessels and d) correct analyst practices. Airborne particulate B contaminant levels may be mitigated via the installation of boron-free HEPA filters in air-handling feeds to geochemical preparation and instrument labs. In addition, sample preparation should be carried out in over-pressured laminar flow hoods, with secondary boron-free HEPA filters installed. Installation of these filters (manufactured by AAF international) at NOCS in the Spring of 2010 reduced fall-in blank from 450 pg/hr to 8 pg/hr: evidence of their efficacy.

Boron in impure reagents is another source of procedural blank that must be mitigated. Because boric acid ($B(OH)_3$) has no charge, it is not removed efficiently by conventional reverse-osmosis laboratory water purification techniques. As such, a Milli-Q *Q-Gard* (© EMD Millipore) pack is used; this system uses electro-deionisation and a chelating adsorbent to improve retention of B (Darbouret and Kano, 2000). All acids used during column chemistry (section 2.2.2) and sample preparation (section 2.3) are Teflon-distilled to ensure high levels of purity, and Na-acetate buffer added to samples prior to column chemistry is first passed through boron-specific Amberlite IRA-143 resin (Kiss, 1988) to remove B.

Another requirement of boron isotope geochemistry is the adherance to effective vial cleaning protocols. Plastic centrifuge tubes and pipette tips are cleaned overnight in ~3 M HCl at 80-90 °C and rinsed 3 times with Milli-Q purified water (hereafter MQ). Subsequently, immediately prior to use, pipette tips and tubes are rinsed with 10% Teflon-distilled HNO_3 and MQ. Between uses, Teflon vials (used for sample storage and analysis) are subject to a lengthy cleaning protocol. First, labels are removed using acetone and vials are rinsed three times with MQ to remove remnant sample. Subsequently, vials are physically wiped, first with MQ and then with acetone, before

being rinsed a further three times in MQ. These are then two-thirds filled with 7M HNO_3, capped, and left to reflux at 140 °C for at least two hours. Next vials are emptied, rinsed three times in MQ, arranged face up in a Teflon jar using tweezers and refluxed in this jar overnight in 7M reagent-grade HNO_3 at 140 °C. After this refluxing, vials are rinsed twice in MQ and replaced upright in the Teflon jar, to be refluxed once more in 2% Reagent-grade HNO_3 overnight. Finally, Teflon is rinsed three times in MQ, shaken dry and stored (capped) in a closed box. As a final precaution, immediately prior to use vials are filled with 10% Teflon-distilled HNO_3 and refluxed at 140 °C for at least 1 hour, and then rinsed twice with MQ. In addition, bottles and jars used to store reagents are subject this cleaning procedure prior to use.

Besides this laboratory hardware and rigorous cleaning protocols, other more general precautions are required to minimise potential for boron contamination. Gloves are worn at all times, and hands are not passed over samples unless absolutely necessary. Pipette tips are changed when switching between reagents or samples, and are never allowed to come into contact with gloves, work surfaces, etc. Samples are kept firmly capped, except during transfer. Columns are only handled using tweezers, and are covered during cleaning and elution with a clean plastic beaker. Working space is kept dry and tidy to more easily detect spillages. Solutions of high [B] (e.g. seawaters, high concentration boric acid standards) are, where possible, handled in an extract hood, outside of the clean laminar flow hood. Finally, laboratory is cleaned weekly (all surfaces and floor wiped down with MQ).

To monitor cleanliness and potential for sample contamination, a total procedural blank (TPB) of 0.5M HNO_3 and buffer is included in each batch of columns. This TPB is then analysed for [B] and $\delta^{11}B$. Typically, TPBs are $\sim$ 20 pg B, and are rarely greater than 50 pg B.

2.2.2 Boron isolation and matrix removal: column chemistry

As described by Foster et al. (2008), analysis via MC-ICPMS entails the prior isolation of pure solutions of boron in HNO_3, using columns of boron specific Amberlite IRA-743 resin (Kiss, 1988, Lemarchand et al., 2002a). This resin has a high affinity for $B(OH)_4^-$ ion, and as a result at high enough pH ($\geq$ 5) virtually all boron is rapidly bound (because of the rapid re-equilibration of aqueous B; Zeebe et al., 2001). Because

of this preference for $B(OH)_4^-$, however, this resin may fractionate boron isotopes upon elution with acid (with ^{11}B-enriched $B(OH)_3$ preferentially eluted; Lemarchand et al., 2002a). Consequently, it is essential that sample elution is complete. Thus column design and rigorous testing is crucial to the generation of accurate data. Since a larger volume of resin requires more acid to complete elution (as a rule of thumb, ~24 column volumes of acid are required to elute to >99% efficiency), small samples requires small column volumes (lest the eluted boron solutions be too dilute). Conversely, although theoretical boron capacity in Amberlite is high (15 μg B/μl, Pinon et al., 1968), too small a column volume will result in boron passing through the resin too quickly to be retained. For the routine analysis of foraminiferal samples at NOCS, 20μl-volume columns are used.

To produce columns for boron isotope geochemistry, teflon must be heat-shrinked around a stainless steel mould. During the course of this study, several dimensions of shapers were trialled, and not all produced effective columns. The dimensions of the most successful design is detailed in Fig. 2.1a. Polyethylene frits of 3.8 mm diameter (pore size 10-30 μm) are then cut using a belt-hole cutter, and firmly inserted into the the narrow base of these shapes using a pipette tip (as in Fig. 2.1c). Columns are trimmed on both ends so that the reservoir holds ~1.6 ml of solution, and such that the column ends flush with the base of the frit (otherwise drips may be retained). These columns are then flushed with water and acetone to remove air bubbles from within the frit before cleaning, first in 7 M reagent-grade HNO_3, then 2% reagent-grade HNO_3, then 10% Teflon-distilled HNO_3 (each step refluxing overnight at ~135 °C). Once cleaned, ~ 20 μl of ground Amberlite resin (sieved to 63-120 μm) is added to each column. MQ is then added and eluted solution is thoroughly screened for resin leakage, either through or around the frit. Furthermore, the rate at which fluids pass through the column must be noted: too slow and future sample preparation time is considerably lengthened, too fast (<~6 minutes for 1.5 ml volume) and fractionation may occur (due to incomplete binding of B, and preferential takeup of ^{10}B-enriched $B(OH)_4^-$; Lemarchand et al., 2002a). Overall success rates for column fabrication are typically < 30 %, with resin loss the most common problem.

Once a set of functioning columns has been isolated, the resin must be pre-cleaned by passing through 15 ml of clean 0.5 M HNO_3, before the boron elution profile is characterised (following Lemarchand et al., 2002a). As aforementioned, complete

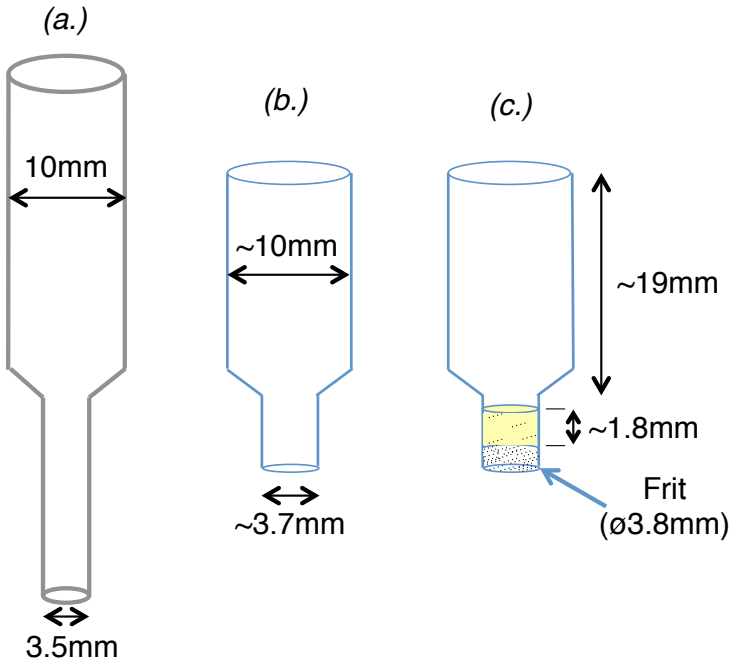

FIGURE 2.1: Schematic of the dimensions of a) the stainless steel shaper upon which teflon is shrunk, b) the resulting column, and c) the fritted column, containing ca. 20 μl of Amberlite resin (shown in yellow).

elution of boron from columns is of utmost importance; characterising elution profiles allows methodological adjustments to be made to ensure this always occurs. To do this, ~20 ng B (from matrix-free boric acid, e.g. NIST SRM 951) is added to columns, and repeat rinses of ~4 column volumes of 0.5M HNO_3 collected and analysed for [B] by ICPMS. Elution profiles for typical 20 μl columns used at NOCS are shown in Fig. 2.2. While total elution is seen at ~480 μl, currently at NOCS 5 x 110 μl elution steps are carried out. This is because uptake rates of the nebuliser used to introduce sample to the Thermo Neptune MC-ICPMS are typically ~80-90 μl/min, and so duplicate analysis of each sample necessitates larger sample volumes than are required for complete elution. To further ensure all boron has been eluted, a further 110 μl of 0.5M HNO_3 is collected as a 'tail' during each column run. This is monitored for [B], with relative contributions from tails greater than 0.1% of total sample B considered suspect.

Standard column chemistry protocol applied at NOCS is outlined in Table 2.1 below. Since retention of B by the resin only occurs at pH $\geq$ 5, samples must first be buffered by addition of 2 M Na-acetate + 0.5 M acetic acid (2 $\times$ the volume of acid used in

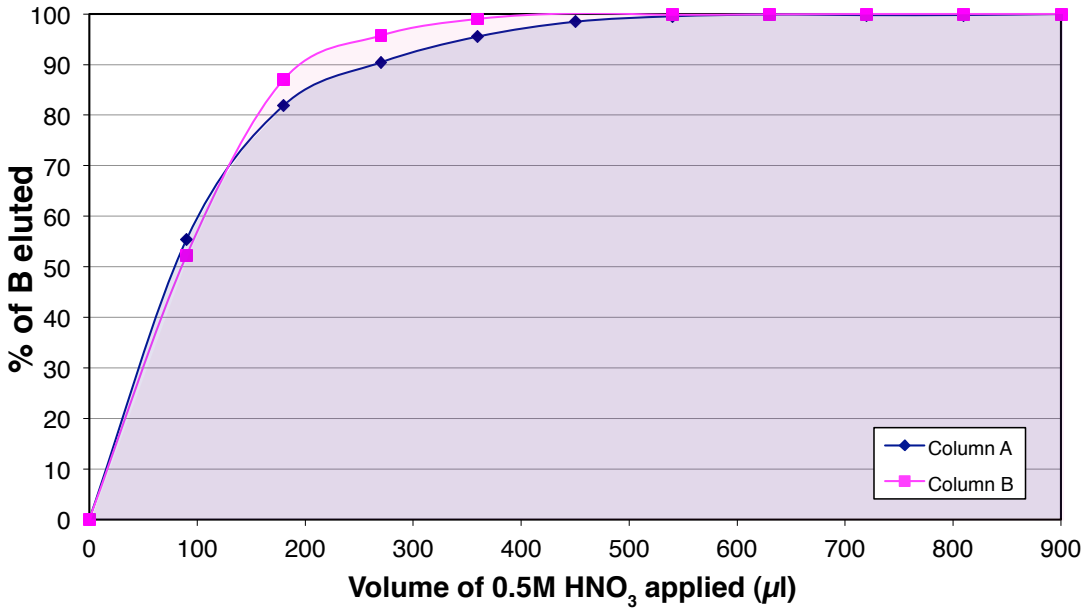

FIGURE 2.2: Elution profiles for two example 20 μl volume boron purification columns at NOCS. Acid is added (in this example) in 90 μl increments, and complete boron elution is seen at ~480 μl. Profiles such as these must be constructed such that protocols for column chemistry may be designed to ensure complete elution.

sample dissolution). Since the introduction of matrix can induce differential instrumental mass fractionation between matrix-contaminated samples and 'clean' standards (Jeffcoate et al., 2004), it is imperative that both dissolved $CaCO_3$ matrix and buffer is rinsed off fully; to this end, 10 × 160 μl of MQ are added to the columns prior to sample elution, ensuring drops rinse the sides of the column reservoir as they are added.

Once elution profiles are understood, and methods honed accordingly, known standards may be passed through to ensure that columns induce no fractionation. Prior to any foraminiferal analysis at NOCS, NIST SRM 951 (Catanzaro et al., 1970), seawater, in-house boric acid standards (BIG-D: 14.71 ‰, BIG-E: 25.12 ‰) and Japanese Geological Survey Porites Coral Standard (JCP-1, Okai et al., 2002) were analysed. The results of these tests are summarised in Table 2.2 below. Testing of the first batch of columns produced at NOCS completed these tests in the Summer of 2011. Good agreement of measured NIST SRM 951 and seawater with published values (Catanzaro et al., 1970, Foster et al., 2010) demonstrates clearly the accuracy of this MC-ICPMS approach.

Step	Solution added	Instructions
Clean columns	2 × 0.5 M HNO_3	First fill to top, second 1ml
Rinse off acid	2 × MQ	2 additions of 1ml
Load sample	Dissolved, buffered sample	Add gently on to resin bed
Rinse off matrix/buffer	10 × 160 μl MQ	Drip round column circumference to rinse walls
Collect sample	5 × 110 μl 0.5M HNO_3	Add gently on to resin bed
Collect tail	1 × 110 μl 0.5M HNO_3	Add gently on to resin bed
Clean columns	2 × 0.5 M HNO_3	First fill to top, second 1ml
Rinse off acid	2 × MQ	2 additions of 1ml

TABLE 2.1: Standard column chemistry protocol at NOCS. Between uses, columns are stored in MQ, in screw-capped Teflon beakers. Samples and tails are collected in airtight, screw-capped Teflon beakers (leached for >1 hour in 10% Teflon-distilled HNO_3 and rinsed twice in MQ).

Sample Material	Measured δ^{11}B
NIST SRM 951	-0.01 ± 0.14 ‰
Seawater	39.68 ± 0.15 ‰
BIG-D	14.75± 0.19 ‰
BIG-E	25.20 ± 0.19 ‰
JCP-1	24.42 ± 0.17 ‰

TABLE 2.2: The results of analyses of standards and reference materials, after having gone through column chemistry, in columns produced at NOCS. Note the close agreement between measurements of NIST SRM 951 and seawaters and published values (Catanzaro et al., 1970, Foster et al., 2010), and between BIG-D, BIG-E and JCP-1 and long-term average values (14.71, 25.12 and 24.31 ‰respectively). Uncertainty on each δ^{11}B measurement is 2σ of measurements from 10 columns. Only after this accuracy was demonstrated were analyses of foraminifera carried out.

2.3 Foraminiferal cleaning protocols

Foraminiferal cleaning throughout is largely as described in Rae et al. (2011), in turn based on the approach of Barker et al. (2003). Foraminifera (cleaned in batches of < 3 mg) are cracked open between two clean glass slides, ultrasonicated and rinsed repeatedly with Milli-Q ultrapure water (18.2 MΩ) to remove clays. For tow and sediment trap samples, where clay is not a major contaminant, as little as three rinses were carried out (to minimise sample loss), while in larger core-top and downcore samples, as many as nine rinses were required to remove all visible clay material.

Culture, sediment trap and tow samples, in agreement with other culturing studies (e.g. Russell et al., 2004), were subject to intensified oxidative cleaning (3 x 20-30 min treatments of 250-400 μl (depending on sample size) 1% H_2O_2 in 0.1 M NH_4OH_4 at 80 °C) to account for the larger organic content. In core-tops, oxidative cleaning was shorter (3 x 5 min) to minimise sample loss. Samples are then subject to a brief weak acid leach in 0.0005 M HNO_3 to remove any readsorbed contaminants. Finally 200 μl of Milli-Q is added to each sample (to slow subsequent dissolution and reduce the likelihood of leaching of B off any remnant contaminants) and 0.5 M HNO_3 (normally <300 μl) added incrementally until dissolved. To further ensure no contaminant organic or mineral matter is added to columns, samples are centrifuged for > 5 min at 1400 rpm, and the bottom $\sim$ 20 μl is not taken for analysis.

Note reductive cleaning is not carried out for foraminiferal samples at NOCS because it has been shown to be unnecessary for B (Yu et al., 2007a, Wara et al., 2003). This is advantageous because reductive cleaning may incur further loss of sample material (see Yu et al., 2007a). The importance of effective cleaning is paramount: clay contamination will result in leaching of adsorbed isotopically-light B from clay minerals (see Palmer et al., 1987, Deyhle and Kopf, 2004) and may hence artificially lighten measurements of $\delta^{11}B_{CaCO_3}$. Fortunately, clay contamination is easily detectable via ICPMS on an aliquot of the same sample material (with values of Al/Ca $>\sim$100 μmol/mol generally likely to result in anomalously low values of $\delta^{11}B$) and so contaminated samples can be recognised and omitted (Rae et al., 2011).

The influence of remnant organic matter, however, is somewhat less certain. Organics are known to bind to boron receptor sites in the resin and to the column interior (eventually hindering effective elution through columns and resulting in slowed elution times and high [B] in 'tails'). During the course of this research, limited attempts were made to better understand the effect of organic contamination in samples. This investigation involved analysis of towed (and thus organic-rich) specimens of *Globigerinita inflata* from the southwest Pacific. Samples were subject to either (i) standard oxidative cleaning as detailed above, (ii) three repetitions of this standard oxidative cleaning, or (iii) intensified cleaning with 15 % H_2O_2 buffered with 0.1M NH_4OH. The results are shown in Fig. 2.3: on this occasion no clear effect was observable, although the detection of any trend may be hindered by the relatively large analytical uncertainties associated with the sample sizes used. Clearly further testing

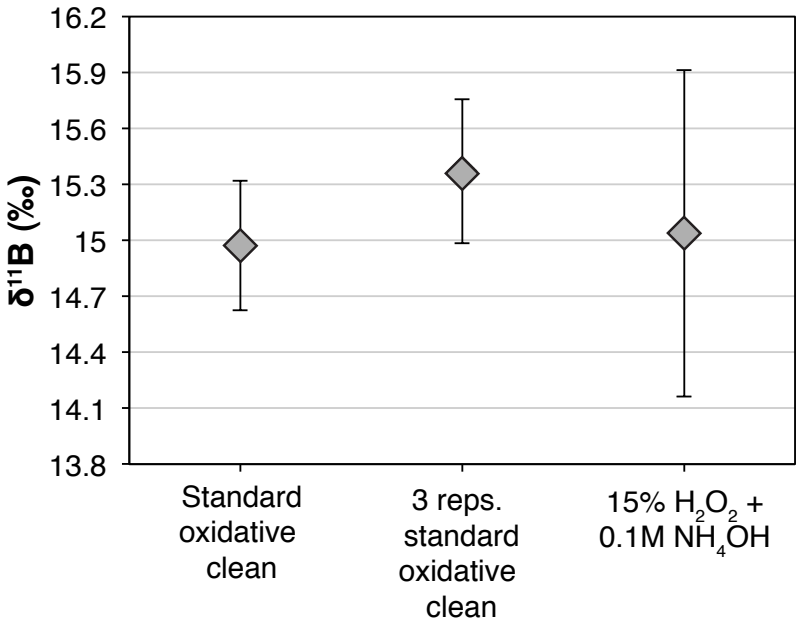

FIGURE 2.3: To test the efficacy of oxidative cleaning, and the potential influence of organic contaminants, cleaning tests were carried out on three splits of *G. inflata* towed from the Southern Ocean. Note the large uncertainty on the strong-peroxide sample, due in part to the loss of sample material through dissolution.

is required before the effects of organics are understood, but since the addition of organic matter shortens the operational lifespan of a column, it would be preferable to address the problem via ICPMS, by finding a trace element/Ca ratio that may act as an indicator for the presence of organic matter (for example P, Se, Cd or Zn).

2.4 Using the Thermo Neptune MC-ICPMS

2.4.1 Hardware used

Boron isotope analysis is carried out on a Thermo Neptune MC-ICPMS at NOCS. This instrument is ideal for boron isotope analysis due to the high sensitivities for B that can be attained (6-8 pA using $10^{11}\Omega$ resistors, or 600-800mV, for a 50ppb B solution), and the ease with which the introduction system can be adapted and customised. Platinum-nickel sample cones and nickel X-geometry skimmer cones are used, for best sensitivities, and faraday cups H3 and L3 used for ^{11}B and ^{10}B respectively.

Wash-out of boron is poor compared to other elements (Al-Ammar et al., 2000), and consequently the sample introduction system used is of crucial importance. Following Foster (2008), a Teflon barrel spray chamber is used, and 2-3 ml/min NH_3 gas is added to the spray chamber immediately after the nebuliser, following Al-Ammar et al. (2000). This raises the pH of the spray chamber interior, and converts volatile boric acid to the less volatile ammonium borate. While Al-Ammar et al. (2000) observe an increase in sensitivity with the addition of NH_3, no such increase is observed here; in fact NH_3 addition can result in some small loss of sensitivity (typically <10%). However, with the addition of NH_3 washout time is dramatically reduced (by a factor of >5 Al-Ammar et al., 2000), with washout to less than 2% signal level typically possible within $\sim$ 2 min. Washout times are measured before each analytical session to ensure efficacy.

Fused teflon nebulisers of uptake $\sim$ 0.75-95 μl/min (manufactured by ESI Ltd.) are used to introduce the sample as a fine aspirated mist into the chamber. Nebulisation efficiency and stability is fundamental to the generation of a stable, high-intensity signal: droplet size affects sample transport efficiency (i.e. how much sample is delivered to the plasma, and thus sensitivity) and plasma stability (too much sample solution may cause plasma to flicker). Fine mists of consistent, uniform droplet size are preferable. These nebulisers were found to offer the best stability when in self-aspirating mode. Unfortunately, in order to pass the required $\sim$1.15 L/min sample gas flow through these nebulisers, it is necessary to operate at back pressures above their designed specification. As a result, they are vulnerable to damage and degradation (typically due to blocking or buckling of the internal capillary). During the course of this study these nebulisers were found to have a limited lifespan of around 4-6 months under typical usage.

2.4.2 Instrument tuning

Critical to the generation of boron isotope measurements via MC-ICPMS is adequate tuning. This is particularly pertinent given relatively low sensitivities and large and variable instrumental mass fractionation ($\sim$15%/amu) seen for boron. At NOCS, the instrument is left to 'warm up' at approximate tuning conditions for 1-2 hours before tuning (using a 50 ppb solution of NIST SRM 951). First, inlet system (primarily

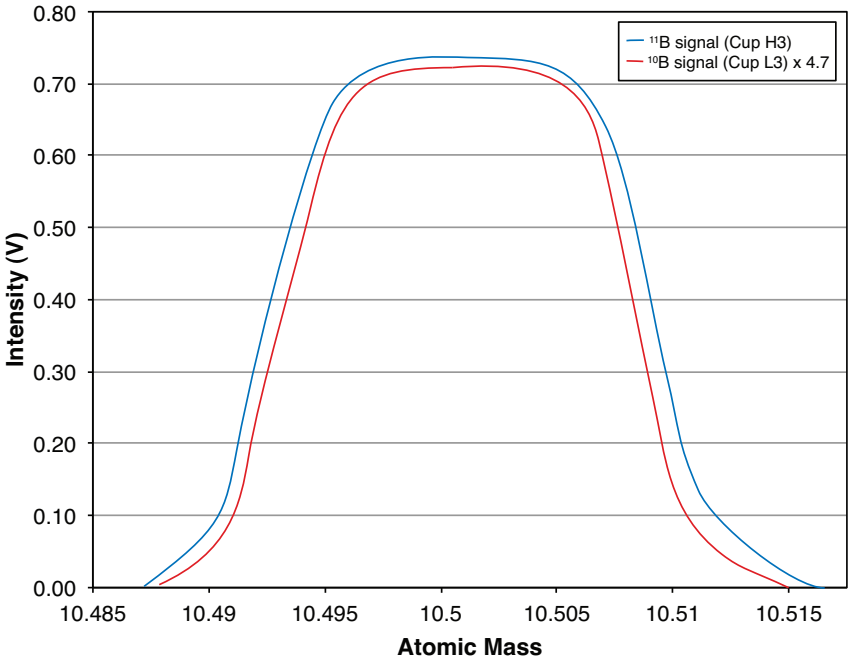

FIGURE 2.4: Peak shape is optimised using focus quad zoom optics to ensure a square shape with flat top, and minimal tailing on either side of the peak.

torch position and sample gas input) and source lenses are tuned for maximum sensitivity. Peak shape may then be optimised using 'shape' and 'focus' under source lenses, and focus quad; best peak shapes (as illustrated in Fig. 2.4) typically require 'shape' to be tuned to +15 to +30 above its optimal intensity. While it possible (and perhaps desirable) to quantitatively assess quality of peak shape (assessing overall symmetry and flatness of the peak through comparison of signal intensity at masses equidistant from peak centre, for example), in practice at the NOC, qualitative assessment has always been sufficient to produce accurate and reproducible data.

Besides peak shape and intensity, it is critical that machine induced isotopic mass fractionation is as stable as possible. To this end, the instrument is tuned for stability by analysing (in blocks of 15 measurements) the isotopic ratio of NIST SRM 951 across a range of sample gas input levels. If properly tuned and nebulising efficiently, it should be possible to detect a stability 'plateau' within which a small change in sample gas flows will not result in large changes in mass fractionation (see Fig. 2.5). The position and character of this plateau will vary between analytical sessions (e.g. Fig. 2.5, A-C), with (among other things) nebuliser condition, condition of guard electrode, etc. It can be manually altered by varying torch Z position, RF power, and auxiliary

Inlet system		Lenses	
X	~3.72	X	~3.09
Y	~3.41	Y	~-2.28
Z	~0.9	Focus	~-588
RF Power	1400	Shape	~ 230
Aux. Gas	0.9	Source Offset	-38
Cool Gas	15.25	Focus Quad	4.5
Sample Gas	~1.16	Rotation Quad	0
Ammonia	0.0025	Dispersion Quad	0

TABLE 2.3: Example of operating parameters for the Thermo Neptune MC-ICPMS used at NOCS for boron isotope analysis. Gas fluxes are in L/min. Note that these values are intended as examples of typical settings; some operating conditions will vary considerably between analytical sessions. Aux. gas, cool gas, ammonia gas flows, source offset, rotation quad and dispersion quad, however, are seldom altered.

gas flow rates, but will typically fall within a range in sample gas of 1.14 - 1.22 L/min. Typically this stability plateau is found at higher sample gas input (+~0.04 L/min, as in Fig. 2.5 A) than peak sensitivity, and will result in a reduction in sensitivity of ~20-30%. The position of the sample gas stability plateau and peak shape are monitored throughout a day's operation to ensure any instrumental drift in this regard is accounted for.

The importance of good tuning (both for sensitivity and stability/peak shape) is demonstrated by Figs. 2.6 and 2.7 below. If tuning and plasma stability is satisfactory, any in-run drift in instrumental mass fractionation is gradual, and measurements of $^{11}B/^{10}B$ ratios in NIST SRM 951 bracketing standards either side of a sample are within uncertainty of each other (Fig. 2.6). In contrast, inadequate tuning and sub-optimal machine performance will result in instability in mass fractionation, manifested in large jumps in measured $^{11}B/^{10}B$ between bracketing standards (Fig. 2.7). In this case, correction for instrumental mass fractionation in intervening samples becomes problematic, as it is not clear which (if either) of the two bracketing standards displays an instrumental mass fractionation more representative of that experienced by the intervening sample. In this way, instability will greatly decrease analytical accuracy.

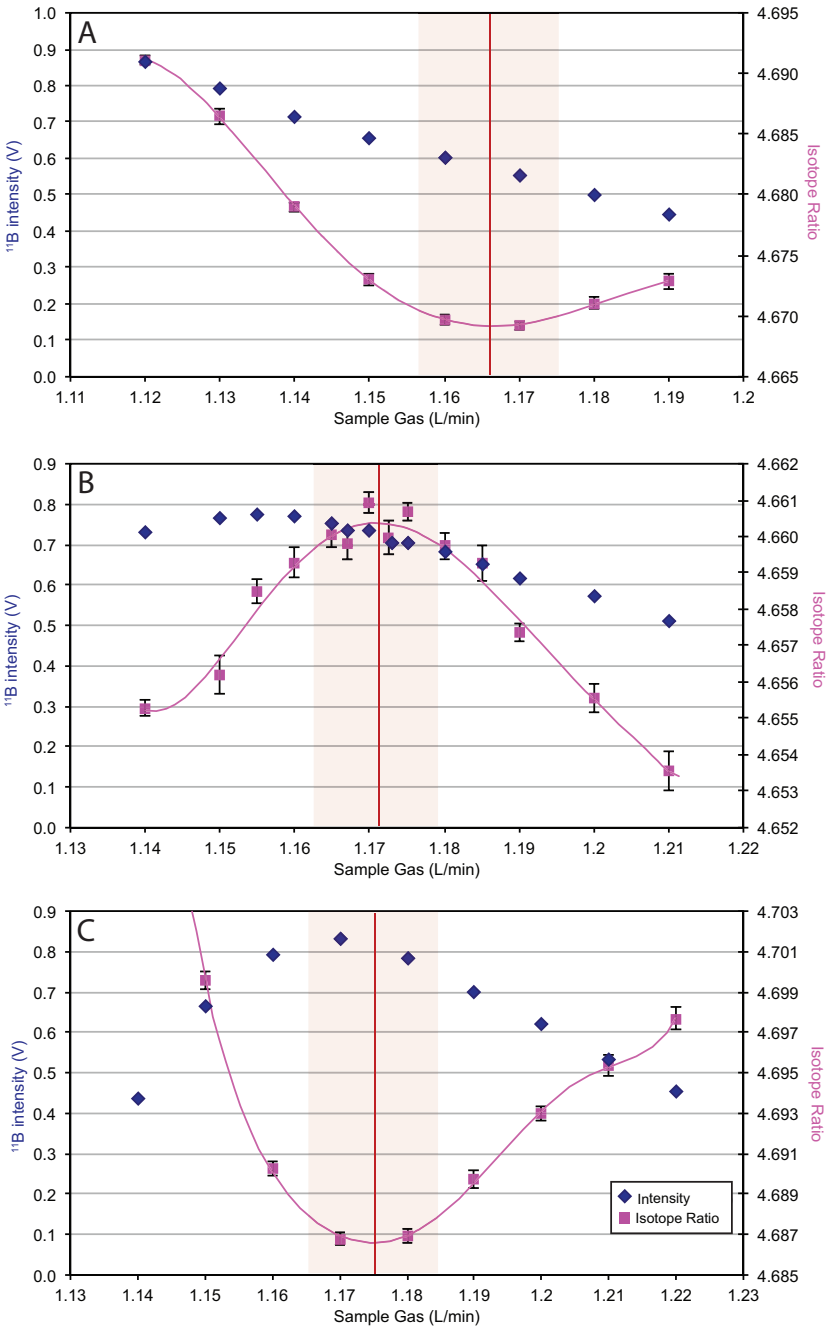

FIGURE 2.5: Examples of typical intensity and isotope ratio profiles as sample gas is increased. Shaded in red is an approximation of the 'stability plateau' in each case, with the red line marking the most appropriate sample gas level to select for analysis. While Panel A represents the 'classic', most typical sample gas profile, very different profiles (see Panels B and C) can still produce good data: in Panel B the broad peak and overall stability (see absolute ranges on ratio axes) make this a suitably stable sample gas zone, while in Panel C while the trough profile appears steep, again, in absolute terms variation in the measured isotope ratio with sample gas is small.

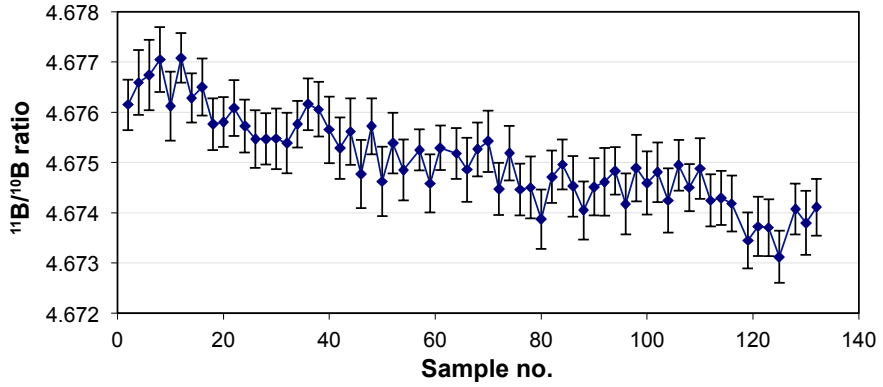

FIGURE 2.6: An example of 'good' machine behaviour/tuning. Note that while some drift is evident, each measurement of NIST SRM 951 is within error of the preceding and subsequent measurement, indicating that samples are well bracketed and reproducibility will be good.

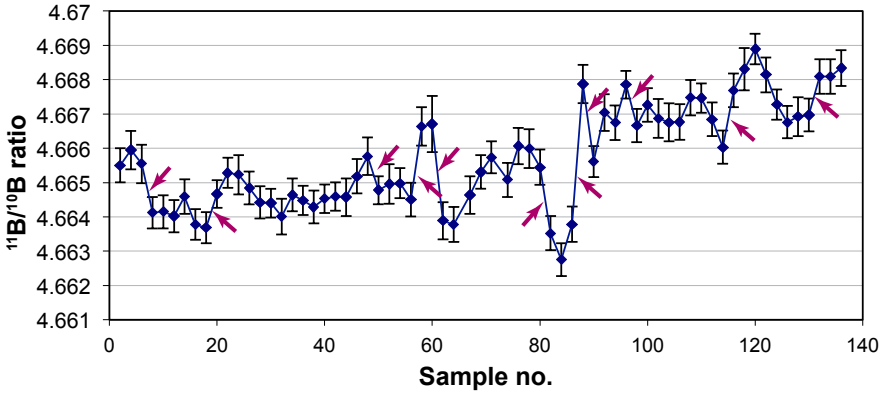

FIGURE 2.7: An example of 'poor' machine behaviour/tuning. Measured isotope ratios in bracketing standards commonly shift by more than the range of uncertainty of each measurement. Sample-standard bracketing then becomes problematic, as it is not clear which (if either) of the two bracketing standards displays a more similar instrumental mass fractionation to that seen by the intervening sample. In this run, such fluctuations occur 11 times (marked by pink arrows).

2.5 Sequence design

Besides careful tuning, the design of method files and analytical sequences is also key. Each sample and standard measurement is made using the same analytical method, consisting of 60 cycles of 2.097s-integrated measurements. Typical measurement block order is described in Table 2.4. Every sample is bracketed by NIST SRM 951 boric acid, meaning that instrumental mass fractionation can be corrected (a major advantage of the MC-ICPMS technique; Foster, 2008). Wash time between

samples/standards is 2 mins (to reduce washout to <2% of sample signal). The reduction in boron memory effect afforded by ammonia addition (section 2.4.1) is such that small samples of ∼ 5 ppb may still be bracketed with 50 ppb B 951 boric acid without any resultant tail-in effect on measured δ^{11}B (see also Section 2.6.2).

Blank pot 1
951-50ppb (+PC)
Sample 1
951-50ppb
Sample 2
951-50ppb
Sample 3
951-50ppb
Blank Pot 2

TABLE 2.4: Standard block order for an analytical sequences on the MC-ICPMS. Note a peak centre (denoted PC) takes place during the measurement of the first 951 boric acid in a block: if changes in plasma behaviour develop in-run, peaks might otherwise drift, to the detriment of internal reproducibility.

Each block of three samples (and associated bracketing standards) is delimited by measurements of 'blank pots'. These are 1.5 ml autosampler vials (the same as those in which samples are held for analysis) filled with a volume of 0.5 M HNO_3 equal to sample volumes, so as to permit accurate characterisation of fall-in blank, reagent-borne blank, and any possible contamination from the autosampler vials themselves. Any such blank (typically small; see Fig. 2.8) is corrected for by subtracting the averaged measured ^{10}B and ^{11}B intensities from bracketing blank pots from the ^{10}B and ^{11}B intensities of intervening samples and their bracketing standards. Although bracketing standards are measure from a large 20 ml standard vial rather than these 1.5 ml autosampler vials, and as such blank correction from blank pots may be an over-estimate (see Fig. 2.8), the effect of such an over-correction on mass-bias-corrected sample δ^{11}B is very small (< 0.02 %).

At NOCS, as at the University of Bristol, standard protocol dictates that samples are analysed twice, and the average of these two replicates reported as the measured value. Note these replicate measurements are fully independent; that is to say that they do not share bracketing standards or blanks. Samples and blank pots are measured once over, then a block of 951 standards are run (to give an indication of machine behaviour

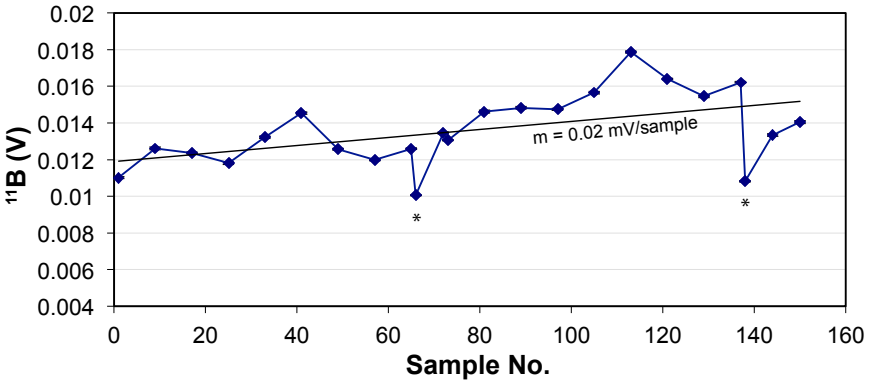

FIGURE 2.8: Typical evolution of measured ^{11}B in blank pots over the course of an analytical run. As may be seen, fall in blank is minimal. That said, ^{11}B measurements in blank pots are higher than measurements of a larger 20 ml blank pot (marked with asterisks), in which any fall-in blank is more diluted: demonstrating why measurements of smaller blank pots are preferred.

mid-way through the run), before all samples and blank pots are measured for a second time.

2.6 Characterising long-term reproducibility

2.6.1 What is reproducibility?

The accurate quantification of uncertainty in analytical science is vital, and this is particularly crucial in the case of boron isotope analysis, where reconstructed CO_2 estimates could shape policy decisions (e.g. IPCC AR4) and so must be reliable to within characterised bounds of certainty. When we speak about uncertainty, it is useful to differentiate between internal, intermediate and external reproducibility. Internal reproducibility, in this context, is the uncertainty in the boron isotope ratio measurement made via mass spectrometry (in our case characterised by a standard error of 60 individual measurements within an analytical cycle of 2 minutes). The size of this uncertainty is generally dependent on sample (signal) size, quality of tuning and machine/introduction system behaviour on any given day.

Intermediate reproducibility in this instance describes how repeatable a measurement would be if you were to carry out the analysis again on a subsample of the same

solution (for instance during another analytical session). Again, in this case sample size, machine/introduction system behaviour and tuning are the main sources of uncertainty, but variation in these factors between days is typically greater than within one run or one measurement (i.e. internal reproducibility).

Finally, full external reproducibility is the variability of measured values of δ^{11}B if one was to run the same sample multiple times through all cleaning protocols, column chemistry and analysis. In addition to the factors that affect internal and intermediate reproducibility, external reproducibility will be influenced by factors such as cleaning efficacy, sample heterogeneity and column elution efficiency.

2.6.2 Results: Long-term reproducibility at the NOC

Following Rae et al. (2011), the long-term external reproducibility of sample measurements is characterised here by the repeat analysis of of carbonate reference materials and in-house standards at a number of different analyte concentrations (5-50 ppb) throughout the duration of this PhD project. Carbonate reference materials used at NOCS are Japanese Geological Survey JCP-1 *Porites* coral (Okai et al., 2002) and JCT-1 *Tridacna* clam (Inoue et al., 2004). The principal factor determining the reproducibility of these measurements is the size of the sample measured (or, more specifically, the size of the ^{11}B signal that is measured on the MC-ICPMS). This is because counting statistics deteriorate (in other words, so-called 'shot noise' increases) as signal intensity drops. Furthermore, as beam intensities drop below a threshold (typically ~100 mV with 10^{11} amplifiers), Johnson noise begins to add further analytical uncertainty (see Rae 2011, Chapter 3, and John and Adkins 2010).

Relationships between sample size (or ^{11}B intensity) and external reproducibility in carbonate reference materials can then be used to approximate the external reproducibility of any given carbonate measurement (as in Rae et al., 2011). The form of this size-reproducibility relationship is described in Equation 2.1 below, where x, y, a, and b are constants. The double exponential form of this equation reflects the two differing regimes of uncertainty: the first (above ~ 100 mV ^{11}B intensity) dominated by shot noise, and the second (at signal intensities below this crossover) dominated by Johnson noise.

$$2\sigma = x \times exp^{a[^{11}B]} + y \times exp^{b[^{11}B]} \tag{2.1}$$

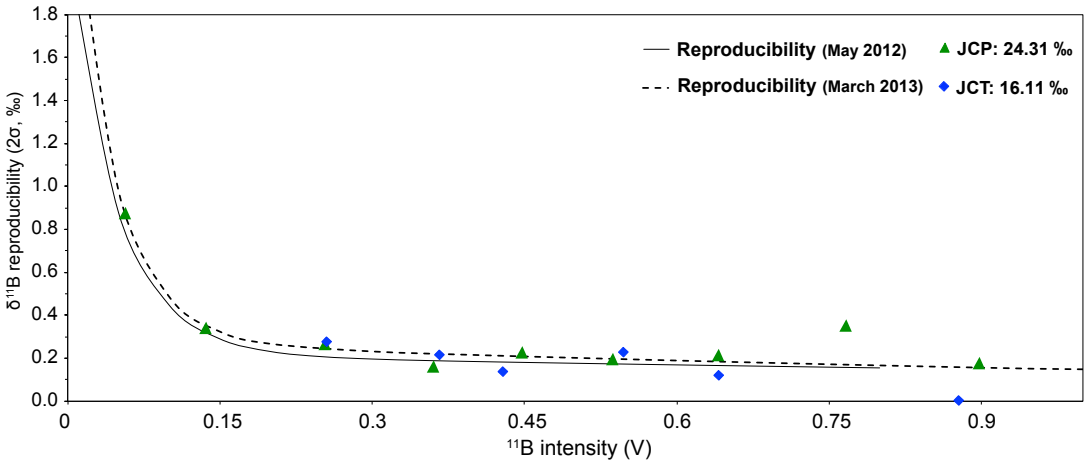

FIGURE 2.9: Plot of external reproducibility of JCP-1 (Okai et al., 2002) and JCT-1 (Inoue et al., 2004) standards as a function of ^{11}B intensity (in volts with 10^{11} ohm resistors) measured by MC-ICPMS, following Rae et al. (2011). The lines-of-best-fit plotted are double exponentials, described by Equations 2.2 and 2.3. External reproducibility may then be approximated from observed ^{11}B intensity, which for the most part is dictated by sample size.

For data analysed prior to March 2013, equation 2.2 was used to characterise reproducibility at NOCS.

$$2\sigma = 1.87 \times exp^{-20.6[^{11}B]} + 0.22 \times exp^{-0.43[^{11}B]} \tag{2.2}$$

Reproducibility of data analysed after this date is estimated via an updated reproducilbility curve described by equation 2.3 below (R^2= 0.85).

$$2\sigma = 2.25 \times exp^{-23.01[^{11}B]} + 0.28 \times exp^{-0.64[^{11}B]} \tag{2.3}$$

These reproducibility curves translate to typical reproducibilities of ±0.17-0.2 ‰ for 20 ng of B (which, after column chemistry, produces a ~50 ppb B solution), ±0.22-0.25 ‰ for 10 ng, ± ~0.3 ‰ for 5 ng B and ~0.7 ‰ for 2 ng B.

As standard, all samples at the NOC are analysed twice during a machine run (see Section 2.5), and the average of these two measurements taken as the measurement value. However, occasional machine problems or nebuliser blockages may mean that only one replicate measurement is run, or that one of the replicate measurements must be discounted as unreliable. Given that the reproducibility equations above (Equations

2.2 and 2.3) are calculated from averaged measurement pairs, it is not appropriate to use these equations to approximate uncertainty in these cases; a degree of variability in measurements is muted by averaging paired replicates. A reproducibility curve calculated from the variability of single replicates, rather than pairs, is shown in Fig. 2.10, and is given in equation 2.4 below (R^2= 0.97).

$$2\sigma = 6.82 \times exp^{-32.61[^{11}B]} + 0.28 \times exp^{-0.18[^{11}B]} \tag{2.4}$$

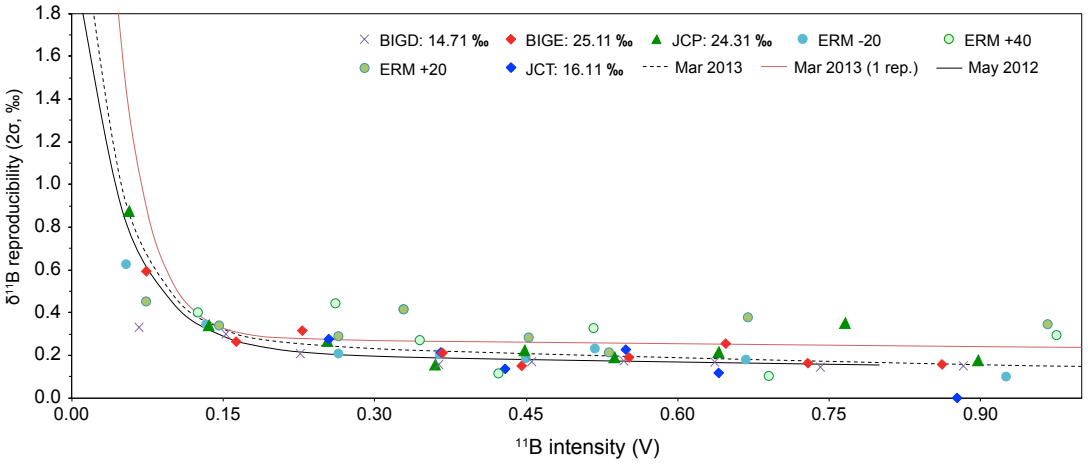

FIGURE 2.10: External reproducibility of pairs of replicate measurements of JCP-1 (Okai et al., 2002) and JCT-1 (Inoue et al., 2004) standards (as a function of ^{11}B intensity) compared to the reproducibility of boric acid standards (paired replicate measurements) and the reproducibility curve produced from single measurements. The lines-of-best-fit plotted are double exponentials, described by Equations 2.2 (May 2012, shown as a black dashed line), 2.3 (March 2013, shown as a solid black line) and 2.4 (March 2013, single measurements, shown in red).

These long-term reproducibility patterns in carbonate standards can be compared with reproducibility of boric acid standards to provide an insight into whether carbonate cleaning or boron separation protocols have any influence on reproducibility. In the case of reproducibility at the NOC, there seems to be little consistent difference (see Figs. 2.10 and 2.11) between full (carbonate) reproducibility and the reproducibility of in-house (BIG-E and BIG-D) and reference material standards (ERM AE120, AE121 and AE122, Vogl and Rosner, 2012), indicating no systematic cleaning or purification-induced bias.

It is worth noting that while the variability of measurements does increase with smaller samples (and ^{11}B signal), we see no systematic bias towards lighter or heavier

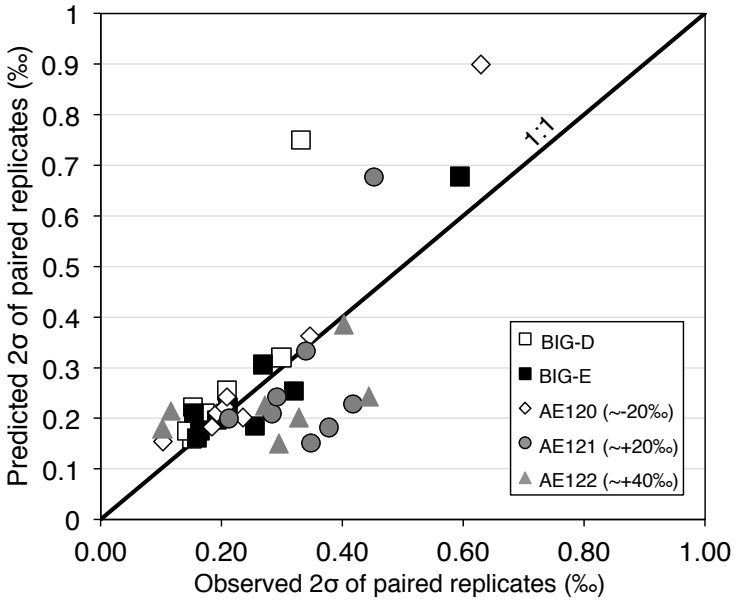

FIGURE 2.11: External reproducibility (2σ) predicted from Equation 2.3 as compared to observed 2σ variability of pairs of replicate measurements of of boric acid in-house standards (BIG-D and BIG-E) and reference materials (AE120, AE121, AE122; Vogl and Rosner, 2012) within discrete ranges of ^{11}B signal intensity. While the fit for BIG-D and BIG-E is generally good, relatively poor fit in AE121 and AE122 boric acid standards is a result of the small number of measurements of these reference materials made to date ($n < 50$, split between 8 signal intensity bins).

values with decreasing sample size (as would occur, for example, with blank or wash-out problems). In fact, absolute values in $\delta^{11}B$ are within analytical uncertainty of each other over the entire range of signal intensities (see Figs. 2.12 and 2.15). This is further evidence of the accuracy of $\delta^{11}B$ measurements at NOCS via this technique.

2.7 Comparability with other Laboratories

2.7.1 Absolute $\delta^{11}B$

As discussed in section 1.4.1, one major hindrance in the development of the $\delta^{11}B$-pH proxy to date has been the poor reproducibility of $\delta^{11}B$ measurements between laboratories. Although absolute accuracy in measurements of non-carbonates at NOCS is evident from analyses of NIST SRM 951 standard and seawater (Table 2.2), no analogous carbonate-matrix standards are available to verify carbonate cleaning methods. Here the results of inter-laboratory comparisons between NOCS and the

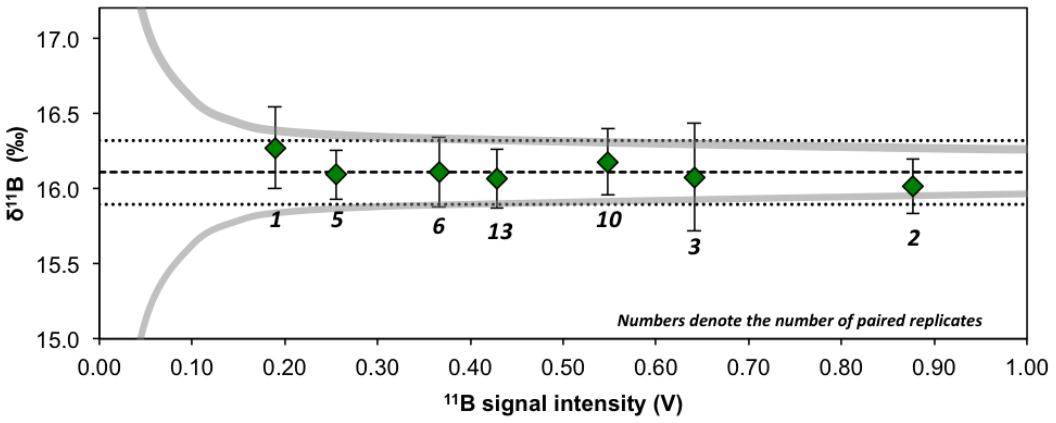

FIGURE 2.12: Measurements of JCT-1 produced at the NOC. The thick dashes line denotes the long-term average of 16.11 ‰, with the thin dashed line either side denoting the overall 2σ of this value (0.21 ‰). Grey lines mark the reproducibility curve from Equation 2.3. Error bars denote the 2σ of pairs of replicates in each bin (except in the case of the smallest sample, where it is a 2σ of paired replicates), with the numbers below each bin denoting the number of pairs of replicates analysed within this intensity bin.

University of Bristol (which has been party to earlier, wider intercomparison studies; Aggarwal et al., 2009, Foster et al., 2013) are presented. Given that the absolute accuracy of MC-ICPMS δ^{11}B measurements made at the University of Bristol has been further demonstrated via standard addition (Ni, 2010), demonstrable agreement between measurements of foraminifera in these two laboratories would also imply absolute accuracy in measurements from NOCS. To test this, downcore samples of *G. ruber* from ODP Site 999A were re-picked and re-cleaned at NOCS as described in section 2.3, and compared to published measurements from Foster (2008). In all cases, measurements made at NOCS are within uncertainty of those made at the University of Bristol (Fig. 2.13), demonstrating good agreement between both laboratories. Furthermore, measurements of seawater and various in-house carbonate and boric acid standards from both laboratories were found to be indistinguishable (Fig. 2.14). As such it would appear that analyses at NOCS are accurate in absolute terms, and that there is no inter-laboratory bias between NOCS and Bristol Isotope Group.

While NOCS has yet to be involved in any published, large-scale intercomparison studies (such as Gonfiantini et al., 2003, Aggarwal et al., 2009, Foster et al., 2013), absolute values reported here for carbonate reference material JCP-1 are similar to those reported elsewhere (Wang et al., 2010, Douville et al., 2010, Ishikawa and

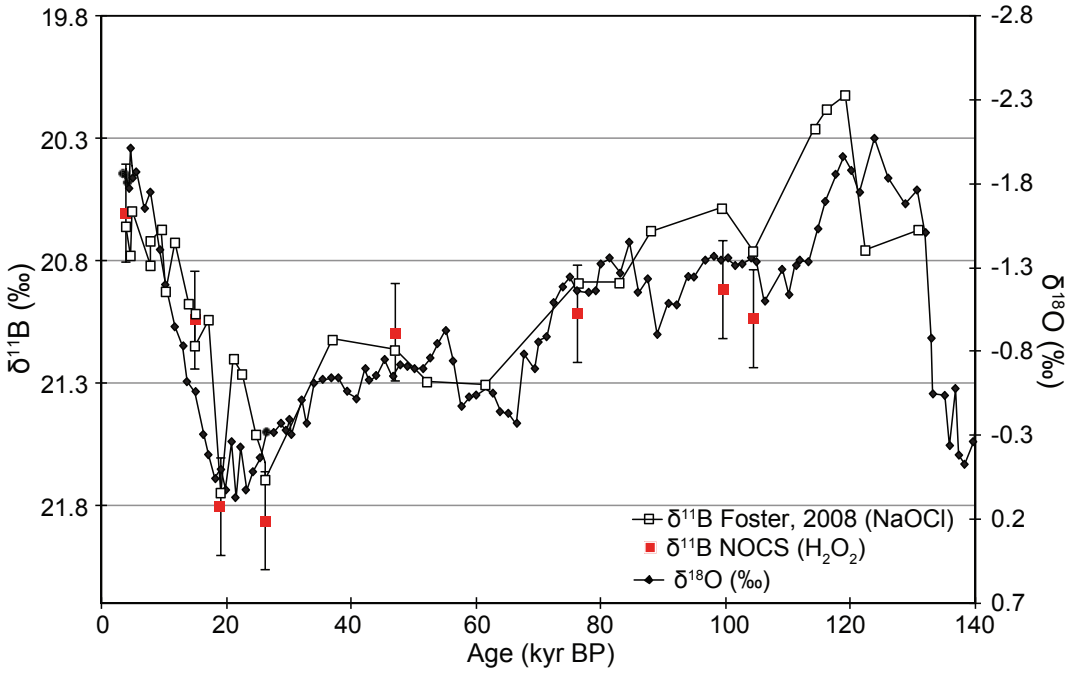

FIGURE 2.13: Boron isotope measurements from ODP999A from Foster (2008) cleaned using NaOCl (white squares), compared to samples repicked and cleaned as described in section 2.3 and measured at NOCS (red squares). The oxygen isotope data from the site are plotted for context.

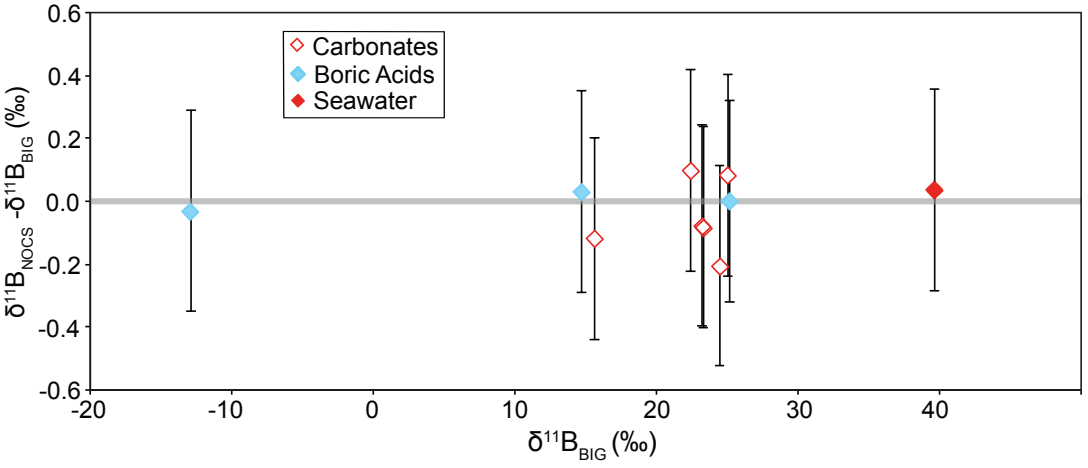

FIGURE 2.14: Comparability of measurements of a range of in house standards between the Thermo Neptune MC-ICPMS machines at the Bristol Isotope Group and the National Oceanography Centre, Southampton. Error margins are the quadratic addition of 2 standard deviations on the mean measurements at Bristol and at Southampton.

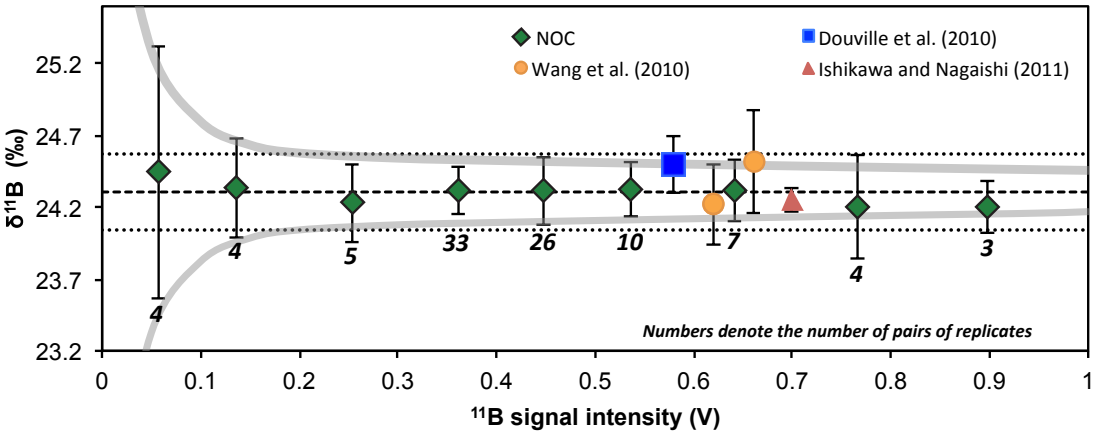

FIGURE 2.15: Measurements of JCP-1 produced at the NOC, plotted for comparison with other published values (Wang et al., 2010, Douville et al., 2010, Ishikawa and Nagaishi, 2011). The thick dashes line denotes the long-term average of 24.31 ‰, with the thin dashed line either side denoting the overall 2σ of this value (0.26 ‰). Grey lines mark the reproducibility curve from Equation 2.3. Error bars denote the 2σ of pairs of replicates in each bin, with the numbers below each bin denoting the number of replicates analysed in this intensity bin.

Nagaishi, 2011, see Figs. 2.15 below), and to preliminary data measured via MC-ICPMS at the University of South Carolina (B. J. Marshall, pers. comm.). In addition, work has begun on a new intercomparison project involving NOCS, co-ordinated by Drs. Ed Hathorne and Marcus Gutjahr (GEOMAR, Kiel), Asst. Prof. Bärbel Hönisch (Lamont-Doherty Earth Observatory) and Dr. Gavin Foster (NOCS).

2.7.2 Reproducibility

Unsurprisingly, given the almost identical procedures and equipment used, the curve of external reproducibility vs. sample signal produced at NOCS is reassuringly similar to that observed at Bristol Isotope Group, University of Bristol, as reported by Rae et al. (2011) and defined by Equation 2.5 below. While it would appear that our reproducibility in smaller samples is somewhat poorer than at BIG, it is likely that this has more to do with the small number of measurements of JCP-1 and JCT-1 at low [B] made to date at the NOC than any systematic issues.

$$2\sigma = 1.7 \times exp^{-29[^{11}B]} + 0.31 \times exp^{-0.75[^{11}B]} \tag{2.5}$$

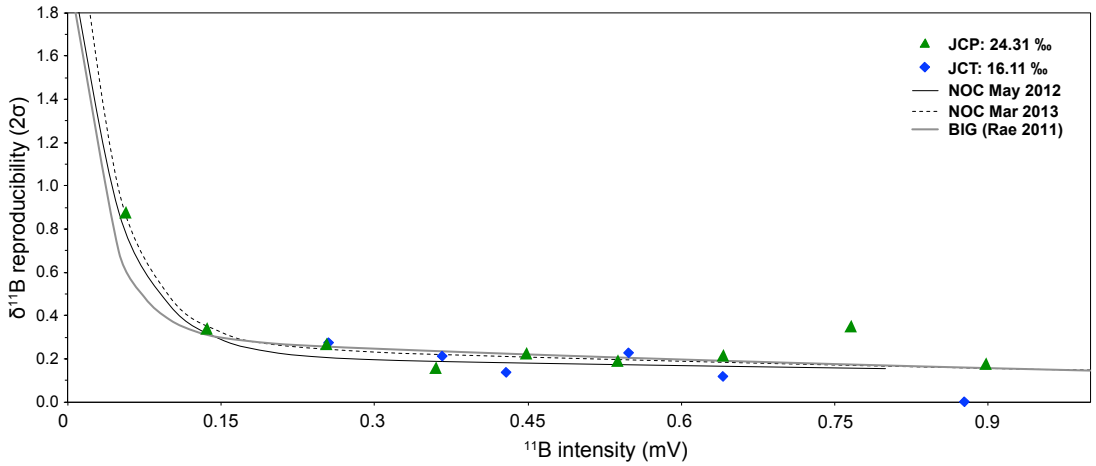

FIGURE 2.16: External reproducibility of pairs of replicate measurements of JCP-1 (Okai et al., 2002) and JCT-1 (Inoue et al., 2004) standards (as a function of ^{11}B intensity) at the NOC compared to reproducibility of at Bristol Isotope Group (from Rae et al., 2011). The lines-of-best-fit plotted are double exponentials, described by Equations 2.2 (May 2012), 2.3 (March 2013) and 2.5 (Bristol).

2.8 Summary

As may be seen from this Chapter, analysis of boron isotopes in foraminiferal carbonates is not a trivial matter. Possible sources of inaccuracy are numerous, and strict protocols must be observed for the generation of data of acceptable quality. That said, as a result of these protocols and practices, it is clear that accurate and precise measurements of δ^{11}B can be routinely achieved at NOCS via MC-ICPMS. Consequently, questions of palaeoceanography and foraminiferal biology (e.g. Chapters 3 and 4) can be approached with confidence.

Chapter 3

Calibration of the boron isotope proxy in the planktic foraminifera *Globigerinoides ruber* for use in palaeo-CO_2 reconstruction

Abstract

The boron isotope-pH proxy, applied to mixed-layer planktic foraminifera, has great potential for estimating past CO_2 levels, which in turn is crucial to advance our understanding of how this greenhouse gas influences Earth's climate. Previous culture experiments have shown that, although the boron isotopic compositions of various planktic foraminifera are pH dependent, they do not agree with the aqueous geochemical basis of the proxy. Here, results are outlined from culture experiments on *Globigerinoides ruber* (white) across a range of pH (∼7.5-8.2) and analysed via multicollector inductively-coupled plasma mass spectrometry (MC-ICPMS). These data are compared to core-top and sediment-trap samples to derive a robust new species-specific boron isotope-pH calibration. Consistent with earlier culture studies, *G. ruber* demonstrates a reduced pH-dependency compared to borate ion in seawater. Evidence for a size fraction effect in the $\delta^{11}B$ of *G. ruber* is also presented. Finally, atmospheric CO_2 concentrations over the last deglacial are reconstructed by applying

this new calibration at two equatorial sites, ODP Site 999A and Site GeoB1523-1. These data provide further grounding for the application of the boron isotope-pH proxy in reconstructions of past atmospheric CO_2 levels.

Acknowledgements

Please note that much of the content within this chapter has been submitted for publication as part of Henehan et al. (2013). As such I acknowledge here the contributions of my co-authors, namely:

- James W. B. Rae *(now Californian Institute of Technology)*, who helped during culturing work in Eilat and who analysed the culture and control samples at the University of Bristol
- Gavin L. Foster *(University of Southampton)* who contributed particularly greatly during drafting of the manuscript in question and who picked and analysed downcore samples from Site GeoB1523-1
- Jonathan Erez *(Hebrew University of Jerusalem)* who supervised culturing work at the IUI, Eilat
- Katherine C. Prentice *(now Imperial College London)* who assisted in culturing work at the IUI, Eilat
- Michal Kucera *(now MARUM)* who sourced samples and facilitated their collection from the archives at the University of Tübingen
- Helen C. Bostock *(National Institute for Water and Atmospheric Research, Wellington)* who sourced and dated core-top material from the Southwest Pacific
- Martínez-Botí, Miguel-Angel *(University of Southampton)* who contributed greatly during the setting up of the laboratory at the University of Southampton
- Milton, J. Andy *(University of Southampton)*, who assisted with MC-ICPMS analysis
- Wilson, Paul A. *(University of Southampton)*, my second supervisor, who assisted in the drafting of this manuscript

- Marshall, Brittney J. *(University of South Carolina)* who sourced and picked sediment- trap material from the Cariaco Basin
- Elliott, Tim *(University of Bristol)* in whose lab culture and control samples were analysed, and whose thinking was key to the formulation of this PhD project.

As authors, each of the above contributed to varying degrees in the drafting of the manuscript for publication.

3.1 Introduction

3.1.1 The Boron isotope-pH proxy in planktonic foraminifera

The use of boron isotopes in surface-dwelling planktic foraminifera to reconstruct ocean pH, and hence past levels of atmospheric CO_2, offers great promise (e.g. Foster, 2008, Hönisch and Hemming, 2005b, Hönisch et al., 2009, Palmer et al., 2010, Pearson and Palmer, 2000, Pearson et al., 2009, Seki et al., 2010, Foster et al., 2012). The boron isotope-pH proxy has a well-understood foundation in inorganic chemistry that, providing biological interferences are understood, should permit greater confidence in boron-based palaeo-pH and -pCO_2 estimates. For a summary of this basis, the reader is referred to Chapter 1. However, because of the range of offsets from the boron isotope composition of ambient borate ion that has been reported to date in planktonic foraminifera (Sanyal et al., 1996, 2001, Hönisch et al., 2003, Hönisch and Hemming, 2004, Foster, 2008), application of the proxy beyond those extant species with species-specific calibrations requires further assumptions to be made. Clearly, then, it is important to extend the range of planktonic foraminiferal species for which empirical calibrations exist, and in doing so better understand exactly how these observed offsets from borate ion, known collectively as "vital effects", arise.

3.1.2 Existing calibrations

Culture studies are an important tool in calibrating foraminifera-based proxies, allowing for manipulation of growth conditions beyond the range seen in the modern oceans (for example the concentration of boron, Allen et al., 2011). In the case of the

boron isotope-pH proxy, attempts have been made to calibrate the symbiont-bearing foraminifera *Orbulina universa* (Sanyal et al., 1996) and *Globigerinoides sacculifer* (Sanyal et al., 2001) across a range of pH (7.6 to 9). These culture studies confirmed that the δ^{11}B of planktic foraminiferal calcite is strongly dependent on pH, but also describe a weaker sensitivity to pH in foraminiferal $\delta^{11}B_{CaCO_3}$compared to $\delta^{11}B_{B(OH)_4^-}$ (see Fig.3.1). However, while undoubtedly pioneering, these studies are not without scope for uncertainty. For instance, some carbonate system parameters during culture in these studies are relatively poorly constrained (e.g. pH only determined using NBS-buffer-calibrated electrodes) and some experiments (Sanyal et al., 2001) were performed at 10 x natural boron concentration, introducing further uncertainty by increasing the buffering capacity of culture seawater and thus potentially dampening vital effects (Zeebe et al., 2003). Furthermore, limited calibration attempts by Foster (2008) suggested a stronger pH sensitivity in the δ^{11}B of *G. ruber*, leading the author to suggest these previous calibrations may have been compromised by having used NTIMS without prior matrix removal, a technique which can result in non-systematic analytical inconsistencies (Rae et al., 2011, Foster et al., 2013, and references within). Therefore, further culture calibrations are required, both to corroborate previously reported pH sensitivities and to extend the applicability of the boron isotope-pH proxy to more species of foraminifera.

3.1.3 *Globigerinoides ruber*: Evolutionary History, Morphotypes, Range and Habitat

Globigerinoides ruber is a symbiont-bearing planktic foraminifera that is ubiquitous in tropical and equatorial waters. The species is a good candidate for use in palaeo-reconstruction, due to its shallow depth habit ($<$ 25 m, Hemleben et al., 1989) and lack of any significant layer of gametogenic calcite (Caron et al., 1990), which reduces the problems of partial dissolution (Ni et al., 2007). It also has a relatively long evolutionary history, having first diverged in the early Miocene approximately 18 Ma (Aurahs et al., 2011). Perhaps because of this it has been used widely in the reconstruction of palaeotemperature (e.g. Oppo et al., 2009) and even palaeo-CO_2 (e.g. Foster, 2008).

However, the morphospecies *G. ruber* is in fact includes a number of other groupings, which, depending on one's taxonomic bent, might be defined as species, subspecies, morphospecies or cryptospecies, and that have been subject to some considerable revision since the first description of the morphospecies (then called *Globigerina rubra*) by d'Orbigny (1839). Although initially the species *G. ruber* was strictly defined, with morphological variants designated as different species (e.g. *Globigerinoides elongatus*; originally *Globigerina elongata* d'Orbigny, 1826), these species were reassigned as phenotypic variants of the broader species *G. ruber* by Parker (1962). Only in the advent of isotopic (e.g., Wang, 2000, Steinke et al., 2005) and genetic analyses (e.g. Darling and Wade, 2008, Aurahs et al., 2009) are these earlier species divisions appearing increasingly prescient. The morphotype or chromotype *G. ruber* (pink) is perhaps the most easily discerned variant, distinguished by its salmon to rose-pink colouration. It is today found only in the equatorial Atlantic and Caribbean, having disappeared in the Indo-Pacific Ocean ca. 120 ka (Thompson et al., 1979). Since it has been shown that this species is geochemically distinct (e.g. Anand et al., 2003), and given that it is easily distinguished from the white morphotype, it is commonly separated in palaeoreconstructions (e.g. Rühlemann et al., 1999, Vink et al., 2001). Within the white chromotype, distinctions between morphotypes becomes somewhat more subtle. Wang (2000) defines two geochemically distinct white morphotypes, *sensu stricto* and *sensu lato*, which have since been corroborated by others (Lin et al., 2004, Kawahata, 2005, Löwemark et al., 2005, Steinke et al., 2005, Numberger et al., 2009). Indeed, more recent phylogenetic analyses (Aurahs et al., 2011) suggest that the *sensu lato* subgroup is in fact more closely related to *G. conglobatus* than *G. ruber sensu stricto*. In addition, the *sensu lato* grouping of Wang (2000) can be further subdivided (Numberger et al., 2009) into *G. pyramidalis* (van den Broeck, 1876) and *G. elongatus* (d'Orbigny, 1826), although, in practice, sample size constraints mean that the separation of these morphotypes for boron isotope analysis is seldom feasible. As such in this study we apply the more general classification system of Wang (2000), combining both *sensu lato* morphotypes, though we suggest that further testing as to the possibility of geochemical differences between *G. ruber pyramidalis* and *G. ruber elongatus* would certainly be beneficial.

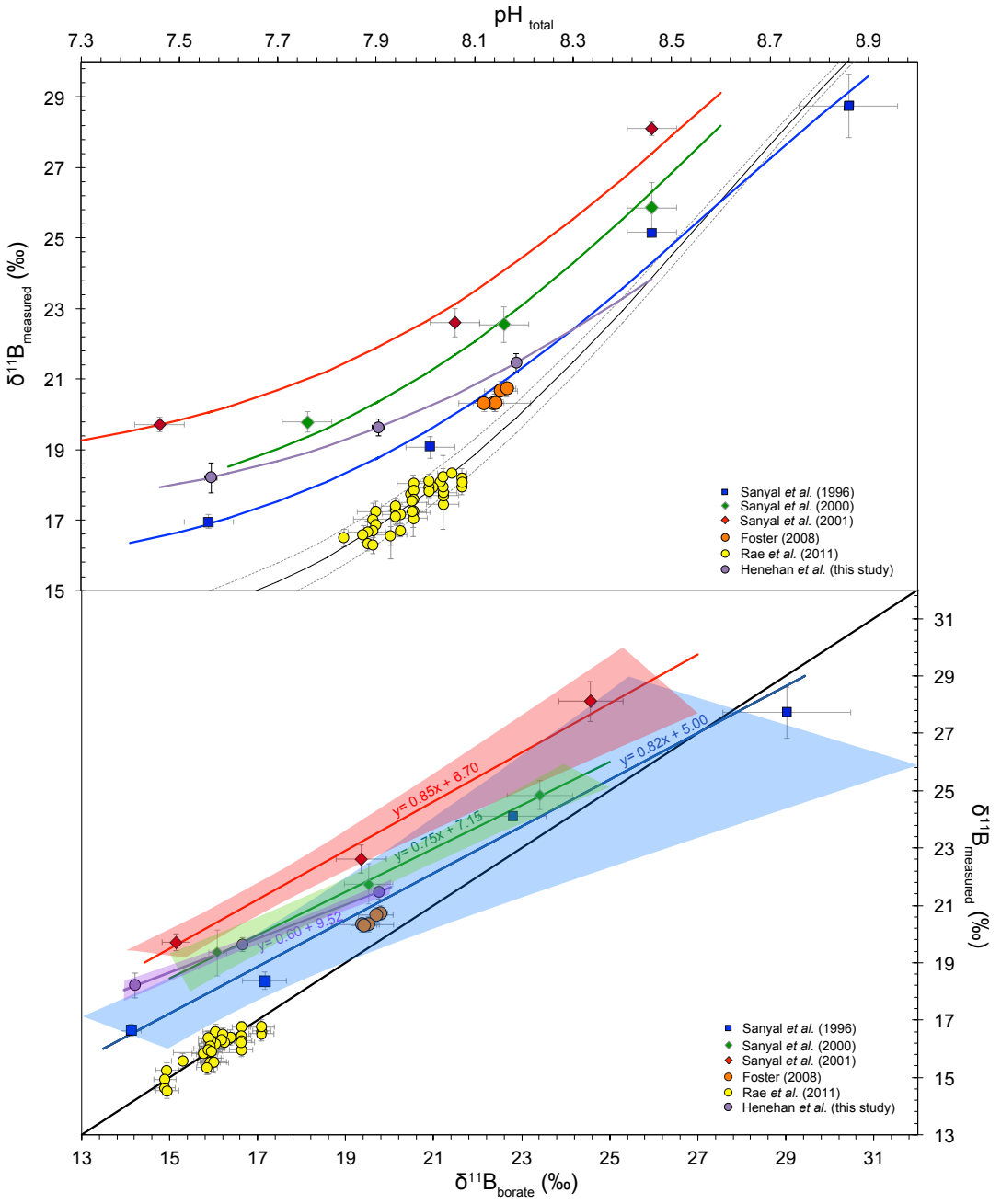

FIGURE 3.1: Published bulk planktic foraminiferal culture and inorganic precipitate experiments, plotted in δ^{11}B-pH space (top panel) and in $\delta^{11}B_{CaCO_3}$-$\delta^{11}B_{B(OH)_4^-}$space (bottom panel). Note that for the purposes of graphical representation, the data were normalised to a $\delta^{11}B_{sw}$= 39.61 ‰ (both panels), and to a temperature of 26 °C and a salinity of 37.2 psu (top panel only; the conditions of our culture calibration). The black line in δ^{11}B-pH space is the inorganic value of $\delta^{11}B_{B(OH)_4^-}$ at these environmental conditions, with the dotted lines representing the error value on the value of $^{11-10}K_B$ (± 0.0006) in seawater at 25 °C reported by Klochko et al. (2006). Coloured calibration lines are best fits, varying $^{11-10}K_B$ and a from Equation 3.4. The black line in $\delta^{11}B_{CaCO_3}$-$\delta^{11}B_{B(OH)_4^-}$ space (bottom panel) is a 1:1 relationship, i.e. a pH sensitivity equal to that of borate ion. Calibrations are represented by York regressions calculated using Isoplot (Ludwig, 2003), with shaded areas representing 95 % confidence intervals for these regressions. Note that it was not possible to calculate statistically significant 95 % confidence intervals for the data of Rae et al. (2011) or Foster (2008) using this method, as the spread in $\delta^{11}B_{B(OH)_4^-}$ is insufficient, but they are included for comparison, having been used elsewhere for downcore reconstruction. Regressions shown here are described in Table 3.1.

3.2 Calibration: Methods

3.2.1 Culture

3.2.1.1 Sampling and Culturing methods

Neanic (typically $\sim$ 250 μm) specimens of *G. ruber* (white) were towed from depths of $<$ 10 m in the Gulf of Aqaba between January and March 2010, at the Interuniversity Institute of Eilat, Israel. Individual foraminifera were transferred to seawater collected at the site of plankton towing within 4-6 hours of capture, and kept under saturated light conditions at $\sim$ 23 °C until fully recovered (i.e. floating, with a halo of spines and symbionts). Those that did not recover fully were retained for boron isotope analysis as control tow samples, and used for mass-balance corrections (as discussed later). Since traits used to distinguish the morphotypes of *G. ruber* (*sensu stricto/lato*; Wang, 2000) are often poorly developed in immature specimens (Aurahs et al., 2011), no distinction could be drawn between morphotypes in culture. For reference, *G. ruber sensu lato* made up 35-45% of the total identifiable population of *G. ruber* from tows and core-top sediment in the Gulf of Aqaba. However, we see no difference in δ^{11}B (or B/Ca) between these morphotypes in core top sediments (see Fig. 3.2).

Recovered foraminifera were transferred to sealed Erlenmeyer flasks filled with prepared seawater (see Section 3.2.1.2). Foraminifera were removed daily,fed one newly-hatched *Artemia* nauplius, observed and measured using a Zeiss inverted light microscope. Condition and approximate symbiont density was noted. In an attempt to avoid damage to the foram and increase the low acceptance rates typically seen in cultured *G. ruber* (Spindler et al., 1984), thereby increasing mass gain, *Artemia* were incapacitated prior to feeding. Illumination was provided by a metal halide lamp (420 W, OsramTM) at levels of 200 μmol photons m^{-2} s^{-1} (13h light:11h dark), equivalent to irradiance at 15 - 20 m depth in the open waters of the northern Gulf of Aqaba (Shaked and Genin, 2006), and in keeping with the reported depth habitat of $<$ 25 m for *G. ruber* (Hemleben et al., 1989). Culture flasks were kept in water baths at a constant temperature of 26 $\pm$ 0.5 °C (see Fig. 3.3).

After gametogenesis (typically after 6-10 days in culture), empty *G. ruber* tests were removed from culture flasks, rinsed in de-ionised water, dried and weighed.

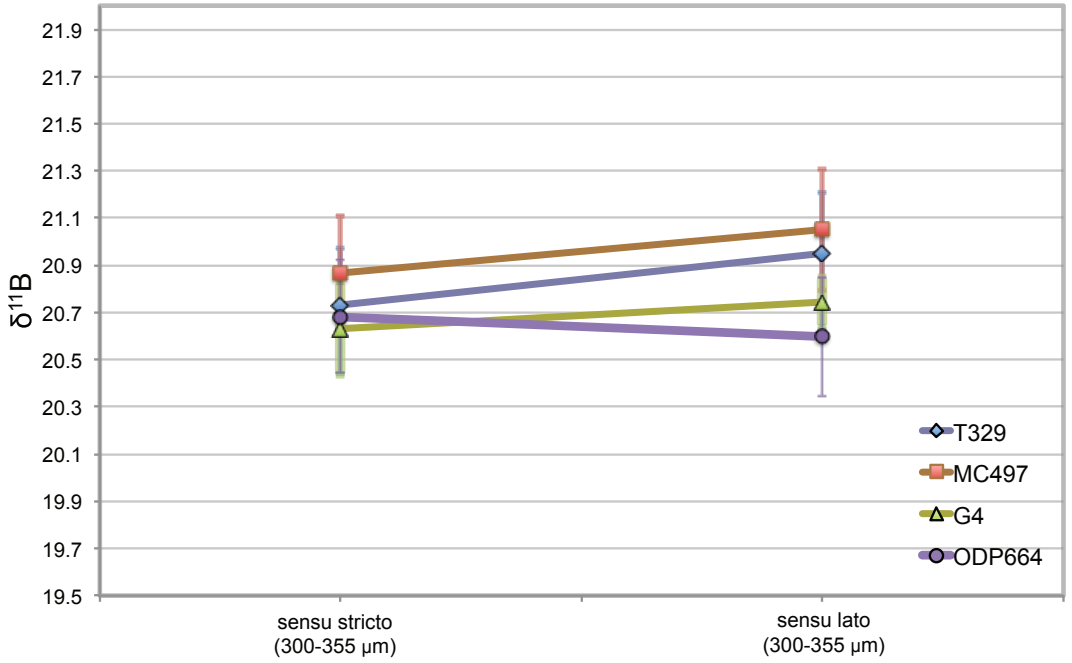

FIGURE 3.2: *G. ruber sensu stricto* vs. *G. ruber sensu lato* (*G. ruber elongatus* and *pyramidalis*) from the same core-top sediment samples, showing no consistent offset. Error bars are calculated according to the characterised long-term reproducibility at the NOC, Equation 2.2.

3.2.1.2 Carbonate System Control

Seawater was prepared in large batches to ensure consistency across all flasks, and a surplus for topping-up was stored in airtight bottles in the dark at ∼ 4 °C. Salinity was reduced from ∼40.7 to 37 via addition of de-ionised water. Following other culturing studies (Sanyal et al., 1996), pH was altered by adjusting alkalinity via addition of NaOH or HCl. Culture experiments were carried out at pH 8.174 ± 0.007, 7.894 ± 0.013, and 7.554 ± 0.013 (total scale; 2 se, n = 48 - 67). pH drift in the culture flasks was monitored periodically using a pH electrode calibrated to NBS buffers, with individuals (n = ∼ 3-5) from flasks that experienced large pH drift discounted. Samples of culture solution were taken at the beginning of each pH experiment, and a composite sample taken from all flasks at the end of culturing. These water samples were poisoned with 50 μl saturated $HgCl_2$ solution and transported for full carbonate system analysis at the UK Ocean Acidification Research Programme (UKOARP) Carbonate Chemistry Facility, at the National Oceanography Centre Southampton (NOCS). Nutrient analyses were also undertaken to ascertain nitrate, nitrite, phosphate and silicate concentrations. NBS-scale pH measurements of

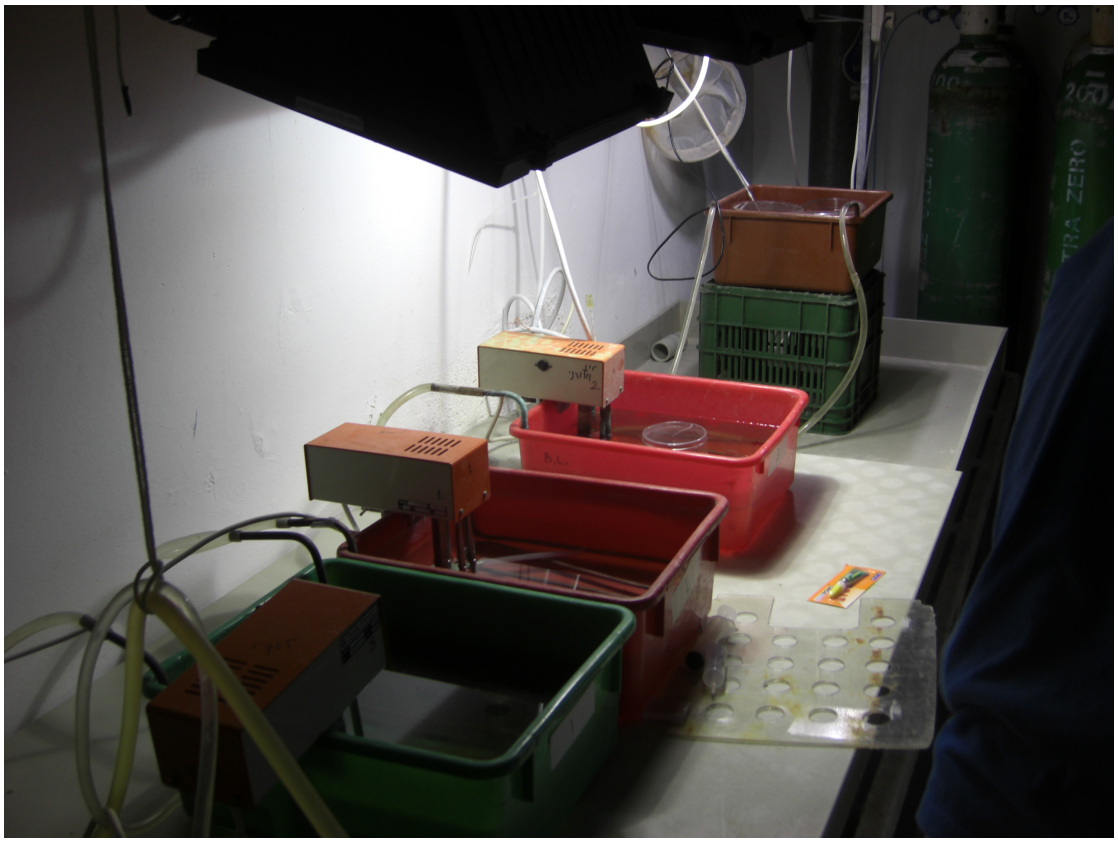

FIGURE 3.3: Culture apparatus, with recovery bath set to 23 °C on the far right and culture baths at 26 °C towards the foreground. Note that subsequent to this photo being taken a third light source was obtained and set up. While the recovery bath was subject to 24 hr light conditions, culture baths were set to 13h light:11h dark cycles. As such a screen was set up to prevent light from the recovery bath reaching culture samples.

these composite samples taken in Eilat were consistently higher than Dissolved Inorganic Carbon(DIC)/Total Alkalinity (TAlk)-derived total scale pH measurements by 0.21 pH units (see Fig.3.4). As such, we judged our in-culture NBS-calibrated potentiometric electrode measurements to be reliable once corrected for this 0.21 pH offset. While the discrepancy between scales reported here is somewhat larger than a 'universal' 0.14 offset that is sometimes advocated elsewhere (Hönisch and Hemming, 2005a), we highlight that conversion between scales is not universal, and may be affected by factors such as instrumental differences (Wedborg et al., 1999) or ionic strength of the solution (Zeebe and Wolf-Gladrow, 2001) - which is particularly high in the Gulf of Aqaba. As we show here (Fig 3.5), the correction used in the conversion of NBS-scale measurements to total scale may have a large bearing on the conclusions to be drawn, and as such we advise that if electrodes are used in culture studies such as

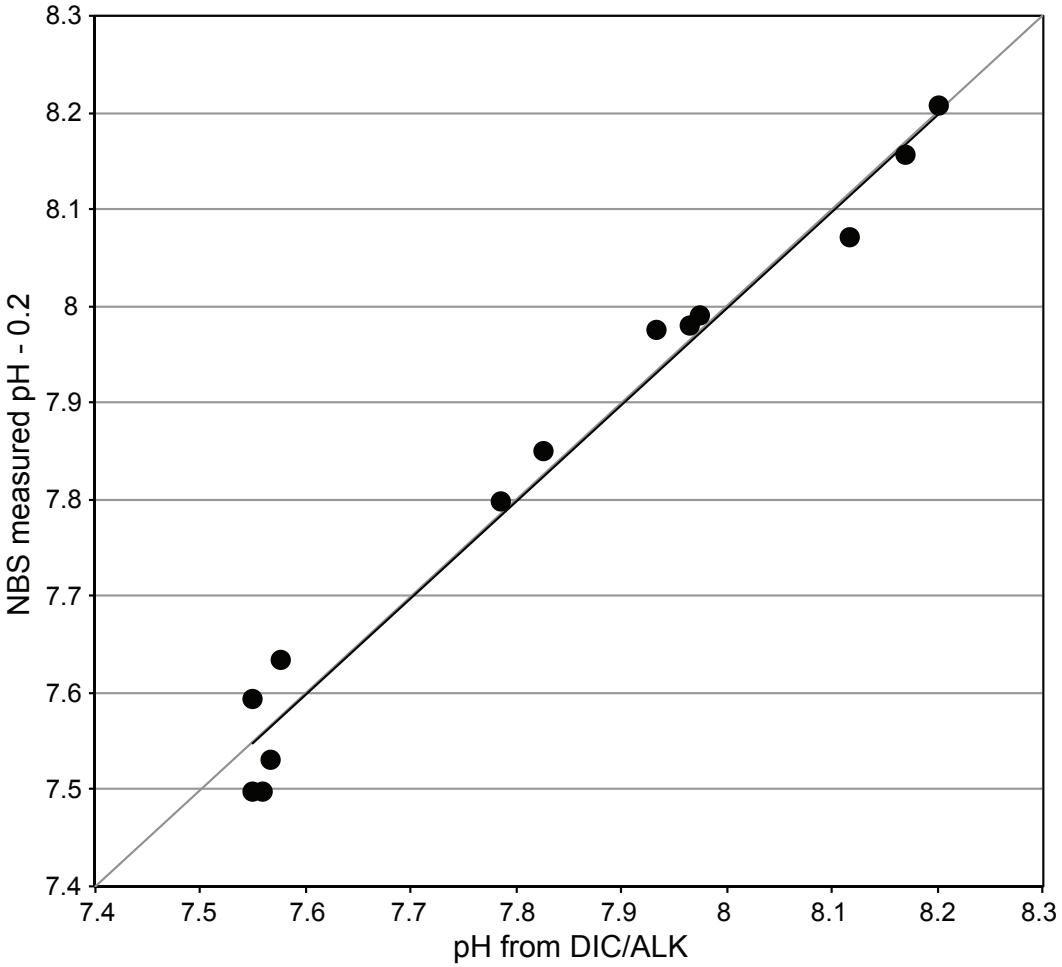

FIGURE 3.4: Illustration of the good fit between pH measurements on the total scale calculated from DIC/Alk using the constants of Lueker et al. 2000 and Dickson 1990 and NBS-buffer-calibrated electrode measurements once a correction of -0.21 has been applied to the latter. On the basis of this, we derived our culture pH uncertainty from NBS electrode measurements taken regularly during culture, corrected to approximate the total scale.

these their offsets from total scale are properly calibrated. Although some authors have suggested a universal correction of - 0.14 pH, neither this study nor Venn et al. (2013) agree with this.

The advantage of using these electrode measurements over a more generalised 'before and after' measurement (of stock solution and composite post-culture solution) is that the pH range experienced by each foram could better quantified using the more high resolution electrode measurements. For example, were we to have replaced the foram in one flask with another half way through the experiment (after it had completed

gametogenesis, for example), but ultimately not included the second foram for analysis (because it died without completing gametogenesis, for example), we can quantify the pH range experienced by the relevant foram and discount any pH variation after this point (that would otherwise be unduly included in our pH estimates via a DIC/Alk measurement of a post-culture composite).

3.2.1.3 Mass-Balance Calculations

To correct for the chemistry of the test grown outside of culture, a mass-balance correction was used, following Erez (1983), Lohmann (1995) and Kisakürek et al. (2008). Dried control samples (i.e. *G. ruber* tests towed at the same time as cultured material) were weighed individually on a microbalance, photographed and measured using Macnification imaging software. A size-mass relationship for all towed control samples was calculated, such that initial size measurements (maximum axis multiplied by its perpendicular axis) of foraminifera made immediately prior to culturing could be used to estimate shell mass (Fig. 3.6). While organic matter was not removed prior to weighing, calculation of $CaCO_3$ mass via ICPMS for a subset of samples gave consistent results, suggesting organics do not contribute much to dried shell mass. Best fit was via power-type regression, as noted by Kisakürek et al. (2011) for *G. ruber* from Eilat. The relationship is best defined by the equation

$$mass = 803.65 * (product\ of\ axes)^{1.957} \tag{3.1}$$

where product of axes is expressed in mm^2 (n= 112, $R^2 = 0.75$, $p < 0.001$). Reassuringly, the exponential of this relationship is the same as that defined by Kisakürek et al. (2011).

The boron isotope composition and boron content (as B/Ca) of control *G. ruber*from each experimental tow (n = 150-200) was then measured (see Section 2 for analytical methodology). Assuming cultured individuals began with this δ^{11}B and B/Ca, and using the size-mass relationship to estimate the mass of calcite grown out of culture, a correction can be made and the composition of the foraminifera grown during culture calculated by

$$\delta^{11}B_{culture} = \frac{\delta^{11}B_{measured} - (\delta^{11}B_{controls} * P^{B}_{controls})}{P^{B}_{culture}} \tag{3.2}$$

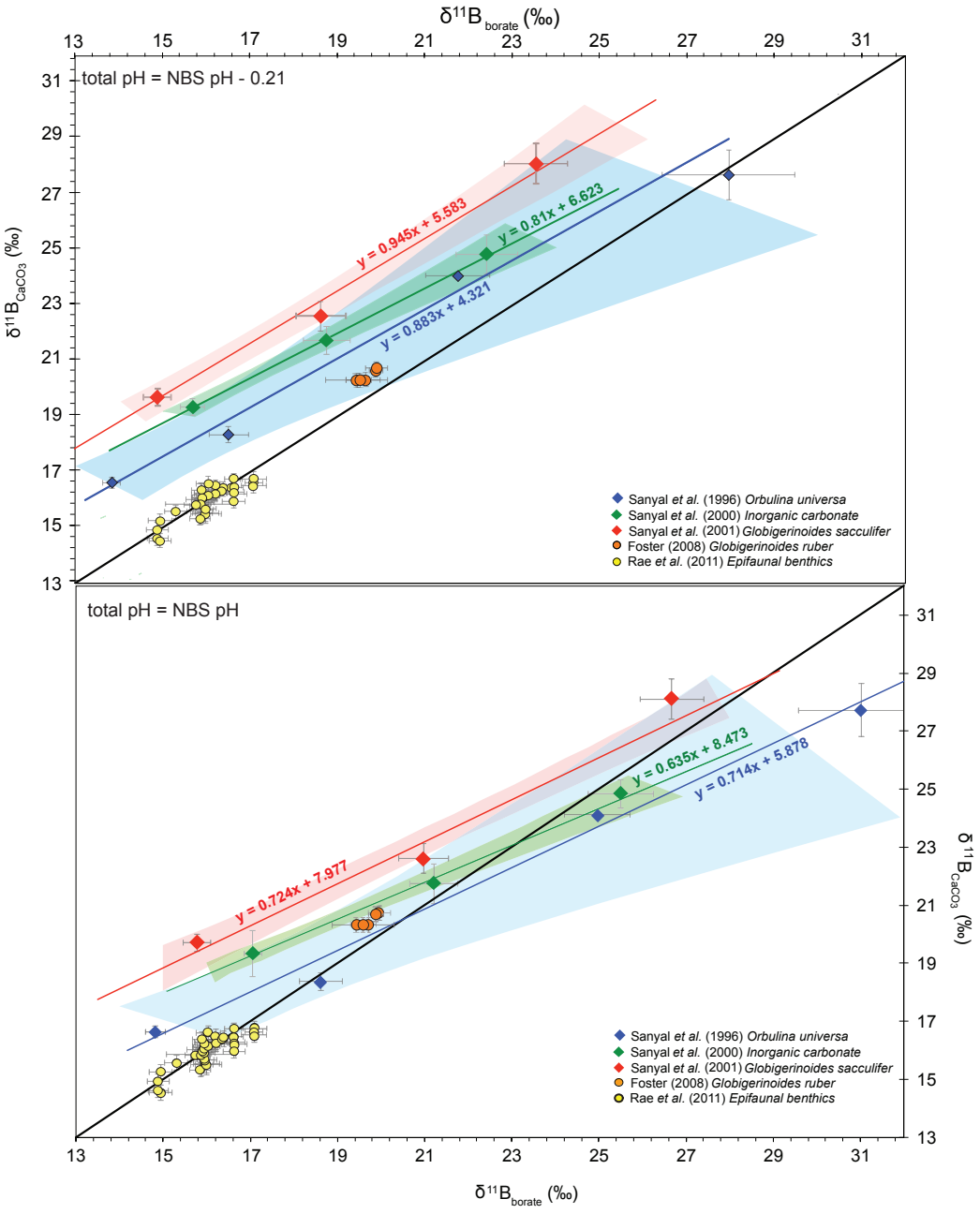

FIGURE 3.5: Illustration of the importance of a good understanding of the correction from NBS-buffer calibrated electrode measurements to the total scale. Note that if using a correction of -0.21 (as required for our calibration), the slopes of the existing calibrations would be within uncertainty of the δ^{11}B of aqueous borate, while without any correction their slopes are much shallower. Since much of the discussion regarding these calibrations to date (e.g. Hemming and Hönisch, 2007, Hönisch et al., 2007) has revolved around the slope of these lines (i.e. the pH sensitivities observed), it is perhaps surprising that this potential source of uncertainty has not been examined more thoroughly.

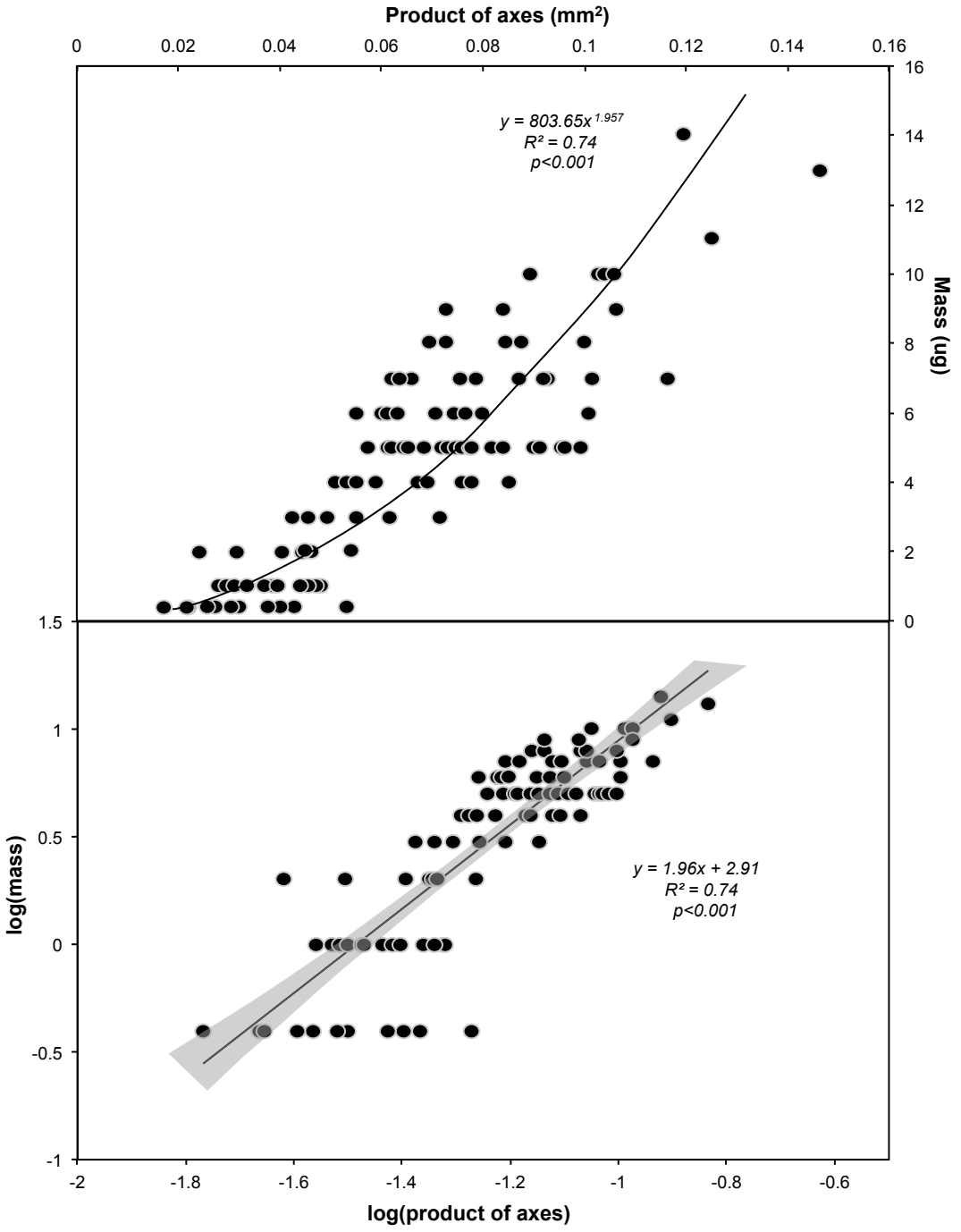

FIGURE 3.6: Size:Mass Relationship constructed from towed samples collected between January and March 2010. Masses were determined by weighing individually, while size is defined as the product of the maximum axis (when viewed from the umbilical side) and the axis perpendicular to it. Measurements were taken with Macnification imaging software. Note that this relationship closely resembles that defined by Kisakürek et al. (2011).

where $\delta^{11}B_{measured}$ is the measured boron isotopic composition of the bulk material, and $\delta^{11}B_{controls}$ is the measured boron isotopic composition of control foraminifera towed at the same time as those cultured. $P^{B}_{controls}$ and $P^{B}_{culture}$ are the proportions of boron in the bulk material coming from the pre-culture and culture-grown calcite respectively. These are calculated based on the B/Ca ratios in the bulk material and in control specimens, and the proportion of calcite mass grown in culture and out of culture, such that

$$P^{B}_{culture} = \frac{B/Ca_{measured} - (B/Ca_{controls} * P^{mass}_{controls})}{B/Ca_{measured}} \tag{3.3}$$

and $P^{B}_{controls} = 1 - P^{B}_{culture}$.

Uncertainty on each mass-balance-corrected culture datapoint was estimated from the 2σ of 10,000 Monte Carlo simulations that incorporated the uncertainty in the size-mass calibration (see Fig. 3.6, Panel B) and uncertainty in B/Ca measurements (5 %) and $\delta^{11}B$ measurements (from Equation 2.5) in 'control' towed specimens and cultured specimens.

3.2.2 Core-tops

3.2.2.1 Sampling

In order to compare the results of our culture calibration with foraminifera grown in natural conditions, we measured specimens of *G. ruber* from globally distributed core-top sites from the core archives at Tübingen, Germany and NIWA, New Zealand, and from sediment trap material from the Cariaco Basin. Samples from NIWA were verified as recent by way of ^{14}C-dating (H. Bostock, pers. comm.), while from the Tübingen repository only undisturbed multicore sediment containing Rose Bengal-stained living benthic foraminifera was selected. In addition, material from sediment traps in the Cariaco Basin was used to further test for biases introduced during sedimentation. This array of sites covers as broad a range of *in situ* $\delta^{11}B_{B(OH)_4^-}$ as possible, and serves to test for any regional differences (as seen in Mg/Ca, Bolton et al., 2011) that might stem from genotype differences, etc. (Darling and Wade, 2008). The locations of these core-top and sediment trap sites are shown in Fig. 3.7

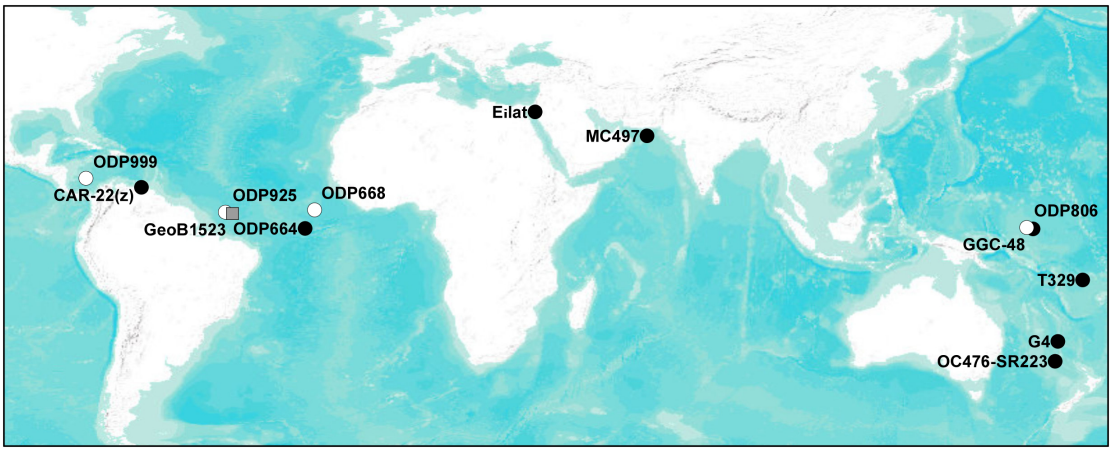

FIGURE 3.7: Locations of core-top, tow and sediment trap samples used in this study. Filled circles are sites from which recent samples are measured (this study), while white circles are core-tops from Foster (2008). Sites of downcore pCO_2 reconstructions are marked by a grey square (GeoB1523-1) and white circle (ODP 999A: also the site of core-top measurement Foster 2008).

(see also Supplementary Table B.2). Samples were also taken from a number of size fractions to examine any influence of test size on measured $\delta^{11}B$, as discussed by Hönisch and Hemming (2004) and Ni et al. (2007).

3.2.2.2 Carbonate System Characterisation

pH, temperature and salinity at the sediment trap site (CAR22(Z), collected January 2007) is interpolated from data from December 2006 and February 2007, downloadable from www.imars.usf.edu/CAR. pH was estimated for core-top sites using surface water oceanographic data from the GLODAP (Key et al., 2004), CARINA (Key et al., 2010) and Takahashi et al. (2009) compendia (see Supplementary Table B.2). First, regional salinity-TAlk correlations were calculated from surface (< 20 m) GLODAP/CARINA measurements. Applying these correlations, monthly-resolved estimates of sea surface salinity from Takahashi et al. (2009) were converted to monthly TAlk estimates. Monthly temperature estimates were also taken from Takahashi et al. (2009). Pre-industrial pCO_2 at each core-top site was estimated by applying monthly ocean-atmosphere ΔpCO_2 from Takahashi et al. (2009) sites (corrected for the anthropogenic changes in flux using the average industrial:pre-industrial ΔpCO_2 ratio found in the models of Gloor et al. 2003) to a pre-industrial atmospheric pCO_2 value. Where samples were ^{14}C-dated, the age-appropriate atmospheric pCO_2 2value was

taken from Lüthi et al. (2008) and references within. Where core-tops were not dated, we assume an average late Holocene (< 4 kyr BP) value of 275 ppm. Combined with approximations of typical local silicate and phosphate concentrations (from GLODAP/CARINA measurements), monthly estimates of pH were calculated using CO2sys.m (van Heuven et al., 2011), and the constants of Lueker et al. (2000), Lee et al. (2010) and Dickson (1990). Note that we did not weight the annual mean carbonate system parameters to any particular bloom season, given that *G. ruber* has a fairly even intraannual flux (Kucera, 2007, Fraile et al., 2009). As such, pH (and thus $\delta^{11}B_{B(OH)_4^-}$) values given are the mean of twelve monthly estimates.

3.2.3 Presentation of Culture Data

3.2.3.1 δ^{11}B vs. pH plots

The most common way to present boron isotope data from cultured foraminifera is in terms of the observed δ^{11}B-pH relationship (Fig. 3.1a). This, however, leads to difficulties in comparing calibrations cultured under differing temperatures and salinities, where the value of pK_B^* differs, thereby introducing the need for normalisation. For example, in Figure 3.1a, disparate calibration datasets are normalised to our culture conditions (26 °C and 37.2 psu), based on the change in inorganic $\delta^{11}B_{B(OH)_4^-}$ expected if pK_B^* were altered to reflect given temperature, salinity and pressure. Similarly, application of these calibrations to open ocean foraminiferal data must include some correction for pK_B^* differences between datasets (though this is often overlooked, e.g. Hönisch and Hemming 2005b).

Furthermore, in order to present boron isotope data in terms of the observed δ^{11}B-pH relationship, it is necessary to characterise species δ^{11}B-pH relationships by forcing them to fit the general equation for boron isotope-pH calculation (Eq. 1.10). This can be done by incorporation of a constant offset or vital effect termed 'a' into equation (1.10), such that

$$pH = pK_B^* - log\left(-\frac{\delta^{11}B_{sw} - (\delta^{11}B_{CaCO_3} - a)}{\delta^{11}B_{sw} - {}^{11-10}K_B * (\delta^{11}B_{CaCO_3} - a) - 1000 * ({}^{11-10}K_B - 1)}\right) \tag{3.4}$$

In addition, the fit of empirical data to an equation of this form can also be optimised by altering the ${}^{11-10}K_B$ constant (Table 1, Hönisch et al., 2007). The addition of an offset '*a*' to an aqueous $\delta^{11}B_{B(OH)_4^-}$-pH curve (e.g. Hönisch and Hemming, 2005b, Foster, 2008), however, implies that any such vital effect is constant across a range of pH. Past modelling efforts (Zeebe et al., 2003) provide some support for this argument, but it must be noted that no previous culture calibration, our own included, shows a constant offset from the ${}^{11-10}K_B$ of Klochko et al. (2006). Furthermore, any optimisation of ${}^{11-10}K_B$ in tandem with an offset 'a', as used by Hönisch et al. (2007) to characterise $\delta^{11}B_{CaCO_3}$-pH curves of published empirical data, might be misconstrued as implying ${}^{11-10}K_B \neq 1.0272$, rather than that these empirical calibrations exhibit pH sensitivities $\neq$ the pH sensitivity of $\delta^{11}B_{B(OH)_4^-}$.

3.2.3.2 $\delta^{11}B_{CaCO_3}$ vs. $\delta^{11}B_{B(OH)_4^-}$ plots

Given these difficulties, we instead describe culture calibration data following Foster et al. (2012). Similar to Rollion-Bard and Erez (2010), who plot calculated pH vs. culture pH, this approach involves a linear regression between calculated $\delta^{11}B_{B(OH)_4^-}$ (at *in situ* conditions) and measured $\delta^{11}B_{CaCO_3}$ (Fig. 3.1b). Thus, given measured $\delta^{11}B_{CaCO_3}$, one can use the appropriate calibration regression to predict the value of ambient $\delta^{11}B_{B(OH)_4^-}$, which may then simply be entered into the general equation (Eq. 1.10) to calculate pH. Necessary transformations for relevant existing calibrations are listed in Table 3.1. On such cross-plots, calibration data define straight lines with slopes (given as 'm, Table 3.1) reflecting the difference between the δ^{11}B-pH sensitivity of $\delta^{11}B_{B(OH)_4^-}$ and $\delta^{11}B_{CaCO_3}$. The slopes and intercepts (given as 'c', 3.1) of these lines are independent of pK_B^* (and hence salinity, temperature and pressure), meaning that culture and core top calibrations can be readily compared without reference to particular environmental conditions. In addition, presentation of culture calibrations in this way allows for the plotting of 95% confidence intervals using York regression, taking into account both uncertainty on culture conditions and measurement uncertainty (York, 1968, Ludwig, 2003). This approach permits better propagation of the uncertainty of culture calibrations into final pH and pCO_2 reconstructions, and confirms the observations of Hönisch et al. (2007) that pH sensitivities seen in published foraminiferal culture calibrations (Sanyal et al., 1996, 2001) are within statistical uncertainty of the pH sensitivity of inorganic $CaCO_3$ (as derived by Sanyal

		Coefficients of Calibration					
Publication	Carbonate	$\delta^{11}B_{B(OH)_4^-}=(\delta^{11}B_{CaCO_3}\text{-c})/\text{m}$				MSWD	p
		c	2σ	m	2σ		
Sanyal et al. (1996)[abc]	*Orbulina universa*	5.0	5.3	0.82	0.32	5.6	<0.01
Sanyal et al. (2000)[a]	Inorganic precipitates	7.1	3	0.75	0.15	0.12	0.73
Sanyal et al. (2001) [ab]	*Globigerinoides sacculifer*	6.7	3.3	0.85	0.19	1.05	0.31
Henehan et al. (this study)	*Globigerinoides ruber*	9.52	1.51	0.60	0.08	0.01	0.96

TABLE 3.1: York-fit regression statistics from Isoplot (Ludwig, 2003); MSWD = Mean Square Weighted Deviation, p = probability of fit at 95 % confidence. [a] pH measurements (from which $\delta^{11}B_{B(OH)_4^-}$ is derived) come from NBS-buffer-calibrated electrode measurements, and as such are in NBS-scale. [b] Salinity assumed to be 35 psu [c] 'Room temperature' assumed to be 20 °C

et al., 2000). Given also the possibility that species-specific offsets (i.e. the observed range in intercepts in Table 3.1) may be at least partially due to inconsistencies in absolute N-TIMS measurements between labs (as highlighted by Hönisch et al. 2003, Rae et al. 2011, Ni 2010), further investigation into the species-specificity of these calibrations is required.

3.2.4 Analytical methods

Analytical methods are as discussed in Chapter 2. Culture, sediment trap and tow samples, in agreement with other culturing studies (e.g. Russell et al., 2004), were subject to intensified oxidative cleaning (3 x 20-30 min treatments of 250 μl 1% H_2O_2 + 0.1 M NH_4OH_4 at 80 °C) to account for the larger organic. In core-tops, oxidative cleaning was shorter (3 x 5 min) to minimise sample loss. Culture and control tow samples were run at the University of Bristol, and as such uncertainty is calculated from the intensity of ^{11}B signal in volts as per (Rae et al., 2011, see Equation 2.5). Uncertainty on core-top and sediment trap data is similarly calculated, but according to the external reproducibility of repeat analyses of Japanese Geological Survey *Porites* coral standard (JCP; $\delta^{11}B$= 24.31‰) at the University of Southampton, as described by Equation 2.2 (see also Fig. 2.9).

3.2.5 Downcore application

3.2.5.1 Site and species selection

G. ruber white (300-355 μm) were picked at roughly even intervals from sediments aged 0 to 30 kyr from core site GeoB1523-1, recovered from the Ceara Rise in the western equatorial Atlantic (3.83 °N, -41.62 °E) at a water depth of 3292 m. The age model for GeoB1523-1 was based on δ^{18}O(Gingele et al., 2000), while the published data from Foster (2008) at ODP 999A use high resolution ^{14}C-based ages (Schmidt et al., 2004).

3.2.5.2 Temperature and salinity estimates

Estimates of sea surface temperature (SST) and salinity (SSS) are required to calculate pH from δ^{11}B, as these parameters influence pK_B^*. It is important to note, however, that calculated pH is only weakly dependent on these environmental parameters (0.012 pH units per °C; 0.003 pH units per psu). For GeoB1523-1, SST was reconstructed using the Mg/Ca ratio of *G. ruber* measured on an aliquot of the same sample used for isotope measurement and the generic SST calibration (Mg/Ca = 0.38 * e$^{[SST*0.09]}$) of Anand et al. (2003). This is preferred over the species-specific calibration as it better fits our dataset of >20 core-top measurements (Henehan, unpublished data). As with Hönisch and Hemming (2005b), palaeo-salinity was estimated using the equation

$$SSS = SSS_{modern} + \left(\frac{\Delta_{sea-level}}{3800} * 34.8 \right) \tag{3.5}$$

where $\Delta_{sea\text{-}level}$ is an estimate of sea-level change in metres, 3800 m is the mean modern ocean depth, 34.8 is mean averaged modern ocean salinity, and SSS_{modern} is the modern salinity at the site of interest (from GLODAP, Key et al., 2004).

3.2.5.3 The second carbonate system parameter

Ocean pH is only one variable of the ocean carbonate system, and to determine $[CO_2]_{aq}$ and hence pCO_2 using Henry's Law, another variable is required (Zeebe and Wolf-Gladrow, 2001). The second variable chosen, TAlk, is calculated from estimated palaeo-salinity (following Palmer and Pearson, 2003, Hönisch et al., 2009), itself

derived from equation 3.5 above, and a TAlk vs. SSS relationship defined by modern ocean data from the equatorial Atlantic ($TAlk = SSS$*61.88 + 162.66, R^2= 0.88, p < 0.001; from GLODAP, Key et al. 2004).

It is important to note, however, that the generated pCO_2 estimate is determined largely by the reconstructed pH, and TAlk has little control. For example, given a pH of 8.2 (and SST of 25 °C and salinity 35 psu), a drastic increase in TAlk from 2400 to 2600 μmol/kg - equivalent to the range modelled by Hönisch et al. (2009) for the last 2 myr - only increases reconstructed pCO_2 by 24 ppm.

Given this reconstruction of TAlk and a δ^{11}B-derived pH, it is possible to reconstruct the entire carbonate system using CO2sys.m (van Heuven et al., 2011). Given the modern disequilibrium of surface waters above GeoB1523-1 (ΔpCO_2 of 15 to 25 ppm; Takahashi et al. 2009), and a correction factor for the pre-industrial ΔpCO_2 in this region of 1.33 (derived from Gloor et al. 2003), a correction for disequilibrium of -27 ppm is applied in order to calculate atmospheric CO_2 concentrations from calculated aqueous pCO_2. We apply an estimate of uncertainty on reconstructed pCO_2 of ± 29 ppm. This is a quadratic addition of the ranges of uncertainty in reconstructed pCO_2 that are produced via propagation of each input parameter uncertainty in turn, namely the calibration equation (uncertainty as in Table 3.1 and discussion below), δ^{11}B measurement (∼ ±0.2‰), and reconstructed salinity (± 1 psu), TAlk (± 100 μmol/kg) and temperature (± 1 °C).

3.3 Calibration: Results

3.3.1 Culture

Results of culturing work are given in Table 3.2. Mortality was greatest at our lowest pH, with most individuals surviving to gametogenesis in the two higher pH experiments (54 % and 64 % at 8.174 and 7.894 pH respectively), but only 40 % surviving to gametogenesis at pH 7.554 (compared to pH in the Gulf of Aqaba of ∼ 8.075). Note that while these values of survivorship are low compared to cultures of other species (e.g. *G. sacculifer*; Hemleben et al., 1987), these authors note *G. ruber* is notoriously difficult to culture, and as such the observed high mortality is not

unexpected. Samples grown at low pH (7.554) were typically surrounded by a much denser shroud of symbionts, with the test outline often entirely obscured by a dense mat of symbionts (Fig. 3.8b). Also, at this low pH individuals often lost most, or all, of their calcitic spines and fed less frequently (every 3-4 days) using unsupported pseudopods only. Larger tests across all pH treatments often showed a proliferation of many small and/or kummerform chambers growing in unusual configurations. While very unusual within the size range 300 - 355 μm, it is not uncommon to see such growth patterns in larger specimens of *G. ruber* ($>$ 400 μm) from Red Sea core-tops, indicating these forms are not simply a response to culture. At higher pH, chambers were usually visibly more heavily calcified (Fig. 3.8c), and growth rates were higher (see Table 3.2). At pH 7.554, tests were visibly thinner and often possessed abnormally wide apertures, with evidence in some cases that chambers may have been partially dissolved or reabsorbed during ontogeny (see Fig. 3.8d).

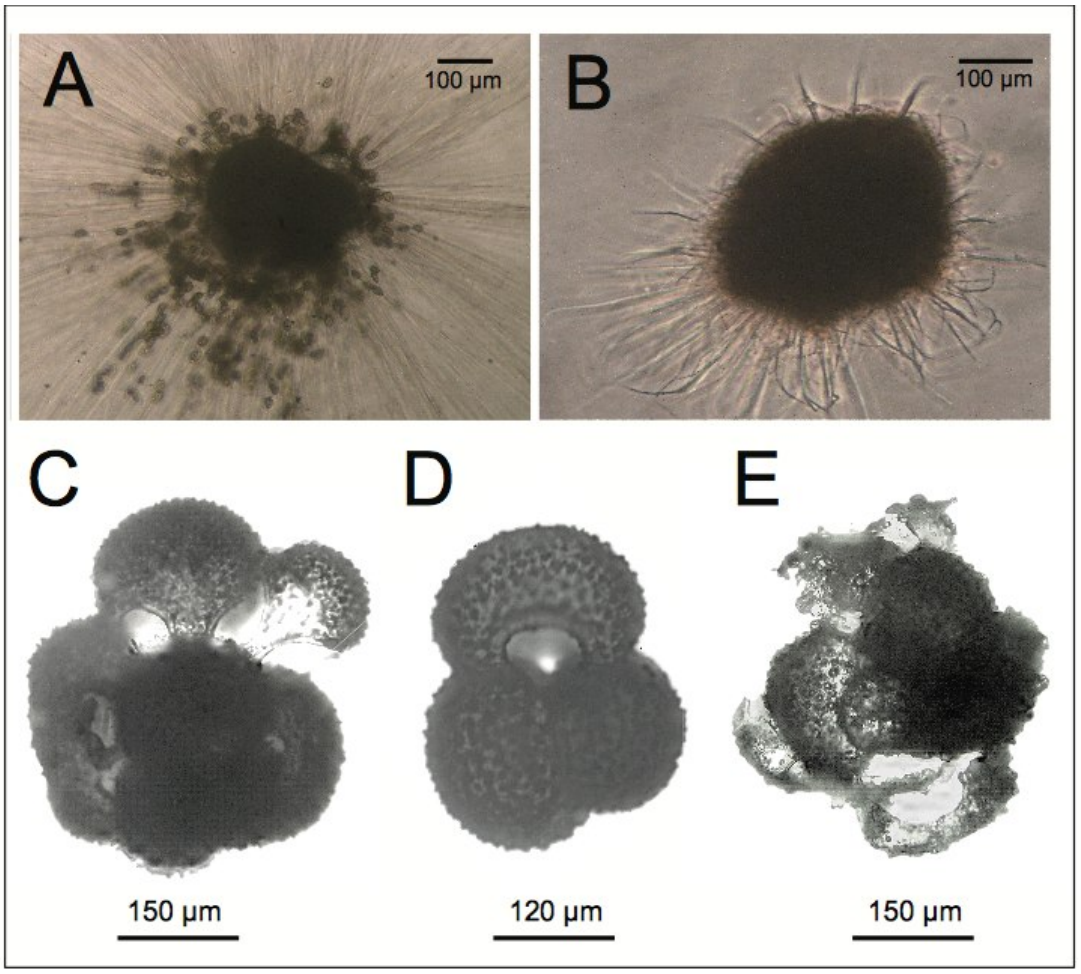

FIGURE 3.8: Examples of foraminifera grown in culture: (A) healthy *G. ruber*, with symbionts spread out within a well-developed halo of spines; (B) Foraminifera grown under low pH, with poorly developed spines and dense shroud of symbionts; (C) Test showing erratic pattern of chamber addition, as sometimes seen under high pH (D) Normal test of *G. ruber*, similar to those seen in sediment samples (Hemleben et al., 1989), as produced in all three pH experiments; (E) Test with large apertures and thinly calcified chambers that may be indicative of dissolution, as sometimes seen under low pH. Note that examples C and E are not representative of the whole experimental group, but are extremes picked for illustration purposes.

Experiment	*Start/ Tow date*	*pH (total)*	*2se*	*T (°C)*	*S*	*N (cultured)*[a]	*N (grown and GAM)*[b]	*Survivorship (%)*[c]	*Mean days in culture*	*Mean starting diameter (μm)*[d]	*Mean end-culture diameter (μm)*	*Mass for analysis (μg)*[e]	*Growth rate (μg/day/ind)*[f]
Culture 1	29/01/2010	8.174	0.007	26	37.2	106	57	54	6	200.0	365.4	590	1.39
Culture 2	10/02/2010	7.894	0.013	26	37.2	105	67	64	10	178.1	441.9	902	1.19
Culture 3	10/03/2010	7.554	0.013	26	37.2	120	48	40	9	197.7	339.6	303	0.35
Tow 1	27/01/2010	8.128	0.005	22	40.4								
Tow 2	08/02/2010	8.116	0.005	23	40.4								
Tow 3	07/03/2010	8.103	0.005	23	40.4								

TABLE 3.2: Results of culturing experiments at Eilat, Spring 2010.

[a] Indicates the number of foraminifera grown at each pH treatment.
[b] Indicates the number of foraminifera that grew in mass during culture and underwent gametogenesis.
[c] The percentage of individuals cultured that grew and survived to gametogenesis in culture.
[d] As determined by micrometer and inverted light microscope.
[e] The total mass of calcite analysed via MC-ICPMS, of which 75-92 % was grown in culture.
[f] Based on the pre-culture mass as estimated from the size-mass relationship in Fig. 3.6 and the end-culture mass as weighed at the University of Bristol, and represents the mean of the growth rates of each individual foraminifera per treatment.

3.3.2 MC-ICPMS Results

The results of boron isotope analyses of culture, core-top, tow, sediment trap and down-core samples (along with the relevant mass-balance corrections in culture experiments) are given in Table 3.3. These data are plotted in $\delta^{11}B_{CaCO_3}$-$\delta^{11}B_{B(OH)_4^-}$ space (Fig. 3.9) and York-fit linear regression of culture data provides a $\delta^{11}B_{CaCO_3}$-$\delta^{11}B_{B(OH)_4^-}$ relationship described by equation 3.6 below.

$$\delta^{11}B_{B(OH)_4^-} = \frac{\delta^{11}B_{measured} - 9.52 \pm 1.51}{0.60 \pm 0.08} \tag{3.6}$$

Uncertainty on this linear fit, accounting for error in analytical and in situ $\delta^{11}B$ values York (1968), is calculated using Isoplot (Ludwig, 2003) and is shown in Fig. 3.9 as a shaded band. The slope (i.e. pH sensitivity) of this culture calibration is within uncertainty of existing culture and inorganic calibrations (see Table 3.1), and is significantly lower than the theoretical pH sensitivity of borate ion in seawater (as indicated by a slope of < 1). For comparison, towed control specimens and coretop specimens are also plotted. There is no discernible effect of geographical location nor sample material type, suggesting that sedimentation or regional differences do not influence recorded $\delta^{11}B$. Although these data are permissively in agreement with the slope (i.e. $\delta^{11}B$-pH sensitivity) of the culture calibration (a York regression, albeit statistically non-significant, of the 300-355 μm size-fraction has a slope of 0.45 $\pm$ 0.25 at 95 % confidence), there is a tendency toward lower values of $\delta^{11}B$ than the culture calibration would predict in size fractions smaller than ~380 μm in diameter, and higher values in larger size fractions (see Fig. 6). As such, and because the spread in pH in the core-top samples alone is too small for a precise $\delta^{11}B$-pH calibration, we suggest modification of the culture calibration equation to reflect the size fractions used down-core. Thus for the commonly-used 300-355 μm size fraction a correction of -0.65 (see Fig. 3.11) should be applied to the intercept value 'c' of the culture $\delta^{11}B_{CaCO_3}$-$\delta^{11}B_{B(OH)_4^-}$ relationship (equation 3.6).

$$\delta^{11}B_{B(OH)_4^-} = \frac{\delta^{11}B_{measured} - 8.87 \pm 1.52}{0.60 \pm 0.08} \tag{3.7}$$

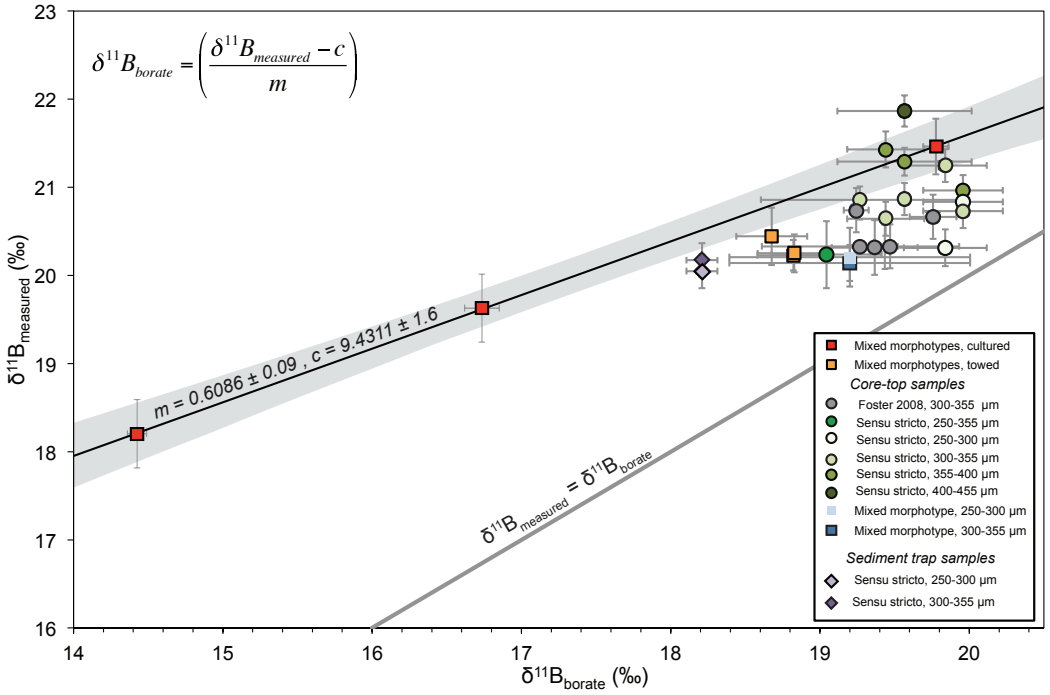

FIGURE 3.9: New culture calibration of *G. ruber*. York-fit regression plotted using Isoplot (Ludwig, 2003), with dotted lines and grey band defining 95 % confidence intervals (MSWD= 0.0031). X-error bars for core-top samples are 2 standard deviations of intra-annual variability in calculated monthly $\delta^{11}B_{B(OH)_4^-}$, while for cultures the error represents 2 standard errors of the mean pH of all culture flasks, and for sediment trap samples it reflects the range of $\delta^{11}B_{B(OH)_4^-}$ between Dec-Feb 2007. Y-error is the analytical reproducibility as calculated by Equation 2.2 (except in the cultured samples, where they reflect a 2 σ of 10,000 Monte Carlo simulations- see Section 3.2.1.3).

The uncertainty on the intercept in this relationship is a quadratic addition of two standard errors of the mean offset from culture for the 300-355 μm fraction of the core-top samples (-0.65 ‰) and the uncertainty in the original culture-calibration York regression intercept. Similarly, we suggest a correction of -0.83 ‰ for the 250-300 μm size fraction, and -0.16 ‰ for samples of 355-400 μm. For other size fractions the culture calibration may be corrected using the relationship between test size and offset from culture in Fig. 3.11 (offset = [0.005*average size] - 2.185, R^2= 0.33), although it must be noted that the narrow size range of *G. ruber* in core-tops and the large ratio of analytical uncertainty to signal mean that the relationship is not statistically robust, and as such wherever possible we would advocate using size fractions tested here. Indeed, given the limitations of our dataset, we encourage prior verification of the consistency of this size fraction effect at the sites of any future downcore reconstructions.

3.4 Downcore reconstruction

The results of boron-based pCO_2 reconstruction at Site GeoB1523-1 are plotted in Fig. 3.10, along with pCO_2 calculated from the *G. ruber* $\delta^{11}B$ data of Foster (2008) from ODP 999A (corrected using a pre-industrial ΔpCO_2 of 21 ppm calculated as discussed above). A cubic spline was plotted using Analyseries (Paillard et al., 1996), and the bounds of uncertainty ($\pm$17 ppm: individual uncertainty of 29 ppm / $\sqrt{2}$) on this spline are shaded. For comparison, the data are plotted with atmospheric pCO_2 derived from ice cores (Lüthi et al. 2008 and references within, Lourantou et al. 2010 with ages recalculated as per Lemieux-Dudon et al. 2010) and are also compared to pCO_2 reconstructed assuming a constant vital effect of 0.8 ‰ (as per Foster 2008). The mean deviation from atmospheric pCO_2 measurements from ice cores and those calculated from 999A and GeoB1523-1 using our new calibration is -5 ppm, with a 2σ of $\pm$ 29 ppm.

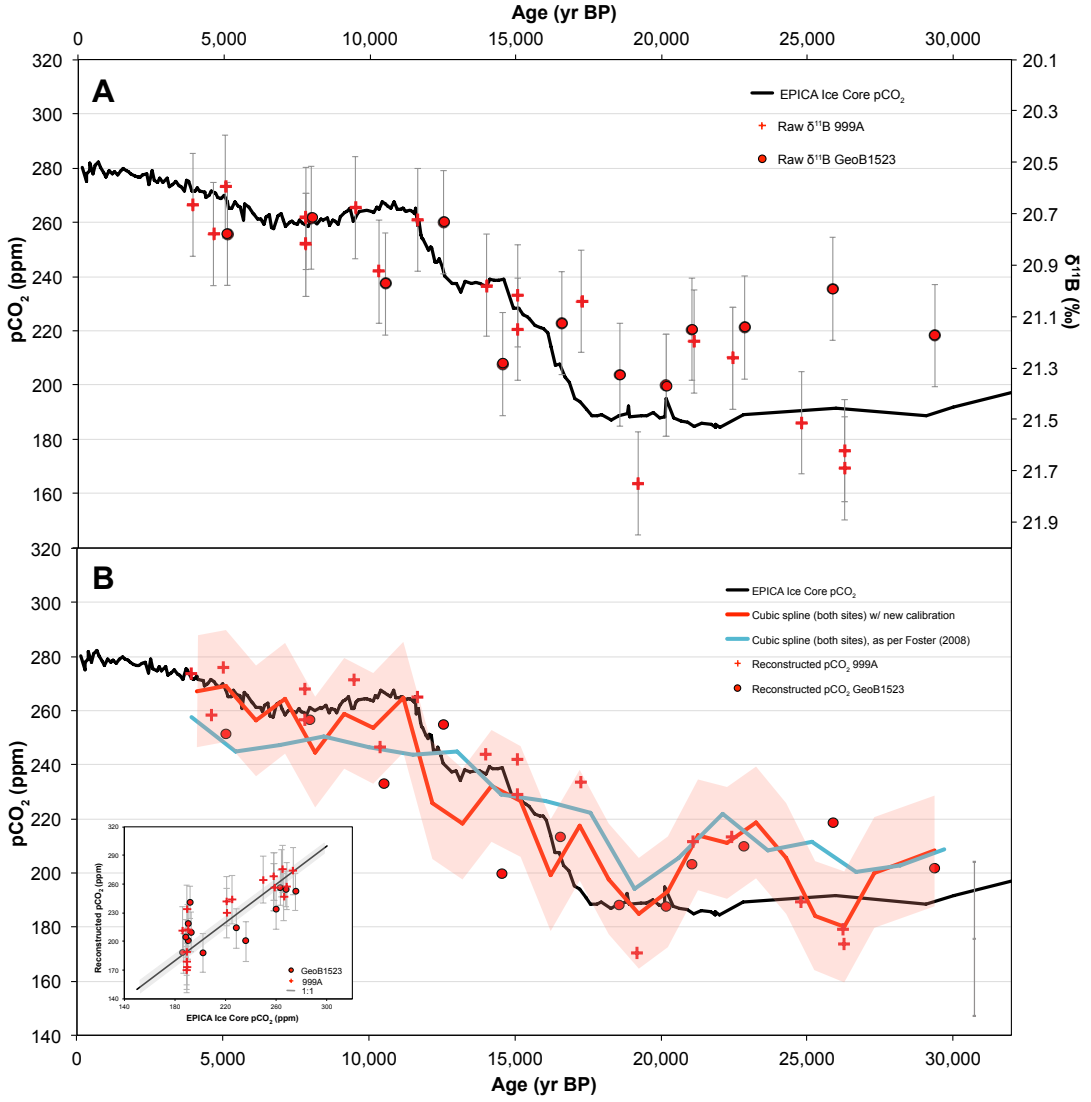

FIGURE 3.10: Down-core reconstructed pCO_2 from ODP site 999A (crosses, Foster (2008)) and GeoB1532-1 (circles, this study), compared to CO_2 concentrations from ice cores (black line). The thick red line is a cubic spline plotted on evenly subsampled values from both sites, as calculated using Analyseries (Paillard et al., 1996), with the shaded area reflecting uncertainty on the spline of ±17 ppm (i.e. 29 ppm individual uncertainty $/\sqrt{2}$). Note that these data are corrected for local ocean-atmosphere disequilibrium, which is taken as the modern mean annual values (from Takahashi et al. (2009)) corrected for the pre-industrial with reference to Gloor et al. (2003): +21 ppm (999A) and +27 ppm (GeoB1523-1). Also plotted (green line) is an equivalent spline through pCO_2 reconstructions based on a constant vital effect 'a' (see Equation 3.4) of +0.8 ‰ as applied by Foster 2008), illustrating the improved fit of the new calibration. Uncertainty on each individual measurement is plotted as a grey bar (bottom right): uncertainty on $\delta^{11}B$ measurements is derived from long term reproducibility at the University of Bristol, while uncertainty on pCO_2 reconstructions is a quadratic addition of the various uncertainties on reconstructed pH, alkalinity and temperature. Within frame is a cross-plot of ice-core derived vs. reconstructed pCO_2, with uncertainty on the 1:1 line (shown as grey shaded region) representing 6 ppm uncertainty on ice-core measurements (from Ahn et al., 2012).

Table 3.3: Measured δ^{11}B, and Calculated and Derived *in situ* conditions, for Culture and Open-Ocean Samples

Sample	Type	Core/ Trap/ Tow Depth (m)	Age (kyr BP)[a]	Latitude (°)	Longitude (°)	T (°C)[b]	S[c]	pK_B^*[d]	TAlk (μmol/kg)[e]	pCO_2 (μatm)[f]	pH (total)[g]	2σ[h]	$\delta^{11}B_{B(OH)_4^-}$[i]	2σ[j]	$\delta^{11}B_{CaCO_3}$[k]	2σ[l]	$P^B_{culture}$[m]	$\delta^{11}B_{corrected}$[n]	2σ[o]
Eilat, Culture 1	Culture	n/a	n/a	29.50	34.92	26	37.2	8.574	2392	277	8.184	0.007	19.76	0.09	21.35	0.23	0.907	21.46	0.26
Eilat, Culture 2	Culture	n/a	n/a	29.50	34.92	26	37.2	8.574	2189	576	7.904	0.013	16.66	0.12	19.66	0.21	0.945	19.63	0.25
Eilat, Culture 3	Culture	n/a	n/a	29.50	34.92	26	37.2	8.574	2027	1415	7.564	0.013	14.22	0.06	18.72	0.31	0.770	18.20	0.43
Eilat, Tow 1	Tow	< 10	n/a	29.50	34.92	22	40.40	8.605	2500	330	8.128	0.005	18.83	0.06	20.25	0.22			
Eilat, Tow 2	Tow	< 10	n/a	29.50	34.92	23	40.32	8.594	2508	342	8.116	0.005	18.82	0.06	20.23	0.33			
Eilat, Tow 3	Tow	< 10	n/a	29.50	34.92	23	40.44	8.593	2500	354	8.103	0.005	18.68	0.06	20.44	0.23			
CAR-22(z), *sensu stricto*, 250-300 μm	Sediment trap	150	n/a	10.50	64.66	24.17	36.70	8.598	2412	388	8.066	0.018	18.21	0.10	20.05	0.19			
CAR-22(z), *sensu stricto*, 300-355 μm	Sediment trap	150	n/a	10.50	64.66	24.17	36.70	8.598	2412	388	8.066	0.018	18.21	0.10	20.17	0.19			
Eilat, *sensu stricto*, 250-300 μm	Grab sample	300	Hol.	29.50	34.92	23.76	40.72	8.582	2510	275	8.188	0.008	19.84	0.28	20.31	0.21			

Sample	**Type**	**Depth (m)**	**Age (kyr BP)**[a]	**Latitude (°)**	**Longitude (°)**	**T (°C)**[b]	**S**[c]	pK_B^{*}[d]	**TAlk (μmol/kg)**[e]	**pCO_2 (μatm)**[f]	**pH (total)**[g]	2σ[h]	$\delta^{11}B_{B(OH)_4^-}$[i]	2σ[j]	$\delta^{11}B_{CaCO_3}$[k]	2σ[l]	$P^{B}_{culture}$[m]	$\delta^{11}B_{corrected}$[n]	2σ[o]
Eilat, *sensu stricto*, 300-355 μm	Grab sample	300	Hol.	29.50	34.92	23.76	40.72	8.582	2510	275	8.188	0.008	19.84	0.28	21.25	0.42			
MC 497, *sensu stricto*, 300-355 μm	Core-top	1000	Hol.	23.53	63.31	26.86	36.37	8.568	2376	295	8.152	0.020	19.57	0.45	20.87	0.18			
MC 497, *sensu stricto*, 355-400 μm	Core-top	1000	Hol.	23.53	63.31	26.86	36.37	8.568	2376	295	8.152	0.020	19.57	0.45	20.97	0.17			
MC 497, *sensu stricto*, 400-455 μm	Core-top	1000	Hol.	23.53	63.31	26.86	36.37	8.568	2376	295	8.152	0.020	19.57	0.45	21.87	0.18			
GGC-48, mixed morphotype, 250-300 μm	Core-top	3055	Hol.	0.00	161.00	29.41	34.61	8.549	2276	329	8.102	0.066	19.20	0.81	20.14	0.20			
GGC-48, mixed morphotype, 300-355 μm	Core-top	3055	Hol.	0.00	161.00	29.41	34.61	8.549	2276	329	8.102	0.066	19.20	0.81	20.21	0.33			
ODP 664, *sensu stricto*, 300-355 μm	Core-top	3817	2.9-3.6	0.10	-23.23	26.81	35.77	8.572	2341	306	8.137	0.073	19.26	0.71	20.82	0.19			

Sample	**Type**	**Depth (m)**	**Age (kyr BP)**[a]	**Latitude (°)**	**Longitude (°)**	**T (°C)**[b]	**S**[c]	pK_B^{*}[d]	**TAlk (μmol/kg)**[e]	**pCO_2 (μatm)**[f]	**pH (total)**[g]	2σ[h]	$\delta^{11}B_{B(OH)_4^-}$[i]	2σ[j]	$\delta^{11}B_{CaCO_3}$[k]	2σ[l]	$P^{B}{}_{culture}$[m]	$\delta^{11}B_{corrected}$[n]	2σ[o]
G4, *sensu stricto*, 300-355 μm	Core-top	831	0.9	-28.42	167.25	21.95	35.82	8.628	2361	260	8.202	0.030	19.44	0.29	20.64	0.19			
G4, *sensu stricto*, 355-400 μm	Core-top	831	0.9	-28.42	167.25	21.95	35.82	8.628	2361	260	8.202	0.030	19.44	0.29	21.43	0.20			
T329, *sensu stricto*, 250-300μm	Core-top	451	2.9	-12.96	173.57	28.63	34.79	8.556	2288	270	8.171	0.024	19.96	0.27	20.83	0.18			
T329, *sensu stricto*, 300-355 μm	Core-top	451	2.9	-12.96	173.57	28.63	34.79	8.556	2288	270	8.171	0.024	19.96	0.27	20.73	0.19			
T329, *sensu stricto*, 355-400 μm	Core-top	451	2.9	-12.96	173.57	28.63	34.79	8.556	2288	270	8.171	0.024	19.96	0.27	21.29	0.16			
OC476-SR223, *sensu stricto*, 250-355 μm	Core-top	2860	0.7	-33.53	166.53	19.33	35.70	8.660	2353	262	8.201	0.013	19.04	0.37	20.24	0.38			
999A	Down-core	2827 +0.05	3.9	12.75	-78.73	28.23	35.5	8.557	2330	282	8.15	0.03			20.67	0.25		19.63	0.35

Sample	Type	Depth (m)	Age (kyr BP)[a]	Latitude (°)	Longitude (°)	T (°C)[b]	S[c]	pK_B^{*}[d]	TAlk (μmol/kg)[e]	pCO_2 (μatm)[f]	pH (total)[g]	2σ[h]	$\delta^{11}B_{B(OH)_4^-}$[i]	2σ[j]	$\delta^{11}B_{CaCO_3}$[k]	2σ[l]	$P^{B}_{culture}$[m]	$\delta^{11}B_{corrected}$[n]	2σ[o]
999A	Down-core	2827 +0.11	4.6	12.75	-78.73	28.44	35	8.557	2301	265	8.16	0.03			20.78	0.25		19.82	0.37
999A	Down-core	2827 +0.15	5	12.75	-78.73	27.77	35	8.561	2301	283	8.14	0.03			20.59	0.25		19.51	0.34
999A	Down-core	2827 +0.31	7.8	12.75	-78.73	28.19	35.55	8.557	2333	264	8.17	0.03			20.82	0.25		19.89	0.38
999A	Down-core	2827 +0.31	7.8 (2)	12.75	-78.73	28.19	35.55	8.557	2333	276	8.15	0.03			20.72	0.25		19.71	0.36
999A	Down-core	2827 +0.39	9.5	12.75	-78.73	27.59	36.1	8.562	2366	279	8.15	0.03			20.68	0.25		19.65	0.36
999A	Down-core	2827 +0.43	10.3	12.75	-78.73	27.50	36.4	8.561	2384	254	8.18	0.03			20.93	0.25		20.06	0.40
999A	Down-core	2827 +0.48	11.7	12.75	-78.73	27.04	36.51	8.567	2390	272	8.16	0.03			20.72	0.25		19.72	0.36
999A	Down-core	2827 +0.57	14	12.75	-78.73	27.38	36.82	8.560	2408	251	8.19	0.03			20.98	0.25		20.15	0.41
999A	Down-core	2827 +0.61	15.1	12.75	-78.73	27.41	37.1	8.559	2425	249	8.19	0.03			21.02	0.25		20.22	0.42

Sample	**Type**	**Depth (m)**	**Age (kyr BP)**[a]	**Latitude (°)**	**Longitude (°)**	**T (°C)**[b]	**S**[c]	pK_B^{*}[d]	**TAlk (μmol/kg)**[e]	**pCO_2 (μatm)**[f]	**pH (total)**[g]	2σ[h]	$\delta^{11}B_{B(OH)_4^-}$[i]	2σ[j]	$\delta^{11}B_{CaCO_3}$[k]	2σ[l]	$P^{B}_{culture}$[m]	$\delta^{11}B_{corrected}$[n]	2σ[o]
999A	Down-core	2827 +0.61	15.1 (2)	12.75	-78.73	27.41	37.1	8.559	2425	237	8.21	0.03			21.15	0.25		20.43	0.44
999A	Down-core	2827 +0.71	17.3	12.75	-78.73	26.69	37.11	8.569	2426	240	8.21	0.03			21.04	0.25		20.25	0.42
999A	Down-core	2827 +0.82	19.2	12.75	-78.73	26.17	37	8.575	2419	176	8.30	0.04			21.75	0.25		21.43	0.57
999A	Down-core	2827 +0.93	21.1	12.75	-78.73	26.01	36.95	8.579	2416	219	8.24	0.03			21.20	0.25		20.51	0.45
999A	Down-core	2827 +1.02	22.5	12.75	-78.73	26.69	37.18	8.569	2430	220	8.23	0.03			21.26	0.25		20.62	0.47
999A	Down-core	2827 +1.13	24.8	12.75	-78.73	26.58	37.05	8.573	2422	195	8.27	0.04			21.51	0.25		21.04	0.52
999A	Down-core	2827 +1.20	26.3	12.75	-78.73	26.34	36.84	8.575	2410	185	8.28	0.04			21.62	0.25		21.22	0.54
999A	Down-core	2827 +1.20	26.3 (2)	12.75	-78.73	26.34	36.84	8.575	2410	180	8.29	0.04			21.69	0.25		21.33	0.56
GeoB1523-1	Down-core	3292 +0.05	3.1	3.83	-41.62	27.76	35.54	8.563	2333	259	8.17	0.03			20.78	0.24		19.81	0.38

Sample	**Type**	**Depth (m)**	**Age (kyr BP)**[a]	**Latitude (°)**	**Longitude (°)**	**T (°C)**[b]	**S**[c]	pK_B^{*}[d]	**TAlk (μmol/kg)**[e]	**pCO_2 (μatm)**[f]	**pH (total)**[g]	2σ[h]	$\delta^{11}B_{B(OH)_4^-}$[i]	2σ[j]	$\delta^{11}B_{CaCO_3}$[k]	2σ[l]	$P^{B}_{culture}$[m]	$\delta^{11}B_{corrected}$[n]	2σ[o]
GeoB1523-1	Down-core	3292 +0.10	6	3.83	-41.62	27.40	35.64	8.566	2338	264	8.16	0.02			20.72	0.23		19.71	0.36
GeoB1523-1	Down-core	3292 +0.15	8.5	3.83	-41.62	27.62	35.86	8.562	2352	240	8.19	0.03			20.97	0.24		20.14	0.42
GeoB1523-1	Down-core	3292 +0.20	10.5	3.83	-41.62	26.94	36.10	8.569	2366	262	8.17	0.03			20.73	0.24		19.74	0.37
GeoB1523-1	Down-core	3292 +0.25	12.6	3.83	-41.62	26.52	36.33	8.572	2379	206	8.24	0.03			21.29	0.23		20.66	0.48
GeoB1523-1	Down-core	3292 +0.30	14.6	3.83	-41.62	26.22	36.52	8.575	2391	220	8.22	0.03			21.13	0.24		20.39	0.45
GeoB1523-1	Down-core	3292 +0.35	16.6	3.83	-41.62	24.83	36.64	8.590	2398	194	8.26	0.04			21.33	0.26		20.73	0.50
GeoB1523-1	Down-core	3292 +0.40	18.2	3.83	-41.62	25.26	36.69	8.585	2401	194	8.26	0.04			21.37	0.26		20.79	0.51
GeoB1523-1	Down-core	3292 +0.45	19.1	3.83	-41.62	24.85	36.69	8.590	2401	209	8.24	0.03			21.15	0.25		20.43	0.46
GeoB1523-1	Down-core	3292 +0.55	20.9	3.83	-41.62	25.76	36.65	8.580	2399	217	8.23	0.03			21.14	0.26		20.42	0.46

Sample	Type	Depth (m)	Age (kyr BP)[a]	Latitude (°)	Longitude (°)	T (°C)[b]	S[c]	pK_B^*[d]	TAlk (μmol/kg)[e]	pCO_2 (μatm)[f]	pH (total)[g]	2σ[h]	$\delta^{11}B_{B(OH)_4^-}$[i]	2σ[j]	$\delta^{11}B_{CaCO_3}$[k]	2σ[l]	$P^B{}_{culture}$[m]	$\delta^{11}B_{corrected}$[n]	2σ[o]
GeoB1523-1	Down-core	3292 +0.65	23.9	3.83	-41.62	25.22	36.51	8.587	2390	225	8.22	0.03			20.99	0.25		20.17	0.43
GeoB1523-1	Down-core	3292 +0.75	27.4	3.83	-41.62	25.31	36.34	8.587	2380	208	8.24	0.03			21.17	0.25		20.47	0.47
GeoB1523-1	Down-core	3292 +0.85	32.9	3.83	-41.62	24.88	36.28	8.592	2376	253	8.18	0.02			20.67	0.25		19.64	0.37

TABLE 3.3: The results of boron isotope analyses on culture, core-top, sediment trap, tow and down-core (GeoB1523-1) samples. All carbonate system and pK_B^* calculations use CO2sys.m (van Heuven et al., 2011) and the constants of Dickson (1990), Lueker et al. (2000) and Lee et al. (2010). Further details may be found in the Supplementary Tables B.1 and B.2. Note that we see no influence of boron from contaminant clays, with Al/Ca ratios all below 100 μmol/mol.

[a] Core-top sediments were where possible determined as undisturbed Holocene by either the presence of stained benthic foraminifera (MC 497), existing age-model (ODP 664, Raymo et al. 1997; GGC48, E. Tappa pers. comm.) or carbon dating (G4, T329, OC476-SR223; Bostock, pers. comm.). Down-core ages derived from existing age models by Schmidt et al. (2004; 999A) and Gingele et al. (2000; GeoB1523-1).

[b] For tow and culture samples, temperature was gauged by direct measurement. For sediment trap samples, temperature is interpolated from data from IMAR (see Supplementary Table B.1), while core-top temperature is mean annual SST interpolated from the Takahashi et al. (2009) database. Downcore temperatures for 999A are interpolated from Schmidt et al. (2004), and at GeoB1523-1 are derived from Mg/Ca data (see Supplementary Information) and the general calibration of Anand et al. (2003).

[c] For tow and culture samples, salinity was gauged by direct measurement. For sediment trap samples, salinity interpolated from data from IMAR (see Supplementary Table B.1). Core-top salinity is mean annual salinity interpolated from the Takahashi et al. (2009) database. Downcore salinity for 999A and GeoB1523-1 are derived from sea level estimates.

[d] Calculated from temperature, salinity and depth.

[e] For tow and culture samples, alkalinity was gauged by direct measurement. For sediment trap samples, alkalinity interpolated from data from IMAR (see Supplementary Table B.1). Core-top alkalinity is derived from regional salinity-alkalinity relationships (from GLODAP/CARINA data <20m deep) and mean annual salinity interpolated from the Takahashi et al. (2009) database. Downcore alkalinity for 999A is from Foster (2008) and for GeoB1523-1 is derived from reconstructed salinity.

[f] For tows, culture and downcore samples, pCO_2 reconstructed from TAlk and either pH reconstructed using the new calibration (Equation 3.7, downcore) or Total DIC as measured directly (tows, cultures). For sediment trap samples, pCO_2 is interpolated from data from IMAR (see Supplementary Table B.1). Core-top ΔpCO_2 is reconstructed by application of the mean annual ΔpCO_2 at each site (interpolated from nearby sites from Takahashi et al. 2009 and corrected for post-industrial changes in ΔpCO_2 according to model results from Gloor et al. 2003) to pre-industrial atmospheric pCO_2.

[g] For tows and sediment traps, pH is calculated from measurements of alkalinity and either DIC (tows) or pCO_2 (sediment traps). For core-tops the pH is a mean annual pH interpolated from Takahashi et al. (2009) and calculated from estimated alkalinity and pCO_2. For cultured samples, pH is calculated as the mean of the mean pH observed by each individual foraminifera during culture (as measured using a potentiometric electrode but cross-calibrated to DIC/TAlk-derived pH, see Fig. 3.4). For down-core samples, pH is derived from $\delta^{11}B$ measurements transformed using the new calibration for *G. ruber*(Eq. 3.7).

[h] Uncertainty on culture pH measurements is 2 standard errors of the mean of the average pHs experienced by constituent forams, while uncertainty on the pH estimates for tows is based on analytical reproducibility at the UK-OARP Carbonate Chemistry Facility. Uncertainty on core-top pH is the interpolated intra-annual variability in pH at that site (see Supplementary Table B.2), while in down-core samples it signifies the pH uncertainty resultant from the uncertainty on corrected $\delta^{11}B_{CaCO_3}$. At Cariaco basin (*), pH is interpolated between cruise measurements taken a month either side of sediment trap deployment, and uncertainty reflects the range in pH between these two months (see Supplementary Table B.1).

[i] As calculated from estimated pH and pK_B^* using the general boron isotope-pH equation (1.10).

[j] Reflecting the uncertainty in pH and pK_B^*.

[k] Includes published data from 999A from Foster (2008) that are re-interpreted here.

[l] Uncertainty on δ^{11}Bmeasurements is derived from Eq. 2.5 (Cultures, Tows, GeoB1523-1), and Eq. 2.2 (core-tops, sediment traps), except for published data from 999A (Foster, 2008) where the published uncertainty is quoted.

[m] Proportion of boron incorporated during culture, see Eq. 3.3.

[n] $\delta^{11}B_{\text{corrected}}$ for culture samples is the $\delta^{11}B$ of carbonate grown under culture conditions, having been mass-balance corrected for test mass grown out of culture (via Eq. 3.3). For downcore samples, it refers to transformations of raw $\delta^{11}B$ data using the new *G. ruber* calibration (Eq. 3.7), and is analogous to $\delta^{11}B_{B(OH)_4^-}$.

[o] Uncertainty on $\delta^{11}B_{\text{corrected}}$ is 2σ of 10,000 Monte Carlo simulations of uncertainty in towed 'control' and culture measurements (for culture samples, see section 3.2.1.3), or quadratic addition of measurement reproducibility and calibration uncertainty (down-core samples).

3.5 Discussion

3.5.1 pH sensitivity of $\delta^{11}B_{G.ruber}$ lower than $\delta^{11}B_{B(OH)_4^-}$

pH is clearly a strong control on δ^{11}B in *G. ruber* (Fig. 3.9), but these new data do not fall on the predicted relationship of seawater borate ion, as epifaunal benthic foraminifera do (Rae et al., 2011). Specifically, our data lie above the $\delta^{11}B_{B(OH)_4^-}$-pH curve, and show a pH sensitivity ~40 % lower than that predicted for $\delta^{11}B_{B(OH)_4^-}$ in seawater, confirming previous observations in other symbiont-bearing planktonic species (Sanyal et al., 1996, 2001, Hönisch et al., 2003). The causes of this deviation from the aqueous geochemical basis of the proxy are potentially manifold. Previous foraminiferal studies have ascribed a lower-than-predicted pH sensitivity in δ^{11}B to: (i) incorporation of boric acid (Klochko et al., 2009); (ii) elevated (compared to ambient) pH inside the seawater vacuoles (Rollion-Bard and Erez, 2010); (iii) modification of the micro-environment around the foraminifera by respiration, calcification and photosynthesis (Hönisch et al., 2003, Zeebe et al., 2003); and (iv) analytical issues relating to the NTIMS approach used by Sanyal et al. (1996, 2001) and Hönisch et al. (2003). These new results for *G. ruber* using MC-ICPMS, where accuracy has been demonstrated (Ni et al., 2010), confirms that analytical issues do not play a role in generating the shallower pH sensitivity in planktic foraminifera. Offsets in absolute δ^{11}B between NTIMS and MC-ICPMS of the order of 1-2 ‰ are observed for a variety of foraminiferal species (e.g., *Cibicidoides weullerstorfi*; see Rae et al. 2011) but, as also supported by an ongoing interlaboratory comparison study (Foster et al., 2013), relative changes do appear to be largely reproducible between NTIMS and MC-ICPMS (see Fig. 8, Rae et al., 2011).

There currently appears to be little consensus regarding the relative importance of the other three phenomena proposed above to explain a shallower than predicted relationship between δ^{11}B and pH. A key observation requiring explanation is that all planktonic foraminiferal calibrations to date show a pH sensitivity (slope 'm') within uncertainty of that seen in inorganic precipitates ($\delta^{11}B_{CaCO_3}$= 0.75 (± 0.15) * the pH sensitivity of $\delta^{11}B_{B(OH)_4^-}$; Sanyal et al. 2000). Similarly reduced pH sensitivity is evident in the symbiont-bearing *Amphistegina lobifera* (Rollion-Bard and Erez, 2010) and in numerous species of coral (Hönisch et al., 2004, Reynaud et al., 2004, Krief

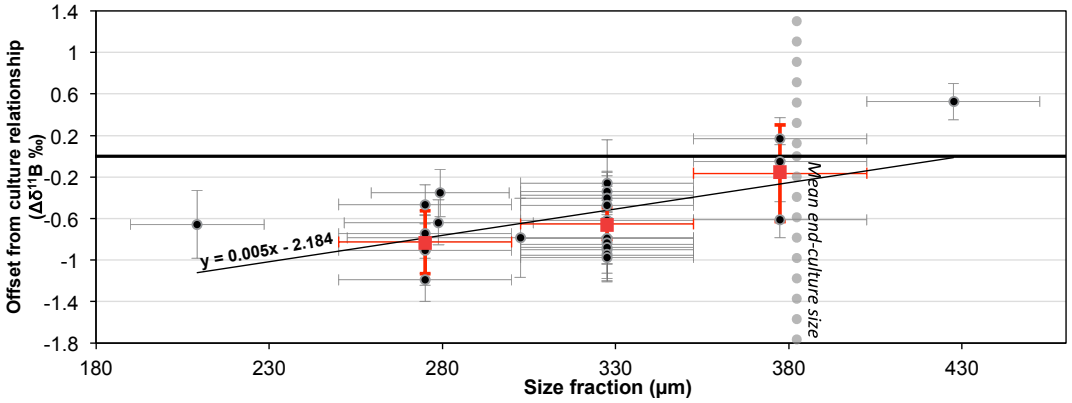

FIGURE 3.11: Offset of core-top, tow and sediment trap samples from our culture calibration, as a function of size fraction. Error bars in size-fraction refer to the sieve fractions, or where available, two standard errors of the mean measured test diameter. Red markers indicate the mean value for the three most commonly used size fractions, with y-errors corresponding to two standard errors of the mean offset. Dotted vertical line denotes the mean end-culture diameter.

et al., 2010, Trotter et al., 2011, Anagnostou et al., 2012). That the sensitivities observed in a broad range of biogenic carbonates are similar to those seen in inorganic precipitates would implicate an inorganic process e.g., a rate dependency in $CaCO_3$ precipitation. A key stumbling block, however, are the epifaunal benthic data of Rae et al. (2011, Fig. 2) and Yu et al. (2010), that lie within uncertainty of the $\delta^{11}B_{B(OH)_4^-}$, seemingly unaffected by any such inorganic process. This implies that the agreement between the $\delta^{11}B$ of aqueous borate and benthic foraminiferal carbonate is either purely fortuitous, the result of a several competing processes operating in tandem to nearly precisely cancel each other out, or that this inorganic process either does not exist or is not universal and benthic foraminifera are the exception to the rule. It is also worth noting that all the other foraminifera so far calibrated are symbiont bearing, and laboratory observations (Jørgensen et al., 1985, Rink et al., 1998, Köhler-Rink and Kühl, 2005) strongly implicate the alteration of the foraminiferal microenvironment by symbionts and life processes. As discussed below, the magnitude of the vital effect in *G. ruber* (and in *G. sacculifer*; Hönisch and Hemming 2004) is dependent on foraminiferal size, therefore life processes may have a role to play in this behaviour. However, a full resolution of this issue is beyond the scope of this current contribution and will require additional studies of both symbiont-bearing and non-symbiont bearing foraminifera, and of inorganic carbonates precipitated in equilibrium at rates comparable to those seen in biogenic carbonates.

3.5.2 δ^{11}B offset between culture and non-culture: a size fraction effect on δ^{11}B in *G. ruber*

While towed, sediment trap and core-top specimens are permissively in agreement with the pH sensitivity of $\delta^{11}B_{CaCO_3}$ observed in our cultures, it is apparent that there is a discrepancy in δ^{11}B values predicted by the culture calibration and some measurements of non-culture specimens of *G. ruber* (Fig. 3.9). The degree of offset from the calibration does not correlate with *in situ* temperature (R^2= 0.04) or the saturation state of bottom water at these coretop sites (R^2= 0.05), suggesting there is no discernible temperature or dissolution effect. Furthermore, there is little evidence for any discrepancy between morphotypes (*G. ruber* sensu stricto or sensu lato) that might effect our mixed morphotype culture (see Fig. 3.2), despite their phylogenetic disparity (Aurahs et al., 2011). Offset from our culture calibration does, however, show some correlation with test size fraction (see Fig. 3.11). Previous evidence (Ni et al., 2007) for a size-fraction effect in *G. ruber* is ambiguous because of large margins of uncertainty in δ^{11}B measurements ($\sim \pm$ 0.8 ‰ vs. $\sim \pm$ 0.25 ‰ here). Increasing δ^{11}B with size is, however, resolvable in the closely-related species *G. sacculifer* (Hönisch and Hemming, 2004, Ni et al., 2007). Moreover, size-fraction effects in *G. ruber* have been noted in δ^{13} C and δ^{18}O (e.g., Kroon and Darling, 1995), B/Ca (Ni et al., 2007), and in Mg/Ca and Sr/Ca (e.g. Friedrich et al., 2012).

The cause of any size fraction effect on δ^{11}B is not clear. Preferential dissolution (Hönisch and Hemming, 2004, Ni et al., 2007) seems unlikely, since a) similar offsets from aqueous $\delta^{11}B_{B(OH)_4^-}$ are reproduced even in towed samples (see Fig. 3.9), b) there is no relationship between degree of offset and deepwater carbonate saturation at the site of deposition, and c) the lack of any geochemically distinct gametogenic calcite in *G. ruber* (Caron et al., 1990) should make the issue of preferential dissolution less pertinent in this species (see also Seki et al., 2010, Fig. 7a). Instead we support the suggestion by Hönisch and Hemming (2004) that a size-fraction effect in δ^{11}B is due to intensified micro-environmental alteration by symbionts in larger specimens. That said, we query the assertion by Hönisch and Hemming (2004) that increasing δ^{13}C and δ^{11}B with size must be due to larger specimens living at shallower depths (thus experiencing a stronger light intensity and stronger microenvironment alteration). While this seems consistent with Caron et al. (1982), we urge some caution in this interpretation

without direct ecological evidence for a bias towards larger test size in *G. ruber* from shallower waters: Bijma et al. (1990) report living individuals measuring anywhere between 125 μm and 708 μm within the uppermost 5 m of the Red Sea at all stages in *G. ruber*'s semilunar life-cycle. Besides, foraminifera towed from $<$ 10 m record lower, not higher, δ^{11}B than foraminifera cultured at light levels equivalent to $\sim$20 m water depth (though we concede these individuals might conceivably have grown to larger size - and heavier δ^{11}B - had they completed their life cycle at this depth).

It is instead likely that the magnitude of these microenvironment effects might change with test size without any need to invoke changes in habitat depth. Photosynthesis by symbionts in the microenvironment surrounding planktic foraminifera raises pH, while respiration and calcification lower pH (Jørgensen et al., 1985, Köhler-Rink and Kühl, 2005, Rink et al., 1998). Crucially, rates of respiration and photosynthesis in culture specimens have been seen to change with test size (Lombard et al., 2009, Rink et al., 1998), with photosynthesis increasing relative to respiration in larger specimens of *G. ruber* (Lombard et al., 2009). In addition, as foraminifera grow, the diffusive boundary layer around their tests is expanded, lengthening timescales for diffusion of carbon through the microenvironment. As such, equilibration of the microenvironment with the ambient seawater slows, and as such any microenvironment pH alteration would be accentuated (see model of Wolf-Gladrow et al., 1999). While more *in situ* microelectrode measurements are required to fully test these hypotheses, they could explain the observed patterns in recorded δ^{11}B we see here. It is also possible that increased test size might be resultant from, not a driver of, increased symbiont activity, with elevated δ^{11}B an inevitable result. Planktonic foraminifera acquire algal symbionts early in their life cycle (Hemleben et al., 1989). Should the activity of symbionts in the foraminiferal microenvironment impart an advantage to the calcification of the host by raising external pH and Ω_{CaCO3} (reflected in δ^{11}B) and thus reducing energetic expenditure needed to raise internal vacuole pH (as suggested by Bentov et al., 2009), foraminifera that happen to succeed in acquiring symbionts earlier in their ontogeny might grow more rapidly, and thus attain larger size prior to gametogenesis. Clearly additional modelling and field observation are required to investigate these hypotheses further.

3.5.3 Applying the *G. ruber* δ^{11}B-pH calibration to downcore data

Reconstructed pCO_2 from Sites GeoB1523-1 and ODP 999A using this new calibration for *G. ruber* tracks reconstructions from ice cores very closely, with average deviation (- 5 ppm) and average absolute deviation (25 ppm) from ice core pCO_2 within propagated uncertainty of ± 29 ppm. Although broadly similar results can be generated with the approach of Foster (2008), the new calibration more accurately reproduces the 90 ppm magnitude of deglacial pCO_2 increase seen in ice core reconstructions (ΔpCO_2= ∼80 ppm vs. ∼50 ppm using Foster 2008. While these sorts of improvements in fit are within uncertainty over these short timescales, the importance of the lower pH sensitivity documented here is magnified in deeper time when pCO_2 is likely to have been higher.

3.6 Conclusions

This contribution represents a further demonstration of the dominance of pH as a control on foraminiferal δ^{11}B. It is the first morphospecies-specific foraminiferal culture calibration analysed using MC-ICPMS, and the first to incorporate globally-distributed cultured, towed, sediment trap and core-top foraminifera. The new method we advocate for presenting culture calibrations allows for greater ease of comparison and uncertainty calculation and propagation. We show that recorded δ^{11}B in *G. ruber* deviates markedly from the simple inorganic basis of the proxy, corroborating previous foraminiferal culture studies analysed using N-TIMS (Sanyal et al., 1996, 2001), and lending some support to the results of published down-core reconstructions based on pH-sensitivities of $\delta^{11}B_{CaCO_3}$ that are lower than $\delta^{11}B_{B(OH)_4^-}$ (e.g., Palmer and Pearson, 2003, Hönisch and Hemming, 2005b, Palmer et al., 2010). We show that, regardless of their phylogenetic separation (Aurahs et al., 2011), sensu stricto and sensu lato morphotypes record similar δ^{11}B. We also document for the first time a size-fraction effect in $\delta^{11}B_{G.\ ruber}$ which must be taken into account in future down-core application. However, as we illustrate for the last 30 kyr BP (Fig. 3.10), by analysing tightly constrained size fractions and applying a species-specific culture calibration, accurate and precise estimates of past levels of atmospheric CO_2 can be reconstructed.

Chapter 4

Exploring vital effects in planktic foraminiferal $\delta^{11}B$

Abstract

The boron isotope proxy can generate be used to accurately and precisely reconstruct atmospheric CO_2 concentrations, providing species- and size-fraction-specific calibrations are used (as shown in Chapter 3). However, further analysis is needed to allow for full exploration of the nature of foraminiferal 'vital effects' in $\delta^{11}B$. Here the nature of vital effects in planktic foraminifera is explored through comparison of symbiont-barren species (including *Globigerina bulloides*) and a deep-dwelling symbiont-bearing species (*Orbulina universa*) to existing calibrations. While affirming the importance of microenvironment alteration in determining both absolute values and the pH sensitivity of $\delta^{11}B_{CaCO_3}$, this chapter highlights some previously unreported complications regarding the microenvironment of the deep-dwelling symbiont-bearing species *O. universa*. This chapter incorporates two new MC-ICPMS-based calibrations, including the first calibration of the symbiont-barren species *Globigerina bulloides*, thereby broadening the range of environments in which the boron isotope-pH proxy can be applied.

4.1 Introduction: Outstanding issues

4.1.1 Understanding pH-sensitivity in foraminifera

In Chapter 3 (Henehan et al., 2013) the pH-sensitivity of δ^{11}B in *Globigerinoides ruber*, a valuable species for palaeo-CO_2 reconstruction because of its reliably mixed-layer depth habit (Hemleben et al., 1989), was calibrated. While this calibration extends the applicability of the boron isotope proxy and corroborates the lowered pH sensitivities seen in previous calibration studies, it does not in itself dramatically improve our understanding of vital effects in the δ^{11}B of planktic foraminifera. As with other published planktic foraminiferal calibrations (Sanyal et al., 1996, 2001), *G. ruber* demonstrates a pH-sensitivity in δ^{11}B that is lower than that of ambient borate ion, in contrast to data from epifaunal benthic foraminifera, that appear to incorporate δ^{11}B signals from $B(OH)_4^-$ without fractionation (Rae et al., 2011).

Clearly, then the issue of pH sensitivity of δ^{11}B recorded in foraminiferal carbonates remains contentious (see Section 1.4.3 for further discussion). Existing models of photosynthesis and respiration in the microenvironment of foraminifera (Zeebe et al., 1999a, 2003) suggest that any micro-environment-derived vital effect on recorded δ^{11}B should be constant across a range of pH (see Section 1.4.2.3). In other words, recorded $\delta^{11}B_{CaCO_3}$ should be elevated above $\delta^{11}B_{B(OH)_4^-}$ in symbiont-bearing foraminifera and lowered below ambient $\delta^{11}B_{B(OH)_4^-}$ in symbiont-barren foraminifera (see Section 1.4.2.3), but the pH sensitivity of recorded δ^{11}B should be dictated by the inorganic aqueous geochemical basis of the proxy (i.e. the value of $^{11-10}K_B$). However, no published calibration of planktic foraminiferal (Sanyal et al., 1996, 2001, Henehan et al., 2013), coral (e.g. Anagnostou et al., 2012, Trotter et al., 2011, McCulloch et al., 2012, Krief et al., 2010) or inorganically precipitated $CaCO_3$ (Sanyal et al., 2000, He et al., 2013) has conclusively described a pH sensitivity in agreement with empirically observed value of $^{11-10}K_B$ of Klochko et al. (2006). Only in epifaunal benthic foraminifera is the δ^{11}B of ambient aqueous $B(OH)_4^-$, and its expected pH sensitivity, recorded in $CaCO_3$ without fractionation (Rae et al., 2011). Perhaps unsurprisingly, then, the similarity of inorganic and planktic foraminiferal calibrations has led some authors to advocate some underlying, universal inorganic cause for the

weaker-than-expected pH sensitivity observed (e.g. Hönisch et al., 2007, Hemming and Hönisch, 2007).

As discussed briefly in Henehan et al. (2013) and Rae et al. (2011), were there some inorganic basis for the similarity in slope of planktic foraminiferal and inorganic calibrations (e.g. a fractionation of δ^{11}B upon incorporation, or an inappropriate value of $^{11-10}K_B$), it would require the > 40 measurements of Rae et al. (2011) to fortuitously record the $\delta^{11}B_{B(OH)_4^-}$ (perhaps through some compensatory 'vital effect'). But equally, advocating a biogenic cause for the weaker-than-expected pH-sensitivity in existing calibrations would necessitate vital effects (e.g. internal pH up-regulation in corals or microenvironment alteration in foraminifera), that are not constant across variations in ambient pH. Although this is seen in corals (Venn et al., 2013), it would be contrary to the modelled results of Zeebe et al. (2003). In addition it would also necessitate some additional factor influencing the published inorganic precipitate data of Sanyal et al. (2000), such as unrepresentative precipitation rates, inconsistent matrix effects on NTIMS measurements, a poorly-defined pK_B^* and/or carbonate system. While new MC-ICPMS-derived measurements of inorganic precipitates (Klein-Gebbinck et al., in prep., see section 1.4.3) cast doubt on the data of Sanyal et al. (2000), and do not support an inorganic cause for low pH-sensitivity, more data at oceanic pH and below are required before any assertions can be made with full confidence.

Expanding the range of planktic foraminifera for which δ^{11}B-pH relationships are characterised would be of great benefit in resolving this issue. As discussed in section 3.5.1, if symbiont-barren foraminifera record a pH-sensitivity that is lower than ambient borate, then it would support an underlying (possibly inorganic) fractionation during precipitation from aqueous borate to $CaCO_3$ (as suggested by Hönisch et al., 2007). If instead the pH-sensitivity is the same as (or greater than) that of aqueous borate, it implies that weaker pH-sensitivity in existing calibrations is not attributable to any flaw in our understanding of the geochemical basis of the proxy and the value of $^{11-10}K_B$, but is likely a result of the influence of photosynthetic symbionts buffering the microenvironment around the test. Moreover, if lowered pH-sensitivity in symbiont-bearing planktic foraminifera were derived from the presence of photosynthetic symbionts, it might be expected that deeper-dwelling symbiont-bearing planktic foraminifera will show pH-sensitivity closer to that of $\delta^{11}B_{B(OH)_4^-}$ than

shallower-dwelling species (since lower light levels at depth will reduce the buffering effect of symbiont photosynthesis). To explore these questions, two new calibrations were constructed and are presented here. Firstly, δ^{11}B-pH relationships in *G. bulloides* were calibrated. Since this species is spinose and typically shallow-dwelling but, crucially, lacks symbionts, it is a useful foil to *G. ruber* (calibrated in Chapter 3). Secondly, *O. universa* was calibrated, as an example of a deep-dwelling symbiont-bearing species. Although often referred to as a surface/mixed-layer species, *O. universa* is typically found at greater depths, even approaching the thermocline (Fairbanks et al., 1982, Spero and Williams, 1988, Sautter and Thunell, 1991). Indeed, in MOCNESS tows from 46 - 52 °S off New Zealand (this study), high incidence of living specimens of *O. universa* was seen at depths of up to 100 m (L. Northcote, pers. comm.). Similarly Morard et al. (2009) found *O. universa* in MOCNESS tows from 100-200 m depth. Consequently, these two species make excellent subjects for comparison with published calibrations of symbiont-bearing species, new and published measurements from other symbiont-barren species (including *Globoconella inflata*) and preliminary data from inorganic precipitation experiments (see section 1.4.3). Through comparison of these calibration data, new insights are gained into the nature of foraminiferal vital effects; insights which go some way to moving future discussion from the issue of causality to the issue of quantification and correction.

4.1.2 Previous foraminiferal calibrations: implications for vital effects

Besides the calibration of *G. ruber* from Chapter 3, the only other published culture calibrations of δ^{11}B in planktic foraminifera are those of the symbiont bearing species *O. universa* (Sanyal et al., 1996) and *G. sacculifer* (Sanyal et al., 2001). As discussed in sections 1.4.2.3 and 3.1.2, considerable issues still surround these culture calibrations that not only limit their downcore application but also cast doubt on the ability of microenvironment alteration (see Wolf-Gladrow et al., 1999, Zeebe et al., 1999a, 2003) to explain vital effects in foraminifera. One such issue is the large offset ($\sim$ 3 ‰) that exists between *G. sacculifer* and *O. universa* calibrations (and between core-top samples of these species). For this offset to be attributable to differences in microenvironment pH, it would suggest microenvironment pH in *G. sacculifer* is $>$ 0.3 pH units higher than in *O. universa* (from Sanyal et al., 1996), and 0.25 - 0.3 pH units higher than in *G. ruber* (Henehan et al., 2013). However, this is incompatible with the

similar observations of microenvironment pH made by microelectrode in *O. universa* (Rink et al., 1998, Köhler-Rink and Kühl, 2005) and *G. sacculifer* (Jørgensen et al., 1985, as given in Zeebe et al. 2003). Indeed, even when differences in day:night calcification (Anderson and Faber, 1984, Lea et al., 1995) are accounted for, the δ^{11}B offset between the two species seems too large to be explained by existing models of microenvironment perturbation (Zeebe et al., 2003).

One variable that hinders interpretation of these calibrations is that of analytical inaccuracy. As discussed by Foster et al. (2013), analysis of boron isotopes in carbonates via differing techniques (MC-ICPMS vs. NTIMS) may reproduce relative differences, but in absolute terms inter-laboratory comparability is poor; in other words, while the pH sensitivities of these calibrations may be reliable, their position in absolute δ^{11}B space is open to re-interpretation. However, since both the *G. sacculifer* (Sanyal et al., 2001) and *O. universa* (Sanyal et al., 1996) calibrations were both analysed at Stony Brook on the same instrument by the same workers, it would seem unlikely that the difference between the measured species calibrations is entirely analytically-derived.

It is possible to approximate the interlaboratory bias at work in these calibrations: Fig. 4.1 shows the ~3.3 ‰ offset between core-top NTIMS measurements of *G. sacculifer* from Sanyal et al. (1995), analysed at Stony Brook, and core-top MC-ICPMS measurements of *G. sacculifer* from nearby sites from Foster (2008), analysed at the Bristol Isotope Group, University of Bristol. However, if this offset were similarly applied to the *O. universa* culture calibration of Sanyal et al. (1996) (Fig. 4.1), the resultant calibration line would imply *O. universa* records pH (and δ^{11}B) values lower than ambient conditions (i.e. it would lie *below* the 1:1 line, where $\delta^{11}B_{CaCO_3}$=$\delta^{11}B_{B(OH)_4^-}$). Although this seems incompatible with micro-electrode observations of higher-than-ambient pH in the microenvironment of this species (Rink et al., 1998, Köhler-Rink and Kühl, 2005), and with microenvironment models for *O. universa* (Zeebe et al., 1999a, 2003), some lines of evidence suggest that this is not unreasonable. Firstly, Sanyal et al. (1996)'s calibration of *O. universa* is lighter in δ^{11}B than their inorganic carbonate calibration line (Sanyal et al., 2000), and not heavier, as microenvironment theory would predict (Zeebe et al., 2003) and as their calibration of *G. sacculifer* is (Sanyal et al., 2001). Secondly, in *G. sacculifer*, the photosynthetic compensation depth (i.e. the depth at which buffering of the microenvironment via

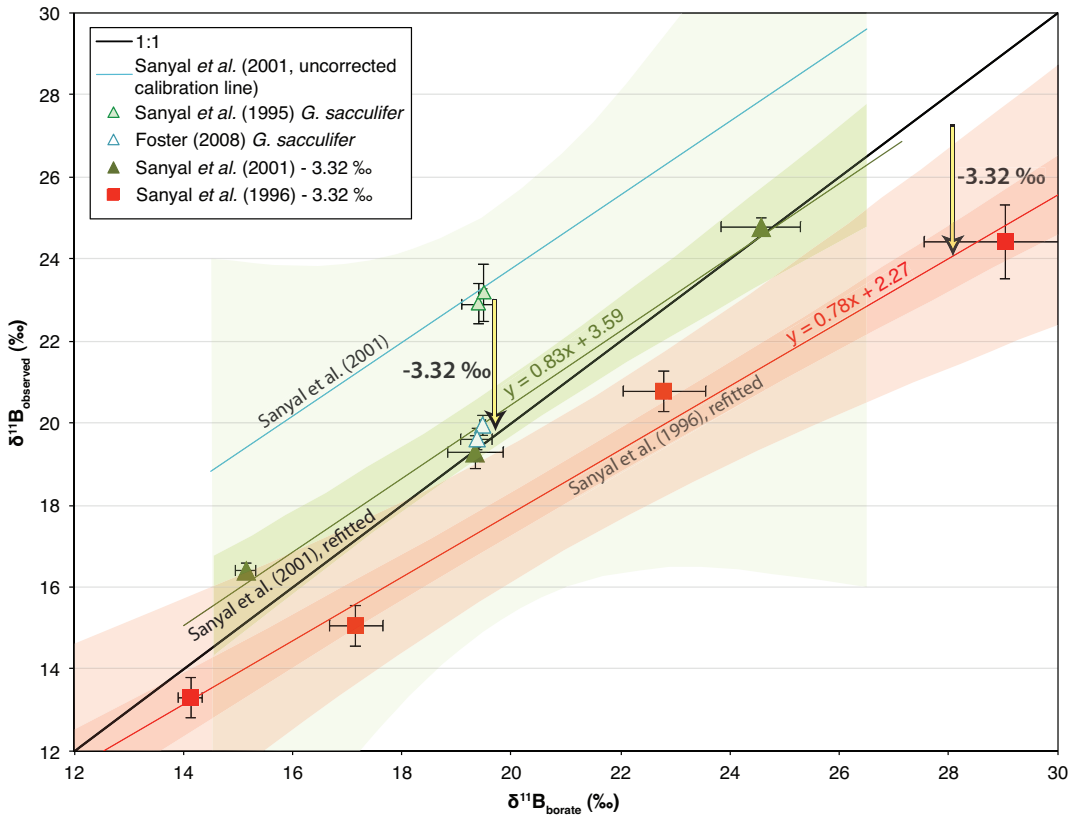

FIGURE 4.1: A representation of existing calibrations of *G. sacculifer* (Sanyal et al., 2001) and *O. universa* (Sanyal et al., 1996) in $\delta^{11}B_{B(OH)_4^-}$-$\delta^{11}B_{CaCO_3}$ space (see section 3.2.3), illustrating possible interlaboratory biases. Core-top *G. sacculifer* NTIMS measurements from Sanyal et al. (1995) are offset by 3.32 ‰ from MC-ICPMS measurements of *G. sacculifer* from adjacent sites (Foster, 2008). Applying this interlaboratory correction to existing calibrations (Sanyal et al., 1996, 2001) results in a *O. universa* calibration line that lies *below* the 1:1 line; implying that *O. universa* records lower-than-ambient pH. Uncertainty on calibration lines are calculated as 2σ (lightly shaded) and 1σ (heavily shaded) as discussed in Section 4.2.3. Slight differences in slope given for these calibrations compared to those quoted in Table 3.1 and Henehan et al. (2013) stem from the differences in line-plotting method used (see section 4.2.3). For culture calibrations, X-error bars represent quoted uncertainty in pH, and Y-error bars quoted uncertainty in NTIMS measurements. For core-tops, X-error represents estimated intra-annual variability of $\delta^{11}B_{B(OH)_4^-}$ for these sites (calculated as in Henehan et al. 2013), and Y-error is quoted analytical uncertainty from Foster (2008) and Sanyal et al. (1995).

photosynthesis is not great enough to cancel out the acidifying effects of respiration and calcification) is estimated at 45 m (Jørgensen et al., 1985). Average depth habitat in *O. universa* may be considerably greater than in either *G. ruber* or *G. sacculifer*, as discussed above (Fairbanks et al., 1982, Spero and Williams, 1988, Sautter and Thunell, 1991, Morard et al., 2009, L. Northcote, unpublished data). Therefore, it is possible that the degree of microenvironment pH elevation in *O. universa* is less than in *G. ruber* or *G. sacculifer*, if not completely cancelled out. This might be supported by the observation by Hönisch et al. (2003) that towed *O. universa* match more closely the δ^{11}B of individuals grown under low-light conditions (in which symbiont photosynthesis is minimal and microenvironment pH and $\delta^{11}B_{B(OH)_4^-}$ should be lowered by respiration) than those grown under saturated light conditions (under which photosynthesis should significantly raise microenvironment pH and $\delta^{11}B_{B(OH)_4^-}$). While clearly the calibration of Sanyal et al. (1996) was not carried out at >45 m water depth, these culture experiments were performed without any additional illumination beyond normal laboratory ceiling lighting, so light levels may have been below P_{max} (i.e. light levels required for optimum photosynthesis), and comparable to those seen at depth. Here a new *in situ* MC-ICPMS-derived calibration for *O. universa*, using tow, sediment trap and core-top sample material, is presented, primarily to inform discussion of vital effects, but also to test and corroborate the existing calibration of Sanyal et al. (1996) in the face of possible inter-laboratory analytical bias shown in Fig. 4.1.

4.1.3 Non-symbiont bearing foraminifera: ecology and existing measurements

Symbiont-barren foraminifera make up a large proportion of global foraminiferal assemblages. Although in oligotrophic low-latitude regions surface water assemblages are dominated by symbiont-bearing Globigerinids, in higher latitudes, surface waters are more likely to harbour symbiont-barren forms such as *Globigerina bulloides* or *Neogloboquadrina pachyderma sinistra*. Furthermore, when approaching palaeoceanographic questions, there are long intervals in Earth history where symbiont-bearing foraminifera are rare even in low latitudes (such as from the late Eocene to the Miocene, Wade, 2004). As such it is vital that we properly understand the relationship between pH and δ^{11}B in symbiont-barren foraminifera, not only to

improve our understanding of foraminiferal vital effects, but to extend both the geographical and temporal range of possible pH and pCO_2 reconstructions.

Very few boron isotope measurements of modern symbiont-barren foraminifera have been published to date. Hönisch et al. (2003) present boron isotope values in *G. bulloides* (measured by N-TIMS) offset from the symbiont-bearing *O. universa* by -1.4 ‰, which they interpreted as being attributable to the absence of photosynthesis in the foraminiferal microenvironment. Foster (2008) report a more pronounced offset of ~ 3 ‰ between the symbiont-bearing species *G. ruber* and *G. sacculifer* and the symbiont-barren *Neogloboquadrina dutertrei*. More recently, Yu et al. (2013) documented $\delta^{11}B$ in *N. pachyderma* below that of ambient $B(OH)_4^-$ ion. These data are all consistent with the hypothesis that the presence of symbionts in the microenvironment around the foraminifera elevates pH (and consequently $\delta^{11}B$), whereas in symbiont-barren species the microenvironment is acidified (and $\delta^{11}B$ lowered) by the release of respired CO_2 from the foraminifera (see section 1.4.2.3). It follows that unless these effects are accounted for, down-core records based on symbiont-barren species will yield artificially low values for pH and artificially high reconstructions of pCO_2. However, to date no calibration of boron isotopes in symbiont-barren foraminifera has been published that spans a pH range wide enough to define pH sensitivity. This is largely because of the challenges involved their capture and culture at a scale large enough for boron isotope analysis (B. Hönisch, pers. comm.). While no attempt is made to culture these species here, core-top and sediment trap data are combined to construct an *in situ* calibration of *G. bulloides* over a broad range in $\delta^{11}B_{B(OH)_4^-}$ (~ 2 ‰). While the primary goal of constructing such a calibration is to extend our understanding of foraminiferal vital effects as discussed above (section 4.1.1), it will also extend the possible range of palaeo-reconstructions to higher latitude oceans, that have no symbiont-bearing populations. In addition, comparison to measurements of $\delta^{11}B$ in other symbiont-barren species (*G. inflata* and *N. pachyderma*) offers insight into the degree of disparity in $\delta^{11}B$ that may occur within the symbiont-barren foraminifera.

4.2 Methods

4.2.1 Sampling

4.2.1.1 Tows and sediment traps

Plankton tows and sediment traps are valuable tools in decoding the relationships between pH and δ^{11}B in planktic foraminifera, because unlike core-top samples they consitute a 'snapshot' in time where pH and $\delta^{11}B_{B(OH)_4^-}$ are fully constrained. With this in mind, foraminifera were towed using a MOCNESS apparatus (Wiebe et al., 1985) on board the RV Tangaroa (Cruise TAN1106, 10th April - 1st May 2011), for boron isotope analysis at NOCS. The MOCNESS apparatus allows for towing over tightly constrained depth ranges, at sites where CTD casts were also taken to determine hydrographic and carbonate system conditions. Unfortunately, the timing of our cruise (late in the Austral autumn) meant that *G. bulloides* were not present in sufficient abundance to incorporate into this study. However, *O. universa* and *Globoconella inflata* were abundant, and these were analysed and are discussed here. Towed foraminifera were separated from soft-bodied plankton using saturated salt solution (Bé, 1959), before being rinsed thoroughly, dried at < 50 °C for 24-48 hours, sieved and picked.

Towed samples were complemented by sediment trap samples from the Cariaco Basin (both *G. bulloides* and *O. universa*, CAR22(Z), collected January 2007 and provided by B. J. Marshall). Trap Z is positioned at 150m water depth. pH, temperature and salinity data for the sediment trap site is interpolated from data from December 2006 and February 2007 downloadable from www.imars.usf.edu/CAR, and is given in Table B.1.

4.2.1.2 Core-tops

Core-top site selection, as in Chapter 3, was intended to maximise the spread in aqueous $\delta^{11}B_{B(OH)_4^-}$, and to sample from multiple ocean basins to investigate any possible regional effects (as noted in Mg/Ca; Marr et al., 2011). Specimens of *G. bulloides* were measured from globally distributed core-top sites from the core archives at Tübingen, Germany and NIWA, New Zealand. Samples from NIWA were verified as

recent by way of ^{14}C-dating (dates from Prebble et al., 2013), while from the Tübingen repository only undisturbed multicored sediments containing Rose Bengal-stained living benthic foraminifera were selected. The locations of core-top and sediment trap sites are shown in Fig. 4.2 (see also Supplementary Table C.1). Samples were also taken from a number of size fractions to examine any influence of test size on measured δ^{11}B, as discussed by Hönisch and Hemming (2004), Henehan et al. (2013) and Ni et al. (2007). As in Chapter 3, pH was estimated for core-top sites using surface water oceanographic data from the GLODAP (Key et al., 2004), CARINA (Key et al., 2010) and Takahashi et al. (2009) compendia (see Supplementary Table C.1). For better comparability with other studies, in newer sites not previously studied for *G. ruber* we use regional salinity-TAlk correlations (Table C.2) from Lee et al. (2006). Applying these correlations, monthly-resolved estimates of salinity from Takahashi et al. (2009) were converted to monthly TAlk estimates. Monthly temperature estimates were also taken from Takahashi et al. (2009). Pre-industrial pCO_2 at each core-top site was estimated by applying monthly ocean-atmosphere ΔpCO_2 from Takahashi et al. (2009) sites (corrected for the post-industrial changes in flux with reference to Gloor et al. 2003) to a pre-industrial atmospheric pCO_2 value. Where samples were ^{14}C-dated, the age-appropriate atmospheric pCO_2 value was taken from Lüthi et al. (2008) and references within. Where core-tops were not dated, we assume an average late Holocene (< 4 kyr BP) value of 275 ppm. Combined with approximations of typical local silicate and phosphate concentrations (from GLODAP/CARINA measurements), monthly estimates of pH were calculated using CO2sys.m (van Heuven et al., 2011), and the constants of Lueker et al. (2000), Lee et al. (2010) and Dickson (1990).

4.2.2 Analytical Methods

Analytical methods are as discussed in Chapter 2. Sediment trap and tow samples, in agreement with other culturing studies (e.g. Russell et al., 2004, Henehan et al., 2013), were subject to intensified oxidative cleaning (3 x 20-30 min treatments of 250 μl 1% H_2O_2 + 0.1 M NH_4OH_4 at 80 °C) to account for the greater presence of organics. In core-tops, oxidative cleaning was shorter (3 x 5 min) to minimise sample loss. Uncertainty is calculated according to the external reproducibility of repeat analyses of Japanese Geological Survey *Porites* coral standard (JCP; δ^{11}B= 24.3 ± 0.19 ‰) at the University of Southampton, as described by Equation 2.3 (see also Fig. 2.9).

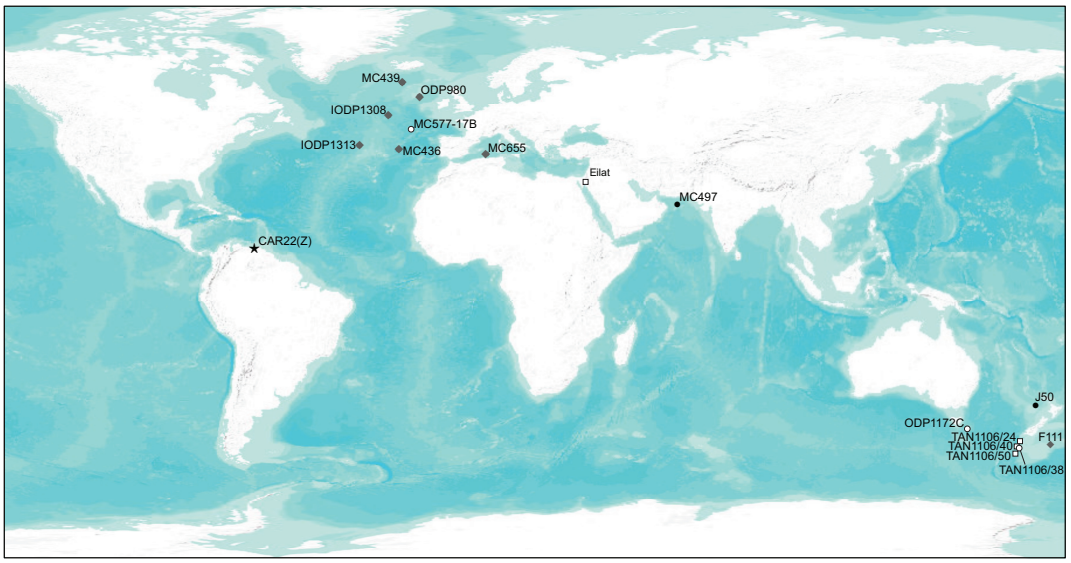

FIGURE 4.2: Locations of core-top, tow and sediment trap samples used in this study. Sites from which recent core-top samples were measured are marked as follows: open circles = *O. universa*, grey diamonds = *G. bulloides*, black circles= both species. Open squares mark the sites of tows, and the star marks site of the Cariaco basin sediment trap.

Because B/Ca ratios in *G. bulloides* are typically very low (30-60 μmol/mol), sample size typically ranged between 3-6 mg of $CaCO_3$ (i.e., 300-500 tests of *G. bulloides*). In *O. universa* B/Ca, while not as low as in *G. bulloides*, is still lower than in *G. ruber* (55 - 75 μmol/mol vs. $>$ 100 μmol/mol in *G. ruber*), and so typically >3 mg of sample material was used. With these larger sample sizes, efficiency of clay removal becomes particularly pertinent. As discussed in Section 2.3, we monitor Al/Ca ratios to screen for clay-contaminated samples (samples with Al/Ca ratios $>$ 100 μmol/mol are discounted). Perhaps partly because of the wide apertures that are characteristic of *G. bulloides* (and thus propensity for contaminants to penetrate the innermost chambers), we found clay contamination to be particularly problematic in this species. This study is not alone in this observation: Marr (2009) observed higher levels of trace element contamination in *G. bulloides*, while Barker et al. (2003) also reported *G. bulloides* to be particularly difficult to clean. In contrast, clay contamination was rarely observed

in specimens of *O. universa*.

4.2.3 Presentation of calibrations: $\delta^{11}B_{CaCO_3}$ vs. $\delta^{11}B_{B(OH)_4^-}$ plots and quantification of uncertainty.

As in Chapter 3, calibration data are described via linear regression between $\delta^{11}B_{B(OH)_4^-}$ (at *in situ* conditions) and measured $\delta^{11}B_{CaCO_3}$. Again, calibration data define straight lines with slopes reflecting the difference between the δ^{11}B-pH sensitivity of $\delta^{11}B_{B(OH)_4^-}$ and $\delta^{11}B_{CaCO_3}$. The slopes and intercepts of these lines are independent of pK_B^* (and hence salinity, temperature and pressure), meaning that tow, sediment trap and core top calibration data can be readily compared without complications from variable *in situ* temperatures and salinities. Previously, in Henehan et al. (2013), York regressions (York, 1968) in Isoplot (Ludwig, 2003) were used to calculate bounds of uncertainty on these sorts of calibrations, but this software is not without its limitations (most notably incompatibility with Mac OS X), and so hereon Monte Carlo approaches are performed. Similarly, though, this approach produces calibrations that account for the uncertainty in individual datapoints' X and Y variables.

One thousand simulated datasets were created. For each data point, a value of $\delta^{11}B_{B(OH)_4^-}$ was randomly generated from within a normal frequency distribution of the uncertainty around quoted mean values. Similarly, random values for $\delta^{11}B_{CaCO_3}$ were generated from within bounds of analytical uncertainty. For each simulated dataset a linear regression was fitted, and slope and intercept calculated. The slope and intercept of the calibration regression line may then be calculated as the mean of these 1,000 calculated slopes and intercepts, and uncertainty on slope and intercept calculated as 2σ of the 1,000 values. Reassuringly, recalculation of the *G. ruber* calibration from Henehan et al. (2013) in this way produced the same equation and bounds of uncertainty as were calculated with a York regression (York, 1968). While this is useful for comparing slopes and intercepts of calibrations, using only these 95% confidence intervals on the slope and intercept to calculate uncertainty for individual datapoints is inadequate: such an approach underestimates uncertainty in the mid-range of the calibration, as illustrated in Fig. 4.3.

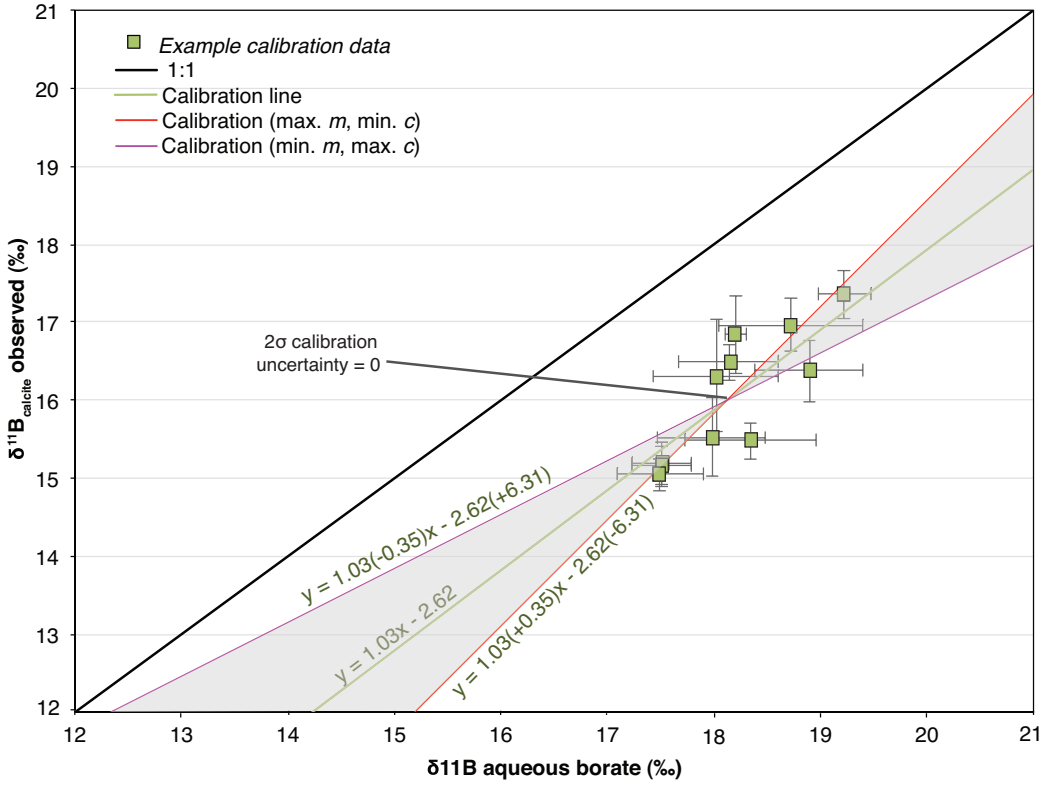

FIGURE 4.3: Illustration of the limitations of a Monte Carlo-only approach used to confidence intervals, using an example calibration dataset. 1,000 Monte Carlo simulations within the bounds of uncertainty of observations can be used to calculate 1,000 values for the slope m and the intercept c, two standard deviations of which may provide 2σ bounds of uncertainty for these values. However, when one uses only the maximum and minimum CIs of slope and intercept to calculate uncertainty, as the shaded region indicates, towards the centre of the calibrated range uncertainty reaches zero, which is clearly inappropriate.

$$CI_y = \pm t(\alpha, df) S_{yx} \sqrt{\frac{1}{n} + \frac{(x_i - \overline{x})^2}{\Sigma(x - \overline{x})^2}} \tag{4.1}$$

To circumvent this issue, for each simulated dataset confidence intervals were calculated via Equation 4.1 above, where CI_y is the calculated uncertainty on y for a given value of x, x_i. In this equation, n is the number of points in the calibration, t is the critical t-statistic, given an uncertainty level (α) and df=$n-2$. S_{yx} is the standard error on a predicted y-value for each x-value in a regression, $\overline{x}$ is the mean value of x in the calibration dataset, and $\Sigma(x-\overline{x})^2$ is the sum of the squared deviations of given x values from the regression line. Confidence intervals (both 1 and 2 σ) on the calibration line are then calculated as the average of 1000 Monte Carlo simulated

Calibration	Study	Slope	Probability of Steeper Slope in *G. bulloides*
G. bulloides	this study	1.01	
O. universa	Sanyal et al. (1996)	0.78	95%
Inorganic $CaCO_3$	Sanyal et al. (2000)	0.78	93%
G. sacculifer	Sanyal et al. (2001)	0.83	89%
G. ruber	Henehan et al. (2013)	0.60	>99%
O. universa	this study	0.80	91%

TABLE 4.1: Slopes (representing pH-sensitivities) in planktic foraminiferal and inorganic carbonate calibrations, and the probability that the new *G. bulloides* demonstrates a steeper slope (i.e. a greater pH-sensitivity) than these calibrations. Probabilities are derived from comparison of slopes in 1,000 Monte Carlo simulations of each calibration line.

confidence intervals. For ease of reproduction, polynomial fits (R^2 >0.999) are plotted to describe the generated bounds of uncertainty for calibration lines. Note that confidence intervals derived via this method are inherently much more sensitive to n, the number of constituent measurements, than those calculated via the alternative standard Monte Carlo approach (i.e. 2σ uncertainty on slopes of 1000 simulated linear regressions). This is why 2σ confidence intervals on the slope of Sanyal et al. (2000) in Fig. 4.1 appear unusually large.

4.3 Results

4.3.1 *G. bulloides* Calibration

The results of this builloides calibration are given in Table 4.2 and are plotted in Figure 4.4. The data record lower δ^{11}B than that of ambient $B(OH)_4^-$ ion (i.e. they plot below the 1:1 line on Fig. 4.4). In addition, the slope of these data is ≃1 (1.01 ± 0.29, 2σ), which suggests that *G. bulloides* has a pH sensitivity permissively equal to that of aqueous $B(OH)_4^-$ ion. Although the residual scatter in this calibration (discussed later) produces large bounds of uncertainty on the calculated slope, the slope of this *G. bulloides* calibration, is, to within 89% confidence, steeper than any previous planktic foraminiferal or inorganic carbonate calibration (see Table 4.1). This is in contrast to all existing planktic foraminifera calibrations, whose slopes are within uncertainty of the inorganic calibration of (Sanyal et al., 2000, see Henehan et al. (2013)), and less than 1.

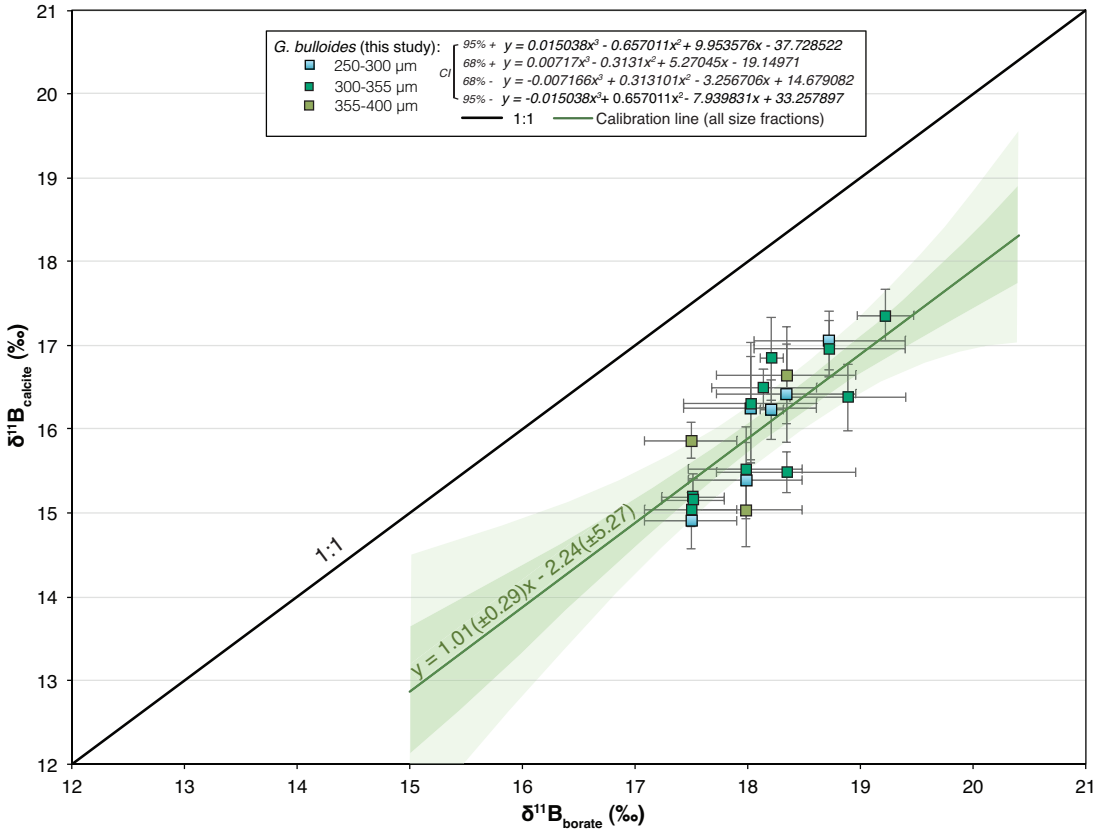

FIGURE 4.4: New calibration of *G. bulloides*, with shaded regions defining 1σ (heavily shaded) and 2σ (lightly shaded) confidence intervals (calculated as per section 4.2.3). X-error bars for core-top samples are 2 standard deviations of intra-annual variability in calculated monthly $\delta^{11}B_{B(OH)_4^-}$, while for sediment trap samples it reflects the range of $\delta^{11}\mathrm{B}_{B(OH)_4^-}$ between Dec-Feb 2007 (see Table B.1). Y-error is the analytical reproducibility as calculated by Equation 2.3.

Sample/site	Sample type	Size fraction (μm)	Latitude (°N)	Longitude (°E)	T (°C)	Salinity	pH	$\pm$ (2σ)	pK^*_B	$\delta^{11}B_{CaCO_3}$ (‰)	$\pm$ (2σ)	$\delta^{11}B_{B(OH)_4^-}$ (‰)	$\pm$ (2σ)	$\Delta\delta^{11}B$ (‰)	$pH_{\delta^{11}B}$	$\Delta pH_{\delta^{11}B}$
MH70 F111	Core-top	355-400	-48.95	174.98	9.08	34.33	8.191	0.003	8.794	15.86	0.21	17.49	0.41	-1.63	8.008	-0.183
MH121 MC577-17B	Core-top	355-400	45.57	-17.40	15.32	35.70	8.188	0.002	8.709	16.65	0.58	18.34	0.62	-1.69	8.019	-0.170
MH68 F111	Core-top	250-300	-48.95	174.98	9.08	34.33	8.191	0.003	8.794	14.90	0.33	17.49	0.41	-2.59	7.863	-0.328
MH108 CAR22(Z)6	Sed. Trap	250-300	10.50	-64.66	24.17	36.70	8.066	0.018	8.597	16.23	0.35	18.21	0.11	-1.98	7.858	-0.208
MH120 MC577-17B	Core-top	250-300	45.57	-17.40	15.32	35.70	8.188	0.002	8.709	16.43	0.58	18.34	0.62	-1.91	7.993	-0.195
MH25 MC436	Core-top	300-355	39.80	-21.06	18.40	36.06	8.201	0.017	8.670	16.37	0.40	18.89	0.51	-2.52	7.948	-0.253
MH61 MC655	Core-top	300-355	38.42	5.40	23.23	37.38	8.161	0.010	8.605	17.36	0.31	19.22	0.25	-1.87	7.992	-0.169
MH69 F111	Core-top	300-355	-48.95	174.98	9.08	34.33	8.191	0.003	8.794	15.04	0.21	17.49	0.41	-2.45	7.887	-0.304
MH102 TAN1106/38 *'flattened'*	Core-top	300-355	-49.69	165.07	9.78	34.49	8.186	0.003	8.783	15.16	0.26	17.51	0.28	-2.36	7.894	-0.292
MH103 TAN1106/38 *'kummerform'*	Core-top	300-355	-49.69	165.07	9.78	34.49	8.186	0.003	8.783	15.19	0.27	17.51	0.28	-2.33	7.899	-0.287
MH107 CAR22(Z)6	Sed. Trap	300-355	10.50	-64.66	24.17	36.70	8.066	0.018	8.597	16.84	0.50	18.21	0.11	-1.37	7.929	-0.137
MH109 ODP1172C	Core-top	300-355	-43.96	149.93	13.72	35.02	8.196	0.004	8.732	16.49	0.23	18.14	0.47	-1.65	8.024	-0.173
MH117 MC577-17B	Core-top	300-355	45.57	-17.40	15.32	35.70	8.188	0.002	8.709	15.48	0.24	18.34	0.62	-2.86	7.869	-0.320
MH125 IODP1313	Core-top	300-355	41.00	-32.96	18.50	36.03	8.182	0.008	8.668	16.96	0.34	18.73	0.67	-1.77	8.013	-0.169
MH126 IODP1308	Core-top	300-355	49.88	-24.24	13.22	35.41	8.183	0.001	8.736	15.52	0.50	17.98	0.50	-2.46	7.903	-0.280
MH127 ODP980	Core-top	300-355	55.49	-14.70	11.71	35.36	8.206	0.016	8.755	16.32	0.72	18.02	0.59	-1.71	8.026	-0.180
MH148 ODP980	Core-top	250-300	55.49	-14.70	11.71	35.36	8.206	0.016	8.755	16.24	0.62	18.02	0.59	-1.78	8.018	-0.188
MH147 IODP1313	Core-top	250-300	41.00	-32.96	18.50	36.03	8.182	0.008	8.668	17.05	0.35	18.73	0.67	-1.67	8.023	-0.159
MH153 IODP1308	Core-top	250-300	49.88	-24.24	13.22	35.41	8.183	0.001	8.736	15.38	0.45	17.98	0.50	-2.60	7.882	-0.301
MH154 IODP1308	Core-top	355-400	49.88	-24.24	13.22	35.41	8.183	0.001	8.736	15.04	0.44	17.98	0.50	-2.94	7.828	-0.355

TABLE 4.2: Results of Boron Isotope analyses of *G. bulloides* from core-tops and sediment traps. Uncertainty on pH in core-tops is 2 standard deviations of twelve monthly reconstructions, while for CAR22(Z) it represents the range in pH between December and February 2006 from IMAR (see Table B.1). Uncertainty on measured $\delta^{11}B$ is from Equation 2.3. $\Delta\delta^{11}B$ is the difference between recorded $\delta^{11}B_{CaCO_3}$ and that of *in situ* $\delta^{11}B_{B(OH)_4^-}$. $pH_{\delta^{11}B}$ is the pH back-calculated from foraminiferal $\delta^{11}B$ measurements, and $\Delta pH_{\delta^{11}B}$ is the difference between this and ambient pH. All carbonate system and pK^*_B calculations use CO2sys.m (van Heuven et al., 2011) and the constants of Dickson (1990), Lueker et al. (2000) and Lee et al. (2010).

4.3.2 Other Symbiont-barren Species

New data from *G. inflata* and *N. pachyderma* from coretops and tows are plotted in Fig. 4.5, along with published measurements from *N. pachyderma* (Yu et al., 2013) and*N. dutertrei* (Foster, 2008) for comparison. Measurements of *N. pachyderma* and most of measurements of *G. inflata* analysed via MC-ICPMS at NOCS plot within uncertainty of the *G. bulloides* calibration line. However, both the *N. pachyderma* data from Yu et al. (2013) and some *G. inflata* datapoints plot lower than the *G. bulloides* calibration line.

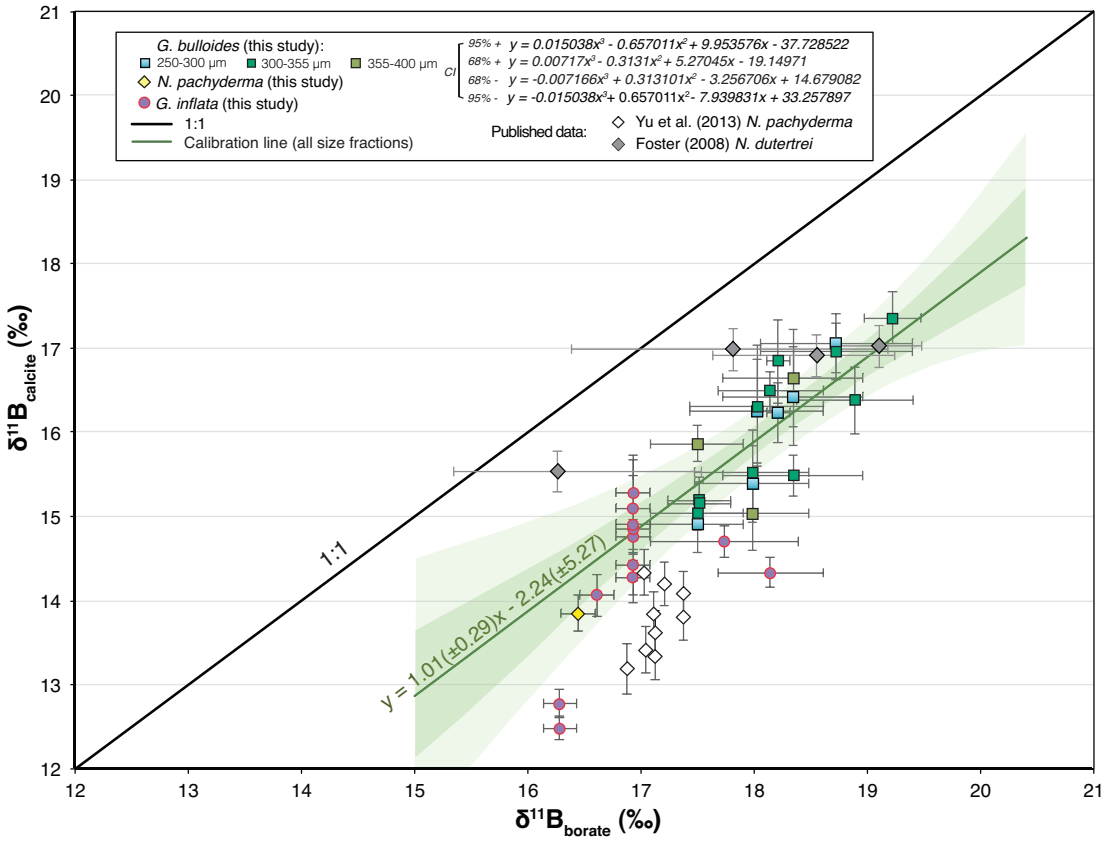

FIGURE 4.5: New MC-ICPMS calibration of *G. bulloides*, compared with new measurements of *N. pachyderma* (core-top, this study) and *G. inflata* (MOCNESS tows and core-top, this study). Published values for *N. pachyderma* (Yu et al., 2013) and *N. dutertrei*(Foster, 2008) are also plotted for comparison. X-error bars for MC-ICPMS data (from this study) are either 2 standard deviations of intra-annual variability in calculated monthly $\delta^{11}B_{B(OH)_4^-}$ (core-tops, see section 4.2.1.2), the range of $\delta^{11}B_{B(OH)_4^-}$ between Dec-Feb 2007 (sediment traps, see Table B.1) or a conservative estimate of the uncertainty in $\delta^{11}B_{B(OH)_4^-}$ between tow depths (*G. inflata* tows). X-error in the data of Yu et al. (2013) and Foster (2008) are as quoted in these studies. Y-error is the analytical reproducibility as calculated by Equation 2.3 for new data, and as quoted in relevant papers for the published data shown.

Sample/site	Sample type	Size fraction (μm)	Latitude (°N)	Longitude (°E)	T (°C)	Salinity	pH	$\pm$ (2σ)	pK^*_B	$\delta^{11}B_{CaCO_3}$ (‰)	$\pm$ (2σ)	$\delta^{11}B_{B(OH)_4^-}$ (‰)	$\pm$ (2σ)	$\Delta\delta^{11}B$ (‰)	$pH_{\delta^{11}B}$	$\Delta pH_{\delta^{11}B}$
TAN1106/24-N8 Clean Test 1	Tow	300-355	-47.98	165.77	12.51	34.70	8.095	0.005	8.746	14.90	0.35	16.93	0.15	-2.03	7.814	-0.273
TAN1106/24-N8 Clean Test 2	Tow	300-355	-47.98	165.77	12.51	34.70	8.095	0.005	8.746	15.29	0.39	16.93	0.15	-1.64	7.877	-0.210
TAN1106/24-N8 Clean Test 3	Tow	300-355	-47.98	165.77	12.51	34.70	8.095	0.005	8.746	14.85	0.88	16.93	0.15	-2.08	7.805	-0.282
MH80 TAN1106/24-N8	Tow	250-300	-47.98	165.77	12.51	34.70	8.095	0.005	8.746	15.10	0.38	16.93	0.15	-1.83	7.848	-0.239
MH82 TAN1106/24-N8	Tow	300-355	-47.98	165.77	12.51	34.70	8.095	0.005	8.746	14.77	0.22	16.93	0.15	-2.16	7.791	-0.296
MH84 TAN1106/24-N8	Tow	355-400	-47.98	165.77	12.51	34.70	8.095	0.005	8.746	14.27	0.20	16.93	0.15	-2.66	7.694	-0.393
MH86 TAN1106/24-N8	Tow	400-455	-47.98	165.77	12.51	34.70	8.095	0.005	8.746	14.42	0.19	16.93	0.15	-2.50	7.726	-0.361
MH95 TAN1106/50-N8	Tow	300-355	-51.56	164.68	9.01	34.39	8.063	0.004	8.789	12.49	0.14	16.21	0.15	-3.80	6.975	-1.082
MH93 TAN1106/50-N8	Tow	355-400	-51.56	164.68	9.01	34.39	8.063	0.004	8.789	12.77	0.17	16.21	0.15	-3.51	7.213	-0.844
MH99 TAN1106/40-N9	Tow	300-355	-49.43	165.26	11.09	34.62	8.071	0.008	8.766	14.06	0.25	16.61	0.15	-2.55	7.667	-0.404
MH111 ODP1172C	Core-top	300-355	-43.96	149.93	13.72	35.02	8.196	0.004	8.732	14.34	0.18	18.14	0.47	-3.81	7.694	-0.503
MH129 MC439	Core-top	355-400	59.46	-20.03	10.09	35.23	8.200	0.019	8.776	14.70	0.19	17.74	0.66	-3.04	7.809	-0.391
MH73 KN7812-6BC	Core-top	250-300	-63.29	174.78	1.36	34.03	8.184	0.008	8.899	13.85	0.21	16.44	0.15	-2.59	7.747	-0.437

TABLE 4.3: Results of Boron Isotope analyses of *G. inflata* and *N. pachyderma* (Sample MH73 KN7812-6BC) from core-tops and tow. Uncertainty on pH in core-tops is 2 standard deviations of twelve monthly reconstructions, while for TAN1106 it represents the range in pH within the depth sampled by the MOCNESS net. Uncertainty on measured δ^{11}B is from Equation 2.3. $\Delta\delta^{11}$B is the difference between recorded $\delta^{11}B_{CaCO_3}$ and that of *in situ* $\delta^{11}B_{B(OH)_4^-}$. $pH_{\delta^{11}B}$ is the pH back-calculated from foraminiferal δ^{11}B measurements, and $\Delta pH_{\delta^{11}B}$ is the difference between this and ambient pH. All carbonate system and pK^*_B calculations use CO2sys.m (van Heuven et al., 2011) and the constants of Dickson (1990), Lueker et al. (2000) and Lee et al. (2010).

4.3.3 *O. universa* calibration

Calibration data for *O. universa* are given in Table 4.4 and are plotted in Figure 4.6. The data record lower δ^{11}B than that of ambient $B(OH)_4^-$ ion, and plot below the 1:1 line. Their slope is almost identical to that observed in Sanyal et al. (1996) (0.80 ± 0.11 vs. 0.78 ± 0.09), meaning that wild *O. universa* display a pH sensitivity equal to those from cultures measured by Sanyal et al. (1996), but are offset in absolute δ^{11}B from the culture calibration (by ∼ 3.3 ‰). However, this MC-ICPMS calibration excludes one data point, shown in parentheses in Fig. 4.6: a towed sample of *O. universa* from the Gulf of Aqaba that recorded very different δ^{11}B signals. This sample had a δ^{11}B that was *elevated* relative to ambient $B(OH)_4^-$, as current understanding of microenvironment alteration would predict (see Zeebe et al., 2003). This datapoint is discussed further in section 4.4.2.2.

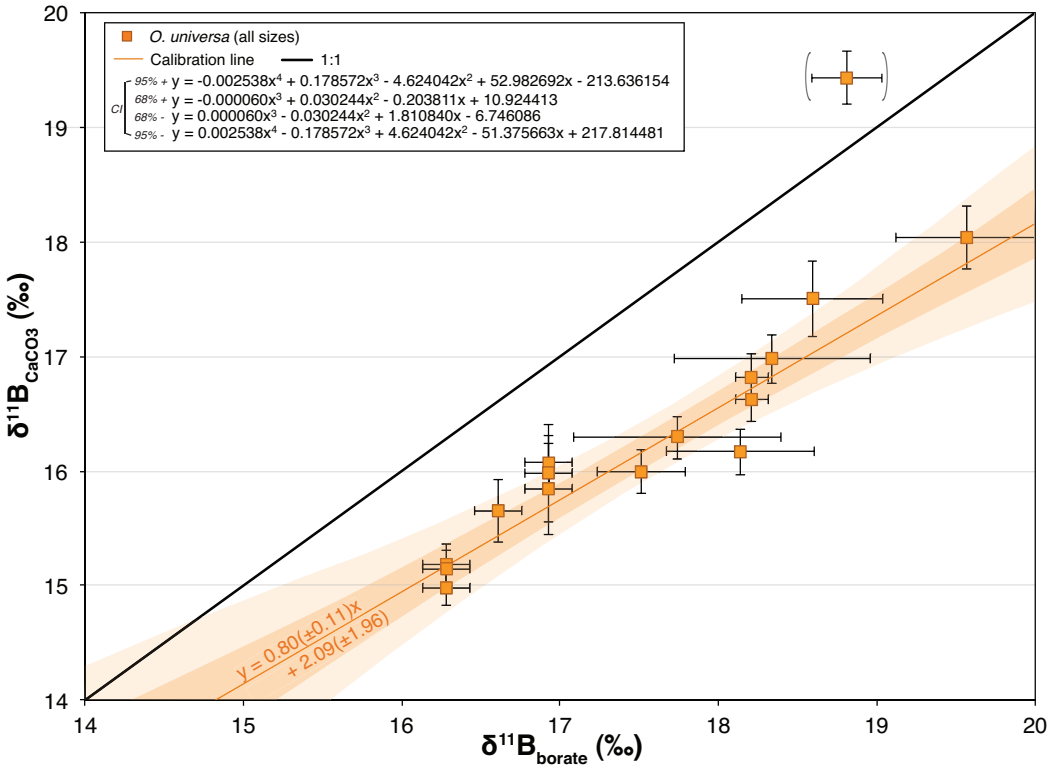

FIGURE 4.6: New calibration of *O. universa*, plotted with uncertainty (shaded regions) calculated as 2σ of 1,000 Monte Carlo simulations (see Section 4.2.3), with shaded regions defining 1σ (heavily shaded) and 2σ (lightly shaded) confidence intervals. X-error bars for core-top samples are 2 standard deviations of intra-annual variability in calculated monthly $\delta^{11}B_{B(OH)_4^-}$, while for sediment trap samples it reflects the range of $\delta^{11}\mathrm{B}_{B(OH)_4^-}$ between Dec-Feb 2007, and for tow samples it reflects CTD-derived hydrographic variability within the depth range of the tow. Y-error is the analytical reproducibility as calculated by Equation 2.2. Note, this calibration excludes one datapoint towed from Eilat, shown in parentheses: see Section 4.4.2.2.

Sample/site	Sample type	Size fraction (μm)	Latitude ($^{\circ}N$)	Longitude ($^{\circ}E$)	T ($^{\circ}C$)	Salinity	pH	$\pm$ (2σ)	pK^*_B	$\delta^{11}B_{CaCO_3}$ (‰)	$\pm$ (2σ)	$\delta^{11}B_{B(OH)_4^-}$ (‰)	$\pm$ (2σ)	$\Delta\delta^{11}B$ (‰)	$pH_{\delta^{11}B}$	$\Delta pH_{\delta^{11}B}$
MH104 J50	Coretop	355-500	-36.67	170.65	17.2	35.49	8.189	0.009	8.687	17.50	0.33	18.59	0.45	-1.09	8.087	-0.102
MH113 ODP1172C	Core-top	300-355	-43.96	149.93	13.7	35.02	8.196	0.004	8.732	16.17	0.20	18.14	0.47	-1.97	7.985	-0.212
MH114 CAR22(Z)	Sed. Trap	>600	10.50	-64.66	24.2	36.70	8.076	0.035	8.598	16.82	0.20	18.21	0.10	-1.39	7.927	-0.149
MH115 CAR22(Z)	Sed. Trap	500-600	10.50	-64.66	24.2	36.70	8.076	0.035	8.598	16.62	0.19	18.21	0.10	-1.59	7.905	-0.171
MH119 MC577-17B	Core-top	300-355	45.57	-17.40	15.3	35.70	8.188	0.002	8.709	16.97	0.21	18.34	0.62	-1.36	8.055	-0.133
MH128 MC439	Core-top	355-400	59.46	-20.03	10.1	35.23	8.200	0.019	8.776	16.29	0.18	17.74	0.66	-1.45	8.044	-0.156
MH130 MC497	Core-top	>355	23.53	63.31	26.9	36.37	8.152	0.020	8.568	18.04	0.27	19.57	0.45	-1.53	8.020	-0.131
MH83 TAN1106/24-N8	Tow	300-355	-47.91	165.79	12.5	34.70	8.087	0.010	8.746	15.98	0.43	16.93	0.15	-0.94	7.975	-0.112
MH85 TAN1106/24-N8	Tow	355-400	-47.91	165.79	12.5	34.70	8.087	0.010	8.746	15.84	0.40	16.93	0.15	-1.08	7.957	-0.130
MH87 TAN1106/24-N8	Tow	400-450	-47.91	165.79	12.5	34.70	8.087	0.010	8.746	16.08	0.23	16.93	0.15	-0.85	7.987	-0.100
MH88 TAN1106/38	Core-top	300-355	-49.69	165.07	9.8	34.49	8.186	0.003	8.784	15.99	0.19	17.51	0.28	-1.52	8.015	-0.171
MH90 TAN1106/50-N8	Tow	>450	-51.71	164.56	9.0	34.41	8.056	0.010	8.789	14.98	0.15	16.28	0.15	-1.30	7.871	-0.185
MH92 TAN1106/50-N8	Tow	355-400	-51.71	164.56	9.0	34.41	8.056	0.010	8.789	15.19	0.18	16.28	0.15	-1.09	7.905	-0.151
MH94 TAN1106/50-N8	Tow	300-355	-51.71	164.56	9.0	34.41	8.056	0.010	8.789	15.15	0.17	16.28	0.15	-1.13	7.899	-0.157
MH98 TAN1106/40-N9	Tow	300-355	-49.72	165.21	11.0	34.61	8.071	0.020	8.766	15.65	0.28	16.61	0.15	-0.95	7.951	-0.120
MH76 Eilat	Tow	>500	29.50	34.92	23	40.40	8.116	0.002	8.598	19.47	0.31	18.78	0.24	0.70	8.174	0.058

TABLE 4.4: Results of Boron Isotope analyses of *O. universa* from tows, core-tops and sediment traps. Uncertainty on pH in core-tops is 2 standard deviations of twelve monthly reconstructions, while for TAN1106 tows it reflects the range in pH in the depth range towed and for CAR22(Z) it represents the range in pH between December and February 2006 from IMAR. Uncertainty on measured $\delta^{11}B$ is from Equation 2.3. $\Delta\delta^{11}B$ is the difference between recorded $\delta^{11}B_{CaCO_3}$ and that of *in situ* $\delta^{11}B_{B(OH)_4^-}$. $pH_{\delta^{11}B}$ is the pH backcalculated from foraminiferal $\delta^{11}B$ measurements, and $\Delta pH_{\delta^{11}B}$ is the difference between this and ambient pH. All carbonate system and pK^*_Bcalculations use CO2sys.m (van Heuven et al., 2011) and the constants of Dickson (1990), Lueker et al. (2000) and Lee et al. (2010).

4.3.4 Size effects

There is no compelling evidence for size-related change in the recorded δ^{11}B of either *G. bulloides* (Fig. 4.7) or *O. universa* (Fig. 4.8). While there is a slight trend towards more negative $\Delta\delta^{11}$B in larger specimens of *O. universa*, this is more likely a site specific difference: within any one site all size fractions give the same value (within analytical uncertainty). In contrast, towed samples of *G. inflata* appear to show a trend in δ^{11}B (and B/Ca, another purported carbonate system proxy; see Chapter 5) that suggests decreasing microenvironment pH with size (see Fig. 4.9).

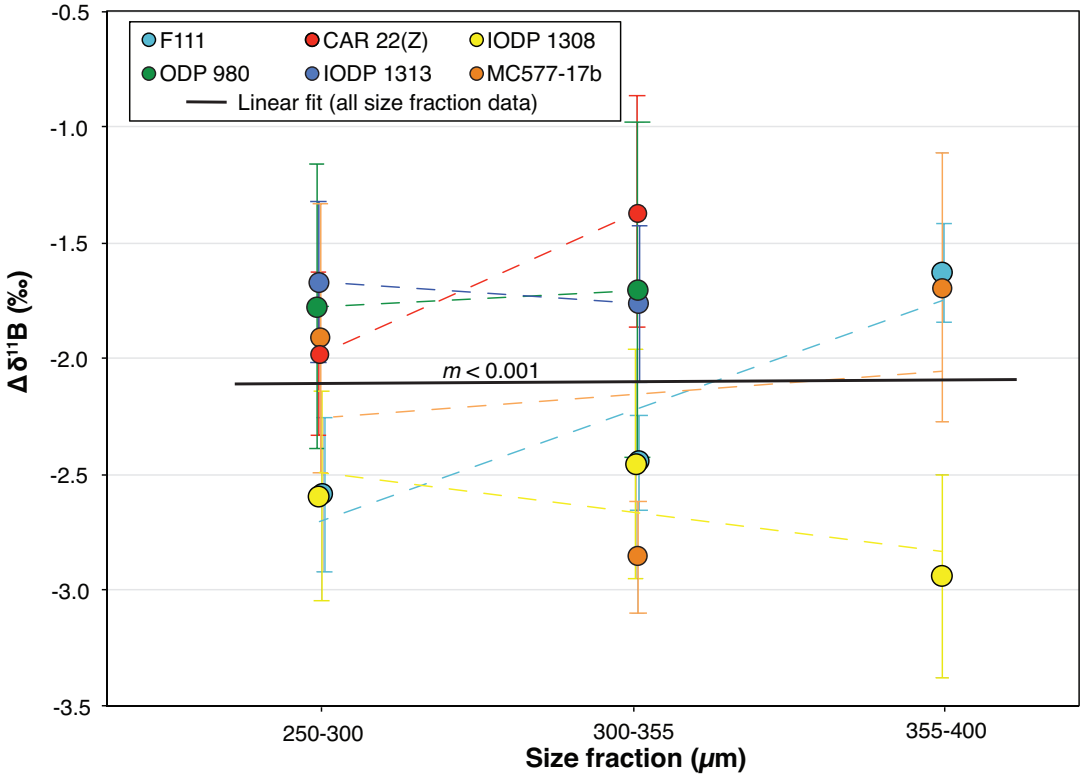

FIGURE 4.7: $\Delta\delta^{11}$B (i.e. deviation of $\delta^{11}B_{CaCO_3}$ from $\delta^{11}B_{B(OH)_4^-}$) with size fraction in *G. bulloides* from Sites CAR 22(Z) (Cariaco Basin sediment trap), F111 (Southern Ocean core-top), ODP 980, IODP 1308, IODP 1313 and MC577-17b (North Atlantic core-tops). Y-error is the analytical reproducibility as calculated by Equation 2.3. While there is often considerable scatter in recorded δ^{11}B between size fractions, there is no consistent size-related pattern. Indeed, a linear fit through the whole dataset (black line) gives a slope of $\simeq$0, suggesting that there is no size effect on δ^{11}B in *G. bulloides*.

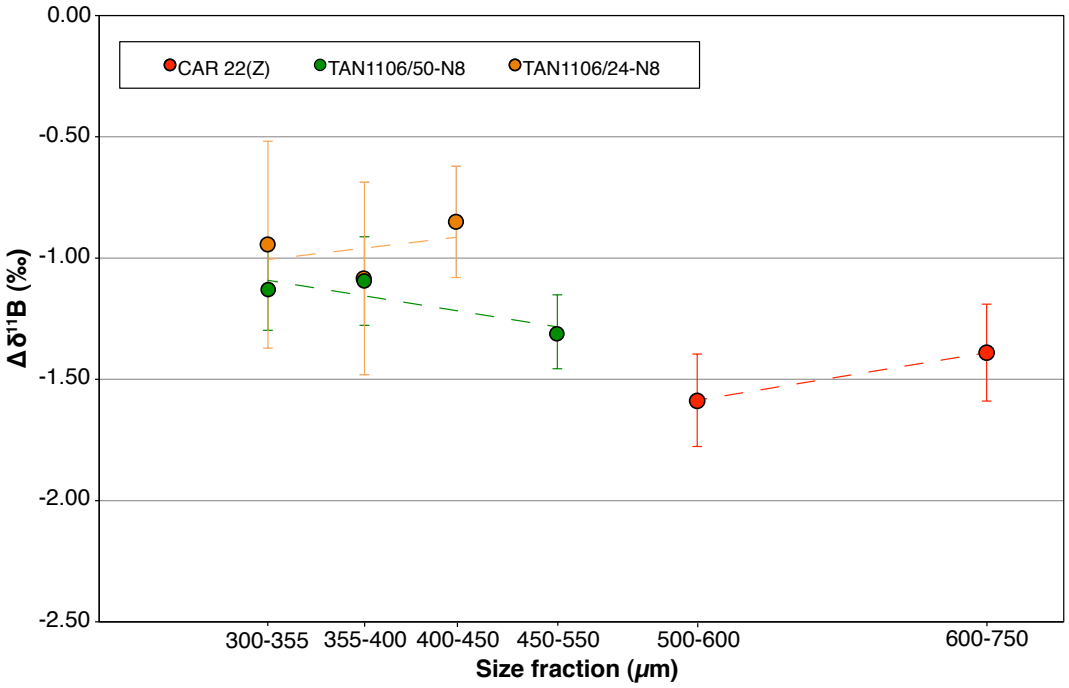

FIGURE 4.8: No unequivocal size-related changes in δ^{11}B were observed in *O. universa*. While there is a slight negative trend in $\Delta\delta^{11}$B in larger samples, this may be driven by site-specific factors; since within each individual site all size fractions are within uncertainty of each other, size fractions are, at best, small. Samples are from Southern Ocean tows (TAN1106/24 and TAN1106/50) and Cariaco Basin sediment traps (CAR22(z)). Y-error is the analytical reproducibility as calculated by Equation 2.3.

4.4 Discussion

4.4.1 *G. bulloides* and symbiont-barren foraminifera

4.4.1.1 Lower-than-ambient δ^{11}B in *G. bulloides*, and other symbiont-barren species.

As shown in Fig. 4.4, *G. bulloides* records δ^{11}B values that are $\sim 2.1‰$ lower than *in situ* $\delta^{11}B_{B(OH)_4^-}$, which, accounting for the pK_B^* of each sample, translates to recorded pH values that are on average 0.23 pH units lower than ambient seawater pH. This is permissively in accordance with modelled values of δ^{11}B for *O. universa* in the absence of photosynthesis (Zeebe et al., 2003), and is roughly midway between the observations of pH reduction at the test boundary in the dark of ~ 0.1 pH (*G. sacculifer*; Jørgensen et al., 1985) and ~ 0.35 pH (*O. universa*; Rink et al., 1998). Thus these δ^{11}B data are consistent with the release of respired CO_2 lowering microenvironment pH. This is

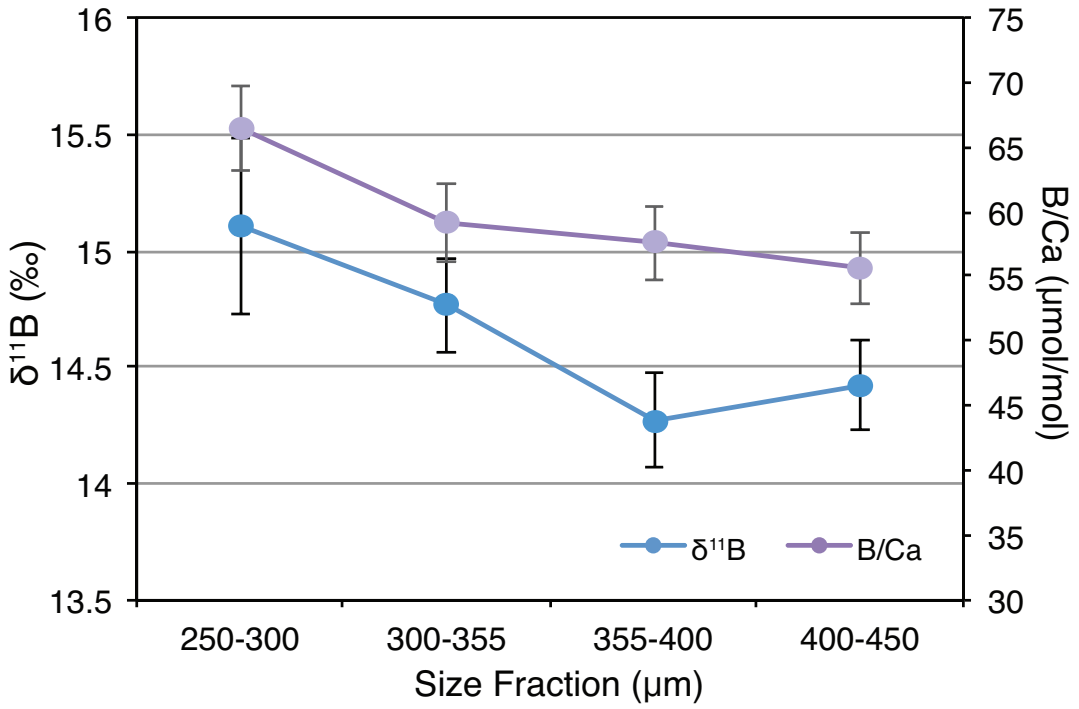

FIGURE 4.9: Size fractions of *G. inflata* from tow TAN1106/24 (-47°58.36',165°46.83') in the Southern Ocean. Although only tested in one site, δ^{11}B and B/Ca ratios seem to suggest that *G. inflata* records progressively lower pH with size (although see Chapter 5 for discussion of the complications in interpreting B/Ca). Y-error is the analytical reproducibility as calculated by Equation 2.3 for δ^{11}B, and 5% for trace element analysis.

corroborated by the observed patterns in other symbiont-barren species (shown in Fig. 4.5), that all record similarly lowered δ^{11}B relative to ambient borate, even if they do not always fall on the *G. bulloides* calibration line. As Foster (2008) notes, there is considerable scatter in measurements of *N. dutertrei*, linked to an uncertainty with regards its depth habitat, but nonetheless each of these points is within uncertainty of the *G. bulloides* calibration line. In the case of the *N. pachyderma* data of Yu et al. (2013), their calibration typically underestimates pCO_2 in reconstructions by 20 - 45 ppm, which might suggest that carbonate system characterisation for calibration samples (using somewhat sparse GLODAP hydrographic data from Key et al., 2004, rather than the approaches used here) may be imperfect, and that *in situ* $\delta^{11}B_{B(OH)_4^-}$ may in fact have been lower.

There is, however, some considerable residual scatter evident in measurements of *G. bulloides*. There are numerous possible causes for this, namely: a) contamination

issues, b) inappropriate characterisation of ambient $\delta^{11}B_{B(OH)_4^-}$, and/or c) cryptospecies variability. Remnant contaminants may cause scatter in $\delta^{11}B$ measurements via the introduction of isotopically divergent boron. For example, boron adsorbed onto clays is typically isotopically light (Palmer et al., 1987), and inefficient clay cleaning may result in anomalously light $\delta^{11}B$ measurements. *G. bulloides* was the species found to be most commonly affected by clay contamination, perhaps as a result of its wide aperture (as also highlighted by Barker et al., 2003). Furthermore, large and apparently non-systematic scatter is seen even between size fractions at the same site, which would perhaps favour a contamination model rather than any biological explanation. However, the residuals from the calibration line do not correlate significantly with Al/Ca (R^2=<0.01), Mn/Ca (R^2=0.07), U/Ca (R^2=0.14), Ba/Ca (R^2=0.01), Cd/Ca (R^2=0.03) or Nd/Ca (R^2=0.12), as one might expect if any of these more common contaminants might be behind the observed scatter. It is possible that contamination by coccolith calcite might produce some variability in $\delta^{11}B$ without being detectable in these trace element values: Martin (2001) examined *G. bulloides* under SEM and found coccoliths often fused and incorporated into apparently secondary diagenetic calcite coatings. That said, mass balance considerations would require $\sim$ 2.5% of the mass of *G. bulloides* sample material to be derived from coccolithophore calcite for contamination to be detectable above analytical uncertainty (Henehan, unpublished data), which seems perhaps unfeasible. Again, more in-depth analysis and SEM study would be desirable, but were not possible within the temporal constraints of this PhD project.

Secondly, it is possible that the characterisation of mean-annual surface $\delta^{11}B_{B(OH)_4^-}$ used here may result in some scatter in *G. bulloides* data. *G. bulloides* is a major constituent of seasonal or transient blooms, which may often be driven by periodic upwelling or deep mixing. As a consequence, *G. bulloides* may not always reflect mean annual pH (and thus $\delta^{11}B_{B(OH)_4^-}$) signals, and so comparison to mean annual $\delta^{11}B_{B(OH)_4^-}$ may be inappropriate. If this were to be the case, however, one might expect the dataset to be uniformly shifted towards the negative bounds of uncertainty in $\delta^{11}B_{B(OH)_4^-}$ (since upwelling waters will typically be of lower pH), rather than being scattered in either direction along the x-axis. Alternatively, but similarly, some of the scatter seen in *G. bulloides* may be as a result of uncertainty in the depth habitat of *G. bulloides*. Although the majority of studies report *G. bulloides* as mainly living in

the upper ~ 30m (e.g. Hemleben et al., 1989, Kahn, 1981), they may also be found (albeit less frequently) in waters of >60m depth (e.g. Schiebel et al., 1997). Thus comparison to surface water $\delta^{11}B_{B(OH)_4^-}$ may be inappropriate. That said, given that much of the intra-annual variability in $\delta^{11}B_{B(OH)_4^-}$ in surface waters at these sites is attributable to changes in the depth of mixing, much of the variability in $\delta^{11}B_{B(OH)_4^-}$ in the top 50-100 m should fall within the bounds of uncertainty in estimated $\delta^{11}B_{B(OH)_4^-}$. Furthermore, given that there is often considerable scatter even between different size-fractions from the same site (see Fig. 4.7 and Section 4.4.1.3), for this scatter to be explained by depth habit it would require not only depth-separation of size fractions, but also variability in size-depth habit relationships between sites.

Thirdly, it is possible that differing proportions of cryptospecies at different sites and in different size fractions may be responsible for some degree of the observed scatter. *G. bulloides* is known to encompass up to seven cryptic species (Darling and Wade, 2008, and references within), and it is possible that these cryptic species may record different $\delta^{11}B$ signals (perhaps as a result of differing metabolic rates, seasonality, etc.). Bemis et al. (1998) and Spero and Lea (1996) report anomalous $\delta^{18}O$ values in samples of *G. bulloides* that possessed distinctly more massive tests and an apparent gametogenic crust, that might conceivably represent a cryptic species, and might also manifest itself in $\delta^{11}B$ signals. At core-top site TAN1106/38, attempts were made to test for $\delta^{11}B$ differences between variant morphotypes of *G. bulloides*, as shown in Fig. 4.10, revealing no observable difference between 'flattened' or 'kummerform' types (see Table 4.2). Unfortunately comparisons such as these are often restricted by the prohibitive sample size requirements of *G. bulloides* (>300 tests of 300-355 μm size per measurement) for the generation of data of acceptable reproducibility, and as such no further tests were carried out. Certainly further testing would be beneficial in assessing the possibility of cryptospecies differences.

4.4.1.2 pH-sensitivity in *G. bulloides*

The slope of the new calibration for *G. bulloides* (m=1.01±0.29, 2σ) is greater than any of the previous calibrations constructed for planktic foraminifera (see Table 3.1), and is effectively equal to 1 (and therefore the pH-sensitivity of aqueous $B(OH)_4^-$; see section 1.3.3.3). This implies that, for *G. bulloides*, recorded pH is consistently offset

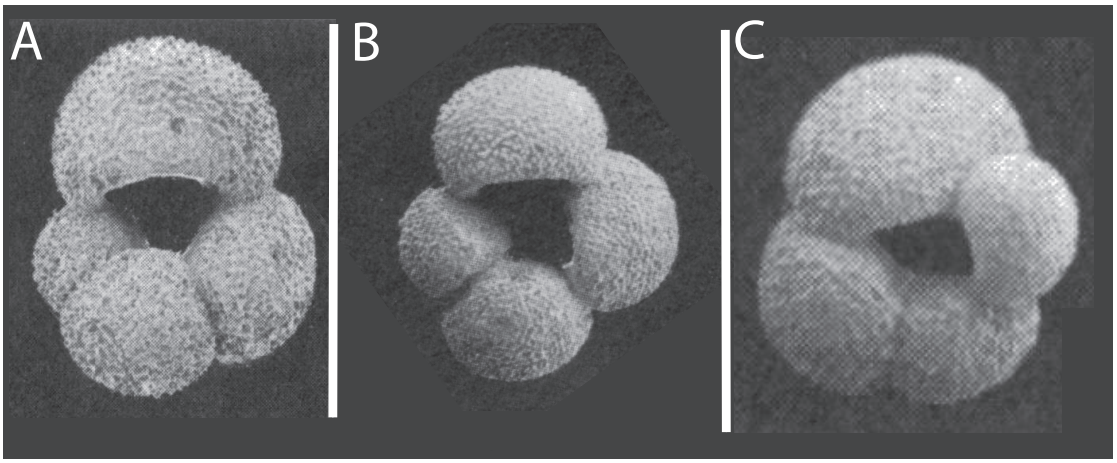

FIGURE 4.10: *G. bulloides* is a very morphologically variable species. Some examples of this variability are shown below: A, a more holotypic *G. bulloides*, B, a 'flattened', more squared morphotype, and C a 'kummerform' variant, with a diminutive final chamber. Images modified after Bandy (1972).

towards negative values compared with ambient pH. Such a pattern is in agreement with the modelled results of Zeebe et al. (2003), and as such constitutes further support for our current understanding of microenvironment alteration. Although the aforementioned scatter in *G. bulloides* data means that the bounds of uncertainty on this slope are large, it is clear from Table 4.1 that the weight of probability suggests that the observed slope for *G. bulloides* is steeper than any analogous calibration in symbiont-bearing species: there is only an 11% likelihood that the slope of the *G. bulloides* calibration equals that of *G. sacculifer* (Sanyal et al., 2001), a 9% likelihood that it equals that of *O. universa* (this study), and <1% likelihood that it equals that of *G. ruber* (Henehan et al., 2013). Moreover, in the context of other symbiont-barren species, it is more difficult to reconcile a shallower slope: if *G. bulloides* were to exhibit a pH sensitivity < 1, it would necessitate some mechanism through which an increasing offset between *G. bulloides* and other symbiont-barren species could arise at lower ambient pH (despite a hypothetically comparable vital effect, driven by the same factors). Nonetheless, although the observed higher pH-sensitivity calculated for *G. bulloides* seems probabilistically robust, culturing and tow collection of *G. bulloides* would be beneficial and would permit greater confidence in this calibration.

It is significant that *G. bulloides*, the only symbiont-barren species for which pH-sensitivity has been investigated to date (Yu et al. 2013 assume a pH-sensitivity equal to aqueous $B(OH)_4^-$ ion), displays the steepest calibration slope observed to

date, and pH-sensitivity permissively equal to that of aqueous $B(OH)_4^-$ ion. This observation implies, firstly, that earlier assertions of some universal boron isotope fractionation factor inherent in foraminiferal biomineralisation (Hönisch et al., 2007, Katz et al., 2010) were premature, and consequently to apply any 'empirical sensitivity' to downcore records (as in Raitzsch and Hönisch, 2013) is inappropriate. It also suggests that internal pH elevation, as advocated by Rollion-Bard and Erez (2010) as an explanation for foraminiferal vital effects, does not have a noticeable effect on planktic foraminiferal $\delta^{11}B$.

Another implication of this finding in symbiont-barren foraminifera is that the weaker-than-predicted pH sensitivity seen elsewhere in symbiont-bearing planktic foraminifera (Sanyal et al., 1996, 2001, Hönisch et al., 2009, Henehan et al., 2013, and *O. universa*, this study), if not a result of some inorganic fractionation, is likely a product of symbiont photosynthesis. While further modelling work, building on the work of Zeebe et al. (1999a, 2003), would be required to adequately test this hypothesis, one line of investigation to pursue might include changes in photosynthetic rate in dinoflagellate symbionts under low pH. For example, Brading et al. (2011) found some species of *Symbiodinium* dinoflagellates (found in corals and some benthic foraminifera, and a sister group of symbionts found in planktic foraminifera - see Spero 1987, Shaked and Vargas 2006) grow more rapidly under higher aqueous CO_2 ($[CO_2]_{aq}$). This is likely because of a preference for $[CO_2]_{aq}$ uptake over HCO_3^- (Colman et al., 2002, Dason et al., 2004). Given the pH-dependence of DIC speciation in seawater, the abundance of $[CO_2]_{aq}$ increases at lowered pH (Zeebe and Wolf-Gladrow, 2001, and references within). Consequently, lowering of ambient seawater pH may be mitigated in the microenvironments of symbiont-bearing foraminifera by photosynthetic symbionts more readily taking up DIC.

4.4.1.3 Size fraction effects in symbiont-barren species

The sizeable non-systematic variation in $\delta^{11}B$ between size fractions of *G. bulloides* is unsettling, and is difficult to explain. It is, however, perhaps not surprising, as this behaviour appears not to be unique to $\delta^{11}B$. Bemis et al. (1998) found that ontogenetic effects in $\delta^{18}O$ produced in culture were not reproduced in towed samples from the Northeast Pacific (Kahn, 1981). Absolute $\delta^{13}C$ disequilibrium and the

magnitude of size-fraction effects in *G. bulloides* have also been shown to differ geographically (specifically between the Chatham Rise, southwest Pacific, and the Southern California Bight Spero and Lea, 1996). In addition, trace element concentrations between and within tests and size fractions of *G. bulloides* are commonly variable (Anand and Elderfield, 2005, Marr, 2009). Most recently, Jonkers et al. (2013) report variable size fraction differences in δ^{13}C and δ^{18}O of *G. bulloides* that are much less consistent than those seen in *N. pachyderma*. These inconsistencies may be linked to variability in the proportion of metabolic carbon that is reincorporated during calcification (Spero and Lea, 1996), the effects of which may be more strongly recorded in δ^{11}B signals in *G. bulloides* because of a lack of pH buffering afforded in other species by the presence of symbionts.

As ever, interpretation of size fractions in core-top samples is limited by the nature of the material: core-tops represent an integrated signal of hundreds (if not thousands) of years, and of all depths in the water column. Therefore seasonality, depth preferences, hydrographic and biogeographic fluctuations, and indeed sampling bias cloud the any underlying signals of metabolism, etc. In addition, individuals above ~150 μm in diameter will all have undergone gametogenesis (Peeters et al., 2002), which must imply that individuals of differing sizes were subject to different conditions during their life cycle (e.g. food supply) to have undergone gametogenesis at different sizes. Recent evidence suggests, that shell size in *G. bulloides* may vary seasonally (Jonkers et al., 2013). As such, size fraction tests in core-tops and sediment traps provide a more holistic signal that also indirectly incorporates local environmental signals through their effect on test size. While core-top size fraction tests are useful in grounding palaeo-application studies, which use similarly time-integrated material, size fraction tests in tow material provide a 'snapshot' signal: an insight into variation in δ^{11}B caused only by intrinsic biological, ontogenetic changes, within fixed, well-characterised environmental conditions. Consequently, these tests are more helpful for understanding issues of foraminiferal physiology.

Our tow data from *G. inflata* suggest that larger individuals record a test-averaged microenvironmental pH that is ~0.12 pH lower than smaller individuals. It is unclear whether this is a trend towards increased respiration rates in larger individuals (consistent with their increase in mass; Zeuthen, 1953), or that those with higher metabolic rates when smaller (and thus respiration rates) had gone on to grow larger

(consistent with Schmidt et al., 2008). Amputation (as per Bemis et al., 1998, for example), or point-measurement via laser ablation ICPMS (LA-ICPMS, as per e.g. Anand and Elderfield, 2005, Marr, 2009), could prove useful in determining this. That said, for the observed differences to be caused by higher rates of respiration early in the ontogeny of those individuals that went on to grow larger, mass balance concerns would require drastically, and perhaps unfeasibly, divergent δ^{11}B in early chambers. It seems more probable, therefore, that the patterns observed are as a result of an increasingly acidified microenvironments as biomass (and therefore respiration rates) increase. This would agree with the models of Zeebe et al. (2003), but makes the lack of a comparable pattern in *G. bulloides* perhaps more puzzling.

4.4.2 Vital effects in *O. universa*

4.4.2.1 pH sensitivity in *O. universa*: comparison with Sanyal et al. (1996)

The slope (i.e. the pH sensitivity) of the new δ^{11}B calibration for *O. universa* presented here is very well constrained, thanks in part to the broad biogeographic (and thus *in situ* $\delta^{11}B_{B(OH)_4^-}$) range of *O. universa*, and in part to less scatter than is seen for *G. bulloides*. The slope of the new calibration is identical to that observed by Sanyal et al. (1996) in cultured *O. universa*, and corroborates their finding that pH sensitivity in *O. universa* is lower than that of aqueous $B(OH)_4^-$. The new calibration is, however, offset from their previous calibration by approximately - 3.3 ‰, and lies below the 1:1 line. Although this is unexpected, there seems little cause query analytical procedures- as shown in Chapter 2, measurements of absolute δ^{11}B in boric acid standards, reference carbonates and foraminifera measured at the NOCS are reliable, comparing favourably with other laboratories and agreeing with certified values where available. Instead it appears that Sanyal et al.'s (1996, 2000, 2001) data are subject to a laboratory-specific bias, presumably linked to analytical differences. As previously mentioned (section 4.1.2), core-top δ^{11}B measurements of *G. sacculifer* measured by MC-ICPMS are on average 3.32 ‰ lighter than those produced at Stonybrook via NTIMS: the same degree to which this new MC-ICPMS calibration of *O. universa* is offset from that of Sanyal et al. (1996)[1]. Correcting for this interlaboratory offset brings the two calibrations into close agreement (see Fig 4.11),

and supports the observation that the *O. universa* data of Sanyal et al. (1996) are lighter in δ^{11}B than inorganic precipitates of Sanyal et al. (2000).

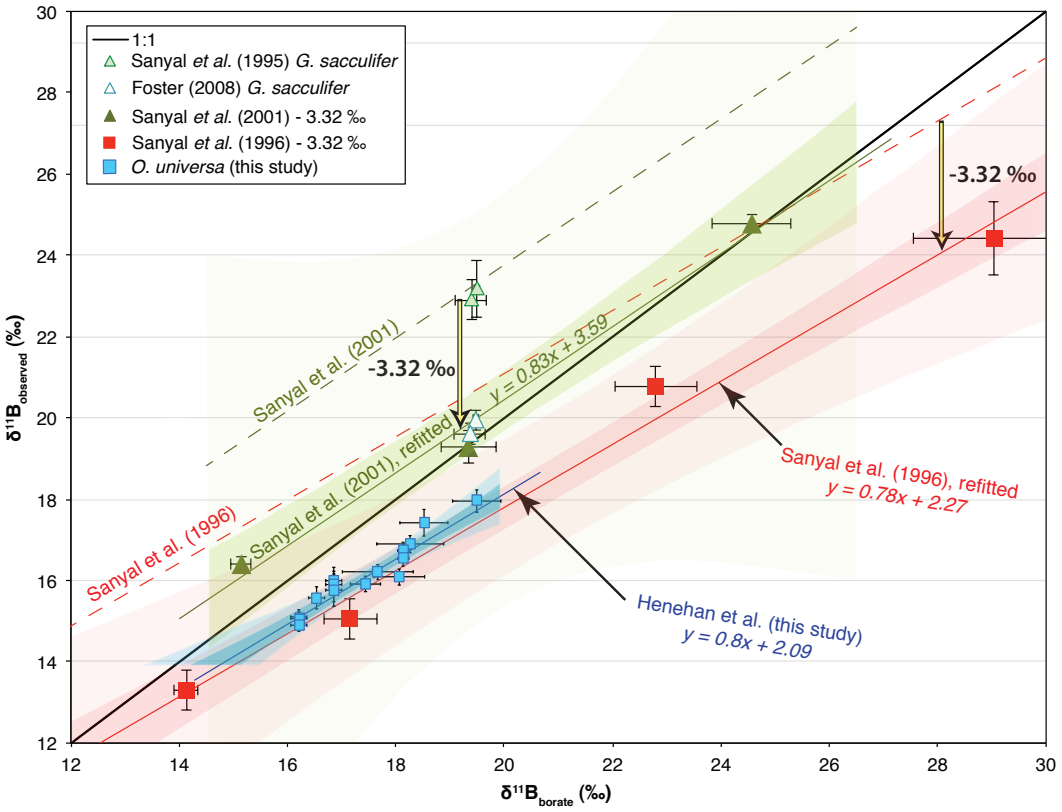

FIGURE 4.11: Illustration of the good agreement between the *O. universa* calibration of Sanyal et al. (1996) and this calibration once an interlaboratory offset is subtracted. For each calibration, uncertainty (shaded regions) is calculated as per Section 4.2.3, with shaded regions defining 1σ (heavily shaded) and 2σ (lightly shaded) confidence intervals. X- and Y-error bars for Sanyal et al. calibrations are derived from quoted uncertainties. Error bars on the new MC-ICPMS calibration of *O. universa* are as in Fig. 4.6.

That this new calibration for *O. universa* displays a pH-sensitivity that is steeper than *G. ruber* (to >99% confidence) may also be support for microenvironment effects being involved in determining pH-sensitivity (as discussed in section 4.4.1.2). If microenvironment pH is buffered by symbiont photosynthesis, dampening δ^{11}B response to reduced seawater pH, it would be expected that symbiont-bearing species that live at greater water depths (and lower light levels) would see weaker buffering effects from symbiont photosynthesis, and thus a greater sensitivity in δ^{11}B to ambient pH changes. Similarly, depth preference in *G. sacculifer* is also deeper than in *G. ruber* (Hemleben et al., 1989), which might explain its observed higher pH-sensitivity.

However, δ^{11}B in *G. sacculifer* is typically higher than in *O. universa*, which would reflect a stronger effect of symbiont photosynthesis, despite a similar pH-sensitivity in both species.

4.4.2.2 Variable vital effects in *O. universa*

While the differences between the *O. universa* calibration of Sanyal et al. (1996) and the one presented here might be explained by analytical differences, there remains an inconsistency within the MC-ICPMS data presented here. As can be seen in Table 4.4, one measurement from *O. universa* towed from the Gulf of Aqaba (Eilat) is considerably offset from other calibration data (by ∼+2.3‰). This datapoint shows no indication from trace element analysis for contamination, and δ^{11}B analysis showed no sign of irregularities, and therefore it must be concluded that (although only one datapoint) the signal is real. Indeed, this datapoint records values more similar to those expected from models of vital effects in *O. universa* (Zeebe et al., 2003).

One possible cause for the deviation seen in tow material from this site is the unusually high salinity levels (> 40) seen in the Gulf of Aqaba. Yet, data from other core-top sites show no correlation between salinity and deviation from predicted $\delta^{11}B_{B(OH)_4^-}$ within a range of salinity of 34.4 and 36.7 (Fig. 4.12), and as such this would seem unlikely.

Another possible explanation for the observed patterns in δ^{11}B is that *O. universa* from higher-productivity, eutrophic waters may have higher respiration rates (perhaps as a result of greater food supply), that outweigh the buffering effect of photosynthetic symbionts. This might be supported by a higher observed occurence of twin-orb *O. universa* in some of the higher-productivity higher-latitude waters sampled here, as the growth of twin orbs is favoured with high feeding rates (Bijma et al., 1992). In contrast, in Eilat, no twin-orbed *O. universa* were observed. Such a hypothesis is worthy of further testing in culture, although it should be noted that feeding rate was shown not to alter δ^{13}C in cultured *O. universa* (Spero, 1998), which might suggest an effect on δ^{11}B is unlikely.

[1]It should also be noted that Sanyal et al. (1996) measured core-top specimens and found them to agree with their culture calibration

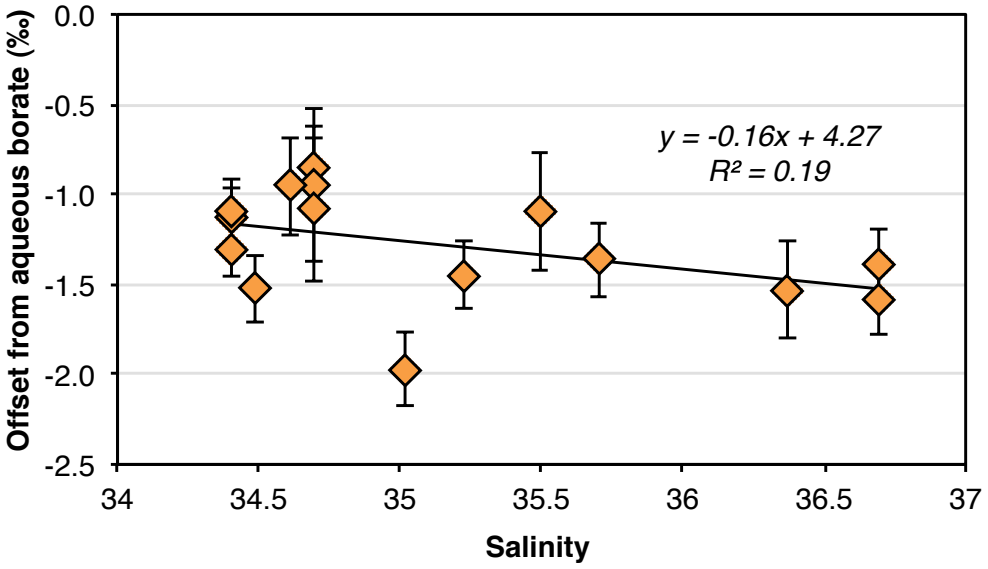

FIGURE 4.12: The difference between observed $\delta^{11}B_{CaCO_3}$ and ambient $\delta^{11}B_{B(OH)_4^-}$ in core-top, tow and trap *O. universa* analysed here is not correlated to ambient salinity. Note the datapoint from Eilat (S = 40.4) is excluded from this figure and the resultant regression, as to include it would skew the regression. Y-error bars are reproducibility of measurements from Equation 2.3.

Alternatively, it may be that the disparity in recorded $\delta^{11}B$ is linked to the presence of cryptic species in *O. universa*. Three genotypes (Types I, II and III) have been defined on the basis of small subunit (SSU) mRNA (Vargas et al., 1999, 2004, Darling and Wade, 2008), with Type I purported to be associated with oligotrophic conditions, Type II with extreme oligotrophic systems and Type III with high-productivity and upwelling regions. These cryptic genetic species have since been shown to correspond to specific morphotypes (similar to those described by Deuser et al., 1981), with high porosity making the Caribbean species (Type I) the most distinctive (Morard et al., 2009). It is possible that boron isotope variations may exist between these genotypes, which might explain the variable vital effects observed here. The mechanisms for differences between genotypes are unclear, however: Morard et al. (2009) see no segregation of genotypes of *O. universa* with depth, so if genotype variability is the cause of the observed variability in $\delta^{11}B$, it is not caused by any disparate depth preferences. It is possible that cryptospecies-specific differences in timing of calcification may exist. Spero and Parker (1985) note that photosynthetic rates in *O. universa* are not uniform within daylight hours. These authors observed that maximum photosynthetic rates in *O. universa* were not reached until midday; as such

$CaCO_3$ precipitated before this point, although perhaps considered 'day' calcite (Lea et al., 1995) may still record a microenvironment where respiration outweighs photosynthesis. Furthermore, although Lea et al. (1995) report ratios of day:night calcification of 3:1, recent studies of day:night banding in *O. universa* (Vetter et al., 2013) show roughly equal quantities of $CaCO_3$ precipitated during day and night (based on the thickness of bands). The variability of day:night calcification observed by Lea et al. (1995), also suggests that there may be some scope for differences in day:night calcification ratios between variants. However, invoking cryptospecies-specific differences in timing is speculative. In addition, although the Gulf of Aqaba (Eilat) is oligotrophic (e.g. Levanon-Spanier et al., 1979), Vargas et al. (1999) report the Type III high-productivity (or Meditteranean-type; Morard et al., 2009) genotype from this region, rather than the Type I oligotrophic variant. Given that this is also the genotype most prevalent in other regions sampled in this study, it seems difficult to explain the dichotomy of δ^{11}B signals through cryptospecies variations.

More likely, perhaps, is that habitat depth is driving the observed patterns, as a result of its association with irradiance (shown to affect vital effects in *O. universa*; Spero, 1992, Hönisch et al., 2003). Because *O. universa* migrates to below the euphotic zone during its life cycle (as observed in MOCNESS tows; Morard et al., 2009, L. Northcote, unpublished data), much of its calcification in the open ocean must occur below the photosynthetic compensation point, and hence a deep, respiration-driven signal should be preserved in core-top samples. In addition, because MOCNESS tows analysed here were from either 0 - 50 m (TAN1106/40-N9) or 50 - 100 m (TAN1106/24-N8, TAN1106/50-N8) depth intervals, it is likely that a large proportion of the $CaCO_3$ analysed was precipitated at low light levels. Spero and Parker (1985) report maximum photosynthetic rate (P_{max}) for *O. universa* at 386 μEinst $m^{-3}s^{-1}$. While Spero and Williams (1989) calculate a depth of approximately 40 m for these light levels (assuming a light attenuation coefficient of 0.04 m^{-1} from Tyler, 1975), in the region of our MOCNESS tows the light attenuation coefficient is 0.07 - 0.1 m^{-1}, and consequently light levels drop to 1% of surface irradiance at depths of between 43 to 70 m (Howard-Williams et al., 1995). As such it is probable that tow material analysed here experienced irradiation levels below those required to compensate for the acidifying effects of respired CO_2. In contrast, in Eilat, *O. universa* was collected from $<$ 10 m water depth, in a region where the euphotic zone stretches to up to 115 m

depth, and light attenuation is low (Stambler, 2006). In this way, high δ^{11}B in tows from Eilat might be caused by sampling individuals from high-light environments (where the effect of symbiont photosynthesis is strongest) before any ontogenetic migration to depth had taken place. However it should be noted that such a hypothesis, if the interlaboratory correction between δ^{11}B measurements at Stonybrook and the NOC (Fig. 4.11) is reliable, requires ambient laboratory lighting in Sanyal et al. (1996)'s culture calibration (no additional lighting was used) to be low enough to resemble conditions below the photosynthetic compensation point. Also, Hönisch et al. (2003) towed *O. universa* from depths of $<$ 20m, where irradiance was still above the light compensation for *O. universa*, yet these specimens still recorded 'dark'-type δ^{11}B signals, which would require these individuals to have recently migrated up from depth. One additional point that requires attention is how *O. universa* maintains symbiosis, if this species lives below the euphotic zone (or at least P_{max}) for a significant proportion of their life. Clearly further sampling (with careful consideration of morphospecies and symbiont density) and research is required to fully understand vital effects in *O. universa*.

4.4.2.3 No size fraction effect in *O. universa*

A further unexpected result, besides *O. universa* recording δ^{11}B below that of ambient $\delta^{11}B_{B(OH)_4^-}$, was the lack of any changes in δ^{11}B between size fractions in *O. universa* (see Fig. 4.8). Modelling of vital effects in *O. universa* (Zeebe et al., 2003) suggests that, if our understanding of microenvironment alteration is correct, one should expect to see increases in δ^{11}B of *O. universa* with size (depending on the proportionality of life processes to test radius that is assumed). In addition, Spero and Parker (1985) show that the number of photosynthetic symbionts found in *O. universa* scales with test size. However, other studies (e.g. Billups and Spero, 1995) also report a lack of size-related change in δ^{13}C in *O. universa*, which would also suggest that microenvironment perturbation due to photosynthetic activity does not affect larger individuals to any larger degree than smaller. Further tows from the Gulf of Aqaba (Eilat), to be carried out in the Autumn of 2013, will seek to address this issue.

4.5 Conclusions

This chapter, in conjunction with inorganic precipitate experiments (Chapter 1) provides good evidence that microenvironment alteration is the most likely cause of widely documented vital effects in planktic foraminifera. Firstly, symbiont-barren foraminifera consistently record δ^{11}B that is lower than that of ambient $\delta^{11}B_{B(OH)_4^-}$, consistent with hypothesised respiration-driven acidification of the diffusive boundary layer around the foraminiferal test. Secondly, pH sensitivity in symbiont-barren foraminifera is approximately equal to that of seawater $B(OH)_4^-$ ion, in agreement with models of vital effects in foraminifera that suggest that offsets in δ^{11}B from ambient $\delta^{11}B_{B(OH)_4^-}$ should be constant regardless of ambient pH. Thirdly, deep-dwelling symbiont-bearing species show lower absolute δ^{11}B and a greater pH-sensitivity than the shallow-dwelling species *G. ruber*, which may be consistent with a weaker buffering effect of photosynthesis at greater depth and thus lower light intensity. Finally, size-fraction changes in the δ^{11}B and trace element composition of *G. inflata* are consistent with increased respiration effects with size, as predicted by working models for the mechanisms of microenvironmental alteration.

This study also highlights areas where our previous understanding was perhaps lacking. The unexpectedly low δ^{11}B in *O. universa* observed here may be evidence of the importance of depth habit in determining the degree and direction of microenvironment alteration. Because these *O. universa* data are still heavier in δ^{11}B than *G. bulloides* and other symbiont-barren species (by $\sim$ 1-1.5 ‰; the same offset observed between *G. bulloides* and *O. universa* by Hönisch et al., 2003), and because the slope that they describe is less than unity, it seems that the effects of symbiont photosynthesis are still evident. However, these data suggest the net effects of respiration and calcification over the lifespan of open-ocean *O. universa* must outweigh those of photosynthesis, seemingly counter to the *in vitro* micro-environment observations of Rink et al. (1998) and the model of Zeebe et al. (2003) that is based, in part, on these observations. These data, then, call into question how representative culture and lab-based measurements of deep-dwelling symbiont-bearing foraminifera are of open ocean conditions. On a positive note, the new calibration is very well constrained and residual scatter in *O. universa* is seen to be low, so accurate and precise surface pH reconstructions using this species may be readily attainable,

providing the outlying tow datum from the Gulf of Aqaba (Eilat) is not evidence for biogeographic differences in vital effects.

In summary, this chapter extends the number of species for which MC-ICPMS δ^{11}B-pH calibration is available, broadening the scope of palaeo-pH reconstruction and providing a more solid basis to approach the question of foraminiferal vital effects. Although in the case of *O. universa* this chapter yields unexpected results and poses numerous questions, it is valuable both in highlighting previously unknown complications and priorities for future research work. While a new calibration for *G. bulloides* is also presented, δ^{11}B signals in this species appear to be more scattered than in other species, either because of variable depth habit, genotype, seasonality, vital effects (e.g. incorporation of metabolic CO_2), and/or propensity for contamination. As such it is advised that prior to downcore application of the calibration presented here, preliminary tests are undertaken at a given site to ensure first that the calibration produces valid estimates of late Holocene pH values. In addition, high resolution sampling and moving-average smoothing of trends may be advisable. Size fraction effects in *G. bulloides* are apparently inconsistent between sites and as such it may be advisable, when applying the calibration downcore, to test for size fraction differences at discrete intervals throughout the sampled core section. Alternatively, if size-fraction changes in δ^{11}B are shown to vary in magnitude and trend within core, it might be advisable to combine a broad range of size fractions for each analysis.

Chapter 5

A Cautionary Tale: assessing the applicability of B/Ca ratios in *G. ruber* as a proxy for the carbonate system

Abstract

Understanding carbon cycling in the past is crucial to deciphering the controls on the Earth's climate system, and hence to better predict the likely effects of future anthropogenic climate change. Given this importance, there has been great interest in the development of new proxies for the ocean carbonate system. One such proxy that is receiving much recent interest, given the well-documented pH-dependent speciation of boron in seawater, is the boron concentration of marine carbonates (expressed as B/Ca ratios). However, the carbonate system controls on B/Ca ratios appear not to be straightforward, with $\Delta[CO_3^{2-}]$, in the case of benthic foraminifera, often correlating best with B/Ca ratios, rather than pH, $\frac{B(OH)_4^-}{HCO_3^-}$ or $\frac{B(OH)_4^-}{DIC}$ as our understanding of the speciation of boron in seawater and its incorporation into $CaCO_3$ would predict. Furthermore, culture experiments have shown that in planktic foraminifera properties such as salinity and $[B]_{sw}$ have profound effects on B/Ca ratios beyond that predicted by simple partition coefficients. Here the controls on B/Ca ratios in *G. ruber* are

determined via a combination of culture experiments and core-top calibration, revealing previously unnoticed drivers of boron incorporation in this species, and suggesting that B/Ca ratios in foraminiferal carbonates are not a reliable proxy for past carbonate system conditions. Instead B/Ca ratios in *G. ruber* show greatest correlation with $[PO_4^{3-}]$ in seawater, suggestive perhaps of a rate or crystallographic control on boron incorporation.

5.1 Introduction

5.1.1 The B/Ca proxy in Planktic Foraminifera: theoretical basis

The B/Ca proxy has generated much interest as a potential carbonate system proxy, and indeed has been used in the reconstruction past atmospheric CO_2 levels (Yu et al., 2007b, Foster, 2008, Tripati et al., 2009, Yu et al., 2013). One reason why the B/Ca proxy has generated such interest is its hypothesised foundation in inorganic aqueous chemistry. Boron is almost exclusively present in seawater in one of two forms: the tetrahedrally-coordinated borate molecule, $B(OH)_4^-$, and the trigonally-coordinated boric acid, or $B(OH)_3$. Some boron does exist in polynuclear forms at typical seawater pH, but this amount is negligible under normal seawater boron concentrations (Su and Suarez, 1995). The relative proportions of the two species is dependent on pH, such that at low pH boron is entirely in the form of $B(OH)_3$, and at high pH it is found as $B(OH)_4^-$ (see Fig 5.1).

Since $B(OH)_4^-$, the charged ion, is thought to be only species of boron incorporated into $CaCO_3$, it was proposed that B/Ca ratios in $CaCO_3$ should increase with increased $[B(OH)_4^-]$ (Hemming and Hanson, 1992). Given that the relative abundance of $B(OH)_4^-$ is pH dependent (Fig. 5.1), B/Ca ratios in $CaCO_3$ should, then, respond to changes in the marine carbonate system. However, the speciation of boron in seawater is not the only control on B/Ca in $CaCO_3$: the site at which boron substitutes into the crystal lattice also has a part to play. Hemming and Hanson (1992) suggest that boron substitutes at the CO_3^{2-} site in $CaCO_3$, given the similarity of B-O and C-O bond lengths (0.137 and 0.128 nm respectively; Kakihana et al., 1977), although they also note the possibility that B resides in defect sites. Based on this assertion, Hemming and Hanson (1992) proposed the formula for boron

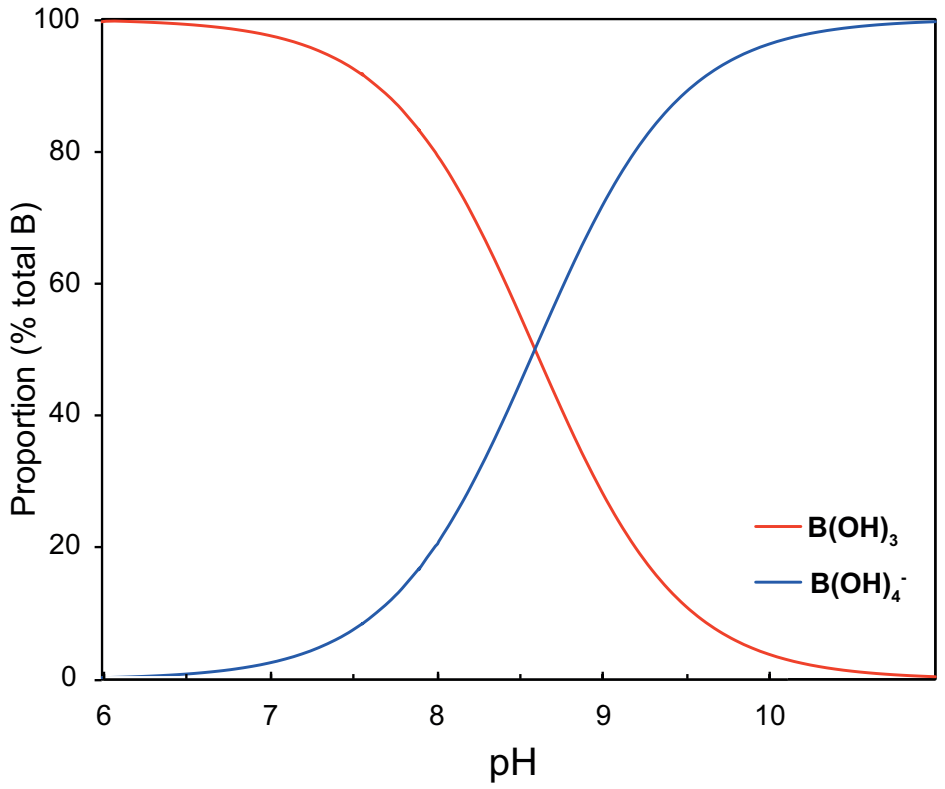

FIGURE 5.1: The relative abundances of the two most abundant boron species in seawater, at 25 °C and S = 35 psu. Boric acid, $B(OH)_3$, is marked in red, while borate ion, $B(OH)_4{}^-$, is marked in blue.

substitution into $CaCO_3$ described in equation 5.1 below.

$$CaCO_{3_{solid}} + B(OH)^-_{4_{aqueous}} \Rightarrow Ca(HBO_3)_{solid} + HCO^-_{3_{aqueous}} + H_2O \tag{5.1}$$

By extension, they defined the exchange distribution coefficient (K_D) for this reaction as

$$K_{D^B_{calcite}} = \frac{[HBO_3^{2-}/CO_3^{2-}]_{solid}}{[B(OH)_4^-/HCO_3^-]_{fluid}} \tag{5.2}$$

which was later shortened (Yu et al., 2007b, Zeebe and Wolf-Gladrow, 2001) to

$$K_{D^B_{calcite}} = \frac{[B/Ca]_{solid}}{[B(OH)_4^-/HCO_3^-]_{fluid}} \quad . \tag{5.3}$$

Consequently, if this mechanism for incorporation is correct, B/Ca ratios in foraminifera should be dependent not only on the pH-driven speciation of boron species, described above, but on the speciation of aqueous dissolved inorganic carbon

(DIC) compounds that compete for incorporation sites (also dependent on pH, temperature, pressure and salinity; Zeebe and Wolf-Gladrow, 2001). Inorganic precipitation experiments (Hemming et al., 1995, Sanyal et al., 2000, He et al., 2013) and culture experiments of marine calcifiers (Sanyal et al., 1996, 2001, Allen et al., 2011, 2012, and this study) suggest that pH (and thereby aqueous $[CO_3^{2-}]$) is indeed a strong control on B/Ca ratios in $CaCO_3$. However, culture experiments (Allen et al., 2011, 2012) also demonstrate that the controls on boron incorporation in foraminifera are more complex and more numerous than previously thought. Other variables (besides pH) that have been suggested to influence recorded B/Ca include temperature (Wara et al., 2003, Yu et al., 2007b, Tripati et al., 2009), salinity (Allen et al., 2011), boron concentrations in seawater (Allen et al., 2011), crystal growth surface processes (Hemming et al., 1995, 1998), post-depositional dissolution (Ni et al., 2007, Seki et al., 2010, Coadic et al., 2013) and foraminiferal physiology and ontogeny (Ni et al., 2007, Allen et al., 2011, 2012). Furthermore, down-core applications of the B/Ca proxy (Yu et al., 2007b, Foster, 2008, Tripati et al., 2009, Palmer et al., 2010) that are based on the pH-dependency of B/Ca and the empirical boron partition coefficient (K_D; defined in equation 5.3 above), have been shown to be flawed: such studies may produce artificial records of carbonate system changes that are in fact wholly derived from variations in the denominator of K_D, entirely independent of variations in measured B/Ca (Allen and Hönisch, 2012). In fact, raw foraminiferal B/Ca ratios in these studies bear little relation to ice core pCO_2 records, and hence ocean pH (see Allen and Hönisch, 2012, Fig. 7), nor $\delta^{11}B$ reconstructions from the same locations (Palmer et al., 2010). In contrast, B/Ca ratios in *N. pachyderma* (Yu et al., 2013) do appear to be controlled by the *in situ* marine carbonate system, and track atmospheric pCO_2 downcore. Clearly, then, there is a need for further research into the controls on boron incorporation in foraminiferal calcite if B/Ca ratios in foraminifera are to prove a useful and reliable tool in palaeoceanography. Below these various factors proposed as influencing B/Ca ratios in foraminifera are discussed: namely, temperature, salinity, boron concentrations in seawater, crystal surface processes, post-depositional dissolution and foraminiferal life processes.

Temperature should influence boron incorporation through its influence on K_1, K_2 and K_B constants, which in turn alter $\frac{B(OH)_4^-}{HCO_3^-}$ ratios in seawater. However, this effect is small, and likely beyond the limits of analytical detectability. Neither cultures of *O.*

universa between 18 - 26 °C by Allen et al. (2011), nor cultures of *G. ruber* and *G. sacculifer* from 24 - 30 °C by Allen et al. (2012) show a significant relationship between B/Ca and temperature. As such, in in spite of the conclusions of some earlier studies (e.g. Wara et al., 2003, Yu et al., 2007b, Tripati et al., 2009), it now seems difficult to support a discernible temperature effect on foraminiferal B/Ca. Instead observed temperature relationships are likely either an artefact of interpreting B/Ca ratios in terms of K_D ($K_D = \frac{B/Ca}{B(OH)_4^-/HCO_3^-}$, as in Yu et al., 2007b, Foster, 2008, Tripati et al., 2009), which may produce artificial relationships (due to the effect of temperature on the denominator; see Allen and Hönisch, 2012, for further discussion), or alternatively a product of the correlation of temperature with $[CO_3^{2-}]$, as may be the case in Yu et al. (2007b). In light of these recent culture observations, also, it seems likely that down-core correlations of B/Ca with Mg/Ca-derived SST (Wara et al., 2003, Yu et al., 2007b) arise either coincidentally, as a result of diagenesis, or as a result of some process that influences both B/Ca and Mg/Ca (e.g. salinity, Kisakürek et al., 2008, Allen et al., 2012).

Although pure thermodynamics would normally imply a temperature effect on trace element partition coefficients between fluid and crystal (see for example Blundy and Wood, 1994), the incorporation of trace elements in calcite has been shown to not adhere to equilibrium thermodynamics (Rimstidt et al., 1998), due to surface site-related and rate-related kinetic effects. Moreover, thermodynamic models and theoretical studies have typically focussed on monoatomic cations (such as Mg^{2+} and Sr^{2+}), whereas boron is incorporated as the molecular anion $B(OH)_4{}^-$, and so the criteria used to estimate surface incorporation in these models (ionic radius and simple point charge distributions) are not sufficient to accurately predict adsorption and incorporation (Cheng, 1998, Masel, 1996, Effenberger et al., 1981). Beyond these considerations, the propensity for biological mechanisms to modulate crystal growth rate (potentially a key factor in determining K_D; Ruiz-Agudo et al., 2010) make comparisons with purely inorganic systems difficult. As such, it is perhaps unsurprising that any influence of temperature on foraminiferal boron incorporation is poorly supported by observation.

As with temperature, salinity will alter the equilibrium constants of seawater, and in turn should affect $\frac{B(OH)_4^-}{HCO_3^-}$, and hence B/Ca. However, Allen et al. (2011, 2012) found salinity to have a much larger effect on B/Ca ratios in planktic foraminifera than that

expected from the alteration of equilibrium constants alone. This salinity effect might be partially explained by an increase in $[B]_{sw}$ at high salinities: Allen et al. (2011) note that increasing $[B(OH)_4^-]$ by raising total $[B]_{sw}$ at a constant pH resulted in a disproportionately large response in B/Ca compared to experiments where $[B(OH)_4^-]$ was increased through pH-dependent speciation. This disproportionate effect of $[B]_{sw}$ may be a product of competition between B and other ions (e.g. CO_3^{2-}, or alternatively, other impurities- see below) for incorporation sites. However, it is also possible that increasing salinity may significantly raise B/Ca without any elevation of $[B]_{sw}$. For example, Kitano et al. (1978a) found that boron incorporation into inorganically precipitated $CaCO_3$ rose with the addition of pure NaCl (i.e. with no concurrent rise in $[B]_{sw}$), which suggests that there is some other effect, perhaps linked to ionic strength affecting crystal surface processes, or ion pairing in solution.

Indeed, crystal surface processes have been shown to have a strong effect on boron incorporation into inorganic precipitates. Hemming et al. (1995) highlight that increased boron incorporation in inorganically-precipitated aragonite (where, they argue, B is incorporated in tetrahedral form without need of re-coordination, following Sen et al., 1994) relative to calcite is evidence for the kinetic requirements of boron re-coordination being an incorporation-limiting factor. Boron doping in inorganic precipitation experiments (e.g. Ruiz-Agudo et al., 2012) disrupts orderly crystal growth patterns, illustrating that incorporation of boron necessitates reorganisation of lattice and growth face structures. These studies suggest that slower rates of calcite crystal precipitation are key to the levels of B incorporated, as they permit more complete re-coordination of tetrahedral boron into trigonal form. In addition, Hemming et al. (1995) and Hemming et al. (1998) also suggest that boron incorporation may be dictated by the availability of defect or anion sites, which in turn is dependent on both the structure of the growing crystal face, and the degree to which these sites may be occupied by other competing impurities. In this way crystallographic processes, or other chemical substitutions that might drive an increase in the number of defects sites, may produce elevated B/Ca ratios. This would also be supported by the findings of Hobbs and Reardon (1999). It is perhaps surprising, then, that these sorts of influences have been largely overlooked by the palaeoceanographic community.

A final inorganic factor which may affect the measured B/Ca of foraminifera is post-mortem dissolution and recrystallisation in the water column, at the

sediment-water interface, and/or following burial. Ni et al. (2007) note decreasing TE/Ca ratios in smaller size fractions of *G. sacculifer* and *G. ruber*, which they interpret as loss of impurities with dissolution (because smaller tests have a large surface:volume ratio and are more susceptible to dissolution). More conclusive, however, are the data of Seki et al. (2010) and Coadic et al. (2013), that show that B/Ca in core-top sediment samples of *G. sacculifer* decreases systematically along depth transects, as waters at the sediment interface become more corrosive. Results for *G. ruber* are less conclusive (Seki et al., 2010), but suggest only a minor dissolution effect on B/Ca in this species (at least at $\Omega_{CaCO_3} > 0.9$). The influence of diagenesis on B/Ca in the sediment column has yet to be investigated. Any dissolution effect could, however, constitute a significant barrier to the successful application of the B/Ca proxy, particularly over large events such as the PETM, where the lysocline may have fluctuated and the intensity of deep-sea carbonate dissolution may have varied.

Inorganic processes aside, the life processes of the foraminifera may also affect boron incorporation into carbonates, and cause further deviation from the the inorganic basis of the proxy. The large interspecific differences in B/Ca between planktic foraminifera (see for example Allen et al., 2012), and between planktic and benthic foraminifera (see for example Foster, 2008), show that boron incorporation must be (to some extent) biologically mediated. The difference in B/Ca between various species of planktic foraminifera seems consistent with existing theories of microenvironment alteration (see Section 1.4.2.3). Firstly, increasing B/Ca from *O. universa*<*G. sacculifer*<*G. ruber* is similar to the increase in δ^{11}B between these species (see Chapter 4), and indeed the progressive shallowing of depth habitats (and increasing illumination and symbiont photosynthesis) in these species (Hemleben et al., 1989). Secondly, symbiont-bearing planktic foraminifera tend to record higher B/Ca ratios than symbiont-barren planktic foraminifera, which would be consistent with a lower microenvironment pH (and thus $\frac{B(OH)_4^-}{DIC}$) in those foraminifera that do not possess photosynthetic symbionts. Thirdly, increasing B/Ca with size fraction, as seen by Ni et al. (2007), if not caused by post-depositional dissolution, might be caused by intensification of vital effects with increasing size, as suggested by Henehan et al. (2013). Finally, observed patterns of intratest variability are permissively consistent with day:night microenvironment pH fluctuations (*O. universa* LA-ICPMS profiles; Allen et al., 2011) or pre-gametogenic expulsion of symbionts (*G. sacculifer* final

chambers; Allen et al., 2012). That said, the scale of disparity in B/Ca between benthics and planktics (a 2× to 4× increase in benthics) might imply some difference in biomineralisation pathways, since the microenvironment of symbiont barren benthic foraminifera experiences no pH elevation (Glas et al., 2012a).

5.1.2 Outstanding issues

To date, the clear carbonate system control on B/Ca ratios of planktic foraminifera that is seen in culture (Allen et al., 2011, 2012) has not always been reproduced in open ocean planktic foraminifera, with correlations between B/Ca and $\frac{B(OH)_4^-}{HCO_3^-}$ or $\frac{B(OH)_4^-}{DIC}$ clouded by a possible temperature effect not seen in culture (Yu et al., 2007b), or in other cases simply absent (Foster, 2008). As such, as encouraged by Allen and Hönisch (2012), core-top calibration over a broad geographic and hydrographic sample set is required, to better determine the dominant environmental controls on boron incorporation. Given also the possibility of dissolution effects on B/Ca ratios (as shown by Coadic et al., 2013, in the related species *G. sacculifer*), comparison of B/Ca ratios in *G. ruber* sample material from varying post-depositional calcite saturation states is required. Finally, in addition to testing the environmental controls on boron incorporation, the potential influence of biotic factors, or 'vital effects' (such as an increase in B/Ca with ontogeny), must also be better understood before B/Ca could be applied to extinct species of planktic foraminifera.

5.2 Methods

5.2.1 Culture experiments in *G. ruber*

Data from cultured *G. ruber* comes from the experiments of Henehan et al. (2013), and therefore the reader is referred to Chapter 3 for details of culturing protocol and carbonate system control (Section 3.2). TE/Ca ratios for cultured material, similar to δ^{11}B, are obtained via mass-balance calculations, as described in equation 5.4 below.

$$\mathrm{TE/Ca}_{culture} = \frac{\mathrm{TE/Ca}_{bulk} - (\mathrm{TE/Ca}_{controls} * P^{mass}_{controls})}{P^{mass}_{culture}} \tag{5.4}$$

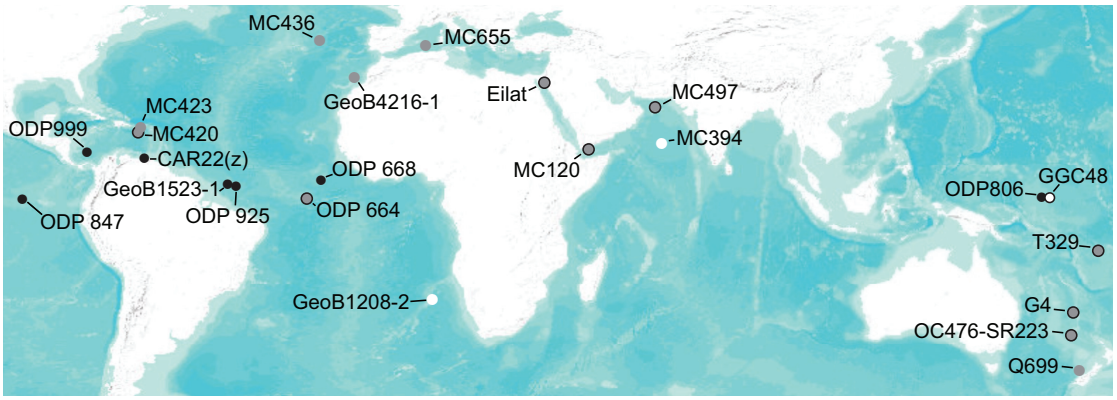

FIGURE 5.2: Locations of core-top and sediment trap samples used in this study. White circles are mixed morphotype coretop sites, grey circles are *G. ruber sensu lato* only, black circles are *G. ruber sensu stricto* only, white circles with a black outline are sites where mixed morphotype and *G. ruber sensu stricto* only measurements were taken, and grey circles with a black outline are sites where both morphotypes were measured.

$P^{mass}_{controls}$ is the proportion of mass calcified prior to culture, while $P^{mass}_{culture}$ is the proportion of mass grown in culture. To determine this, initial pre-culture mass was estimated from starting diameter using a calculated size:mass relationship (equation 3.1 and figure 3.6) of Henehan et al. (2013), and end-culture mass was determined by weighing of cultured tests. $TE/Ca_{controls}$ is the trace element composition of *G. ruber* towed at the time of the collection of cultured individuals, while TE/Ca_{bulk} is the measured trace element ratio composition of post-culture material.

5.2.2 Site and Sample Selection

To investigate the controls on B/Ca ratios in foraminifera outside of controlled culture conditions, *G. ruber* were analysed from geographically disparate core-top sites (from archives at Tübingen and NIWA, Wellington). In addition, sediment trap sample material from the Cariaco Basin and towed specimens from Eilat were analysed, with the aim of investigating post-depositional alteration. To expand the dataset still further, core-top B/Ca data from Foster (2008) are also included in analyses, but with carbonate system parameters re-estimated following Henehan et al. (2013) for consistency.

5.2.3 Carbonate System Characterisation

Carbonate system calculations for culture experiments are described in Henehan et al. (2013). For core-top samples, also following Henehan et al. (2013), pre-industrial carbonate system parameters are estimated using the Takahashi et al. (2009) database of global SST, salinity and CO_2 fluxes, modelled post-industrial carbon system changes from Gloor et al. (2003), and nutrient data from GLODAP and CARINA databases (Key et al., 2004, 2010). For full discussion of these methods the reader is referred to Section 3.2.2.2. In addition, mean annual surface water $[PO_4^{3-}]$ at each site is obtained from World Ocean Atlas (WOA; Garcia et al., 2010).

5.2.4 Sample Preparation

Foram cleaning throughout is largely as described in Rae et al. (2011) and (Henehan et al., 2013), in turn based on the approach of Barker et al. (2003). Foraminifera (cleaned in batches of < 3 mg[1]) are cracked open between two clean glass slides, ultrasonicated and rinsed repeatedly with Milli-Q ultrapure water (18.2 MΩ) to remove clays. For tow and sediment trap samples, where clay is not a major contaminant, as little as three rinses were carried out (to minimise sample loss), but usually the in core-top samples, five or more rinses are required to remove all visible clay material. Culture, sediment trap and tow samples, in agreement with other culturing studies (e.g. Russell et al., 2004), were subject to intensified oxidative cleaning (3 x 20-30 min treatments of 250-400 μl (depending on sample size) 1% H_2O_2 in 0.1 M NH_4OH_4 at 80 °C) to account for the larger organic content. In core-tops, oxidative cleaning was shorter (3 x 5 min) to minimise sample loss. Samples are then subject to a brief weak acid leach in 0.0005 M HNO_3 to remove any readsorbed contaminants. Finally 200 μl of Milli-Q is added to each sample (to slow subsequent dissolution and reduce the likelihood of leaching of B off any remnant contaminants) and 0.5 M HNO_3 (normally <300 μl) added incrementally until dissolved. To ensure complete removal of clays and other contaminants, samples are centrifuged for > 5 min at 1400 rpm, and the last ~ 20 μl discarded.

[1]Such large sample sizes were used because these same samples were often, but not always successfully, analysed for boron isotopes; see Chapter 2.

5.2.5 ICP-MS analysis

Trace element analysis was carried out on Thermo Element ICP-MS at the National Oceanography Centre, Southampton (NOCS; core-tops and sediment traps) and the Bristol Isotope Group (BIG; cultures and tows). Analysis of common consistency standards ensures no bias exists between these two laboratories in measurements of the trace elements (e.g. B/Ca, Li/Ca, Mg/Ca, Sr/Ca etc). This is despite slight differences in sample introduction system: typical Ar sample gas flow through the nebuliser at BIG is ∼1.2 L/min, while at NOCS sample gas input is fixed at 0.7 L/min, and an additional gas supply (typically to ∼ 0.4-0.45 L/min) is added directly into the spray chamber to reduce strain on nebuliser tips. In both laboratories a Teflon barrel spray chamber is used, and ammonia gas (0.07 L/min) is added to convert sample $B(OH)_3$ to $B(OH)_4^-$ (which is more easily washed out), following Al-Ammar et al. (2000).

Tuning is performed on a 0.1 ppb multielement tune solution (with 0.5 ppb of Boron) to optimise sensitivity while minimising the presence of oxides (to this end, UO is monitored and the ratio of UO to U counts kept to below 7%). Typical counts for B, In and U are 20-50 kcps, 70-100 kcps and 100-140 kcps respectively. Prior to each analytical session, in-house consistency standards (CS1, 2 and 3; B/Ca ratios of ∼ 196, 492 and 38 μmol/mol respectively) are analysed at a range of concentrations (typically 0.5 mM Ca, 1mM Ca and 2mM Ca) to monitor machine performance. The best reproducibility of element ratios on measured via ICPMS is found when samples and their bracketing standards are measured at the same concentration (Yu et al., 2005). To this end, an aliquot of each sample (typically 20 μl) is further diluted in 0.5 M HNO_3 (typically 200 μl) and analysed for [Ca] and (at lower confidence) [B]. Based on these results, samples are diluted with 0.5 M HNO_3 to match standard concentration. The bracketing standard used is an in-house gravimetric standard (BSGS+B2), with measurement blocks as shown in Table 5.1.

5.2.6 Statistical analyses

Multiple linear regressions were carried out using *R* statistical software (www.r-project.org). Non-contributing parameters were removed from models according to their contribution to the model's Akaike Information Criterion (AIC;

Blank
BSGS+B2
Blank
Sample 1
Blank
Sample 2
Blank
Sample 3
Blank
BSGS+B2
Blank

TABLE 5.1: Typical measurement block for trace element analysis on the Element MC-ICPMS. Blank used is 0.5M teflon-distilled 0.5M HNO_3. BSGS+B2 and samples are diluted to the same [Ca].

Akaike, 1974). This parameter describes the relative quality of each of a set of statistical models derived from a set of data, based on the compromise between the complexity of each model and its goodness-of-fit. Thus, if the addition of a parameter makes no positive contribution to the AIC, the parameter is omitted from the model. To better illustrate the relative importance of each environmental parameter (in addition to the t and p values given), the *relaimpo* package (Groemping, 2006) is used. Following the recommendation of Groemping (2006), we estimate relative importances via the *lmg* approach, based on the work of Lindemann et al. (1980). This removes the otherwise sizeable influence of factor ordering (i.e. which factor is entered into the model first) on the relative importance metric, by averaging out relative importances computed from all factor ordering permutations. 95% confidence intervals on these relative importances are calculated via bootstrapping: 1000 repeated samplings from the residuals of the regression model (following Hesterberg et al., 2005).

5.3 Results

5.3.1 *G. ruber* from culture

B/Ca ratios from culture data are shown in Figure 5.3 below. These data show a strong positive correlation with pH, $\frac{B(OH)_4^-}{DIC}$ and $\frac{B(OH)_4^-}{HCO_3^-}$. Compared to cultures of *G. ruber* (pink) (Allen et al., 2012), these new data show a much more linear relationship.

5.3.2 *G. ruber* from core-tops and sediment traps

The results of B/Ca measurements in coretop and sediment trap samples of *G. ruber* are given in Table 5.2. Coretop and sediment trap data show no strong relationship with either pH, $\frac{B(OH)_4^-}{HCO_3^-}$, or $\frac{B(OH)_4^-}{DIC}$ (see Fig. 5.4). Also, unlike in benthic foraminifera (Yu and Elderfield, 2007, Rae et al., 2011, Brown et al., 2011), there is no correlation evident between B/Ca and $\Delta[CO_3^{2-}]$ (R^2=0.02). Regression plots with other environmental parameters ($[PO_4^{3-}]$, salinity, Ω_{CaCO_3} at the site of deposition, and sea surface temperature), morphotype and test size are given in Fig. 5.5. To better determine the nature of other controlling factors on boron incorporation, the effect of $\frac{B(OH)_4^-}{DIC}$ from culture (the strongest controlling factor in Allen et al. (2012) and in this study, Fig. 5.3) was removed, and the residual variation from the linear B/Ca-$\frac{B(OH)_4^-}{DIC}$ culture calibration (B/Ca= 1378.2($\frac{B(OH)_4^-}{DIC}$) + 97.51; see Fig. 5.3) was also tested. Correlations between these environmental parameters and residual variation from the culture B/Ca-$\frac{B(OH)_4^-}{DIC}$ relationship are shown in blue. Note that residual B/Ca (i.e. the deviation from the culture calibration of B/Ca-$\frac{B(OH)_4^-}{DIC}$) is always negative, signifying that cultures were always elevated in B/Ca relative to open ocean samples.

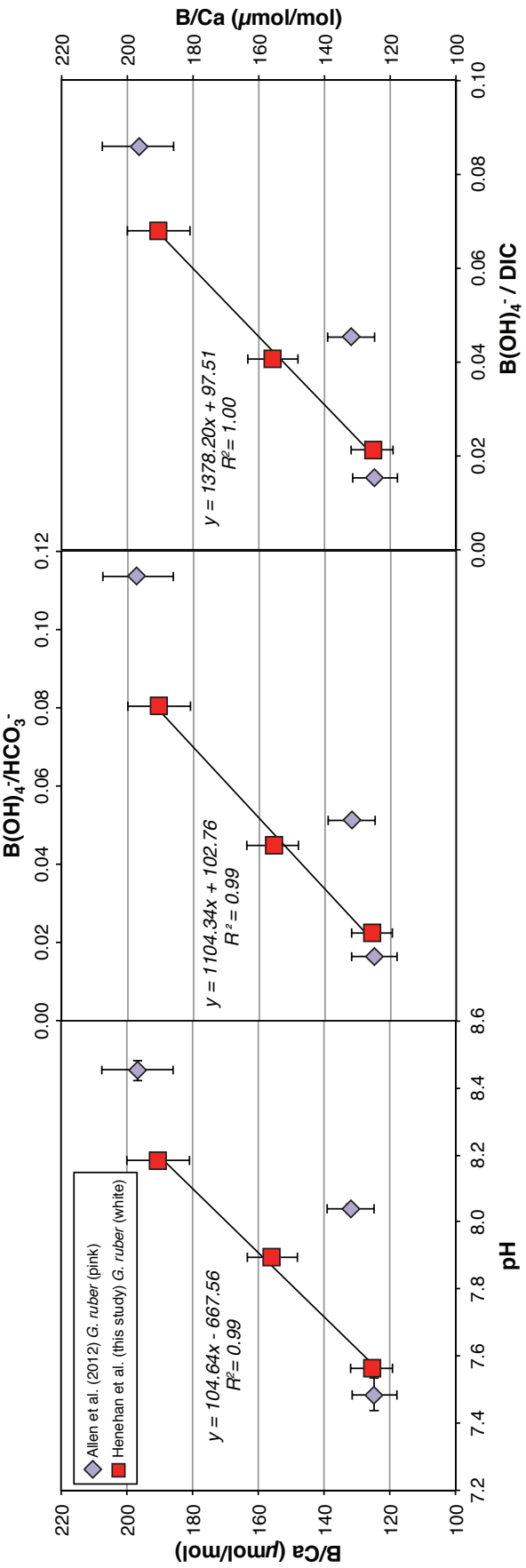

FIGURE 5.3: Changes in B/Ca ratios observed in cultures of *G. ruber*, in response to carbonate system changes. Also plotted are data from *G. ruber* (pink) from Allen et al. (2012). Error bars for B/Ca ratios in *G. ruber* (white) are 5% analytical uncertainty, while for *G. ruber* (pink) they are as stated in Allen et al. (2012).

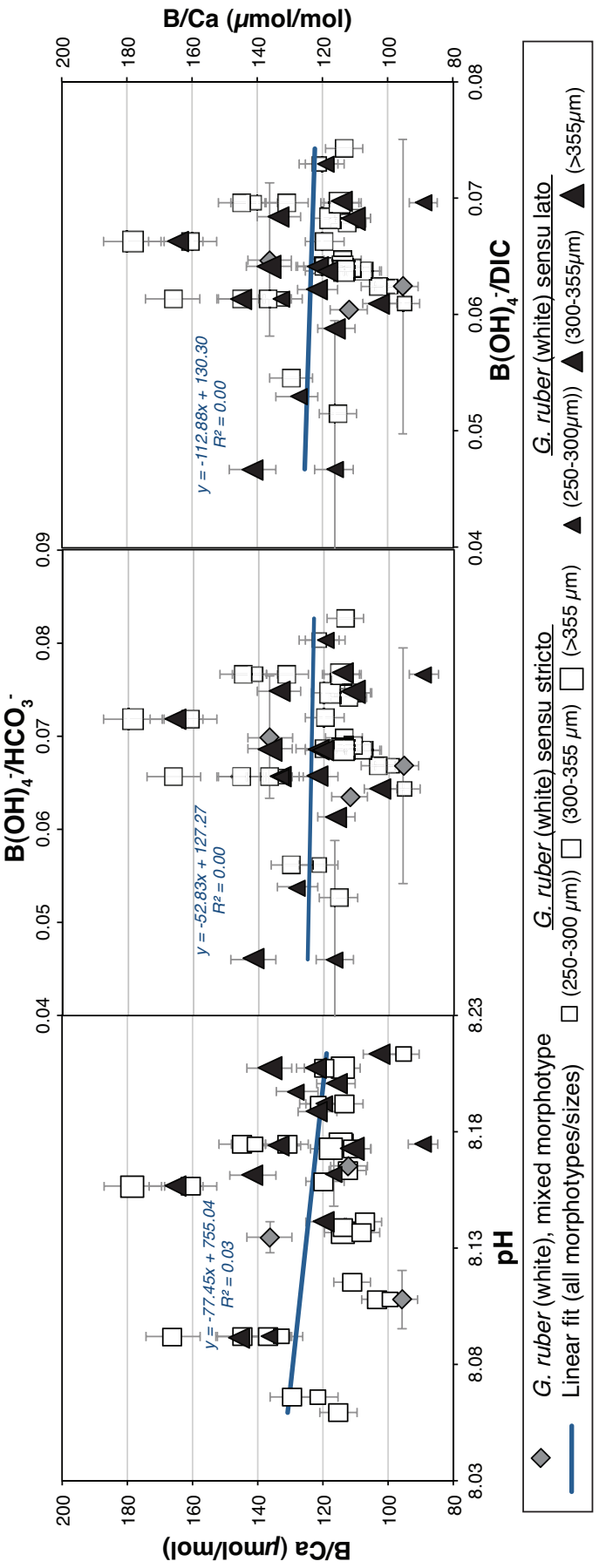

FIGURE 5.4: Core-top and sediment trap *G. ruber* show no correlation between B/Ca and either pH, $\frac{B(OH)_4^-}{HCO_3^-}$, or $\frac{B(OH)_4^-}{DIC}$. Grey diamonds denote mixed morphotype samples, open squares denote *sensu stricto*, and black triangles denote *sensu lato*. Error bars are 5% analytical uncertainty (on B/Ca) and 2σ of intraannual variability in pH at each coretop site.

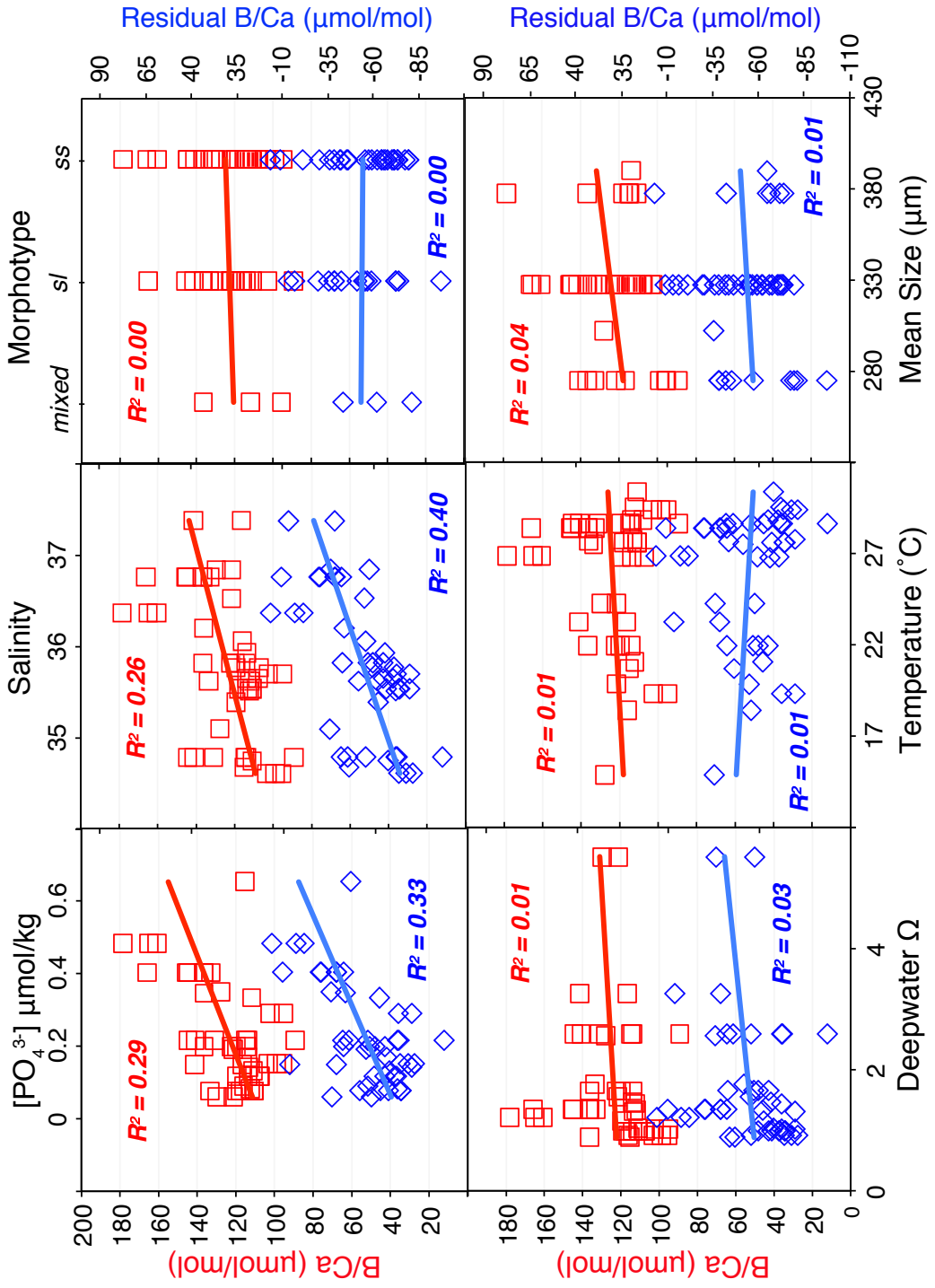

FIGURE 5.5: B/Ca ratios (red) and residual B/Ca once the effect of $\frac{B(OH)_4^-}{DIC}$ from culture is removed (blue) in open-ocean specimens of *G. ruber* (white, both morphotypes), compared to environmental parameters. Note that despite no correlation between B/Ca and $\frac{B(OH)_4^-}{DIC}$ being evident (Fig. 5.4), plotting against the residuals from the relationship seen in culture (assuming this relationship is reproduced in the open-ocean but is obscured by other controls) often results in improvements in fit.

Site	**Description**	**Size fraction**	**Lat (°N)**	**Long (°E)**	**Temp (°C)**	$\pm 2\sigma$	**Salinity**	$\pm 2\sigma$	**Deep** Ω	$\mathbf{PO_4^{3-}}$	**pH**	$\pm 2\sigma$	$\frac{B(OH)_4^-}{HCO_3^-}$	$\frac{B(OH)_4^-}{DIC}$	**B/Ca (μmol/mol)**	**Residual B/Ca**
MC394	mixed morph	300-355	14.38	64.57	27.67	2.24	36.20	0.35	0.88	0.346	8.135	0.020	0.0699	0.0597	136.3	-43.6
GGC48	mixed morph	250-300	0.00	161.00	29.41	0.36	34.61	0.51	0.92	0.151	8.108	0.064	0.0668	0.0574	95.6	-81.1
GeoB1208-2 **	mixed morph	300-355	-24.49	7.11	21.05	3.64	35.62	0.19	1.33	0.334	8.165	0.044	0.0635	0.0555	112.0	-62.0
MC655	*sensu lato*	250-300	38.42	5.40	23.23	3.00	37.38	0.20	3.26	0.15	8.161	0.050	0.0460	0.0418	116.6	-38.5
T329	*sensu lato*	250-300	-12.96	173.57	28.63	1.45	34.79	0.24	2.59	0.215	8.175	0.023	0.0766	0.0647	89.2	-97.4
MC120	*sensu lato*	250-300	12.47	45.38	28.38	5.55	36.76	1.23	1.34	0.403	8.092	0.068	0.0656	0.0564	136.4	-38.8
Eilat	*sensu lato*	250-300	29.50	34.92	23.76	4.25	40.40	0.22	4.48	0.129	8.192	0.008	0.0803	0.0679	119.4	-71.8
Q699	*sensu lato*	250-355	-42.42	169.30	14.88	3.53	35.10	0.25	2.57	0.35	8.197	0.005	0.0538	0.0480	127.9	-35.7
MC655	*sensu lato*	300-355	38.42	5.40	23.23	3.00	37.38	0.20	3.26	0.15	8.161	0.050	0.0460	0.0418	141.5	-13.5
MC120	*sensu lato*	300-355	12.47	45.38	28.38	5.55	36.76	1.23	1.34	0.403	8.092	0.068	0.0656	0.0564	145.5	-29.8
ODP 664	*sensu lato*	300-355	0.10	-23.23	26.81	3.97	35.77	0.35	0.98	0.117	8.141	0.008	0.0685	0.0588	119.4	-59.1
G4	*sensu lato*	300-355	-28.42	167.25	21.95	3.98	35.82	0.11	1.65	0.199	8.207	0.030	0.0686	0.0592	122.2	-56.8
MC436	*sensu lato*	300-355	39.80	-21.06	18.40	3.74	36.06	0.09	0.92	0.091	8.201	0.018	0.0614	0.0538	116.0	-55.7
MC497	*sensu lato*	300-355	23.53	63.31	26.86	3.64	36.37	0.21	1.22	0.482	8.156	0.020	0.0719	0.0613	165.1	-16.9
MC423	*sensu lato*	300-355	17.75	-65.59	27.50	2.00	35.62	0.82	1.76	0.077	8.174	0.012	0.0748	0.0634	133.5	-51.4
T329	*sensu lato*	300-355	-12.96	173.57	28.63	1.45	34.79	0.24	2.59	0.215	8.175	0.023	0.0766	0.0647	113.9	-72.7
GeoB4216-1 **	*sensu lato*	300-355	30.63	-12.40	19.83	3.84	36.53	0.13	1.56	0.19	8.188	0.006	0.0657	0.0572	121.6	-54.8
OC476-SR223	*sensu lato*	300-355	-33.53	166.53	19.33	3.74	35.70	0.13	1.02	0.291	8.213	0.014	0.0643	0.0560	102.5	-72.3
MC420	*sensu lato*	355-400	17.04	-66.00	27.59	1.08	35.54	0.48	0.98	0.077	8.173	0.013	0.0747	0.0633	110.8	-74.0
G4	*sensu lato*	355-400	-28.42	167.25	21.95	3.98	35.82	0.11	1.65	0.199	8.207	0.030	0.0686	0.0592	136.4	-42.6
MC120	*sensu stricto*	250-300	12.47	45.38	28.38	5.55	36.76	1.23	1.34	0.403	8.092	0.068	0.0656	0.0564	132.9	-42.4
CAR22(z)	*sensu stricto*	250-300	10.50	-64.66	24.26	1.97	36.84	0.11	5.52	0.06	8.066	0.018	0.0562	0.0592	121.5	-57.6
T329	*sensu stricto*	250-300	-12.96	173.57	28.63	1.45	34.79	0.24	2.59	0.215	8.175	0.023	0.0766	0.0647	141.0	-45.6
GGC48	*sensu stricto*	250-300	0.00	161.00	29.41	0.36	34.61	0.51	0.92	0.151	8.108	0.064	0.0668	0.0574	99.1	-77.5
Eilat	*sensu stricto*	250-300	29.50	34.92	23.76	4.25	40.40	0.22	4.48	0.129	8.192	0.008	0.0803	0.0679	121.3	-69.8
OC476-SR223	*sensu stricto*	250-355	-33.53	166.53	19.33	3.74	35.70	0.13	1.02	0.291	8.213	0.014	0.0643	0.0560	95.1	-79.6
MC120	*sensu stricto*	300-355	12.47	45.38	28.38	5.55	36.76	1.23	1.34	0.403	8.092	0.068	0.0656	0.0564	144.9	-30.4
MC120	*sensu stricto*	300-355	12.47	45.38	28.38	5.55	36.76	1.23	1.34	0.403	8.092	0.068	0.0656	0.0564	166.0	-9.3
MC120	*sensu stricto*	300-355	12.47	45.38	28.38	5.55	36.76	1.23	1.34	0.403	8.092	0.068	0.0656	0.0564	136.7	-38.6
MC497	*sensu stricto*	300-355	23.53	63.31	26.86	3.64	36.37	0.21	1.22	0.482	8.156	0.020	0.0719	0.0613	160.6	-21.4
ODP 664	*sensu stricto*	300-355	0.10	-23.23	26.81	3.97	35.77	0.35	0.98	0.117	8.141	0.008	0.0685	0.0588	107.4	-71.1
G4	*sensu stricto*	300-355	-28.42	167.25	21.95	3.98	35.82	0.11	1.65	0.199	8.207	0.030	0.0686	0.0592	119.7	-59.4
CAR22(z)	*sensu stricto*	300-355	10.50	-64.66	24.26	1.97	36.84	0.11	5.52	0.06	8.066	0.018	0.0562	0.0496	129.7	-36.2
GGC48	*sensu stricto*	300-355	0.00	161.00	29.41	0.36	34.61	0.51	0.92	0.151	8.108	0.064	0.0668	0.0574	103.2	-73.5
T329	*sensu stricto*	300-355	-12.96	173.57	28.63	1.45	34.79	0.24	2.59	0.215	8.175	0.023	0.0766	0.0647	131.1	-55.6
T329	*sensu stricto*	300-355	-12.96	173.57	28.63	1.45	34.79	0.24	2.59	0.215	8.175	0.023	0.0766	0.0647	144.7	-42.0

Site	Description	Size fraction	Lat (°N)	Long (°E)	Temp (°C)	$\pm 2\sigma$	Salinity	$\pm 2\sigma$	Deep Ω	PO_4^{3-}	pH	$\pm 2\sigma$	$\frac{B(OH)_4^-}{HCO_3^-}$	$\frac{B(OH)_4^-}{DIC}$	B/Ca (μmol/mol)	Residual B/Ca
MC420	*sensu stricto*	300-355	17.04	-66.00	27.59	1.08	35.54	0.48	0.98	0.077	8.173	0.013	0.0747	0.0633	110.9	-73.8
MC420	*sensu stricto*	355-400	17.04	-66.00	27.59	1.08	35.54	0.48	0.98	0.077	8.173	0.013	0.0747	0.0633	117.8	-66.9
MC497	*sensu stricto*	355-400	23.53	63.31	26.86	3.64	36.37	0.21	1.22	0.482	8.156	0.020	0.0719	0.0613	178.4	-3.6
G4	*sensu stricto*	355-400	-28.42	167.25	21.95	3.98	35.82	0.11	1.65	0.199	8.207	0.030	0.0686	0.0592	114.1	-65.0
T329	*sensu stricto*	355-400	-12.96	173.57	28.63	1.45	34.79	0.24	2.59	0.215	8.175	0.023	0.0766	0.0647	114.7	-71.9
ODP 847 *	*sensu stricto*	300-355	0.20	-95.32	20.71	1.40	34.68	0.26	0.88	0.653	8.059	0.056	0.0526	0.0465	115.3	-46.4
ODP 925 *	*sensu stricto*	300-355	4.20	-43.48	26.78	0.77	35.93	0.81	1.47	0.168	8.138	0.004	0.0699	0.0597	113.8	-66.0
ODP 664 *	*sensu stricto*	300-355	0.10	-23.23	28.81	3.97	35.65	0.35	0.98	0.117	8.137	0.073	0.0685	0.0588	108.0	-70.5
ODP 668 *	*sensu stricto*	300-355	4.77	-20.93	29.54	0.70	35.51	0.24	1.44	0.082	8.163	0.018	0.0741	0.0629	112.4	-71.8
ODP 999 *	*sensu stricto*	300-355	12.75	-78.73	28.63	0.98	35.39	0.32	1.15	0.077	8.158	0.019	0.0720	0.0613	119.5	-62.5
ODP 806 *	*sensu stricto*	300-355	0.32	159.37	30.36	0.19	34.75	0.25	1.03	0.132	8.115	0.023	0.0689	0.0590	111.0	-67.8
GeoB1523-1 **	*sensu stricto*	300-355	3.83	-41.62	27.76	0.74	35.54	0.62	1.31	0.142	8.192	0.042	0.0826	0.0693	113.4	-79.6
ODP 664 **	*sensu stricto*	355-425	0.10	-23.23	28.81	3.97	35.65	0.35	0.98	0.117	8.137	0.073	0.0685	0.0588	113.7	-64.9

TABLE 5.2: Summary of core-top and sediment trap (CAR 22(z) only) samples of *G. ruber* analysed for B/Ca. Sites marked * are taken from Foster (2008), while samples marked ** were analysed by G. L. Foster (unpublished data), and are reproduced here with permission. For these sites, carbonate system parameters were re-estimated via the methods of Henehan et al. (2013) for consistency with the rest of the dataset. Carbonate system parameters are estimated as per Section 3.2.2.2. PO_4^{3-} measurements are surface measurements from the nearest World Ocean Atlas datapoint (Garcia et al., 2010). Uncertainty on temperature, salinity and pH is the two standard deviations of intraannual variability in these parameters at each site. Residual B/Ca is the measured B/Ca minus the predicted B/Ca from the culture B/Ca-$\frac{B(OH)_4^-}{DIC}$ relationship, and is used to better test for other controlling factors.

5.4 Statistical Analyses

5.4.1 Tests for Collinearity

Tests for collinearity in the environmental parameters incorporated in the model (Fig. 5.6) show that $[PO_4^{3-}]$ is not significantly correlated with other carbonate system or hydrographic variables. While salinity correlates with $\frac{B(OH)_4^-}{DIC}$ to some degree (R^2= -0.5), correlation of B/Ca with $\frac{B(OH)_4^-}{DIC}$ is poor (Fig. 5.4), and if the influence of $\frac{B(OH)_4^-}{DIC}$ is stripped from the dataset using the relationship observed in culture (i.e. the residuals from this relationship measured), the effect of salinity is strengthened (see Fig. 5.5). As such it seems that the effect of salinity on B/Ca is independent of any collinearity with $\frac{B(OH)_4^-}{DIC}$.

5.4.2 Multiple Regression Models

Core-top and tow samples (both sensu stricto and sensu lato) from Eilat are strong outliers that bias the regressions, as signified by Cook's distances[2]of >1 (Cook and Weisberg, 1982). This deviance stems from salinity: although the salinity of the Gulf of Aqaba is unusually high (∼40.4), B/Ca measurements are not as high as the salinity trends in the rest of the data would suggest. Since the inclusion of core-top and tow data from Eilat significantly alters regression model fits (removing an otherwise strong salinity component of the linear model, and artificially implicating temperature as a small but significant control), we omit these datapoints from statistical tests below. The significance of this is discussed in section 5.5.7. Fitting of multiplicative models (allowing interaction of variables) resulted in poorer fits, and as such these models are not discussed here.

Results of multiple regression analyses are given in Tables 5.3, 5.4 and 5.5. In analysis of *G. ruber*(all morphotypes; Table 5.3), morphotype is discounted from the model on the basis of a deterioration in AIC score. Despite this, multivariate regression analysis of the *sensu stricto* morphotypes alone results in better model fits (all sizes, $R^2_{(adj.)}$ = 72.04%, Table 5.4) than analyses of either the whole dataset (either morphotype and

[2]Cook's distance is a statistical method for detection of datapoints that have high leverage and/or large residuals, i.e. outliers. Put simply, it is a measure of the effect of the deletion of a given observation upon the overall regression model.

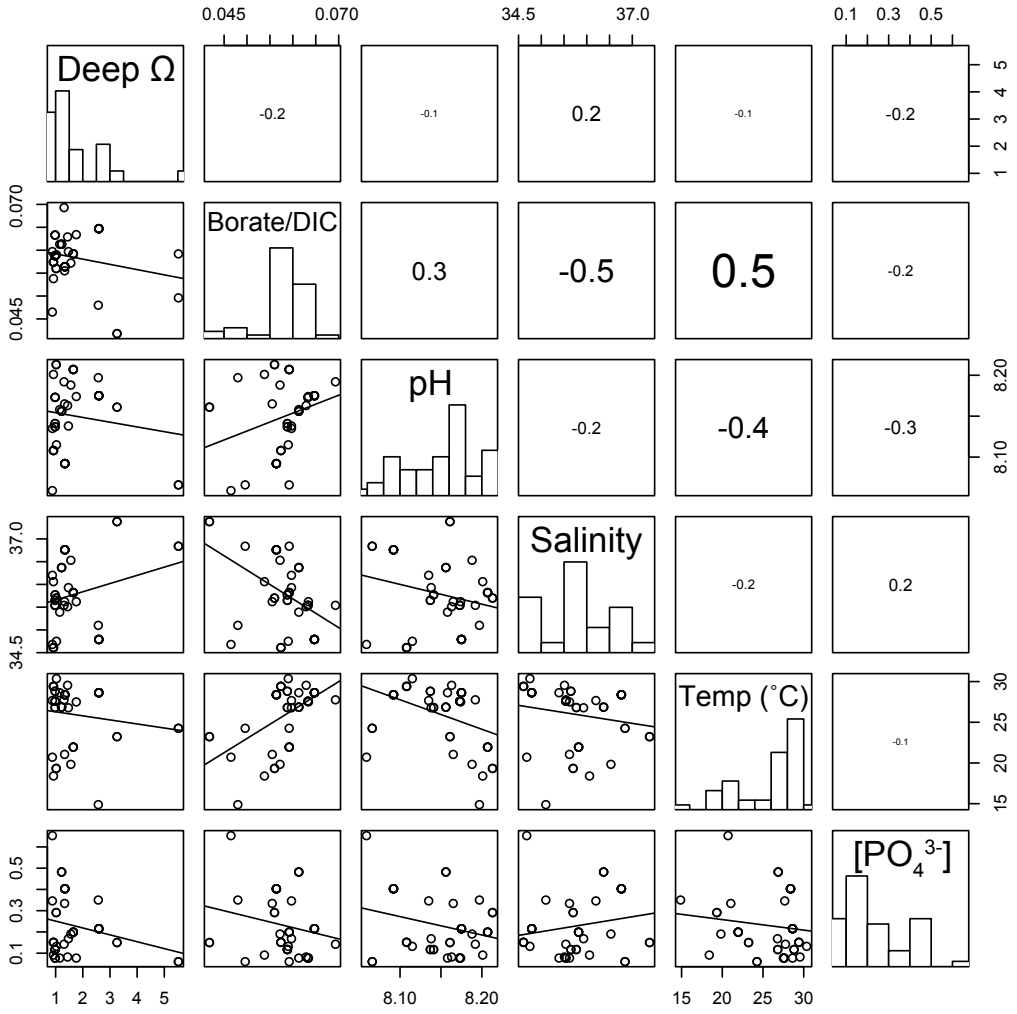

FIGURE 5.6: A matrix of regression plots and R^2 values of these linear regressions between some of the environmental parameters used in multiple regression models. Font size in R^2 values scales with the strength of the relationship, with a negative R^2 value describing a negative correlation. Histograms for each variable describe frequency distributions in each case.

all size fractions; $R^{2(adj.)} = 59.7\%$, Table 5.3) or *sensu lato* data only (all size fractions; $R^2_{(adj.)} = 53.5\%$, Table 5.5), suggesting there is some influence of morphotype that is not in itself statistically detectable. This improved fit of *sensu stricto* data to environmental parameters compared to *sensu lato* is despite there being no significant difference in B/Ca (paired two-tail t-test, p=0.520, n=10) between the two morphotypes where both *G. ruber sensu stricto* and *sensu lato* were measured from the same site and in the same size fraction.

Linear Model:				
	Estimated Coefficient	*Std. Error*	*t*	*p*
(Intercept)	-432.626	104.777	-4.129	1.8×10^{-4} ***
PO_4^{3-}	81.906	14.005	5.849	7.72×10^{-7} ***
Salinity	11.427	2.704	4.226	1.34×10^{-4} ***
Size	0.166	0.063	2.630	0.012 *
Bottom Water Ω	4.918	1.952	2.519	0.016 *
Temperature	0.980	0.586	1.673	0.102
$\frac{B(OH)_4^-}{DIC}$	707.540	438.534	1.613	0.115
Significance codes:				
	*** = 0.001	** = 0.01	*= 0.05	. = 0.1
Residuals:				
Min.	*1st Quart.*	*Median*	*3rd Quart*	*Max.*
-25.450	-8.408	-1.171	7.980	26.350
Residual standard error: 12.25 (*d.f.* = 40)				
Multiple R^2: 65.02%			Adjusted R^2: 59.77%	
F-statistic: 12.39			$p = 7.734 \times 10^{-8}$	

TABLE 5.3: Multiple linear regression statistics output from core-top and sediment trap *G. ruber* (all sizes and morphotypes) once Eilat outliers were removed. Note that temperature and $\frac{B(OH)_4^-}{DIC}$ have no significant effect on B/Ca ratios, but they are left in for illustration, given their inclusion raises the model AIC. Omission of these factors results in no change in the significance of the other factors, nor their relative importance.

5.4.3 Changes in B/Ca with size

Just as morphotypes produced differing strengths of regression model, *G. ruber sensu stricto* and *G. ruber sensu lato* show different patterns with regards size-related changes in B/Ca. Multiple regression models of *G. ruber sensu stricto* detect no significant effect of size on B/Ca; a point further illustrated by Figure 5.10. However, incorporation of measurements in *G. ruber sensu lato* introduces a significant size effect (Tables 5.3, 5.5, Figs. 5.7, 5.9). This size-related change in B/Ca in *G. ruber sensu lato* is shown in isolation in Fig. 5.11.

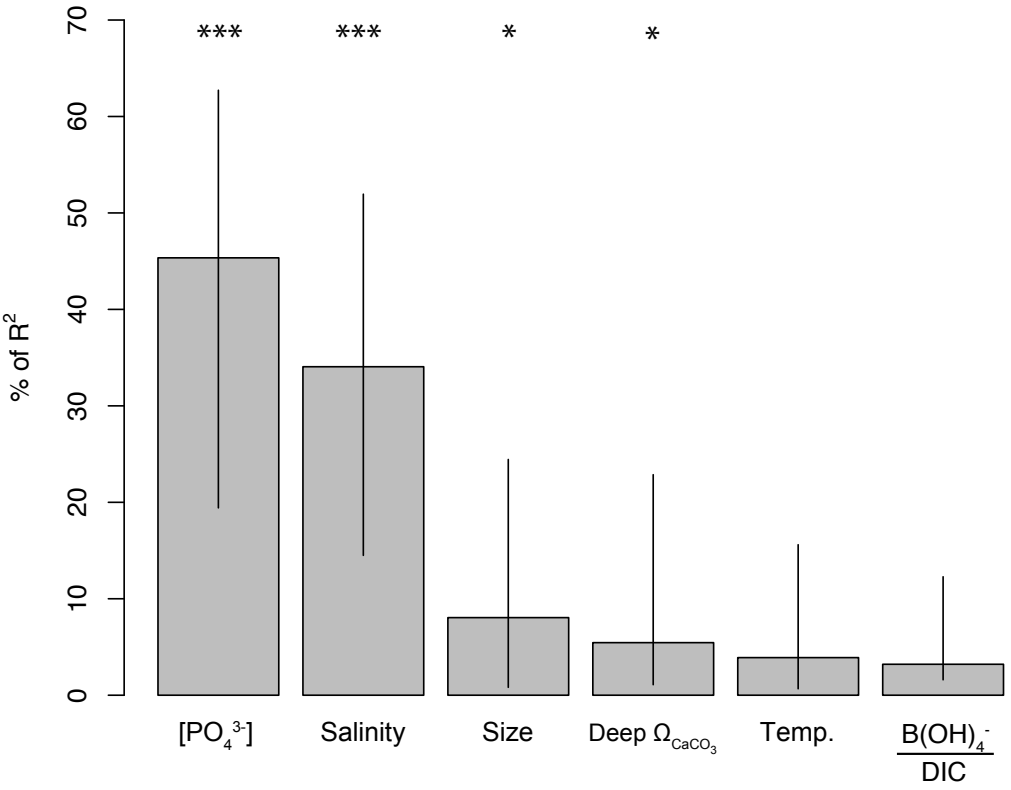

FIGURE 5.7: The relative importance of $[PO_4^{3-}]$, salinity, size, bottom water Ω, size, temperature and $\frac{B(OH)_4^-}{DIC}$ as controls on residual B/Ca variability. Relative importance is calculated as per Lindemann et al. (1980) using the 'lmg' method of Groemping (2006), using 'R', with uncertainty on relative importance (at 2σ) determined via 1000 bootstrap subsamples. Note that the overall $R^2_{(adj.)}$ of the model is 59.77%; the metrics are normalised to sum to 100% of this R^2. As in Table 5.3, *** indicates that a factor is a significant contributor to the model to $p < 0.001$, while * indicates $p < 0.05$. Neither temperature nor $\frac{B(OH)_4^-}{DIC}$ are statistically significant contributors to the regression model.

5.5 Discussion

5.5.1 The effect of the carbonate system on B/Ca ratios

These new data suggest that the marine carbonate system has very little influence on B/Ca in open ocean samples of *G. ruber*, and that $[PO_4^{3-}]$, followed by salinity, are instead the dominant controls. This is despite well-documented evidence from culture (Sanyal et al., 1996, Allen et al., 2011, 2012, this study) that demonstrates the importance of the carbonate system in determining boron incorporation. Therefore it must be assumed that this is a result of the interaction of other competing factors.

Linear Model:				
	Coefficient	*Std. Error*	*t*	*p*
(Intercept)	-421.219	115.008	-3.663	1.45×10^{-3} **
PO_4^{3-}	106.962	15.924	6.717	1.2×10^{-6} ***
Bottom Water Ω	6.725	2.009	3.347	0.003 **
Salinity	9.138	2.992	3.054	0.006 **
Temperature	2.410	0.831	2.899	0.009 **
$\frac{B(OH)_4^-}{DIC}$	1421.271	542.985	2.618	0.016 *
Size	0.104	0.067	1.560	0.134
Significance codes:				
	*** = 0.001	** = 0.01	*= 0.05	. = 0.1
Residuals:				
Min.	*1st Quart.*	*Median*	*3rd Quart*	*Max.*
-22.733	-4.644	-0.798	4.679	16.478
Residual standard error: 10.48 (*d.f.* = 22)				
Multiple R^2: 78.25%			Adjusted R^2: 72.04%	
F-statistic: 12.59			$p = 5.1 \times 10^{-6}$	

TABLE 5.4: Multiple linear regression statistics output from core-top and sediment trap *G. ruber sensu stricto* (all sizes) once Eilat outliers were removed. Note that size has no significant effect B/Ca ratios, but it is left in the model for illustration, given that its inclusion does not detrimentally affect the model's AIC. Omission of test size produces no change in the significance of the other factors, nor their relative importance.

Multiple regression in *G. ruber sensu stricto* only does detect a small but statistically significant (to 95% confidence) effect of $\frac{B(OH)_4^-}{DIC}$ on B/Ca, but when combined with data from *G. ruber sensu lato* this effect disappears (note that inclusion of pH or $\frac{B(OH)_4^-}{HCO_3^-}$ in lieu of $\frac{B(OH)_4^-}{DIC}$ has no bearing on this finding). Clearly this could well preclude the use of B/Ca for palaeo-pH and palaeo-CO_2 reconstruction.

However, while the carbonate system cannot be considered a strong control on B/Ca in open ocean samples, in all cases multiple regression models were more powerful (i.e. had a higher $R^2_{(adj.)}$) when the residuals from the culture $\frac{B(OH)_4^-}{DIC}$-B/Ca relationship were analysed in lieu of raw B/Ca ratios: *sensu stricto* $R^2_{(adj.)}$ 74.02% → 74.79%, *sensu lato* $R^2_{(adj.)}$ 53.5% → 62.73%, both $R^2_{(adj.)}$ 59.77% → 64.76%. This implies that the carbonate system does have some underlying influence on B/Ca ratios that is obscured by conflicting factors. It should be noted, though, that analysis of these residuals rather than B/Ca did not affect which of environmental parameters proved to be controls, nor the relative importance of these factors, except in the case of *G. ruber*

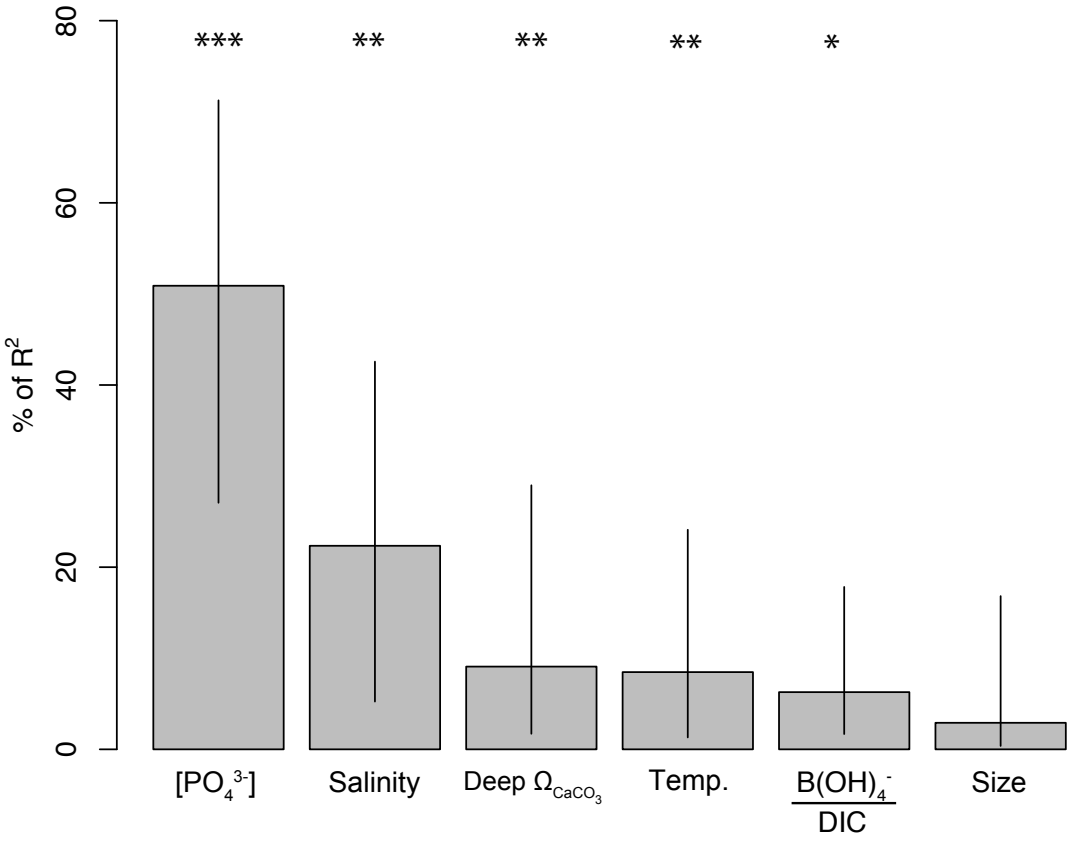

FIGURE 5.8: The relative importance of $[PO_4^{3-}]$, salinity, bottom water Ω, temperature, $\frac{B(OH)_4^-}{DIC}$ and size as controls on residual B/Ca variability in *G. ruber sensu stricto* . Relative importance is calculated as per Lindemann et al. (1980) using the 'lmg' method of Groemping (2006), using 'R', with uncertainty on relative importance (at 2σ) determined via 1000 bootstrap subsamples. Note that the overall $R^2_{(adj.)}$ of the model is 72.04%; the metrics are normalised to sum to 100% of this R^2. As in Table 5.4, *** indicates that a factor is a significant contributor to the model to $p < 0.001$, ** indicates significance to $p < 0.01$, while * indicates $p < 0.05$. Note also that size does not contribute significantly to the regression model.

sensu lato , where size was no longer found to be a significant contributor in multiple regression analysis of residual B/Ca. No notable difference arose from using the residuals from the $\frac{B(OH)_4^-}{DIC}$-B/Ca of *G. ruber* (pink) (Allen et al., 2012).

Although carbonate system control in B/Ca is not clearly evident in numerous other open ocean planktic foraminifera (see Allen and Hönisch, 2012, for review), B/Ca ratios in *N. pachyderma* do appear to show a correlation with $\frac{B(OH)_4^-}{DIC}$ (Yu et al., 2013). It is unclear why boron incorporation in open ocean*N. pachyderma* might be carbonate-system-dependent, but boron incorporation in *G. ruber* is not. It is possible that the presence of symbionts in *G. ruber* may dampen the effect of ambient

Linear Model:				
	Coefficient	*Std. Error*	*t*	*p*
(Intercept)	-394.433	154.799	-2.548	0.026 *
PO_4^{3-}	82.520	26.737	3.086	0.009 **
Salinity	11.552	4.046	2.855	0.014 *
Size	0.263	0.113	2.331	0.038 *
Significance codes:				
	*** = 0.001	** = 0.01	*= 0.05	. = 0.1
Residuals:				
Min.	*1st Quart.*	*Median*	*3rd Quart*	*Max.*
-25.558	-6.004	-0.499	5.086	24.025
Residual standard error: 12.4 (*d.f.* = 12)				
Multiple R^2: 62.8%			Adjusted R^2: 53.5%	
F-statistic: 6.753			$p = 0.0064$	

TABLE 5.5: Multiple linear regression statistics output from core-top and sediment trap *G. ruber sensu lato* (all sizes) once Eilat outliers are removed. Note that temperature, $\frac{B(OH)_4^-}{DIC}$ and bottom water Ω are not significant contributors, and indeed these are removed via stepwise model selection, as to include them results in inferior AIC values.

.

carbonate system changes upon the microenvironment of the foram (and hence B/Ca). This is supported by the lower-than-expected pH-sensitivity seen in *G. ruber* (see Chapter 3). However, preliminary investigations in *G. bulloides* (also a symbiont-barren species) currently in preparation has revealed similar controls (namely salinity and phosphate) in this species (Henehan et al., in prep.). Since correlation between B/Ca and $\frac{B(OH)_4^-}{DIC}$ in this data set is perhaps not unassailable (R^2= 44%, calibration data are largely within quoted 5% analytical uncertainty of each other, and carbonate system parameterisation relies on somewhat sparse GLODAP measurements), more measurements, including analyses from towed samples where the *in situ* carbonate system is well characterised, might prove valuable.

5.5.2 $[PO_4^{3-}]$: a previously overlooked control on B/Ca ratios

The positive correlation between phosphate concentrations ($[PO_4^{3-}]$) and B/Ca seen in these core-top data is the first suggestion of $[PO_4^{3-}]$ being relevant to foraminiferal B/Ca ratios. The root cause of this phosphate correlation, however, is unclear. It is

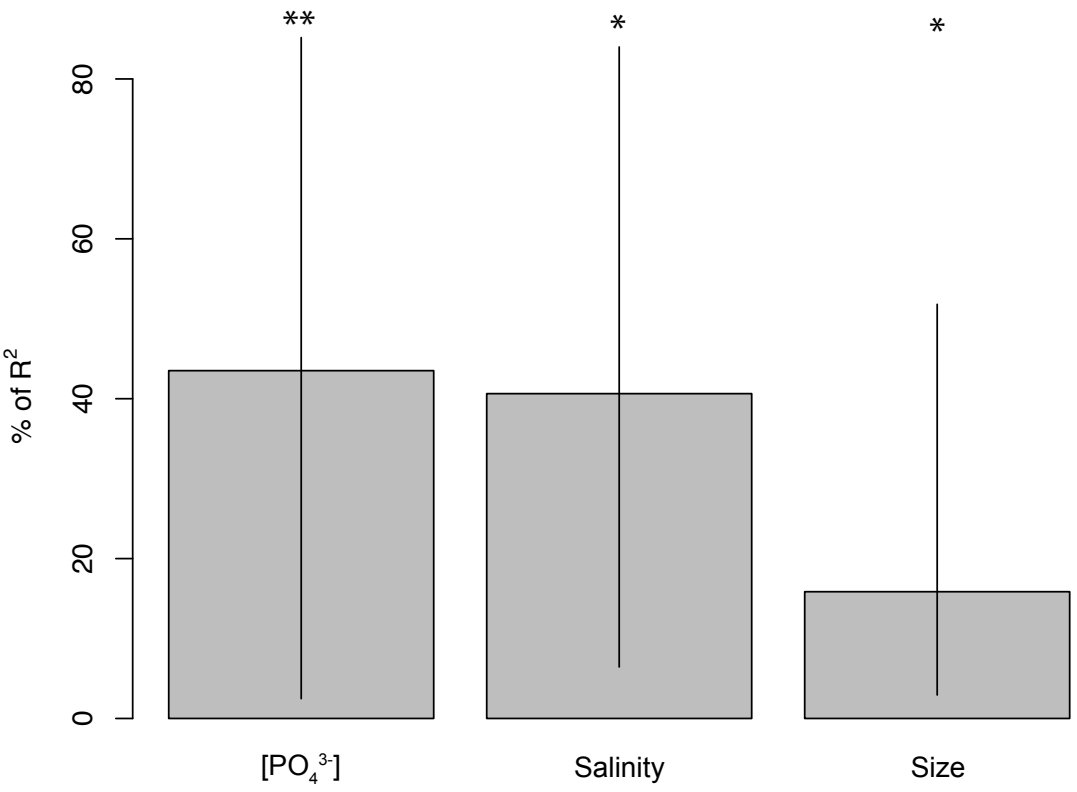

FIGURE 5.9: The relative importance of $[PO_4^{3-}]$, salinity and size as controls on B/Ca ratios in *G. ruber sensu lato* . Relative importance is calculated as per Lindemann et al. (1980) using the 'lmg' method of Groemping (2006), using 'R', with uncertainty on relative importance (at 2σ) determined via 1000 bootstrap subsamples. Note that the overall $R^2_{(adj.)}$ of the model is 53.5%; the metrics are normalised to sum to 100% of this R^2. Note also that temperature, $\frac{B(OH)_4^-}{DIC}$ and bottom water Ω do not contribute significantly to the regression model, and are removed from the model by stepwise model selection due to their detrimental effect on model AIC.

possible that the apparent influence of PO_4^{3-} on B/Ca is not as a direct result of any interaction with biomineralisation processs, but rather it is a proxy for some other hydrographic conditions that induce a vital effect in foraminiferal B/Ca. For example, areas of high PO_4^{3-} conditions are often associated with seasonal upwelling or deep mixing, and may have higher levels of primary productivity (see Fig. 5.12). It is possible that a more plentiful food supply in areas of high productivity may result in higher growth rates, and that this in turn might induce some kind of vital effect. This might be supported by the finding that foraminifera grown in culture, where food was offered every day, have higher B/Ca than those grown in the open ocean (this study). However, any mechanisms for an elevation of boron incorporation with enhanced feeding rate are not clear. Higher feeding should result in higher respiration rates, and

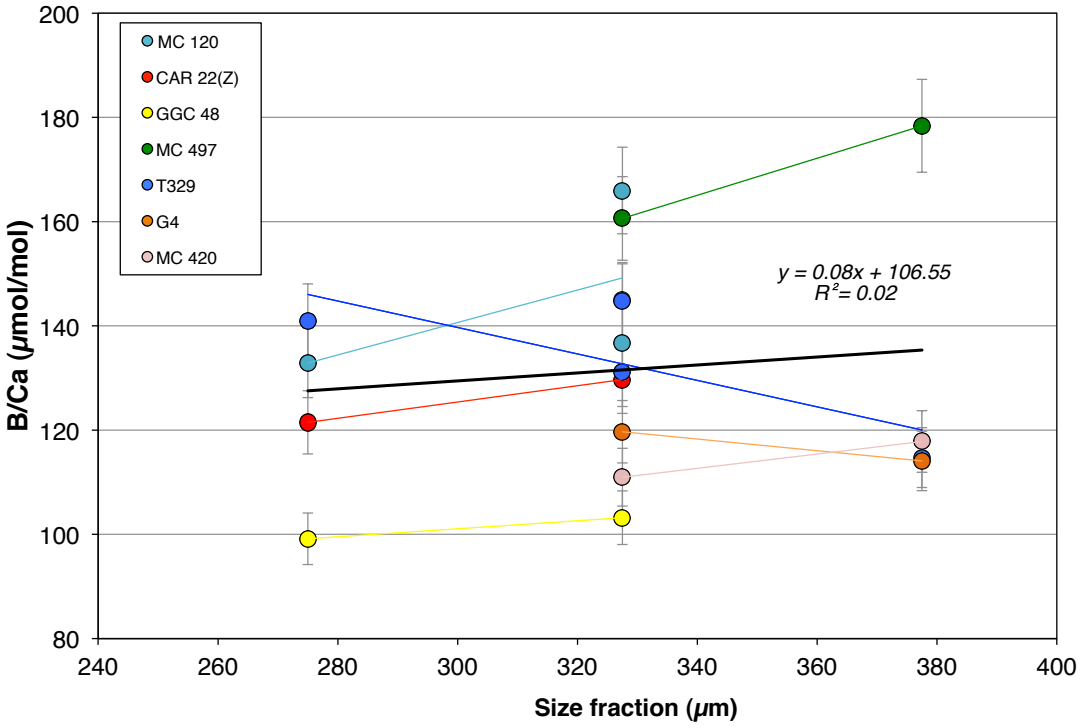

FIGURE 5.10: No significant, systematic change in B/Ca ratios with size fraction was detectable in *G. ruber sensu stricto* measured from a number of sites. Y-error bars are 5% analytical uncertainty.

hence acidification of the foraminiferal microenvironment and reduction in $\frac{B(OH)_4^-}{DIC}$ (Zeebe et al., 1999a), which should reduce B/Ca. Furthermore, light attenuation is greater in areas of higher productivity, which would suggest that the buffering of the microenvironment of *G. ruber* by photosynthetic symbionts should be less effective, and should again result in lower $\frac{B(OH)_4^-}{DIC}$ in these high productivity regions.

Alternatively, the observed correlation between B/Ca and $[PO_4^{3-}]$ may be due to inorganic processes. Phosphorous compounds are known to interact with $CaCO_3$ in seawater and are readily incorporated into, and adsorbed onto, $CaCO_3$, with incorporation rate dependent on ambient $[PO_4^{3-}]$ (Berner and Morse, 1974, Ishikawa and Ichikuni, 1981). Phosphorous compounds have also been known to retard $CaCO_3$ nucleation (Simkiss, 1964, Pytkowicz, 1973) and precipitation (Reddy, 1977, Kitano et al., 1978b, Berner et al., 1978, Mucci, 1986, Burton and Walter, 1990) rates. The possible effect of phosphorous on boron incorporation, however, is unclear. Ruiz-Agudo et al. (2012) hypothesise that one of the limiting factors on the incorporation of boron is the time permitted for the re-coordination of tetrahedral boron to trigonal form, and

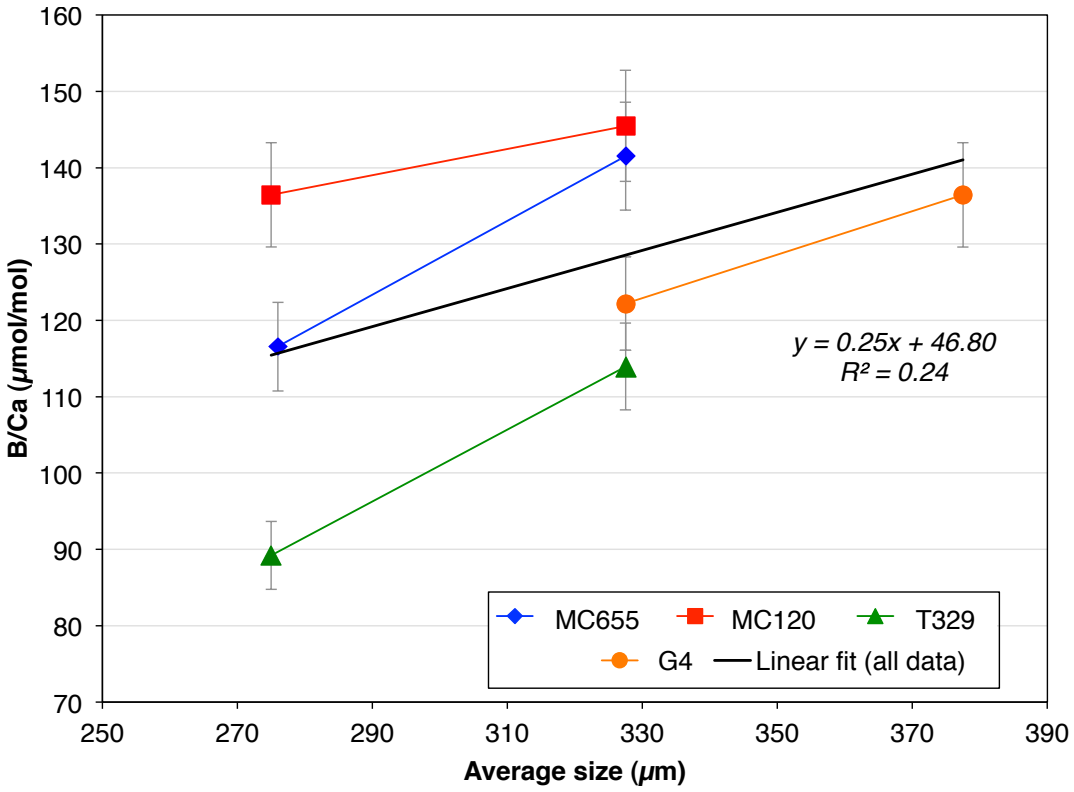

FIGURE 5.11: Change in B/Ca ratios with size fraction was detectable in *G. ruber sensu lato* from multiple sites, and is likewise detected as a significant factor in multiple regression analyses (Tables 5.3, 5.5). Y-error bars are 5% analytical uncertainty.

that at slower precipitation rates more boron can be incorporated in the crystal lattice. As such the retardation of $CaCO_3$ growth by ambient inorganic PO_4^{3-} may result in higher B/Ca ratios. A decrease in shell weight in *G. bulloides* with ambient $[PO_4^{3-}]$ (Aldridge et al., 2012), may constitute evidence for retardation of calcification in foraminifera caused by PO_4^{3-} ion, although this finding may also result from collinearity of $[PO_4^{3-}]$ and $[CO_3^{2-}]$ in this study (Marshall et al., 2013, see Appendix E attached).

Alternatively, if P is incorporated into $CaCO_3$ as orthophosphate (PO_4^{3-} ion), as suggested by Ishikawa and Ichikuni (1981) and Mucci (1986), then it may be possible that paired substitution is required to balance valency, and that boron may be incorporated as a result. For example, $2(CO_3^{2-})$ might substitute for one PO_4^{3-} and one $B(OH)_4^-$ ion. While this too could explain the positive correlation between B/Ca and $[PO_4^{3-}]$, it is not certain that PO_4^{3-} ion alone is the species incorporated into the

crystal lattice, with Burton and Walter (1990) suggesting HPO_4^{2-} may also be incorporated, and Lin and Singer (2006) advocating $CaHPO^0_{4(aq)}$ instead. Regardless of the form of P incorporated, however, it is likely that the reorganisation of such a large molecule into the carbonate lattice would result in considerable disorder and an increase in kink sites, where boron might more easily be incorporated (Hemming et al., 1995). One possible problem with invoking a crystallographic cause for the observed correlation between $[PO_4^{3-}]$ and B/Ca is that some other lines of evidence would suggest that PO_4^{3-} might compete with $B(OH)_4{}^-$ for incorporation sites. Both molecules are thought to compete to incorporate in place of CO_3^{2-} ion (Ishikawa and Ichikuni, 1981, Allen et al., 2012) and both $B(OH)_4{}^-$ (Hemming et al., 1995) and PO_4^{3-} (Dove and Hochella Jr., 1993, Berner and Morse, 1974) are incorporated into growing crystal faces at kink sites. However, as aforementioned, it is possible that the two ions are incorporated together in a paired substitution, or that the disruption of the $CaCO_3$ lattice by PO_4^{3-} ion creates binding sites for $B(OH)_4{}^-$.

Another alternative means by which phosphate may promote the incorporation of boron is via the facilitation of amorphous calcium carbonate (ACC) formation. Dove and Hochella Jr. (1993) note that the presence of PO_4^{3-} tends to result in rounded or amorphous precipitation nucleii. Meanwhile, Bentov et al. (2010) and Hild et al. (2008) show that organic phosphorous compounds promote the production of ACC, and suggest that inorganic dissolved PO_4^{3-} may also play a co-operative role in the stabilisation of ACC. Therefore, given that ACC more readily incorporates trace elements (Bentov and Erez, 2006, Cusack and Freer, 2008), it is possible that enhanced ACC formation may allow for greater incorporation of boron.

It is worth noting that pH-dependent changes in the speciation of P in culture experiments (towards increasing abundance of orthophosphate ion with increasing pH; Atlas, 1975, Zeebe and Wolf-Gladrow, 2001) might produce an apparent carbonate system control, should orthophosphate (PO_4^{3-} ion) be the species incorporated into $CaCO_3$ (as suggested by Ishikawa and Ichikuni, 1981). In this way, changes in carbonate system parameters might produce (or at least accentuate) changes in B/Ca in culture, but in the open ocean where $[PO_4^{3-}]$ is controlled not only by pH-dependent speciation, but also by nutrient cycling processes, this correlation is lost. Allen et al. (2011) cite a mismatch between predicted and observed B/Ca in culture experiments as evidence that "other pH-sensitive ions may be involved in calcification". While

additional culturing experiments where aqueous [PO_4^{3-}] is altered are required, it is possible that PO_4^{3-} might be one such pH-sensitive ion.

5.5.3 Morphotype differences in B/Ca controls

While *G. ruber sensu lato* is not significantly different in B/Ca from *sensu stricto* at sites where both were analysed (section 5.4), regression models using *sensu lato* are poorer in fit. Not only this, but salinity appears to be a relatively more powerful control on B/Ca ratios in this group compared to [PO_4^{3-}]. This poorer fit is likely the result of either a) morphospecies-specific variability in boron incorporation or b) uncertainty in the depth habit of *G. ruber sensu lato*.

While comparisons at core-top sites between two morphotypes reveal no offset, *G. ruber sensu lato* is an umbrella term (from Wang, 2000) for what are in reality two separate species: *G. ruber pyramidalis* and *G. ruber elongatus* (Aurahs et al., 2011). In this study, both of these species were combined, but it is conceivable that these groups differ in B/Ca. While no quantitative data as to the relative contributions of these species were collected here, *G. ruber pyramidalis* was relatively more abundant at sites where *sensu stricto* were absent (such as in higher-latitude, transitional waters). In this way, sites where *G. ruber sensu stricto* was not present may have comprised more *G. ruber pyramidalis* and produced more scattered data (thus reducing the power of regression models of *sensu lato*). However, there is no statistically significant difference detectable between B/Ca measurements at sites where *sensu stricto* were also present and those taken from higher-latitude waters where it was not. Further investigation to ascertain the variability of the relative contributions of *G. ruber pyramidalis* and *G. ruber elongatus* between sites, and comparison of B/Ca values between these two morphotypes, would be beneficial, but at present it seems that morphotype differences within *G. ruber sensu lato* can not easily explain the relatively higher residual scatter in this group.

It is possible that the poorer fit in *G. ruber sensu lato* is due to a deeper habitat in this group. MOCNESS tows by Kuroyanagi and Kawahata (2004) found living *G. ruber sensu lato* in abundance at depths of >50 m, while *G. ruber sensu stricto* was only abundant in surface waters. This deeper habit is corroborated by lower reconstructed temperatures in *G. ruber sensu lato* noted by Wang (2000), Löwemark

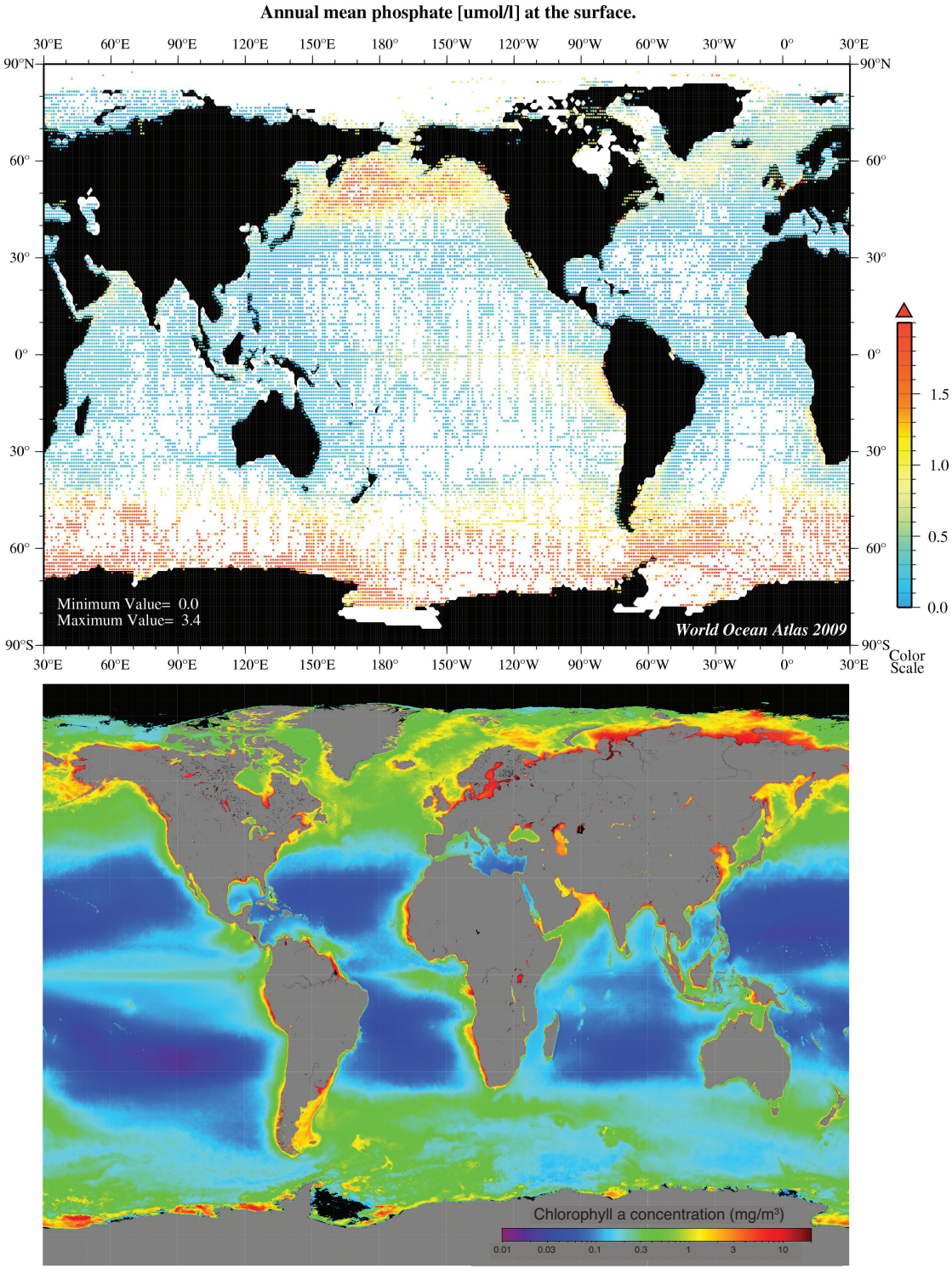

FIGURE 5.12: A demonstration of the coincidence of areas of high primary productivity in areas where $[PO_4^{3-}]$ is high. The upper plot was produced from World Ocean Atlas (Garcia et al., 2010) and the lower was produced at NASA's OceanColour Web. Colour scales are given in each plot.

et al. (2005), Kawahata (2005), Steinke et al. (2005, 2008). Although calculations of pre-industrial pH used here rely on the Takahashi et al. (2009) surface water database, if a similar surface-50m pH, temperature and salinity gradient at these sites (from GLODAP (Key et al., 2004) and CARINA (Key et al., 2010) datasets) is assumed for the pre-industrial, one may apply this offset to reconstructed pre-industrial surface values. Fitting of a regression model to *sensu lato* data with conditions at ~50m depth (Table 5.6), using 50m depth $[PO_4^{3-}]$ values from WOA (Garcia et al., 2010), improves the fit considerably ($R^2_{(adj.)} = 65.41\%$ vs. 53.5%), and puts $[PO_4^{3-}]$ over salinity as the primary control in *G. ruber sensu lato* (Fig. 5.13). Testing residual B/Ca (removing the $\frac{B(OH)_4^-}{DIC}$-B/Ca relationship from culture, using $\frac{B(OH)_4^-}{DIC}$ estimated at 50m) results in even stronger models for both *sensu lato* only ($R^2_{(adj.)} = 73.66\%$) and whole species ($R^2_{(adj.)} = 70.43\%$) datasets when a depth habit of 50m is assumed (with $[PO_4^{3-}]$ and salinity the only significant factors in both cases). However, further work is needed to validate this assumption. Such depth segregation between morphotypes may not always be present, with Kuroyanagi and Kawahata (2004) observing contrasting patterns between sites, and Mohtadi et al. (2011) prescribing only a slightly more uncertain depth habitat in *G. ruber sensu lato* compared to *G. ruber sensu stricto* (as inferred from Mg/Ca and $\delta^{18}O$). In addition, in the Gulf of Aqaba (Eilat) both morphotypes were found in tows from <10m depth (this study). One final problem with assuming such a deep habitat for *G. ruber sensu lato* is that no difference in $\delta^{11}B$ is observed between *sensu stricto* and *sensu lato* where these two species co-habit (Henehan et al., 2013); if *sensu lato* were to live at such depths, lower light levels should result in a reduction in symbiont photosynthesis and thus a less pronounced vital effect in $\delta^{11}B$ (as in *O. universa*; see Chapter 4). Clearly, then, further work is required to determine the drivers of B/Ca differences in these morphotypes.

5.5.4 The influence of salinity on foraminiferal B/Ca

Open ocean data presented here support the findings of Allen et al. (2011, 2012) that salinity is positively correlated with B/Ca in *G. ruber*, although the slope of this relationship seen here ($m = 12.46$) is greater than that seen in *G. ruber* (pink) ($m = 4.5$; Allen et al., 2012). Notably, even when the effect of $\frac{B(OH)_4^-}{DIC}$ from culture is stripped from the data and residual B/Ca is tested, salinity remains a significant control: the effect of salinity appears greater than its influence on $\frac{B(OH)_4^-}{DIC}$ alone

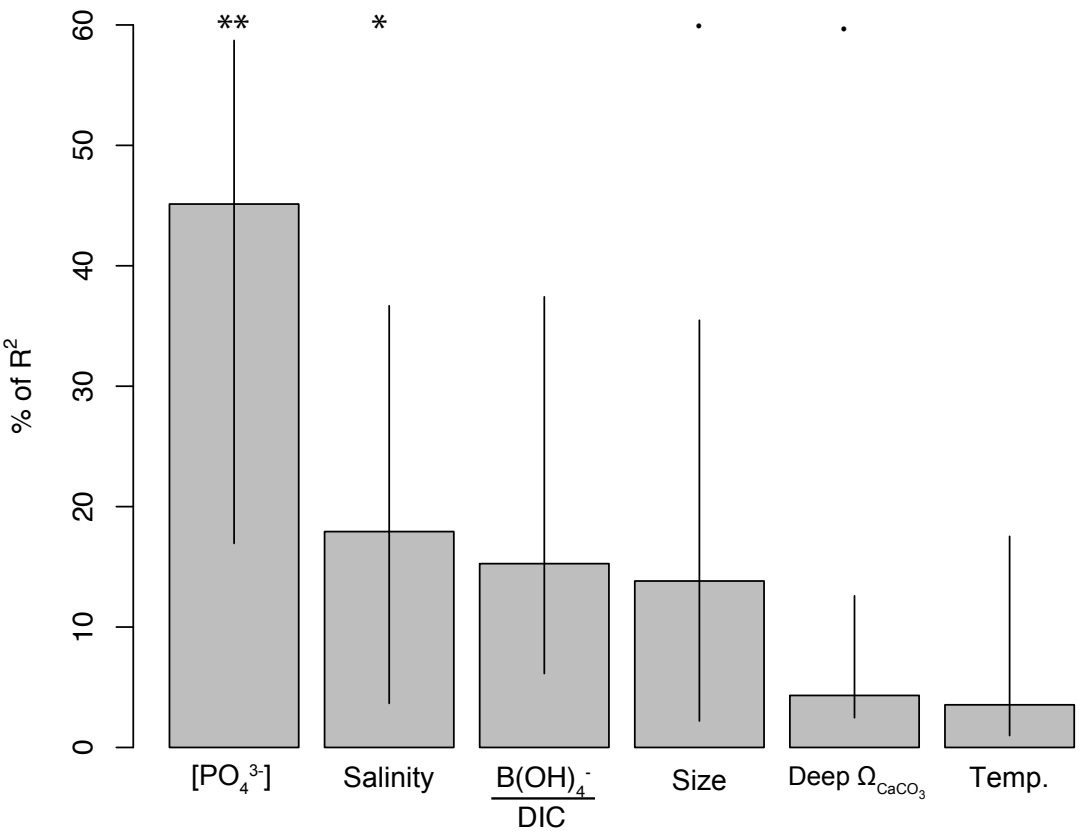

FIGURE 5.13: Assuming a habitat depth of 50m for *G. ruber sensu lato* , the relative importance of $[PO_4^{3-}]$ in controlling residual B/Ca variability (once the known relationship between B/Ca and $\frac{B(OH)_4^-}{DIC}$ from cultures is removed) is increased. Relative importance is calculated as per Lindemann et al. (1980) using the 'lmg' method of Groemping (2006), using 'R', with uncertainty on relative importance (at 2σ) determined via 1000 bootstrap subsamples. Note that the overall $R^2_{(adj.)}$ of the model is 65.41%; the metrics are normalised to sum to 100% of this R^2. Note also that size, temperature, $\frac{B(OH)_4^-}{DIC}$ and bottom water Ω do not contribute significantly to the regression model, despite the relative importance metric suggesting $\frac{B(OH)_4^-}{DIC}$ is the third most important factor. Significance codes are as in Table 5.6: ** $= p < 0.01$, * $= p < 0.05$, . $= p < 0.1$.

(again, corroborating Allen et al., 2011). However, it is not clear whether this is due to the effects of elevated $[B]_{sw}$ (as suggested by Allen et al., 2011), or a more direct effect of higher salinity and ionic strength (as seen in Kitano et al., 1978a). Higher ionic strength will raise the activity of molecules involved in biomineralisation, for example. In addition, should $[PO_4^{3-}]$ play a role in crystal growth and boron incorporation, higher salinity (and thus ionic strength) will alter the speciation of aqueous phosphorous compounds (Atlas, 1975).

Linear Model				
	Coefficient	*Std. Error*	*t*	*p*
(Intercept)	-482.750	185.026	-2.609	0.031 *
PO_4^{3-}	63.017	15.649	4.027	0.004 **
Salinity	13.467	5.074	2.654	0.029 *
Size	0.289	0.127	2.270	0.053 .
Bottom Water Ω	8.793	6.593	1.915	0.092 .
Temperature	-1.477	0.834	-1.771	0.115
$\frac{B(OH)_4^-}{DIC}$	501.257	410.664	1.221	0.257
Significance codes:				
	*** = 0.001	** = 0.01	*= 0.05	. = 0.1
Residuals:				
Min.	*1st Quart.*	*Median*	*3rd Quart*	*Max.*
-15.576	-5.523	2.491	4.425	12.795
Residual standard error: 11.05 (*d.f.* = 8)				
Multiple R^2: 80.24%			Adjusted R^2: 65.41%	
F-statistic: 5.413			$p = 0.016$	

TABLE 5.6: Multiple linear regression statistics output from core-top and sediment trap *G. ruber sensu lato* (all sizes) once Eilat outliers were removed, assuming a depth habitat in *G. ruber sensu lato* of 50 m. Note that temperature, size, deepwater Ω and $\frac{B(OH)_4^-}{DIC}$ have no significant effect on B/Ca ratios at 95% confidence, but they are left in for illustration, and since stepwise model selection does not remove them from the model on the basis of AIC. Omission of these factors results in no change in the significance of the other factors, nor their relative importance.

.

It is difficult (at least within the range of environmental parameters studied here) to quantify accurately the relative importance of salinity compared to other variables (e.g. $[PO_4^{3-}]$). Although in most cases salinity appears to be a secondary control behind $[PO_4^{3-}]$, in *G. ruber sensu lato* the dominance of $[PO_4^{3-}]$ is less clear (not least due to the smaller number of *sensu lato* measurements). Should *G. ruber sensu lato* inhabit a deeper depth habitat (see section 5.5.3), however, this strong salinity influence is diminished and $[PO_4^{3-}]$ again becomes the dominant control in this group (see Fig.5.13). As a result of this uncertainty in depth habit, and the smaller number of *sensu lato* measurements, it is as yet difficult to express these factors in the form of a multivariate regression equation (which might, if well defined, be useful in palaeo-reconstructions). To this end, further culturing work, varying both salinity and phosphate, would be beneficial.

5.5.5 The influence of size-fraction on *G. ruber* B/Ca ratios.

Although its contribution to the regression model for all morphotypes (Table 5.3) is statistically significant, this is driven only by size-related changes in *G. ruber sensu lato* . In *G. ruber sensu stricto* , no change in B/Ca is seen with size (R^2= 0.02 %, Fig. 5.10). Given that size fraction effects have previously been noted in *G. ruber* (white) (Ni et al., 2007), this lack of size fraction effect seen here in *G. ruber sensu stricto* B/Ca ratios might be considered surprising. However, examining the data of Ni et al. (2007), much of the trend in B/Ca with size is driven by *G. ruber* (pink). In *G. ruber* (white), apart from relatively lower B/Ca ratios in samples < 250 μm, values of B/Ca are invariant: Ni et al. (2007) observe no trend outside of analytical uncertainty between 280 and 390 μm in diameter. Here, *G. ruber sensu lato* show a similar slope in B/Ca with size (m=0.25) as in *G. ruber*(pink) analysed by (Ni et al., 2007, m=0.23). This similarity is striking, and merits further investigation.

The mechanism by which *G. ruber sensu lato* and *G. ruber sensu stricto* may demonstrate differing trends in B/Ca with size are unclear. It is possible that both *G. ruber* (pink) and *sensu lato* may deposit a greater proportion of gametogenic (GAM) calcite than *G. ruber sensu stricto* , causing intratest heterogeneity, and prompting dissolution trends in a similar way to those seen in *G. sacculifer* (see Ni et al., 2007, Seki et al., 2010, Coadic et al., 2013). However, post-mortem dissolution seems counter-intuitive given the lack of significant effect of deep-water Ω_{CaCO_3} in *G. ruber sensu lato* (see Table. 5.5; though this parameter may not be an ideal measure of dissolution pressures, see Section 5.5.6). Instead it is possible that *sensu lato* grow larger in times of upwelling or deep mixing (conditions which they are thought to favour; Wang, 2000), such that larger foraminifera also saw higher $[PO_4^{3-}]$. Such an explanation would not explain similar trends in *G. ruber* (pink), however, given that this species is most commonly found in the extremely oligotrophic Caribbean sea. Moreover, the lack of similar patterns in δ^{11}B (Henehan et al., 2013) is puzzling.

5.5.6 Deepwater Ω: assessing the evidence for a dissolution effect of B/Ca

While Ω_{CaCO_3} at the site of deposition has been shown elsewhere to effect B/Ca ratios in *G. sacculifer* (Seki et al., 2010, Coadic et al., 2013), it accounts for a very small percentage of the variation seen in the coretop *G. ruber* data presented here (at least within the range of Ω_{CaCO_3} tested: 0.9<5.2). If this lack of a dissolution effect is reliable, it would support *G. ruber*'s being a preferable candidate for the application of boron-based proxies, in agreement with Seki et al. (2010). This apparent resistance to loss of B via dissolution may be due to the homogeneity of *G. ruber* compared to *G. sacculifer*, given a lack of gametogenic calcite in *G. ruber* (Caron et al., 1990). However, it might be that dissolution upon deposition is controlled not only by the saturation state of the waters above the sediments, but by processes within the sediments, such as the supply of organic matter to sediments or the degree of bioturbation (see Peterson and Prell, 1985, Schulte and Bard, 2003, Hönisch and Hemming, 2004), and as such this analysis cannot properly account for it. Furthermore, all core-top samples were taken from within the top 1cm of sediment, and as such it should still be noted that corrosion from porewaters deeper within sediments may still have some effect on B/Ca that cannot be explored here, and that must still be borne in mind when approaching down-core records.

5.5.7 Unusual conditions in Eilat

As discussed in Section 5.4, core-top data from the Gulf of Aqaba (Eilat) were removed from analyses as outliers. While salinity in Eilat is very high, core-top *G. ruber* from this site do not show the same elevated B/Ca as would be expected from the B/Ca-salinity relationships of Allen et al. (2012), or from the trends in other core-top data (Fig. 5.5). Since the salinity experiments of Allen et al. (2012) reach salinities comparable to Eilat and see a rise in B/Ca as a result, it is not merely that the relationship with salinity is non-linear. As yet this discrepancy is difficult to explain, in light of a lack of any similar discrepancy in $\delta^{11}B$ in *G. ruber* (see Chapter 3). It is not an artefact of preservation, as tows of *G. ruber* from the Gulf recorded similar B/Ca ratios as specimens from sediments. It is possible that $[PO_4^{3-}]$ and salinity affect B/Ca ratios synergistically (for example by changes in salinity/ionic strength influencing

aqueous P speciation Atlas, 1975), but that this interaction was not distinguishable within the limited range of these parameters examined for *G. ruber*. If salinity were to have a greater effect at higher $[PO_4^{3-}]$, for example, the low $[PO_4^{3-}]$ seen in the Gulf of Aqaba (Eilat) may mean that the effects of high salinity at this site are dampened. At this juncture, however, these data remain unexplained, and require further investigation in future trips to Eilat.

5.6 Conclusions

This study constitutes the first combined culture and *in situ* open-ocean calibration study for B/Ca ratios in *G. ruber*, and highlights that the strong response of B/Ca to carbonate system changes that is seen in culture is not reproduced in the open ocean. The finding that B/Ca in *G. ruber* in the open ocean is not predominantly controlled by pH, $\frac{B(OH)_4^-}{HCO_3^-}$ or $\frac{B(OH)_4^-}{DIC}$, but by $[PO_4^{3-}]$ (hitherto unnoted) and salinity (supporting Allen et al., 2011, 2012), has implications for palaeo-application, as it implies that B/Ca ratios are not a reliable recorder of past carbonate system conditions. While the absence of the clear relationships seen in culture in open-ocean samples is puzzling, it is possible that the changing speciation of phosphorous compounds in culture pH experiments (Atlas, 1975, Zeebe and Wolf-Gladrow, 2001) may drive (or at the very least accentuate) changes in B/Ca (should orthophosphate ion be incorporated into $CaCO_3$, as in Burton and Walter, 1990, Mucci, 1986, Ishikawa and Ichikuni, 1981). In the open-ocean, however, where $[PO_4^{3-}]$ is influenced by other factors besides pH, this carbonate system correlation is obscured.

These data support the findings of Allen et al. (2011, 2012) that temperature does not significantly affect B/Ca in *G. ruber*. Downcore correlations between Mg/Ca and B/Ca (e.g. Wara et al., 2003, Yu et al., 2007b) may arise via other means, for example as a result of a common salinity effect on B/Ca (Allen et al., 2011, 2012, this study) and Mg/Ca (Kisakürek et al., 2008) ratios. Deepwater Ω_{CaCO_3} was not seen to have a strong influence on B/Ca ratios in *G. ruber* (as least within the range of Ω_{CaCO_3} studied), unlike in *G. sacculifer* (Seki et al., 2010, Coadic et al., 2013), suggesting that at least for this species post-mortem alteration does not cloud primary signals. In addition, no clear size fraction effect was observed for *G. ruber sensu stricto*, despite

the change in micro-environment pH (and thus $\frac{B(OH)_4^-}{DIC}$) with size implied by δ^{11}B (Henehan et al., 2013).

Chapter 6

Synthesis

6.1 Thesis Summary/Chapter Synopsis

To summarise, this thesis has made a number of novel contributions to the field of boron isotope geochemistry. In chapter 3, pH sensitivity in the δ^{11}B of *G. ruber* was calibrated for the first time, incorporating not just measurements from culture, but for the first time combining these measurements with those from open-ocean samples from tows, sediment traps and core-tops. In chapter 4, the symbiont-barren *G. bulloides* and deep-dwelling symbiont-bearing *O. universa* are calibrated, providing insights into the drivers of vital effects in planktic foraminifera. In chapter 5, the drivers of B/Ca ratios in open-ocean *G. ruber* are determined via statistical means, revealing that the carbonate system is not a strong control on B/Ca ratios, and throwing considerable doubt on its potential as a palaeo-environmental proxy.

6.2 Objectives met

6.2.1 Aim 1: Examining the sources of vital effects, and lowered pH-sensitivity, in foraminiferal δ^{11}B

The main goal of this PhD project was to determine the cause(s) of vital effects in planktic foraminiferal δ^{11}B. Through the comparison of the symbiont-bearing surface-dwelling foraminifera *G. ruber* (Chapter 3) with the deeper-dwelling *O.*

universa and the symbiont-barren *G. bulloides* (both Chapter 4), this PhD project provides further evidence that the action of symbionts in the foraminiferal microenvironment is key in determining both the direction and the magnitude of vital effects. Moreover, analyses of inorganic carbonate precipitates (Section 1.4.3), together with the seemingly steeper pH-sensitivity seen in symbiont-barren species (Chapter 4), suggests that photosynthetic symbionts may not only cause offsets in $\delta^{11}B_{CaCO_3}$ from the $\delta^{11}B_{B(OH)_4^-}$, but they may also be the cause of the reduced pH-sensitivity of $\delta^{11}B_{CaCO_3}$observed in *G. ruber*, *O. universa* and *G. sacculifer* (Sanyal et al., 1996, 2001, Henehan et al., 2013).

This project has yielded unexpected results from the symbiont-bearing species *O. universa*; namely that it records $\delta^{11}B$ that is *lower* than the $\delta^{11}B$ of ambient $B(OH)_4^-$ ion, not higher, as previous work would suggest (Sanyal et al., 1996, Zeebe et al., 2003). Previous calibration by Sanyal et al. (1996) appears to be subject to an interlaboratory bias. This is an powerful demonstration of the dangers of relying on NTIMS calibrations that may be accurate in terms of slope (i.e. pH-sensitivity), but whose position in terms of absolute $\delta^{11}B$ is not reliable. It also serves as a warning when applying the boron isotope-pH proxy to extinct foraminifera, that symbiont-bearing foraminifera do not necessarily produce $\delta^{11}B$ values above those of ambient $\delta^{11}B_{B(OH)_4^-}$: should their habitat depth extend to depths below their photosynthetic compensation point, they may record low $\delta^{11}B$ values more typical of symbiont-barren species.

6.2.2 Aim 2: Extending the applicability of the δ^{11}B-pH proxy through species-specific calibrations

This PhD project has extended the applicability of the $\delta^{11}B$-pH proxy both in increasing the number of calibrated species available to palaeoceanographers, and in investigating the possibility of using broad size-fractions in palaeo-applications (thereby mitigating sample-size constraints that can otherwise prove prohibitive).

The calibration of *G. ruber*, thought to be the shallowest-dwelling of the tropical foraminifera (Hemleben et al., 1989) and thus a better tool for reconstructing past atmospheric CO_2 levels, constitutes a major advance in boron isotope geochemistry and palaeo-CO_2 reconstruction. However, this species is restricted to low latitudes,

and so the reappraisal of δ^{11}B-pH relationships in *O. universa*, and the first characterisation of pH-sensitivity in a symbiont-barren species (*G. bulloides*), are valuable in extending the geographical range of the boron isotope-pH proxy.

Finally, investigations into size-related changes in δ^{11}B revealed a significant size-effect in *G. ruber*. In contrast, no such effect was discernible in *O. universa* or *G. bulloides*. While it is possible that size-related changes in δ^{11}B do exist in symbiont-barren forms like *G. bulloides* (as preliminary investigation in *G. inflata* suggest; see fig 4.9), trends may be obscured by a large degree of residual scatter, and as such further investigation is encouraged. In *O. universa*, however, no such scatter is observed, and the lack of size-related δ^{11}B changes seems robust. While site-specific corroboration of this observation is encouraged prior to downcore application, it seems that broad size-fractions in *O. universa* may be pooled for analysis, thereby reducing the sample-size restrictions that may often hinder application of the proxy.

6.2.3 Aim 3: Testing the applicability of the B/Ca proxy

This PhD project includes the first attempt to determine the controls on B/Ca ratios in *in situ* open-ocean planktic foraminifera, and yields surprising results. Although in culture B/Ca ratios in *G. ruber* were seen to be strongly influenced by the carbonate system (as also observed by Allen et al., 2012), in the open ocean the effect was undetectable. Instead, B/Ca ratios appear to be controlled by a combination of salinity and, more unexpectedly, $[PO_4^{3-}]$. Although further work is needed to better determine the relative importance of these two factors, and the specific mechanisms through which they might control B/Ca ratios, the observation that B/Ca is not a reliable recorder of past carbonate systems (at least in planktic foraminifera) is an important one.

If boron incorporation in foraminifera is controlled mainly by crystal growth surface processes, as the effects of salinity and PO_4^{3-} might suggest, it may imply that vacuolisation of seawater has limited effect on boron systematics in foraminifera. If incorporated boron is sourced not from the original vacuolised seawater (as implied by Rollion-Bard and Erez, 2010, Rae et al., 2011), but rather as the growing crystal face comes into contact with ambient seawater, it may explain how microenvironment

effects can be recorded in δ^{11}B even in the face of known elevation of internal pH. Further research, is required before this may be fully understood, however.

6.3 Future work

6.3.1 Foraminifera

6.3.1.1 Culturing of planktic foraminifera

While this PhD project has gone some way to improving our understanding of planktic foraminiferal vital effects, it has also prompted some questions. Firstly, it is clear that while most measurements of *O. universa* show a low level of residual scatter from the calibration line (Fig. 4.6), one measurement of towed *O. universa* from the Gulf of Aqaba (Eilat) records strikingly different δ^{11}B signals. It is important, therefore, that this matter is investigated, lest this be an indicator of cryptospecies or biogeographic variability. To this end, during an EU-funded research visit to the IUI, Eilat in the Autumn of 2013, we will undertake investigations into the cause of this variability. Namely, *O. universa* will be sampled from different depth habits, and will be cultured under light and dark conditions to investigate the controls on δ^{11}B signals in this area. Moreover, more detailed description of porosity and symbiont type will be undertaken, with a view to understanding the morphospecies (Morard et al., 2009) and the symbiont types (Shaked and Vargas, 2006) that are present in the Gulf of Aqaba (Eilat). Similarly, discrete measurements of the three morphotypes outlined by (Morard et al., 2009) would be desirable, particularly since cultures of *O. universa* from Puerto Rico (Hönisch et al., 2003, B. Hönisch, pers. comm.), and therefore presumably of the 'Caribbean' morphotype, appear to be offset from the calibration presented in Chapter 4.

Secondly, (Lombard et al., 2009) suggest that rates of net photosynthesis in planktic foraminifera should increase with temperature. Despite this, there is no clear relationship between deviation from $\delta^{11}B_{B(OH)_4^-}$ and temperature in calibration datasets of *G. ruber* (see Fig. 6.1) or *O. universa* (see Fig. 6.2). In light of this, we will attempt to culture *O. universa* under differing temperature conditions at the IUI, Eilat, and investigate whether there are any discernible effects on $\delta^{11}B_{CaCO_3}$.

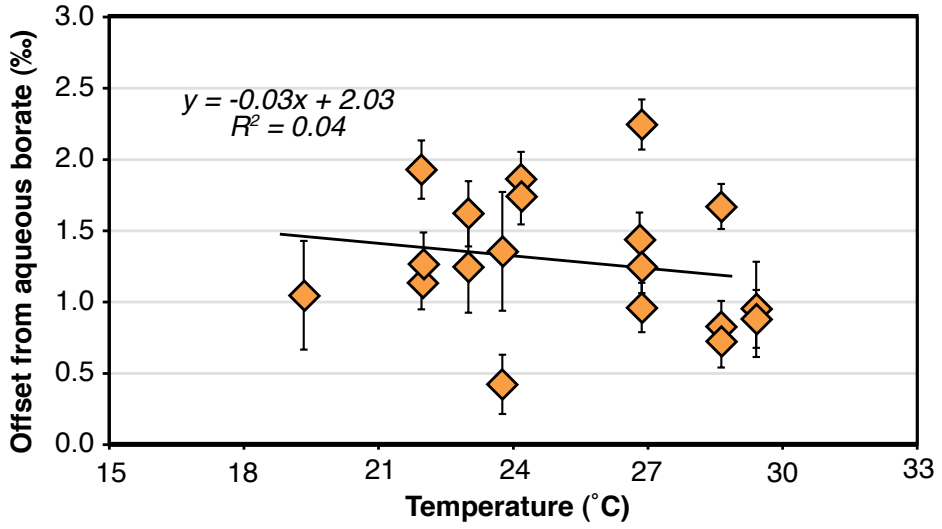

FIGURE 6.1: No correlation between the deviation from ambient $\delta^{11}B_{B(OH)_4^-}$ and temperature in *G. ruber*, suggesting no discernible temperature dependence beyond its documented effect on pK_B^*.

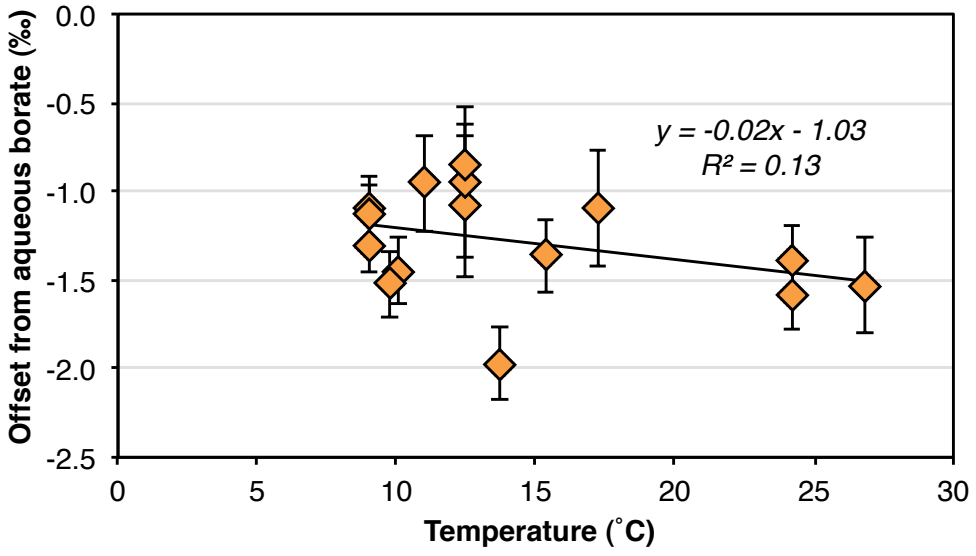

FIGURE 6.2: No correlation between the deviation from ambient $\delta^{11}B_{B(OH)_4^-}$ and temperature in *O. universa*, suggesting no discernible temperature dependence beyond its documented effect on pK_B^*. Note that the datapoint from Eilat (23 °C) is not included on this plot, because to do so would skew the regression unduly. In any case, inclusion of this measurement weakens the R^2 further.

6.3.1.2 Culturing of benthic foraminifera

Because of the limited range in pH (and hence $\delta^{11}B_{B(OH)_4^-}$) in the deep ocean, it is difficult to determine the pH-sensitivity of benthic foraminiferal $\delta^{11}B$ via *in situ* calibration alone. While the data of Rae et al. (2011) agree well with the ambient $\delta^{11}B$ of aqueous $B(OH)_4{}^-$ (calculated using a $^{11-10}K_B$ of 1.0272, following Klochko et al., 2006), they cannot, over such a limited range in aqueous $\delta^{11}B_{B(OH)_4^-}$, conclusively prove that pH-sensitivity in benthic foraminifera is equal to that of aqueous $B(OH)_4{}^-$. Therefore culturing of symbiont-barren benthic foraminifera over a broader range in ambient pH would be helpful in contributing to discussion of pH-sensitivity in biogenic $CaCO_3$.

6.3.1.3 B/Ca

The elevated B/Ca in epifaunal benthic foraminifera (Yu and Elderfield, 2007, Brown et al., 2011, Rae et al., 2011) relative to planktic foraminifera is perhaps counter-intuitive given the lower pH and $\frac{B(OH)_4^-}{DIC}$ in deep waters, and might imply some species-specificity of biomineralisation pathways. However, if PO_4^{3-} were the dominant control on foraminiferal B/Ca ratios, it would go some way to explaining the elevated B/Ca of benthic foraminifera. PO_4^{3-} levels are much higher in bottom waters than in surface waters, as a result of remineralisation of sinking organic matter, and may be even higher still in sediments as a result of the remobilisation of inorganic phosphates Froelich et al. (1979). Plotting benthic foraminiferal B/Ca ratios from *Cibicidoides wuellerstorfi* (Yu and Elderfield, 2007, Brown et al., 2011, Rae et al., 2011) against $[PO_4^{3-}]$ (Fig. 6.3) sees some overlap with the B/Ca-$[PO_4^{3-}]$ trend derived from *G. ruber*, but the overall agreement in benthic foraminiferal B/Ca data with the trend is poor, particularly at higher levels of $[PO_4^{3-}]$.

As shown in (Fig. 6.4), however, the degree of deviation from the *G. ruber* B/Ca-$[PO_4^{3-}]$ trend is strongly correlated to salinity ($R^2 = 0.82$). As such it seems possible that a combination of PO_4^{3-} and salinity might also explain published benthic data. Moreover, the correlation of residual variation with salinity is both stronger and of steeper slope than the similar relationship in *G. ruber*. This might suggest that salinity and phosphate affect B/Ca in a synergistic manner, with B/Ca ratios more

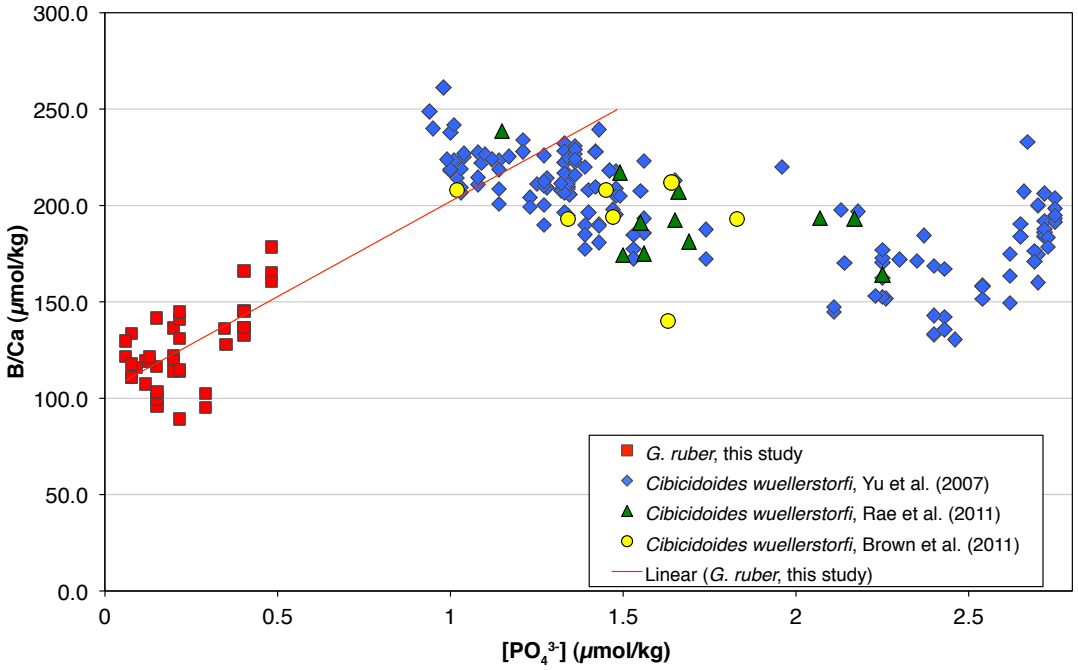

FIGURE 6.3: Some data from the benthic foraminifera *Cibicidoides wuellerstorfi* (taken from Yu and Elderfield, 2007, Brown et al., 2011, Rae et al., 2011) shows consistency with the B/Ca-$[PO_4^{3-}]$ relationship seen in *G. ruber*. However, some other factor is clearly at work; there is considerable deviation from the *G. ruber* relationship (see Fig. 6.4 below).

sensitive to changes in salinity at higher $[PO_4^{3-}]$. Such a finding might also explain anomalous B/Ca ratios in *G. ruber* from the Gulf of Aqaba: while salinity is very high, oligotrophic, low PO_4^{3-} waters may mean that the effect of this high salinity is dampened. The correlations seen elsewhere between benthic foraminiferal data and ΔCO_3^{2-} (Yu and Elderfield, 2007, Brown et al., 2011, Rae et al., 2011) might well be at least partly explained by the correlation of ΔCO_3^{2-} and salinity in each of these datasets. While further culturing and core-top calibration (including data from *O. universa* and *G. bulloides*) is required to more fully disentangle the effects of these factors, their relative importance, and possible interactions between the two, it may well be that B/Ca ratios in both planktic and benthic foraminifera are controlled by the same environmental variables (i.e. $[PO_4^{3-}]$ and salinity). If so, this would suggests a universal abiotic control on B/Ca ratios in foraminiferal carbonates, more strongly linked to crystal surface processes (as was previously advocated by Hemming et al., 1995) than concentrations of aqueous $B(OH)_4^-$ ion alone.

Clearly there is cause to pursue these lines of investigation further, as if such a

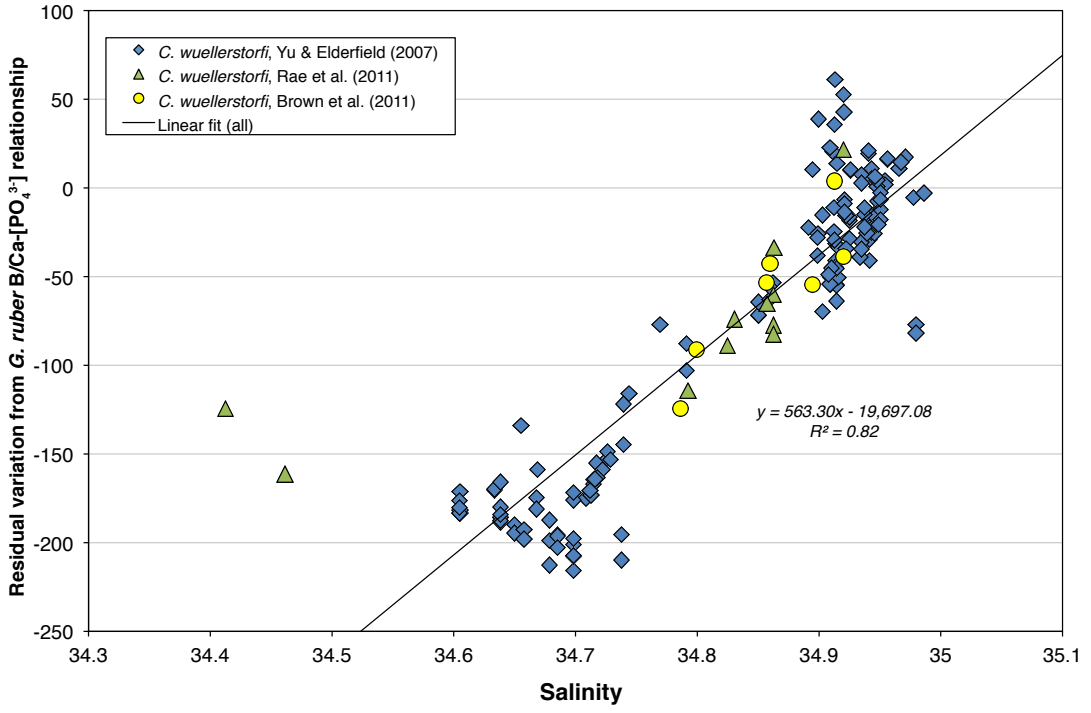

FIGURE 6.4: Residual variation from the PO_4^{3-} relationship identified in *G. ruber* (Fig. 6.3) in *Cibicidoides wuellerstorfi* (Yu and Elderfield, 2007, Brown et al., 2011, Rae et al., 2011) correlates strongly with salinity, and with a steeper slope than that seen in *G. ruber*.

hypothesis were correct it would throw considerable doubt on the use of B/Ca as a carbonate system proxy. As part of our next trip to Eilat in the Autumn of 2013, we will grow planktic foraminifera under varying $[PO_4^{3-}]$ and salinity levels, varying feeding rates and varying light levels, to investigate possible effects on B/Ca ratios. In this way we can directly test the effects of P on boron incorporation in foraminiferal tests, and test whether the correlation seen in core-top material is as a result of the direct interaction of P at the crystal growth face, or whether factors such as food availability (which may correlated with $[PO_4^{3-}]$ in the open ocean), and hence metabolic rates, may be at play. In addition, similar statistical treatment to that carried out for *G. ruber* (Chapter 5) will be applied to measurements of *O. universa*, *G. bulloides* and *G. inflata*, to determine whether the controls are comparable. Beyond this, culturing benthic foraminifera under different $\Delta[CO_3^{2-}]$, salinity and nutrient levels would be of great benefit, and allow us to better determine the controls on B/Ca ratios in this group: *in situ* calibration studies to date are limited by the covariance of carbonate system parameters with salinity and nutrient concentrations.

6.3.2 Coccolithophore δ^{11}B and B/Ca

While foraminiferal carbonates are thought to be precipitated from vacuolised seawater (e.g. Bentov et al., 2009), calcification in coccolithophores is more fully internalised: all component molecules are transported to an internal coccolith vesicle via the Golgi body (Young et al., 1999, and references within). Consequently boron incorporation and boron isotope systematics in coccolithophores constitute an interesting contrast with the boron systematics of foraminifera. Current modelled understanding of boron incorporation in coccolithophores (Stoll et al., 2012) suggests boron diffuses into the cell as boric acid (as this form of boron is more prone to diffusion through membranes Dordas and Brown, 2000, 2001, Tanaka and Fujiwara, 2008). After equilibration in the cytosol, the resultant boric acid then diffuses into the coccolith vacuole, where it again re-equilibrated to modified pH and is incorporated into coccolith calcite (see Fig. 6.5).

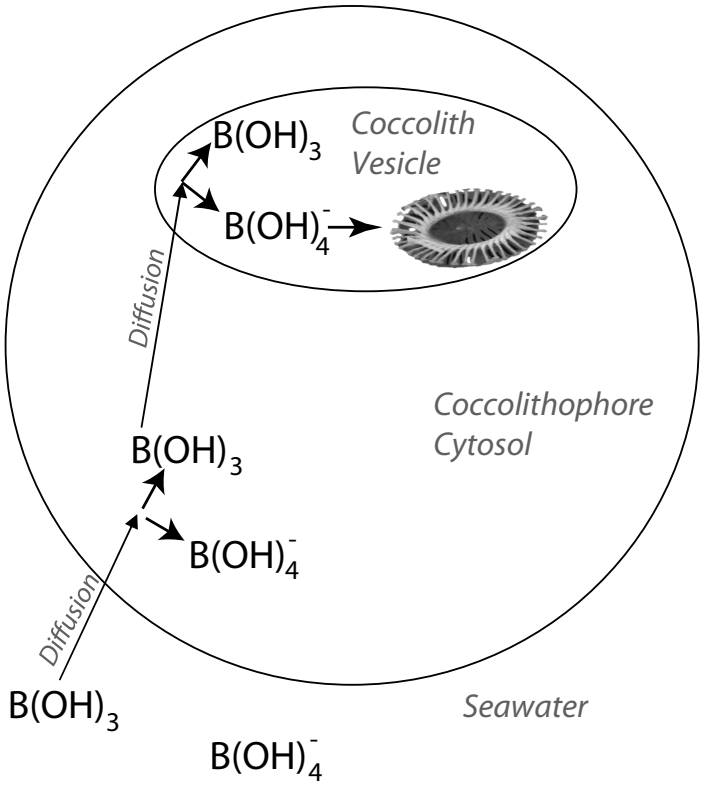

FIGURE 6.5: A model for the incorporation of boron into coccoliths, based on sequential diffusion and re-coordination of boric acid. Modifed from Stoll et al. (2012).

Assuming boron substitutes into $CaCO_3$ via substitution at the CO_3^{2-} site, B/Ca in

coccolith calcite should then vary with DIC concentrations in the coccolith vesicle, to a degree that is dependent on the partition coefficient (K_D) for B. Meanwhile, δ^{11}B should infer some information as to the pH of the coccolith vesicIe, given an estimate of cytosol (e.g. Anning et al., 1996). Therefore, application of both of these geochemical measurement techniques may provide some information as to biomineralisation pathways in coccolithophores, and their vulnerability to ocean acidification stress (Stoll et al., 2012). The only published measurements of B/Ca ratios in coccoliths (Stoll et al., 2012) come from ion probe analyses, and reveal a high level of inter-strain variation (from <10 - 60 μmol/mol), with faster-growing strains reporting higher B/Ca. These authors highlight the need to develop boron isotope measurement techniques in coccolithophores, to shed further light on biomineralisation pathways.

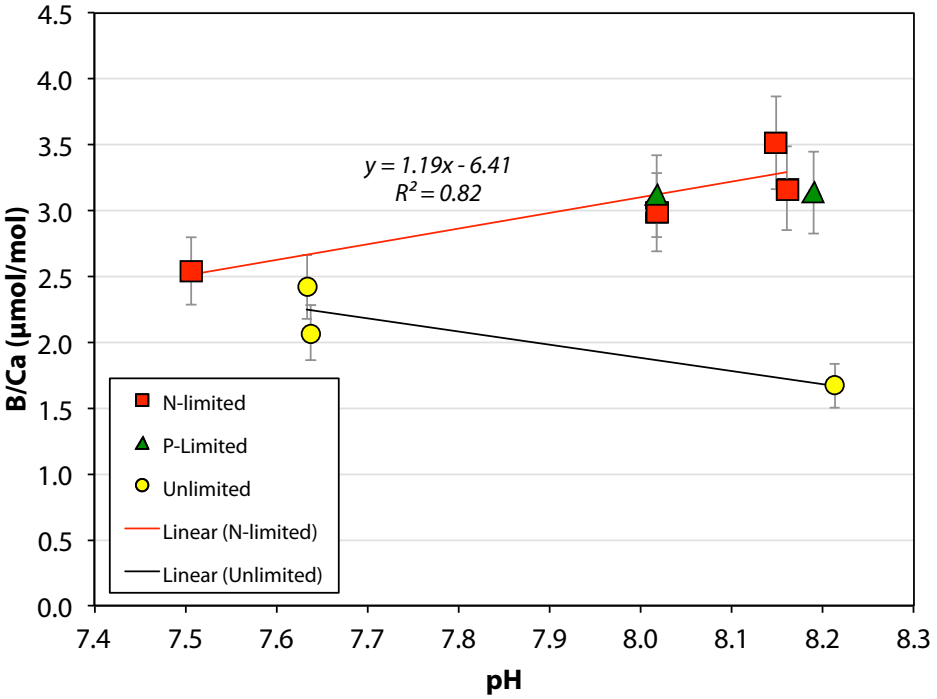

FIGURE 6.6: B/Ca ratios in *E. huxleyi*, cultured across a range in pH. Observed ratios were much lower than in previous studies (Stoll et al., 2012). Note that B/Ca increases slightly with pH in nutrient-limited cultures, but decreases in unlimited (Redfield ratio) nutrient conditions.

With this study in mind, a collaboration has begun between myself, Dr. Gavin Foster, Mr. Oscar Branson (now University of Cambridge) and Prof. Heather Stoll (University of Oviedo), to determine the relationship between ambient pH and coccolith δ^{11}B. *Emiliania huxleyi* were cultured across a range in pH and nutrient availability,

concentrated by centrifuge and freeze-dried. Due to the high organic content in the resultant sample agglomerate, considerable research was required to ascertain the most effective cleaning method. Cleaning methods used by Stoll et al. (2012) were found to be ineffective in this case, and so new methods were developed (detailed in Appendix D). Samples were then dissolved in 0.5M HNO_3, with an aliquot taken for trace element analysis. While data collection is in progress, B/Ca ratios measured to date are shown in Fig. 6.6. Observed boron concentrations are low (1.5 - 4 μmol/mol B/Ca), but appear in nutrient-limited samples to increase with increasing ambient pH. In contrast, in nutrient-unlimited samples (i.e. C, N and P, all present in Redfield Ratio), B/Ca ratios show no such increase.

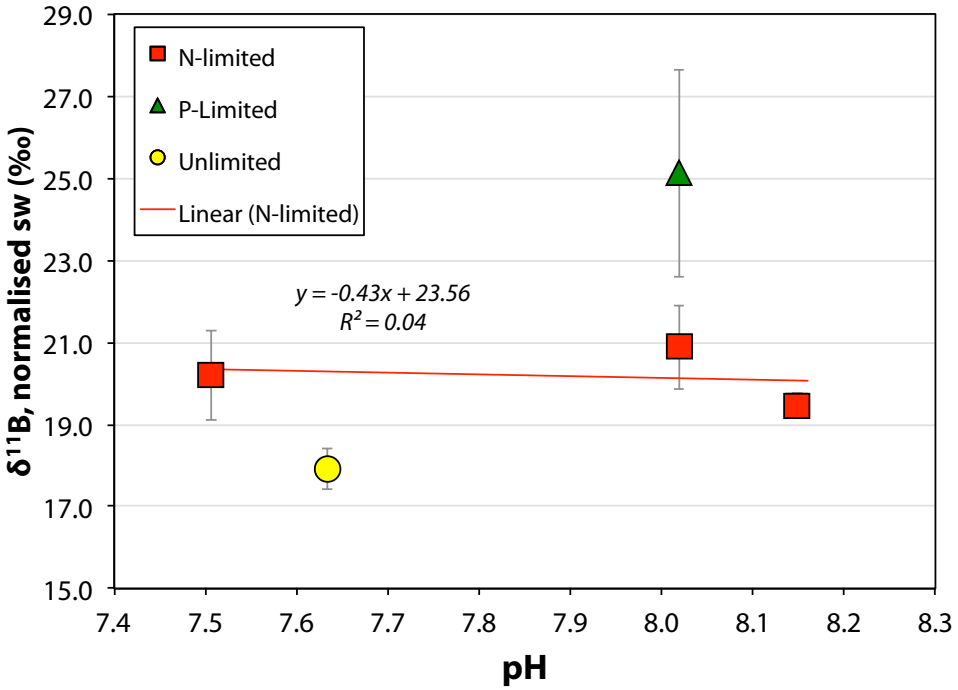

FIGURE 6.7: δ^{11}B measurements from *E. huxleyi*, cultured across a range in pH. In N-limited cultures, δ^{11}B does not increase with pH, suggesting that pH in the calcifying vesicle remains constant regardless of ambient pH. Divergent values in P-limited and nutrient-unlimited cultures suggest that calcifying vesicle pH is affected by nutrient availability.

Once B/Ca ratios were determined, boron was isolated using ion-specific resin (see Section 2.2.2), and boron isotopes determined via MC-ICPMS (Section 2.4). Because of the low boron concentrations seen in *E. huxleyi*, and thus the smaller sample sizes (as little as < 1 ng in some cases) analytical reproducibility is rather poorer than in

foraminiferal measurements (as much as ± 2 ‰). Nonetheless, it seems clear that where all three pH treatments have been analysed for $\delta^{11}B$ (the low-N treatment; see Fig. 6.7), there is no discernible change in $\delta^{11}B_{CaCO_3}$ with change in ambient pH. However, again, nutrient treatment appears to be key, with P-limited and nutrient-unlimited samples showing very disparate $\delta^{11}B$ signals.

Since this work is still in progress, and more data is still to be collected, it is somewhat premature to draw conclusions as to the significance of this data. Moreover, it will be necessary to more fully investigate the reliability of measurements of B/Ca ratios at such low [B] before trends in B/Ca data can be interpreted. That said, comparison with the model of Stoll et al. (2012) does permit some tentative conclusions to be drawn (see Fig. 6.8). For example, the low B/Ca ratios of these cultured coccolithophores do seem to imply that coccolith vesicle pH in *E. huxleyi* is likely to be variable, but low (< 7.6), and that coccolith vesicles probably contain variable, but very high, concentrations of DIC (potentially exceeding 10,000 μmol/kg; see Fig. 6.9). While perhaps surprising, these values are not inconsistent with published internal pH estimates for coccolithophores (see Anning et al., 1996, and references within).

While further analyses and modelling is required to fully understand these data, they constitute the first ever boron isotope measurements in coccoliths, and the first analysis of B/Ca ratios in coccoliths via ICPMS. Although separation of coccolith calcite from clay remains problematic (Minoletti et al., 2009), and thus the use of coccolith calcite in palaeo-reconstructions, is still some way off, these data may yet offer unique insight into the biomineralisation pathways of coccolithophores and their potential vulnerability to ocean acidification.

6.3.3 Prospects for Analytical Advances

6.3.3.1 Sample Size Limitations: $10^{12}\Omega$ resistors

As demonstrated in this thesis, the boron isotope-pH proxy has enormous potential. However, to meet the practical demands of the palaeoceanographic community, and to extend the proxy to low-[B] sample material like coccoliths, sample size constraints must be eased. Despite considerable recent advances, one of the biggest problems with the analysis of boron isotopes in foraminifera by MC-ICPMS remains the relatively

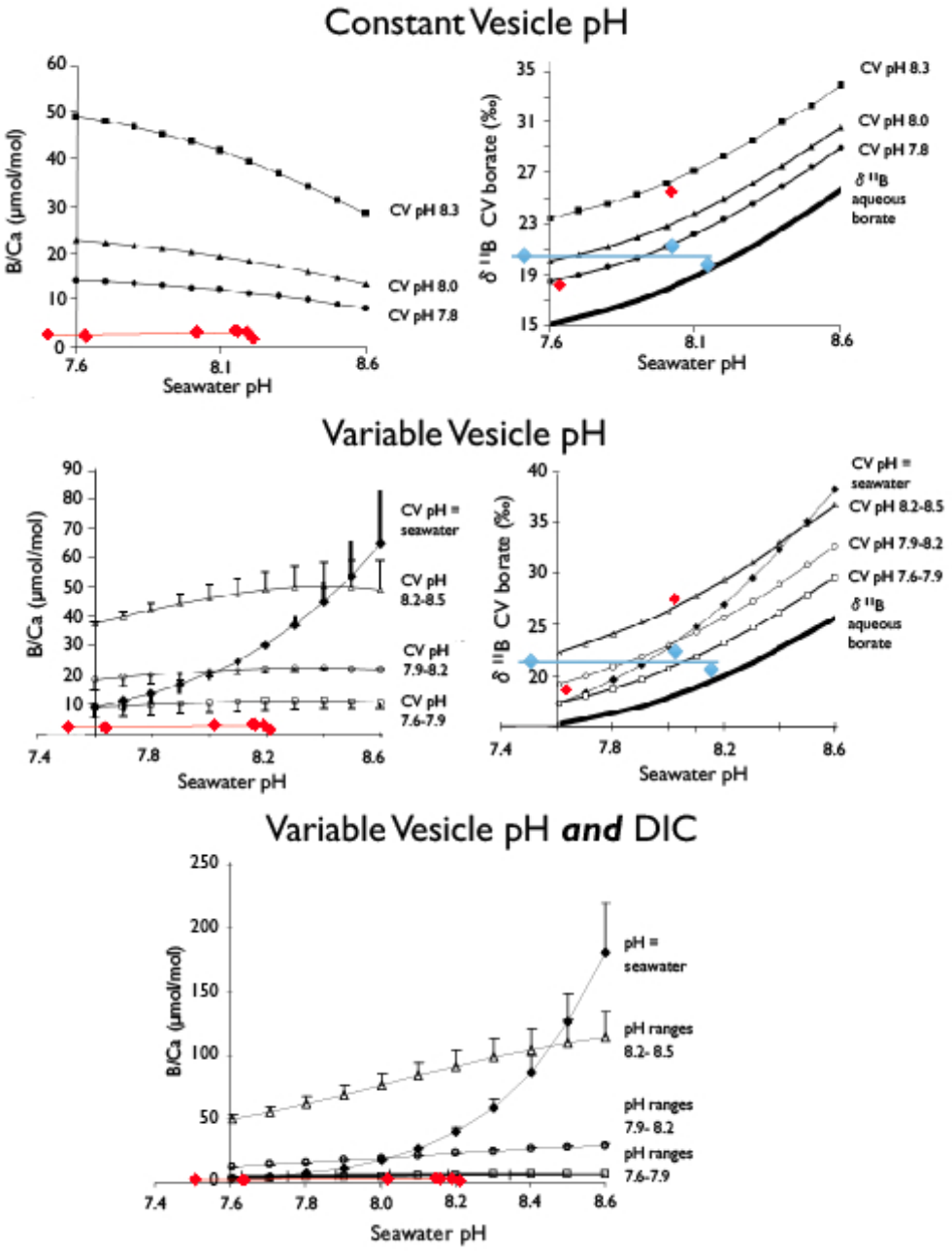

FIGURE 6.8: Comparison of B/Ca and δ^{11}B variation with pH in *Emiliana huxleyi* with model results from Stoll et al. (2012). Low B/Ca ratios fit best with a low, variable pH and [DIC] coccolith vesicle. In panels referring to δ^{11}B, blue datapoints (and the blue trendline) denote a full pH-range experiment at one nutrient treatment (low-N), while the remaining red datapoints are at different nutrient conditions. Note for B/Ca all data are marked in red, regardless of nutrient treatment.

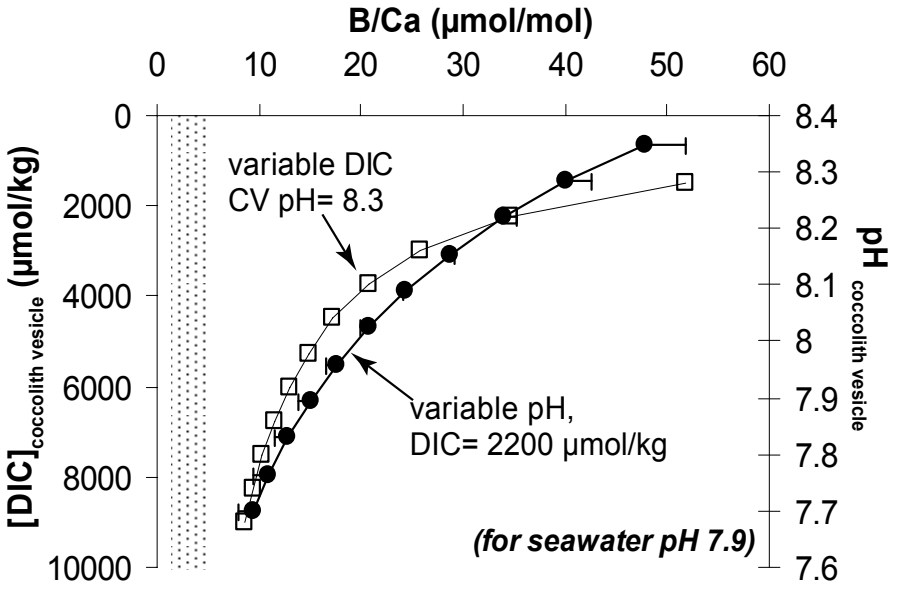

FIGURE 6.9: For a given pH of seawater (7.9), this figure illustrates the degree of variation in coccolith vesicle pH or [DIC] which would be required to produce a given B/Ca ratio (according to the model of Stoll et al., 2012) Open squares assume varying DIC in the coccolith vesicle, but a stable pH (8.3), while black circles assume a constant DIC (2200 μmol/kg) but a varying pH. The shaded region indicates the typical B/Ca ratios observed in cultures of *E. huxleyi*. Model assumes a constant K_D of 0.0005. Modified from Stoll et al. (2012).

large sample size required. Depending on the typical [B] of the species and the size fraction used, between 50 (*Orbulina universa*, >600 μm diameter) and 450 (*Globigerina bulloides*, 250-300 μm diameter) individual foram tests must be combined to attain enough B to generate a strong ^{11}B signal (typically 15-20 ng B translates to 600-800 mV at optimal stability). One of the reasons for this, discussed in detail in (Rae, 2011, Chapter 3), is that below a threshold level ($\sim$ 100mV), Johnson noise (background baseline noise) on the $10^{11}\Omega$ resistor will contribute an increasingly significant amount to the total uncertainty. Uncertainty (1 SE) resulting from Johnson Noise (σ_{JN} is calculated via Equation 6.1 below, where k is the Boltzmann constant (1.30×10^{-23} J K^{-1}), R is the amplifier resistance, T is the operating temperature ($\sim$300 °K), and t is the length of time taken for a measurement (125.82 s).

$$\sigma_{\mathrm{JN}} = \sqrt{\frac{4kRT}{t}} \tag{6.1}$$

One possible improvement in this area is the utilisation of $10^{12}\Omega$ resistors. Given the derivation of Johnson noise above (Equation 6.1) a decrease in the resistance associated with amplifiers (R) by an order of magnitude should significantly reduce Johnson Noise. These amplifiers have been installed at NOCS, and initial testing by Rosanna Greenop has revealed a marked improvement in precision in small samples. After some further testing, these amplifiers will soon be in operation at NOCS, and as a consequence reproducibility of small samples is likely to improve in the near future.

6.3.3.2 Automation

Besides reducing sample size requirements, if we are to reach a point where boron isotope measurements can be made on scales approaching that of stable oxygen and carbon isotopes (see for example Zachos et al., 2008), sample throughput must be improved. To this end, members of the B-Team at the NOC (Dr. Miguel-Angel Martínez-Botí and Dr. Eleni Anagnostou) are currently working with ESI Instruments to design an automated device to perform column chemistry. Although testing is still in progress, this system could vastly improve the time-efficiency of boron isotope analysis and hence contribute significantly to a deeper understanding of carbon cycle-climate dynamics.

6.4 Concluding Remarks

To conclude, this PhD project has made significant steps forward in extending the applicability of the boron isotope-pH proxy, by contributing to our understanding of the inorganic basis of the proxy, the causes behind (and variability in) foraminiferal 'vital effects', and the mechanisms of boron incorporation in foraminiferal calcite. This project will permit greater confidence in future reconstructions of palaeo-CO_2, by provision of accurate new species-specific calibrations, and new approaches for uncertainty propagation. Through these improved estimates of past CO_2 levels, we can gain a greater understanding of the climate's sensitivity to changes in greenhouse gas concentrations, and of the role of CO_2 in important climate transitions and events, including the end-Cretaceous extinction, the Palaeocene-Eocene Thermal Maximum and other Eocene hyperthermals, and the underlying rise in Eocene temperatures in

the run up to the Middle-Eocene Climatic Optimum, as well as the Eocene-Oligocene and Plio-Pleistocene transitions.

Appendix A

Published Manuscript: Henehan et al. (2013)

Michael J. Henehan, James W. B. Rae, Gavin L. Foster, Jonathan Erez, Katy Prentice, Michal Kucera, Helen C. Bostock, Miguel A. Martínez-Botí, J. Andy Milton, Paul A. Wilson, Brittney J. Marshall, and Tim R. Elliott, (2013). *Calibration of the boron isotope proxy in the planktonic foraminifera Globigerinoides ruber for use in palaeo-CO_2 reconstruction.* Earth and Planetary Science Letters **(364)** 111-122.

Earth and Planetary Science Letters 364 (2013) 111–122

Contents lists available at SciVerse ScienceDirect

Earth and Planetary Science Letters

journal homepage: www.elsevier.com/locate/epsl

Calibration of the boron isotope proxy in the planktonic foraminifera *Globigerinoides ruber* for use in palaeo-CO_2 reconstruction

Michael J. Henehan [a,*], James W.B. Rae [b], Gavin L. Foster [a], Jonathan Erez [c], Katherine C. Prentice [d], Michal Kucera [e], Helen C. Bostock [f], Miguel A. Martínez-Botí [a], J. Andy Milton [a], Paul A. Wilson [a], Brittney J. Marshall [g], Tim Elliott [b]

[a] Ocean and Earth Science, National Oceanography Centre Southampton, University of Southampton Waterfront Campus, European Way, Southampton SO14 3ZH, UK
[b] Bristol Isotope Group, Department of Earth Sciences, Bristol University, Wills Memorial Building, Queens Road, Bristol BS8 1RJ, UK
[c] Institute of Earth Sciences, The Hebrew University, Givat Ram, Jerusalem 91904, Israel
[d] Department of Earth Science and Engineering, Imperial College London, South Kensington SW7 2AZ, UK
[e] MARUM-Centre for Marine Environmental Sciences and Faculty of Geosciences, University of Bremen, Loebener Strasse, 28359 Bremen, Germany
[f] National Institute for Water and Atmospheric Research, Evans Bay Parade, Wellington, New Zealand
[g] Department of Earth and Ocean Sciences, University of South Carolina, Columbia, SC 29208, USA

ARTICLE INFO

Article history:
Received 17 July 2012
Received in revised form
20 December 2012
Accepted 21 December 2012
Editor: G. Henderson

Keywords:
boron isotopes
Globigerinoides ruber
MC-ICPMS
culture calibration
pCO_2 reconstruction
planktic foraminifera

ABSTRACT

The boron isotope-pH proxy, applied to mixed-layer planktic foraminifera, has great potential for estimating past CO_2 levels, which in turn is crucial to advance our understanding of how this greenhouse gas influences Earth's climate. Previous culture experiments have shown that, although the boron isotopic compositions of various planktic foraminifera are pH dependent, they do not agree with the aqueous geochemical basis of the proxy. Here we outline the results of culture experiments on *Globigerinoides ruber* (white) across a range of pH (~7.5–8.2) and analysed via multicollector inductively-coupled plasma mass spectrometry (MC-ICPMS), and compare these data to core-top and sediment-trap samples to derive a robust new species-specific boron isotope-pH calibration. Consistent with earlier culture studies, we show a reduced pH dependency of the boron isotopic composition of symbiont-bearing planktonic foraminifera compared to borate ion in seawater. We also present evidence for a size fraction effect in the $\delta^{11}B$ of *G. ruber*. Finally, we reconstruct atmospheric CO_2 concentrations over the last deglacial using our new calibration at two equatorial sites, ODP Site 999A and Site GeoB1523-1. These data provide further grounding for the application of the boron isotope-pH proxy in reconstructions of past atmospheric CO_2 levels.

1. Introduction

1.1. The boron isotope-pH proxy

The use of boron isotopes in surface-dwelling planktic foraminifera to reconstruct ocean pH, and hence past levels of atmospheric CO_2 (expressed as partial pressure: pCO_2), offers great promise (Foster, 2008; Hönisch and Hemming, 2005; Hönisch et al., 2009; Palmer et al., 2010; Pearson and Palmer, 2000; Pearson et al., 2009; e.g. Sanyal et al., 1995). However, because of the range of offsets from the boron isotope composition of ambient borate ion that has been reported to date in planktonic foraminifera (Sanyal et al., 1996, 2001; Hönisch et al., 2003; Hönisch and Hemming, 2004; Foster, 2008), application of the proxy beyond those extant species with species-specific calibrations requires further assumptions to be made. Clearly, then, it is important to extend the range of planktonic foraminiferal species for which empirical calibrations exist, and in doing so better understand exactly how the observed offsets from borate ion, known collectively as "vital effects", arise.

The boron isotope-pH proxy has a well-understood foundation in inorganic chemistry that sets it apart from more empirically-derived proxies (e.g. Li/Ca) and that, providing biological interferences are understood, should permit greater confidence in boron-based palaeo-pH and -pCO_2 estimates. This chemical basis, summarised briefly here, is dealt with in more detail elsewhere (Foster, 2008; Hemming and Hanson, 1992; Hemming and Hönisch, 2007; Pagani et al., 2005; Rae et al., 2011; Sanyal et al., 2000; e.g. Vengosh et al., 1991).

Boron has two stable isotopes, ^{11}B and ^{10}B (approximately 80% and 20% of total B respectively), with isotopic composition expressed in delta notation as $\delta^{11}B$ relative to NIST-SRM 951 boric acid (Catanzaro et al., 1970), where

$$\delta^{11}B = \left(\frac{^{11}B/^{10}B_{sample}}{^{11}B/^{10}B_{NISTSRM\ 951}} - 1 \right) \times 1000 \quad (1)$$

* Corresponding author. Tel.: +44 2380 596539.
E-mail address: M.J.Henehan@soton.ac.uk (M.J. Henehan).

0012-821X/$ - see front matter © 2012 Elsevier B.V. All rights reserved.
http://dx.doi.org/10.1016/j.epsl.2012.12.029

Boron is present in seawater almost exclusively as either tetrahedrally-coordinated borate ion, $B(OH)_4^-$, or trigonally-coordinated boric acid, $B(OH)_3$, with the relative abundances of these compounds dependent on pH (see Fig. 1A). Equilibration is rapid (Zeebe et al., 2001) and described by the following disassociation equation:

$$B(OH)_3 + H_2O \Leftrightarrow B(OH)_4^- + H^+ \quad (2)$$

Associated with this equilibration is an isotopic fractionation, described as

$$^{10}B(OH)_3 + {}^{11}B(OH)_4^- \Leftrightarrow {}^{11}B(OH)_3 + {}^{10}B(OH)_4^- \quad (3)$$

where the equilibrium constant $^{11-10}K_B$ is defined in Eq. (4) below

$$^{11-10}K_B = \frac{[^{11}B(OH)_3] \times [^{10}B(OH)_4^-]}{[^{10}B(OH)_3] \times [^{11}B(OH)_4^-]}. \quad (4)$$

This constant is often termed α_{3-4} or α_B (e.g. Rae et al., 2011) but, following Klochko et al. (2006), we use $^{11-10}K_B$ here. This equilibrium constant was derived experimentally by Klochko et al. (2006) as 1.0272 ± 0.0006 (in seawater and at 25 °C). This value is in-keeping with the results of numerous independent theoretical studies (e.g. Oi, 2000; Liu and Tossell, 2005; Zeebe, 2005; Rustad and Bylaska, 2007) advocating values in the range of 1.025–1.035. Given a value for $^{11-10}K_B$, the isotopic composition of both boron species in seawater varies predictably with pH (see Fig. 1B). Correspondingly, pH can be calculated from the $\delta^{11}B$ of either boron species, for instance for $\delta^{11}B$ of borate as

$$pH = pK_B^* - \log\left(-\frac{\delta^{11}B_{sw} - \delta^{11}B_{borate}}{\delta^{11}B_{sw} - (^{11-10}K_B \times \delta^{11}B_{borate}) - 1000(^{11-10}K_B - 1)}\right) \quad (5)$$

where pK_B^* is the disassociation constant for boric acid at *in situ* temperature, salinity and pressure (most commonly calculated as per Dickson, 1990). $\delta^{11}B_{sw}$ is the isotopic composition of seawater (39.61‰; Foster et al., 2010), and $^{11-10}K_B$ is 1.0272 ± 0.0006 (Klochko et al., 2006). Since only the charged borate ion is thought to be incorporated into biogenic calcite (Hemming and Hanson, 1992; Hemming et al., 1995), the boron isotopic composition of $CaCO_3$ can be used to calculate ocean pH (as $\delta^{11}B_{borate}$ in Eq. (5)) provided any vital effects have been accounted for.

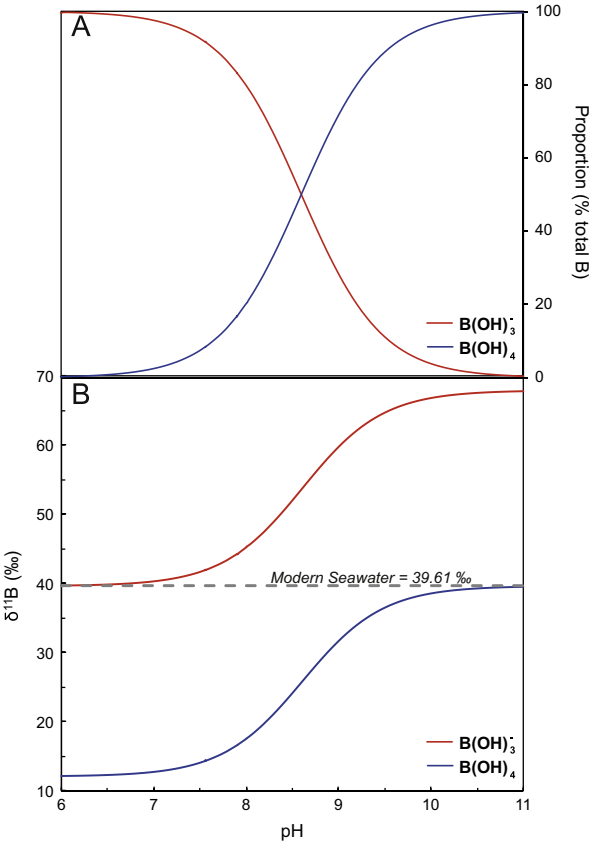

Fig. 1. (A) The relative distribution of boron species in seawater over a range of pH at 25 °C and 35 psu, with pK_B^* calculated according to Dickson (1990). (B) The changing isotopic composition of each species according to Eq. (3) in the text.

1.2. Calibration attempts to date

Culture studies are an important tool in calibrating foraminifera-based proxies, allowing for manipulation of growth conditions beyond the range seen in the modern oceans (e.g. Allen et al., 2011). In the case of the boron isotope-pH proxy, attempts have been made to calibrate the symbiont-bearing foraminifera *Orbulina universa* (Sanyal et al., 1996) and *Globigerinoides sacculifer* (Sanyal et al., 2001) across a range of pH (7.6–9). These culture studies confirmed that the $\delta^{11}B$ of planktic foraminiferal calcite is strongly dependent on pH, but also describe a weaker sensitivity to pH in foraminiferal $\delta^{11}B_{CaCO_3}$ compared to $\delta^{11}B_{borate}$ (Fig. 2A). While these studies were pioneering, some uncertainty still remains in the robustness of these relationships. For instance, some carbonate system parameters during culture in these studies are relatively poorly constrained (e.g. pH only determined using NBS-buffer-calibrated electrodes, with the magnitude of any correction to total scale greatly influencing conclusions to be made: see Supplementary Fig. S1) and some experiments (e.g. Sanyal et al., 2001) were performed at 10× natural boron concentration, introducing additional uncertainty by increasing the buffering capacity of culture seawater and thus potentially dampening 'vital effects' (Zeebe et al., 2003). Furthermore, limited core-top calibration attempts by Foster (2008) (measured by multicollector inductively coupled plasma mass spectrometry; MC-ICPMS) suggested a stronger pH sensitivity in the $\delta^{11}B$ of *G. ruber* and *G. sacculifer* (close to that of borate ion), leading to the suggestion that these previous calibrations may have been compromised by analytical issues related to the analytical technique used (negative ion thermal ionisation mass spectrometry; NTIMS; e.g., Foster, 2008; Ni et al., 2010). Therefore, further culture calibrations are required, both to corroborate previously reported pH sensitivities and to extend the applicability of the boron isotope-pH proxy to more species of foraminifera.

1.3. Presentation of species calibrations

The most common way to present boron isotope data from cultured foraminifera is in terms of the observed $\delta^{11}B$–pH relationship (Fig. 2A). This, however, leads to difficulties in comparing calibrations generated under differing temperatures and salinities, where the value of pK_B^* differs, introducing the need for normalisation. For example, in Fig. 2A, calibration datasets are normalised to our culture conditions (26 °C and 37.2 psu), based on the change in aqueous $\delta^{11}B_{borate}$ expected if pK_B^* were altered to reflect these conditions. Similarly, application of these calibrations to open ocean foraminiferal data must include some correction for pK_B^* differences between datasets.

Furthermore, in order to present boron isotope data in terms of the observed $\delta^{11}B$–pH relationship, it is necessary to characterise

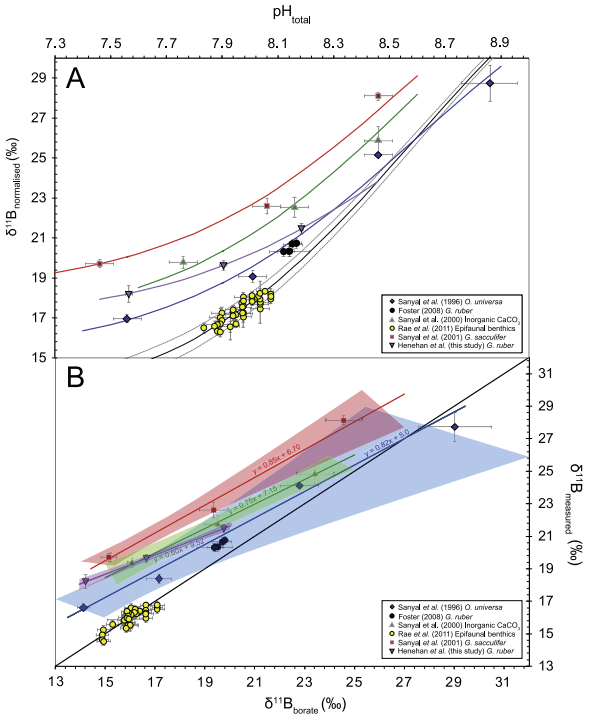

Fig. 2. Published planktic foraminiferal culture and inorganic precipitate experiments, plotted in δ^{11}B–pH space (top panel) and in $\delta^{11}B_{CaCO_3}-\delta^{11}B_{borate}$ space (bottom panel). Note that for the purposes of graphical representation, the data were normalised to a $\delta^{11}B_{sw}=39.61‰$ (both panels), and to a temperature of 26 °C and a salinity of 37.2 psu (the conditions of our culture calibration, top panel only). The black line in δ^{11}B–pH space is the aqueous value of $\delta^{11}B_{borate}$ at these environmental conditions, with the dotted lines representing the uncertainty on the value of $^{11-10}K_B$ (0.0006) in seawater at 25 °C reported by Klochko et al. (2006). Coloured calibration lines are best fits, varying $^{11-10}K_B$ and a from Eq. (6). The black line in $\delta^{11}B_{CaCO_3}-\delta^{11}B_{borate}$ space (bottom panel) is a 1:1 relationship, i.e. a pH sensitivity equal to that of borate ion. Calibrations are represented by the York regressions calculated using Isoplot (Ludwig, 2003), with shaded areas representing 95% confidence intervals for these regressions. Note that it was not possible to calculate 95% confidence intervals for the data of Rae et al. (2011) or Foster (2008) using this method, as the spread in $\delta^{11}B_{borate}$ is insufficient, but they are included for comparison, having been used elsewhere in downcore reconstructions. Carbonate system parameters for Sanyal et al. (1996, 2000, 2001) are adjusted from NBS scale to total scale by subtraction of −0.14. While this is no doubt more representative than no correction at all, we emphasise that NBS-total scale conversions are not necessarily universal and that the correction used is critical to the resultant slope (see Supplementary Fig. S1). As such we emphasise that the Sanyal calibrations are plotted more for comparison of trend than for comparison of exact positioning of that trend on any one axis. (For interpretation of the references to colour in this figure legend, the reader is referred to the web version of this article.)

species' δ^{11}B–pH relationships by forcing them to fit the general equation for boron isotope–pH calculation (Eq. (5) above). This can be done by incorporation of a constant offset or 'vital effect' termed 'a' into Eq. (5), such that $\delta^{11}B_{borate}=\delta^{11}B_{CaCO_3}-a$.

$$pH=pK_B^*-\log\left(-\frac{\delta^{11}B_{sw}-(\delta^{11}B_{CaCO_3}-a)}{\delta^{11}B_{sw}-{}^{11-10}K_B(\delta^{11}B_{CaCO_3}-a)-1000({}^{11-10}K_B-1)}\right) \quad (6)$$

In addition, the fit of empirical data to an equation of this form can also be optimised by altering the $^{11-10}K_B$ constant (Table 1; Hönisch et al., 2007). The addition of an offset 'a' to an aqueous $\delta^{11}B_{borate}$–pH curve (Foster, 2008; as in Hönisch and Hemming, 2005), however, implies that any such 'vital effect' is constant across a range of pH. Past modelling efforts (Zeebe et al., 2003) provide some support for this argument, but it must be noted that no culture calibration performed to date (our own included) shows a constant offset from the $^{11-10}K_B$ of Klochko et al. (2006). In addition, any optimisation of $^{11-10}K_B$ in tandem with an offset 'a', as used by Hönisch et al. (2007) to characterise $\delta^{11}B_{carbonate}$–pH curves of published empirical data, might be misconstrued as implying $^{11-10}K_B$ is not 1.0272, rather than that these empirical calibrations exhibit pH sensitivities different from the pH sensitivity of $\delta^{11}B_{borate}$.

Given these difficulties, we instead describe culture calibration data following Foster et al. (2012). Similar to Rollion-Bard and Erez (2010), who plot calculated pH vs. culture pH, this approach involves a linear regression between aqueous $\delta^{11}B_{borate}$ (at *in situ* conditions) and measured $\delta^{11}B_{CaCO_3}$ (Fig. 2B). Given measured $\delta^{11}B_{CaCO_3}$, one can use the appropriate calibration regression to predict the value of ambient $\delta^{11}B_{borate}$, which may then be entered into the general Eq. (5) to calculate pH. On such cross-plots, calibration data define straight lines with slopes (given as 'm', Table 1) reflecting the difference between the δ^{11}B–pH sensitivity of $\delta^{11}B_{borate}$ and $\delta^{11}B_{CaCO_3}$. Transformations for relevant existing calibrations are listed in Table 1. The slopes and intercepts (given as 'c', Table 1) of these lines are independent of pK_B^* (and hence salinity, temperature and pressure), meaning that culture and core top calibrations can be readily compared without reference to *in situ* environmental conditions. In addition, presentation of culture calibrations in this way allows for the plotting of 95% confidence intervals using the York regression, accounting for uncertainty in culture conditions and measurement (Ludwig, 2003; York, 1968). This approach permits better propagation of the uncertainty of culture calibrations into final pH and pCO_2 reconstructions, and confirms the observations of Hönisch et al. (2007) that pH sensitivities seen in published foraminiferal culture calibrations (Sanyal et al., 1996, 2001) are within statistical uncertainty of the pH sensitivity of inorganic $CaCO_3$ derived by Sanyal et al. (2000). Given also the possibility that species-specific offsets (i.e. the observed range in intercept

Table 1
Planktic foraminiferal and inorganic carbonate calibrations (York-fit regression statistics from Isoplot (Ludwig, 2003)).

Publication	Carbonate type	Coefficients of calibration $\delta^{11}B_{borate}=(\delta^{11}B_{CaCO_3}-c)/m$				MSWD[a]	p[b]
		c	2σ	m	2σ		
Sanyal et al. (1996)[c,d,e]	*Orbulina universa*	5	5.3	0.82	0.32	5.6	0.004
Sanyal et al. (2000)[c]	Inorganic precipitates	7.1	3	0.75	0.15	0.118	0.73
Sanyal et al. (2001)[c,d]	*Globigerinoides sacculifer*	6.7	3.3	0.85	0.19	1.05	0.3
This study	*Globigerinoides ruber*	9.52	1.51	0.6	0.08	0.01	0.96

[a] MSWD = Mean Square Weighted Deviation.
[b] p = probability of fit at 95% confidence.
[c] pH measurements (from which $\delta^{11}B_{borate}$ is derived) come from NBS-buffer-calibrated electrode measurements, and are approximated to total scale by subtraction of 0.14.
[d] Salinity assumed to be 35 psu.
[e] 'Room temperature' assumed to be 20 °C.

on Table 1) may be partially due to inconsistencies in absolute N-TIMS measurements between labs (as highlighted by Hönisch et al., 2003; Ni et al., 2010; Rae et al., 2011), further investigation into the species-specificity of these calibrations is required.

2. Methods

2.1. Culture calibration

2.1.1. Sampling and culturing

Neanic (typically ~250 μm in diameter) specimens of *G. ruber* (white) were towed from depths of <10 m in the Gulf of Aqaba between January and March 2010, at the Interuniversity Institute of Eilat, Israel. Individual foraminifera were transferred to seawater collected at the site of plankton towing within 4–6 h of capture, and kept under saturated light conditions at ~23 °C until fully recovered (i.e. floating, with a halo of spines and symbionts). Those that did not recover fully were retained for boron isotope analysis as 'control' tow samples, and used for mass-balance corrections (as discussed later). Since traits used to distinguish the morphotypes of *G. ruber* (sensu stricto/lato; Wang, 2000) are often poorly developed in immature specimens (Aurahs et al., 2011), no distinction could be drawn between morphotypes in culture. For reference, *G. ruber* sensu lato made up 35–45% of the total identifiable population of *G. ruber* from tows and core-top sediment in the Gulf of Aqaba. However, we see no difference in $\delta^{11}B$ (or B/Ca) between these morphotypes in core top sediments (see Supplementary Fig. S2).

Recovered foraminifera were transferred to sealed 100 ml Erlenmeyer flasks filled with prepared filtered seawater (see below). Foraminifera were removed daily, fed one newly-hatched *Artemia* nauplius, observed and measured using a Zeiss inverted light microscope. Condition and approximate symbiont density was noted. In an attempt to avoid damage to the foraminifera and increase the low acceptance rates typically seen in cultured *G. ruber* (Spindler et al., 1984), thereby increasing mass gain, *Artemia* were physically incapacitated prior to feeding. Illumination was provided by a metal halide lamp (420 W, Osram™) at levels of 200 μmol photons m^{-2} s^{-1} (13 h light:11 h dark), equivalent to irradiance at 15–20 m depth in the open waters of the northern Gulf of Aqaba (Shaked and Genin, 2006). Culture flasks were kept in water baths at a constant temperature of 26 ± 0.5 °C.

Seawater was prepared in large batches to ensure consistency across all flasks, with surplus for topping up stored in airtight bottles in the dark at ~4 °C. Salinity was reduced from ~40.7 to 37 via addition of de-ionised water. Following other culturing studies (e.g. Sanyal et al., 1996, 2001), pH was altered by adjusting alkalinity via addition of NaOH or HCl. Culture experiments were carried out at pH 8.174 ± 0.007, 7.894 ± 0.013, and 7.554 ± 0.013 (total scale; 2 se, n=48–67). pH drift in culture flasks was monitored periodically using a pH electrode calibrated to NBS buffers, with individuals from flasks that experienced large pH drift discounted (n=5). Culture solution was sampled at the beginning of each pH experiment, and a composite sample taken from all flasks at the end of culturing. These water samples were poisoned with 50 μl saturated $HgCl_2$ solution and transported for full carbonate system analysis at the UK Ocean Acidification Research Programme (UKOARP) Carbonate Chemistry Facility, at the National Oceanography Centre Southampton (NOCS). Nutrient analyses were also undertaken to ascertain nitrate, nitrite, phosphate and silicate concentrations. NBS-scale pH measurements of these composite samples taken in Eilat were consistently higher than Dissolved Inorganic Carbon (DIC) and Total Alkalinity (TAlk)-derived total scale pH measurements by 0.21 pH units (see Supplementary Fig. S3). As such, in-culture NBS-scale electrode measurements could be used once corrected for this 0.21 pH offset.

After gametogenesis (typically after 6–10 days in culture), empty *G. ruber* tests were removed from culture flasks, rinsed in de-ionised water, dried and weighed.

2.1.2. Mass balance calculations and estimates of growth rate

To correct for the chemistry of the test grown outside of culture, a mass-balance correction was used, following Erez and Luz (1983), Lohmann (1995) and Kısakürek et al. (2008, 2011). Dried 'control' samples (i.e. *G. ruber* tests towed at the same time as cultured material) were weighed on a microbalance, photographed and measured using Macnification® imaging software. A size-mass relationship for all towed control samples was calculated, such that initial size measurements (maximum axis multiplied by its perpendicular axis) of foraminifera made immediately prior to culturing could be used to estimate shell mass (Supplementary Fig. S4). While organic matter was not removed prior to weighing, calculation of $CaCO_3$ mass via ICPMS (as per Villiers et al., 2002) for a subset of samples gave consistent results, suggesting organics did not significantly contribute to dried shell mass. Best fit was via power-type regression, as noted by Kısakürek et al. (2011) for *G. ruber* from Eilat. The relationship is best defined by the equation mass = 803.65 × (product of axes)$^{1.957}$ (n=112, R^2=0.75, p<0.001). Note the exponential of this relationship is the same as that defined by Kısakürek et al. (2011).

The $\delta^{11}B$ and B/Ca of control *G. ruber* from each experimental tow (n=150–200) was then measured (see below for analytical methodology). Assuming cultured individuals began with this $\delta^{11}B$ and B/Ca, and using the size–mass relationship to estimate the mass of calcite grown out of culture, a correction can be made and the composition of the foraminifera grown during culture calculated by

$$\delta^{11}B_{culture} = -\frac{\delta^{11}B_{measured} - (\delta^{11}B_{controls} \times P^{B}_{controls})}{P^{B}_{culture}} \quad (7)$$

where $\delta^{11}B_{measured}$ is the measured boron isotopic composition of the bulk material, and $\delta^{11}B_{controls}$ is the measured boron isotopic composition of 'control' foraminifera towed at the same time as those cultured. $P^{B}_{controls}$ and $P^{B}_{culture}$ are the proportions of boron in the bulk material coming from the pre-culture and culture-grown calcite respectively. These are calculated based on the B/Ca ratios in the bulk material and in control specimens, and the proportion of calcite mass grown in culture and out of culture, such that

$$P^{B}_{culture} = -\frac{B/Ca_{measured} - (B/Ca_{controls} \times P^{mass}_{controls})}{B/Ca_{measured}} \quad (8)$$

and $P^{B}_{controls} = 1 - P^{B}_{culture}$. Uncertainty on $\delta^{11}B_{culture}$ data was calculated as two standard deviations of 10,000 Monte Carlo simulations accounting for the uncertainty in the size:mass relationship (Supplementary Fig. S4b), B/Ca measurements (5% at 2σ) and $\delta^{11}B$ measurements (from Eq. (9)).

2.2. Core-top calibration

2.2.1. Sampling

To compare the results of our culture calibration with foraminifera grown in natural conditions, we measured *G. ruber* from globally distributed core-top sites from archives at Tübingen, Germany and NIWA, New Zealand. Samples from NIWA were verified as recent by way of ^{14}C-dating (H. Bostock, pers. comm.), while from the Tübingen repository only undisturbed multicore

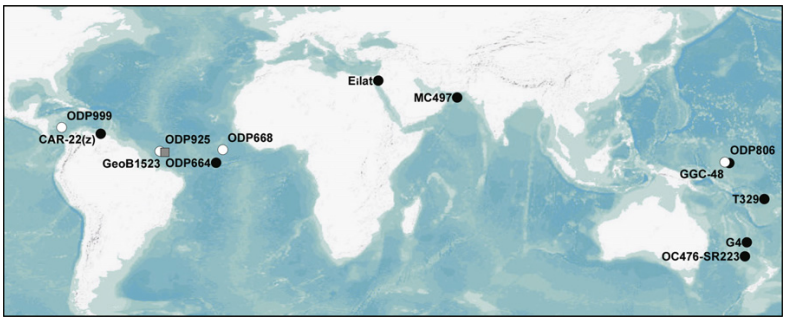

Fig. 3. Locations of core-top, tow and sediment trap samples used in this study. Filled circles are sites from which recent samples are measured (this study), while white circles are core-tops from Foster (2008). Sites of down-core pCO_2 reconstructions are marked by a grey square (GeoB1523-1) and white circle (ODP 999A: also the site of core-top measurement; Foster, 2008).

sediment containing Rose Bengal-stained living benthic foraminifera was selected. In addition, material from sediment traps in the Cariaco Basin was used to further test for biases introduced during sedimentation. This array of sites covered as broad a range of *in situ* $\delta^{11}B_{borate}$ as possible for regions inhabited by *G. ruber*, and serves to test for regional variations (as seen in Mg/Ca, Bolton et al., 2011) that might stem from genotype differences (Darling and Wade, 2008). The locations of these core-top and sediment trap sites are shown in Fig. 3 (see also Supplementary materials). Samples were also taken from a number of size fractions to examine the influence of test size on measured $\delta^{11}B$.

2.2.2. Carbonate system parameters

pH, temperature and salinity at the sediment trap site (Cariaco Basin, collected January 2007) is interpolated from data from December 2006 and February 2007, downloadable from http://www.imars.usf.edu/CAR. pH was estimated for core-top sites using surface water oceanographic data from the GLODAP (Key et al., 2004), CARINA (Key et al., 2010) and Takahashi et al. (2009) compendia (see Supplementary materials). First, regional salinity-TAlk correlations were calculated from surface (<20 m) GLODAP/CARINA measurements. Applying these correlations, monthly-resolved values of salinity from Takahashi et al. (2009) were converted to monthly TAlk estimates. Monthly temperature was also taken from Takahashi et al. (2009). Pre-industrial pCO_2 at each core-top site was estimated by applying ocean–atmosphere ΔpCO_2 from Takahashi et al. (2009) sites (corrected for post-industrial changes in flux with reference to Gloor et al., 2003) to a pre-industrial atmospheric pCO_2 value. Where samples were ^{14}C-dated, the age-appropriate atmospheric pCO_2 value was taken from Lüthi et al. (2008), and references within. Where core-tops were not dated, we assume an average late Holocene (<4 kyr BP) value of 275 ppm. Combined with approximations of typical local silicate and phosphate concentrations (from GLODAP/CARINA measurements), monthly estimates of pH were calculated using CO_2sys.m (Van Heuven et al., 2011), and the constants of Lueker et al. (2000), Lee et al. (2010) and Dickson (1990).

2.3. Analytical techniques

2.3.1. Sample cleaning and preparation

Foraminiferal cleaning is largely as described in Rae et al. (2011), in turn based on the approach of Barker et al. (2003). Foraminifera were cracked open between two clean glass slides, ultrasonicated and rinsed repeatedly with MilliQ ultrapure water (18.2 MΩ) to remove clays. Culture, sediment trap and tow samples, in agreement with other culturing studies (e.g. Russell et al., 2004), were subject to intensified oxidative cleaning (3×20–30 min treatments of 250 µl 1% H_2O_2 + 0.1 M NH_4OH_4 at 80 °C) to account for the larger organic content. In core-tops, oxidative cleaning was shorter (3×5 min) to minimise sample loss. Samples were subject to a brief weak acid leach in 0.0005 M HNO_3 to remove readsorbed contaminants, before dissolution by incremental addition of 0.5 M HNO_3 (typically <100 µl).

An aliquot (~20 µl) of dissolved sample was taken for elemental analysis, before the remaining sample was buffered and boron separated from matrix using 20 µl-volume columns of Amberlite IRA743 boron-specific resin (Kiss, 1988). Typical column yields for boron are $>99.9\%$, with an extra acid elution step monitored for boron concentration to check elution efficiency. All sample preparation work and column chemistry were carried out in a dedicated flow hood within an over-pressured clean lab fitted with boron-free HEPA filters, permitting typical total procedural blanks of <20 pg.

2.3.2. MC-ICPMS and ICPMS

Samples were measured for boron isotope composition on Thermo Scientific Neptune MC-ICPMS at the University of Bristol (cultures, 'control' tows and GeoB-1523-1), and the University of Southampton (core-tops and sediment trap) according to methods described elsewhere (Rae et al., 2011; Foster, 2008). Repeat analysis of a range of carbonate (including *G. ruber*, Supplementary Fig. S5) and boric acid consistency standards (Supplementary Fig. S6) reveals no significant differences between these laboratories.

External reproducibility of the MC-ICPMS $\delta^{11}B$ method (at 95% confidence, 2σ) is typically <0.25‰ on ~1 mg of $CaCO_3$ (sample size requirement varies with $[B]_{calcite}$, but in the case of *G. ruber* equates to 75–100 tests of diameter 300–355 µm). Following Rae et al. (2011), uncertainty on culture and tow data run at Bristol is calculated as

$$2\sigma = 1.7(e^{-29[^{11}B]}) + 0.31(\exp^{-0.75[^{11}B]}) \quad (9)$$

where $[^{11}B]$ is the intensity of ^{11}B signal in volts. Uncertainty on core-top and sediment trap data is similarly calculated, according to the external reproducibility of repeat analyses of Japanese Geological Survey *Porites* coral standard (JCP; $\delta^{11}B = 24.3$‰) at the University of Southampton (Supplementary Fig. S7). This relationship is described by.

$$2\sigma = 1.87(e^{-20.6[^{11}B]}) + 0.22(exp^{-0..43[^{11}B]}) \quad (10)$$

Trace element–calcium ratios (Mg, B, Al, Mn, Ba, Sr, Li, Na, Cd, U, Nd, and Fe) were analysed using Thermo Element 2 ICP-MS at the University of Bristol (cultures, down-core and control tows) and the University of Southampton (core-tops and sediment trap). Here, these data are only used to assess adequacy of clay removal

(Al/Ca < 100 μmol/mol; Rae et al., 2011), to generate down-core temperature estimates (Mg/Ca; see Supplementary materials), and to correct for boron incorporated outside of culture. A full exploration of trace element data is beyond the scope of this paper, and will follow in later publications.

2.4. Downcore application

2.4.1. Site and species selection

G. ruber white sensu stricto (300–355 μm) were picked from sediments aged 0–30 kyr from core site GeoB1523-1, recovered from the Ceara Rise in the western equatorial Atlantic (3.83°N, −41.62°E) at a water depth of 3292 m. We use the previously published age model for this site based on $\delta^{18}O$ (Gingele et al., 2000).

2.4.2. Temperature and salinity estimates

Estimates of sea surface temperature (SST) and salinity (SSS) are required to calculate pH from $\delta^{11}B$, as these parameters influence pK_B^*. It is important to note, however, that calculated pH is only weakly dependent on these environmental parameters (0.012 pH units/°C; 0.003 pH units/psu). For GeoB1523-1, SST was reconstructed using the Mg/Ca ratio of *G. ruber* measured on an aliquot of the same sample used for isotope measurement and the generic SST calibration (Mg/Ca = 0.38 × exp[SST*0.09]) of Anand et al. (2003). This is preferred over the species-specific calibration as it better fits our dataset of >20 core-top measurements (Henehan, unpublished data). As with Hönisch and Hemming (2005), palaeo-salinity was estimated using the following equation:

$$SSS = SSS_{modern} + \Delta_{sea\text{-}level}/3800 * 34.8 \quad (11)$$

where $\Delta_{sea\text{-}level}$ is an estimate of sea-level change in metres, 3800 m is the average ocean depth, 34.8 is mean averaged modern ocean salinity, and SSS_{modern} is the modern salinity at the site of interest (from GLODAP; Key et al., 2004).

2.4.3. The second carbonate system parameter

Ocean pH is only one variable of the ocean carbonate system, and to determine $[CO_2]_{aq}$ and hence pCO_2 using Henry's Law, another variable is required (Zeebe and Wolf-Gladrow, 2001). The second variable chosen, TAlk, is calculated from estimated palaeo-salinity (Hönisch et al., 2009; as per Palmer and Pearson, 2003), itself derived from Eq. (11) above, and a TAlk vs. SSS relationship defined by modern ocean data from the equatorial Atlantic (TAlk = SSS × 61.88 + 162.66, $R^2 = 0.88$, $p < 0.001$; from GLODAP; Key et al., 2004). However it is important to note that the generated pCO_2 estimate is determined largely by the reconstructed pH, and TAlk has little control. For example, given a pH of 8.2 (and SST of 25 °C and salinity 35 psu) drastically increasing TAlk from 2400 to 2600 μmol/kg—equivalent to the range modelled by Hönisch et al. (2009) for the last 2 myr—only increases reconstructed pCO_2 by 24 ppm.

Given this reconstruction of TAlk and a $\delta^{11}B$–derived pH, it is possible to reconstruct the entire carbonate system using CO_2sys.m (Van Heuven et al., 2011). Given the modern disequilibrium of surface waters above GeoB1523-1 (ΔpCO_2 of 15–25 ppm; Takahashi et al., 2009), and a correction factor for the pre-industrial ΔpCO_2 in this region of 1.33 (derived from Gloor et al., 2003), a correction for disequilibrium of −27 ppm is applied in order to calculate atmospheric CO_2 concentrations from calculated aqueous pCO_2. We apply a conservative approximation of uncertainty on reconstructed aqueous pCO_2 of 29 ppm. This is a quadratic addition of the ranges of uncertainty in reconstructed pCO_2 that are produced via propagation of each input parameter uncertainty in turn, namely the calibration equation (uncertainty as in Table 1 and discussion below), $\delta^{11}B$ measurement (~±0.2‰), and reconstructed salinity (±1 psu), TAlk (±100 μmol/kg) and temperature (±1 °C).

3. Results

3.1. Culturing

Mortality was greatest at our lowest pH, with most individuals surviving to gametogenesis in the two higher pH experiments (54% and 64% at 8.174 and 7.894 pH respectively), but only 40% surviving to gametogenesis at pH 7.554 (compared to pH in the Gulf of Aqaba of ~8.075). Note that while these values of survivorship are low compared to cultures of other species, *G. ruber* is notoriously difficult to culture (e.g. Hemleben et al., 1987), and as such the observed high mortality is not unexpected.

Samples grown at low pH (7.554) were typically surrounded by a much denser shroud of symbionts that often entirely obscured the outline of the test (Fig. 4B). Also, at this low pH individuals often lost most, or all, of their calcitic spines and fed less frequently (every 3–4 days) using short, unsupported, pseudopods. Larger tests across all pH treatments often showed a proliferation of many small and/or kummerform chambers growing in unusual configurations. While unusual within the 300–355 μm size range, it is not uncommon to find such growth patterns in larger *G. ruber* (>400 μm) from core-tops, indicating these forms are not simply a response to culture. At higher pH, chambers were usually visibly more heavily calcified (Fig. 4C), and growth rates were higher (see Table 2). At pH 7.554, tests were visibly thinner and often possessed abnormally wide apertures, with evidence in some cases that chambers may have been partially dissolved or reabsorbed during ontogeny (see Fig. 4E).

3.2. MC-ICPMS results

The results of boron isotope analyses of culture, core-top, tow, sediment trap and down-core samples (along with the relevant mass-balance corrections in culture experiments) can be found in the Supplementary materials. These data are plotted in $\delta^{11}B_{CaCO_3}$–$\delta^{11}B_{borate}$ space (Fig. 5). The York-fit linear regression of culture data produces a $\delta^{11}B_{CaCO_3}$–$\delta^{11}B_{borate}$ relationship described by Eq. (12) below, with uncertainty (2σ, 95%) on this fit, accounting for error in analytical and *in situ* $\delta^{11}B_{borate}$ values, shown as a shaded band.

$$\delta^{11}B_{borate} = (\delta^{11}B_{measured} - 9.52 \pm 1.51)/(0.60 \pm 0.08) \quad (12)$$

The slope (i.e. pH sensitivity) of this culture calibration is within uncertainty of existing culture and inorganic calibrations (see Table 1), and is significantly lower than the theoretical pH sensitivity of borate ion in seawater (as indicated by a slope of <1). For comparison, towed 'control' specimens and core-top specimens are also plotted. We see no discernible effect of geographical location nor sample material type, suggesting that sedimentation or regional differences do not influence recorded $\delta^{11}B$. Although these data are permissively in agreement with the slope (i.e. $\delta^{11}B$–pH sensitivity) of the culture calibration (a York regression of the 300–355 μm size-fraction has a slope of 0.45 ± 0.25 at 95% confidence), there is a tendency towards lower values of $\delta^{11}B$ than the culture calibration would predict in size fractions smaller than ~380 μm, and higher values in larger size fractions (see Fig. 6). As such, and because the spread in pH in the core-top samples alone is too small for a precise $\delta^{11}B$–pH calibration, we suggest modification of the culture calibration equation to reflect the size fractions used down-core. Thus for the commonly-used 300–355 μm size fraction a correction of −0.65

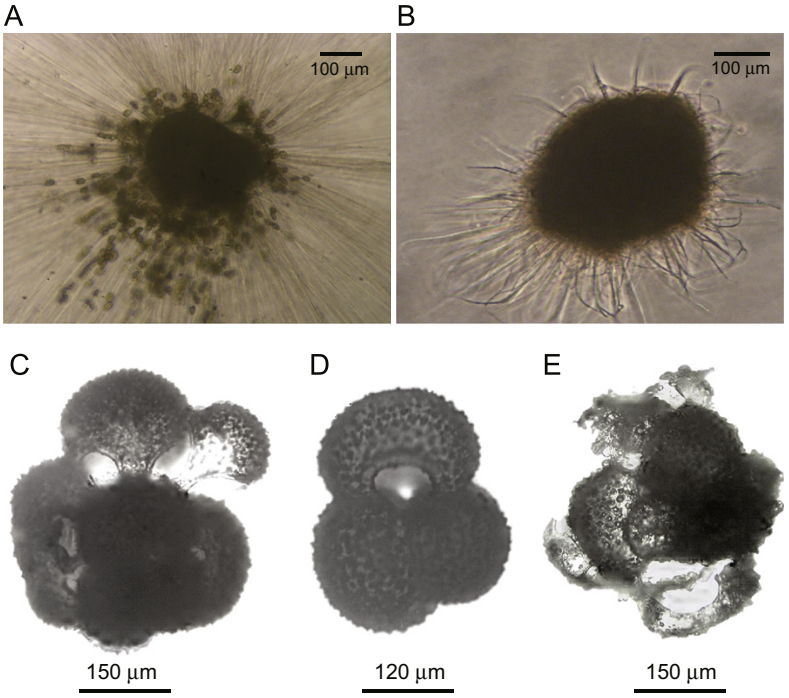

Fig. 4. Examples of foraminifera grown in culture: (A) healthy *G. ruber* at ambient pH, with symbionts spread out within a well-developed halo of spines; (B) foraminifera grown under low pH (~7.55), with poorly developed spines and dense shroud of symbionts; (C) test grown at high pH (~8.17) showing erratic pattern of chamber addition, also seen (albeit less frequently) at mid-range pH; (D) 'Normal' test of *G. ruber*, similar to those seen in sediment samples (e.g. Hemleben et al., 1989), as produced in all three pH experiments; (E) test with large apertures and thinly calcified chambers that may be indicative of dissolution, as sometimes seen at low pH (~7.55). Note that examples (C) and (E) are not representative of the whole experimental group, but are extremes picked for illustration purposes.

Table 2
Culturing and tows, Eilat.

Experiment	Start/tow date	pH (total)	2se	*T* (°C)	*S*	*N* (cultured)[a]	N (grown and GAM)[b]	Survivorship (%)[c]	Mean days in culture	Mean starting diameter (µm)[d]	Mean end-culture diameter (µm)[d]	Mass for analysis (µg)[e]	Growth rate (µg/day/ind.)[f]
Culture 1	29/01/10	8.174	0.007	26	37.2	106	57	54	6	200.0	365.4	590	1.39
Culture 2	10/02/10	7.894	0.013	26	37.2	105	67	64	10	178.1	441.9	902	1.19
Culture 3	10/03/10	7.554	0.013	26	37.2	120	48	40	9	197.7	339.6	303	0.35
Tow 1	27/01/10	8.128	0.005	22	40.4								
Tow 2	08/02/10	8.116	0.005	23	40.4								
Tow 3	07/03/10	8.103	0.005	23	40.4								

[a] Indicates the number of foraminifera grown at each pH treatment.
[b] Indicates the number of foraminifera that grew in mass during culture and underwent gametogenesis.
[c] The percentage of individuals cultured that grew and survived to gametogenesis in culture.
[d] As determined by micrometre and inverted light microscope.
[e] The total mass of calcite analysed via MC-ICPMS, of which 75–92% was grown in culture.
[f] Based on the pre-culture mass as estimated from the size–mass relationship in Supplementary Fig. S2 and the end-culture mass as weighed at the University of Bristol, and represents the mean of the growth rates of each individual foraminifera per treatment.

(see Fig. 6) should be applied to the intercept value '*c*' of the culture $\delta^{11}B_{CaCO_3}-\delta^{11}B_{borate}$ relationship (Eq. (12))

$$\delta^{11}B_{borate} = (\delta^{11}B_{measured} - 8.87 \pm 1.52)/(0.60 \pm 0.09) \quad (13)$$

Uncertainty on the intercept in this relationship is a quadratic addition of two standard errors of the mean offset from culture in 300–355 µm fraction core-top samples and the uncertainty in the original culture calibration York regression intercept. Similarly, we suggest a correction of −0.83‰ for the 250–300 µm size fraction, and −0.16‰ for samples of 355–400 µm. For other size fractions the culture calibration may be corrected using the relationship between test size and offset from culture in Fig. 6 (offset = [0.005 × average size] − 2.185, $R^2 = 0.33$), although the narrow size range of *G. ruber* in core-tops and the large ratio of analytical uncertainty to signal mean that the relationship is not statistically robust, and as such wherever possible we would advocate using size fractions tested here. Indeed, despite the general similarity of size-fraction effects seen across our sample sites (Supplementary Fig. S8), given the limitations of our dataset, we encourage prior verification of the consistency of this size fraction effect at the sites of any future down-core reconstructions.

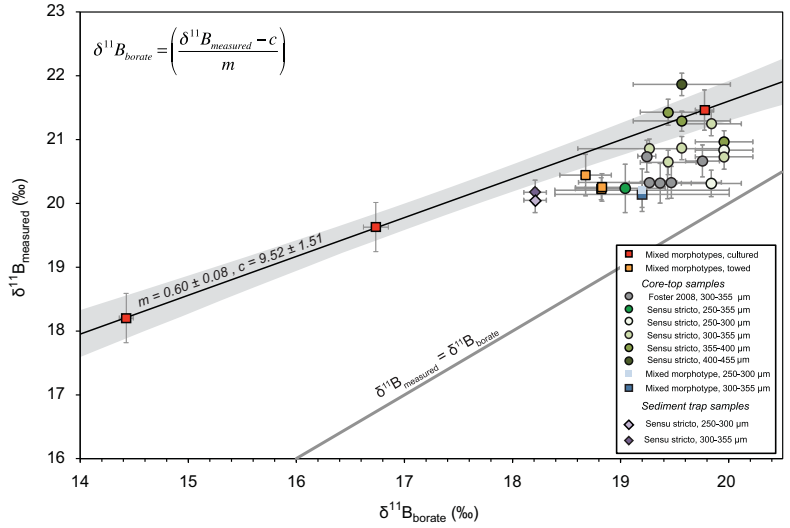

Fig. 5. New culture calibration of *G. ruber*. The York-fit regression plotted using Isoplot (Ludwig, 2003), with dotted lines and grey band defining 95% confidence intervals (mean standard weighted deviance (MSWD)=0.01). X-error bars for core-top samples are 2 standard deviations of intra-annual variability in calculated monthly $\delta^{11}B_{borate}$, while for cultures the error represents 2 standard errors of the mean pH of all culture flasks, and for sediment trap samples it reflects the range of $\delta^{11}B_{borate}$ between Dec and Feb 2007. Y-error in non-culture samples is the analytical reproducibility as calculated by Eq. (10). In cultured samples, error bars reflect 2 standard deviations of 10,000 Monte Carlo simulations that also incorporate the uncertainties in the size–mass relationship (see Supp. Fig. S4b) and reproducibility of boron isotope and B/Ca measurements in 'control' pre-culture tows and bulk post-culture measurements.

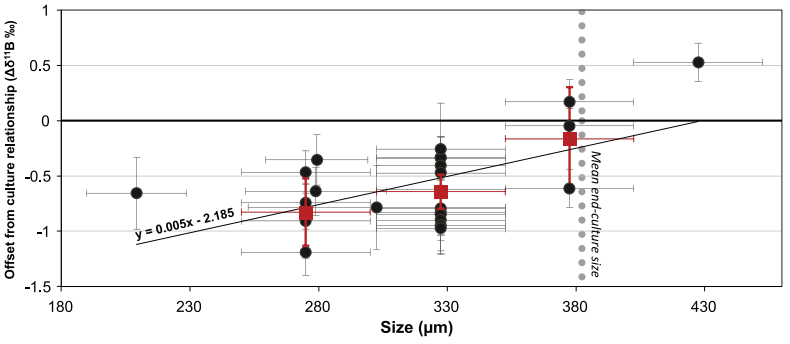

Fig. 6. Offset of core-top, tow and sediment trap samples from our culture calibration, as a function of size fraction. Error bars in size-fraction refer to the sieve fractions, or where available, two standard errors of the measured test diameter. Red markers indicate the mean value for the three most commonly used size fractions, with y-errors corresponding to two standard errors of the mean offset. Dotted vertical line denotes the mean end-culture diameter. (For interpretation of the references to colour in this figure legend, the reader is referred to the web version of this article.)

3.3. pCO_2 reconstruction

The $\delta^{11}B$ of *G. ruber* from Site GeoB1523-1 are plotted in Fig. 7A, along with the *G. ruber* data from ODP 999A for comparison, from Foster (2008). The results of boron-based pCO_2 reconstruction at these sites are also plotted in Fig. 7B, with the estimates from ODP 999A corrected using a pre-industrial ΔpCO_2 of −21 ppm calculated as discussed above. A cubic spline was plotted using Analyseries (Paillard et al., 1996), and the bounds of uncertainty (17 ppm: individual uncertainty of 29 ppm/$\sqrt{2}$) on this spline are shaded. For comparison, the data are plotted with atmospheric pCO_2 derived from ice cores (Lüthi et al., 2008 and references within; Lourantou et al., 2010; ages recalculated as per Lemieux-Dudon et al., 2010) and pCO_2 reconstructed assuming a constant vital effect of 0.8‰ (as per Foster, 2008). The mean deviation from atmospheric pCO_2 measurements from ice cores and those calculated from 999A and GeoB1523-1 using our new calibration is −5 ppm, with a 2σ of ±19 ppm. All data may be found in the Supplementary materials.

4. Discussion

4.1. pH sensitivity of $\delta^{11}B_{G.ruber}$ lower than $\delta^{11}B_{borate}$

pH is clearly a strong control on $\delta^{11}B$ in *G. ruber*, yet these new data do not fall on the predicted relationship of seawater borate ion, as epifaunal benthic foraminifera do (albeit within a limited range of $\delta^{11}B_{borate}$; Rae et al., 2011). Specifically, our data lie above the $\delta^{11}B_{borate}$–pH curve, and show a pH sensitivity ~40% lower than that predicted for aqueous $\delta^{11}B_{borate}$, confirming previous observations in other symbiont-bearing planktonic species (Hönisch et al., 2003; Sanyal et al., 2001, 1996) using NTIMS. This suggests that, absolute values aside, relative changes in $\delta^{11}B$ are still accurately described using N-TIMS (Foster et al., in preparation). The causes of this deviation from the aqueous geochemical basis of the proxy are potentially manifold. Previous studies have ascribed a lower-than-predicted pH sensitivity in $\delta^{11}B$ for (i) incorporation of $B(OH)_3$ (Klochko et al., 2009); (ii) elevated (compared to ambient) pH inside seawater vacuoles

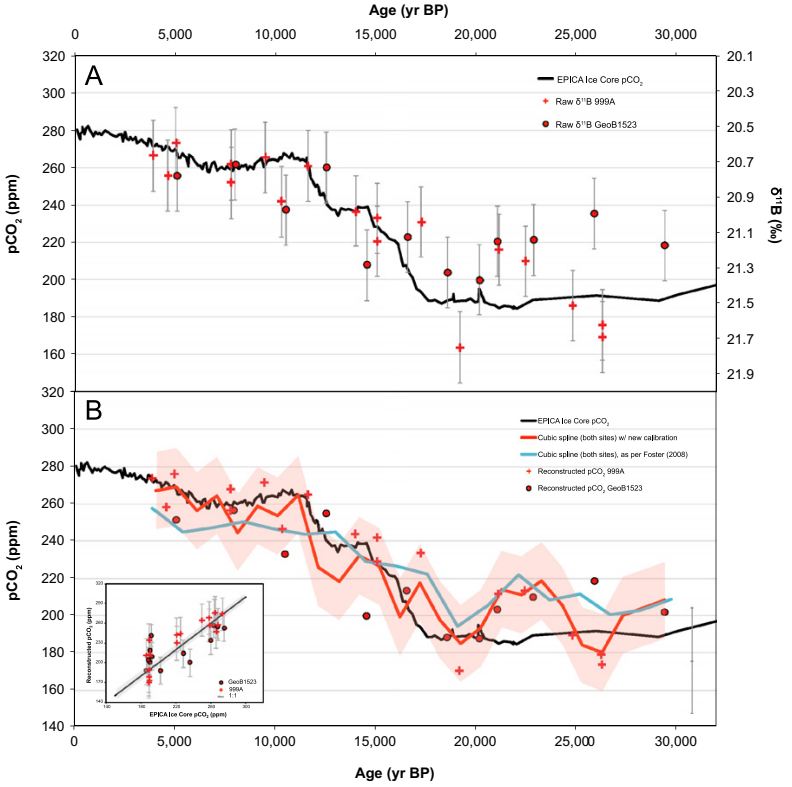

Fig. 7. Down-core δ^{11}B (Panel A) and reconstructed pCO_2 (Panel B) from ODP site 999A (crosses, Foster, 2008) and GeoB1532-1 (circles, this study), compared to CO_2 concentrations from ice cores (black line). The thick red line in Panel B is a cubic spline plotted on evenly subsampled values from both sites, as calculated using Analyseries (Paillard et al., 1996), with the shaded area reflecting uncertainty on the spline of ± 17 ppm (i.e. 29 ppm individual uncertainty/$\sqrt{2}$). Note that these data are corrected for local ocean–atmosphere disequilibrium, which is taken as the modern mean annual values (from Takahashi et al., 2009) corrected for the pre-industrial with reference to Gloor et al. (2003): +21 ppm (999A) and +27 ppm (GeoB1523-1). Also plotted (green line) is a similar spline through pCO_2 reconstructions based on a constant vital effect '*a*' (see Eq. (6) above) of +0.8‰ as applied by Foster (2008), illustrating the improved fit of the new calibration. Uncertainty on each individual measurement is plotted (Panel A), with uncertainty on pCO_2 reconstructions (Panel B) a quadratic addition of the various uncertainties on reconstructed pH, alkalinity and temperature. Insert in panel B is a cross-plot of ice-core derived vs. reconstructed pCO_2, with uncertainty on the 1:1 line (shown as grey shaded region) representing 6 ppm uncertainty on ice-core measurements (from Ahn et al., 2012). (For interpretation of the references to colour in this figure legend, the reader is referred to the web version of this article.)

(Rollion-Bard and Erez, 2010); (iii) modification of the micro-environment around the foraminifera by respiration, calcification and photosynthesis (Hönisch et al., 2003; Zeebe et al., 2003); and (iv) analytical issues relating to the NTIMS approach used in past studies (Foster, 2008). These new results for *G. ruber* using MC-ICPMS, where accuracy has been demonstrated (Ni et al., 2010), show that analytical issues do not play a role in generating the shallower pH sensitivity in planktic foraminifera. Offsets in *absolute* δ^{11}B between NTIMS and MC-ICPMS of the order of 1–2‰ are observed for a variety of foraminiferal species (e.g., *Cibicidoides weullerstorfi*; see Rae et al., 2011) but, as also supported by an ongoing interlaboratory comparison study (Foster et al., in preparation), *relative* changes appear to be largely reproducible between NTIMS and MC-ICPMS (e.g. Fig. 8 of Rae et al., 2011). There currently appears to be little consensus regarding the relative importance of the other three phenomena proposed above to explain a shallower-than-predicted relationship between δ^{11}B and pH. A key observation requiring explanation is that all planktonic foraminiferal calibrations to date show a pH sensitivity (slope '*m*') within uncertainty of that seen in inorganic precipitates ($\delta^{11}B_{CaCO_3} = \sim 0.75(\pm 0.15)$*the pH sensitivity of $\delta^{11}B_{borate}$; Sanyal et al., 2000). Similarly reduced pH sensitivity is evident in the symbiont-bearing *Amphistegina lobifera* (Rollion-Bard and Erez, 2010) and in numerous species of coral (Anagnostou et al., 2012; Hönisch et al., 2004; Krief et al., 2010; Reynaud et al., 2004; Trotter et al., 2011). That the sensitivities observed in a broad range of biogenic carbonates are similar to those seen in inorganic precipitates would implicate an inorganic process—e.g., a rate dependency in $CaCO_3$ precipitation. However, the epifaunal benthic data of Rae et al. (2011) (Fig. 2) and Yu et al. (2010) lie within uncertainty of the $\delta^{11}B_{borate}$, implying that either the agreement between the $\delta^{11}B_{borate}$ and benthic foraminiferal carbonate is either purely fortuitous (the result of a several competing processes operating in tandem to cancel each other out), or that any inorganic process, if it exists, is not universal and benthic foraminifera are the exception to the rule. It is also worth noting that all the other foraminifera so far calibrated are symbiont bearing, and laboratory observations (Jørgensen et al., 1985; Köhler-Rink and Kühl, 2005; Rink et al., 1998) would strongly implicate the alteration of the foraminiferal microenvironment by symbionts and life processes. However, a full resolution of this issue is beyond the scope of this current contribution and will require additional studies of both symbiont-bearing and non-symbiont bearing foraminifera, and of inorganic carbonates precipitated in equilibrium at rates comparable to those seen in biogenic carbonates.

4.2. $\delta^{11}B$ offset between culture and non-culture: a size fraction effect on $\delta^{11}B$ in *G. ruber*

While towed, sediment trap and core-top specimens are permissively in agreement with the pH-sensitivity of $\delta^{11}B_{CaCO_3}$ observed in our cultures, it is clear there is a discrepancy in $\delta^{11}B$ values predicted by the culture calibration and some measurements of non-culture specimens of *G. ruber* (Fig. 5). The degree of offset from the calibration does not correlate with *in situ* temperature ($R^2=0.04$) or the saturation state of bottom water at these core-top sites ($R^2=0.05$), suggesting there is no discernible temperature or dissolution effect. This offset does, however, show some correlation with test size fraction (see Fig. 6, Supplementary Fig. S8). Previous evidence (Ni et al., 2007) for a size-fraction effect in *G. ruber* is ambiguous because of prohibitive uncertainty in $\delta^{11}B$ measurements ($\sim \pm 0.8$‰ vs. $\sim \pm 0.25$‰ here). Increasing $\delta^{11}B$ with size is, however, resolvable in the closely-related species *G. sacculifer* (Hemming and Hönisch, 2007; Ni et al., 2007). Moreover, size-fraction effects in *G. ruber* have been noted in $\delta^{13}C$ and $\delta^{18}O$ (e.g. Kroon and Darling, 1995), B/Ca (Ni et al., 2007), and in Mg/Ca and Sr/Ca (e.g. Friedrich et al., 2012).

The cause of any size fraction effect on $\delta^{11}B$ is not clear. Preferential dissolution (Hönisch and Hemming, 2004; Ni et al., 2007) seems unlikely, since (a) similar offsets from aqueous $\delta^{11}B_{borate}$ are reproduced even in towed samples (see Fig. 5), (b) there is no relationship between degree of offset and deepwater carbonate saturation at the site of deposition, and (c) the lack of any geochemically distinct gametogenic calcite in *G. ruber* (Caron et al., 1990) should make the issue of preferential dissolution less pertinent in this species (see also Seki et al., 2010; Fig. 7A). Instead we support the suggestion by Hönisch and Hemming (2004) that a size-fraction effect in $\delta^{11}B$ is due to intensified micro-environmental alteration by symbionts in larger specimens. That said, we query the assertion by Hönisch and Hemming (2004) that increasing $\delta^{13}C$ and $\delta^{11}B$ with size must be due to larger specimens living at shallower depths (thus experiencing a stronger light intensity and stronger microenvironment alteration). While this seems consistent with Caron et al. (1990), we urge some caution in this interpretation without direct ecological evidence for a bias towards larger test size in *G. ruber* from shallower waters: Bijma et al. (1990) report living individuals measuring anywhere between 125 μm and 708 μm within the uppermost 5 m of the Red Sea at all stages in *G. ruber*'s semilunar life-cycle. Besides, foraminifera towed from <10 m record lower, not higher, $\delta^{11}B$ than foraminifera cultured at light levels equivalent to $\sim$20 m water depth (though we concede these individuals might conceivably have grown to larger size—and heavier $\delta^{11}B$—had they completed their life cycle at this depth).

It is instead likely that the magnitude of these microenvironment effects might change with test size without any need to invoke changes in habitat depth. Photosynthesis by symbionts in the microenvironment surrounding planktic foraminifera raises pH, while respiration and calcification lower pH (Jørgensen et al., 1985; Köhler-Rink and Kühl, 2005; Rink et al., 1998). Crucially, rates of respiration and photosynthesis in culture specimens have been seen to change with test size (Lombard et al., 2009; Rink et al., 1998), with photosynthesis increasing relative to respiration in larger specimens of *G. ruber* (Lombard et al., 2009). In addition, as foraminifera grow, the diffusive boundary layer around their tests is expanded, lengthening timescales for diffusion of carbon through the microenvironment. As such, equilibration of the microenvironment with the ambient seawater slows, and as such any microenvironment pH alteration would be accentuated (see model of Wolf-Gladrow et al., 1999). While more *in situ* microelectrode measurements are required to fully test these hypotheses, they could explain the observed patterns in recorded $\delta^{11}B$ we see here.

It is also possible that increased test size might be resultant from, not a driver of, increased symbiont activity, with elevated $\delta^{11}B$ an inevitable result. Planktonic foraminifera acquire algal symbionts early in their life cycle (Hemleben et al., 1989). Should the activity of symbionts in the foraminiferal microenvironment impart an advantage to the calcification of the host by raising external pH and Ω_{CaCO_3} (reflected in $\delta^{11}B$) and thus reducing energetic expenditure needed to raise internal vacuole pH (as suggested by Bentov et al., 2009), foraminifera that happen to succeed in acquiring symbionts earlier in their ontogeny might grow more rapidly, and thus attain larger size prior to gametogenesis. Clearly additional modelling and field observation are required to investigate these hypotheses further.

4.3. Applying the *G. ruber* $\delta^{11}B$–pH calibration to downcore data

Reconstructed pCO_2 from Sites GeoB1523-1 and ODP 999A using this new calibration for *G. ruber* tracks reconstructions from ice cores very closely, with average deviation (-5 ppm) from ice core pCO_2 within propagated uncertainty of ± 29 ppm. Although broadly similar results can be generated with the approach of Foster (2008) (Eq. (6) above), the new calibration more accurately reproduces the 90 ppm magnitude of deglacial pCO_2 increase seen in ice core reconstructions ($\Delta pCO_2 = \sim 80$ ppm vs. ~ 50 ppm using Foster, 2008). What is more, while these sorts of improvements in fit are within uncertainty over these short timescales, the importance of the lower pH sensitivity documented here is magnified in deeper time when pCO_2 is likely to have been higher.

5. Conclusions

This contribution represents a further demonstration of the dominance of pH as a control on foraminiferal $\delta^{11}B$. It is the first species-specific foraminiferal culture calibration analysed using MC-ICPMS, and the first to incorporate globally-distributed cultured, towed, sediment trap and core-top foraminifera. The new method we advocate for presenting culture calibrations allows for greater ease of comparison and uncertainty calculation and propagation. We show that recorded $\delta^{11}B$ in *G. ruber* deviates markedly from the simple inorganic basis of the proxy, corroborating previous foraminiferal culture studies analysed using N-TIMS (Sanyal et al., 2001, 1996), and supporting the results of published down-core reconstructions that are based on pH-sensitivities of $\delta^{11}B_{CaCO_3}$ that are lower than $\delta^{11}B_{borate}$. We also document for the first time a size-fraction effect in $\delta^{11}B_{G.\ ruber}$, which must be taken into account in down-core application. As we illustrate for the last 30 kyr (Fig. 7), however, by analysing well-constrained size fractions and applying a species-specific culture calibration, accurate and precise estimates of past levels of atmospheric CO_2 can be reconstructed.

Acknowledgements

The authors would like to acknowledge the contributions of a number of people. We thank the other members of 'The B-Team' at the National Oceanography Centre, Southampton for their contributions, Barbara Donner from MARUM for supplying core material from Site GeoB1523-1 and Basak Kısakürek for advice and provision of core-top Eilat sample material. MH, KP and JR thank Asaph and Tanya Rivlin, Itay Cohen and rest of the students and staff at the IUI for their assistance during culturing experiments. We thank Mark Stinchcombe (NOC) for nutrient data from culture solutions, Wolfram Schinko, Hartmut Schulz, Margret Bayer, Christoph Hemleben and Ralf Aurahs for assistance and

discussion during sampling work at Tübingen, and Emmanuel Gloor and Matthew Humphries for discussion of pre-industrial pH. Gemma Smith and Gary Bilotta are thanked for GIS contributions and helpful discussion, respectively. The manuscript was also much improved by input from Rachael James, Jimin Yu, and two other anonymous reviewers. This work was made possible by a NERC PhD studentship granted to M.H., NERC grant NE/D00876X/2 awarded to G.L.F., and ISF grant 551/10 awarded to J.E.

Appendix A. Supporting information

Supplementary data associated with this article can be found in the online version at http://dx.doi.org/10.1016/j.epsl.2012.12.029.

References

Ahn, J., Brook, E.J., Mitchell, L., Rosen, J., McConnell, J.R., Taylor, K., Etheridge, D., Rubino, M., 2012. Atmospheric CO_2 over the last 1000 years: a high-resolution record from the West Antarctic Ice Sheet (WAIS) divide ice core. Global Biogeochem. Cycles 26, 11.

Allen, K.A., Hönisch, B., Eggins, S.M., Yu, J., Spero, H.J., Elderfield, H., 2011. Controls on boron incorporation in cultured tests of the planktic foraminifer Orbulina universa. Earth Planet. Sci. Lett. 309, 291–301.

Anagnostou, E., Huang, K.-F., You, C.-F., Sikes, E.L., Sherrell, R.M., 2012. Evaluation of boron isotope ratio as a pH proxy in the deep sea coral Desmophyllum dianthus: evidence of physiological pH adjustment. Earth Planet. Sci. Lett. 349, 251–260.

Anand, P., Elderfield, H., Conte, M.H., 2003. Calibration of Mg/Ca thermometry in planktonic foraminifera from a sediment trap time series. Paleoceanography 18, 1050–1064.

Aurahs, R., Treis, Y., Darling, K., Kucera, M., 2011. A revised taxonomic and phylogenetic concept for the planktonic foraminifer species *Globigerinoides ruber* based on molecular and morphometric evidence. Mar. Micropaleontol. 79, 1–14.

Barker, S., Greaves, M., Elderfield, H., 2003. A study of cleaning procedures used for foraminiferal Mg/Ca paleothermometry. Geochem. Geophys. Geosyst. 4, 8407–8426.

Bentov, S., Brownlee, C., Erez, J., 2009. The role of seawater endocytosis in the biomineralization process in calcareous foraminifera. Proc. Natl. Acad. Sci. USA 106, 21500–21504.

Bijma, J., Erez, J., Hemleben, C., 1990. Lunar and semi-lunar reproductive cycles in some spinose planktonic foraminifers. J. Foraminiferal Res. 20, 117–127.

Bolton, A., Baker, J.A., Dunbar, G.B., Carter, L., Smith, E.G.C., Neil, H.L., 2011. Environmental versus biological controls on Mg/Ca variability in *Globigerinoides ruber* (white) from core top and plankton tow samples in the southwest Pacific Ocean. Paleoceanography 26, 14.

Caron, D.A., Roger Anderson, O., Lindsey, J.L., Faber Jr., W.W., Lin Lim, E.E., 1990. Effects of gametogenesis on test structure and dissolution of some spinose planktonic foraminifera and implications for test preservation. Mar. Micropaleontol. 16, 93–116.

Catanzaro, E.J., Champion, C., Garner, E., Marinenko, G., Sappenfield, K., Shields, W., 1970. Boric Acid: Isotopic and Assay Standard Reference Materials. NBS (US) Special Publications. National Bureau of Standards, Institute for Materials Research, Washington, DC.

Darling, K.F., Wade, C.M., 2008. The genetic diversity of planktic foraminifera and the global distribution of ribosomal RNA genotypes. Mar. Micropaleontol. 67, 216–238.

Dickson, A.G., 1990. Thermodynamics of the dissociation of boric acid in synthetic seawater from 273.15 to 318.15 K. Deep-Sea Res. Pt. A 37, 755–766.

Erez, J., Luz, B., 1983. Experimental paleotemperature equation for planktonic foraminifera. Geochim. Cosmochim. Acta 47, 1025–1031.

Foster, G.L., 2008. Seawater pH, pCO_2 and CO_3^{2-} variations in the Caribbean Sea over the last 130 kyr: a boron isotope and B/Ca study of planktic foraminifera. Earth Planet. Sci. Lett. 271, 254–266.

Foster, G.L., Hönisch, B., Paris, G., Dwyer, G.S., Rae, J.W.B., Elliott, T.R., Gaillardet, J., Hemming, N.G., Louvat, P., Vengosh, A. Interlaboratory comparison of boron isotope analyses of boric acid, seawater and marine $CaCO_3$ by MC-ICPMS and NTIMS. Chem. Geol., in preparation.

Foster, G.L., Lear, C.H., Rae, J.W.B., 2012. The evolution of pCO2, ice volume and climate during the middle Miocene. Earth Planet. Sci. Lett. 341–344, 243–254.

Foster, G.L., Strandmann, P.A.E.P., von Rae, J.W.B., 2010. Boron and magnesium isotopic composition of seawater. Geochem. Geophys. Geosyst. 11, 10.

Friedrich, O., Schiebel, R., Wilson, P.A., Weldeab, S., Beer, C.J., Cooper, M.J., Fiebig, J., 2012. Influence of test size, water depth, and ecology on Mg/Ca, Sr/Ca, $\delta^{18}O$ and $\delta^{13}C$ in nine modern species of planktic foraminifers. Earth Planet. Sci. Lett. 319–320, 133–145.

Gingele, F., Kasten, S., Mulitza, S., Rühlemann, C., 2000. Age Model and Isotopes of Sediment Core GeoB1523-1. Available from: 〈www.pangaea.de〉 doi: 10.1594/PANGAEA.56532.

Gloor, M., Gruber, N., Sarmiento, J., Sabine, C.L., Feely, R.A., Rödenbeck, C., 2003. A first estimate of present and preindustrial air-sea CO_2 flux patterns based on ocean interior carbon measurements and models. Geophys. Res. Lett. 30, 1010.

Hemleben, C., Spindler, M., Breitinger, I., Ott, R., 1987. Morphological and physiological responses of *Globigerinoides sacculifer* (Brady) under varying laboratory conditions. Mar. Micropaleontol. 12, 305–324.

Hemleben, C., Spindler, M., Erson, O.R., 1989. Modern Planktonic Foraminifera. Springer, Berlin.

Hemming, N.G., Hanson, G.N., 1992. Boron isotopic composition and concentration in modern marine carbonates. Geochim. Cosmochim. Acta 56, 537–543.

Hemming, N.G., Hönisch, B., 2007. Boron isotopes in marine carbonate sediments and the pH of the ocean. In: Hillaire-Marcel, C., de Vernal, A. (Eds.), Proxies in Late Cenozoic Paleoceanography, 1, Developments in Marine Geology. Elsevier, Oxford, pp. 717–734.

Hemming, N.G., Reeder, R.J., Hanson, G.N., 1995. Mineral-fluid partitioning and isotopic fractionation of boron in synthetic calcium carbonate. Geochim. Cosmochim. Acta 59, 371–379.

Hönisch, B., Bijma, J., Russell, A.D., Spero, H.J., Palmer, M.R., Zeebe, R.E., Eisenhauer, A., 2003. The influence of symbiont photosynthesis on the boron isotopic composition of foraminifera shells. Mar. Micropaleontol. 49, 87–96.

Hönisch, B., Hemming, N.G., 2004. Ground-truthing the boron isotope-paleo-pH proxy in planktonic foraminifera shells: partial dissolution and shell size effects. Paleoceanography 19, 13.

Hönisch, B., Hemming, N.G., 2005. Surface ocean pH response to variations in pCO_2 through two full glacial cycles. Earth Planet. Sci. Lett. 236, 305–314.

Hönisch, B., Hemming, N.G., Archer, D., Siddall, M., McManus, J.F., 2009. Atmospheric carbon dioxide concentration across the mid-pleistocene transition. Science 324, 1551–1554.

Hönisch, B., Hemming, N.G., Grottoli, A.G., Amat, A., Hanson, G.N., Bijma, J., 2004. Assessing scleractinian corals as recorders for paleo-pH: empirical calibration and vital effects. Geochim. Cosmochim. Acta 68, 3675–3685.

Hönisch, B., Hemming, N.G., Loose, B., 2007. Comment on "A critical evaluation of the boron isotope-pH proxy: The accuracy of ancient ocean pH estimates" by M. Pagani, D. Lemarchand, A. Spivack and J. Gaillardet. Geochim. Cosmochim. Acta 71, 1636–1641.

Jørgensen, B.B., Erez, J., Revsbech, N.P., Cohen, Y., 1985. Symbiotic photosynthesis in a planktonic foraminiferan, *Globigerinoides sacculifer* (Brady), studied with microelectrodes. Limnol. Oceanogr. 30, 1253–1267.

Key, R.M., Kozyr, A., Sabine, C.L., Lee, K., Wanninkhof, R., Bullister, J.L., Feely, R.A., Millero, F.J., Mordy, C., Peng, T.-H., 2004. A global ocean carbon climatology: results from Global Data Analysis Project (GLODAP). Global Biogeochem. Cycles 18, 23.

Key, R.M., Tanhua, T., Olsen, A., Hoppema, M., Jutterström, S., Schirnick, C., Van Heuven, S., Kozyr, A., Lin, X., Velo, A., Wallace, D.W.R., Mintrop, L., 2010. The CARINA data synthesis project: introduction and overview. Earth Syst. Sci. Data 2, 105–121.

Kiss, E., 1988. Ion-exchange separation and spectrophotometric determination of boron in geological materials. Anal. Chim. Acta 211, 243–256.

Kisakürek, B., Eisenhauer, A., Böhm, F., Garbe-Schönberg, D., Erez, J., 2008. Controls on shell Mg/Ca and Sr/Ca in cultured planktonic foraminiferan, *Globigerinoides ruber* (white). Earth Planet. Sci. Lett. 273, 260–269.

Kısakürek, B., Eisenhauer, A., Böhm, F., Hathorne, E.C., Erez, J., 2011. Controls on calcium isotope fractionation in cultured planktic foraminifera, *Globigerinoides ruber* and *Globigerinella siphonifera*. Geochim. Cosmochim. Acta 75, 427–443.

Klochko, K., Cody, G.D., Tossell, J.A., Dera, P., Kaufman, A.J., 2009. Re-evaluating boron speciation in biogenic calcite and aragonite using ^{11}B MAS NMR. Geochim. Cosmochim. Acta 73, 1890–1900.

Klochko, K., Kaufman, A.J., Yao, W., Byrne, R.H., Tossell, J.A., 2006. Experimental measurement of boron isotope fractionation in seawater. Earth Planet. Sci. Lett. 248, 276–285.

Köhler-Rink, S., Kühl, M., 2005. The chemical microenvironment of the symbiotic planktonic foraminifer *Orbulina universa*. Mar. Biol. Res. 1, 68–78.

Krief, S., Hendy, E.J., Fine, M., Yam, R., Meibom, A., Foster, G.L., Shemesh, A., 2010. Physiological and isotopic responses of scleractinian corals to ocean acidification. Geochim. Cosmochim. Acta 74, 4988–5001.

Kroon, D., Darling, K., 1995. Size and upwelling control of the stable isotope composition of *Neogloboquadrina dutertrei* (d'Orbigny), *Globigerinoides ruber* (d'Orbigny) and *Globigerina bulloides* d'Orbigny; examples from the Panama Basin and Arabian Sea. J. Foraminiferal Res. 25, 39–52.

Lee, K., Kim, T.-W., Byrne, R.H., Millero, F.J., Feely, R.A., Liu, Y.-M., 2010. The universal ratio of boron to chlorinity for the North Pacific and North Atlantic oceans. Geochim. Cosmochim. Acta 74, 1801–1811.

Lemieux-Dudon, B., Blayo, E., Petit, J.R., Waelbroeck, C., Svensson, A., Ritz, C., Barnola, J.-M., Narcisi, B.M., Parrenin, F., 2010. Consistent dating for Antarctic and Greenland ice cores. Q. Sci. Rev. 29, 8–20.

Liu, Y., Tossell, J.A., 2005. Ab initio molecular orbital calculations for boron isotope fractionations on boric acids and borates. Geochim. Cosmochim. Acta 69, 3995–4006.

Lohmann, G.P., 1995. A model for variation in the chemistry of planktonic foraminifera due to secondary calcification and selective dissolution. Paleoceanography 10, 445–457.

Lombard, F., Erez, J., Michel, E., Labeyrie, L., 2009. Temperature effect on respiration and photosynthesis of the symbiont-bearing planktonic foraminifera *Globigerinoides ruber*, *Orbulina universa*, and *Globigerinella siphonifera*. Limnol. Oceanogr. 54, 210–218.

Lourantou, A., Lavrič, J.V., Köhler, P., Barnola, J.-M., Paillard, D., Michel, E., Raynaud, D., Chappellaz, J., 2010. Constraint of the CO_2 rise by new atmospheric carbon isotopic measurements during the last deglaciation. Global Biogeochem. Cycles 24, 15.

Ludwig, K.R., 2003. Isoplot, A Geochronological Toolkit for Microsoft Excel. Berkeley Geochronology Center, Berkeley, CA.

Lueker, T.J., Dickson, A.G., Keeling, C.D., 2000. Ocean pCO_2 calculated from dissolved inorganic carbon, alkalinity, and equations for K_1 and K_2: validation based on laboratory measurements of CO_2 in gas and seawater at equilibrium. Mar. Chem. 70, 105–119.

Lüthi, D., Le Floch, M., Bereiter, B., Blunier, T., Barnola, J.-M., Siegenthaler, U., Raynaud, D., Jouzel, J., Fischer, H., Kawamura, K., Stocker, T.F., 2008. High-resolution carbon dioxide concentration record 650,000–800,000 years before present. Nature 453, 379–382.

Ni, Y., Foster, G.L., Bailey, T., Elliott, T.R., Schmidt, D.N., Pearson, P., Haley, B., Coath, C., 2007. A core top assessment of proxies for the ocean carbonate system in surface-dwelling foraminifers. Paleoceanography 22, 3212–3226.

Ni, Y., Foster, G.L., Elliott, T., 2010. The accuracy of $\delta^{11}B$ measurements of foraminifers. Chem. Geol. 274, 187–195.

Oi, T., 2000. Ab initio molecular orbital calculations of reduced partition function ratios of polyboric acids and polyborate anions. Z. Naturforsch. 55, 623–628.

Pagani, M., Lemarchand, D., Spivack, A., Gaillardet, J., 2005. A critical evaluation of the boron isotope-pH proxy: the accuracy of ancient ocean pH estimates. Geochim. Cosmochim. Acta 69, 953–961.

Paillard, D., Labeyrie, L., Yiou, P., 1996. Analyseries 1.0: a macintosh software for the analysis of geographical time-series. EOS, 77.

Palmer, M.R., Brummer, G.J., Cooper, M.J., Elderfield, H., Greaves, M.J., Reichart, G.J., Schouten, S., Yu, J.M., 2010. Multi-proxy reconstruction of surface water pCO\sub 2\nosupersub in the northern Arabian Sea since 29 ka. Earth Planet. Sci. Lett. 295, 49–57.

Palmer, M.R., Pearson, P.N., 2003. A 23,000-year record of surface water pH and PCO_2 in the Western Equatorial Pacific Ocean. Science 300, 480–482.

Pearson, P.N., Foster, G.L., Wade, B.S., 2009. Atmospheric carbon dioxide through the Eocene–Oligocene climate transition. Nature 461, 1110–1113.

Pearson, P.N., Palmer, M.R., 2000. Atmospheric carbon dioxide concentrations over the past 60 million years. Nature 406, 695–699.

Rae, J.W.B., Foster, G.L., Schmidt, D.N., Elliott, T., 2011. Boron isotopes and B/Ca in benthic foraminifera: proxies for the deep ocean carbonate system. Earth Planet. Sci. Lett. 302, 403–413.

Reynaud, S., Hemming, N.G., Juillet-Leclerc, A., Gattuso, J.-P., 2004. Effect of pCO_2 and temperature on the boron isotopic composition of the zooxanthellate coral *Acropora* sp. Coral Reefs 23, 539–546.

Rink, S., Kühl, M., Bijma, J., Spero, H.J., 1998. Microsensor studies of photosynthesis and respiration in the symbiotic foraminifer *Orbulina universa*. Mar. Biol. 131, 583–595.

Rollion-Bard, C., Erez, J., 2010. Intra-shell boron isotope ratios in the symbiont-bearing benthic foraminiferan *Amphistegina lobifera*: Implications for $\delta^{11}B$ vital effects and paleo-pH reconstructions. Geochim. Cosmochim. Acta 74, 1530–1536.

Russell, A.D., Hönisch, B., Spero, H.J., Lea, D.W., 2004. Effects of seawater carbonate ion concentration and temperature on shell U, Mg, and Sr in cultured planktonic foraminifera. Geochim. Cosmochim. Acta 68, 4347–4361.

Rustad, J.R., Bylaska, E.J., 2007. Ab initio calculation of isotopic fractionation in $B(OH)_3(aq)$ and $BOH_4^-(aq)$. J. Am. Chem. Soc. 129, 2222–2223.

Sanyal, A., Bijma, J., Spero, H., Lea, D.W., 2001. Empirical relationship between pH and the boron isotopic composition of *Globigerinoides sacculifer*: Implications for the boron isotope paleo-pH proxy. Paleoceanography 16, 515–519.

Sanyal, A., Hemming, N.G., Broecker, W.S., Lea, D.W., Spero, H.J., Hanson, G.N., 1996. Oceanic pH control on the boron isotopic composition of foraminifera: evidence from culture experiments. Paleoceanography 11, 513–517.

Sanyal, A., Hemming, N.G., Hanson, G.N., Broecker, W.S., 1995. Evidence for a higher pH in the glacial ocean from boron isotopes in foraminifera. Nature 373, 234–236.

Sanyal, A., Nugent, M., Reeder, R.J., Bijma, J., 2000. Seawater pH control on the boron isotopic composition of calcite: evidence from inorganic calcite precipitation experiments. Geochim. Cosmochim. Acta 64, 1551–1555.

Seki, O., Foster, G.L., Schmidt, D.N., Mackensen, A., Kawamura, K., Pancost, R.D., 2010. Alkenone and boron-based Pliocene pCO_2 records. Earth Planet. Sci. Lett. 292, 201–211.

Shaked, Y., Genin, A., 2006. The Israel National Monitoring Program at the Gulf of Eilat (NMP). (Scientific Report), Scientific Report. Interuniversity Institute, Eilat.

Spindler, M., Hemleben, C., Salomons, J.B., Smit, L.P., 1984. Feeding behavior of some planktonic foraminifers in laboratory cultures. J. Foraminiferal Res. 14, 237–249.

Takahashi, T., Sutherland, S.C., Wanninkhof, R., Sweeney, C., Feely, R.A., Chipman, D.W., Hales, B., Friederich, G., Chavez, F., Sabine, C., Watson, A., Bakker, D.C.E., Schuster, U., Metzl, N., Yoshikawa-Inoue, H., Ishii, M., Midorikawa, T., Nojiri, Y., Körtzinger, A., Steinhoff, T., Hoppema, M., Olafsson, J., Arnarson, T.S., Tilbrook, B., Johannessen, T., Olsen, A., Bellerby, R., Wong, C.S., Delille, B., Bates, N.R., de Baar, H.J.W, 2009. Climatological mean and decadal change in surface ocean pCO_2, and net sea–air CO_2 flux over the global oceans. Deep-Sea Res. Pt. II 56, 554–577.

Trotter, J., Montagna, P., McCulloch, M., Silenzi, S., Reynaud, S., Mortimer, G., Martin, S., Ferrier-Pagès, C., Gattuso, J.-P., Rodolfo-Metalpa, R., 2011. Quantifying the pH "vital effect" in the temperate zooxanthellate coral *Cladocora caespitosa*: validation of the boron seawater pH proxy. Earth Planet. Sci. Lett. 303, 163–173.

van Heuven, S., Pierrot, D., Rae, J.W.B., Lewis, E., Wallace, D.W.R., 2011. MATLAB program developed for CO_2 system calculations, CO_2sys. Carbon Dioxide Information Analysis Center, Oak Ridge National Laboratory, US.

Vengosh, A., Kolodny, Y., Starinsky, A., Chivas, A.R., McCulloch, M.T., 1991. Coprecipitation and isotopic fractionation of boron in modern biogenic carbonates. Geochim. Cosmochim. Acta 55, 2901–2910.

Villiers, S.de, Greaves, M., Elderfield, H., 2002. An intensity ratio calibration method for the accurate determination of Mg/Ca and Sr/Ca of marine carbonates by ICP-AES. Geochem. Geophys. Geosyst. 3, 1001.

Wang, L., 2000. Isotopic signals in two morphotypes of *Globigerinoides ruber* (white) from the South China Sea: implications for monsoon climate change during the last glacial cycle. Palaeogeogr. Palaeoclimatol. Palaeoecol. 161, 381–394.

Wolf-Gladrow, D.A., Bijma, J., Zeebe, R.E., 1999. Model simulation of the carbonate system in the microenvironment of symbiont bearing foraminifera. Mar. Chem. 64, 181–198.

York, D., 1968. Least squares fitting of a straight line with correlated errors. Earth Planet. Sci. Lett. 5, 320–324.

Yu, J., Foster, G.L., Elderfield, H., Broecker, W.S., Clark, E., 2010. An evaluation of benthic foraminiferal B/Ca and $\delta^{11}B$ for deep ocean carbonate ion and pH reconstructions. Earth Planet. Sci. Lett. 293, 114–120.

Zeebe, R.E., 2005. Stable boron isotope fractionation between dissolved $B(OH)_3$ and $B(OH)_4^-$. Geochim. Cosmochim. Acta 69, 2753–2766.

Zeebe, R.E., Sanyal, A., Ortiz, J.D., Wolf-Gladrow, D.A., 2001. A theoretical study of the kinetics of the boric acid–borate equilibrium in seawater. Mar. Chem. 73, 113–124.

Zeebe, R.E., Wolf-Gladrow, D.A., 2001. CO_2 in Seawater: Equilibrium, Kinetics, Isotopes. Elsevier Oceanography Series. Elsevier, Amsterdam.

Zeebe, R.E., Wolf-Gladrow, D.A., Bijma, J., Hönisch, B., 2003. Vital effects in foraminifera do not compromise the use of $\delta^{11}B$ as a paleo-pH indicator: evidence from modeling. Paleoceanography 18, 9.

Appendix B

Supplementary Materials: Henehan et al. (2013)

SITE	Archive	Long (°E)	Lat (°N)		Month	SST (°C)	S	pK^*_B	TAlk (μmol/ kg)	pCO_2	SiO_4^{2-}	PO_4^-	pH	$\delta^{11}B_{B(OH)_4^-}$
CAR22(Z)-7	Marshall, B.	-64.67	10.50	Collected Jan-07	Dec-06	26.9	36.5	8.567	2385	408	1.77	0.04	8.042	18.39
					Feb-07	22.9	36.8	8.612	2424	379	0.37	0.08	8.077	18.28
	Date-weighted average												8.066	8.31
	Uncertainty (± Half of the December-February range)												0.018	0.052

TABLE B.1: Sediment Trap Carbonate System Calculations. *Data downloadable from IMARS*

		Site		Nearest Takahashi Sites				From Takahashi et al. (2009)										
Site	**Archive**	**Long (°)**	**Lat (°)**	**Long (°)**	**Lat (°)**	**1/(s.s. dist. from site)**	**Month**	**SST (C)**	**S (psu)**	pK_B^*	**Regional Sal/Alk correlation used**	**TAlk (μmol/kg)**	**ΔpCO_2(ppm)**	**Poor correction factor**	**pCO_2**	**SiO_4^{2-}**	**PO_4^-**	**pH**	**$\delta^{11}B_{B(OH)_4^-}$**
G4	Bostock, H.	167.25	-28.42	162.5	-32	0.0282	1	22.9	35.81	8.617	Alk = Sal*65.91	2360.2	-26.21	0.591	261.1	0.9	0.12	8.199	19.54
G4	Bostock, H.	167.25	-28.42	162.5	-32	0.0282	2	23.5	35.73	8.611	Alk = Sal*65.91	2355.0	-14.65	0.591	267.9	0.9	0.12	8.189	19.49
G4	Bostock, H.	167.25	-28.42	162.5	-32	0.0282	3	23.2	35.77	8.614	Alk = Sal*65.91	2357.6	-19.79	0.591	264.9	0.9	0.12	8.193	19.50
G4	Bostock, H.	167.25	-28.42	162.5	-32	0.0282	4	22.3	35.87	8.624	Alk = Sal*65.91	2364.2	-33.79	0.591	256.6	0.9	0.12	8.206	19.54
G4	Bostock, H.	167.25	-28.42	162.5	-32	0.0282	5	21.1	35.81	8.638	Alk = Sal*65.91	2360.2	-34.5	0.591	256.2	0.9	0.12	8.208	19.39
G4	Bostock, H.	167.25	-28.42	162.5	-32	0.0282	6	19.9	35.85	8.653	Alk = Sal*65.91	2362.9	-32.78	0.591	257.2	0.9	0.12	8.208	19.21
G4	Bostock, H.	167.25	-28.42	162.5	-32	0.0282	7	18.9	35.77	8.665	Alk = Sal*65.91	2357.6	-40.1	0.591	252.9	0.9	0.12	8.215	19.14
G4	Bostock, H.	167.25	-28.42	162.5	-32	0.0282	8	18.4	35.74	8.671	Alk = Sal*65.91	2355.6	-47.25	0.591	248.7	0.9	0.12	8.221	19.15
G4	Bostock, H.	167.25	-28.42	162.5	-32	0.0282	9	18.4	35.75	8.670	Alk = Sal*65.91	2356.3	-45.15	0.591	249.9	0.9	0.12	8.219	19.13
G4	Bostock, H.	167.25	-28.42	162.5	-32	0.0282	10	19.0	35.77	8.664	Alk = Sal*65.91	2357.6	-47.94	0.591	248.3	0.9	0.12	8.221	19.23
G4	Bostock, H.	167.25	-28.42	162.5	-32	0.0282	11	20.1	35.7	8.651	Alk = Sal*65.91	2353.0	-39.08	0.591	253.5	0.9	0.12	8.212	19.29
G4	Bostock, H.	167.25	-28.42	162.5	-32	0.0282	12	21.6	35.75	8.633	Alk = Sal*65.91	2356.3	-33.75	0.591	256.7	0.9	0.12	8.206	19.43
G4	Bostock, H.	167.25	-28.42	162.5	-28	0.0440	1	24.4	35.85	8.599	Alk = Sal*65.91	2362.9	3.39	0.591	278.6	0.9	0.12	8.175	19.46
G4	Bostock, H.	167.25	-28.42	162.5	-28	0.0440	2	24.9	35.81	8.594	Alk = Sal*65.91	2360.2	-2.01	0.591	275.4	0.9	0.12	8.178	19.57
G4	Bostock, H.	167.25	-28.42	162.5	-28	0.0440	3	24.6	35.74	8.598	Alk = Sal*65.91	2355.6	-13.53	0.591	268.6	0.9	0.12	8.186	19.62

		Site		Nearest Takahashi Sites				From Takahashi et al. (2009)										
Site	**Archive**	**Long (°)**	**Lat (°)**	**Long (°)**	**Lat (°)**	**1/(s.s. dist. from site)**	**Month**	**SST (C)**	**S (psu)**	pK_B^*	**Regional Sal/Alk correlation used**	**TAlk (μmol/kg)**	**ΔpCO_2(ppm)**	**Poor correction factor**	**pCO_2**	**SiO_4^{2-}**	**PO_4^-**	**pH**	**$\delta^{11}B_{B(OH)_4^-}$**
G4	Bostock, H.	167.25	-28.42	162.5	-28	0.0440	4	23.7	35.84	8.607	Alk = Sal*65.91	2362.2	-20.05	0.591	264.8	0.9	0.12	8.193	19.59
G4	Bostock, H.	167.25	-28.42	162.5	-28	0.0440	5	22.6	35.87	8.620	Alk = Sal*65.91	2364.2	-18.39	0.591	265.7	0.9	0.12	8.194	19.44
G4	Bostock, H.	167.25	-28.42	162.5	-28	0.0440	6	21.4	35.91	8.634	Alk = Sal*65.91	2366.8	-30.35	0.591	258.7	0.9	0.12	8.205	19.40
G4	Bostock, H.	167.25	-28.42	162.5	-28	0.0440	7	20.5	35.84	8.646	Alk = Sal*65.91	2362.2	-44.51	0.591	250.3	0.9	0.12	8.217	19.41
G4	Bostock, H.	167.25	-28.42	162.5	-28	0.0440	8	20.0	35.81	8.652	Alk = Sal*65.91	2360.2	-47.7	0.591	248.4	0.9	0.12	8.220	19.37
G4	Bostock, H.	167.25	-28.42	162.5	-28	0.0440	9	20.1	35.89	8.650	Alk = Sal*65.91	2365.5	-38.27	0.591	254.0	0.9	0.12	8.213	19.30
G4	Bostock, H.	167.25	-28.42	162.5	-28	0.0440	10	20.7	35.86	8.642	Alk = Sal*65.91	2363.5	-22.37	0.591	263.4	0.9	0.12	8.199	19.23
G4	Bostock, H.	167.25	-28.42	162.5	-28	0.0440	11	21.9	35.8	8.629	Alk = Sal*65.91	2359.6	-16.73	0.591	266.7	0.9	0.12	8.193	19.32
G4	Bostock, H.	167.25	-28.42	162.5	-28	0.0440	12	23.2	35.84	8.613	Alk = Sal*65.91	2362.2	-24.03	0.591	262.4	0.9	0.12	8.197	19.56
G4	Bostock, H.	167.25	-28.42	167.5	-32	0.0775	1	21.9	35.71	8.629	Alk = Sal*65.91	2353.6	-26.99	0.591	260.7	0.9	0.12	8.200	19.41
G4	Bostock, H.	167.25	-28.42	167.5	-32	0.0775	2	22.6	35.69	8.621	Alk = Sal*65.91	2352.3	-17.58	0.591	266.2	0.9	0.12	8.192	19.40
G4	Bostock, H.	167.25	-28.42	167.5	-32	0.0775	3	22.3	35.76	8.624	Alk = Sal*65.91	2356.9	-24.12	0.591	262.3	0.9	0.12	8.198	19.43
G4	Bostock, H.	167.25	-28.42	167.5	-32	0.0775	4	21.4	35.84	8.634	Alk = Sal*65.91	2362.2	-27.72	0.591	260.2	0.9	0.12	8.202	19.37
G4	Bostock, H.	167.25	-28.42	167.5	-32	0.0775	5	20.3	35.86	8.647	Alk = Sal*65.91	2363.5	-34.17	0.591	256.4	0.9	0.12	8.209	19.29
G4	Bostock, H.	167.25	-28.42	167.5	-32	0.0775	6	19.1	35.77	8.663	Alk = Sal*65.91	2357.6	-31.44	0.591	258.0	0.9	0.12	8.208	19.09

		Site		Nearest Takahashi Sites				From Takahashi et al. (2009)										
Site	**Archive**	**Long (°)**	**Lat (°)**	**Long (°)**	**Lat (°)**	**1/(s.s. dist. from site)**	**Month**	**SST (C)**	**S (psu)**	pK_B^*	**Regional Sal/Alk correlation used**	**TAlk (μmol/kg)**	**ΔpCO_2(ppm)**	**Coor correction factor**	**pCO_2**	**SiO_4^{2-}**	**PO_4^-**	**pH**	**$\delta^{11}B_{B(OH)_4^-}$**
G4	Bostock, H.	167.25	-28.42	167.5	-32	0.0775	7	18.2	35.74	8.674	Alk = Sal*65.91	2355.6	-35.02	0.591	255.9	0.9	0.12	8.211	19.00
G4	Bostock, H.	167.25	-28.42	167.5	-32	0.0775	8	17.7	35.69	8.680	Alk = Sal*65.91	2352.3	-42.38	0.591	251.6	0.9	0.12	8.217	19.00
G4	Bostock, H.	167.25	-28.42	167.5	-32	0.0775	9	17.7	35.66	8.679	Alk = Sal*65.91	2350.4	-44.44	0.591	250.3	0.9	0.12	8.219	19.02
G4	Bostock, H.	167.25	-28.42	167.5	-32	0.0775	10	18.2	35.73	8.673	Alk = Sal*65.91	2355.0	-45.64	0.591	249.6	0.9	0.12	8.220	19.11
G4	Bostock, H.	167.25	-28.42	167.5	-32	0.0775	11	19.3	35.66	8.660	Alk = Sal*65.91	2350.4	-34.75	0.591	256.1	0.9	0.12	8.209	19.14
G4	Bostock, H.	167.25	-28.42	167.5	-32	0.0775	12	20.7	35.71	8.643	Alk = Sal*65.91	2353.6	-38.11	0.591	254.1	0.9	0.12	8.210	19.36
G4	Bostock, H.	167.25	-28.42	167.5	-28	4.2348	1	24.0	35.9	8.604	Alk = Sal*65.91	2366.2	-3.69	0.591	274.4	0.9	0.12	8.181	19.48
G4	Bostock, H.	167.25	-28.42	167.5	-28	4.2348	2	24.5	35.77	8.598	Alk = Sal*65.91	2357.6	0.22	0.591	276.7	0.9	0.12	8.176	19.49
G4	Bostock, H.	167.25	-28.42	167.5	-28	4.2348	3	24.2	35.74	8.602	Alk = Sal*65.91	2355.6	-22.05	0.591	263.6	0.9	0.12	8.193	19.66
G4	Bostock, H.	167.25	-28.42	167.5	-28	4.2348	4	23.3	35.8	8.612	Alk = Sal*65.91	2359.6	-35.28	0.591	255.8	0.9	0.12	8.205	19.68
G4	Bostock, H.	167.25	-28.42	167.5	-28	4.2348	5	22.3	35.89	8.624	Alk = Sal*65.91	2365.5	-28.31	0.591	259.9	0.9	0.12	8.202	19.49
G4	Bostock, H.	167.25	-28.42	167.5	-28	4.2348	6	21.0	35.83	8.639	Alk = Sal*65.91	2361.6	-32.19	0.591	257.6	0.9	0.12	8.206	19.36
G4	Bostock, H.	167.25	-28.42	167.5	-28	4.2348	7	20.2	35.8	8.650	Alk = Sal*65.91	2359.6	-43.02	0.591	251.2	0.9	0.12	8.216	19.35
G4	Bostock, H.	167.25	-28.42	167.5	-28	4.2348	8	19.7	35.83	8.655	Alk = Sal*65.91	2361.6	-47.78	0.591	248.4	0.9	0.12	8.220	19.34
G4	Bostock, H.	167.25	-28.42	167.5	-28	4.2348	9	19.8	35.81	8.653	Alk = Sal*65.91	2360.2	-47.73	0.591	248.4	0.9	0.12	8.220	19.35

		Site		Nearest Takahashi Sites				From Takahashi et al. (2009)										
Site	**Archive**	**Long (°)**	**Lat (°)**	**Long (°)**	**Lat (°)**	**1/(s.s. dist. from site)**	**Month**	**SST (C)**	**S (psu)**	pK_B^*	**Regional Sal/Alk correlation used**	**TAlk (μmol/kg)**	**ΔpCO_2(ppm)**	**Poor correction factor**	**pCO_2**	**SiO_4^{2-}**	**PO_4^-**	**pH**	**$\delta^{11}B_{B(OH)_4^-}$**
G4	Bostock, H.	167.25	-28.42	167.5	-28	4.2348	10	20.5	35.85	8.646	Alk = Sal*65.91	2362.9	-36.2	0.591	255.2	0.9	0.12	8.210	19.33
G4	Bostock, H.	167.25	-28.42	167.5	-28	4.2348	11	21.6	35.79	8.633	Alk = Sal*65.91	2358.9	-20.05	0.591	264.8	0.9	0.12	8.196	19.31
G4	Bostock, H.	167.25	-28.42	167.5	-28	4.2348	12	22.9	35.82	8.617	Alk = Sal*65.91	2360.9	-23.39	0.591	262.8	0.9	0.12	8.197	19.51
													Interpolated average					**8.202**	**19.44**
													Interpolated intraannual variation					**0.030**	**0.29**
MC497	Kucera, M.	63.31	23.53	62.5	20	0.0762	1	24.1	36.54	8.599	Alk = (62.9*Sal) + 87.77	2386.1	27.96	0.591	291.5	3.19	0.51	8.161	19.30
MC497	Kucera, M.	63.31	23.53	62.5	20	0.0762	2	23.7	36.44	8.604	Alk = (62.9*Sal) + 87.77	2379.8	6.86	0.591	279.1	3.19	0.51	8.176	19.41
MC497	Kucera, M.	63.31	23.53	62.5	20	0.0762	3	24.6	36.49	8.593	Alk = (62.9*Sal) + 87.77	2383.0	12.89	0.591	282.6	3.19	0.51	8.171	19.48
MC497	Kucera, M.	63.31	23.53	62.5	20	0.0762	4	26.6	36.54	8.570	Alk = (62.9*Sal) + 87.77	2386.1	24.48	0.591	289.5	3.19	0.51	8.159	19.64
MC497	Kucera, M.	63.31	23.53	62.5	20	0.0762	5	28.8	36.57	8.545	Alk = (62.9*Sal) + 87.77	2388.0	36.75	0.591	296.7	3.19	0.51	8.148	19.80
MC497	Kucera, M.	63.31	23.53	62.5	20	0.0762	6	29.6	36.59	8.535	Alk = (62.9*Sal) + 87.77	2389.3	44.33	0.591	301.2	3.19	0.51	8.141	19.84
MC497	Kucera, M.	63.31	23.53	62.5	20	0.0762	7	28.6	36.35	8.548	Alk = (62.9*Sal) + 87.77	2374.2	79.13	0.591	321.8	3.19	0.51	8.119	19.42

		Site		Nearest Takahashi Sites				From Takahashi et al. (2009)										
Site	**Archive**	**Long (°)**	**Lat (°)**	**Long (°)**	**Lat (°)**	**1/(s.s. dist. from site)**	**Month**	**SST (C)**	**S (psu)**	pK_B^*	**Regional Sal/Alk correlation used**	**TAlk (μmol/kg)**	**ΔpCO_2(ppm)**	**G loor correction factor**	**pCO_2**	**SiO_4^{2-}**	**PO_4^-**	**pH**	**$\delta^{11}B_{B(OH)_4^-}$**
MC497	Kucera, M.	63.31	23.53	62.5	20	0.0762	8	27.5	36.53	8.560	Alk = (62.9*Sal) + 87.77	2385.5	85.26	0.591	325.4	3.19	0.51	8.119	19.26
MC497	Kucera, M.	63.31	23.53	62.5	20	0.0762	9	27.6	36.37	8.559	Alk = (62.9*Sal) + 87.77	2375.4	90.85	0.591	328.7	3.19	0.51	8.114	19.21
MC497	Kucera, M.	63.31	23.53	62.5	20	0.0762	10	28.1	36.37	8.553	Alk = (62.9*Sal) + 87.77	2375.4	50.14	0.591	304.6	3.19	0.51	8.139	19.58
MC497	Kucera, M.	63.31	23.53	62.5	20	0.0762	11	27.2	36.55	8.563	Alk = (62.9*Sal) + 87.77	2386.8	27.28	0.591	291.1	3.19	0.51	8.157	19.69
MC497	Kucera, M.	63.31	23.53	62.5	20	0.0762	12	25.5	36.54	8.583	Alk = (62.9*Sal) + 87.77	2386.1	29.04	0.591	292.2	3.19	0.51	8.158	19.46
MC497	Kucera, M.	63.31	23.53	62.5	24	1.1403	1	24.8	36.38	8.592	Alk = (62.9*Sal) + 87.77	2376.1	37	0.591	296.9	3.19	0.51	8.153	19.29
MC497	Kucera, M.	63.31	23.53	62.5	24	1.1403	2	24.7	36.37	8.593	Alk = (62.9*Sal) + 87.77	2375.4	24.41	0.591	289.4	3.19	0.51	8.162	19.37
MC497	Kucera, M.	63.31	23.53	62.5	24	1.1403	3	25.8	36.41	8.580	Alk = (62.9*Sal) + 87.77	2378.0	36.1	0.591	296.3	3.19	0.51	8.152	19.42
MC497	Kucera, M.	63.31	23.53	62.5	24	1.1403	4	27.7	36.49	8.558	Alk = (62.9*Sal) + 87.77	2383.0	28.73	0.591	292.0	3.19	0.51	8.154	19.73
MC497	Kucera, M.	63.31	23.53	62.5	24	1.1403	5	28.9	36.48	8.543	Alk = (62.9*Sal) + 87.77	2382.4	24.76	0.591	289.6	3.19	0.51	8.155	19.92

		Site		Nearest Takahashi Sites				From Takahashi et al. (2009)										
Site	**Archive**	**Long (°)**	**Lat (°)**	**Long (°)**	**Lat (°)**	**1/(s.s. dist. from site)**	**Month**	**SST (C)**	**S (psu)**	pK_B^*	**Regional Sal/Alk correlation used**	**TAlk (μmol/kg)**	**ΔpCO_2(ppm)**	**Poor correction factor**	**pCO_2**	**SiO_4^{2-}**	**PO_4^-**	**pH**	$\delta^{11}B_{B(OH)_4^-}$
MC497	Kucera, M.	63.31	23.53	62.5	24	1.1403	6	28.9	36.35	8.545	Alk = (62.9*Sal) + 87.77	2374.2	31.37	0.591	293.5	3.19	0.51	8.150	19.83
MC497	Kucera, M.	63.31	23.53	62.5	24	1.1403	7	27.1	36.35	8.565	Alk = (62.9*Sal) + 87.77	2374.2	23.7	0.591	289.0	3.19	0.51	8.158	19.68
MC497	Kucera, M.	63.31	23.53	62.5	24	1.1403	8	26.0	36.35	8.578	Alk = (62.9*Sal) + 87.77	2374.2	63.6	0.591	312.6	3.19	0.51	8.133	19.22
MC497	Kucera, M.	63.31	23.53	62.5	24	1.1403	9	26.8	36.19	8.570	Alk = (62.9*Sal) + 87.77	2364.1	40.51	0.591	298.9	3.19	0.51	8.146	19.47
MC497	Kucera, M.	63.31	23.53	62.5	24	1.1403	10	28.0	36.26	8.555	Alk = (62.9*Sal) + 87.77	2368.5	33.42	0.591	294.7	3.19	0.51	8.149	19.69
MC497	Kucera, M.	63.31	23.53	62.5	24	1.1403	11	27.5	36.38	8.560	Alk = (62.9*Sal) + 87.77	2376.1	22.95	0.591	288.6	3.19	0.51	8.158	19.74
MC497	Kucera, M.	63.31	23.53	62.5	24	1.1403	12	26.0	36.41	8.578	Alk = (62.9*Sal) + 87.77	2378.0	39.47	0.591	298.3	3.19	0.51	8.150	19.42
MC497	Kucera, M.	63.31	23.53	67.5	20	0.0333	1	25.3	36.33	8.586	Alk = (62.9*Sal) + 87.77	2372.9	29.04	0.591	292.2	3.19	0.51	8.157	19.41
MC497	Kucera, M.	63.31	23.53	67.5	20	0.0333	2	25.3	36.12	8.588	Alk = (62.9*Sal) + 87.77	2359.7	5.45	0.591	278.2	3.19	0.51	8.172	19.58
MC497	Kucera, M.	63.31	23.53	67.5	20	0.0333	3	26.2	36.12	8.577	Alk = (62.9*Sal) + 87.77	2359.7	-1.6	0.591	274.1	3.19	0.51	8.176	19.76

		Site		Nearest Takahashi Sites				From Takahashi et al. (2009)										
Site	**Archive**	**Long (°)**	**Lat (°)**	**Long (°)**	**Lat (°)**	**1/(s.s. dist. from site)**	**Month**	**SST (C)**	**S (psu)**	pK_B^*	**Regional Sal/Alk correlation used**	**TAlk (μmol/kg)**	**ΔpCO_2(ppm)**	**Poor correction factor**	**pCO_2**	**SiO_4^{2-}**	**PO_4^-**	**pH**	**$\delta^{11}B_{B(OH)_4^-}$**
MC497	Kucera, M.	63.31	23.53	67.5	20	0.0333	4	27.7	36.23	8.559	Alk = (62.9*Sal) + 87.77	2366.6	14.35	0.591	283.5	3.19	0.51	8.163	19.82
MC497	Kucera, M.	63.31	23.53	67.5	20	0.0333	5	29.0	36.3	8.543	Alk = (62.9*Sal) + 87.77	2371.0	21.25	0.591	287.6	3.19	0.51	8.156	19.93
MC497	Kucera, M.	63.31	23.53	67.5	20	0.0333	6	29.4	36.51	8.538	Alk = (62.9*Sal) + 87.77	2384.2	22.68	0.591	288.4	3.19	0.51	8.155	20.00
MC497	Kucera, M.	63.31	23.53	67.5	20	0.0333	7	28.5	36.45	8.549	Alk = (62.9*Sal) + 87.77	2380.5	20.22	0.591	286.9	3.19	0.51	8.158	19.89
MC497	Kucera, M.	63.31	23.53	67.5	20	0.0333	8	27.6	36.49	8.559	Alk = (62.9*Sal) + 87.77	2383.0	27.47	0.591	291.2	3.19	0.51	8.156	19.72
MC497	Kucera, M.	63.31	23.53	67.5	20	0.0333	9	27.9	36.19	8.557	Alk = (62.9*Sal) + 87.77	2364.1	36.97	0.591	296.8	3.19	0.51	8.147	19.64
MC497	Kucera, M.	63.31	23.53	67.5	20	0.0333	10	28.4	36.05	8.552	Alk = (62.9*Sal) + 87.77	2355.3	32.79	0.591	294.4	3.19	0.51	8.148	19.72
MC497	Kucera, M.	63.31	23.53	67.5	20	0.0333	11	27.9	36.27	8.557	Alk = (62.9*Sal) + 87.77	2369.2	16.05	0.591	284.5	3.19	0.51	8.161	19.83
MC497	Kucera, M.	63.31	23.53	67.5	20	0.0333	12	26.4	36.34	8.573	Alk = (62.9*Sal) + 87.77	2373.6	15.72	0.591	284.3	3.19	0.51	8.165	19.66
													Interpolated average					**8.152**	**19.57**
													Interpolated intraannual variation					**0.020**	**0.55**
OC476-SR223	Bostock, H.	166.53	-33.53	162.5	-36	0.0448	1	20.6	35.74	8.644	Alk = Sal*65.91	2355.6	-26.81	0.591	266.4	0.9	0.25	8.195	19.15

		Site		Nearest Takahashi Sites				From Takahashi et al. (2009)										
Site	**Archive**	**Long (°)**	**Lat (°)**	**Long (°)**	**Lat (°)**	**1/(s.s. dist. from site)**	**Month**	**SST (C)**	**S (psu)**	pK_B^*	**Regional Sal/Alk correlation used**	**TAlk (μmol/kg)**	**ΔpCO_2(ppm)**	**Cfloor correction factor**	**pCO_2**	**SiO_4^{2-}**	**PO_4^-**	**pH**	**$\delta^{11}B_{B(OH)_4^-}$**
OC476-SR223	Bostock, H.	166.53	-33.53	162.5	-36	0.0448	2	21.3	35.59	8.637	Alk = Sal*65.91	2345.7	-20.32	0.591	270.2	0.9	0.25	8.188	19.16
OC476-SR223	Bostock, H.	166.53	-33.53	162.5	-36	0.0448	3	21.0	35.71	8.641	Alk = Sal*65.91	2353.6	-29.64	0.591	264.7	0.9	0.25	8.196	19.22
OC476-SR223	Bostock, H.	166.53	-33.53	162.5	-36	0.0448	4	20.0	35.66	8.652	Alk = Sal*65.91	2350.4	-39.62	0.591	258.8	0.9	0.25	8.205	19.18
OC476-SR223	Bostock, H.	166.53	-33.53	162.5	-36	0.0448	5	18.8	35.83	8.666	Alk = Sal*65.91	2361.6	-35.79	0.591	261.1	0.9	0.25	8.204	19.01
OC476-SR223	Bostock, H.	166.53	-33.53	162.5	-36	0.0448	6	17.6	35.8	8.681	Alk = Sal*65.91	2359.6	-33.92	0.591	262.2	0.9	0.25	8.204	18.83
OC476-SR223	Bostock, H.	166.53	-33.53	162.5	-36	0.0448	7	16.7	35.72	8.692	Alk = Sal*65.91	2354.3	-40.09	0.591	258.5	0.9	0.25	8.209	18.76
OC476-SR223	Bostock, H.	166.53	-33.53	162.5	-36	0.0448	8	16.2	35.64	8.698	Alk = Sal*65.91	2349.0	-45.86	0.591	255.1	0.9	0.25	8.213	18.73
OC476-SR223	Bostock, H.	166.53	-33.53	162.5	-36	0.0448	9	16.2	35.56	8.699	Alk = Sal*65.91	2343.8	-48.98	0.591	253.3	0.9	0.25	8.215	18.75
OC476-SR223	Bostock, H.	166.53	-33.53	162.5	-36	0.0448	10	16.6	35.62	8.693	Alk = Sal*65.91	2347.7	-50.34	0.591	252.5	0.9	0.25	8.216	18.83
OC476-SR223	Bostock, H.	166.53	-33.53	162.5	-36	0.0448	11	17.7	35.55	8.680	Alk = Sal*65.91	2343.1	-44.45	0.591	255.9	0.9	0.25	8.210	18.91
OC476-SR223	Bostock, H.	166.53	-33.53	162.5	-36	0.0448	12	19.2	35.6	8.662	Alk = Sal*65.91	2346.4	-45.33	0.591	255.4	0.9	0.25	8.210	19.12
OC476-SR223	Bostock, H.	166.53	-33.53	162.5	-32	0.0537	1	22.9	35.81	8.617	Alk = Sal*65.91	2360.2	-26.21	0.591	266.7	0.9	0.25	8.191	19.45
OC476-SR223	Bostock, H.	166.53	-33.53	162.5	-32	0.0537	2	23.5	35.73	8.611	Alk = Sal*65.91	2355.0	-14.65	0.591	273.5	0.9	0.25	8.182	19.40
OC476-SR223	Bostock, H.	166.53	-33.53	162.5	-32	0.0537	3	23.2	35.77	8.614	Alk = Sal*65.91	2357.6	-19.79	0.591	270.5	0.9	0.25	8.186	19.42
OC476-SR223	Bostock, H.	166.53	-33.53	162.5	-32	0.0537	4	22.3	35.87	8.624	Alk = Sal*65.91	2364.2	-33.79	0.591	262.2	0.9	0.25	8.199	19.45

		Site		Nearest Takahashi Sites				From Takahashi et al. (2009)										
Site	**Archive**	**Long (°)**	**Lat (°)**	**Long (°)**	**Lat (°)**	**1/(s.s. dist. from site)**	**Month**	**SST (C)**	**S (psu)**	pK_B^*	**Regional Sal/Alk correlation used**	**TAlk (μmol/kg)**	**ΔpCO_2(ppm)**	**Poor correction factor**	**pCO_2**	**SiO_4^{2-}**	**PO_4^-**	**pH**	**$\delta^{11}B_{B(OH)_4^-}$**
OC476-SR223	Bostock, H.	166.53	-33.53	162.5	-32	0.0537	5	21.1	35.81	8.638	Alk = Sal*65.91	2360.2	-34.5	0.591	261.8	0.9	0.25	8.200	19.30
OC476-SR223	Bostock, H.	166.53	-33.53	162.5	-32	0.0537	6	19.9	35.85	8.653	Alk = Sal*65.91	2362.9	-32.78	0.591	262.8	0.9	0.25	8.201	19.12
OC476-SR223	Bostock, H.	166.53	-33.53	162.5	-32	0.0537	7	18.9	35.77	8.665	Alk = Sal*65.91	2357.6	-40.1	0.591	258.5	0.9	0.25	8.207	19.05
OC476-SR223	Bostock, H.	166.53	-33.53	162.5	-32	0.0537	8	18.4	35.74	8.671	Alk = Sal*65.91	2355.6	-47.25	0.591	254.3	0.9	0.25	8.213	19.06
OC476-SR223	Bostock, H.	166.53	-33.53	162.5	-32	0.0537	9	18.4	35.75	8.670	Alk = Sal*65.91	2356.3	-45.15	0.591	255.5	0.9	0.25	8.211	19.04
OC476-SR223	Bostock, H.	166.53	-33.53	162.5	-32	0.0537	10	19.0	35.77	8.664	Alk = Sal*65.91	2357.6	-47.94	0.591	253.9	0.9	0.25	8.213	19.14
OC476-SR223	Bostock, H.	166.53	-33.53	162.5	-32	0.0537	11	20.1	35.7	8.651	Alk = Sal*65.91	2353.0	-39.08	0.591	259.1	0.9	0.25	8.204	19.19
OC476-SR223	Bostock, H.	166.53	-33.53	162.5	-32	0.0537	12	21.6	35.75	8.633	Alk = Sal*65.91	2356.3	-33.75	0.591	262.3	0.9	0.25	8.199	19.34
OC476-SR223	Bostock, H.	166.53	-33.53	167.5	-36	0.1424	1	19.9	35.6	8.654	Alk = Sal*65.91	2346.4	-29.3	0.591	264.9	0.9	0.25	8.196	19.06
OC476-SR223	Bostock, H.	166.53	-33.53	167.5	-36	0.1424	2	20.6	35.57	8.645	Alk = Sal*65.91	2344.4	-19.7	0.591	270.6	0.9	0.25	8.188	19.06
OC476-SR223	Bostock, H.	166.53	-33.53	167.5	-36	0.1424	3	20.2	35.6	8.650	Alk = Sal*65.91	2346.4	-22.71	0.591	268.8	0.9	0.25	8.191	19.05
OC476-SR223	Bostock, H.	166.53	-33.53	167.5	-36	0.1424	4	19.3	35.63	8.660	Alk = Sal*65.91	2348.4	-28.39	0.591	265.4	0.9	0.25	8.197	18.98
OC476-SR223	Bostock, H.	166.53	-33.53	167.5	-36	0.1424	5	18.1	35.68	8.675	Alk = Sal*65.91	2351.7	-35.06	0.591	261.5	0.9	0.25	8.203	18.89
OC476-SR223	Bostock, H.	166.53	-33.53	167.5	-36	0.1424	6	16.8	35.69	8.691	Alk = Sal*65.91	2352.3	-31.88	0.591	263.4	0.9	0.25	8.202	18.69
OC476-SR223	Bostock, H.	166.53	-33.53	167.5	-36	0.1424	7	15.9	35.66	8.701	Alk = Sal*65.91	2350.4	-33.53	0.591	262.4	0.9	0.25	8.204	18.59

		Site		Nearest Takahashi Sites				From Takahashi et al. (2009)										
Site	**Archive**	**Long (°)**	**Lat (°)**	**Long (°)**	**Lat (°)**	**1/(s.s. dist. from site)**	**Month**	**SST (C)**	**S (psu)**	pK_B^*	**Regional Sal/Alk correlation used**	**TAlk (μmol/kg)**	**ΔpCO_2(ppm)**	**Poor correction factor**	**pCO_2**	**SiO_4^{2-}**	**PO_4^-**	**pH**	**$\delta^{11}B_{B(OH)_4^-}$**
OC476-SR223	Bostock, H.	166.53	-33.53	167.5	-36	0.1424	8	15.4	35.53	8.708	Alk = Sal*65.91	2341.8	-35.94	0.591	261.0	0.9	0.25	8.205	18.53
OC476-SR223	Bostock, H.	166.53	-33.53	167.5	-36	0.1424	9	15.4	35.48	8.708	Alk = Sal*65.91	2338.5	-40.7	0.591	258.2	0.9	0.25	8.209	18.56
OC476-SR223	Bostock, H.	166.53	-33.53	167.5	-36	0.1424	10	15.9	35.58	8.702	Alk = Sal*65.91	2345.1	-38.39	0.591	259.5	0.9	0.25	8.207	18.62
OC476-SR223	Bostock, H.	166.53	-33.53	167.5	-36	0.1424	11	17.0	35.47	8.689	Alk = Sal*65.91	2337.8	-32.98	0.591	262.7	0.9	0.25	8.201	18.70
OC476-SR223	Bostock, H.	166.53	-33.53	167.5	-36	0.1424	12	18.4	35.6	8.671	Alk = Sal*65.91	2346.4	-43.83	0.591	256.3	0.9	0.25	8.209	19.01
OC476-SR223	Bostock, H.	166.53	-33.53	167.5	-32	0.3042	1	21.9	35.71	8.629	Alk = Sal*65.91	2353.6	-26.99	0.591	266.3	0.9	0.25	8.193	19.32
OC476-SR223	Bostock, H.	166.53	-33.53	167.5	-32	0.3042	2	22.6	35.69	8.621	Alk = Sal*65.91	2352.3	-17.58	0.591	271.8	0.9	0.25	8.185	19.31
OC476-SR223	Bostock, H.	166.53	-33.53	167.5	-32	0.3042	3	22.3	35.76	8.624	Alk = Sal*65.91	2356.9	-24.12	0.591	267.9	0.9	0.25	8.190	19.34
OC476-SR223	Bostock, H.	166.53	-33.53	167.5	-32	0.3042	4	21.4	35.84	8.634	Alk = Sal*65.91	2362.2	-27.72	0.591	265.8	0.9	0.25	8.195	19.28
OC476-SR223	Bostock, H.	166.53	-33.53	167.5	-32	0.3042	5	20.3	35.86	8.647	Alk = Sal*65.91	2363.5	-34.17	0.591	262.0	0.9	0.25	8.201	19.20
OC476-SR223	Bostock, H.	166.53	-33.53	167.5	-32	0.3042	6	19.1	35.77	8.663	Alk = Sal*65.91	2357.6	-31.44	0.591	263.6	0.9	0.25	8.200	19.00
OC476-SR223	Bostock, H.	166.53	-33.53	167.5	-32	0.3042	7	18.2	35.74	8.674	Alk = Sal*65.91	2355.6	-35.02	0.591	261.5	0.9	0.25	8.204	18.91
OC476-SR223	Bostock, H.	166.53	-33.53	167.5	-32	0.3042	8	17.7	35.69	8.680	Alk = Sal*65.91	2352.3	-42.38	0.591	257.2	0.9	0.25	8.210	18.91
OC476-SR223	Bostock, H.	166.53	-33.53	167.5	-32	0.3042	9	17.7	35.66	8.679	Alk = Sal*65.91	2350.4	-44.44	0.591	255.9	0.9	0.25	8.211	18.93
OC476-SR223	Bostock, H.	166.53	-33.53	167.5	-32	0.3042	10	18.2	35.73	8.673	Alk = Sal*65.91	2355.0	-45.64	0.591	255.2	0.9	0.25	8.212	19.02

		Site		Nearest Takahashi Sites				From Takahashi et al. (2009)										
Site	**Archive**	**Long (°)**	**Lat (°)**	**Long (°)**	**Lat (°)**	**1/(s.s. dist. from site)**	**Month**	**SST (C)**	**S (psu)**	pK_B^*	**Regional Sal/Alk correlation used**	**TAlk (μmol/kg)**	**ΔpCO_2(ppm)**	**Poor correction factor**	**pCO_2**	**SiO_4^{2-}**	**PO_4^-**	**pH**	**$\delta^{11}B_{B(OH)_4^-}$**
OC476-SR223	Bostock, H.	166.53	-33.53	167.5	-32	0.3042	11	19.3	35.66	8.660	Alk = Sal*65.91	2350.4	-34.75	0.591	261.7	0.9	0.25	8.202	19.05
OC476-SR223	Bostock, H.	166.53	-33.53	167.5	-32	0.3042	12	20.7	35.71	8.643	Alk = Sal*65.91	2353.6	-38.11	0.591	259.7	0.9	0.25	8.203	19.26
													Interpolated average					**8.201**	**19.04**
													Interpolated intraannual variation					**0.013**	**0.37**
T329	Bostock, H.	173.57	-12.96	172.5	-16	0.0961	1	28.9	35.02	8.553	Alk = (66.275*Sal) - 18.256	2302.7	-8.84	1.786	258.8	2	0.13	8.185	20.20
T329	Bostock, H.	173.57	-12.96	172.5	-16	0.0961	2	29.1	34.79	8.551	Alk = (66.275*Sal) - 18.256	2287.5	-11.68	1.786	253.7	2	0.13	8.190	20.28
T329	Bostock, H.	173.57	-12.96	172.5	-16	0.0961	3	29.1	34.94	8.550	Alk = (66.275*Sal) - 18.256	2297.4	-15.03	1.786	247.8	2	0.13	8.199	20.40
T329	Bostock, H.	173.57	-12.96	172.5	-16	0.0961	4	28.8	34.89	8.554	Alk = (66.275*Sal) - 18.256	2294.1	-13.88	1.786	249.8	2	0.13	8.196	20.32
T329	Bostock, H.	173.57	-12.96	172.5	-16	0.0961	5	28.0	34.89	8.563	Alk = (66.275*Sal) - 18.256	2294.1	-14	1.786	249.6	2	0.13	8.198	20.23
T329	Bostock, H.	173.57	-12.96	172.5	-16	0.0961	6	27.2	35.1	8.571	Alk = (66.275*Sal) - 18.256	2308.0	-19.46	1.786	239.9	2	0.13	8.214	20.33
T329	Bostock, H.	173.57	-12.96	172.5	-16	0.0961	7	26.6	35.07	8.579	Alk = (66.275*Sal) - 18.256	2306.0	-37.19	1.786	208.2	2	0.13	8.261	20.87
T329	Bostock, H.	173.57	-12.96	172.5	-16	0.0961	8	26.3	35.15	8.582	Alk = (66.275*Sal) - 18.256	2311.3	-42.49	1.786	198.7	2	0.13	8.277	21.05

		Site		Nearest Takahashi Sites				From Takahashi et al. (2009)										
Site	**Archive**	**Long (°)**	**Lat (°)**	**Long (°)**	**Lat (°)**	**1/(s.s. dist. from site)**	**Month**	**SST (C)**	**S (psu)**	pK_B^*	**Regional Sal/Alk correlation used**	**TAlk (μmol/kg)**	**ΔpCO_2(ppm)**	**Floor correction factor**	**pCO_2**	**SiO_4^{2-}**	**PO_4^-**	**pH**	**$\delta^{11}B_{B(OH)_4^-}$**
T329	Bostock, H.	173.57	-12.96	172.5	-16	0.0961	9	26.3	35.2	8.581	Alk = (66.275*Sal) - 18.256	2314.6	-33.02	1.786	215.6	2	0.13	8.251	20.70
T329	Bostock, H.	173.57	-12.96	172.5	-16	0.0961	10	26.8	35.02	8.576	Alk = (66.275*Sal) - 18.256	2302.7	-30.37	1.786	220.4	2	0.13	8.242	20.64
T329	Bostock, H.	173.57	-12.96	172.5	-16	0.0961	11	27.6	35.02	8.567	Alk = (66.275*Sal) - 18.256	2302.7	-18.85	1.786	240.9	2	0.13	8.211	20.35
T329	Bostock, H.	173.57	-12.96	172.5	-16	0.0961	12	28.4	34.99	8.558	Alk = (66.275*Sal) - 18.256	2300.7	-9.75	1.786	257.2	2	0.13	8.188	20.16
T329	Bostock, H.	173.57	-12.96	172.5	-12	0.4887	1	29.4	34.79	8.547	Alk = (66.275*Sal) - 18.256	2287.5	8.04	1.786	289.0	2	0.13	8.146	19.76
T329	Bostock, H.	173.57	-12.96	172.5	-12	0.4887	2	29.6	34.54	8.547	Alk = (66.275*Sal) - 18.256	2270.9	5.46	1.786	284.4	2	0.13	8.150	19.81
T329	Bostock, H.	173.57	-12.96	172.5	-12	0.4887	3	29.5	34.73	8.546	Alk = (66.275*Sal) - 18.256	2283.5	6.09	1.786	285.5	2	0.13	8.150	19.81
T329	Bostock, H.	173.57	-12.96	172.5	-12	0.4887	4	29.4	34.57	8.549	Alk = (66.275*Sal) - 18.256	2272.9	6.25	1.786	285.8	2	0.13	8.149	19.77
T329	Bostock, H.	173.57	-12.96	172.5	-12	0.4887	5	29.0	34.53	8.553	Alk = (66.275*Sal) - 18.256	2270.2	3.99	1.786	281.7	2	0.13	8.154	19.78
T329	Bostock, H.	173.57	-12.96	172.5	-12	0.4887	6	28.5	34.69	8.558	Alk = (66.275*Sal) - 18.256	2280.8	-0.29	1.786	274.1	2	0.13	8.165	19.85

		Site		Nearest Takahashi Sites				From Takahashi et al. (2009)										
Site	**Archive**	**Long (°)**	**Lat (°)**	**Long (°)**	**Lat (°)**	**1/(s.s. dist. from site)**	**Month**	**SST (C)**	**S (psu)**	pK_B^*	**Regional Sal/Alk correlation used**	**TAlk (μmol/kg)**	**ΔpCO_2(ppm)**	**Poor correction factor**	**pCO_2**	**SiO_4^{2-}**	**PO_4^-**	**pH**	**$\delta^{11}B_{B(OH)_4^-}$**
T329	Bostock, H.	173.57	-12.96	172.5	-12	0.4887	7	28.1	34.67	8.564	Alk = (66.275*Sal) - 18.256	2279.5	-5.29	1.786	265.2	2	0.13	8.177	19.94
T329	Bostock, H.	173.57	-12.96	172.5	-12	0.4887	8	27.9	34.86	8.565	Alk = (66.275*Sal) - 18.256	2292.1	-8.34	1.786	259.7	2	0.13	8.185	20.03
T329	Bostock, H.	173.57	-12.96	172.5	-12	0.4887	9	28.1	34.87	8.562	Alk = (66.275*Sal) - 18.256	2292.8	-7.15	1.786	261.8	2	0.13	8.182	20.02
T329	Bostock, H.	173.57	-12.96	172.5	-12	0.4887	10	28.4	34.78	8.560	Alk = (66.275*Sal) - 18.256	2286.8	-2.76	1.786	269.7	2	0.13	8.171	19.92
T329	Bostock, H.	173.57	-12.96	172.5	-12	0.4887	11	28.9	34.88	8.553	Alk = (66.275*Sal) - 18.256	2293.4	2.44	1.786	279.0	2	0.13	8.160	19.86
T329	Bostock, H.	173.57	-12.96	172.5	-12	0.4887	12	29.4	34.83	8.548	Alk = (66.275*Sal) - 18.256	2290.1	6.76	1.786	286.7	2	0.13	8.149	19.79
T329	Bostock, H.	173.57	-12.96	177.5	-16	0.0404	1	28.9	34.93	8.553	Alk = (66.275*Sal) - 18.256	2296.7	-5.95	1.786	264.0	2	0.13	8.178	20.10
T329	Bostock, H.	173.57	-12.96	177.5	-16	0.0404	2	29.2	34.92	8.550	Alk = (66.275*Sal) - 18.256	2296.1	-12.42	1.786	252.4	2	0.13	8.192	20.33
T329	Bostock, H.	173.57	-12.96	177.5	-16	0.0404	3	29.2	34.92	8.549	Alk = (66.275*Sal) - 18.256	2296.1	-11.95	1.786	253.3	2	0.13	8.191	20.31
T329	Bostock, H.	173.57	-12.96	177.5	-16	0.0404	4	28.9	35.01	8.553	Alk = (66.275*Sal) - 18.256	2302.0	3.76	1.786	281.3	2	0.13	8.158	19.84

		Site		Nearest Takahashi Sites				From Takahashi et al. (2009)										
Site	**Archive**	**Long (°)**	**Lat (°)**	**Long (°)**	**Lat (°)**	**1/(s.s. dist. from site)**	**Month**	**SST (C)**	**S (psu)**	pK_B^*	**Regional Sal/Alk correlation used**	**TAlk (μmol/kg)**	**ΔpCO_2(ppm)**	**Poor correction factor**	**pCO_2**	**SiO_4^{2-}**	**PO_4^-**	**pH**	**$\delta^{11}B_{B(OH)_4^-}$**
T329	Bostock, H.	173.57	-12.96	177.5	-16	0.0404	5	28.1	35.01	8.561	Alk = (66.275*Sal) - 18.256	2302.0	-4.33	1.786	266.9	2	0.13	8.177	19.97
T329	Bostock, H.	173.57	-12.96	177.5	-16	0.0404	6	27.3	35.07	8.570	Alk = (66.275*Sal) - 18.256	2306.0	-14.05	1.786	249.5	2	0.13	8.201	20.16
T329	Bostock, H.	173.57	-12.96	177.5	-16	0.0404	7	26.7	35.02	8.578	Alk = (66.275*Sal) - 18.256	2302.7	-24.37	1.786	231.1	2	0.13	8.227	20.41
T329	Bostock, H.	173.57	-12.96	177.5	-16	0.0404	8	26.3	35.16	8.581	Alk = (66.275*Sal) - 18.256	2312.0	-29.19	1.786	222.5	2	0.13	8.241	20.56
T329	Bostock, H.	173.57	-12.96	177.5	-16	0.0404	9	26.5	35.13	8.579	Alk = (66.275*Sal) - 18.256	2310.0	-28.74	1.786	223.3	2	0.13	8.239	20.55
T329	Bostock, H.	173.57	-12.96	177.5	-16	0.0404	10	27.0	35.05	8.574	Alk = (66.275*Sal) - 18.256	2304.7	-18.4	1.786	241.7	2	0.13	8.212	20.26
T329	Bostock, H.	173.57	-12.96	177.5	-16	0.0404	11	27.7	35.07	8.565	Alk = (66.275*Sal) - 18.256	2306.0	-3.92	1.786	267.6	2	0.13	8.177	19.92
T329	Bostock, H.	173.57	-12.96	177.5	-16	0.0404	12	28.5	35.03	8.557	Alk = (66.275*Sal) - 18.256	2303.4	2.85	1.786	279.7	2	0.13	8.160	19.82
T329	Bostock, H.	173.57	-12.96	177.5	-12	0.0610	1	29.5	34.73	8.547	Alk = (66.275*Sal) - 18.256	2283.5	4.53	1.786	282.7	2	0.13	8.153	19.85
T329	Bostock, H.	173.57	-12.96	177.5	-12	0.0610	2	29.5	34.85	8.546	Alk = (66.275*Sal) - 18.256	2291.4	5.03	1.786	283.6	2	0.13	8.153	19.86

		Site		Nearest Takahashi Sites				From Takahashi et al. (2009)										
Site	**Archive**	**Long (°)**	**Lat (°)**	**Long (°)**	**Lat (°)**	**1/(s.s. dist. from site)**	**Month**	**SST (C)**	**S (psu)**	pK_B^*	**Regional Sal/Alk correlation used**	**TAlk (μmol/kg)**	**ΔpCO_2(ppm)**	**Poor correction factor**	**pCO_2**	**SiO_4^{2-}**	**PO_4^-**	**pH**	**$\delta^{11}B_{B(OH)_4^-}$**
T329	Bostock, H.	173.57	-12.96	177.5	-12	0.0610	3	29.5	34.65	8.548	Alk = (66.275*Sal) - 18.256	2278.2	6.26	1.786	285.8	2	0.13	8.149	19.79
T329	Bostock, H.	173.57	-12.96	177.5	-12	0.0610	4	29.4	34.79	8.548	Alk = (66.275*Sal) - 18.256	2287.5	6.64	1.786	286.5	2	0.13	8.149	19.79
T329	Bostock, H.	173.57	-12.96	177.5	-12	0.0610	5	29.1	34.71	8.552	Alk = (66.275*Sal) - 18.256	2282.1	4.36	1.786	282.4	2	0.13	8.154	19.80
T329	Bostock, H.	173.57	-12.96	177.5	-12	0.0610	6	28.6	34.82	8.557	Alk = (66.275*Sal) - 18.256	2289.4	0	n/a	274.6	2	0.13	8.165	19.88
T329	Bostock, H.	173.57	-12.96	177.5	-12	0.0610	7	28.2	34.8	8.561	Alk = (66.275*Sal) - 18.256	2288.1	-3.51	1.786	268.3	2	0.13	8.173	19.92
T329	Bostock, H.	173.57	-12.96	177.5	-12	0.0610	8	28.0	34.97	8.562	Alk = (66.275*Sal) - 18.256	2299.4	0.62	1.786	275.7	2	0.13	8.166	19.82
T329	Bostock, H.	173.57	-12.96	177.5	-12	0.0610	9	28.2	34.96	8.560	Alk = (66.275*Sal) - 18.256	2298.7	12.45	1.786	296.8	2	0.13	8.141	19.52
T329	Bostock, H.	173.57	-12.96	177.5	-12	0.0610	10	28.5	34.92	8.557	Alk = (66.275*Sal) - 18.256	2296.1	6.99	1.786	287.1	2	0.13	8.151	19.69
T329	Bostock, H.	173.57	-12.96	177.5	-12	0.0610	11	29.0	34.87	8.552	Alk = (66.275*Sal) - 18.256	2292.8	4.91	1.786	283.4	2	0.13	8.154	19.80
T329	Bostock, H.	173.57	-12.96	177.5	-12	0.0610	12	29.4	34.78	8.548	Alk = (66.275*Sal) - 18.256	2286.8	6.8	1.786	286.7	2	0.13	8.149	19.79
													Interpolated average					**8.171**	**19.96**

		Site		Nearest Takahashi Sites				From Takahashi et al. (2009)										
Site	**Archive**	**Long (°)**	**Lat (°)**	**Long (°)**	**Lat (°)**	**1/(s.s. dist. from site)**	**Month**	**SST (C)**	**S (psu)**	pK_B^*	**Regional Sal/Alk correlation used**	**TAlk (μmol/kg)**	**ΔpCO_2(ppm)**	**Poor correction factor**	**pCO_2**	**SiO_4^{2-}**	**PO_4^-**	**pH**	**$\delta^{11}B_{B(OH)_4^-}$**
													Interpolated intraannual variation					**0.024**	**0.27**
GGC48	Marshall, B.	161	0	157.5	0	0.0816	1	29.7	34.57	8.545	Alk = (69.547*Sal) - 130.95	2273.3	34.02	1.786	335.8	0.8	0.02	8.094	19.14
GGC48	Marshall, B.	161	0	157.5	0	0.0816	2	29.6	34.52	8.547	Alk = (69.547*Sal) - 130.95	2269.8	35.45	1.786	338.3	0.8	0.02	8.092	19.08
GGC48	Marshall, B.	161	0	157.5	0	0.0816	3	29.4	34.83	8.547	Alk = (69.547*Sal) - 130.95	2291.4	37.07	1.786	341.2	0.8	0.02	8.091	19.08
GGC48	Marshall, B.	161	0	157.5	0	0.0816	4	29.4	34.70	8.548	Alk = (69.547*Sal) - 130.95	2282.3	25.18	1.786	320.0	0.8	0.02	8.112	19.31
GGC48	Marshall, B.	161	0	157.5	0	0.0816	5	29.5	34.71	8.547	Alk = (69.547*Sal) - 130.95	2283.0	14.02	1.786	300.0	0.8	0.02	8.133	19.60
GGC48	Marshall, B.	161	0	157.5	0	0.0816	6	29.5	34.81	8.547	Alk = (69.547*Sal) - 130.95	2290.0	8.37	1.786	289.9	0.8	0.02	8.146	19.75
GGC48	Marshall, B.	161	0	157.5	0	0.0816	7	29.6	34.58	8.547	Alk = (69.547*Sal) - 130.95	2274.0	4.56	1.786	283.1	0.8	0.02	8.152	19.83
GGC48	Marshall, B.	161	0	157.5	0	0.0816	8	29.4	34.77	8.548	Alk = (69.547*Sal) - 130.95	2287.2	1.13	1.786	277.0	0.8	0.02	8.161	19.93
GGC48	Marshall, B.	161	0	157.5	0	0.0816	9	29.5	34.32	8.549	Alk = (69.547*Sal) - 130.95	2255.9	16.69	1.786	304.8	0.8	0.02	8.125	19.47
GGC48	Marshall, B.	161	0	157.5	0	0.0816	10	29.7	34.32	8.547	Alk = (69.547*Sal) - 130.95	2255.9	39.12	1.786	344.9	0.8	0.02	8.083	18.99

		Site		Nearest Takahashi Sites				From Takahashi et al. (2009)										
Site	**Archive**	**Long (°)**	**Lat (°)**	**Long (°)**	**Lat (°)**	**1/(s.s. dist. from site)**	**Month**	**SST (C)**	**S (psu)**	pK_B^*	**Regional Sal/Alk correlation used**	**TAlk (μmol/kg)**	**ΔpCO_2(ppm)**	**Floor correction factor**	**pCO_2**	**SiO_4^{2-}**	**PO_4^-**	**pH**	**$\delta^{11}B_{B(OH)_4^-}$**
GGC48	Marshall, B.	161	0	157.5	0	0.0816	11	29.8	34.39	8.545	Alk = (69.547*Sal) - 130.95	2260.8	44.41	1.786	354.3	0.8	0.02	8.075	18.90
GGC48	Marshall, B.	161	0	157.5	0	0.0816	12	29.8	34.14	8.547	Alk = (69.547*Sal) - 130.95	2243.4	31.44	1.786	331.1	0.8	0.02	8.096	19.14
GGC48	Marshall, B.	161	0	162.5	0	0.4444	1	29.5	34.61	8.548	Alk = (69.547*Sal) - 130.95	2276.1	43.51	1.786	352.7	0.8	0.02	8.078	18.92
GGC48	Marshall, B.	161	0	162.5	0	0.4444	2	29.3	34.37	8.551	Alk = (69.547*Sal) - 130.95	2259.4	41.78	1.786	349.6	0.8	0.02	8.080	18.89
GGC48	Marshall, B.	161	0	162.5	0	0.4444	3	29.1	34.80	8.551	Alk = (69.547*Sal) - 130.95	2289.3	41.31	1.786	348.8	0.8	0.02	8.084	18.94
GGC48	Marshall, B.	161	0	162.5	0	0.4444	4	29.0	35.10	8.550	Alk = (69.547*Sal) - 130.95	2310.1	23.96	1.786	317.8	0.8	0.02	8.118	19.36
GGC48	Marshall, B.	161	0	162.5	0	0.4444	5	29.3	34.86	8.549	Alk = (69.547*Sal) - 130.95	2293.5	21.05	1.786	312.6	0.8	0.02	8.121	19.42
GGC48	Marshall, B.	161	0	162.5	0	0.4444	6	29.3	34.86	8.548	Alk = (69.547*Sal) - 130.95	2293.5	30.73	1.786	329.9	0.8	0.02	8.103	19.21
GGC48	Marshall, B.	161	0	162.5	0	0.4444	7	29.5	34.55	8.548	Alk = (69.547*Sal) - 130.95	2271.9	26.77	1.786	322.8	0.8	0.02	8.108	19.27
GGC48	Marshall, B.	161	0	162.5	0	0.4444	8	29.4	34.81	8.547	Alk = (69.547*Sal) - 130.95	2290.0	9.62	1.786	292.2	0.8	0.02	8.143	19.72

		Site		Nearest Takahashi Sites			From Takahashi et al. (2009)											
Site	**Archive**	**Long (°)**	**Lat (°)**	**Long (°)**	**Lat (°)**	**1/(s.s. dist. from site)**	**Month**	**SST (C)**	**S (psu)**	pK_B^*	**Regional Sal/Alk correlation used**	**TAlk (μmol/kg)**	**ΔpCO_2(ppm)**	**G. loor correction factor**	**pCO_2**	**SiO_4^{2-}**	**PO_4^-**	**pH**	$\delta^{11}B_{B(OH)_4^-}$
GGC48	Marshall, B.	161	0	162.5	0	0.4444	9	29.5	34.32	8.549	Alk = (69.547*Sal) - 130.95	2255.9	18.08	1.786	307.3	0.8	0.02	8.123	19.43
GGC48	Marshall, B.	161	0	162.5	0	0.4444	10	29.5	34.22	8.550	Alk = (69.547*Sal) - 130.95	2248.9	43.05	1.786	351.9	0.8	0.02	8.076	18.86
GGC48	Marshall, B.	161	0	162.5	0	0.4444	11	29.6	34.67	8.546	Alk = (69.547*Sal) - 130.95	2280.2	28.61	1.786	326.1	0.8	0.02	8.105	19.26
GGC48	Marshall, B.	161	0	162.5	0	0.4444	12	29.7	34.27	8.548	Alk = (69.547*Sal) - 130.95	2252.4	48.75	1.786	362.1	0.8	0.02	8.066	18.78
													Interpolated average					**8.102**	**19.20**
													Interpolated intraannual variation					**0.066**	**0.81**
Eilat	Kısakürek, B.	34.92	29.50	Periodic data from Eilat Monitoring Program			1/21/04	25.9	40.65	8.557	n/a: Data from NMP	2499	G. of Aqaba assumed to be well mixed		275	0.95	0.02	8.182	20.09
Eilat	Kısakürek, B.	34.92	29.50	Periodic data from Eilat Monitoring Program			2/24/04	21.3	40.76	8.611	n/a: Data from NMP	2498	G. of Aqaba assumed to be well mixed		275	1.03	0.05	8.190	19.51
Eilat	Kısakürek, B.	34.92	29.50	Periodic data from Eilat Monitoring Program			3/23/04	21.2	40.83	8.612	n/a: Data from NMP	2488	G. of Aqaba assumed to be well mixed		275	1.28	0.08	8.189	19.48
Eilat	Kısakürek, B.	34.92	29.50	Periodic data from Eilat Monitoring Program			4/20/04	21.7	40.78	8.607	n/a: Data from NMP	2489	G. of Aqaba assumed to be well mixed		275	0.83	0.01	8.188	19.54
Eilat	Kısakürek, B.	34.92	29.50	Periodic data from Eilat Monitoring Program			5/17/04	23.2	40.63	8.589	n/a: Data from NMP	2524	G. of Aqaba assumed to be well mixed		275	0.88	0.01	8.191	19.79

		Site		Nearest Takahashi Sites			From Takahashi et al. (2009)										
Site	**Archive**	**Long (°)**	**Lat (°)**	**Long (°)**	**Lat (°)**	**1/(s.s. dist. from site)**	**Month**	**SST (C)**	**S (psu)**	pK_B^*	**Regional Sal/Alk correlation used**	**TAlk (μmol/kg)**	**ΔpCO_2(ppm) G)loor correction factor**	**pCO_2**	**SiO_4^{2-}**	**PO_4^-**	**pH**	**$\delta^{11}B_{B(OH)_4^-}$**
Eilat	Kısakürek, B.	34.92	29.50	Periodic data from Eilat Monitoring Program			6/21/04	25.85	40.82	8.557	n/a: Data from NMP	2515	G. of Aqaba assumed to be well mixed	275	0.66	0.02	8.184	20.12
Eilat	Kısakürek, B.	34.92	29.50	Periodic data from Eilat Monitoring Program			12/22/04	22.5	40.78	8.597	n/a: Data from NMP	2518	G. of Aqaba assumed to be well mixed	275	0.69	0.06	8.191	19.70
Eilat	Kısakürek, B.	34.92	29.50	Periodic data from Eilat Monitoring Program			1/19/05	22	40.95	8.602	n/a: Data from NMP	2514	G. of Aqaba assumed to be well mixed	275	0.94	0.04	8.191	19.63
Eilat	Kısakürek, B.	34.92	29.50	Periodic data from Eilat Monitoring Program			2/16/05	21.4	41.02	8.609	n/a: Data from NMP	2499	G. of Aqaba assumed to be well mixed	275	1.08	0.07	8.190	19.53
Eilat	Kısakürek, B.	34.92	29.50	Periodic data from Eilat Monitoring Program			3/20/05	21.8	40.95	8.605	n/a: Data from NMP	2512	G. of Aqaba assumed to be well mixed	275	0.61	0.04	8.191	19.60
Eilat	Kısakürek, B.	34.92	29.50	Periodic data from Eilat Monitoring Program			4/14/05	22.8	40.68	8.594	n/a: Data from NMP	2513	G. of Aqaba assumed to be well mixed	275	0.71	0.05	8.190	19.72
Eilat	Kısakürek, B.	34.92	29.50	Periodic data from Eilat Monitoring Program			5/18/05	24	40.70	8.580	n/a: Data from NMP	2506	G. of Aqaba assumed to be well mixed	275	0.72	0.03	8.187	19.86
Eilat	Kısakürek, B.	34.92	29.50	Periodic data from Eilat Monitoring Program			6/14/05	25.8	40.80	8.558	n/a: Data from NMP	2526	G. of Aqaba assumed to be well mixed	275	0.70	0.04	8.186	20.13
Eilat	Kısakürek, B.	34.92	29.50	Periodic data from Eilat Monitoring Program			8/10/05	27	40.78	8.544	n/a: Data from NMP	2526	G. of Aqaba assumed to be well mixed	275	0.48	0.04	8.183	20.28
Eilat	Kısakürek, B.	34.92	29.50	Periodic data from Eilat Monitoring Program			8/10/05	26.5	40.75	8.550	n/a: Data from NMP	2522	G. of Aqaba assumed to be well mixed	275	0.78	0.03	8.184	20.21

		Site		Nearest Takahashi Sites			From Takahashi et al. (2009)										
Site	**Archive**	**Long (°)**	**Lat (°)**	**Long (°)**	**Lat (°)**	**1/(s.s. dist. from site)**	**Month**	**SST (C)**	**S (psu)**	pK_B^*	**Regional Sal/Alk correlation used**	**TAlk (μmol/kg)**	**ΔpCO_2(ppm)**	**G.loor correction factor**	**pCO_2**	**SiO_4^{2-}**	**PO_4^-**	**pH**	**$\delta^{11}B_{B(OH)_4^-}$**
Eilat	Kısakürek, B.	34.92	29.50	Periodic data from Eilat Monitoring Program			10/27/05	24.4	40.73	8.575	n/a: Data from NMP	2518	G. of Aqaba assumed to be well mixed		275	0.43	0.04	8.188	19.94
Eilat	Kısakürek, B.	34.92	29.50	Periodic data from Eilat Monitoring Program			11/22/05	23.2	40.76	8.589	n/a: Data from NMP	2531	G. of Aqaba assumed to be well mixed		275	0.86	0.03	8.192	19.81
Eilat	Kısakürek, B.	34.92	29.50	Periodic data from Eilat Monitoring Program			12/13/05	22.8	40.74	8.594	n/a: Data from NMP	2549	G. of Aqaba assumed to be well mixed		275	0.32	0.05	8.195	19.79
Eilat	Kısakürek, B.	34.92	29.50	Periodic data from Eilat Monitoring Program			1/17/06	21.5	40.78	8.609	n/a: Data from NMP	2497	G. of Aqaba assumed to be well mixed		275	0.90	0.04	8.190	19.53
Eilat	Kısakürek, B.	34.92	29.50	Periodic data from Eilat Monitoring Program			2/19/06	21.5	40.64	8.610	n/a: Data from NMP	2507	G. of Aqaba assumed to be well mixed		275	0.61	0.03	8.192	19.54
Eilat	Kısakürek, B.	34.92	29.50	Periodic data from Eilat Monitoring Program			3/20/06	22.8	40.52	8.595	n/a: Data from NMP	2525	G. of Aqaba assumed to be well mixed		275	1.01	0.02	8.192	19.74
Eilat	Kısakürek, B.	34.92	29.50	Periodic data from Eilat Monitoring Program			6/13/06	23.3	40.61	8.588	n/a: Data from NMP	2508	G. of Aqaba assumed to be well mixed		275	0.39	0.07	8.189	19.78
Eilat	Kısakürek, B.	34.92	29.50	Periodic data from Eilat Monitoring Program			7/11/06	25.6	40.64	8.561	n/a: Data from NMP	2513	G. of Aqaba assumed to be well mixed		275	0.64	0.01	8.185	20.08
Eilat	Kısakürek, B.	34.92	29.50	Periodic data from Eilat Monitoring Program			8/6/06	27.2	40.78	8.542	n/a: Data from NMP	2521	G. of Aqaba assumed to be well mixed		275	0.47	0.02	8.182	20.30
Eilat	Kısakürek, B.	34.92	29.50	Periodic data from Eilat Monitoring Program			9/19/06	26.2	40.72	8.554	n/a: Data from NMP	2513	G. of Aqaba assumed to be well mixed		275	0.47	0.00	8.183	20.16

		Site		Nearest Takahashi Sites			From Takahashi et al. (2009)										
Site	**Archive**	**Long (°)**	**Lat (°)**	**Long (°)**	**Lat (°)**	**1/(s.s. dist. from site)**	**Month**	**SST (C)**	**S (psu)**	pK_B^*	**Regional Sal/Alk correlation used**	**TAlk (μmol/kg)**	**ΔpCO_2(ppm) Poor correction factor**	**pCO_2**	**SiO_4^{2-}**	**PO_4^-**	**pH**	**$\delta^{11}B_{B(OH)_4^-}$**
Eilat	Kısakürek, B.	34.92	29.50	Periodic data from Eilat Monitoring Program			10/16/06	25.8	40.73	8.558	n/a: Data from NMP	2510	G. of Aqaba assumed to be well mixed	275	0.53	0.02	8.184	20.10
Eilat	Kısakürek, B.	34.92	29.50	Periodic data from Eilat Monitoring Program			11/20/06	23.9	40.79	8.580	n/a: Data from NMP	2514	G. of Aqaba assumed to be well mixed	275	0.47	0.02	8.188	19.87
Eilat	Kısakürek, B.	34.92	29.50	Periodic data from Eilat Monitoring Program			12/14/06	22.7	40.82	8.594	n/a: Data from NMP	2522	G. of Aqaba assumed to be well mixed	275	0.55	0.00	8.191	19.73
Eilat	Kısakürek, B.	34.92	29.50	Periodic data from Eilat Monitoring Program			1/14/07	21.5	40.79	8.609	n/a: Data from NMP	2524	G. of Aqaba assumed to be well mixed	275	0.67	0.03	8.194	19.58
Eilat	Kısakürek, B.	34.92	29.50	Periodic data from Eilat Monitoring Program			2/11/07	21.2	40.76	8.613	n/a: Data from NMP	2518	G. of Aqaba assumed to be well mixed	275	0.88	0.07	8.193	19.53
Eilat	Kısakürek, B.	34.92	29.50	Periodic data from Eilat Monitoring Program			3/11/07	21.1	40.75	8.614	n/a: Data from NMP	2516	G. of Aqaba assumed to be well mixed	275	1.03	0.11	8.193	19.51
Eilat	Kısakürek, B.	34.92	29.50	Periodic data from Eilat Monitoring Program			4/15/07	21.1	40.67	8.614	n/a: Data from NMP	2502	G. of Aqaba assumed to be well mixed	275	1.03	0.05	8.191	19.48
Eilat	Kısakürek, B.	34.92	29.50	Periodic data from Eilat Monitoring Program			5/13/07	23.4	40.68	8.587	n/a: Data from NMP	2506	G. of Aqaba assumed to be well mixed	275	0.55	0.01	8.188	19.79
Eilat	Kısakürek, B.	34.92	29.50	Periodic data from Eilat Monitoring Program			6/17/07	23.7	40.68	8.583	n/a: Data from NMP	2501	G. of Aqaba assumed to be well mixed	275	0.72	0.04	8.187	19.82
Eilat	Kısakürek, B.	34.92	29.50	Periodic data from Eilat Monitoring Program			7/16/07	26.8	40.79	8.546	n/a: Data from NMP	2500	G. of Aqaba assumed to be well mixed	275	0.60	0.00	8.180	20.21

		Site		Nearest Takahashi Sites			From Takahashi et al. (2009)										
Site	**Archive**	**Long (°)**	**Lat (°)**	**Long (°)**	**Lat (°)**	**1/(s.s. dist. from site)**	**Month**	**SST (C)**	**S (psu)**	pK_B^*	**Regional Sal/Alk correlation used**	**TAlk (μmol/kg)**	**ΔpCO_2(ppm) Correction factor**	**pCO_2**	**SiO_4^{2-}**	**PO_4^-**	**pH**	**$\delta^{11}B_{B(OH)_4^-}$**
Eilat	Kısakürek, B.	34.92	29.50	Periodic data from Eilat Monitoring Program			8/8/07	27.4	40.83	8.539	n/a: Data from NMP	2509	G. of Aqaba assumed to be well mixed	275	0.71	0.10	8.180	20.30
Eilat	Kısakürek, B.	34.92	29.50	Periodic data from Eilat Monitoring Program			9/2/07	27.7	40.86	8.535	n/a: Data from NMP	2506	G. of Aqaba assumed to be well mixed	275	0.59	0.03	8.179	20.34
Eilat	Kısakürek, B.	34.92	29.50	Periodic data from Eilat Monitoring Program			10/21/07	24.8	40.78	8.570	n/a: Data from NMP	2508	G. of Aqaba assumed to be well mixed	275	0.67	0.02	8.185	19.97
Eilat	Kısakürek, B.	34.92	29.50	Periodic data from Eilat Monitoring Program			11/12/07	24.1	40.83	8.578	n/a: Data from NMP	2525	G. of Aqaba assumed to be well mixed	275	0.69	0.02	8.189	19.92
Eilat	Kısakürek, B.	34.92	29.50	Periodic data from Eilat Monitoring Program			12/20/07	22.8	40.82	8.593	n/a: Data from NMP	2506	G. of Aqaba assumed to be well mixed	275	0.86	0.05	8.189	19.71
Eilat	Kısakürek, B.	34.92	29.50	Periodic data from Eilat Monitoring Program			1/15/08	21.6	40.82	8.608	n/a: Data from NMP	2499	G. of Aqaba assumed to be well mixed	275	0.88	0.07	8.190	19.55
Eilat	Kısakürek, B.	34.92	29.50	Periodic data from Eilat Monitoring Program			2/11/08	21	40.73	8.615	n/a: Data from NMP	2516	G. of Aqaba assumed to be well mixed	275	1.30	0.15	8.193	19.50
Eilat	Kısakürek, B.	34.92	29.50	Periodic data from Eilat Monitoring Program			3/17/08	21	40.68	8.615	n/a: Data from NMP	2505	G. of Aqaba assumed to be well mixed	275	1.67	0.17	8.192	19.48
Eilat	Kısakürek, B.	34.92	29.50	Periodic data from Eilat Monitoring Program			4/13/08	21.4	40.64	8.611	n/a: Data from NMP	2501	G. of Aqaba assumed to be well mixed	275	0.81	0.02	8.191	19.52
Eilat	Kısakürek, B.	34.92	29.50	Periodic data from Eilat Monitoring Program			5/11/08	22.3	40.59	8.600	n/a: Data from NMP	2505	G. of Aqaba assumed to be well mixed	275	0.83	0.05	8.190	19.64

		Site		Nearest Takahashi Sites			From Takahashi et al. (2009)										
Site	**Archive**	**Long (°)**	**Lat (°)**	**Long (°)**	**Lat (°)**	**1/(s.s. dist. from site)**	**Month**	**SST (C)**	**S (psu)**	pK_B^*	**Regional Sal/Alk correlation used**	**TAlk (μmol/kg)**	**ΔpCO_2(ppm) Correction factor**	**pCO_2**	**SiO_4^{2-}**	**PO_4^-**	**pH**	**$\delta^{11}B_{B(OH)_4^-}$**
Eilat	Kısakürek, B.	34.92	29.50	Periodic data from Eilat Monitoring Program			6/16/08	23.9	40.69	8.581	n/a: Data from NMP	2506	G. of Aqaba assumed to be well mixed	275	0.77	0.04	8.187	19.85
Eilat	Kısakürek, B.	34.92	29.50	Periodic data from Eilat Monitoring Program			7/9/08	25.9	40.81	8.557	n/a: Data from NMP	2508	G. of Aqaba assumed to be well mixed	275	0.84	0.02	8.183	20.11
Eilat	Kısakürek, B.	34.92	29.50	Periodic data from Eilat Monitoring Program			8/17/08	27.5	40.83	8.538	n/a: Data from NMP	2509	G. of Aqaba assumed to be well mixed	275	0.92	0.06	8.180	20.32
Eilat	Kısakürek, B.	34.92	29.50	Periodic data from Eilat Monitoring Program			9/14/08	27.4	40.79	8.539	n/a: Data from NMP	2505	G. of Aqaba assumed to be well mixed	275	0.98	0.06	8.180	20.30
Eilat	Kısakürek, B.	34.92	29.50	Periodic data from Eilat Monitoring Program			10/26/08	25	40.74	8.568	n/a: Data from NMP	2501	G. of Aqaba assumed to be well mixed	275	0.91	0.07	8.184	19.98
Eilat	Kısakürek, B.	34.92	29.50	Periodic data from Eilat Monitoring Program			12/14/08	23.3	40.51	8.589	n/a: Data from NMP	2511	G. of Aqaba assumed to be well mixed	275	1.09	0.05	8.189	19.78
Eilat	Kısakürek, B.	34.92	29.50	Periodic data from Eilat Monitoring Program			1/13/09	22	40.67	8.603	n/a: Data from NMP	2491	G. of Aqaba assumed to be well mixed	275	0.22	0.39	8.188	19.58
Eilat	Kısakürek, B.	34.92	29.50	Periodic data from Eilat Monitoring Program			2/22/09	21.6	40.59	8.609	n/a: Data from NMP	2512	G. of Aqaba assumed to be well mixed	275	0.21	0.23	8.192	19.56
Eilat	Kısakürek, B.	34.92	29.50	Periodic data from Eilat Monitoring Program			3/17/09	21.4	40.52	8.611	n/a: Data from NMP	2516	G. of Aqaba assumed to be well mixed	275	0.04	0.88	8.193	19.54
Eilat	Kısakürek, B.	34.92	29.50	Periodic data from Eilat Monitoring Program			4/19/09	21.5	40.55	8.610	n/a: Data from NMP	2490	G. of Aqaba assumed to be well mixed	275	0.03	0.06	8.189	19.51

		Site		Nearest Takahashi Sites			From Takahashi et al. (2009)										
Site	**Archive**	**Long (°)**	**Lat (°)**	**Long (°)**	**Lat (°)**	**1/(s.s. dist. from site)**	**Month**	**SST (C)**	**S (psu)**	pK_B^*	**Regional Sal/Alk correlation used**	**TAlk (μmol/kg)**	**ΔpCO_2(ppm)**	**G.C. correction factor**	**pCO_2**	**SiO_4^{2-}**	**PO_4^-**	**pH**	**$\delta^{11}B_{B(OH)_4^-}$**
Eilat	Kısakürek, B.	34.92	29.50	Periodic data from Eilat Monitoring Program			5/10/09	22.1	40.57	8.603	n/a: Data from NMP	2492	G. of Aqaba assumed to be well mixed		275	0.00	0.00	8.189	19.59
Eilat	Kısakürek, B.	34.92	29.50	Periodic data from Eilat Monitoring Program			6/18/09	24.1	40.56	8.579	n/a: Data from NMP	2501	G. of Aqaba assumed to be well mixed		275	0.01	0.09	8.186	19.86
Eilat	Kısakürek, B.	34.92	29.50	Periodic data from Eilat Monitoring Program			7/20/09	26.7	40.57	8.548	n/a: Data from NMP	2513	G. of Aqaba assumed to be well mixed		275	0.02	0.12	8.183	20.22
Eilat	Kısakürek, B.	34.92	29.50	Periodic data from Eilat Monitoring Program			8/18/09	26.7	40.62	8.548	n/a: Data from NMP	2516	G. of Aqaba assumed to be well mixed		275	0.04	0.02	8.183	20.22
Eilat	Kısakürek, B.	34.92	29.50	Periodic data from Eilat Monitoring Program			9/13/09	26.8	40.66	8.547	n/a: Data from NMP	2507	G. of Aqaba assumed to be well mixed		275	0.04	0.03	8.182	20.22
Eilat	Kısakürek, B.	34.92	29.50	Periodic data from Eilat Monitoring Program			10/18/09	25.8	40.55	8.559	n/a: Data from NMP	2496	G. of Aqaba assumed to be well mixed		275	0.10	0.06	8.182	20.07
Eilat	Kısakürek, B.	34.92	29.50	Periodic data from Eilat Monitoring Program			11/16/09	25.3	40.58	8.565	n/a: Data from NMP	2496	G. of Aqaba assumed to be well mixed		275	0.02	0.47	8.183	20.01
Eilat	Kısakürek, B.	34.92	29.50	Periodic data from Eilat Monitoring Program			12/28/09	23	40.63	8.592	n/a: Data from NMP	2507	G. of Aqaba assumed to be well mixed		275	0.22	0.22	8.189	19.74
													Average					**8.188**	**19.84**
													Intraannual variation (2σ)					**0.008**	**0.56**

TABLE B.2: Carbonate System Parameters for Coretop Sites

Appendix C

Supplementary Information, Chapter 4

		Site		Nearest Takahashi Sites																			
Site	**Archive**[ℵ]	**Long** (°E)	**Lat** (°N)	**Long** (°E)	**Lat** (°N)	$\frac{1}{SSS_D}$ [∀]	**Month**	**SST** (°C)[§]	**Salinity**[§]	pK_B^* [◇]	**TAlk** (μmol/kg)[♣]	Δ**pCO$_2$ (ppm)**[§]	**Gloor corr.**[♯]	**pCO$_2$**[†]	**SiO$_2^-$**[♭]	**PO$_4^{3-}$**[♭]	**pH**	$\delta^{11}B_{B(OH)_4^-}$ (‰)	**DIC** (μmol/kg)	**B(OH)$_4^-$ /HCO$_3^-$**	**B(OH)$_4^-$/DIC**	**CO$_3^{2-}$** (μmol/kg)	Ω_{CaCO_3}	**[B] (μmol/kg)**
MC497	Tübingen	63.31	23.53	62.5	20	0.076	1	24.10	36.54	8.599	2386.1	28.0	0.59	291.5	3.19	0.51	8.161	19.30	2001.0	0.0678	0.0584	268	6.34	451.6
MC497	Tübingen	63.31	23.53	62.5	20	0.076	2	23.69	36.44	8.604	2379.8	6.9	0.59	279.1	3.19	0.51	8.176	19.41	1990.6	0.0691	0.0595	270	6.40	450.4
MC497	Tübingen	63.31	23.53	62.5	20	0.076	3	24.61	36.49	8.593	2383.0	12.9	0.59	282.6	3.19	0.51	8.171	19.48	1986.9	0.0702	0.0602	275	6.52	451.0
MC497	Tübingen	63.31	23.53	62.5	20	0.076	4	26.62	36.54	8.570	2386.1	24.5	0.59	289.5	3.19	0.51	8.159	19.64	1975.2	0.0728	0.0620	285	6.78	451.6
MC497	Tübingen	63.31	23.53	62.5	20	0.076	5	28.75	36.57	8.545	2388.0	36.8	0.59	296.7	3.19	0.51	8.148	19.80	1961.7	0.0755	0.0638	296	7.06	452.0
MC497	Tübingen	63.31	23.53	62.5	20	0.076	6	29.58	36.59	8.535	2389.3	44.3	0.59	301.2	3.19	0.51	8.141	19.84	1958.0	0.0763	0.0644	299	7.15	452.3
MC497	Tübingen	63.31	23.53	62.5	20	0.076	7	28.62	36.35	8.548	2374.2	79.1	0.59	321.8	3.19	0.51	8.119	19.42	1972.8	0.0702	0.0600	279	6.68	449.3
MC497	Tübingen	63.31	23.53	62.5	20	0.076	8	27.47	36.53	8.560	2385.5	85.3	0.59	325.4	3.19	0.51	8.119	19.26	1993.9	0.0680	0.0584	273	6.50	451.5
MC497	Tübingen	63.31	23.53	62.5	20	0.076	9	27.59	36.37	8.559	2375.4	90.9	0.59	328.7	3.19	0.51	8.114	19.21	1988.3	0.0673	0.0579	270	6.44	449.5
MC497	Tübingen	63.31	23.53	62.5	20	0.076	10	28.11	36.37	8.553	2375.4	50.1	0.59	304.6	3.19	0.51	8.139	19.58	1965.7	0.0724	0.0616	285	6.80	449.5
MC497	Tübingen	63.31	23.53	62.5	20	0.076	11	27.22	36.55	8.563	2386.8	27.3	0.59	291.1	3.19	0.51	8.157	19.69	1971.2	0.0736	0.0626	288	6.87	451.8
MC497	Tübingen	63.31	23.53	62.5	20	0.076	12	25.50	36.54	8.583	2386.1	29.0	0.59	292.2	3.19	0.51	8.158	19.46	1988.1	0.0702	0.0601	276	6.57	451.6
MC497	Tübingen	63.31	23.53	62.5	24	1.14	1	24.80	36.38	8.592	2376.1	37.0	0.59	296.9	3.19	0.51	8.153	19.29	1991.7	0.0677	0.0584	267	6.35	449.7
MC497	Tübingen	63.31	23.53	62.5	24	1.14	2	24.66	36.37	8.593	2375.4	24.4	0.59	289.4	3.19	0.51	8.162	19.37	1986.8	0.0688	0.0592	270	6.41	449.5
MC497	Tübingen	63.31	23.53	62.5	24	1.14	3	25.79	36.41	8.580	2378.0	36.1	0.59	296.3	3.19	0.51	8.152	19.42	1983.1	0.0697	0.0598	274	6.52	450.0
MC497	Tübingen	63.31	23.53	62.5	24	1.14	4	27.67	36.49	8.558	2383.0	28.7	0.59	292.0	3.19	0.51	8.154	19.73	1965.0	0.0742	0.0630	290	6.91	451.0
MC497	Tübingen	63.31	23.53	62.5	24	1.14	5	28.94	36.48	8.543	2382.4	24.8	0.59	289.6	3.19	0.51	8.155	19.92	1950.3	0.0771	0.0650	299	7.15	450.9
MC497	Tübingen	63.31	23.53	62.5	24	1.14	6	28.89	36.35	8.545	2374.2	31.4	0.59	293.5	3.19	0.51	8.150	19.83	1948.6	0.0759	0.0641	295	7.06	449.3
MC497	Tübingen	63.31	23.53	62.5	24	1.14	7	27.12	36.35	8.565	2374.2	23.7	0.59	289.0	3.19	0.51	8.158	19.68	1962.1	0.0734	0.0624	286	6.82	449.3
MC497	Tübingen	63.31	23.53	62.5	24	1.14	8	26.02	36.35	8.578	2374.2	63.6	0.59	312.6	3.19	0.51	8.133	19.22	1990.7	0.0671	0.0578	267	6.36	449.3
MC497	Tübingen	63.31	23.53	62.5	24	1.14	9	26.77	36.19	8.570	2364.1	40.5	0.59	298.9	3.19	0.51	8.146	19.47	1966.5	0.0705	0.0603	276	6.59	447.3
MC497	Tübingen	63.31	23.53	62.5	24	1.14	10	28.00	36.26	8.555	2368.5	33.4	0.59	294.7	3.19	0.51	8.149	19.69	1954.4	0.0738	0.0626	287	6.87	448.2
MC497	Tübingen	63.31	23.53	62.5	24	1.14	11	27.52	36.38	8.560	2376.1	23.0	0.59	288.6	3.19	0.51	8.158	19.74	1959.1	0.0743	0.0631	289	6.90	449.7
MC497	Tübingen	63.31	23.53	62.5	24	1.14	12	25.98	36.41	8.578	2378.0	39.5	0.59	298.3	3.19	0.51	8.150	19.42	1982.9	0.0697	0.0597	275	6.53	450.0
MC497	Tübingen	63.31	23.53	67.5	20	0.033	1	25.33	36.33	8.586	2372.9	29.0	0.59	292.2	3.19	0.51	8.157	19.41	1980.9	0.0694	0.0596	272	6.48	449.0
MC497	Tübingen	63.31	23.53	67.5	20	0.033	2	25.25	36.12	8.588	2359.7	5.4	0.59	278.2	3.19	0.51	8.172	19.58	1961.5	0.0715	0.0611	276	6.58	446.4
MC497	Tübingen	63.31	23.53	67.5	20	0.033	3	26.19	36.12	8.577	2359.7	-1.6	0.59	274.1	3.19	0.51	8.176	19.76	1949.0	0.0741	0.0630	284	6.79	446.4
MC497	Tübingen	63.31	23.53	67.5	20	0.033	4	27.72	36.23	8.559	2366.6	14.4	0.59	283.5	3.19	0.51	8.163	19.82	1946.7	0.0754	0.0638	291	6.95	447.8
MC497	Tübingen	63.31	23.53	67.5	20	0.033	5	29.03	36.30	8.543	2371.0	21.3	0.59	287.6	3.19	0.51	8.156	19.93	1940.3	0.0773	0.0651	298	7.14	448.7
MC497	Tübingen	63.31	23.53	67.5	20	0.033	6	29.42	36.51	8.538	2384.2	22.7	0.59	288.4	3.19	0.51	8.155	20	1945.9	0.0784	0.0659	304	7.26	451.3
MC497	Tübingen	63.31	23.53	67.5	20	0.033	7	28.48	36.45	8.549	2380.5	20.2	0.59	286.9	3.19	0.51	8.158	19.89	1951.4	0.0767	0.0647	297	7.10	450.5
MC497	Tübingen	63.31	23.53	67.5	20	0.033	8	27.55	36.49	8.559	2383.0	27.5	0.59	291.2	3.19	0.51	8.156	19.72	1965.6	0.0741	0.0629	290	6.90	451.0

		Site		Nearest Takahashi Sites																			
Site	**Archive**[ϰ]	**Long (°E)**	**Lat (°N)**	**Long (°E)**	**Lat (°N)**	$\frac{1}{SSD}$[∀]	**Month**	**SST (°C)**[§]	**Salinity**[§]	pK_B^*[◇]	**TAlk (μmol/kg)**[♣]	**ΔpCO$_2$ (ppm)**[§]	**Gloor corr.**[♯]	**pCO$_2$**[†]	**SiO$_2$**[♭]	**PO$_4^-$**[♭]	**pH**	$\delta^{11}B_{B(OH)_4^-}$ (‰)	**DIC (μmol/kg)**	**B(OH)$_4^-$/HCO$_3^-$**	**B(OH)$_4^-$/DIC**	**CO$_3^{2-}$ (μmol/kg)**	Ω_{CaCO_3}	**[B] (μmol/kg)**
MC497	Tübingen	63.31	23.53	67.5	20	0.033	9	27.86	36.19	8.557	2364.1	37.0	0.59	296.8	3.19	0.51	8.147	19.64	1954.5	0.0730	0.0621	284	6.80	447.3
MC497	Tübingen	63.31	23.53	67.5	20	0.033	10	28.41	36.05	8.552	2355.3	32.8	0.59	294.4	3.19	0.51	8.148	19.72	1941.5	0.0741	0.0629	287	6.88	445.6
MC497	Tübingen	63.31	23.53	67.5	20	0.033	11	27.85	36.27	8.557	2369.2	16.1	0.59	284.5	3.19	0.51	8.161	19.83	1948.0	0.0755	0.0639	292	6.97	448.3
MC497	Tübingen	63.31	23.53	67.5	20	0.033	12	26.43	36.34	8.573	2373.6	15.7	0.59	284.3	3.19	0.51	8.165	19.66	1964.4	0.0730	0.0622	284	6.76	449.2
n/d, Pre-ind. CO_2 ≃275 ppm			**Interpolated[▽] average**					**26.86**	**36.37**	**8.568**	**2375.7**	**34.0**		**295.1**			**8.152**	**19.57**	**1970.2**	**0.0719**	**0.0613**	**281**	**6.71**	**449.6**
			Interpolated[▽] intraannual variation					**3.64**	**0.21**	**0.042**	**13.2**	**24.6**		**18.1**			**0.020**	**0.45**	**39.3**	**0.0082**	**0.0058**	**27**	**0.69**	**2.7**
MC436	Tübingen	-21.06	39.80	-22.5	36	0.061	1	17.72	36.25	8.676	2375.6	-21.1	0.50	264.4	0.80	0.10	8.202	18.86	2033.1	0.0609	0.0535	238	5.62	448.1
MC436	Tübingen	-21.06	39.80	-22.5	36	0.061	2	17.12	36.26	8.684	2376.1	-47.1	0.50	251.5	0.80	0.10	8.220	18.99	2028.1	0.0623	0.0546	241	5.69	448.2
MC436	Tübingen	-21.06	39.80	-22.5	36	0.061	3	16.98	36.22	8.685	2374.0	-37.4	0.50	256.3	0.80	0.10	8.213	18.88	2032.1	0.0610	0.0536	237	5.60	447.7
MC436	Tübingen	-21.06	39.80	-22.5	36	0.061	4	17.40	36.22	8.680	2374.0	-31.1	0.50	259.5	0.80	0.10	8.209	18.89	2030.8	0.0612	0.0537	238	5.62	447.7
MC436	Tübingen	-21.06	39.80	-22.5	36	0.061	5	18.42	36.24	8.668	2375.1	-24.1	0.50	263.0	0.80	0.10	8.203	18.97	2025.0	0.0623	0.0545	243	5.74	447.9
MC436	Tübingen	-21.06	39.80	-22.5	36	0.061	6	20.45	36.28	8.643	2377.2	-19.1	0.50	265.5	0.80	0.10	8.198	19.20	2009.5	0.0655	0.0569	255	6.04	448.4
MC436	Tübingen	-21.06	39.80	-22.5	36	0.061	7	22.69	36.35	8.617	2381.0	15.3	0.50	282.6	0.80	0.10	8.174	19.23	2005.0	0.0664	0.0575	262	6.20	449.3
MC436	Tübingen	-21.06	39.80	-22.5	36	0.061	8	24.20	36.43	8.598	2385.4	25.2	0.50	287.6	0.80	0.10	8.166	19.36	1997.5	0.0684	0.0589	270	6.41	450.3
MC436	Tübingen	-21.06	39.80	-22.5	36	0.061	9	23.99	36.43	8.601	2385.4	-1.3	0.50	274.4	0.80	0.10	8.182	19.53	1988.7	0.0705	0.0605	276	6.54	450.3
MC436	Tübingen	-21.06	39.80	-22.5	36	0.061	10	22.39	36.44	8.620	2385.9	-10.7	0.50	269.7	0.80	0.10	8.190	19.40	2000.4	0.0685	0.0591	268	6.34	450.4
MC436	Tübingen	-21.06	39.80	-22.5	36	0.061	11	20.48	36.35	8.643	2381.0	-24.0	0.50	263.0	0.80	0.10	8.201	19.25	2009.7	0.0662	0.0574	258	6.10	449.3
MC436	Tübingen	-21.06	39.80	-22.5	36	0.061	12	18.84	36.29	8.663	2377.8	-23.1	0.50	263.4	0.80	0.10	8.202	19.02	2023.3	0.0630	0.0551	246	5.81	448.5
MC436	Tübingen	-21.06	39.80	-22.5	40	0.473	1	15.72	35.93	8.702	2358.2	-20.7	0.50	264.7	0.80	0.10	8.201	18.55	2039.6	0.0569	0.0504	221	5.23	444.1
MC436	Tübingen	-21.06	39.80	-22.5	40	0.473	2	15.23	35.94	8.708	2358.8	-29.9	0.50	260.1	0.80	0.10	8.208	18.56	2040.7	0.0569	0.0505	221	5.22	444.2
MC436	Tübingen	-21.06	39.80	-22.5	40	0.473	3	15.18	35.98	8.709	2361.0	-23.6	0.50	263.2	0.80	0.10	8.204	18.51	2045.2	0.0563	0.0500	219	5.18	444.7
MC436	Tübingen	-21.06	39.80	-22.5	40	0.473	4	15.64	35.93	8.703	2358.2	-25.5	0.50	262.2	0.80	0.10	8.205	18.58	2038.4	0.0572	0.0507	222	5.25	444.1
MC436	Tübingen	-21.06	39.80	-22.5	40	0.473	5	16.69	35.98	8.690	2361.0	-34.3	0.50	257.8	0.80	0.10	8.210	18.79	2027.1	0.0598	0.0527	232	5.48	444.7
MC436	Tübingen	-21.06	39.80	-22.5	40	0.473	6	18.60	36.04	8.667	2364.2	-17.8	0.50	266.1	0.80	0.10	8.198	18.92	2018.5	0.0616	0.0540	240	5.68	445.5
MC436	Tübingen	-21.06	39.80	-22.5	40	0.473	7	21.14	36.09	8.636	2366.9	-13.4	0.50	268.3	0.80	0.10	8.192	19.22	1998.5	0.0658	0.0571	256	6.07	446.1
MC436	Tübingen	-21.06	39.80	-22.5	40	0.473	8	22.54	36.07	8.620	2365.8	14.7	0.50	282.3	0.80	0.10	8.173	19.18	1996.0	0.0656	0.0569	257	6.11	445.8
MC436	Tübingen	-21.06	39.80	-22.5	40	0.473	9	22.06	36.12	8.625	2368.5	8.0	0.50	279.0	0.80	0.10	8.178	19.18	1999.6	0.0655	0.0568	257	6.09	446.4
MC436	Tübingen	-21.06	39.80	-22.5	40	0.473	10	20.19	36.03	8.648	2363.7	-15.4	0.50	267.3	0.80	0.10	8.194	19.11	2004.3	0.0642	0.0559	250	5.92	445.3
MC436	Tübingen	-21.06	39.80	-22.5	40	0.473	11	18.20	36.00	8.672	2362.0	-24.7	0.50	262.6	0.80	0.10	8.202	18.92	2017.9	0.0615	0.0540	239	5.66	445.0
MC436	Tübingen	-21.06	39.80	-22.5	40	0.473	12	16.77	35.98	8.689	2361.0	-33.8	0.50	258.1	0.80	0.10	8.210	18.80	2026.6	0.0599	0.0527	232	5.49	444.7

		Site		Nearest Takahashi Sites																			
Site	**Archive**[ж]	**Long (°E)**	**Lat (°N)**	**Long (°E)**	**Lat (°N)**	$\frac{1}{SSS_D}$[∀]	**Month**	**SST (°C)**[§]	**Salinity**[§]	pK_B^*[◇]	**TAlk** (μmol/kg)[♣]	Δ**pCO$_2$ (ppm)**[§]	**Gloor corr.**[♯]	**pCO$_2$**[†]	**SiO$_2$**[♭]	**PO$_4^-$**[♭]	**pH**	$\delta^{11}B_{B(OH)_4^-}$ (‰)	**DIC** (μmol/kg)	**B(OH)$_4^-$ /HCO$_3^-$**	**B(OH)$_4^-$/DIC**	**CO$_3^{2-}$** (μmol/kg)	Ω_{CaCO_3}	**[B] (μmol/kg)**
MC436	Tübingen	-21.06	39.80	-17.5	36	0.037	1	17.53	36.29	8.678	2377.8	-21.5	0.50	264.2	0.80	0.10	8.202	18.84	2036.2	0.0606	0.0533	237	5.60	448.5
MC436	Tübingen	-21.06	39.80	-17.5	36	0.037	2	16.94	36.25	8.686	2375.6	-28.5	0.50	260.7	0.80	0.10	8.207	18.81	2037.3	0.0602	0.0530	235	5.54	448.1
MC436	Tübingen	-21.06	39.80	-17.5	36	0.037	3	16.80	36.23	8.688	2374.5	-38.8	0.50	255.6	0.80	0.10	8.214	18.87	2033.6	0.0609	0.0535	236	5.58	447.8
MC436	Tübingen	-21.06	39.80	-17.5	36	0.037	4	17.16	36.24	8.683	2375.1	-44.0	0.50	253.0	0.80	0.10	8.218	18.96	2028.4	0.0620	0.0544	240	5.67	447.9
MC436	Tübingen	-21.06	39.80	-17.5	36	0.037	5	18.12	36.26	8.671	2376.1	-27.0	0.50	261.5	0.80	0.10	8.205	18.96	2027.3	0.0621	0.0544	242	5.72	448.2
MC436	Tübingen	-21.06	39.80	-17.5	36	0.037	6	20.07	36.31	8.648	2378.9	-6.9	0.50	271.6	0.80	0.10	8.190	19.06	2019.3	0.0637	0.0556	250	5.91	448.8
MC436	Tübingen	-21.06	39.80	-17.5	36	0.037	7	22.13	36.38	8.623	2382.7	33.3	0.50	291.6	0.80	0.10	8.164	19.04	2018.4	0.0639	0.0556	254	6.01	449.7
MC436	Tübingen	-21.06	39.80	-17.5	36	0.037	8	23.62	36.49	8.605	2388.6	23.4	0.50	286.7	0.80	0.10	8.168	19.31	2004.5	0.0676	0.0583	267	6.34	451.0
MC436	Tübingen	-21.06	39.80	-17.5	36	0.037	9	23.55	36.50	8.606	2389.2	21.9	0.50	285.9	0.80	0.10	8.169	19.31	2004.9	0.0677	0.0584	267	6.34	451.1
MC436	Tübingen	-21.06	39.80	-17.5	36	0.037	10	22.08	36.47	8.623	2387.5	3.0	0.50	276.5	0.80	0.10	8.182	19.26	2010.2	0.0667	0.0577	262	6.21	450.8
MC436	Tübingen	-21.06	39.80	-17.5	36	0.037	11	20.19	36.43	8.646	2385.4	-27.5	0.50	261.3	0.80	0.10	8.204	19.25	2013.9	0.0661	0.0574	258	6.09	450.3
MC436	Tübingen	-21.06	39.80	-17.5	36	0.037	12	18.60	36.39	8.665	2383.2	-24.2	0.50	262.9	0.80	0.10	8.204	19.01	2028.8	0.0629	0.0550	246	5.81	449.8
MC436	Tübingen	-21.06	39.80	-17.5	40	0.079	1	15.57	35.96	8.704	2359.9	-17.2	0.50	266.4	0.80	0.10	8.199	18.51	2043.5	0.0564	0.0501	220	5.20	444.5
MC436	Tübingen	-21.06	39.80	-17.5	40	0.079	2	15.07	35.92	8.710	2357.7	-33.5	0.50	258.2	0.80	0.10	8.211	18.56	2039.9	0.0569	0.0505	220	5.21	444.0
MC436	Tübingen	-21.06	39.80	-17.5	40	0.079	3	14.97	35.98	8.711	2361.0	-28.4	0.50	260.8	0.80	0.10	8.207	18.52	2045.2	0.0564	0.0501	219	5.18	444.7
MC436	Tübingen	-21.06	39.80	-17.5	40	0.079	4	15.34	35.96	8.707	2359.9	-35.4	0.50	257.3	0.80	0.10	8.212	18.62	2038.2	0.0576	0.0510	223	5.27	444.5
MC436	Tübingen	-21.06	39.80	-17.5	40	0.079	5	16.38	35.99	8.694	2361.5	-39.9	0.50	255.1	0.80	0.10	8.214	18.80	2028.0	0.0598	0.0527	231	5.47	444.8
MC436	Tübingen	-21.06	39.80	-17.5	40	0.079	6	18.39	36.02	8.669	2363.1	-16.0	0.50	267.0	0.80	0.10	8.197	18.88	2020.5	0.0611	0.0536	238	5.63	445.2
MC436	Tübingen	-21.06	39.80	-17.5	40	0.079	7	20.75	36.08	8.641	2366.4	18.2	0.50	284.1	0.80	0.10	8.173	18.93	2014.4	0.0622	0.0544	245	5.81	445.9
MC436	Tübingen	-21.06	39.80	-17.5	40	0.079	8	22.15	36.09	8.624	2366.9	10.9	0.50	280.5	0.80	0.10	8.176	19.16	1998.9	0.0653	0.0567	256	6.08	446.1
MC436	Tübingen	-21.06	39.80	-17.5	40	0.079	9	21.81	36.14	8.628	2369.6	6.0	0.50	278.0	0.80	0.10	8.179	19.16	2001.9	0.0653	0.0566	256	6.07	446.7
MC436	Tübingen	-21.06	39.80	-17.5	40	0.079	10	20.03	36.09	8.649	2366.9	-13.4	0.50	268.3	0.80	0.10	8.193	19.08	2008.9	0.0638	0.0556	249	5.89	446.1
MC436	Tübingen	-21.06	39.80	-17.5	40	0.079	11	18.03	36.06	8.674	2365.3	-26.4	0.50	261.8	0.80	0.10	8.204	18.91	2021.0	0.0615	0.0539	239	5.65	445.7
MC436	Tübingen	-21.06	39.80	-17.5	40	0.079	12	16.59	36.04	8.691	2364.2	-26.9	0.50	261.5	0.80	0.10	8.206	18.73	2033.3	0.0591	0.0521	230	5.43	445.5
n/d, Pre-ind. CO_2 ≃275 ppm			**Interpolated[▽] average**					**18.40**	**36.06**	**8.669**	**2365.2**	**-17.4**		**266.3**			**8.198**	**18.89**	**2021.0**	**0.0614**	**0.0538**	**239**	**5.66**	**445.7**
			Interpolated[▽] intraannual variation					**3.74**	**0.09**	**0.045**	**5.1**	**23.5**		**11.8**			**0.018**	**0.51**	**23.7**	**0.0049**	**0.0036**	**20**	**0.48**	**1.2**
F111	NIWA	174.98	-48.95	172.5	-52	0.065	1	9.51	34.30	8.789	2284.3	-21.7	0.30	265.0	1.8	0.73	8.196	17.56	2042.8	0.0442	0.0403	168	4.02	423.9
F111	NIWA	174.98	-48.95	172.5	-52	0.065	2	9.72	34.32	8.786	2284.8	-5.1	0.30	270.0	1.8	0.73	8.189	17.52	2044.8	0.0439	0.0400	167	4.00	424.2
F111	NIWA	174.98	-48.95	172.5	-52	0.065	3	9.30	34.29	8.791	2284.3	-15.0	0.30	267.0	1.8	0.73	8.193	17.51	2045.9	0.0437	0.0399	166	3.97	423.8
F111	NIWA	174.98	-48.95	172.5	-52	0.065	4	8.68	34.30	8.799	2286.2	-3.7	0.30	270.4	1.8	0.73	8.189	17.38	2054.7	0.0424	0.0388	162	3.86	423.9

		Site		Nearest Takahashi Sites																			
Site	**Archive**[ℵ]	**Long** (°E)	**Lat** (°N)	**Long** (°E)	**Lat** (°N)	$\frac{1}{SS_D}$ [∀]	**Month**	**SST** (°C)[§]	**Salinity**[§]	pK_B^* [◇]	**TAlk** (μmol/kg)[♣]	Δ**pCO$_2$ (ppm)**[§]	**Gloor corr.**[♯]	**pCO$_2$**[†]	**SiO$_2$**[♭]	**PO$_4^-$**[♭]	**pH**	$\delta^{11}B_{B(OH)_4^-}$ (‰)	**DIC** (μmol/kg)	**B(OH)$_4^-$ /HCO$_3^-$**	**B(OH)$_4^-$/DIC**	**CO$_3^{2-}$** (μmol/kg)	Ω_{CaCO_3}	**[B] (μmol/kg)**
F111	NIWA	174.98	-48.95	172.5	-52	0.065	5	7.97	34.21	8.809	2283.7	-3.8	0.30	270.4	1.8	0.73	8.188	17.29	2058.6	0.0413	0.0379	157	3.76	422.8
F111	NIWA	174.98	-48.95	172.5	-52	0.065	6	7.43	34.16	8.816	2282.7	-9.3	0.30	268.7	1.8	0.73	8.190	17.24	2061.2	0.0408	0.0374	155	3.71	422.2
F111	NIWA	174.98	-48.95	172.5	-52	0.065	7	7.18	34.28	8.819	2289.1	-7.9	0.30	269.1	1.8	0.73	8.190	17.21	2068.4	0.0406	0.0373	155	3.69	423.7
F111	NIWA	174.98	-48.95	172.5	-52	0.065	8	7.08	34.14	8.821	2282.7	-7.2	0.30	269.4	1.8	0.73	8.189	17.18	2064.5	0.0402	0.0370	153	3.66	422.0
F111	NIWA	174.98	-48.95	172.5	-52	0.065	9	7.07	34.27	8.820	2288.9	-6.0	0.30	269.7	1.8	0.73	8.190	17.19	2069.5	0.0403	0.0371	154	3.67	423.6
F111	NIWA	174.98	-48.95	172.5	-52	0.065	10	7.26	34.52	8.816	2300.7	-0.5	0.30	271.4	1.8	0.73	8.189	17.22	2077.9	0.0407	0.0374	156	3.72	426.7
F111	NIWA	174.98	-48.95	172.5	-52	0.065	11	7.79	34.60	8.809	2303.3	-10.8	0.30	268.3	1.8	0.73	8.193	17.33	2073.5	0.0419	0.0384	161	3.83	427.7
F111	NIWA	174.98	-48.95	172.5	-52	0.065	12	8.69	34.37	8.799	2289.6	-14.3	0.30	267.2	1.8	0.73	8.193	17.44	2055.1	0.0429	0.0393	164	3.91	424.8
F111	NIWA	174.98	-48.95	172.5	-48	0.142	1	11.84	34.32	8.759	2280.4	-49.0	0.30	256.8	1.8	0.73	8.206	17.98	2014.5	0.0488	0.0440	185	4.41	424.2
F111	NIWA	174.98	-48.95	172.5	-48	0.142	2	12.29	34.35	8.753	2281.0	-20.3	0.30	265.4	1.8	0.73	8.194	17.91	2017.3	0.0482	0.0436	183	4.38	424.6
F111	NIWA	174.98	-48.95	172.5	-48	0.142	3	11.70	34.36	8.760	2282.6	-29.1	0.30	262.8	1.8	0.73	8.198	17.88	2021.6	0.0477	0.0432	181	4.33	424.7
F111	NIWA	174.98	-48.95	172.5	-48	0.142	4	10.66	34.37	8.774	2285.1	-25.5	0.30	263.9	1.8	0.73	8.197	17.73	2033.0	0.0461	0.0419	175	4.19	424.8
F111	NIWA	174.98	-48.95	172.5	-48	0.142	5	9.50	34.33	8.789	2285.7	-12.2	0.30	267.8	1.8	0.73	8.192	17.53	2045.9	0.0439	0.0400	167	3.99	424.3
F111	NIWA	174.98	-48.95	172.5	-48	0.142	6	8.55	34.29	8.801	2286.1	-17.4	0.30	266.3	1.8	0.73	8.194	17.42	2053.0	0.0427	0.0391	163	3.89	423.8
F111	NIWA	174.98	-48.95	172.5	-48	0.142	7	7.99	34.45	8.807	2295.3	-17.1	0.30	266.4	1.8	0.73	8.195	17.37	2064.6	0.0422	0.0387	161	3.85	425.8
F111	NIWA	174.98	-48.95	172.5	-48	0.142	8	7.79	34.20	8.811	2283.6	-15.0	0.30	267.0	1.8	0.73	8.193	17.31	2057.9	0.0415	0.0381	158	3.77	422.7
F111	NIWA	174.98	-48.95	172.5	-48	0.142	9	7.86	34.39	8.809	2292.7	-23.0	0.30	264.6	1.8	0.73	8.197	17.37	2062.5	0.0422	0.0386	161	3.84	425.1
F111	NIWA	174.98	-48.95	172.5	-48	0.142	10	8.30	34.62	8.802	2303.0	-17.2	0.30	266.4	1.8	0.73	8.196	17.43	2067.7	0.0429	0.0392	164	3.91	427.9
F111	NIWA	174.98	-48.95	172.5	-48	0.142	11	9.28	34.68	8.789	2303.6	-16.4	0.30	266.6	1.8	0.73	8.196	17.55	2060.2	0.0443	0.0404	170	4.04	428.6
F111	NIWA	174.98	-48.95	172.5	-48	0.142	12	10.61	34.39	8.774	2286.2	-23.9	0.30	264.3	1.8	0.73	8.197	17.72	2034.6	0.0460	0.0418	175	4.18	425.1
F111	NIWA	174.98	-48.95	177.5	-52	0.064	1	9.27	34.24	8.792	2281.9	-11.7	0.30	268.0	1.8	0.73	8.191	17.48	2045.1	0.0434	0.0397	165	3.95	423.2
F111	NIWA	174.98	-48.95	177.5	-52	0.064	2	9.55	34.26	8.788	2282.2	-8.1	0.30	269.1	1.8	0.73	8.190	17.51	2043.7	0.0437	0.0399	166	3.98	423.5
F111	NIWA	174.98	-48.95	177.5	-52	0.064	3	9.08	34.25	8.794	2282.8	-16.7	0.30	266.5	1.8	0.73	8.194	17.48	2046.3	0.0434	0.0396	165	3.94	423.3
F111	NIWA	174.98	-48.95	177.5	-52	0.064	4	8.30	34.22	8.805	2283.3	-5.3	0.30	269.9	1.8	0.73	8.189	17.34	2055.4	0.0418	0.0383	159	3.81	423.0
F111	NIWA	174.98	-48.95	177.5	-52	0.064	5	7.43	34.10	8.816	2279.8	-3.9	0.30	270.3	1.8	0.73	8.188	17.21	2060.1	0.0405	0.0372	154	3.68	421.5
F111	NIWA	174.98	-48.95	177.5	-52	0.064	6	6.82	34.07	8.825	2280.1	-9.6	0.30	268.6	1.8	0.73	8.190	17.15	2064.1	0.0399	0.0367	151	3.62	421.1
F111	NIWA	174.98	-48.95	177.5	-52	0.064	7	6.51	34.23	8.828	2288.5	-7.7	0.30	269.2	1.8	0.73	8.190	17.12	2073.4	0.0396	0.0365	151	3.61	423.1
F111	NIWA	174.98	-48.95	177.5	-52	0.064	8	6.39	34.20	8.830	2287.4	-6.5	0.30	269.6	1.8	0.73	8.189	17.10	2073.8	0.0394	0.0363	150	3.59	422.7
F111	NIWA	174.98	-48.95	177.5	-52	0.064	9	6.45	34.27	8.828	2290.6	-7.0	0.30	269.4	1.8	0.73	8.190	17.12	2075.6	0.0396	0.0364	151	3.61	423.6
F111	NIWA	174.98	-48.95	177.5	-52	0.064	10	6.72	34.35	8.824	2293.8	-10.0	0.30	268.5	1.8	0.73	8.192	17.17	2075.2	0.0401	0.0369	153	3.66	424.6
F111	NIWA	174.98	-48.95	177.5	-52	0.064	11	7.32	34.43	8.816	2296.1	-8.0	0.30	269.1	1.8	0.73	8.191	17.25	2072.5	0.0409	0.0376	157	3.74	425.6
F111	NIWA	174.98	-48.95	177.5	-52	0.064	12	8.33	34.29	8.804	2286.6	-11.1	0.30	268.2	1.8	0.73	8.192	17.37	2056.4	0.0422	0.0386	161	3.84	423.8

		Site		Nearest Takahashi Sites																			
Site	**Archive**[ϰ]	**Long (°E)**	**Lat (°N)**	**Long (°E)**	**Lat (°N)**	$\frac{1}{SS_D}$ [∀]	**Month**	**SST (°C)**[§]	**Salinity**[§]	pK_B^* [◇]	**TAlk** (μmol/kg)[♣]	Δ**pCO$_2$ (ppm)**[§]	**Gloor corr.**[♯]	**pCO$_2$**[†]	**SiO$_2$**[♭]	**PO$_4^-$**[♭]	**pH**	$\delta^{11}B_{B(OH)_4^-}$ (‰)	**DIC** (μmol/kg)	**B(OH)$_4^-$ /HCO$_3^-$**	**B(OH)$_4^-$/DIC**	**CO$_3^{2-}$** (μmol/kg)	Ω_{CaCO_3}	**[B] (μmol/kg)**
F111	NIWA	174.98	-48.95	177.5	-48	0.137	1	11.67	34.30	8.761	2279.7	-16.1	0.30	266.7	1.8	0.73	8.193	17.81	2022.5	0.0471	0.0426	179	4.27	423.9
F111	NIWA	174.98	-48.95	177.5	-48	0.137	2	12.21	34.31	8.754	2279.2	-15.3	0.30	266.9	1.8	0.73	8.192	17.88	2017.7	0.0478	0.0432	182	4.34	424.1
F111	NIWA	174.98	-48.95	177.5	-48	0.137	3	11.66	34.32	8.761	2280.7	-33.9	0.30	261.3	1.8	0.73	8.200	17.89	2019.5	0.0478	0.0433	181	4.33	424.2
F111	NIWA	174.98	-48.95	177.5	-48	0.137	4	10.56	34.36	8.775	2284.9	-24.9	0.30	264.0	1.8	0.73	8.197	17.72	2033.8	0.0459	0.0417	175	4.17	424.7
F111	NIWA	174.98	-48.95	177.5	-48	0.137	5	9.33	34.31	8.791	2285.2	-12.4	0.30	267.8	1.8	0.73	8.192	17.50	2046.8	0.0436	0.0398	166	3.97	424.1
F111	NIWA	174.98	-48.95	177.5	-48	0.137	6	8.37	34.11	8.804	2277.9	-18.9	0.30	265.8	1.8	0.73	8.194	17.39	2048.1	0.0423	0.0387	161	3.84	421.6
F111	NIWA	174.98	-48.95	177.5	-48	0.137	7	7.84	34.27	8.810	2286.9	-19.7	0.30	265.6	1.8	0.73	8.195	17.34	2059.0	0.0419	0.0384	159	3.80	423.6
F111	NIWA	174.98	-48.95	177.5	-48	0.137	8	7.64	34.20	8.813	2284.0	-20.3	0.30	265.4	1.8	0.73	8.195	17.31	2058.4	0.0415	0.0381	158	3.77	422.7
F111	NIWA	174.98	-48.95	177.5	-48	0.137	9	7.65	34.39	8.812	2293.2	-15.8	0.30	266.7	1.8	0.73	8.194	17.31	2066.1	0.0416	0.0382	159	3.79	425.1
F111	NIWA	174.98	-48.95	177.5	-48	0.137	10	8.05	34.44	8.807	2294.6	-21.1	0.30	265.2	1.8	0.73	8.197	17.39	2062.8	0.0424	0.0388	162	3.86	425.7
F111	NIWA	174.98	-48.95	177.5	-48	0.137	11	8.99	34.47	8.794	2293.8	-11.3	0.30	268.1	1.8	0.73	8.193	17.47	2056.3	0.0434	0.0396	166	3.95	426.0
F111	NIWA	174.98	-48.95	177.5	-48	0.137	12	10.39	34.36	8.777	2285.2	-17.9	0.30	266.1	1.8	0.73	8.194	17.66	2036.9	0.0454	0.0413	173	4.13	424.7
^{14}C age = 4.582ka, CO_2 = 271.5 ppm			**Interpolated[∇] average**					**9.08**	**34.33**	**8.794**	**2287.2**	**-16.9**		**266.4**			**8.194**	**17.49**	**2049.4**	**0.0436**	**0.0398**	**166**	**3.96**	**424.4**
			Interpolated[∇] intraannual variation					**2.99**	**0.23**	**0.024**	**13.4**	**4.1**		**4.1**			**0.003**	**0.41**	**20.4**	**0.0028**	**0.0023**	**10**	**0.25**	**1.7**
ODP1172C	NIWA	149.93	-43.96	147.5	-44	0.170	1	14.74	34.98	8.719	2308.9	-40.9	0.30	263.0	2	0.75	8.199	18.33	2012.0	0.0539	0.0481	206	4.91	432.4
ODP1172C	NIWA	149.93	-43.96	147.5	-44	0.170	2	15.19	35.01	8.714	2309.9	-43.8	0.30	262.1	2	0.75	8.200	18.41	2008.0	0.0548	0.0488	210	4.99	432.7
ODP1172C	NIWA	149.93	-43.96	147.5	-44	0.170	3	15.10	35.08	8.714	2313.7	-41.2	0.30	262.9	2	0.75	8.200	18.39	2012.1	0.0547	0.0487	209	4.98	433.6
ODP1172C	NIWA	149.93	-43.96	147.5	-44	0.170	4	14.25	35.05	8.725	2313.3	-37.6	0.30	264.0	2	0.75	8.199	18.26	2020.2	0.0531	0.0475	204	4.84	433.2
ODP1172C	NIWA	149.93	-43.96	147.5	-44	0.170	5	13.45	35.05	8.735	2314.5	-27.9	0.30	266.9	2	0.75	8.195	18.12	2030.3	0.0514	0.0462	198	4.70	433.2
ODP1172C	NIWA	149.93	-43.96	147.5	-44	0.170	6	12.61	34.89	8.746	2307.6	-18.2	0.30	269.9	2	0.75	8.191	17.95	2034.8	0.0495	0.0446	190	4.52	431.2
ODP1172C	NIWA	149.93	-43.96	147.5	-44	0.170	7	12.16	34.79	8.752	2303.2	-9.6	0.30	272.4	2	0.75	8.187	17.85	2037.3	0.0483	0.0436	185	4.41	430.0
ODP1172C	NIWA	149.93	-43.96	147.5	-44	0.170	8	11.68	34.83	8.758	2306.2	2.0	0.30	275.9	2	0.75	8.183	17.74	2046.0	0.0471	0.0427	182	4.32	430.5
ODP1172C	NIWA	149.93	-43.96	147.5	-44	0.170	9	11.61	34.86	8.759	2307.9	0.4	0.30	275.4	2	0.75	8.184	17.75	2047.5	0.0472	0.0427	182	4.32	430.9
ODP1172C	NIWA	149.93	-43.96	147.5	-44	0.170	10	11.84	34.87	8.756	2308.0	-18.0	0.30	269.9	2	0.75	8.191	17.85	2041.7	0.0483	0.0436	185	4.41	431.0
ODP1172C	NIWA	149.93	-43.96	147.5	-44	0.170	11	12.66	34.86	8.746	2305.9	-32.6	0.30	265.5	2	0.75	8.197	18.02	2030.0	0.0501	0.0451	192	4.57	430.9
ODP1172C	NIWA	149.93	-43.96	147.5	-44	0.170	12	13.76	34.82	8.732	2302.1	-33.9	0.30	265.1	2	0.75	8.196	18.16	2017.3	0.0518	0.0464	198	4.71	430.4
ODP1172C	NIWA	149.93	-43.96	152.5	-44	0.151	1	14.88	35.04	8.717	2311.9	-34.6	0.30	264.9	2	0.75	8.197	18.33	2014.3	0.0539	0.0481	207	4.92	433.1
ODP1172C	NIWA	149.93	-43.96	152.5	-44	0.151	2	15.40	34.97	8.711	2307.5	-23.5	0.30	268.2	2	0.75	8.192	18.34	2009.1	0.0541	0.0482	207	4.94	432.2
ODP1172C	NIWA	149.93	-43.96	152.5	-44	0.151	3	15.21	35.02	8.713	2310.4	-34.2	0.30	265.0	2	0.75	8.196	18.37	2010.4	0.0544	0.0485	208	4.96	432.8
ODP1172C	NIWA	149.93	-43.96	152.5	-44	0.151	4	14.45	35.12	8.722	2316.7	-36.2	0.30	264.4	2	0.75	8.198	18.29	2021.2	0.0535	0.0478	205	4.88	434.1

		Site		Nearest Takahashi Sites																			
Site	**Archive**[ϰ]	**Long (°E)**	**Lat (°N)**	**Long (°E)**	**Lat (°N)**	$\frac{1}{SS_D}$[∀]	**Month**	**SST (°C)**[§]	**Salinity**[§]	pK_B^*[◇]	**TAlk (μmol/kg)**[♣]	**ΔpCO_2 (ppm)**[§]	**Gloor corr.**[♯]	**pCO_2**[†]	**SiO_2**[♭]	**PO_4^-**[♭]	**pH**	$\delta^{11}B_{B(OH)_4^-}$ (‰)	**DIC (μmol/kg)**	$B(OH)_4^-/HCO_3^-$	$B(OH)_4^-$/DIC	CO_3^{2-} (μmol/kg)	Ω_{CaCO_3}	**[B] (µmol/kg)**
ODP1172C	NIWA	149.93	-43.96	152.5	-44	0.151	5	13.71	35.16	8.731	2320.0	-24.4	0.30	268.0	2	0.75	8.194	18.15	2032.7	0.0519	0.0465	200	4.75	434.6
ODP1172C	NIWA	149.93	-43.96	152.5	-44	0.151	6	12.79	35.06	8.743	2316.2	-22.8	0.30	268.5	2	0.75	8.194	18.01	2038.4	0.0502	0.0452	193	4.59	433.3
ODP1172C	NIWA	149.93	-43.96	152.5	-44	0.151	7	12.17	34.94	8.751	2311.0	-15.8	0.30	270.6	2	0.75	8.191	17.89	2041.5	0.0488	0.0440	188	4.46	431.9
ODP1172C	NIWA	149.93	-43.96	152.5	-44	0.151	8	11.68	34.92	8.758	2310.8	-0.4	0.30	275.2	2	0.75	8.185	17.76	2048.9	0.0474	0.0429	183	4.35	431.6
ODP1172C	NIWA	149.93	-43.96	152.5	-44	0.151	9	11.65	35.02	8.758	2316.1	-1.3	0.30	274.9	2	0.75	8.185	17.78	2052.9	0.0475	0.0430	184	4.37	432.8
ODP1172C	NIWA	149.93	-43.96	152.5	-44	0.151	10	11.92	34.97	8.754	2313.0	-25.0	0.30	267.8	2	0.75	8.195	17.90	2043.2	0.0489	0.0441	188	4.47	432.2
ODP1172C	NIWA	149.93	-43.96	152.5	-44	0.151	11	12.75	34.97	8.744	2311.5	-29.5	0.30	266.5	2	0.75	8.196	18.03	2033.9	0.0503	0.0453	193	4.59	432.2
ODP1172C	NIWA	149.93	-43.96	152.5	-44	0.151	12	13.84	34.94	8.731	2308.1	-28.0	0.30	266.9	2	0.75	8.194	18.16	2022.3	0.0518	0.0465	199	4.73	431.9
ODP1172C	NIWA	149.93	-43.96	152.5	-40	0.045	1	18.59	35.42	8.670	2328.4	-30.7	0.30	266.1	2	0.75	8.194	18.83	1993.3	0.0605	0.0532	233	5.53	437.8
ODP1172C	NIWA	149.93	-43.96	152.5	-40	0.045	2	19.45	35.42	8.660	2327.8	-18.7	0.30	269.7	2	0.75	8.188	18.89	1988.0	0.0613	0.0538	236	5.62	437.8
ODP1172C	NIWA	149.93	-43.96	152.5	-40	0.045	3	19.20	35.50	8.662	2332.4	-33.2	0.30	265.3	2	0.75	8.195	18.93	1989.9	0.0618	0.0542	238	5.65	438.8
ODP1172C	NIWA	149.93	-43.96	152.5	-40	0.045	4	18.29	35.45	8.674	2330.3	-33.3	0.30	265.3	2	0.75	8.195	18.81	1996.8	0.0602	0.0529	231	5.50	438.2
ODP1172C	NIWA	149.93	-43.96	152.5	-40	0.045	5	17.17	35.46	8.687	2331.8	-24.2	0.30	268.0	2	0.75	8.193	18.63	2010.2	0.0579	0.0512	223	5.30	438.3
ODP1172C	NIWA	149.93	-43.96	152.5	-40	0.045	6	15.87	35.39	8.703	2329.4	-30.0	0.30	266.3	2	0.75	8.196	18.48	2018.9	0.0559	0.0497	216	5.12	437.4
ODP1172C	NIWA	149.93	-43.96	152.5	-40	0.045	7	14.94	35.45	8.714	2333.9	-39.4	0.30	263.5	2	0.75	8.201	18.41	2028.3	0.0550	0.0490	212	5.03	438.2
ODP1172C	NIWA	149.93	-43.96	152.5	-40	0.045	8	14.35	35.32	8.722	2327.6	-37.6	0.30	264.0	2	0.75	8.200	18.31	2029.5	0.0537	0.0480	207	4.92	436.6
ODP1172C	NIWA	149.93	-43.96	152.5	-40	0.045	9	14.36	35.35	8.722	2329.2	-34.7	0.30	264.9	2	0.75	8.199	18.30	2031.2	0.0537	0.0479	207	4.91	436.9
ODP1172C	NIWA	149.93	-43.96	152.5	-40	0.045	10	14.75	35.34	8.717	2328.1	-31.4	0.30	265.9	2	0.75	8.197	18.34	2027.7	0.0541	0.0483	209	4.95	436.8
ODP1172C	NIWA	149.93	-43.96	152.5	-40	0.045	11	15.83	35.35	8.704	2327.3	-42.1	0.30	262.7	2	0.75	8.201	18.52	2014.9	0.0564	0.0501	217	5.15	436.9
ODP1172C	NIWA	149.93	-43.96	152.5	-40	0.045	12	17.27	35.34	8.687	2325.2	-46.9	0.30	261.2	2	0.75	8.201	18.73	1999.2	0.0590	0.0520	226	5.37	436.8
^{14}C age = 2.622ka, CO_2 = 275.3 ppm			**Interpolated[∇] average**					**13.72**	**35.02**	**8.732**	**2312.8**	**-25.2**		**267.7**			**8.194**	**18.14**	**2027.0**	**0.0518**	**0.0464**	**199**	**4.73**	**432.8**
			Interpolated[∇] intraannual variation					**2.86**	**0.17**	**0.017**	**7.4**	**26.7**		**8.0**			**0.004**	**0.47**	**13.3**	**0.0025**	**0.0020**	**9**	**0.22**	**1.4**
MC439	Tübingen	-20.03	59.46	-22.5	56	0.055	1	9.42	35.17	8.785	2322.0	-17.7	0.50	266.2	0.96	0.34	8.198	17.62	2064.3	0.0477	0.0433	178	4.22	434.7
MC439	Tübingen	-20.03	59.46	-22.5	56	0.055	2	9.06	35.27	8.789	2327.7	-16.4	0.50	266.8	0.96	0.34	8.198	17.58	2072.0	0.0472	0.0429	176	4.19	435.9
MC439	Tübingen	-20.03	59.46	-22.5	56	0.055	3	8.98	35.26	8.790	2327.1	-12.8	0.50	268.6	0.96	0.34	8.195	17.54	2073.6	0.0468	0.0426	175	4.15	435.8
MC439	Tübingen	-20.03	59.46	-22.5	56	0.055	4	9.21	35.21	8.788	2324.3	-3.6	0.50	273.2	0.96	0.34	8.189	17.50	2072.8	0.0464	0.0422	174	4.13	435.2
MC439	Tübingen	-20.03	59.46	-22.5	56	0.055	5	10.02	35.17	8.777	2321.8	-24.8	0.50	262.6	0.96	0.34	8.203	17.75	2056.4	0.0491	0.0445	183	4.34	434.7
MC439	Tübingen	-20.03	59.46	-22.5	56	0.055	6	11.44	35.22	8.759	2324.0	-44.9	0.50	252.6	0.96	0.34	8.217	18.09	2037.9	0.0530	0.0476	196	4.66	435.3
MC439	Tübingen	-20.03	59.46	-22.5	56	0.055	7	12.85	35.22	8.741	2323.3	-42.0	0.50	254.0	0.96	0.34	8.214	18.26	2026.1	0.0550	0.0492	204	4.85	435.3
MC439	Tübingen	-20.03	59.46	-22.5	56	0.055	8	13.58	35.21	8.732	2322.3	-47.3	0.50	251.3	0.96	0.34	8.217	18.39	2016.7	0.0567	0.0505	210	4.98	435.2

		Site		Nearest Takahashi Sites																			
Site	**Archive**[ℵ]	**Long** (°E)	**Lat** (°N)	**Long** (°E)	**Lat** (°N)	$\frac{1}{SSS_D}$ [∀]	**Month**	**SST** (°C)[§]	**Salinity**[§]	pK_B^* [◇]	**TAlk** (μmol/kg)[♣]	Δ**pCO$_2$ (ppm)**[§]	**Gloor corr.**[♯]	**pCO$_2$**[†]	**SiO$_2^-$**[♭]	**PO$_4^{--}$**[♭]	**pH**	$\delta^{11}B_{B(OH)_4^-}$ (‰)	**DIC** (μmol/kg)	**B(OH)$_4^-$ /HCO$_3^-$**	**B(OH)$_4^-$/DIC**	**CO$_3^{2-}$** (μmol/kg)	Ω_{CaCO_3}	**[B] (μmol/kg)**
MC439	Tübingen	-20.03	59.46	-22.5	56	0.055	9	13.02	35.14	8.740	2318.8	-38.9	0.50	255.6	0.96	0.34	8.211	18.24	2022.6	0.0549	0.0491	203	4.83	434.3
MC439	Tübingen	-20.03	59.46	-22.5	56	0.055	10	11.86	35.22	8.754	2323.8	-27.4	0.50	261.3	0.96	0.34	8.205	18.02	2041.0	0.0522	0.0470	195	4.62	435.3
MC439	Tübingen	-20.03	59.46	-22.5	56	0.055	11	10.75	35.22	8.768	2324.3	-23.9	0.50	263.1	0.96	0.34	8.202	17.84	2052.3	0.0502	0.0454	187	4.45	435.3
MC439	Tübingen	-20.03	59.46	-22.5	56	0.055	12	10.06	35.23	8.777	2325.1	-21.2	0.50	264.4	0.96	0.34	8.201	17.74	2059.9	0.0490	0.0444	183	4.34	435.4
MC439	Tübingen	-20.03	59.46	-22.5	60	0.156	1	8.38	35.11	8.799	2319.0	17.4	0.50	283.7	0.96	0.34	8.174	17.25	2082.8	0.0437	0.0400	164	3.89	434.0
MC439	Tübingen	-20.03	59.46	-22.5	60	0.156	2	8.11	35.23	8.802	2325.7	8.2	0.50	279.1	0.96	0.34	8.181	17.29	2087.0	0.0441	0.0403	165	3.93	435.4
MC439	Tübingen	-20.03	59.46	-22.5	60	0.156	3	8.01	35.23	8.803	2325.7	-2.6	0.50	273.7	0.96	0.34	8.188	17.34	2084.2	0.0447	0.0408	167	3.97	435.4
MC439	Tübingen	-20.03	59.46	-22.5	60	0.156	4	8.08	35.18	8.802	2322.9	-11.1	0.50	269.5	0.96	0.34	8.193	17.40	2078.6	0.0453	0.0413	169	4.01	434.8
MC439	Tübingen	-20.03	59.46	-22.5	60	0.156	5	8.78	35.18	8.793	2322.8	-25.9	0.50	262.1	0.96	0.34	8.204	17.60	2067.3	0.0474	0.0430	176	4.18	434.8
MC439	Tübingen	-20.03	59.46	-22.5	60	0.156	6	10.21	35.16	8.775	2321.2	-59.5	0.50	245.2	0.96	0.34	8.227	18.03	2040.8	0.0522	0.0470	192	4.57	434.6
MC439	Tübingen	-20.03	59.46	-22.5	60	0.156	7	11.52	35.14	8.759	2319.6	-54.5	0.50	247.8	0.96	0.34	8.223	18.17	2030.1	0.0538	0.0483	198	4.72	434.3
MC439	Tübingen	-20.03	59.46	-22.5	60	0.156	8	12.17	35.19	8.750	2322.0	-38.0	0.50	256.0	0.96	0.34	8.212	18.13	2032.8	0.0535	0.0480	199	4.72	434.9
MC439	Tübingen	-20.03	59.46	-22.5	60	0.156	9	11.43	35.13	8.760	2319.1	-26.6	0.50	261.7	0.96	0.34	8.204	17.94	2041.6	0.0513	0.0462	191	4.54	434.2
MC439	Tübingen	-20.03	59.46	-22.5	60	0.156	10	10.29	35.19	8.774	2322.8	-9.4	0.50	270.3	0.96	0.34	8.192	17.68	2060.5	0.0484	0.0438	181	4.30	434.9
MC439	Tübingen	-20.03	59.46	-22.5	60	0.156	11	9.33	35.19	8.786	2323.2	-2.1	0.50	274.0	0.96	0.34	8.188	17.50	2071.5	0.0464	0.0423	174	4.13	434.9
MC439	Tübingen	-20.03	59.46	-22.5	60	0.156	12	8.84	35.19	8.792	2323.3	7.1	0.50	278.6	0.96	0.34	8.181	17.38	2078.8	0.0451	0.0412	169	4.02	434.9
MC439	Tübingen	-20.03	59.46	-17.5	56	0.054	1	9.92	35.34	8.778	2331.3	-18.6	0.50	265.7	0.96	0.34	8.200	17.71	2066.6	0.0487	0.0442	182	4.33	436.8
MC439	Tübingen	-20.03	59.46	-17.5	56	0.054	2	9.64	35.35	8.781	2331.9	-18.7	0.50	265.7	0.96	0.34	8.200	17.68	2069.4	0.0483	0.0438	181	4.29	436.9
MC439	Tübingen	-20.03	59.46	-17.5	56	0.054	3	9.56	35.36	8.782	2332.5	-20.8	0.50	264.6	0.96	0.34	8.201	17.68	2069.8	0.0484	0.0439	181	4.30	437.0
MC439	Tübingen	-20.03	59.46	-17.5	56	0.054	4	9.74	35.31	8.780	2329.7	-30.2	0.50	259.9	0.96	0.34	8.208	17.77	2062.6	0.0493	0.0447	184	4.36	436.4
MC439	Tübingen	-20.03	59.46	-17.5	56	0.054	5	10.52	35.31	8.770	2329.4	-44.2	0.50	252.9	0.96	0.34	8.217	17.98	2050.2	0.0516	0.0465	192	4.55	436.4
MC439	Tübingen	-20.03	59.46	-17.5	56	0.054	6	11.85	35.36	8.753	2331.6	-55.8	0.50	247.1	0.96	0.34	8.225	18.25	2035.3	0.0549	0.0491	203	4.82	437.0
MC439	Tübingen	-20.03	59.46	-17.5	56	0.054	7	13.21	35.32	8.736	2328.6	-46.2	0.50	251.9	0.96	0.34	8.217	18.35	2025.0	0.0562	0.0501	208	4.95	436.6
MC439	Tübingen	-20.03	59.46	-17.5	56	0.054	8	14.00	35.34	8.727	2329.2	-49.6	0.50	250.2	0.96	0.34	8.220	18.48	2016.8	0.0578	0.0514	214	5.09	436.8
MC439	Tübingen	-20.03	59.46	-17.5	56	0.054	9	13.34	35.29	8.735	2326.8	-39.1	0.50	255.4	0.96	0.34	8.212	18.31	2025.4	0.0557	0.0497	207	4.91	436.2
MC439	Tübingen	-20.03	59.46	-17.5	56	0.054	10	12.11	35.28	8.750	2327.0	-24.8	0.50	262.6	0.96	0.34	8.203	18.04	2042.1	0.0525	0.0472	196	4.65	436.1
MC439	Tübingen	-20.03	59.46	-17.5	56	0.054	11	11.04	35.36	8.763	2332.0	-21.8	0.50	264.1	0.96	0.34	8.202	17.88	2056.2	0.0507	0.0458	190	4.50	437.0
MC439	Tübingen	-20.03	59.46	-17.5	56	0.054	12	10.46	35.37	8.771	2332.8	-21.3	0.50	264.4	0.96	0.34	8.202	17.81	2062.0	0.0498	0.0450	186	4.42	437.2
MC439	Tübingen	-20.03	59.46	-17.5	60	0.149	1	8.66	35.25	8.794	2326.7	15.4	0.50	282.7	0.96	0.34	8.176	17.31	2085.6	0.0444	0.0406	167	3.97	435.7
MC439	Tübingen	-20.03	59.46	-17.5	60	0.149	2	8.44	35.29	8.797	2328.9	5.2	0.50	277.6	0.96	0.34	8.183	17.35	2085.7	0.0448	0.0409	168	4.00	436.2
MC439	Tübingen	-20.03	59.46	-17.5	60	0.149	3	8.35	35.31	8.798	2330.1	-3.7	0.50	273.2	0.96	0.34	8.189	17.40	2084.3	0.0453	0.0414	170	4.03	436.4
MC439	Tübingen	-20.03	59.46	-17.5	60	0.149	4	8.41	35.25	8.798	2326.7	-9.8	0.50	270.1	0.96	0.34	8.193	17.44	2079.1	0.0458	0.0417	171	4.06	435.7

		Site		Nearest Takahashi Sites																			
Site	**Archive**[ϰ]	**Long (°E)**	**Lat (°N)**	**Long (°E)**	**Lat (°N)**	$\frac{1}{SSS_D}$ [∀]	**Month**	**SST (°C)**[§]	**Salinity**[§]	pK_B^* [◇]	**TAlk (μmol/kg)**[♣]	**ΔpCO$_2$ (ppm)**[§]	**Gloor corr.**[♯]	**pCO$_2$**[†]	**SiO$_2$**[♭]	**PO$_4^-$**[♭]	**pH**	$\delta^{11}B_{B(OH)_4^-}$ (‰)	**DIC (μmol/kg)**	**B(OH)$_4^-$ /HCO$_3^-$**	**B(OH)$_4^-$/DIC**	**CO$_3^{2-}$ (μmol/kg)**	Ω_{CaCO_3}	**[B] (μmol/kg)**
MC439	Tübingen	-20.03	59.46	-17.5	60	0.149	5	9.05	35.25	8.789	2326.6	-27.3	0.50	261.4	0.96	0.34	8.205	17.65	2067.3	0.0480	0.0436	179	4.24	435.7
MC439	Tübingen	-20.03	59.46	-17.5	60	0.149	6	10.45	35.26	8.771	2326.6	-59.8	0.50	245.1	0.96	0.34	8.228	18.08	2042.5	0.0528	0.0475	195	4.62	435.8
MC439	Tübingen	-20.03	59.46	-17.5	60	0.149	7	11.84	35.18	8.754	2321.6	-59.5	0.50	245.3	0.96	0.34	8.227	18.25	2026.7	0.0549	0.0491	202	4.80	434.8
MC439	Tübingen	-20.03	59.46	-17.5	60	0.149	8	12.57	35.22	8.745	2323.4	-37.5	0.50	256.2	0.96	0.34	8.211	18.18	2030.5	0.0542	0.0485	201	4.78	435.3
MC439	Tübingen	-20.03	59.46	-17.5	60	0.149	9	11.74	35.17	8.756	2321.1	-16.2	0.50	266.9	0.96	0.34	8.197	17.91	2044.3	0.0510	0.0460	191	4.53	434.7
MC439	Tübingen	-20.03	59.46	-17.5	60	0.149	10	10.52	35.20	8.771	2323.3	-9.0	0.50	270.5	0.96	0.34	8.192	17.71	2059.1	0.0487	0.0441	182	4.33	435.1
MC439	Tübingen	-20.03	59.46	-17.5	60	0.149	11	9.56	35.28	8.783	2328.1	-2.8	0.50	273.6	0.96	0.34	8.189	17.55	2072.9	0.0470	0.0427	176	4.18	436.1
MC439	Tübingen	-20.03	59.46	-17.5	60	0.149	12	9.07	35.27	8.789	2327.7	5.7	0.50	277.9	0.96	0.34	8.183	17.43	2079.7	0.0456	0.0416	172	4.07	435.9
n/d, Pre-ind. CO_2 ≃275 ppm			**Interpolated[▽] average**					**10.09**	**35.23**	**8.776**	**2324.8**	**-20.0**		**265.0**			**8.200**	**17.74**	**2059.4**	**0.0491**	**0.0444**	**183**	**4.34**	**435.4**
			Interpolated[▽] intraannual variation					**3.06**	**0.08**	**0.024**	**4.9**	**43.6**		**21.8**			**0.019**	**0.66**	**26.7**	**0.0047**	**0.0038**	**16**	**0.38**	**0.6**
TAN1106/38	NIWA	165.07	-49.69	162.5	-52	0.084	1	9.73	34.30	8.786	2283.8	-18.3	0.23	270.7	3	1.2	8.188	17.51	2036.5	0.0461	0.0419	170	4.07	423.9
TAN1106/38	NIWA	165.07	-49.69	162.5	-52	0.084	2	9.93	34.22	8.784	2279.5	-14.1	0.23	271.7	3	1.2	8.186	17.51	2032.4	0.0461	0.0420	170	4.07	423.0
TAN1106/38	NIWA	165.07	-49.69	162.5	-52	0.084	3	9.54	34.27	8.788	2282.7	-12.3	0.23	272.1	3	1.2	8.186	17.46	2038.3	0.0456	0.0415	168	4.02	423.6
TAN1106/38	NIWA	165.07	-49.69	162.5	-52	0.084	4	8.90	34.28	8.796	2284.7	-17.9	0.23	270.8	3	1.2	8.188	17.40	2044.2	0.0449	0.0409	166	3.96	423.7
TAN1106/38	NIWA	165.07	-49.69	162.5	-52	0.084	5	8.37	34.42	8.803	2292.9	-14.3	0.23	271.7	3	1.2	8.187	17.34	2055.3	0.0442	0.0404	164	3.91	425.4
TAN1106/38	NIWA	165.07	-49.69	162.5	-52	0.084	6	7.93	34.19	8.810	2282.8	-11.8	0.23	272.3	3	1.2	8.185	17.25	2051.8	0.0432	0.0396	160	3.81	422.6
TAN1106/38	NIWA	165.07	-49.69	162.5	-52	0.084	7	7.66	34.34	8.812	2290.7	-7.6	0.23	273.2	3	1.2	8.185	17.22	2060.7	0.0429	0.0393	159	3.80	424.4
TAN1106/38	NIWA	165.07	-49.69	162.5	-52	0.084	8	7.53	34.46	8.813	2297.0	-2.5	0.23	274.4	3	1.2	8.184	17.20	2067.2	0.0427	0.0392	159	3.79	425.9
TAN1106/38	NIWA	165.07	-49.69	162.5	-52	0.084	9	7.53	34.41	8.814	2294.5	-0.7	0.23	274.8	3	1.2	8.183	17.19	2065.6	0.0426	0.0391	158	3.78	425.3
TAN1106/38	NIWA	165.07	-49.69	162.5	-52	0.084	10	7.66	34.41	8.812	2294.2	10.0	0.23	277.3	3	1.2	8.180	17.18	2065.9	0.0425	0.0390	158	3.77	425.3
TAN1106/38	NIWA	165.07	-49.69	162.5	-52	0.084	11	8.18	34.48	8.805	2296.3	20.2	0.23	279.7	3	1.2	8.177	17.22	2064.8	0.0430	0.0394	160	3.82	426.2
TAN1106/38	NIWA	165.07	-49.69	162.5	-52	0.084	12	8.90	34.38	8.796	2289.6	6.6	0.23	276.5	3	1.2	8.181	17.34	2051.7	0.0442	0.0404	164	3.92	424.9
TAN1106/38	NIWA	165.07	-49.69	162.5	-48	0.105	1	12.13	34.69	8.753	2298.2	-26.4	0.23	268.9	3	1.2	8.191	17.88	2025.2	0.0505	0.0456	188	4.47	428.8
TAN1106/38	NIWA	165.07	-49.69	162.5	-48	0.105	2	12.51	34.52	8.749	2289.0	-21.4	0.23	270.0	3	1.2	8.189	17.89	2016.1	0.0506	0.0456	187	4.47	426.7
TAN1106/38	NIWA	165.07	-49.69	162.5	-48	0.105	3	12.11	34.40	8.755	2283.8	-13.7	0.23	271.8	3	1.2	8.186	17.81	2017.1	0.0495	0.0448	183	4.38	425.2
TAN1106/38	NIWA	165.07	-49.69	162.5	-48	0.105	4	11.38	34.57	8.763	2293.6	-22.4	0.23	269.8	3	1.2	8.190	17.76	2029.0	0.0490	0.0444	182	4.34	427.3
TAN1106/38	NIWA	165.07	-49.69	162.5	-48	0.105	5	10.73	34.70	8.771	2301.4	-20.4	0.23	270.3	3	1.2	8.190	17.69	2040.7	0.0482	0.0437	179	4.27	428.9
TAN1106/38	NIWA	165.07	-49.69	162.5	-48	0.105	6	10.13	34.52	8.779	2293.7	-19.0	0.23	270.6	3	1.2	8.189	17.59	2040.3	0.0470	0.0427	174	4.16	426.7
TAN1106/38	NIWA	165.07	-49.69	162.5	-48	0.105	7	9.70	34.64	8.784	2300.6	-13.9	0.23	271.8	3	1.2	8.188	17.53	2049.9	0.0464	0.0422	173	4.11	428.2
TAN1106/38	NIWA	165.07	-49.69	162.5	-48	0.105	8	9.50	34.80	8.786	2309.2	-1.9	0.23	274.6	3	1.2	8.185	17.48	2059.9	0.0460	0.0419	172	4.09	430.1

		Site		Nearest Takahashi Sites																			
Site	**Archive**[ж]	**Long (°E)**	**Lat (°N)**	**Long (°E)**	**Lat (°N)**	$\frac{1}{SS_D}$ [∀]	**Month**	**SST (°C)**[§]	**Salinity**[§]	pK_B^* [◇]	**TAlk (μmol/kg)**[♣]	**ΔpCO$_2$ (ppm)**[§]	**Gloor corr.**[♯]	**pCO$_2$**[†]	**SiO$_2$**[♭]	**PO$_4^-$**[♭]	**pH**	$\delta^{11}B_{B(OH)_4^-}$ (‰)	**DIC (μmol/kg)**	**B(OH)$_4^-$ /HCO$_3^-$**	**B(OH)$_4^-$/DIC**	**CO$_3^{2-}$ (μmol/kg)**	Ω_{CaCO_3}	**[B] (μmol/kg)**
TAN1106/38	NIWA	165.07	-49.69	162.5	-48	0.105	9	9.47	34.72	8.787	2305.2	-11.1	0.23	272.4	3	1.2	8.188	17.50	2055.7	0.0461	0.0420	172	4.09	429.1
TAN1106/38	NIWA	165.07	-49.69	162.5	-48	0.105	10	9.63	34.71	8.785	2304.3	-7.1	0.23	273.4	3	1.2	8.186	17.51	2054.4	0.0462	0.0421	172	4.10	429.0
TAN1106/38	NIWA	165.07	-49.69	162.5	-48	0.105	11	10.31	34.71	8.776	2302.8	11.0	0.23	277.5	3	1.2	8.181	17.54	2050.4	0.0466	0.0424	174	4.14	429.0
TAN1106/38	NIWA	165.07	-49.69	162.5	-48	0.105	12	11.21	34.57	8.765	2293.9	5.4	0.23	276.3	3	1.2	8.181	17.65	2035.3	0.0478	0.0434	178	4.25	427.3
TAN1106/38	NIWA	165.07	-49.69	167.5	-52	0.089	1	9.82	34.34	8.784	2285.5	-27.6	0.23	268.6	3	1.2	8.191	17.56	2035.5	0.0466	0.0424	172	4.11	424.4
TAN1106/38	NIWA	165.07	-49.69	167.5	-52	0.089	2	10.05	34.32	8.782	2284.0	-14.3	0.23	271.7	3	1.2	8.186	17.54	2034.7	0.0464	0.0422	172	4.10	424.2
TAN1106/38	NIWA	165.07	-49.69	167.5	-52	0.089	3	9.72	34.34	8.786	2285.7	-13.3	0.23	271.9	3	1.2	8.186	17.50	2038.9	0.0460	0.0418	170	4.06	424.4
TAN1106/38	NIWA	165.07	-49.69	167.5	-52	0.089	4	9.11	34.40	8.793	2290.1	-8.2	0.23	273.1	3	1.2	8.185	17.41	2048.0	0.0450	0.0411	167	3.98	425.2
TAN1106/38	NIWA	165.07	-49.69	167.5	-52	0.089	5	8.57	34.42	8.800	2292.4	-12.2	0.23	272.2	3	1.2	8.187	17.36	2053.6	0.0444	0.0406	165	3.93	425.4
TAN1106/38	NIWA	165.07	-49.69	167.5	-52	0.089	6	8.15	34.28	8.806	2286.6	-11.6	0.23	272.3	3	1.2	8.186	17.29	2052.9	0.0436	0.0399	161	3.85	423.7
TAN1106/38	NIWA	165.07	-49.69	167.5	-52	0.089	7	7.88	34.35	8.809	2290.7	-8.7	0.23	273.0	3	1.2	8.185	17.25	2058.6	0.0432	0.0396	160	3.83	424.6
TAN1106/38	NIWA	165.07	-49.69	167.5	-52	0.089	8	7.69	34.24	8.812	2285.8	-7.5	0.23	273.3	3	1.2	8.184	17.22	2056.7	0.0428	0.0392	158	3.78	423.2
TAN1106/38	NIWA	165.07	-49.69	167.5	-52	0.089	9	7.63	34.31	8.813	2289.4	-6.2	0.23	273.6	3	1.2	8.184	17.21	2060.1	0.0428	0.0392	158	3.78	424.1
TAN1106/38	NIWA	165.07	-49.69	167.5	-52	0.089	10	7.84	34.53	8.809	2299.6	4.3	0.23	276.0	3	1.2	8.182	17.23	2067.7	0.0431	0.0395	160	3.82	426.8
TAN1106/38	NIWA	165.07	-49.69	167.5	-52	0.089	11	8.37	34.58	8.802	2300.8	-5.9	0.23	273.6	3	1.2	8.186	17.33	2062.5	0.0442	0.0404	164	3.92	427.4
TAN1106/38	NIWA	165.07	-49.69	167.5	-52	0.089	12	9.04	34.39	8.794	2289.7	-31.8	0.23	267.6	3	1.2	8.193	17.48	2044.6	0.0457	0.0416	169	4.03	425.1
TAN1106/38	NIWA	165.07	-49.69	167.5	-48	0.114	1	12.07	34.48	8.755	2287.8	-30.8	0.23	267.8	3	1.2	8.192	17.87	2017.5	0.0502	0.0453	186	4.43	426.2
TAN1106/38	NIWA	165.07	-49.69	167.5	-48	0.114	2	12.46	34.47	8.750	2286.6	-16.5	0.23	271.2	3	1.2	8.187	17.87	2015.7	0.0503	0.0454	186	4.44	426.0
TAN1106/38	NIWA	165.07	-49.69	167.5	-48	0.114	3	12.09	34.32	8.756	2279.9	-15.3	0.23	271.5	3	1.2	8.186	17.80	2014.2	0.0494	0.0447	183	4.36	424.2
TAN1106/38	NIWA	165.07	-49.69	167.5	-48	0.114	4	11.37	34.52	8.764	2291.1	-0.8	0.23	274.8	3	1.2	8.183	17.68	2030.9	0.0482	0.0437	179	4.27	426.7
TAN1106/38	NIWA	165.07	-49.69	167.5	-48	0.114	5	10.67	34.62	8.772	2297.5	-14.5	0.23	271.6	3	1.2	8.188	17.65	2039.3	0.0478	0.0434	178	4.23	427.9
TAN1106/38	NIWA	165.07	-49.69	167.5	-48	0.114	6	10.11	34.53	8.780	2294.2	-18.1	0.23	270.8	3	1.2	8.189	17.58	2041.0	0.0470	0.0427	174	4.15	426.8
TAN1106/38	NIWA	165.07	-49.69	167.5	-48	0.114	7	9.73	34.69	8.784	2303.1	-15.6	0.23	271.4	3	1.2	8.189	17.54	2051.2	0.0466	0.0424	173	4.13	428.8
TAN1106/38	NIWA	165.07	-49.69	167.5	-48	0.114	8	9.56	34.59	8.786	2298.5	-7.5	0.23	273.3	3	1.2	8.186	17.49	2050.5	0.0459	0.0418	171	4.07	427.5
TAN1106/38	NIWA	165.07	-49.69	167.5	-48	0.114	9	9.52	34.60	8.787	2299.0	-2.4	0.23	274.4	3	1.2	8.184	17.47	2052.1	0.0457	0.0417	170	4.06	427.7
TAN1106/38	NIWA	165.07	-49.69	167.5	-48	0.114	10	9.71	34.71	8.784	2304.2	0.1	0.23	275.0	3	1.2	8.184	17.49	2054.7	0.0461	0.0420	172	4.09	429.0
TAN1106/38	NIWA	165.07	-49.69	167.5	-48	0.114	11	10.32	34.68	8.776	2301.3	-7.0	0.23	273.4	3	1.2	8.186	17.59	2046.3	0.0471	0.0428	176	4.18	428.6
TAN1106/38	NIWA	165.07	-49.69	167.5	-48	0.114	12	11.20	34.38	8.767	2284.5	-21.0	0.23	270.1	3	1.2	8.188	17.71	2024.2	0.0484	0.0439	179	4.27	424.9
n/d, Pre-ind. CO_2 ≃275 ppm			Interpolated[▽] average					**9.78**	**34.49**	**8.784**	**2293.1**	**-10.6**		**272.5**			**8.186**	**17.51**	**2044.1**	**0.0462**	**0.0421**	**172**	**4.09**	**426.3**
			Interpolated[▽] intraannual variation					**2.00**	**0.22**	**0.014**	**13.6**	**21.2**		**4.9**			**0.003**	**0.28**	**16.2**	**0.0018**	**0.0015**	**6**	**0.15**	**1.6**

		Site		Nearest Takahashi Sites																			
Site	**Archive**[ℵ]	**Long** (°E)	**Lat** (°N)	**Long** (°E)	**Lat** (°N)	$\frac{1}{SS_D}$ [∀]	**Month**	**SST** (°C)[§]	**Salinity**[§]	pK_B^* [◇]	**TAlk** (μmol/kg)[♣]	Δ**pCO$_2$ (ppm)**[§]	**Gloor corr.**[♯]	**pCO$_2$**[†]	**SiO$_2^-$**[♭]	**PO$_4^{--}$**[♭]	**pH**	$\delta^{11}B_{B(OH)_4^-}$ (‰)	**DIC** (μmol/kg)	**B(OH)$_4^-$ /HCO$_3^-$**	**B(OH)$_4^-$/DIC**	**CO$_3^{2-}$** (μmol/kg)	Ω_{CaCO_3}	**[B] (μmol/kg)**
J50	NIWA	170.65	-36.67	167.5	-40	0.048	1	17.77	35.29	8.681	2322.0	-31.0	0.23	271.7	1.6	0.13	8.187	18.63	1995.2	0.0602	0.0531	225	5.36	436.2
J50	NIWA	170.65	-36.67	167.5	-40	0.048	2	18.58	35.36	8.671	2325.1	-22.5	0.23	273.7	1.6	0.13	8.184	18.71	1991.6	0.0613	0.0540	230	5.47	437.0
J50	NIWA	170.65	-36.67	167.5	-40	0.048	3	18.05	35.19	8.678	2316.4	-21.7	0.23	273.9	1.6	0.13	8.183	18.62	1990.5	0.0600	0.0530	225	5.35	434.9
J50	NIWA	170.65	-36.67	167.5	-40	0.048	4	17.05	35.23	8.690	2319.4	-26.3	0.23	272.8	1.6	0.13	8.186	18.52	2000.8	0.0586	0.0519	220	5.22	435.4
J50	NIWA	170.65	-36.67	167.5	-40	0.048	5	15.87	35.35	8.703	2327.2	-28.7	0.23	272.2	1.6	0.13	8.188	18.39	2016.5	0.0570	0.0507	214	5.09	436.9
J50	NIWA	170.65	-36.67	167.5	-40	0.048	6	14.70	35.45	8.717	2334.2	-32.6	0.23	271.3	1.6	0.13	8.191	18.27	2031.2	0.0555	0.0495	209	4.95	438.2
J50	NIWA	170.65	-36.67	167.5	-40	0.048	7	13.93	35.33	8.727	2328.8	-39.0	0.23	269.8	1.6	0.13	8.193	18.17	2033.1	0.0542	0.0485	204	4.84	436.7
J50	NIWA	170.65	-36.67	167.5	-40	0.048	8	13.48	35.31	8.733	2328.4	-43.8	0.23	268.7	1.6	0.13	8.194	18.13	2036.0	0.0537	0.0481	202	4.78	436.4
J50	NIWA	170.65	-36.67	167.5	-40	0.048	9	13.49	35.29	8.733	2327.3	-45.5	0.23	268.3	1.6	0.13	8.195	18.13	2034.8	0.0537	0.0481	202	4.78	436.2
J50	NIWA	170.65	-36.67	167.5	-40	0.048	10	13.86	35.44	8.728	2334.9	-43.1	0.23	268.9	1.6	0.13	8.195	18.19	2037.4	0.0545	0.0487	205	4.86	438.0
J50	NIWA	170.65	-36.67	167.5	-40	0.048	11	14.84	35.22	8.717	2321.5	-45.8	0.23	268.3	1.6	0.13	8.194	18.30	2018.6	0.0558	0.0497	209	4.96	435.3
J50	NIWA	170.65	-36.67	167.5	-40	0.048	12	16.28	35.29	8.699	2323.5	-41.9	0.23	269.2	1.6	0.13	8.192	18.48	2007.7	0.0581	0.0515	218	5.17	436.2
J50	NIWA	170.65	-36.67	167.5	-36	0.096	1	19.85	35.60	8.654	2337.6	-29.3	0.23	272.1	1.6	0.13	8.186	18.93	1987.2	0.0643	0.0562	241	5.74	440.0
J50	NIWA	170.65	-36.67	167.5	-36	0.096	2	20.64	35.57	8.645	2335.6	-19.7	0.23	274.3	1.6	0.13	8.182	18.99	1980.3	0.0652	0.0569	245	5.83	439.6
J50	NIWA	170.65	-36.67	167.5	-36	0.096	3	20.24	35.60	8.650	2337.4	-22.7	0.23	273.6	1.6	0.13	8.183	18.96	1984.7	0.0647	0.0565	243	5.78	440.0
J50	NIWA	170.65	-36.67	167.5	-36	0.096	4	19.31	35.63	8.660	2339.6	-28.4	0.23	272.3	1.6	0.13	8.186	18.86	1993.7	0.0634	0.0555	238	5.66	440.4
J50	NIWA	170.65	-36.67	167.5	-36	0.096	5	18.10	35.68	8.675	2343.2	-35.1	0.23	270.8	1.6	0.13	8.190	18.74	2006.2	0.0616	0.0542	232	5.51	441.0
J50	NIWA	170.65	-36.67	167.5	-36	0.096	6	16.79	35.69	8.691	2345.0	-31.9	0.23	271.5	1.6	0.13	8.190	18.56	2020.1	0.0593	0.0524	224	5.31	441.1
J50	NIWA	170.65	-36.67	167.5	-36	0.096	7	15.90	35.66	8.701	2344.3	-33.5	0.23	271.1	1.6	0.13	8.191	18.45	2027.4	0.0578	0.0513	218	5.18	440.8
J50	NIWA	170.65	-36.67	167.5	-36	0.096	8	15.41	35.53	8.708	2337.7	-35.9	0.23	270.6	1.6	0.13	8.192	18.38	2026.7	0.0569	0.0506	214	5.08	439.2
J50	NIWA	170.65	-36.67	167.5	-36	0.096	9	15.41	35.48	8.708	2334.9	-40.7	0.23	269.4	1.6	0.13	8.193	18.39	2023.9	0.0570	0.0507	214	5.08	438.5
J50	NIWA	170.65	-36.67	167.5	-36	0.096	10	15.87	35.58	8.702	2339.9	-38.4	0.23	270.0	1.6	0.13	8.192	18.45	2023.6	0.0578	0.0513	218	5.17	439.8
J50	NIWA	170.65	-36.67	167.5	-36	0.096	11	16.97	35.47	8.689	2332.6	-33.0	0.23	271.2	1.6	0.13	8.189	18.56	2009.5	0.0592	0.0524	223	5.29	438.4
J50	NIWA	170.65	-36.67	167.5	-36	0.096	12	18.42	35.60	8.671	2338.5	-43.8	0.23	268.7	1.6	0.13	8.192	18.80	1998.3	0.0624	0.0548	234	5.56	440.0
J50	NIWA	170.65	-36.67	172.5	-40	0.069	1	18.05	35.10	8.678	2311.6	-29.4	0.23	272.1	1.6	0.13	8.185	18.64	1985.7	0.0602	0.0531	225	5.35	433.8
J50	NIWA	170.65	-36.67	172.5	-40	0.069	2	18.96	35.25	8.667	2318.9	-24.7	0.23	273.2	1.6	0.13	8.184	18.76	1983.4	0.0618	0.0543	231	5.51	435.7
J50	NIWA	170.65	-36.67	172.5	-40	0.069	3	18.46	35.11	8.673	2311.8	-20.2	0.23	274.2	1.6	0.13	8.182	18.66	1983.8	0.0605	0.0533	226	5.39	434.0
J50	NIWA	170.65	-36.67	172.5	-40	0.069	4	17.34	35.28	8.686	2321.8	-21.0	0.23	274.0	1.6	0.13	8.184	18.54	2000.8	0.0590	0.0522	221	5.26	436.1
J50	NIWA	170.65	-36.67	172.5	-40	0.069	5	16.10	35.29	8.701	2323.7	-19.7	0.23	274.3	1.6	0.13	8.185	18.38	2013.5	0.0569	0.0506	214	5.08	436.2
J50	NIWA	170.65	-36.67	172.5	-40	0.069	6	14.87	35.33	8.716	2327.4	-31.1	0.23	271.7	1.6	0.13	8.190	18.27	2025.1	0.0555	0.0495	208	4.95	436.7
J50	NIWA	170.65	-36.67	172.5	-40	0.069	7	14.04	35.36	8.726	2330.2	-22.8	0.23	273.6	1.6	0.13	8.188	18.14	2036.1	0.0539	0.0482	203	4.82	437.0
J50	NIWA	170.65	-36.67	172.5	-40	0.069	8	13.56	35.24	8.733	2324.5	-41.4	0.23	269.3	1.6	0.13	8.193	18.12	2032.9	0.0536	0.0480	201	4.77	435.6

		Site		Nearest Takahashi Sites																			
Site	**Archive**[ℵ]	**Long (°E)**	**Lat (°N)**	**Long (°E)**	**Lat (°N)**	$\frac{1}{SS_D}$ [∀]	**Month**	**SST (°C)**[§]	**Salinity**[§]	pK_B^* [◇]	**TAlk** (μmol/kg)[♣]	Δ**pCO$_2$ (ppm)**[§]	**Gloor corr.**[♯]	**pCO$_2$**[†]	**SiO$_2$**[♭]	**PO$_4^-$**[♭]	**pH**	$\delta^{11}B_{B(OH)_4^-}$ (‰)	**DIC** (μmol/kg)	**B(OH)$_4^-$ /HCO$_3^-$**	**B(OH)$_4^-$/DIC**	**CO$_3^{2-}$** (μmol/kg)	Ω_{CaCO_3}	**[B] (μmol/kg)**
J50	NIWA	170.65	-36.67	172.5	-40	0.069	9	13.56	35.33	8.732	2329.4	-49.4	0.23	267.4	1.6	0.13	8.196	18.16	2035.0	0.0541	0.0484	203	4.81	436.7
J50	NIWA	170.65	-36.67	172.5	-40	0.069	10	14.02	35.31	8.726	2327.5	-77.5	0.23	260.9	1.6	0.13	8.205	18.31	2024.4	0.0559	0.0498	209	4.95	436.4
J50	NIWA	170.65	-36.67	172.5	-40	0.069	11	15.13	35.17	8.714	2318.4	-26.6	0.23	272.7	1.6	0.13	8.187	18.27	2017.2	0.0554	0.0494	208	4.94	434.7
J50	NIWA	170.65	-36.67	172.5	-40	0.069	12	16.58	35.22	8.696	2319.4	-35.4	0.23	270.7	1.6	0.13	8.189	18.49	2003.3	0.0582	0.0516	218	5.18	435.3
J50	NIWA	170.65	-36.67	172.5	-36	0.259	1	19.92	35.56	8.654	2335.3	-13.5	0.23	275.8	1.6	0.13	8.181	18.88	1988.0	0.0636	0.0557	239	5.69	439.5
J50	NIWA	170.65	-36.67	172.5	-36	0.259	2	20.72	35.53	8.644	2333.3	-11.7	0.23	276.2	1.6	0.13	8.179	18.97	1979.6	0.0649	0.0566	244	5.81	439.2
J50	NIWA	170.65	-36.67	172.5	-36	0.259	3	20.28	35.52	8.650	2332.9	-19.5	0.23	274.4	1.6	0.13	8.182	18.94	1981.9	0.0645	0.0563	242	5.76	439.0
J50	NIWA	170.65	-36.67	172.5	-36	0.259	4	19.19	35.63	8.662	2339.6	-27.4	0.23	272.5	1.6	0.13	8.186	18.84	1995.1	0.0631	0.0553	237	5.64	440.4
J50	NIWA	170.65	-36.67	172.5	-36	0.259	5	17.92	35.57	8.677	2337.2	-34.7	0.23	270.9	1.6	0.13	8.189	18.70	2003.7	0.0611	0.0538	230	5.45	439.6
J50	NIWA	170.65	-36.67	172.5	-36	0.259	6	16.59	35.62	8.693	2341.3	-33.0	0.23	271.2	1.6	0.13	8.190	18.53	2019.1	0.0589	0.0521	222	5.27	440.3
J50	NIWA	170.65	-36.67	172.5	-36	0.259	7	15.68	35.63	8.704	2342.9	-32.7	0.23	271.3	1.6	0.13	8.191	18.41	2028.6	0.0574	0.0510	217	5.13	440.4
J50	NIWA	170.65	-36.67	172.5	-36	0.259	8	15.17	35.49	8.711	2335.8	-35.2	0.23	270.7	1.6	0.13	8.192	18.34	2027.7	0.0564	0.0502	212	5.04	438.7
J50	NIWA	170.65	-36.67	172.5	-36	0.259	9	15.17	35.54	8.711	2338.5	-54.4	0.23	266.3	1.6	0.13	8.198	18.41	2026.1	0.0572	0.0509	215	5.10	439.3
J50	NIWA	170.65	-36.67	172.5	-36	0.259	10	15.68	35.51	8.705	2336.2	-69.0	0.23	262.9	1.6	0.13	8.202	18.52	2017.1	0.0586	0.0520	220	5.21	438.9
J50	NIWA	170.65	-36.67	172.5	-36	0.259	11	16.89	35.46	8.691	2332.1	-25.4	0.23	273.0	1.6	0.13	8.187	18.52	2011.3	0.0588	0.0520	221	5.25	438.3
J50	NIWA	170.65	-36.67	172.5	-36	0.259	12	18.44	35.54	8.671	2335.1	-36.0	0.23	270.5	1.6	0.13	8.189	18.76	1997.3	0.0620	0.0545	233	5.53	439.3
^{14}C age =1.564ka, CO_2 = 278.9 ppm			**Interpolated[∇] average**					**17.20**	**35.49**	**8.687**	**2333.9**	**-33.0**		**271.2**			**8.189**	**18.59**	**2008.2**	**0.0597**	**0.0527**	**224**	**5.33**	**438.7**
			Interpolated[∇] intraannual variation					**4.00**	**0.13**	**0.037**	**8.2**	**27.3**		**6.3**			**0.009**	**0.45**	**27.5**	**0.0046**	**0.0035**	**17**	**0.41**	**1.2**
IODP 1308	IODP (T. Chalk)	-24.24	49.88	-27.5	40	0.071	1	12.40	35.52	8.745	2340.3	-25.3	0.04	278.1	0.34	0.04	8.184	17.88	2061.2	0.0509	0.0459	193	4.57	439.0
IODP 1308	IODP (T. Chalk)	-24.24	49.88	-27.5	40	0.071	2	12.12	35.54	8.749	2341.6	-22.0	0.04	278.2	0.34	0.04	8.184	17.85	2064.6	0.0505	0.0455	191	4.54	439.3
IODP 1308	IODP (T. Chalk)	-24.24	49.88	-27.5	40	0.071	3	12.14	35.53	8.749	2341.0	-25.2	0.04	278.1	0.34	0.04	8.184	17.85	2064.0	0.0505	0.0456	192	4.54	439.2
IODP 1308	IODP (T. Chalk)	-24.24	49.88	-27.5	40	0.071	4	12.48	35.53	8.744	2340.8	-30.4	0.04	277.9	0.34	0.04	8.184	17.90	2060.7	0.0511	0.0460	194	4.59	439.2
IODP 1308	IODP (T. Chalk)	-24.24	49.88	-27.5	40	0.071	5	13.36	35.53	8.733	2340.3	-27.6	0.04	278.0	0.34	0.04	8.184	18.01	2052.7	0.0524	0.0471	199	4.71	439.2
IODP 1308	IODP (T. Chalk)	-24.24	49.88	-27.5	40	0.071	6	14.67	35.55	8.717	2340.6	-45.2	0.04	277.3	0.34	0.04	8.184	18.19	2040.8	0.0546	0.0488	207	4.91	439.4
IODP 1308	IODP (T. Chalk)	-24.24	49.88	-27.5	40	0.071	7	16.56	35.53	8.694	2337.9	-32.0	0.04	277.8	0.34	0.04	8.182	18.42	2022.4	0.0575	0.0510	218	5.17	439.2
IODP 1308	IODP (T. Chalk)	-24.24	49.88	-27.5	40	0.071	8	17.53	35.47	8.683	2333.6	-14.9	0.04	278.5	0.34	0.04	8.180	18.53	2011.1	0.0589	0.0521	223	5.29	438.4
IODP 1308	IODP (T. Chalk)	-24.24	49.88	-27.5	40	0.071	9	16.99	35.48	8.689	2334.7	-13.2	0.04	278.6	0.34	0.04	8.180	18.46	2016.8	0.0580	0.0514	220	5.21	438.5
IODP 1308	IODP (T. Chalk)	-24.24	49.88	-27.5	40	0.071	10	15.44	35.48	8.708	2336.0	-17.1	0.04	278.4	0.34	0.04	8.182	18.26	2031.5	0.0555	0.0495	210	4.99	438.5
IODP 1308	IODP (T. Chalk)	-24.24	49.88	-27.5	40	0.071	11	13.96	35.46	8.726	2336.0	-14.6	0.04	278.5	0.34	0.04	8.182	18.07	2044.7	0.0531	0.0476	201	4.77	438.3
IODP 1308	IODP (T. Chalk)	-24.24	49.88	-27.5	40	0.071	12	13.15	35.47	8.736	2337.0	-30.2	0.04	277.9	0.34	0.04	8.183	17.98	2052.1	0.0520	0.0467	197	4.67	438.4

		Site		Nearest Takahashi Sites																			
Site	**Archive**[ж]	**Long (°E)**	**Lat (°N)**	**Long (°E)**	**Lat (°N)**	$\frac{1}{SS_D}$[∀]	**Month**	**SST (°C)**[§]	**Salinity**[§]	pK_B^*[◇]	**TAlk** (μmol/kg)[♣]	Δ**pCO$_2$ (ppm)**[§]	**Gloor corr.**[♯]	**pCO$_2$**[†]	**SiO$_2$**[♭]	**PO$_4^-$**[♭]	**pH**	$\delta^{11}B_{B(OH)_4^-}$ (‰)	**DIC** (μmol/kg)	**B(OH)$_4^-$ /HCO$_3^-$**	**B(OH)$_4^-$/DIC**	**CO$_3^{2-}$** (μmol/kg)	Ω_{CaCO_3}	**[B] (μmol/kg)**
IODP 1308	IODP (T. Chalk)	-24.24	49.88	-27.5	52	0.066	1	9.57	35.17	8.783	2322.0	-21.4	0.04	278.2	0.34	0.04	8.182	17.48	2071.9	0.0462	0.0420	173	4.12	434.7
IODP 1308	IODP (T. Chalk)	-24.24	49.88	-27.5	52	0.066	2	9.22	35.26	8.787	2327.1	-20.5	0.04	278.3	0.34	0.04	8.182	17.44	2078.6	0.0458	0.0417	172	4.09	435.8
IODP 1308	IODP (T. Chalk)	-24.24	49.88	-27.5	52	0.066	3	9.34	35.26	8.786	2327.0	-21.8	0.04	278.2	0.34	0.04	8.182	17.46	2077.5	0.0460	0.0419	173	4.10	435.8
IODP 1308	IODP (T. Chalk)	-24.24	49.88	-27.5	52	0.066	4	9.77	35.20	8.780	2323.6	-29.3	0.04	277.9	0.34	0.04	8.182	17.51	2071.1	0.0465	0.0423	175	4.15	435.1
IODP 1308	IODP (T. Chalk)	-24.24	49.88	-27.5	52	0.066	5	10.76	35.17	8.768	2321.6	-41.4	0.04	277.4	0.34	0.04	8.183	17.64	2061.0	0.0480	0.0435	180	4.28	434.7
IODP 1308	IODP (T. Chalk)	-24.24	49.88	-27.5	52	0.066	6	12.17	35.18	8.750	2321.4	-53.5	0.04	277.0	0.34	0.04	8.183	17.83	2048.5	0.0502	0.0453	189	4.48	434.8
IODP 1308	IODP (T. Chalk)	-24.24	49.88	-27.5	52	0.066	7	13.73	35.19	8.731	2321.1	-45.5	0.04	277.3	0.34	0.04	8.182	18.03	2035.0	0.0525	0.0471	198	4.69	434.9
IODP 1308	IODP (T. Chalk)	-24.24	49.88	-27.5	52	0.066	8	14.50	35.08	8.722	2314.5	-27.7	0.04	278.0	0.34	0.04	8.180	18.10	2024.1	0.0534	0.0478	201	4.77	433.6
IODP 1308	IODP (T. Chalk)	-24.24	49.88	-27.5	52	0.066	9	14.05	35.05	8.727	2313.2	-15.3	0.04	278.5	0.34	0.04	8.180	18.03	2027.4	0.0526	0.0472	197	4.70	433.2
IODP 1308	IODP (T. Chalk)	-24.24	49.88	-27.5	52	0.066	10	12.56	35.14	8.745	2319.0	-17.0	0.04	278.4	0.34	0.04	8.181	17.85	2044.5	0.0505	0.0455	190	4.51	434.3
IODP 1308	IODP (T. Chalk)	-24.24	49.88	-27.5	52	0.066	11	11.21	35.10	8.763	2317.5	-24.0	0.04	278.1	0.34	0.04	8.181	17.68	2054.7	0.0484	0.0439	182	4.32	433.8
IODP 1308	IODP (T. Chalk)	-24.24	49.88	-27.5	52	0.066	12	10.32	35.11	8.774	2318.5	-24.2	0.04	278.1	0.34	0.04	8.182	17.57	2062.9	0.0472	0.0428	177	4.20	434.0
IODP 1308	IODP (T. Chalk)	-24.24	49.88	-22.5	48	0.153	1	12.50	35.54	8.744	2341.4	-26.7	0.04	278.0	0.34	0.04	8.184	17.90	2061.1	0.0511	0.0460	194	4.59	439.3
IODP 1308	IODP (T. Chalk)	-24.24	49.88	-22.5	48	0.153	2	12.20	35.55	8.748	2342.1	-16.1	0.04	278.5	0.34	0.04	8.184	17.86	2064.5	0.0506	0.0456	192	4.55	439.4
IODP 1308	IODP (T. Chalk)	-24.24	49.88	-22.5	48	0.153	3	12.17	35.58	8.748	2343.9	-15.7	0.04	278.5	0.34	0.04	8.184	17.86	2066.0	0.0506	0.0456	192	4.55	439.8
IODP 1308	IODP (T. Chalk)	-24.24	49.88	-22.5	48	0.153	4	12.46	35.55	8.745	2342.0	-23.6	0.04	278.2	0.34	0.04	8.184	17.89	2061.9	0.0510	0.0460	194	4.59	439.4
IODP 1308	IODP (T. Chalk)	-24.24	49.88	-22.5	48	0.153	5	13.35	35.58	8.733	2343.2	-47.9	0.04	277.2	0.34	0.04	8.185	18.03	2054.3	0.0526	0.0472	200	4.73	439.8
IODP 1308	IODP (T. Chalk)	-24.24	49.88	-22.5	48	0.153	6	14.89	35.57	8.714	2341.5	-84.5	0.04	275.7	0.34	0.04	8.186	18.24	2038.4	0.0552	0.0493	209	4.96	439.6
IODP 1308	IODP (T. Chalk)	-24.24	49.88	-22.5	48	0.153	7	16.77	35.58	8.691	2340.6	-26.2	0.04	278.1	0.34	0.04	8.182	18.45	2022.5	0.0579	0.0514	220	5.21	439.8
IODP 1308	IODP (T. Chalk)	-24.24	49.88	-22.5	48	0.153	8	17.75	35.58	8.679	2339.6	-32.7	0.04	277.8	0.34	0.04	8.181	18.58	2012.8	0.0596	0.0526	226	5.36	439.8
IODP 1308	IODP (T. Chalk)	-24.24	49.88	-22.5	48	0.153	9	17.18	35.55	8.687	2338.5	-24.9	0.04	278.1	0.34	0.04	8.181	18.50	2017.4	0.0585	0.0518	222	5.26	439.4
IODP 1308	IODP (T. Chalk)	-24.24	49.88	-22.5	48	0.153	10	15.62	35.59	8.705	2342.1	-30.3	0.04	277.9	0.34	0.04	8.183	18.31	2033.9	0.0561	0.0499	213	5.05	439.9
IODP 1308	IODP (T. Chalk)	-24.24	49.88	-22.5	48	0.153	11	14.08	35.51	8.725	2338.7	-22.2	0.04	278.2	0.34	0.04	8.183	18.10	2045.4	0.0535	0.0479	203	4.80	438.9
IODP 1308	IODP (T. Chalk)	-24.24	49.88	-22.5	48	0.153	12	13.19	35.52	8.736	2339.8	-32.2	0.04	277.8	0.34	0.04	8.184	17.99	2053.7	0.0522	0.0469	198	4.69	439.0
IODP 1308	IODP (T. Chalk)	-24.24	49.88	-22.5	52	0.133	1	10.59	35.31	8.769	2329.4	-20.3	0.04	278.3	0.34	0.04	8.183	17.62	2068.8	0.0478	0.0434	180	4.28	436.4
IODP 1308	IODP (T. Chalk)	-24.24	49.88	-22.5	52	0.133	2	10.25	35.36	8.773	2332.3	-19.3	0.04	278.3	0.34	0.04	8.183	17.59	2073.9	0.0474	0.0431	179	4.24	437.0
IODP 1308	IODP (T. Chalk)	-24.24	49.88	-22.5	52	0.133	3	10.23	35.39	8.774	2334.0	-15.0	0.04	278.5	0.34	0.04	8.183	17.58	2075.4	0.0474	0.0430	179	4.25	437.4
IODP 1308	IODP (T. Chalk)	-24.24	49.88	-22.5	52	0.133	4	10.60	35.31	8.769	2329.4	-3.9	0.04	278.9	0.34	0.04	8.182	17.62	2069.2	0.0478	0.0433	180	4.27	436.4
IODP 1308	IODP (T. Chalk)	-24.24	49.88	-22.5	52	0.133	5	11.52	35.29	8.758	2327.8	-44.7	0.04	277.3	0.34	0.04	8.184	17.75	2059.1	0.0493	0.0446	186	4.41	436.2
IODP 1308	IODP (T. Chalk)	-24.24	49.88	-22.5	52	0.133	6	12.93	35.36	8.740	2331.0	-50.6	0.04	277.1	0.34	0.04	8.184	17.95	2049.0	0.0516	0.0464	195	4.62	437.0
IODP 1308	IODP (T. Chalk)	-24.24	49.88	-22.5	52	0.133	7	14.49	35.38	8.720	2331.1	-47.0	0.04	277.2	0.34	0.04	8.183	18.15	2035.5	0.0540	0.0483	204	4.84	437.3
IODP 1308	IODP (T. Chalk)	-24.24	49.88	-22.5	52	0.133	8	15.25	35.32	8.711	2327.2	-44.8	0.04	277.3	0.34	0.04	8.182	18.24	2026.1	0.0551	0.0492	208	4.94	436.6

		Site		Nearest Takahashi Sites																			
Site	**Archive**[ж]	**Long (°E)**	**Lat (°N)**	**Long (°E)**	**Lat (°N)**	$\frac{1}{SS_D}$ [∀]	**Month**	**SST (°C)**[§]	**Salinity**[§]	pK_B^* [◇]	**TAlk** (μmol/kg)[♣]	Δ**pCO$_2$ (ppm)**[§]	**Gloor corr.**[♯]	**pCO$_2$**[†]	**SiO$_2$**[♭]	**PO$_4^-$**[♭]	**pH**	$\delta^{11}B_{B(OH)_4^-}$ (‰)	**DIC** (μmol/kg)	**B(OH)$_4^-$ /HCO$_3^-$**	**B(OH)$_4^-$/DIC**	**CO$_3^{2-}$** (μmol/kg)	Ω_{CaCO_3}	**[B] (μmol/kg)**
IODP 1308	IODP (T. Chalk)	-24.24	49.88	-22.5	52	0.133	9	14.78	35.24	8.717	2323.1	-31.1	0.04	277.9	0.34	0.04	8.181	18.16	2027.7	0.0541	0.0484	204	4.85	435.6
IODP 1308	IODP (T. Chalk)	-24.24	49.88	-22.5	52	0.133	10	13.38	35.32	8.734	2328.5	-23.3	0.04	278.2	0.34	0.04	8.182	17.98	2044.1	0.0521	0.0468	197	4.66	436.6
IODP 1308	IODP (T. Chalk)	-24.24	49.88	-22.5	52	0.133	11	12.09	35.27	8.751	2326.4	-24.5	0.04	278.1	0.34	0.04	8.182	17.81	2053.7	0.0500	0.0452	189	4.48	435.9
IODP 1308	IODP (T. Chalk)	-24.24	49.88	-22.5	52	0.133	12	11.29	35.30	8.761	2328.5	-23.0	0.04	278.2	0.34	0.04	8.183	17.71	2062.1	0.0489	0.0442	184	4.37	436.3
Age = 0.390ka, CO_2 = 279.1 ppm			**Interpolated[▽] average**					**13.22**	**35.41**	**8.736**	**2333.6**	**-29.3**		**277.9**			**8.183**	**17.98**	**2048.8**	**0.0521**	**0.0468**	**197**	**4.67**	**437.7**
			Interpolated[▽] intraannual variation					**3.90**	**0.08**	**0.029**	**5.3**	**29.5**		**1.2**			**0.001**	**0.50**	**37.1**	**0.0061**	**0.0048**	**23**	**0.55**	**1.0**
IODP 1313	IODP (T. Chalk)	-32.96	41.00	-37.5	40	0.046	1	16.83	36.16	8.688	2374.6	-26.2	0.04	278.1	0.66	0.02	8.185	18.53	2046.1	0.0591	0.0523	227	5.36	446.9
IODP 1313	IODP (T. Chalk)	-32.96	41.00	-37.5	40	0.046	2	16.33	36.10	8.694	2371.4	-15.0	0.04	278.5	0.66	0.02	8.185	18.46	2048.8	0.0581	0.0515	223	5.27	446.2
IODP 1313	IODP (T. Chalk)	-32.96	41.00	-37.5	40	0.046	3	16.21	36.14	8.695	2373.9	-30.3	0.04	277.9	0.66	0.02	8.186	18.45	2051.2	0.0581	0.0515	223	5.26	446.7
IODP 1313	IODP (T. Chalk)	-32.96	41.00	-37.5	40	0.046	4	16.56	36.13	8.691	2373.0	-26.3	0.04	278.0	0.66	0.02	8.185	18.50	2047.4	0.0586	0.0519	225	5.31	446.6
IODP 1313	IODP (T. Chalk)	-32.96	41.00	-37.5	40	0.046	5	17.60	36.24	8.678	2378.7	-33.7	0.04	277.8	0.66	0.02	8.185	18.65	2041.6	0.0606	0.0534	233	5.50	447.9
IODP 1313	IODP (T. Chalk)	-32.96	41.00	-37.5	40	0.046	6	19.44	36.19	8.656	2373.7	-23.5	0.04	278.2	0.66	0.02	8.182	18.87	2021.2	0.0636	0.0557	243	5.76	447.3
IODP 1313	IODP (T. Chalk)	-32.96	41.00	-37.5	40	0.046	7	22.30	36.22	8.622	2372.0	-7.7	0.04	278.8	0.66	0.02	8.178	19.22	1993.3	0.0687	0.0594	261	6.20	447.7
IODP 1313	IODP (T. Chalk)	-32.96	41.00	-37.5	40	0.046	8	23.94	36.14	8.603	2364.9	4.9	0.04	279.3	0.66	0.02	8.174	19.41	1973.1	0.0715	0.0614	270	6.43	446.7
IODP 1313	IODP (T. Chalk)	-32.96	41.00	-37.5	40	0.046	9	23.20	36.13	8.612	2365.4	2.0	0.04	279.2	0.66	0.02	8.175	19.32	1980.5	0.0701	0.0604	266	6.31	446.6
IODP 1313	IODP (T. Chalk)	-32.96	41.00	-37.5	40	0.046	10	21.34	36.03	8.634	2361.9	-19.4	0.04	278.3	0.66	0.02	8.179	19.08	1995.2	0.0667	0.0579	253	6.00	445.3
IODP 1313	IODP (T. Chalk)	-32.96	41.00	-37.5	40	0.046	11	19.34	36.09	8.658	2367.8	-22.5	0.04	278.2	0.66	0.02	8.182	18.84	2018.1	0.0632	0.0554	241	5.72	446.1
IODP 1313	IODP (T. Chalk)	-32.96	41.00	-37.5	40	0.046	12	17.83	36.10	8.676	2370.0	-33.2	0.04	277.8	0.66	0.02	8.184	18.66	2033.3	0.0607	0.0535	232	5.50	446.2
IODP 1313	IODP (T. Chalk)	-32.96	41.00	-37.5	44	0.034	1	14.92	35.84	8.713	2357.1	-13.4	0.04	278.6	0.66	0.02	8.184	18.24	2051.4	0.0553	0.0493	211	5.00	443.0
IODP 1313	IODP (T. Chalk)	-32.96	41.00	-37.5	44	0.034	2	14.48	35.87	8.718	2359.2	-21.3	0.04	278.2	0.66	0.02	8.185	18.19	2056.6	0.0547	0.0489	209	4.94	443.4
IODP 1313	IODP (T. Chalk)	-32.96	41.00	-37.5	44	0.034	3	14.38	35.87	8.719	2359.3	-36.5	0.04	277.6	0.66	0.02	8.186	18.19	2057.1	0.0546	0.0488	209	4.94	443.4
IODP 1313	IODP (T. Chalk)	-32.96	41.00	-37.5	44	0.034	4	14.68	35.85	8.715	2357.9	-24.1	0.04	278.1	0.66	0.02	8.185	18.22	2053.8	0.0550	0.0491	210	4.97	443.1
IODP 1313	IODP (T. Chalk)	-32.96	41.00	-37.5	44	0.034	5	15.55	35.95	8.704	2363.1	-30.2	0.04	277.9	0.66	0.02	8.185	18.35	2049.5	0.0566	0.0504	217	5.12	444.3
IODP 1313	IODP (T. Chalk)	-32.96	41.00	-37.5	44	0.034	6	16.90	35.93	8.688	2360.8	-45.4	0.04	277.3	0.66	0.02	8.185	18.52	2035.1	0.0589	0.0521	225	5.32	444.1
IODP 1313	IODP (T. Chalk)	-32.96	41.00	-37.5	44	0.034	7	19.45	35.79	8.658	2350.0	-22.1	0.04	278.2	0.66	0.02	8.180	18.81	2004.7	0.0628	0.0551	238	5.66	442.4
IODP 1313	IODP (T. Chalk)	-32.96	41.00	-37.5	44	0.034	8	20.99	35.69	8.640	2342.4	5.9	0.04	279.3	0.66	0.02	8.176	18.98	1985.9	0.0651	0.0568	246	5.85	441.1
IODP 1313	IODP (T. Chalk)	-32.96	41.00	-37.5	44	0.034	9	20.51	35.61	8.646	2338.3	-16.1	0.04	278.5	0.66	0.02	8.177	18.92	1987.0	0.0643	0.0562	243	5.77	440.1
IODP 1313	IODP (T. Chalk)	-32.96	41.00	-37.5	44	0.034	10	18.72	35.61	8.668	2340.4	-34.0	0.04	277.7	0.66	0.02	8.180	18.71	2004.4	0.0613	0.0539	232	5.51	440.1
IODP 1313	IODP (T. Chalk)	-32.96	41.00	-37.5	44	0.034	11	17.02	35.71	8.688	2347.8	-24.8	0.04	278.1	0.66	0.02	8.182	18.50	2025.4	0.0586	0.0519	223	5.28	441.4
IODP 1313	IODP (T. Chalk)	-32.96	41.00	-37.5	44	0.034	12	15.82	35.79	8.702	2353.5	-34.6	0.04	277.7	0.66	0.02	8.184	18.36	2040.1	0.0568	0.0505	216	5.12	442.4

		Site		Nearest Takahashi Sites																			
Site	**Archive**[ϰ]	**Long (°E)**	**Lat (°N)**	**Long (°E)**	**Lat (°N)**	$\frac{1}{SS_D}$[∀]	**Month**	**SST (°C)**[§]	**Salinity**[§]	pK_B^*[◇]	**TAlk (μmol/kg)**[♣]	**ΔpCO_2 (ppm)**[§]	**Gloor corr.**[♯]	**pCO_2**[†]	**SiO_2**[♭]	**PO_4^-**[♭]	**pH**	$\delta^{11}B_{B(OH)_4^-}$ (‰)	**DIC (μmol/kg)**	$B(OH)_4^-/HCO_3^-$	$B(OH)_4^-$/DIC	CO_3^{2-} (μmol/kg)	Ω_{CaCO_3}	**[B] (µmol/kg)**
IODP 1313	IODP (T. Chalk)	-32.96	41.00	-32.5	40	0.826	1	16.36	36.03	8.694	2367.2	-34.4	0.04	277.7	0.66	0.02	8.185	18.46	2044.9	0.0581	0.0515	223	5.26	445.3
IODP 1313	IODP (T. Chalk)	-32.96	41.00	-32.5	40	0.826	2	15.90	36.00	8.700	2365.8	-18.6	0.04	278.4	0.66	0.02	8.185	18.39	2048.6	0.0572	0.0508	219	5.18	445.0
IODP 1313	IODP (T. Chalk)	-32.96	41.00	-32.5	40	0.826	3	15.81	36.07	8.700	2370.0	-21.4	0.04	278.2	0.66	0.02	8.185	18.39	2052.4	0.0572	0.0508	219	5.18	445.8
IODP 1313	IODP (T. Chalk)	-32.96	41.00	-32.5	40	0.826	4	16.19	36.01	8.696	2366.1	-28.9	0.04	277.9	0.66	0.02	8.185	18.43	2045.9	0.0578	0.0512	221	5.23	445.1
IODP 1313	IODP (T. Chalk)	-32.96	41.00	-32.5	40	0.826	5	17.23	36.09	8.683	2370.0	-33.8	0.04	277.7	0.66	0.02	8.185	18.58	2038.9	0.0597	0.0527	229	5.40	446.1
IODP 1313	IODP (T. Chalk)	-32.96	41.00	-32.5	40	0.826	6	19.08	36.13	8.661	2370.5	-24.8	0.04	278.1	0.66	0.02	8.183	18.82	2022.3	0.0629	0.0551	240	5.69	446.6
IODP 1313	IODP (T. Chalk)	-32.96	41.00	-32.5	40	0.826	7	21.81	36.12	8.628	2366.7	-3.5	0.04	279.0	0.66	0.02	8.178	19.14	1994.5	0.0676	0.0586	257	6.09	446.4
IODP 1313	IODP (T. Chalk)	-32.96	41.00	-32.5	40	0.826	8	23.29	36.14	8.611	2365.8	15.1	0.04	279.7	0.66	0.02	8.175	19.32	1980.4	0.0702	0.0605	266	6.32	446.7
IODP 1313	IODP (T. Chalk)	-32.96	41.00	-32.5	40	0.826	9	22.64	36.14	8.618	2366.7	7.8	0.04	279.4	0.66	0.02	8.176	19.24	1987.0	0.0691	0.0597	262	6.22	446.7
IODP 1313	IODP (T. Chalk)	-32.96	41.00	-32.5	40	0.826	10	20.72	36.03	8.642	2362.6	-14.6	0.04	278.5	0.66	0.02	8.179	19.00	2001.7	0.0655	0.0571	249	5.91	445.3
IODP 1313	IODP (T. Chalk)	-32.96	41.00	-32.5	40	0.826	11	18.76	36.03	8.665	2364.9	-19.2	0.04	278.3	0.66	0.02	8.182	18.76	2021.5	0.0621	0.0545	237	5.61	445.3
IODP 1313	IODP (T. Chalk)	-32.96	41.00	-32.5	40	0.826	12	17.32	36.00	8.682	2364.5	-66.6	0.04	276.4	0.66	0.02	8.186	18.60	2033.2	0.0599	0.0529	229	5.41	445.0
IODP 1313	IODP (T. Chalk)	-32.96	41.00	-32.5	44	0.109	1	14.58	35.83	8.717	2356.8	-21.8	0.04	278.2	0.66	0.02	8.185	18.20	2054.0	0.0548	0.0489	209	4.95	442.9
IODP 1313	IODP (T. Chalk)	-32.96	41.00	-32.5	44	0.109	2	14.26	35.79	8.721	2354.7	-28.3	0.04	278.0	0.66	0.02	8.185	18.16	2055.1	0.0543	0.0485	207	4.90	442.4
IODP 1313	IODP (T. Chalk)	-32.96	41.00	-32.5	44	0.109	3	14.27	35.86	8.720	2358.8	-28.3	0.04	278.0	0.66	0.02	8.185	18.17	2058.0	0.0544	0.0486	208	4.91	443.2
IODP 1313	IODP (T. Chalk)	-32.96	41.00	-32.5	44	0.109	4	14.62	35.81	8.716	2355.6	-27.4	0.04	278.0	0.66	0.02	8.185	18.21	2052.6	0.0549	0.0490	209	4.95	442.6
IODP 1313	IODP (T. Chalk)	-32.96	41.00	-32.5	44	0.109	5	15.51	35.87	8.705	2358.4	-36.3	0.04	277.6	0.66	0.02	8.185	18.33	2046.3	0.0565	0.0502	216	5.10	443.4
IODP 1313	IODP (T. Chalk)	-32.96	41.00	-32.5	44	0.109	6	16.96	35.93	8.687	2360.7	-43.4	0.04	277.4	0.66	0.02	8.184	18.53	2034.5	0.0590	0.0522	225	5.33	444.1
IODP 1313	IODP (T. Chalk)	-32.96	41.00	-32.5	44	0.109	7	19.43	35.84	8.658	2352.9	-26.8	0.04	278.0	0.66	0.02	8.180	18.82	2006.7	0.0629	0.0552	239	5.67	443.0
IODP 1313	IODP (T. Chalk)	-32.96	41.00	-32.5	44	0.109	8	20.69	35.81	8.643	2349.7	-11.6	0.04	278.6	0.66	0.02	8.178	18.97	1993.2	0.0650	0.0567	246	5.84	442.6
IODP 1313	IODP (T. Chalk)	-32.96	41.00	-32.5	44	0.109	9	20.17	35.77	8.649	2348.0	-6.3	0.04	278.8	0.66	0.02	8.178	18.89	1997.1	0.0639	0.0559	242	5.75	442.1
IODP 1313	IODP (T. Chalk)	-32.96	41.00	-32.5	44	0.109	10	18.33	35.67	8.672	2344.2	-27.3	0.04	278.0	0.66	0.02	8.181	18.66	2010.8	0.0607	0.0535	230	5.46	440.9
IODP 1313	IODP (T. Chalk)	-32.96	41.00	-32.5	44	0.109	11	16.61	35.77	8.692	2351.7	-32.5	0.04	277.8	0.66	0.02	8.183	18.46	2031.6	0.0581	0.0515	221	5.23	442.1
IODP 1313	IODP (T. Chalk)	-32.96	41.00	-32.5	44	0.109	12	15.45	35.78	8.706	2353.2	-23.5	0.04	278.2	0.66	0.02	8.184	18.31	2043.5	0.0561	0.0500	214	5.06	442.2
Age = 1.097ka, CO_2 = 279.1 ppm			**Interpolated[∇] average**					**18.50**	**36.03**	**8.668**	**2365.1**	**-21.0**		**278.3**			**8.182**	**18.73**	**2023.7**	**0.0618**	**0.0542**	**236**	**5.58**	**445.4**
			Interpolated[∇] intraannual variation					**5.38**	**0.12**	**0.066**	**5.9**	**38.8**		**1.6**			**0.008**	**0.67**	**52.0**	**0.0094**	**0.0070**	**34**	**0.82**	**1.5**
ODP 980	ODP (T. Chalk)	-14.70	55.49	-17.5	52	0.050	1	11.14	35.42	8.762	2335.3	-19.5	0.55	268.4	0.55	0.23	8.196	17.84	2061.1	0.0503	0.0454	189	4.48	437.8
ODP 980	ODP (T. Chalk)	-14.70	55.49	-17.5	52	0.050	2	10.84	35.43	8.766	2336.0	-18.5	0.55	269.0	0.55	0.23	8.196	17.80	2064.6	0.0498	0.0450	187	4.44	437.9
ODP 980	ODP (T. Chalk)	-14.70	55.49	-17.5	52	0.050	3	10.78	35.46	8.766	2337.7	-14.1	0.55	271.3	0.55	0.23	8.193	17.76	2068.2	0.0494	0.0447	186	4.41	438.3
ODP 980	ODP (T. Chalk)	-14.70	55.49	-17.5	52	0.050	4	11.05	35.40	8.763	2334.2	-8.4	0.55	274.5	0.55	0.23	8.188	17.74	2065.6	0.0492	0.0445	186	4.40	437.5

		Site		Nearest Takahashi Sites																			
Site	**Archive**[ℵ]	**Long (°E)**	**Lat (°N)**	**Long (°E)**	**Lat (°N)**	$\frac{1}{SSS_D}$ [∀]	**Month**	**SST (°C)**[§]	**Salinity**[§]	pK_B^* [◇]	**TAlk** (μmol/kg)[♣]	Δ**pCO$_2$ (ppm)**[§]	**Gloor corr.**[♯]	**pCO$_2$**[†]	**SiO$_2$**[♭]	**PO$_4^-$**[♭]	**pH**	$\delta^{11}B_{B(OH)_4^-}$ (‰)	**DIC** (μmol/kg)	**B(OH)$_4^-$ /HCO$_3^-$**	**B(OH)$_4^-$/DIC**	**CO$_3^{2-}$** (μmol/kg)	Ω_{CaCO_3}	**[B] (μmol/kg)**
ODP 980	ODP (T. Chalk)	-14.70	55.49	-17.5	52	0.050	5	11.91	35.44	8.752	2336.0	-55.1	0.55	248.8	0.55	0.23	8.223	18.24	2039.5	0.0548	0.0491	203	4.82	438.0
ODP 980	ODP (T. Chalk)	-14.70	55.49	-17.5	52	0.050	6	13.34	35.47	8.734	2336.9	-65.1	0.55	243.3	0.55	0.23	8.231	18.52	2022.5	0.0583	0.0518	216	5.11	438.4
ODP 980	ODP (T. Chalk)	-14.70	55.49	-17.5	52	0.050	7	14.97	35.46	8.714	2335.2	-45.3	0.55	254.2	0.55	0.23	8.214	18.56	2015.8	0.0589	0.0522	219	5.21	438.3
ODP 980	ODP (T. Chalk)	-14.70	55.49	-17.5	52	0.050	8	15.79	35.46	8.704	2334.6	-44.6	0.55	254.6	0.55	0.23	8.213	18.66	2008.2	0.0603	0.0532	224	5.32	438.3
ODP 980	ODP (T. Chalk)	-14.70	55.49	-17.5	52	0.050	9	15.28	35.40	8.710	2331.6	-35.2	0.55	259.7	0.55	0.23	8.206	18.51	2015.0	0.0583	0.0517	218	5.17	437.5
ODP 980	ODP (T. Chalk)	-14.70	55.49	-17.5	52	0.050	10	13.86	35.41	8.728	2333.2	-26.0	0.55	264.8	0.55	0.23	8.200	18.25	2033.0	0.0551	0.0492	207	4.90	437.7
ODP 980	ODP (T. Chalk)	-14.70	55.49	-17.5	52	0.050	11	12.55	35.38	8.744	2332.3	-23.2	0.55	266.4	0.55	0.23	8.198	18.05	2045.1	0.0527	0.0474	198	4.69	437.3
ODP 980	ODP (T. Chalk)	-14.70	55.49	-17.5	52	0.050	12	11.76	35.46	8.754	2337.2	-22.0	0.55	267.0	0.55	0.23	8.198	17.95	2056.1	0.0515	0.0464	194	4.59	438.3
ODP 980	ODP (T. Chalk)	-14.70	55.49	-17.5	56	0.124	1	9.92	35.34	8.778	2331.3	-18.6	0.55	268.9	0.55	0.23	8.195	17.67	2069.0	0.0483	0.0438	181	4.29	436.8
ODP 980	ODP (T. Chalk)	-14.70	55.49	-17.5	56	0.124	2	9.64	35.35	8.781	2331.9	-18.7	0.55	268.8	0.55	0.23	8.196	17.63	2071.8	0.0479	0.0435	179	4.26	436.9
ODP 980	ODP (T. Chalk)	-14.70	55.49	-17.5	56	0.124	3	9.56	35.36	8.782	2332.5	-20.8	0.55	267.7	0.55	0.23	8.197	17.64	2072.1	0.0479	0.0435	180	4.26	437.0
ODP 980	ODP (T. Chalk)	-14.70	55.49	-17.5	56	0.124	4	9.74	35.31	8.780	2329.7	-30.2	0.55	262.5	0.55	0.23	8.204	17.73	2064.6	0.0489	0.0443	183	4.33	436.4
ODP 980	ODP (T. Chalk)	-14.70	55.49	-17.5	56	0.124	5	10.52	35.31	8.770	2329.4	-44.2	0.55	254.8	0.55	0.23	8.215	17.95	2051.8	0.0513	0.0463	191	4.53	436.4
ODP 980	ODP (T. Chalk)	-14.70	55.49	-17.5	56	0.124	6	11.85	35.36	8.753	2331.6	-55.8	0.55	248.4	0.55	0.23	8.224	18.23	2036.5	0.0546	0.0489	202	4.80	437.0
ODP 980	ODP (T. Chalk)	-14.70	55.49	-17.5	56	0.124	7	13.21	35.32	8.736	2328.6	-46.2	0.55	253.7	0.55	0.23	8.215	18.32	2026.6	0.0558	0.0498	207	4.92	436.6
ODP 980	ODP (T. Chalk)	-14.70	55.49	-17.5	56	0.124	8	14.00	35.34	8.727	2329.2	-49.6	0.55	251.8	0.55	0.23	8.217	18.46	2018.3	0.0575	0.0512	213	5.07	436.8
ODP 980	ODP (T. Chalk)	-14.70	55.49	-17.5	56	0.124	9	13.34	35.29	8.735	2326.8	-39.1	0.55	257.6	0.55	0.23	8.209	18.27	2027.3	0.0553	0.0494	206	4.89	436.2
ODP 980	ODP (T. Chalk)	-14.70	55.49	-17.5	56	0.124	10	12.11	35.28	8.750	2327.0	-24.8	0.55	265.5	0.55	0.23	8.199	17.99	2044.4	0.0520	0.0468	195	4.62	436.1
ODP 980	ODP (T. Chalk)	-14.70	55.49	-17.5	56	0.124	11	11.04	35.36	8.763	2332.0	-21.8	0.55	267.1	0.55	0.23	8.198	17.84	2058.6	0.0502	0.0454	188	4.47	437.0
ODP 980	ODP (T. Chalk)	-14.70	55.49	-17.5	56	0.124	12	10.46	35.37	8.771	2332.8	-21.3	0.55	267.4	0.55	0.23	8.198	17.76	2064.4	0.0493	0.0446	185	4.39	437.2
ODP 980	ODP (T. Chalk)	-14.70	55.49	-12.5	52	0.059	1	10.84	35.42	8.766	2335.4	-19.5	0.55	268.4	0.55	0.23	8.196	17.81	2063.8	0.0499	0.0451	187	4.44	437.8
ODP 980	ODP (T. Chalk)	-14.70	55.49	-12.5	52	0.059	2	10.54	35.43	8.769	2336.1	-20.8	0.55	267.7	0.55	0.23	8.198	17.78	2066.4	0.0495	0.0448	186	4.41	437.9
ODP 980	ODP (T. Chalk)	-14.70	55.49	-12.5	52	0.059	3	10.48	35.44	8.770	2336.7	-24.4	0.55	265.7	0.55	0.23	8.200	17.80	2065.8	0.0498	0.0450	187	4.43	438.0
ODP 980	ODP (T. Chalk)	-14.70	55.49	-12.5	52	0.059	4	10.80	35.42	8.766	2335.4	-43.3	0.55	255.3	0.55	0.23	8.214	17.99	2054.1	0.0519	0.0467	193	4.58	437.8
ODP 980	ODP (T. Chalk)	-14.70	55.49	-12.5	52	0.059	5	11.81	35.43	8.753	2335.5	-74.5	0.55	238.1	0.55	0.23	8.239	18.40	2030.9	0.0566	0.0505	209	4.94	437.9
ODP 980	ODP (T. Chalk)	-14.70	55.49	-12.5	52	0.059	6	13.40	35.43	8.733	2334.6	-53.3	0.55	249.8	0.55	0.23	8.221	18.42	2025.9	0.0570	0.0508	212	5.02	437.9
ODP 980	ODP (T. Chalk)	-14.70	55.49	-12.5	52	0.059	7	15.12	35.38	8.713	2330.6	-43.3	0.55	255.3	0.55	0.23	8.212	18.55	2012.1	0.0588	0.0522	219	5.19	437.3
ODP 980	ODP (T. Chalk)	-14.70	55.49	-12.5	52	0.059	8	15.91	35.37	8.703	2329.4	-31.7	0.55	261.7	0.55	0.23	8.202	18.56	2009.3	0.0590	0.0522	220	5.23	437.2
ODP 980	ODP (T. Chalk)	-14.70	55.49	-12.5	52	0.059	9	15.30	35.34	8.711	2328.2	-28.9	0.55	263.2	0.55	0.23	8.201	18.45	2015.2	0.0576	0.0512	215	5.11	436.8
ODP 980	ODP (T. Chalk)	-14.70	55.49	-12.5	52	0.059	10	13.81	35.36	8.729	2330.4	-26.8	0.55	264.3	0.55	0.23	8.200	18.24	2031.1	0.0550	0.0492	206	4.89	437.0
ODP 980	ODP (T. Chalk)	-14.70	55.49	-12.5	52	0.059	11	12.38	35.38	8.746	2332.4	-20.0	0.55	268.1	0.55	0.23	8.196	18.00	2048.0	0.0522	0.0469	196	4.65	437.3
ODP 980	ODP (T. Chalk)	-14.70	55.49	-12.5	52	0.059	12	11.45	35.46	8.758	2337.4	-21.2	0.55	267.4	0.55	0.23	8.198	17.90	2059.3	0.0510	0.0460	192	4.54	438.3

		Site		Nearest Takahashi Sites																			
Site	**Archive**[ж]	**Long (°E)**	**Lat (°N)**	**Long (°E)**	**Lat (°N)**	$\frac{1}{SS_D}$ [∀]	**Month**	**SST (°C)**[§]	**Salinity**[§]	pK_B^* [◇]	**TAlk (μmol/kg)**[♣]	**ΔpCO_2 (ppm)**[§]	**Gloor corr.**[♯]	**pCO_2**[†]	**SiO_2**[♭]	**PO_4^-**[♭]	**pH**	$\delta^{11}B_{B(OH)_4^-}$ (‰)	**DIC (μmol/kg)**	$B(OH)_4^-/HCO_3^-$	$B(OH)_4^-$/DIC	CO_3^{2-} (μmol/kg)	Ω_{CaCO_3}	**[B] (μmol/kg)**
ODP 980	ODP (T. Chalk)	-14.70	55.49	-12.5	56	0.196	1	9.93	35.40	8.777	2334.7	-20.2	0.55	268.0	0.55	0.23	8.197	17.69	2070.7	0.0485	0.0440	182	4.32	437.5
ODP 980	ODP (T. Chalk)	-14.70	55.49	-12.5	56	0.196	2	9.69	35.37	8.781	2333.1	-20.5	0.55	267.8	0.55	0.23	8.197	17.66	2071.5	0.0481	0.0437	180	4.28	437.2
ODP 980	ODP (T. Chalk)	-14.70	55.49	-12.5	56	0.196	3	9.63	35.38	8.781	2333.6	-22.3	0.55	266.8	0.55	0.23	8.198	17.66	2071.7	0.0482	0.0437	181	4.29	437.3
ODP 980	ODP (T. Chalk)	-14.70	55.49	-12.5	56	0.196	4	9.86	35.35	8.779	2331.9	-34.5	0.55	260.1	0.55	0.23	8.207	17.79	2063.5	0.0495	0.0448	185	4.38	436.9
ODP 980	ODP (T. Chalk)	-14.70	55.49	-12.5	56	0.196	5	10.71	35.35	8.768	2331.5	-61.5	0.55	245.3	0.55	0.23	8.228	18.12	2044.0	0.0533	0.0479	197	4.68	436.9
ODP 980	ODP (T. Chalk)	-14.70	55.49	-12.5	56	0.196	6	12.06	35.37	8.751	2332.0	-63.3	0.55	244.3	0.55	0.23	8.229	18.32	2031.5	0.0557	0.0498	206	4.89	437.2
ODP 980	ODP (T. Chalk)	-14.70	55.49	-12.5	56	0.196	7	13.50	35.31	8.733	2327.8	-40.3	0.55	256.9	0.55	0.23	8.210	18.31	2026.1	0.0557	0.0497	207	4.92	436.4
ODP 980	ODP (T. Chalk)	-14.70	55.49	-12.5	56	0.196	8	14.28	35.30	8.723	2326.8	-33.6	0.55	260.6	0.55	0.23	8.205	18.35	2021.3	0.0563	0.0502	210	4.99	436.3
ODP 980	ODP (T. Chalk)	-14.70	55.49	-12.5	56	0.196	9	13.60	35.27	8.732	2325.6	-31.1	0.55	262.0	0.55	0.23	8.203	18.24	2027.6	0.0549	0.0491	205	4.87	435.9
ODP 980	ODP (T. Chalk)	-14.70	55.49	-12.5	56	0.196	10	12.32	35.28	8.748	2326.9	-27.6	0.55	263.9	0.55	0.23	8.201	18.04	2041.3	0.0526	0.0473	197	4.67	436.1
ODP 980	ODP (T. Chalk)	-14.70	55.49	-12.5	56	0.196	11	11.16	35.36	8.762	2331.9	-23.7	0.55	266.1	0.55	0.23	8.199	17.87	2056.7	0.0506	0.0457	190	4.50	437.0
ODP 980	ODP (T. Chalk)	-14.70	55.49	-12.5	56	0.196	12	10.45	35.39	8.771	2333.9	-22.8	0.55	266.6	0.55	0.23	8.199	17.78	2064.7	0.0495	0.0448	186	4.40	437.4
Age = 1.076ka, CO_2= 279.1 ppm			**Interpolated[▽] average**					**11.71**	**35.36**	**8.755**	**2331.5**	**-33.0**		**260.9**			**8.206**	**18.02**	**2047.4**	**0.0524**	**0.0471**	**196**	**4.64**	**437.0**
			Interpolated[▽] intraannual variation					**3.42**	**0.07**	**0.029**	**5.4**	**30.2**		**16.6**			**0.016**	**0.59**	**27.3**	**0.0046**	**0.0037**	**16**	**0.39**	**0.7**
MC577-17b	Tübingen	-17.40	45.57	-17.5	44	0.407	1	13.63	35.73	8.729	2351.6	-14.4	0.04	274.4	0.71	0.02	8.189	18.12	2055.9	0.0537	0.0481	204	4.83	441.6
MC577-17b	Tübingen	-17.40	45.57	-17.5	44	0.407	2	13.17	35.71	8.735	2350.8	-24.2	0.04	274.0	0.71	0.02	8.190	18.06	2059.0	0.0530	0.0476	201	4.77	441.4
MC577-17b	Tübingen	-17.40	45.57	-17.5	44	0.407	3	13.10	35.73	8.736	2352.0	-15.2	0.04	274.4	0.71	0.02	8.190	18.05	2060.8	0.0529	0.0475	201	4.76	441.6
MC577-17b	Tübingen	-17.40	45.57	-17.5	44	0.407	4	13.41	35.71	8.732	2350.6	-23.7	0.04	274.1	0.71	0.02	8.190	18.09	2056.8	0.0534	0.0479	203	4.80	441.4
MC577-17b	Tübingen	-17.40	45.57	-17.5	44	0.407	5	14.40	35.76	8.719	2352.8	-39.8	0.04	273.4	0.71	0.02	8.190	18.24	2049.1	0.0552	0.0492	210	4.96	442.0
MC577-17b	Tübingen	-17.40	45.57	-17.5	44	0.407	6	16.42	35.75	8.695	2350.7	-32.7	0.04	273.7	0.71	0.02	8.189	18.49	2029.5	0.0584	0.0517	222	5.25	441.9
MC577-17b	Tübingen	-17.40	45.57	-17.5	44	0.407	7	18.63	35.79	8.668	2350.9	-33.3	0.04	273.7	0.71	0.02	8.187	18.78	2009.2	0.0622	0.0547	236	5.59	442.4
MC577-17b	Tübingen	-17.40	45.57	-17.5	44	0.407	8	19.81	35.80	8.654	2350.1	-17.8	0.04	274.3	0.71	0.02	8.184	18.92	1998.3	0.0642	0.0561	243	5.76	442.5
MC577-17b	Tübingen	-17.40	45.57	-17.5	44	0.407	9	19.31	35.83	8.659	2352.5	-23.2	0.04	274.1	0.71	0.02	8.185	18.86	2004.4	0.0634	0.0555	240	5.70	442.9
MC577-17b	Tübingen	-17.40	45.57	-17.5	44	0.407	10	17.61	35.79	8.680	2351.9	-21.2	0.04	274.2	0.71	0.02	8.187	18.64	2019.8	0.0604	0.0533	229	5.43	442.4
MC577-17b	Tübingen	-17.40	45.57	-17.5	44	0.407	11	15.79	35.74	8.702	2350.6	-25.9	0.04	274.0	0.71	0.02	8.189	18.41	2035.4	0.0573	0.0509	218	5.15	441.7
MC577-17b	Tübingen	-17.40	45.57	-17.5	44	0.407	12	14.52	35.73	8.718	2351.0	-25.8	0.04	274.0	0.71	0.02	8.189	18.24	2047.1	0.0552	0.0493	210	4.97	441.6
MC577-17b	Tübingen	-17.40	45.57	-17.5	48	0.168	1	12.40	35.57	8.745	2343.2	-17.1	0.04	274.3	0.71	0.02	8.189	17.94	2060.5	0.0516	0.0464	195	4.62	439.6
MC577-17b	Tübingen	-17.40	45.57	-17.5	48	0.168	2	12.08	35.57	8.749	2343.3	-13.7	0.04	274.5	0.71	0.02	8.189	17.90	2063.5	0.0510	0.0460	193	4.58	439.6
MC577-17b	Tübingen	-17.40	45.57	-17.5	48	0.168	3	12.06	35.59	8.749	2344.5	-35.4	0.04	273.6	0.71	0.02	8.190	17.91	2063.9	0.0512	0.0461	194	4.59	439.9
MC577-17b	Tübingen	-17.40	45.57	-17.5	48	0.168	4	12.30	35.55	8.747	2342.1	-26.0	0.04	274.0	0.71	0.02	8.189	17.93	2060.3	0.0514	0.0463	195	4.61	439.4

		Site		Nearest Takahashi Sites																			
Site	**Archive**[ж]	**Long (°E)**	**Lat (°N)**	**Long (°E)**	**Lat (°N)**	$\frac{1}{SS_D}$ [∀]	**Month**	**SST (°C)**[§]	**Salinity**[§]	pK_B^* [◇]	**TAlk** (μmol/kg)[♣]	Δ**pCO$_2$ (ppm)**[§]	**Gloor corr.**[♯]	**pCO$_2$**[†]	**SiO$_2^-$**[♭]	**PO$_4^{--}$**[♭]	**pH**	$\delta^{11}B_{B(OH)_4^-}$ (‰)	**DIC** (μmol/kg)	**B(OH)$_4^-$ /HCO$_3^-$**	**B(OH)$_4^-$/DIC**	**CO$_3^{2-}$** (μmol/kg)	Ω_{CaCO_3}	**[B] (μmol/kg)**
MC577-17b	Tübingen	-17.40	45.57	-17.5	48	0.168	5	13.18	35.60	8.735	2344.4	-60.2	0.04	272.6	0.71	0.02	8.191	18.07	2053.3	0.0531	0.0476	201	4.76	440.0
MC577-17b	Tübingen	-17.40	45.57	-17.5	48	0.168	6	14.90	35.59	8.714	2342.7	-65.6	0.04	272.4	0.71	0.02	8.190	18.29	2036.5	0.0558	0.0498	211	5.01	439.9
MC577-17b	Tübingen	-17.40	45.57	-17.5	48	0.168	7	16.87	35.61	8.690	2342.2	-22.9	0.04	274.1	0.71	0.02	8.187	18.52	2019.7	0.0588	0.0521	223	5.28	440.1
MC577-17b	Tübingen	-17.40	45.57	-17.5	48	0.168	8	17.89	35.63	8.678	2342.4	-25.9	0.04	274.0	0.71	0.02	8.186	18.66	2010.4	0.0606	0.0534	229	5.43	440.4
MC577-17b	Tübingen	-17.40	45.57	-17.5	48	0.168	9	17.25	35.62	8.685	2342.4	-17.3	0.04	274.3	0.71	0.02	8.186	18.57	2016.6	0.0594	0.0525	225	5.33	440.3
MC577-17b	Tübingen	-17.40	45.57	-17.5	48	0.168	10	15.63	35.60	8.705	2342.7	-26.5	0.04	273.9	0.71	0.02	8.188	18.37	2031.2	0.0568	0.0505	215	5.10	440.0
MC577-17b	Tübingen	-17.40	45.57	-17.5	48	0.168	11	14.05	35.51	8.725	2338.7	-20.4	0.04	274.2	0.71	0.02	8.188	18.15	2042.6	0.0540	0.0484	204	4.85	438.9
MC577-17b	Tübingen	-17.40	45.57	-17.5	48	0.168	12	13.06	35.58	8.737	2343.3	-22.5	0.04	274.1	0.71	0.02	8.189	18.03	2054.7	0.0526	0.0472	199	4.72	439.8
MC577-17b	Tübingen	-17.40	45.57	-12.5	44	0.038	1	13.36	35.73	8.732	2351.8	-10.4	0.04	274.6	0.71	0.02	8.189	18.08	2058.5	0.0533	0.0478	203	4.79	441.6
MC577-17b	Tübingen	-17.40	45.57	-12.5	44	0.038	2	12.94	35.70	8.738	2350.3	-21.3	0.04	274.1	0.71	0.02	8.190	18.03	2060.8	0.0526	0.0473	200	4.73	441.3
MC577-17b	Tübingen	-17.40	45.57	-12.5	44	0.038	3	12.89	35.70	8.738	2350.3	-17.4	0.04	274.3	0.71	0.02	8.190	18.02	2061.4	0.0525	0.0472	200	4.72	441.3
MC577-17b	Tübingen	-17.40	45.57	-12.5	44	0.038	4	13.17	35.68	8.735	2349.0	-23.4	0.04	274.1	0.71	0.02	8.190	18.06	2057.8	0.0530	0.0475	201	4.76	441.0
MC577-17b	Tübingen	-17.40	45.57	-12.5	44	0.038	5	14.25	35.69	8.722	2348.9	-42.6	0.04	273.3	0.71	0.02	8.190	18.21	2047.5	0.0548	0.0490	208	4.93	441.1
MC577-17b	Tübingen	-17.40	45.57	-12.5	44	0.038	6	16.25	35.69	8.697	2347.3	-31.3	0.04	273.7	0.71	0.02	8.188	18.46	2028.7	0.0580	0.0514	220	5.21	441.1
MC577-17b	Tübingen	-17.40	45.57	-12.5	44	0.038	7	18.24	35.73	8.673	2347.8	-42.9	0.04	273.3	0.71	0.02	8.187	18.73	2010.4	0.0615	0.0541	233	5.52	441.6
MC577-17b	Tübingen	-17.40	45.57	-12.5	44	0.038	8	19.43	35.72	8.659	2345.9	-12.9	0.04	274.5	0.71	0.02	8.184	18.86	1999.0	0.0633	0.0555	239	5.68	441.5
MC577-17b	Tübingen	-17.40	45.57	-12.5	44	0.038	9	18.95	35.76	8.664	2348.8	-15.0	0.04	274.4	0.71	0.02	8.185	18.80	2005.4	0.0626	0.0549	237	5.62	442.0
MC577-17b	Tübingen	-17.40	45.57	-12.5	44	0.038	10	17.40	35.75	8.683	2349.8	-22.7	0.04	274.1	0.71	0.02	8.187	18.61	2020.2	0.0600	0.0529	227	5.39	441.9
MC577-17b	Tübingen	-17.40	45.57	-12.5	44	0.038	11	15.65	35.72	8.704	2349.6	-25.3	0.04	274.0	0.71	0.02	8.189	18.38	2035.9	0.0570	0.0507	216	5.13	441.5
MC577-17b	Tübingen	-17.40	45.57	-12.5	44	0.038	12	14.28	35.70	8.721	2349.4	-25.1	0.04	274.0	0.71	0.02	8.189	18.21	2048.2	0.0548	0.0489	208	4.92	441.3
MC577-17b	Tübingen	-17.40	45.57	-12.5	40	0.033	1	12.10	35.54	8.749	2341.6	-10.5	0.04	274.6	0.71	0.02	8.189	17.90	2062.2	0.0510	0.0460	193	4.57	439.3
MC577-17b	Tübingen	-17.40	45.57	-12.5	40	0.033	2	11.76	35.56	8.753	2342.9	-16.2	0.04	274.4	0.71	0.02	8.189	17.86	2065.9	0.0506	0.0456	191	4.53	439.5
MC577-17b	Tübingen	-17.40	45.57	-12.5	40	0.033	3	11.71	35.55	8.754	2342.4	-11.0	0.04	274.6	0.71	0.02	8.189	17.85	2066.1	0.0504	0.0455	191	4.52	439.4
MC577-17b	Tübingen	-17.40	45.57	-12.5	40	0.033	4	11.97	35.55	8.751	2342.2	-25.8	0.04	274.0	0.71	0.02	8.190	17.89	2063.3	0.0509	0.0459	193	4.56	439.4
MC577-17b	Tübingen	-17.40	45.57	-12.5	40	0.033	5	13.00	35.56	8.738	2342.2	-52.7	0.04	272.9	0.71	0.02	8.191	18.04	2053.5	0.0527	0.0473	199	4.72	439.5
MC577-17b	Tübingen	-17.40	45.57	-12.5	40	0.033	6	14.83	35.56	8.715	2341.0	-53.8	0.04	272.8	0.71	0.02	8.190	18.28	2036.3	0.0556	0.0496	210	4.98	439.5
MC577-17b	Tübingen	-17.40	45.57	-12.5	40	0.033	7	16.82	35.57	8.691	2339.9	-27.6	0.04	273.9	0.71	0.02	8.187	18.52	2018.4	0.0587	0.0520	222	5.26	439.6
MC577-17b	Tübingen	-17.40	45.57	-12.5	40	0.033	8	17.87	35.56	8.678	2338.4	-15.5	0.04	274.4	0.71	0.02	8.185	18.64	2008.1	0.0604	0.0532	228	5.41	439.5
MC577-17b	Tübingen	-17.40	45.57	-12.5	40	0.033	9	17.25	35.57	8.686	2339.5	-15.7	0.04	274.4	0.71	0.02	8.186	18.56	2014.6	0.0593	0.0525	224	5.32	439.6
MC577-17b	Tübingen	-17.40	45.57	-12.5	40	0.033	10	15.65	35.55	8.705	2339.8	-23.6	0.04	274.1	0.71	0.02	8.187	18.36	2029.0	0.0567	0.0504	214	5.09	439.4
MC577-17b	Tübingen	-17.40	45.57	-12.5	40	0.033	11	14.01	35.54	8.725	2340.5	-24.2	0.04	274.0	0.71	0.02	8.188	18.15	2044.1	0.0541	0.0484	205	4.85	439.3
MC577-17b	Tübingen	-17.40	45.57	-12.5	40	0.033	12	12.85	35.58	8.740	2343.5	-25.4	0.04	274.0	0.71	0.02	8.189	18.01	2056.5	0.0523	0.0470	198	4.69	439.8

		Site		Nearest Takahashi Sites																			
Site	**Archive**[ϰ]	**Long (°E)**	**Lat (°N)**	**Long (°E)**	**Lat (°N)**	$\frac{1}{SSD}$[∀]	**Month**	**SST (°C)**[§]	**Salinity**[§]	pK_B^*[◇]	**TAlk (μmol/kg)**[♣]	**ΔpCO_2 (ppm)**[§]	**Gloor corr.**[♯]	**pCO_2**[†]	**SiO_2**[♭]	**PO_4^-**[♭]	**pH**	$\delta^{11}B_{B(OH)_4^-}$ (‰)	**DIC (μmol/kg)**	$B(OH)_4^-/HCO_3^-$	$B(OH)_4^-$/DIC	CO_3^{2-} (μmol/kg)	Ω_{CaCO_3}	**[B] (μmol/kg)**
n/d, Pre-ind. CO_2 ≃275 ppm			Interpolated[▽] average					**15.32**	**35.70**	**8.709**	**2348.4**	**-26.0**		**274.0**			**8.188**	**18.34**	**2037.8**	**0.0565**	**0.0503**	**214**	**5.08**	**441.2**
			Interpolated[▽] intraannual variation					**4.78**	**0.07**	**0.039**	**2.2**	**20.9**		**0.8**			**0.002**	**0.62**	**43.7**	**0.0080**	**0.0061**	**30**	**0.71**	**0.9**
MC655	Tübingen	5.40	38.42	n/a	n/a	n/a	n/a	23.230	37.382	8.605	2629	n/a	n/a	321.9	1.5	0.25	8.161	19.22	2212.5	0.0641	0.0553	296	6.95	462.0
**NOTE: MC655 in the Mediterranean is not covered by Takahashi et al. (2009) dataset. Pre-industrial carbonate system from Touratier and Goyet (2011), with additional parameters from CARINA*																							
TAN1106 /24-N8	TAN1106	-47.98	165.77	n/a	n/a	n/a	n/a	12.51	34.70	8.746	2296.7	n/a	n/a	348.2	3	0.3	8.095	17.00	2070.9	0.0412	0.0378	159	3.76	428.9
TAN1106 /40-N8	TAN1106	-49.72	165.21	n/a	n/a	n/a	n/a	11.03	34.62	8.764	2347.3	n/a	n/a	368.4	5	0.6	8.072	16.63	2087.6	0.0375	0.0346	145	3.40	427.9
TAN1106 /50-N8	TAN1106	-51.72	164.56	n/a	n/a	n/a	n/a	9.00	34.41	8.789	2282.3	n/a	n/a	380.0	2	0.7	8.056	16.28	2100.9	0.0340	0.0316	130	3.05	425.2

TABLE C.1: Supplementary Information to accompany Chapter 4. [ϰ] Samples from Tübingen were provided by M. Kucera, those from NIWA were provided by H. Bostock, and those from IODP/ODP were provided by T. Chalk. TAN1106 material was collected from the TAN1106 Cruise from NIWA in 2011. [∀] The inversed sum of squares distance from the sample site to the Takahashi site (in °) [§] From Takahashi et al. (2009) [♣]from regional Salinity/Alk relationships [◇] Calculated via Dickson (1990) at 10m depth from SST and Salinity. [♯]Derived from Gloor et al. (2003): the ratio of average modelled values of pre-industrial CO_2 flux to average modelled modern values. [♭]Lamentably we have no data for intraannual variability and so these values are taken from nearby measurements in the GLODAP/CARINA datasets. [†]Applying modified ΔpCO_2 to pre-industrial atmospheric CO_2 [▽]Interpolated between surrounding Takahashi datapoints by weighting the mean value to the inverse of the sum-of-squares distance from the core sites

Sample Site	Salinity/TAlk correlation used
MC497	TAlk=(62.9*S)+87.77
MC436	TAlk=(54.24*S)+409.4
F111	TAlk=2305+(52.48*(S-35))+(2.85*((S-35)^2))-(0.49*(T-20))+(0.086*((T-20)^2))
ODP1172C	TAlk=2305+(52.48*(S-35))+(2.85*((S-35)^2))-(0.49*(T-20))+(0.086*((T-20)^2))
MC439	TAlk=2305+(53.97*(S-35))+(2.74*((S-35)^2))-(1.16*(T-20))-(0.04*((T-20)^2))
TAN1106/38	TAlk=2305+(52.48*(S-35))+(2.85*((S-35)^2))-(0.49*(T-20))+(0.086*((T-20)^2))
J50	TAlk=2305+(52.48*(S-35))+(2.85*((S-35)^2))-(0.49*(T-20))+(0.086*((T-20)^2))
IODP 1308	TAlk=2305+(53.97*(S-35))+(2.74*((S-35)^2))-(1.16*(T-20))-(0.04*((T-20)^2))
IODP 1313	TAlk=2305+(53.97*(S-35))+(2.74*((S-35)^2))-(1.16*(T-20))-(0.04*((T-20)^2))
IODP 980	TAlk=2305+(53.97*(S-35))+(2.74*((S-35)^2))-(1.16*(T-20))-(0.04*((T-20)^2))
MC577-17b	TAlk=2305+(53.97*(S-35))+(2.74*((S-35)^2))-(1.16*(T-20))-(0.04*((T-20)^2))

TABLE C.2: Salinity/TAlk correlations used, Chapter 4. For MC497 and MC436, consistent with Chapter 3, local Sal:Talk relationships were constructed from surface water data from GLODAP. For more recently-added sites, Sal:Alk correlations are from Lee et al. (2006).

Appendix D

Coccolithophore Cleaning Protocol

Cleaning Coccolithophore Calcite for Trace Element and Boron Isotope Analysis

As part of this PhD project, a new cleaning protocol for cultured coccolithophores was developed, in collaboration with Dr. Heather Stoll's working group in Oviedo, Spain. This material presents a significant challenge, due to (i) the large amount of organic matter present (which can lead to formation of a red substance, presumed to be iron oxyhydroxides) and (ii) susceptibility to dissolution. Since Milli-Q de-ionised water (hereafter MQ) is mildly acidic (pH 5), all MQ used in the following procedure was buffered to pH 9 to prevent dissolution by addition of a few drops of NH_3.

Cultured coccolithophores (cultivated by Oscar Branson at the NOC as part of his Masters thesis) were provided as dried centrifuged pellets. As such, the first step was to crush these pellets in a clean agate pestle and mortar, and to disaggregate material in MQ (in acid-cleaned 15ml plastic centrifuge tubes) using a vortex agitator. Samples were then centrifuged at 1400 rpm for 5 minutes and the supernatant extracted to waste. To each tube, 1ml of reductive reagent was added before boiling for 30 minutes. Preliminary attempts found NH_4OH-buffered Hydroxylamine Hydrochloride to be an ineffective reductant, and instead, following Hernandez-Sanchez et al. (2011), the following reagent was used: 25 ml 0.15M Na-citrate + 0.5M $NaHCO_3$ + 1.125g Na-dithionate (Reitz et al., 2004).

Samples were then centrifuged (1400 rpm, 5 min), and the supernatant extracted to waste, before a reagitating the sample in a further 500 μl of reductive reagent, ultrasonicating (30 s) and subjecting to a further 30 minutes boiling. After centrifuging and 3 MQ rinses (each time reagitating using a vortex and centrifuging), the samples were then transferred to new acid-cleaned centrifuge tubes and rinsed again. 1ml of oxidative solution (100 μl 30% H_2O_2 + 100 μl NaOH + 10 ml MQ) was then added to each tube, with samples then boiled for 30 mins. This oxidative step was repeated three times in total, with centrifuging, extraction of supernatant, reagitation and ultrasonication (15s) in new oxidative reagent each time.

Samples were then centrifuged and reagitated/rinsed in buffered MQ three times, before finally centrifuging for 8 minutes, extracting supernatant and drying (overnight, $\sim$ 40 °C). In some cases samples were still faintly red in colour after the full cleaning

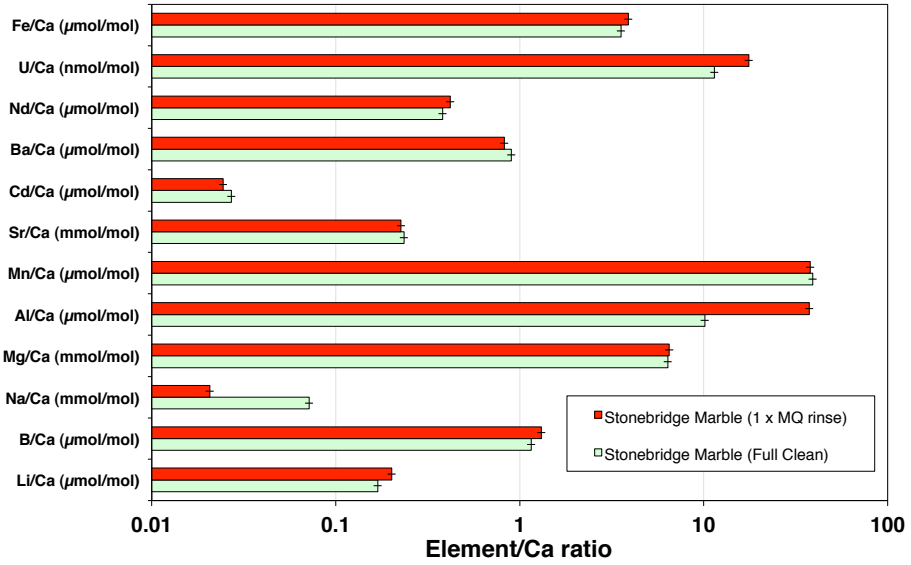

FIGURE D.1: Comparison of El/Ca ratios in samples of in-house Stonebridge Marble standard, one subject to the full coccolith cleaning protocol, and the other simply rinsed once with MQ prior to dissolution. Note that key element ratios of potential interest in coccolith geochemistry (e.g. B, Sr, Mg, Li), there is no discernible difference between the two samples. While the cause of differences in Al/Ca is not clear, Na is a common laboratory procedural contaminant, and consequently may be a result of increased handling of the cleaned sample.

protocol; in these cases samples were subject to alternating reductive and oxidative cleaning steps until fully clean. Samples were then transported back to NOCS, where samples were reagitated in MQ, centrifuged and supernatant extracted. Samples were then dissolved in 0.5M HNO_3 for trace element and boron isotope analysis. It is also important to note that coccoliths contain considerable quantities of interstitial organic matter, so following dissolution further centrifuging (1400 rpm, 15 mins) is required before sample is extracted.

To test for the possibility that this vigourous cleaning protocol might leach boron, or fractionate boron in some way, the full cleaning protocol was applied to a sample of in-house marble standard, with another dissolved and analysed uncleaned as a control. No difference in the trace element profiles of the cleaned and uncleaned marble was found (see Fig. D.1), and therefore the cleaning protocol was deemed non-destructive.

Appendix E

Published Manuscript: Marshall et al. (2013)

Marshall, Brittney J., Thunell, Robert C., Henehan, Michael J., Astor, Yrene and Wejnert, Katherine E. (2013) *Planktonic foraminiferal area density as a proxy for carbonate ion concentration: A calibration study using the Cariaco Basin Ocean Time Series* Paleoceanography **(28)**1-14.

PALEOCEANOGRAPHY, VOL. 28, 1–14, doi:10.1002/palo.20034, 2013

Planktonic foraminiferal area density as a proxy for carbonate ion concentration: A calibration study using the Cariaco Basin ocean time series

Brittney J. Marshall,[1] Robert C. Thunell,[1] Michael J. Henehan,[2] Yrene Astor,[3] and Katherine E. Wejnert[4]

Received 13 March 2013; revised 3 June 2013; accepted 4 June 2013.

[1] Biweekly sediment trap samples and concurrent hydrographic measurements collected between March 2005 and October 2008 from the Cariaco Basin, Venezuela, are used to assess the relationship between [CO_3^{2-}] and the area densities (ρ_A) of two species of planktonic foraminifera (*Globigerinoides ruber* (pink) and *Globigerinoides sacculifer*). Calcification temperatures were calculated for each sample using species-appropriate oxygen isotope ($\delta^{18}O$) temperature equations that were then compared to monthly temperature profiles taken at the study site in order to determine calcification depth. Ambient [CO_3^{2-}] was determined for these calcification depths using alkalinity, pH, temperature, salinity, and nutrient concentration measurements taken during monthly hydrographic cruises. The ρ_A, which is representative of calcification efficiency, is determined by dividing individual foraminiferal shell weights (±0.43 μg) by their associated silhouette areas and taking the sample average. The results of this study show a strong correlation between ρ_A and ambient [CO_3^{2-}] for both *G. ruber* and *G. sacculifer* ($R^2 = 0.89$ and 0.86, respectively), confirming that [CO_3^{2-}] has a pronounced effect on the calcification of these species. Though the ρ_A for both species reveal a highly significant ($p < 0.001$) relationship with ambient [CO_3^{2-}], linear regression reveals that the extent to which [CO_3^{2-}] influences foraminiferal calcification is species specific. Hierarchical regression analyses indicate that other environmental parameters (temperature and [PO_4^{3-}]) do not confound the use of *G. ruber* and *G. sacculifer* ρ_A as a predictor for [CO_3^{2-}]. This study suggests that *G. ruber* and *G. sacculifer* ρ_A can be used as reliable proxies for past surface ocean [CO_3^{2-}].

Citation: Marshall, B. J., R. C. Thunell, M. J. Henehan, Y. Astor, and K. E. Wejnert (2013), Planktonic foraminiferal area density as a proxy for carbonate ion concentration: A calibration study using the Cariaco Basin ocean time series, *Paleoceanography*, *28*, doi:10.1002/palo.20034.

1. Introduction

[2] Changes in the carbon dioxide (pCO_{2aq}) concentration of the oceans alter surface ocean pH and in turn seawater carbonate ion concentrations [CO_3^{2-}]. Over the last two centuries, anthropogenic input of carbon into the atmosphere and oceans has resulted in an unprecedented rapid decline in surface ocean pH, a process referred to as ocean acidification (OA) [*Caldiera and Wickett*, 2003; *Honisch et al*., 2012; *Zeebe*, 2012]. Though the uptake of ~30% of the anthropogenic CO_2 by the ocean has mitigated modern pCO_{2atm} rise [*Sabine et al*., 2004], the resulting decline in calcite and aragonite saturation states has had an adverse effect on several key marine organisms and ecosystems [*Riebesell et al*., 2000; *Caldiera and Wickett*, 2003; *Orr et al*., 2005; *Hoegh-Guldberg et al*., 2007, *Moy et al*., 2009]. With some exceptions [*Iglesias-Rodriguez et al*., 2008; *Ries et al*., 2009], marine calcifiers—including several species of planktonic foraminifera—have exhibited reduced rates of calcification when grown in low pH and low [CO_3^{2-}] waters (Table 1) [*Spero et al*., 1997; *Bijma et al*., 1999, 2002; *Wolf-Gladrow et al*., 1999; *Riebesell et al*., 2000; *Russell et al*., 2004; *Lombard et al*., 2010; *Manno et al*., 2012]. In addition to having an adverse effect on the calcification efficiency of these organisms, a reduction in calcification rates of marine plankton will likely have a significant impact on the marine carbon cycle, as calcification is a process that increases aqueous CO_2 [*Wolf-Gladrow et al*., 1999; *Zeebe and Wolf-Gladrow*, 2001]. Thus, on short time scales, a decrease in calcification will result

Additional supporting information may be found in the online version of this article.

[1]Department of Earth and Ocean Sciences, University of South Carolina, Columbia, South Carolina, USA.
[2]Ocean and Earth Science, National Oceanography Centre Southampton, Southampton, UK.
[3]Estacion de Investigaciones de Margarita, Fundacion La Salle de Ciencias Naturales, Porlamar, Venezuela.
[4]School of Earth and Atmospheric Sciences, Georgia Institute of Technology, Atlanta, Georgia, USA.

Corresponding author: B. J. Marshall, Department of Earth and Ocean Sciences, University of South Carolina, 701 Sumter St., EWCS Rm. 617, Columbia, SC 29208, USA. (bmarshall@geol.sc.edu)

0883-8305/13/10.1002/palo.20034

Table 1. Compilation of Previous Studies Assessing the Relationship Between Planktonic Foraminiferal Calculation and [CO_3^{2-}]

Species/Study	Sample Type	Size Fraction(μm)	Size-Normalizing Method	Range in [CO_3^{2-}](μm/kg)	Correlation With [CO_3^{2-}]	%Δ [CO_3^{2-}]$_{200–300}$
			Orbulina universa			
Spero et al. [1997]	culture	–	–	75–774 (699)	positive	37[d]
Bijma et al. [1999]	culture	500–600 (100)	SBW	40–150 (110)[b]	positive, $R^2 = 0.55$	24.3
	culture	500–600 (100)	SBW	180–640 (460)[b]	positive, $R^2 = 0.67$	12.8
Russell et al. [2004]	culture	427–653 (226)	shell thickness	76–468 (392)[b]	positive, $R^2 = 0.97$	15.1
	culture	427–667 (240)	SBW	77–480 (404)[b]	positive, $R^2 = 0.65$	18.3
Lombard et al. [2010][a]	culture	427–667 (240)	calcification rate	77–480 (404)[b]	positive, $R^2 = 0.04$	7.7–14.7
			Globigerina bulloides			
Barker and Elderfield [2002]	core top	300–355 (55)	MBW	206–257 (51)[c]	positive, $R^2 = 0.67$	155.5
	core top	300–355 (55)	SBW	199–264 (65)[c]	positive, $R^2 = 0.31$	63.9
Gonzalez-Mora et al. [2008]	core	250–300 (50)	SBW	150–250 (100)[c]	positive	–
Moy et al. [2009]	sediment trap/core top	300–355 (55)	SBW	153–189 (36)[c]	positive	35[e]
	sediment trap/core top	355–425 (70)	SBW	153–189 (36)[c]	positive	30[e]
Beer et al. [2010a]	plankton net	200–250 (50)	MBW	166–276 (110)[c]	positive, $R^2 = 0.38$	16.6
Aldridge et al. [2012]	plankton net	150–200 (50)	MBW	148–181 (40)[c]	positive, $R^2 = 0.35$	62.6
	plankton net	200–250 (50)	MBW	148–181 (40)[c]	positive, $R^2 = 0.56$	47.5
			Pulleniatina obliquiloculata			
Naik and Naidu [2007]	core top	350–420 (70)	MBW	–	positive	–
Mekik and Raterink [2008]	core top	420–520 (100)	MBW	145–225 (80)[b]	positive, $R^2 = 0.67$	200.0
			Neogloboquadrina dutertrei			
Naik and Naidu [2007]	core top	350–420 (70)	MBW	–	positive	–
Mekik and Raterink [2008]	core top	355–415 (60)	MBW	120–225 (105)[b]	positive, $R^2 = 0.64$	76.8
			Globorotalia truncatulinoides			
Barker and Elderfield [2002]	core	300–355(55)	SBW	216–264 (48)[c]	positive, $R^2 = 0.44$	38.2
			Neogloboquadrina pachyderma			
Barker and Elderfield [2002]	core	250–300 (50)	MBW	199–264 (65)	positive, $R^2 = 0.65$	53.3
Gonzalez-Mora et al. [2008]	core	250–300 (50)	SBW	–	no response	–
Manno et al. [2012]	culture	100–200 (100)	calcification rate	60–120 (60)[c]	positive	21–30
			Globorotalia inflata			
Barker and Elderfield [2002]	core	300–355(55)	SBW	200–268 (68)[c]	positive, $R^2 = 0.77$	70.7
			Globogerinoides ruber			
Gonzalez-Mora et al. [2008]	core	250–300 (50)	SBW	–	positive	–
de Moel et al. [2009]	core	250–300 (50)	SBW	(6.5; 18)	positive	25.0[f]
	core	300–355 (55)	SBW	(6.5; 18)	positive	25.0[f]
	core	250–500 (250)	shell thickness	(6.5; 18)	positive	35.0[f]
Beer et al. [2010a]	plankton net	200–250 (50)	MBW	251–284 (33)[c]	negative, $R^2 = 0.78$	−88.6
	plankton net	250–315 (65)	MBW	261–285 (24)[c]	negative, $R^2 = 0.64$	−74.2
	plankton net	315–355 (40)	MBW	262–284 (22)[c]	negative, $R^2 = 0.50$	−71.5
This study (pink)	sediment trap	355–650 (295)	ρ_A	215–270 (55)[b]	positive, $R^2 = 0.89$	44.1
	sediment trap	355–500 (145)	ρ_A	215–270 (55)[b]	positive, $R^2 = 0.73$	49.6
	sediment trap	500–650 (150)	ρ_A	215–270 (55)[b]	positive, $R^2 = 0.82$	43.8
			Globogerinoides sacculifer			
Bijma et al. [2002]	culture	493–575 (82)	SBW	100–620 (520)[b]	positive, $R^2 = 0.39$	7.7
	culture	582–663 (81)	SBW	100–620 (520)[b]	positive, $R^2 = 0.22$	4.6
	culture	762–845 (83)	SBW	100–620 (520)[b]	positive, $R^2 = 0.28$	5.4
Naik and Naidu [2007]	core top	350–420 (70)	MBW	240–250 (10)[b]	positive	157.7
Lombard et al. [2010][a]	culture	372–446 (74)	calcification rate	72–566 (494)[b]	positive, $R^2 = 0.03–0.07$	6.3–8.1
Naik et al. [2010]	core	503–699 (196)	SBW	61–106 (36)[c]	positive	32.3[g]
This study (no sac)	sediment trap	425–800 (350)	ρ_A	165–240 (70)[b]	positive, $R^2 = 0.86$	27.1
	sediment trap	425–650 (225)	ρ_A	165–240 (70)[b]	positive, $R^2 = 0.79$	29.1
	sediment trap	650–850 (200)	ρ_A	165–240 (70)[b]	positive, $R^2 = 0.55$	19.5

[a]This study uses data from *Russell et al*. [2004] and unpublished data from R. da Rocha, A. Kuroyanagi, G. J. Reichart, and J. Bijma.
[b]Ambient [CO_3^{2-}].
[c]Sea surface [CO_3^{2-}].
[d]Percent change in mass of *O. universa* at high [CO_3^{2-}] (over 600 μmol/kg) relative to the mass at ambient [CO_3^{2-}].
[e]Percent change in SBW from preindustrial (core top) *G. bulloides* to present (sediment trap) *G. bulloides*.
[f]Percent change represents the difference between the SBW from thin (younger) and thick (older) shelled populations with ^{14}C-derived age differences of 35–140 years.
[g]Percent change in SBW from 25,000 years B.P. to 1000 years B.P.

in an increase in the ocean's ability to take up atmospheric CO_2 [*Feely et al*., 2004], but would ultimately reduce the total flux of calcite and organic carbon to the deep ocean over longer time scales, which serves as a significant long-term carbon sink [*Armstrong et al*., 2001; *Klaas and Archer*, 2002; *Ridgwell and Zeebe*, 2005; *Zeebe*, 2012].

[3] Since planktonic foraminifera are responsible for up to 80% of the total calcium carbonate ($CaCO_3$) accumulated in surface sediments [*Schiebel*, 2002], it is important to understand the extent to which their calcification will be affected by decreasing [CO_3^{2-}] associated with OA. The quantification of the relationship between [CO_3^{2-}] and planktonic foraminiferal calcification provides a useful proxy for determining past changes in ocean carbonate chemistry, as well as estimates of past pCO_{2atm}. It has been shown that a positive linear relationship exists between planktonic foraminiferal size-normalized shell weight (SNW) and ambient [CO_3^{2-}] [*Spero et al*., 1997; *Bijma et al*., 1999; *Barker and Elderfield*, 2002]. Rates of calcification increase in conjunction with increasing seawater [CO_3^{2-}], resulting in a thickening of the shell wall and an increase in mean shell weight [*Spero et al*., 1997; *Bijma et al*., 1999; *Russell et al*., 2004].

[4] Culture studies have shown a decline in calcification efficiency with decreasing [CO_3^{2-}] for a wide variety of foraminiferal species commonly used in paleoclimatic and paleoceanographic reconstructions (Table 1). Most studies of sediment core and water column material (plankton tow and sediment trap) report a stronger influence of [CO_3^{2-}] on foraminiferal calcification than what has been reported in culture studies (Table 1). It has been suggested that the shallower slopes reported in culture studies could have been a result of the foraminifera not having completed their entire life cycle in culture conditions [*Bijma et al*., 2002].

[5] Additional differences amongst studies investigating the influence of [CO_3^{2-}] on foraminiferal calcification arise from the variety of methodologies used to estimate changes in calcification. While some studies estimate or measure calcification rate or shell thickness, most studies use SNW to estimate a change in shell thickness or density in response to changes in [CO_3^{2-}] (Table 1). In order to isolate the contribution of shell thickness to weight measurements, the influence of size on the overall weight of the foraminiferal test must be taken into account. Prior studies have examined the relationship between [CO_3^{2-}] and shell weight using two general methods for size normalization: sieve-based weight (SBW) [*Broecker and Clark*, 2001; *Naik et al*., 2010; *de Villiers*, 2004] and measurement-based weight (MBW) [*Barker and Elderfield*, 2002; *Beer et al*., 2010a; *Aldridge et al*., 2012]. The SBW is the simpler of the two methods, in which the mean bulk weights are determined from traditionally used narrow size fractions. The use of MBW, which is a more effective method for reducing the influence of size on weight measurements [*Beer et al*., 2010b], normalizes mean bulk weights taken from narrow size fractions using equation (1) below, where *parameter* refers to either silhouette area or diameter:

$$\mathrm{MBW}_{\mathrm{parameter}} = \frac{\text{mean SB}W_{\mathrm{sample}} \times \text{mean parameter}_{\text{size fraction}}}{\text{mean parameter}_{\mathrm{sample}}}. \quad (1)$$

[6] Most SNW studies, regardless of the normalization method used, reveal a positive linear relationship between foraminiferal shell weights and [CO_3^{2-}], although there are significant inter and intraspecies differences (Table 1). However, a number of studies have found contradictory results, reporting either a negative (*Globigerinoides ruber* (white)) [*Beer et al*., 2010a] or no relationship (*Neogloboquadrina pachyderma*) [*de Villiers*, 2004; *Gonzalez-Mora et al*., 2008] between shell weight and [CO_3^{2-}]. In these cases, it was suggested that other environmental parameters, or more generally optimal growth conditions [*de Villiers*, 2004], govern calcification efficiency for these species.

[7] A temperature effect on foraminiferal calcification has been reported in a number of studies [*Bé et al*., 1973; *Hecht*, 1976; *Hemleben et al*., 1987; *Schmidt et al*., 2004; *Lombard et al*., 2009]. These studies indicate that the size of foraminiferal tests varies with temperature, giving an additional reason for size normalization when using shell weight as a proxy for [CO_3^{2-}]. Likewise, several studies have reported a potential relationship between SNW and temperature [*Barker and Elderfield*, 2002; *Beer et al*., 2010a; *Aldridge et al*., 2012]. However, this observed relationship between SNW and temperature can also be explained by a [CO_3^{2-}] effect as the two parameters covary in surface waters. *Barker and Elderfield* [2002] evaluated the influence of temperature on *Globigerina bulloides* SNW by comparing shell weights across the most recent glacial-interglacial transition. They found that average shell weights were higher during the last glacial period when SST was low and [CO_3^{2-}] was high, concluding that [CO_3^{2-}], not temperature, was the dominant factor influencing calcification rates. A recent culture study using *N. pachyderma* (sinistral) specimens showed that the calcification rates of both juvenile and adult specimens decreased by 30% and 21%, respectively, when grown in low [CO_3^{2-}] waters, but were unaffected by an increase in ambient temperature while keeping [CO_3^{2-}] constant [*Manno et al*., 2012].

[8] Other authors have suggested that nutrient concentrations ([PO_4^{3-}] and [NO^{3-}]) may affect foraminiferal calcification efficiency—either by enhancing calcification [*Bijma et al*., 1992; *Barker and Elderfield*, 2002] or by hindering it [*Aldridge et al*., 2012]. For example, based on a North Atlantic plankton tow study, *Aldridge et al*. [2012] found that the MBW of *G. bulloides* had a strong negative correlation with [PO_4^{3-}]. However, *Aldridge et al*. [2012] do not consider the strong collinearity that exists between [PO_4^{3-}] and [CO_3^{2-}] ($R^2 = -0.85$). Simply put, when [PO_4^{3-}] is increasing in surface waters, [CO_3^{2-}] is decreasing, making it difficult to determine which environmental parameter best explains the observed variability in *G. bulloides* MBW.

[9] The objective of the current study is to better quantify the relationship between foraminiferal calcification and [CO_3^{2-}] by utilizing a more precise method of eliminating the contribution of shell size to shell weight through area density (ρ_A; μg/μm^2) calculations. The method for deriving ρ_A presented in this study uses the weight and silhouette area of individual shells of *Globigerinoides ruber* (355–650 μm) and *Globigerinoides sacculifer* (425–850 μm), allowing for the use of a broad size fraction while investigating the relationship between calcification efficiency and ambient [CO_3^{2-}]. The Cariaco Basin, Venezuela, is an ideal study area to investigate the relationship between seawater [CO_3^{2-}] and planktonic foraminiferal ρ_A as this region is

characterized by the seasonal upwelling of low pH, low temperature, and low [CO_3^{2-}] waters. In this study, we use linear regression modeling to investigate the relationships amongst foraminiferal ρ_A, ambient [CO_3^{2-}], temperature, and [PO_4^{3-}] at the depth of calcification.

2. The Cariaco Basin

2.1. Regional Setting

[10] The Cariaco Basin is located on the continental shelf of northern Venezuela and is divided into two subbasins by a 900 m saddle (Figure 1). Climatological conditions in the basin are controlled by the seasonal migration of the Intertropical Convergence Zone (ITCZ) and the associated latitudinal position of the easterly trade winds. The ITCZ is in its most southerly position during the boreal winter and early spring (November–May). During this time, the easterlies are positioned over the basin and generate Ekman-induced upwelling, which results in minimum sea surface temperatures (~22°C), maximum salinity (>36.8), elevated nutrient concentrations, and high primary production [*Thunell et al*., 2000; *Muller-Karger et al*., 2001; *Goñi et al*., 2003]. During the summer and early fall (August–October), the ITCZ migrates to its most northerly position; trade winds decrease over the basin and upwelling ceases, allowing sea surface temperatures to reach their maximum (~28–29°C), while nutrient concentrations and primary production are mutually diminished. The northerly position of the ITCZ over the Cariaco Basin at this time also increases precipitation, resulting in lower salinities in the surface waters (<36.6).

[11] The Carbon Retention in a Colored Ocean Project (CARIACO) oceanographic time series began in November 1995 with the goal of providing a link between surface processes and the sediment record [*Muller-Karger et al*., 2000, 2001; *Thunell et al*., 2000; *Goñi et al*., 2003]. A bottom-tethered mooring (10°30′N and 65°31′W) with automated sediment traps at five depths (150, 230, 410, 800, and 1200 m) continuously measures the flux of settling particles and provides biweekly samples that can be examined and compared to monthly hydrographic data. The samples used in this study are from the upper three sediment traps. The planktonic foraminifera collected from these samples display excellent preservation, with specimens frequently having intact spines. Since its inception, the program has collected a wide range of hydrographic data at discrete depths throughout the water column (0–1300 m) on a monthly basis. All hydrographic data for the Cariaco Time Series are archived at http://www.imars.usf.edu/CAR.

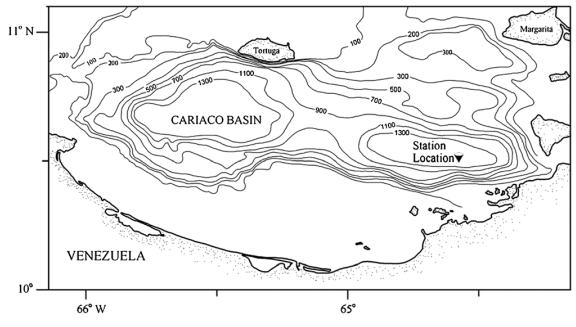

Figure 1. Bathymetric map of the Cariaco Basin showing the location of the sediment trap mooring (10°30′N and 65°31′W).

2.2. The Carbonate System in the Cariaco Basin

[12] The ocean carbonate system can be quantitatively defined by the following six parameters: total dissolved inorganic carbon, total alkalinity (A_T), pH, [CO_3^{2-}], total CO_2 in seawater ([CO_2] = [$CO_{2(aq)}$] + H_2CO_3), and bicarbonate ([HCO^{3-}]). One can use the combination of any two of these parameters, in combination with temperature, salinity, pressure, and nutrient concentrations, to calculate the entire carbonate system (see *Zeebe and Wolf-Gladrow* [2001] and *Zeebe* [2012] for a review of the carbonate system). For our study, pH and total alkalinity are the only two parameters directly measured during the monthly hydrographic cruises. The carbonate system in the Cariaco Basin is influenced by a number of water column biogeochemical processes including primary production and respiration, $CaCO_3$ precipitation and dissolution, and the remineralization and consumption of organic matter [*Astor et al*., 2005]. Additionally, physical factors such as seasonal upwelling, changes in evaporation and precipitation ratios, advection of Caribbean waters into the basin, air-sea gas exchange, and riverine input also impact the carbonate system in the basin. These processes collectively yield surface water (1 m depth) pH values that range from 8.03 to 8.11 during the study period (March 2005 to September 2008; http://www.imars.usf.edu/CAR). The oxidation of organic matter in the basin, coupled with increased CO_2 solubility associated with decreasing water temperatures, causes a rapid decline in pH values with increasing depth. These processes, in combination with a lower average alkalinity at intermediate depths (2407 μmol/kg at 100 m versus 2418 μmol/kg at the surface), yield an average pH value of 7.91 at 100 m depth throughout the course of the study period.

3. Materials and Methods

3.1. Foraminiferal Collection

[13] Biweekly sediment trap samples were collected between May 2005 and September 2008 in cups containing a buffered formalin solution, ensuring good preservation of the foraminiferal tests. Shells of planktonic foraminiferal species *G. ruber* and *G. sacculifer* were separated from the sediment trap samples using the settling method described by *Bé* [1959]. The shells were washed, wet sieved (>125 μm), and examined under a stereo binocular microscope. After washing, microscopic observation of the foraminiferal tests revealed clean surfaces, free of surficial organic matter (OM). All *G. ruber* (pink) and *G. sacculifer* (sac-less) individuals were wet picked and allowed to dry (>1 week) prior to weighing in an environmentally controlled weighing room. Following a 45 min oxidative treatment (30% H_2O_2 with 0.1 *M* NH_4OH) on a select number of samples (n = 4), it was determined that differences between the pretreatment and posttreatment shell weights were within the analytical error associated with the weight measurements (±0.43 μg, repeat weighing of individual *Orbulina universa*; n = 60). This indicates that the settling and washing techniques were efficient in

removing surficial OM and that oxidative cleaning is unnecessary for the samples used in this study. The microscopic imaging program Macnification 2.0 (Orbicule, Mac OS X Leopard) was used to sort *G. ruber* (355–650 μm) and *G. sacculifer* (425–850 μm) into their corresponding size fractions based on Feret's diameter (the longest distance between two points on the test).

3.2. Area Density Analysis

[14] Individual foraminiferal shells from each sample population were weighed using a Metler Toledo microbalance and photographed with an inverted light microscope for size analysis. Macnification 2.0 uses an RGB filter to determine individual foraminiferal 2-D (silhouette) areas. Calibration for the silhouette area and Feret's diameter measurements was performed using a microscale image taken at the same magnification as the foraminiferal images (50×). Foraminiferal shells are positioned to capture the maximum silhouette area of each individual, corresponding to the umbilical or spiral sides for both *G. ruber* and *G. sacculifer*. The difference in average areas for the spiral and umbilical orientations was determined to be negligible based on analyses performed on sample populations of *G. ruber* ($n = 15$, area difference between orientations is 0.15%) and *G. sacculifer* ($n = 12$, area difference between orientations is 0.40%). The ρ_A (μg/μm^2) is determined by dividing individual weights by their corresponding silhouette area and taking the sample average ($n > 10$, mean = 18).

3.3. Temperature Calculations and Calcification Depths

[15] Randomly selected individuals ($n = 4$ to 8) from each sample population were analyzed for oxygen isotope composition to determine calcification temperature. Oxygen isotope analyses were performed on a GV IsoPrime stable isotope ratio mass spectrometer (long-term standard reproducibility is ±0.07‰) and are reported relative to Vienna Pee Dee Belemnite (V-PDB). Calcification temperatures for each sample were determined using the following species-appropriate $\delta^{18}O$ temperature equations:

for *G. ruber* [*Bemis et al.*, 1998],

$$T(\text{°C}) = 14.90\text{–}4.80(\delta_c\text{–}\delta_w), \quad (2)$$

and for *G. sacculifer* [*Mulitza et al.*, 2003],

$$T(\text{°C}) = 14.91\text{–}4.35(\delta_c\text{–}\delta_w), \quad (3)$$

where δ_c is the $\delta^{18}O$ of the foraminiferal calcite, and δ_w is the $\delta^{18}O$ of the calcifying waters. Time-equivalent $\delta^{18}O_w$ estimates were established using the $\delta^{18}O_w$ salinity equations from *McConnell et al.* [2009] for the Cariaco Basin for both upwelling (equation (4)) and nonupwelling conditions (equation (5)):

$$\delta^{18}O_w = 0.80(\pm0.08) \times (\text{salinity})\text{–}28.53(\pm3.0), \quad (4)$$

$$\delta^{18}O_w = 0.27(\pm0.04) \times (\text{salinity})\text{–}8.77(\pm1.3). \quad (5)$$

[16] The $\delta^{18}O_w$ values are scaled from SMOW to PDB by subtracting 0.27‰ [*Bemis et al.*, 1998]. The $\delta^{18}O$-derived calcification temperatures were then compared to the measured water column temperatures to determine calcification depths and the associated instrumental temperature, salinity, nutrient, pH, and alkalinity needed for calculating [CO_3^{2-}]. It should be noted that a [CO_3^{2-}]-δ_c relationship has been observed in culture studies [*Spero et al.*, 1997]. To our knowledge, no calibration of this relationship exists for either *G. ruber* or *G. sacculifer* making it difficult to model this effect on the samples used in this study. Using the $\Delta\delta^{18}O$-[CO_3^{2-}] model presented in *King and Howard* [2005], where $\Delta\delta^{18}O$ is the difference between the measured δ_c from the foraminiferal samples and the predicted δ_c based on the instrumental temperatures, we find that there is no correlation between [CO_3^{2-}] and $\Delta\delta^{18}O$ for the sediment trap samples used in this study, suggesting that [CO_3^{2-}] is not a controlling factor for this offset.

3.4. Carbonate Parameter Calculations

[17] Monthly records of aqueous [CO_3^{2-}] were generated for the study site using CO2SYS.xls [*Pelletier et al.* 2007] (version 16) and the constants of *Lueker et al.* [2000] and *Dickson* [1990]. [CO_3^{2-}] values were calculated for the upper 130 m at discrete depth intervals (1, 7, 15, 25, 35, 55, 75, 100, and 130 m) using A_T, pH, temperature, salinity, and nutrient concentration measurements taken during monthly hydrographic cruises, and accounting for the depth (i.e., pressure) of collection. The measurement error for [CO_3^{2-}], calculated from the errors associated with each carbonate parameter used for its calculation, is less than ±1.3 μmol/kg for all the samples used in this study. A comprehensive description of the methodologies used to collect monthly hydrographic data in the Cariaco Basin can be found at http://www.imars.usf.edu/CAR.

[18] Assuming an average 3 week life span for both *G. ruber* and *G. sacculifer* [*Bijma et al.*, 1990] and a 1 day settling period to reach the trap depths of 150 and 410 m (sinking speed = 300 m/day) [*Takahashi and Bé*, 1984], the foraminifera collected in the biweekly sediment traps calcified in waters 8 to 22 days prior to the time the trap opened for collection. Thus, in all possible cases, we used hydrographic data that fell close to or within this range of day difference to pair with the average foraminiferal ρ_A.

3.5. Regression Analyses

[19] Simple, multiple, and hierarchical regression analyses (IBM SPSS) [*Miles and Shevlin*, 2001] were used to quantify the relationships between the response variable (foraminiferal ρ_A) and the predictor variables ([CO_3^{2-}], temperature, and [PO_4^{3-}]). Simple linear regression analysis (SLR) was used to determine the bivariate relationship between individual response and predictor variables. Various types of multiple linear regression analyses (MLR) were performed to examine the relationships between ρ_A and the predictor variables, as well as to examine the covariance amongst the predictor variables themselves. Both SLR and MLR can yield unreliable statistical outcomes for cases of multiple covarying predictor variables—a condition called collinearity or multicollinearity. Collinearity can be an issue in upwelling systems such as the Cariaco Basin as it is difficult to decouple covarying environmental variables and determine the actual amount each variable contributes to changes in the response variable (e.g., ρ_A). To examine the collinearity amongst the three predictor variables, two types of MLR were performed. The first used each predictor variable in turn as the dependent variable and the other two predictor variables as the dependent variables (Table

S2 in the supporting information). The coefficient of determination (R^2) resulting from these multivariate regression analyses is indicative of the amount of variance shared by the dependent variable (one of the predictor variables) with the independent variables (the other two predictor variables), essentially quantifying the redundancy one predictor variable shares with the other predictor variables. Two other collinearity diagnostics, tolerance ($1 - R^2$) and variance inflation factor (VIF; $(1 - R^2)^{-1}$), were determined using MLR with ρ_A as the dependent variable and [CO_3^{2-}], temperature, and [PO_4^{3-}] as the independent variables (Table S3). Collinearity in two or more predictor variables will inflate the variance and standard errors associated with a regression analysis; thus, a strong R^2 is the result of redundant predictor variables as opposed to a set of good independent predictor variables. In general, tolerance values below 0.50 and VIF values above 2 are indicative of an issue with collinearity amongst the independent variables [*Miles and Shevlin*, 2001].

[20] One way the current study addresses the issue of collinearity is by leaving the values for one predictor variable (X_1) unchanged, but removing its covariance with the other two predictor variables (X_2, X_3) by regressing them on X_1 and generating their residuals. For example, the residuals of temperature and [PO_4^{3-}] (T_{Cres}, [CO_3^{2-}] and [PO_4^{3-}]$_{res}$, [CO_3^{2-}]) were quantified using equations (11) and (12) for *G. ruber* and (17) and (18) for *G. sacculifer* from Table 2 in order to determine the predicted values for calcification temperature and phosphate concentrations based on their relationship with [CO_3^{2-}]. The residuals were then calculated by subtracting the predicted values from the measured values. The residuals represent the variability in temperature and phosphate that is unrelated to their covariance with [CO_3^{2-}]. By using the residuals as opposed to the original calcification temperature and phosphate concentrations, we are able to estimate what additional influence these parameters have on *G. ruber* and *G. sacculifer* ρ_A once [CO_3^{2-}] has been considered. Hierarchical multiple regression analysis (HMR) was used to determine the relative predictive capabilities of each variable for *G. ruber* and *G. sacculifer* ρ_A by assessing the change in R^2 (ΔR^2) and the significance of this change ($p\ \Delta R^2$) as each predictor variable is added sequentially to the regression model. In addition to the R^2, ΔR^2, and $p\ \Delta R^2$, the beta or standardized coefficient (β) is also reported as this is indicative of the percentage of a standard deviation (SD) that the response variable (ρ_A) would change for a 1 SD change in the predictor variable (Tables S4 and 3). Each model assumes that X_1 is the dominant predictor variable and assesses the relative contributions of X_2 and X_3 while holding all previously added variable(s) constant (Table 3). When using HMR, each predictor variable is added to the regression equation in an order specified by the researcher based on prior observations or an established theory. For the first model, we use the results of previous studies [*Barker and Elderfield*, 2002; *Naik et al*., 2010; *Manno et al*., 2012] to establish the order of the variables, using [CO_3^{2-}] as X_1 and T_{Cres}, [CO_3^{2-}] and [PO_4^{3-}]$_{res}$, [CO_3^{2-}] as X_2 and X_3, respectively. Models 2–4 placed the residuals of [CO_3^{2-}] either second or third during HMR to determine if it still contributed significantly to predicting ρ_A once the other variables had been considered.

Table 2. SLR Equations and Associated Correlation Statistics[a]

Species	Equation Number	$Y = a + b(X)$								Standard Error of Estimate
		Y	X	a	b	n	R	R^2	p	
G. ruber (pink)	7	[CO_3^{2-}] (μmol/kg)	ρ_A (355–650 μm; 10^{-4} μg/μm^2)	2.390 (±52.66)	201.663 (±44.50)	14	0.94	0.89	<0.001	±6.34
	8	ρ_A (355–650 μm; 10^{-4} μg/μm^2)	[CO_3^{2-}] (μmol/kg)	0.119 (±0.24)	0.00442 (±0.001)	14	0.94	0.89	<0.001	±0.03
	9	ρ_A (355–500 μm; 10^{-4} μg/μm^2)	[CO_3^{2-}] (μmol/kg)	0.00801 (±0.47)	0.00488 (±0.002)	13	0.86	0.73	<0.001	±0.06
	10	ρ_A (500–650 μm; 10^{-4} μg/μm^2)	[CO_3^{2-}] (μmol/kg)	0.126 (±0.33)	0.00441 (±0.001)	13	0.91	0.82	<0.001	±0.04
	11		T_C (°C)	7.516 (±5.72)	0.075 (±0.02)	14	0.89	0.80	<0.001	±0.72
	12	[PO_4^{3-}] (μmol/kg)	[CO_3^{2-}] (μmol/kg)	0.392 (±0.29)	−0.001 (±0.002)	4	0.60	−0.36	<0.05	±0.04
G. sacculifer	13	[CO_3^{2-}] (μmol/kg)	ρ_A (425–850 μm; 10^{-4} μg/μm^2)	−118.224 (±84.74)	195.687 (±52.10)	13	0.93	0.86	<0.001	±9.63
	14	ρ_A (425–850 μm; 10^{-4} μg/μm^2)	[CO_3^{2-}] (μmol/kg)	0.745 (±0.24)	0.00440 (±0.001)	13	0.93	0.86	<0.001	±0.05
	15	ρ_A (425–650 μm; 10^{-4} μg/μm^2)	[CO_3^{2-}] (μmol/kg)	0.669 (±0.36)	0.00465 (±0.002)	12	0.65	0.77	<0.001	±0.07
	16	ρ_A (650–850 μm; 10^{-4} μg/μm^2)	[CO_3^{2-}] (μmol/kg)	1.022 (±0.53)	0.00328 (±0.003)	12	0.88	0.43	<0.001	±0.09
	17		[CO_3^{2-}] (μmol/kg)	10.577 (±1.31)	0.064 (±0.006)	13	0.99	0.98	<0.001	±0.25
	18	[PO_4^{3-}] (μmol/kg)	[CO_3^{2-}] (μmol/kg)	0.863 (±0.52)	−0.003 (±0.004)	13	0.48	−0.23	<0.1	±0.15

[a]Reported error with slopes and intercepts are 95% confidence limits.

Table 3. Hierarchical Regression Model and Statistical Output for the Predictors of ρ_A

	$Y = a + b_1(X_1) + b_2(X_2) + b_3(X_3)$							Beta		
Species Model	Y	X_1	X_2	X_3	R^2	ΔR^2	$p\ \Delta R^2$	β_1	β_2	β_3
				G. ruber						
G. ruber - 1	ρ_A (10^{-4} µg/µm^2)	$[CO_3^{2-}]$ (µmol/kg)	–	–	0.89	0.89	<0.001	0.94	–	–
	ρ_A (10^{-4} µg/µm^2)	$[CO_3^{2-}]$ (µmol/kg)	T_{Cres}, $[CO_3^{2-}]$ (°C)	–	0.91	0.02	ns	0.94	0.13	–
	ρ_A (10^{-4} µg/µm^2)	$[CO_3^{2-}]$ (µmol/kg)	T_{Cres}, $[CO_3^{2-}]$ (°C)	$[PO_4^{3-}]_{res}$, $[CO_3^{2-}]$ (µmol/kg)	0.92	0.01	ns	0.94	0.17	−0.01
2	ρ_A (10^{-4} µg/µm^2)	T_C (°C)	–	–	0.81	0.81	<0.001	0.90	–	–
	ρ_A (10^{-4} µg/µm^2)	T_C (°C)	$[CO_3^{2-}]_{res}$, T_C (µmol/kg)	–	0.90	0.10	<0.01	0.90	0.31	–
	ρ_A (10^{-4} µg/µm^2)	T_C (°C)	$[CO_3^{2-}]_{res}$, T_C (µmol/kg)	$[PO_4^{3-}]_{res}$, T_C (µmol/kg)	0.91	0.01	ns	0.90	0.25	−0.10
3	ρ_A (10^{-4} µg/µm^2)	$[PO_4^{3-}]$ (µmol/kg)	–	–	0.36	0.36	<0.05	−0.60	–	–
	ρ_A (10^{-4} µg/µm^2)	$[PO_4^{3-}]$ (µmol/kg)	$[CO_3^{2-}]_{res}$, $[PO_4^{3-}]$ (µmol/kg)	–	0.89	0.54	<0.001	−0.60	0.73	–
	ρ_A (10^{-4} µg/µm^2)	$[PO_4^{3-}]$ (µmol/kg)	$[CO_3^{2-}]_{res}$, $[PO_4^{3-}]$ (µmol/kg)	T_{Cres}, $[PO_4^{3-}]$ (°C)	0.92	0.02	ns	−0.60	0.43	0.34
4	ρ_A (10^{-4} µg/µm^2)	$[PO_4^{3-}]$ (µmol/kg)	–	–	0.36	0.36	<0.05	−0.60	–	–
	ρ_A (10^{-4} µg/µm^2)	$[PO_4^{3-}]$ (µmol/kg)	T_{Cres}, $[PO_4^{3-}]$ (°C)	–	0.88	0.52	<0.001	−0.60	0.72	–
	ρ_A (10^{-4} µg/µm^2)	$[PO_4^{3-}]$ (µmol/kg)	T_{Cres}, $[PO_4^{3-}]$ (°C)	$[CO_3^{2-}]_{res}$, $[PO_4^{3-}]$ (µmol/kg)	0.92	0.04	<0.05	−0.60	0.34	0.43
				G. sacculifer						
G. sacculifer - 1	ρ_A (10^{-4} µg/µm^2)	$[CO_3^{2-}]$ (µmol/kg)	–	–	0.86	0.86	<0.001	0.93	–	–
	ρ_A (10^{-4} µg/µm^2)	$[CO_3^{2-}]$ (µmol/kg)	T_{Cres}, $[CO_3^{2-}]$ (°C)	–	0.87	0.00	ns	0.93	0.09	–
	ρ_A (10^{-4} µg/µm^2)	$[CO_3^{2-}]$ (µmol/kg)	T_{Cres}, $[CO_3^{2-}]$ (°C)	$[PO_4^{3-}]_{res}$, $[CO_3^{2-}]$ (µmol/kg)	0.87	0.00	ns	0.93	0.08	0.04
2	ρ_A (10^{-4} µg/µm^2)	T_C (°C)	–	–	0.86	0.86	<0.001	0.93	–	–
	ρ_A (10^{-4} µg/µm^2)	T_C (°C)	$[CO_3^{2-}]_{res}$, T_C (µmol/kg)	–	0.87	0.00	ns	0.93	0.06	–
	ρ_A (10^{-4} µg/µm^2)	T_C (°C)	$[CO_3^{2-}]_{res}$, T_C (µmol/kg)	$[PO_4^{3-}]_{res}$, T_C (µmol/kg)	0.87	0.00	ns	0.93	0.07	0.04
3	ρ_A (10^{-4} µg/µm^2)	$[PO_4^{3-}]$ (µmol/kg)	–	–	0.16	0.16	ns	−0.40	–	–
	ρ_A (10^{-4} µg/µm^2)	$[PO_4^{3-}]$ (µmol/kg)	$[CO_3^{2-}]_{res}$, $[PO_4^{3-}]$ (µmol/kg)	–	0.86	0.70	<0.001	−0.40	0.84	–
	ρ_A (10^{-4} µg/µm^2)	$[PO_4^{3-}]$ (µmol/kg)	$[CO_3^{2-}]_{res}$, $[PO_4^{3-}]$ (µmol/kg)	T_{Cres}, $[PO_4^{3-}]$ (°C)	0.87	0.01	ns	−0.40	0.40	0.47
4	ρ_A (10^{-4} µg/µm^2)	$[PO_4^{3-}]$ (µmol/kg)	–	–	0.16	0.16	ns	−0.40	–	–
	ρ_A (10^{-4} µg/µm^2)	$[PO_4^{3-}]$ (µmol/kg)	T_{Cres}, $[PO_4^{3-}]$ (°C)	–	0.86	0.71	<0.001	−0.40	0.84	–
	ρ_A (10^{-4} µg/µm^2)	$[PO_4^{3-}]$ (µmol/kg)	T_{Cres}, $[PO_4^{3-}]$ (°C)	$[CO_3^{2-}]_{res}$, $[PO_4^{3-}]$ (µmol/kg)	0.87	0.00	ns	−0.40	0.47	0.38

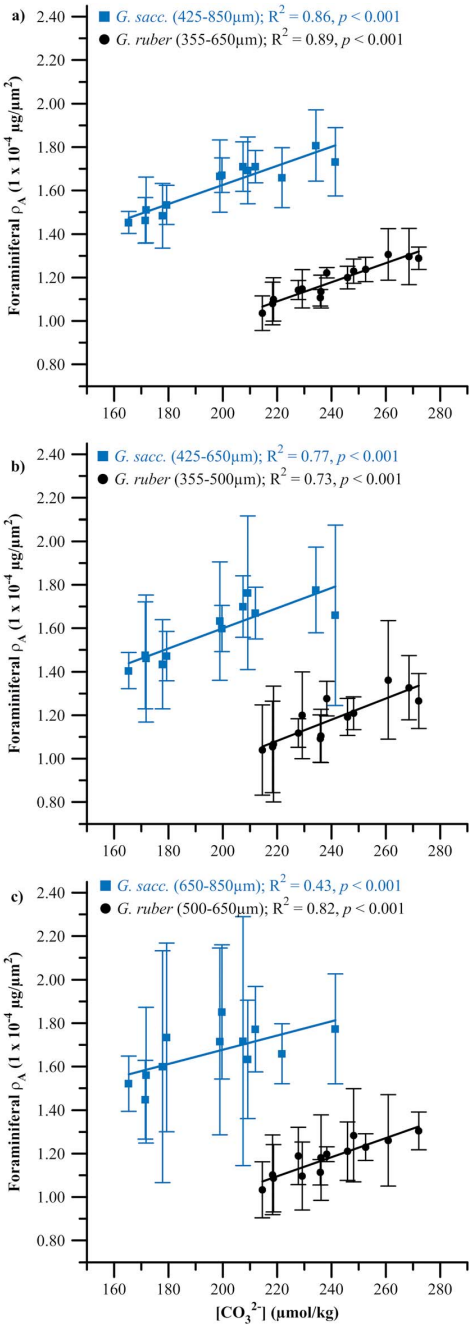

Figure 2. [CO_3^{2-}]-ρ_A relationships for both *G. ruber* and *G. sacculifer* for size fractions (a) 355–650 and 425–850 µm, (b) 355–500 and 425–650 µm, and (c) 500–650 and 650–850 µm. Error bars represent the ρ_A multiplied by the reciprocal of the number of individuals in each sample populations. Samples with $n > 2$ were included for Figures 2b and 2c in order to compare to the broader size-fraction samples presented in Figure 2a ($n \geq 10$).

4. Results and Discussion

4.1. Size-Fraction Relevance and Utilization

[21] A potential limiting factor in traditional SNW studies is the requirement that samples be restricted to narrow size fractions in an attempt to eliminate the contribution of size to the measured weights. However, the use of narrow size fractions may limit the number of foraminiferal shells per sample, and a small sample size increases the error associated with size-normalized weight or ρ_A estimations as defined by the following error estimation equation [*Beer et al.*, 2010a; *Aldridge et al.*, 2012]:

$$\text{SNW or } \rho_A \text{ error} = \text{SNW or } \rho_A \times (n)^{-1} \quad (6)$$

[22] A large number of individuals per sample greatly decrease the chances of having biased weight or ρ_A estimations. In this study, shell weight and silhouette area estimates were made for individual foraminifera as opposed to groupings of individuals, allowing for the application of ρ_A analysis over a wider size fraction (425–850 µm for *G. sacculifer* and 355–650 µm for *G. ruber*). SLR comparing ρ_A to the mean silhouette area for each sample reveals no statistically significant relationship for either species (Figure S1; $R^2 = 0.02$, p = ns for *G. ruber*; $R^2 = 0.00$, p = ns for *G. sacculifer*). We therefore conclude that the area density method used in this study is very effective at removing the influence of *G. ruber* and *G. sacculifer* shell size on ρ_A. These results support the use of broader shell size fractions in ρ_A studies.

[23] A concern with using broader size fractions for ρ_A and SNW analysis is that the morphology and calcification of foraminifera can change throughout ontogeny [*Bé*, 1980; *Hemleben et al.*, 1989]. For example, during gametogenesis and following the formation of a sac-like final chamber, *G. sacculifer* secretes a calcite crust over its entire shell, increasing the thickness of the shell by an average of 9 µm [*Bé*, 1980]. In this study, only sac-less *G. sacculifer* individuals were used for ρ_A analysis in the effort to eliminate the complication of gametogenic calcite formation in this species. *Globigerinoides ruber* does not precipitate gametogenic calcite [*Caron et al.*, 1990], but it is possible that the influence of [CO_3^{2-}] on calcification could vary throughout ontogeny for both *G. ruber* and *G. sacculifer*. Both field and culture studies have shown that ontogeny, and by extension size-fraction utilization, does not have a significant influence on *G. ruber* (white) and *O. universa* SNW-[CO_3^{2-}] calibrations [*Beer et al.*, 2010a; *Bijma et al.*, 2002]. To test whether the use of broader size fractions has an impact on the calibration equations derived for ρ_A and [CO_3^{2-}], we examined the relationship between these two variables for three different size fractions of both *G. ruber* (355–500, 500–650, and 355–650 µm) and *G. sacculifer* (425–650, 650–850, and 425–850 µm; Figure 2). We found that the percent change in ρ_A that occurred with a change in [CO_3^{2-}] from 200 to 300 µmol/kg (%$\Delta[CO_3^{2-}]_{200-300}$) ranged from 44 to 50% for the three *G. ruber* size fractions (Table 2; equations (8)–(10)) and from 20 to 29% for the various *G. sacculifer* size fractions (Table 2; equations (14)–(16)). The correlation coefficients are lower and the ρ_A error higher for the narrower size fractions due to the smaller number of individuals per sample in these size fractions ($n > 2$; Figure 2). We speculate that the small

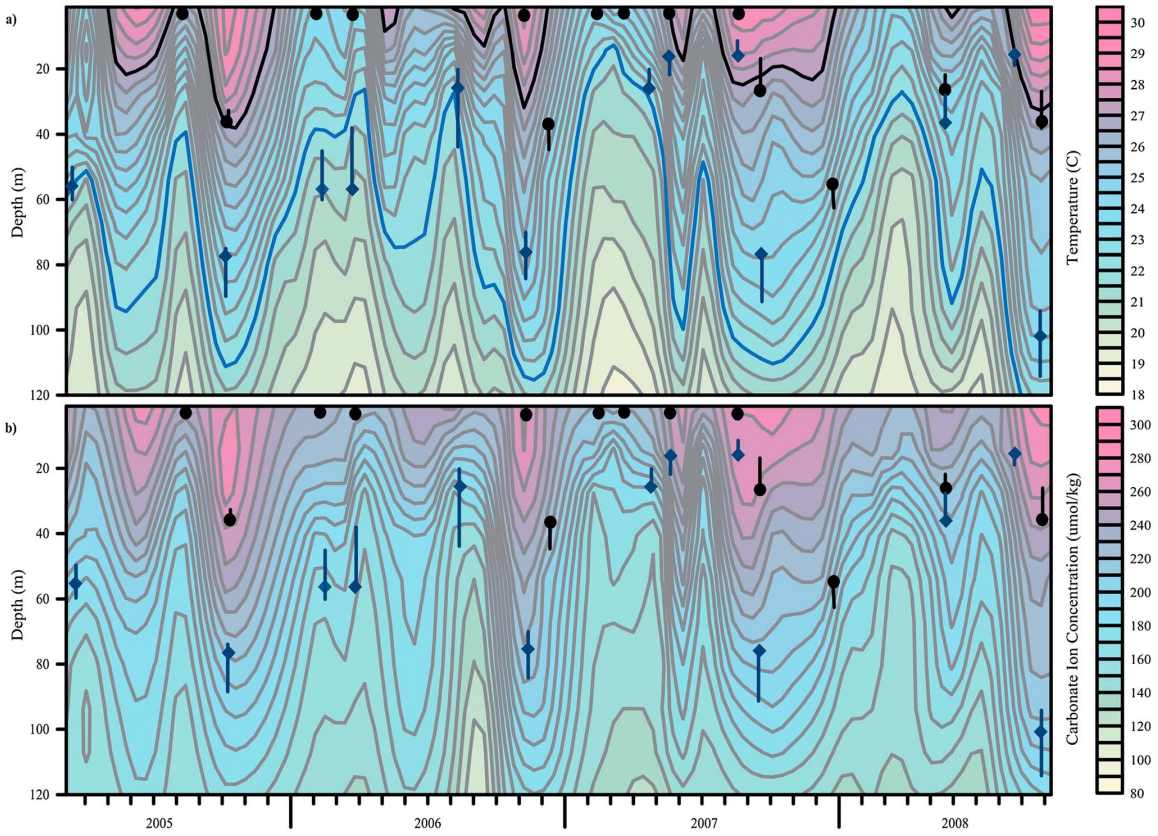

Figure 3. Contour plots of (a) temperature and (b) [CO_3^{2-}] from March 2005 to October 2008 in the Cariaco Basin for the upper 160 m of the water column. Calcification depths, estimated from δ^{18}O-derived calcification temperatures, are shown for *G. ruber* (black circles) and *G. sacculifer* (blue diamonds). Also shown are the estimated depth ranges for each sample estimated from the instrumental and δ^{18}O-derived calcification temperatures (see the supporting information for more details). Optimal growth temperatures for both *G. ruber* (black line) and *G. sacculifer* (blue line) are also plotted [*Mulitza et al.*, 1998] to compare to the estimated calcification depths for both species.

difference in ρ_A change between the different size fractions is likely due to the difference in the number of individuals per sample, resulting in significant errors associated with the average ρ_A calculations for the narrower size fractions. Based on these observations, we conclude that the small range in $\%\Delta[CO_3^{2-}]_{200-300}$ for ρ_A exhibited by the different size fractions illustrates that ontogeny does not significantly affect the relationship between ρ_A and [CO_3^{2-}]. The broader size fractions (355–650 µm for *G. ruber*, 425–850 µm for *G. sacculifer*) used in this study yield the largest number of individuals per sample and smallest errors and are therefore optimal for generating the calibration equations. Thus, only the data for the broader size fractions will be considered from here on.

4.2. Calcification Depth and Temperature Estimates

[24] Calcification temperatures derived from the δ^{18}O analyses for each sample were paired with the closest time-equivalent measured water column temperatures. The instrumental temperatures rather than the δ^{18}O-derived temperatures are used for the carbonate calculations and statistical analyses in order to maintain consistency with the rest of the hydrographic data used in this study. Average temperatures were comparable to previously published optimum temperatures for both *G. ruber* (26°C for this study versus 27°C from *Mulitza et al.* [1998]) and *G. sacculifer* (23°C for this study versus 22°C from *Mulitza et al.* [1998]). The instrumental temperature values for the upper 130 m for the 3 year study period, along with the estimated calcification depths for *G. ruber* (black circles) and *G. sacculifer* (blue diamonds) from each sediment trap sample are shown in Figure 3a. The mean calcification depth for *G. ruber* is 16 (±19) m, which is consistent with this species living in the surface mixed layer in the Cariaco Basin [*Miro*, 1971; *Tedesco et al.*, 2007] and falls within the previously observed depth range of 0–50 m [*Hemleben et al.*, 1989; *Farmer et al.*, 2007].

[25] The estimated calcification depths for *G. sacculifer* range from 15 to 100 m, with the mean being ~50 (±28) m. These results are in line with previous depth estimates for the species from the Cariaco Basin [*Wejnert*, 2011]. For

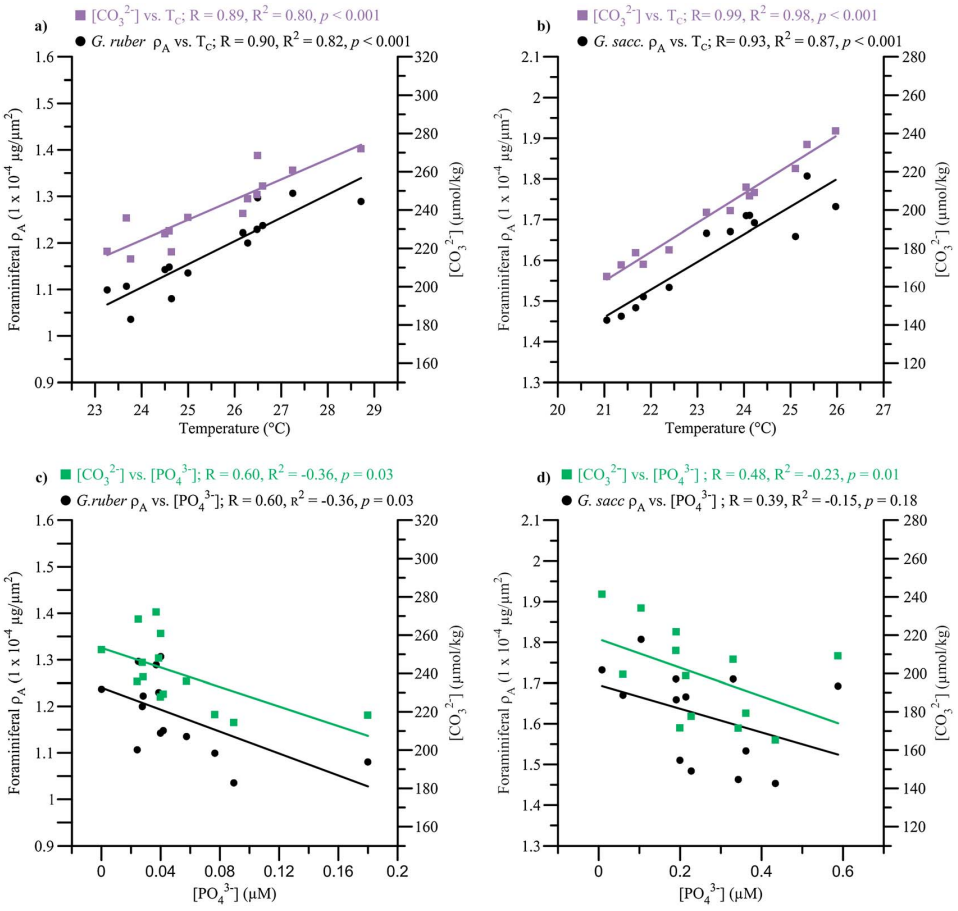

Figure 4. Temperature-ρ_A and temperature-[CO_3^{2-}] relationships for (a) *G. ruber* and (b) *G. sacculifer*. Also shown are [PO_4^{3-}]-ρ_A and [PO_4^{3-}]-[CO_3^{2-}] relationships for (c) *G. ruber* and (d) *G. sacculifer*.

both species, calcification depth changes seasonally in response to shifts between upwelling and nonupwelling regimes in the basin (Figure 3a). Changes in calcification depth are likely a response to changes in ambient water density at depth due to transitions between upwelling and nonupwelling regimes and to a certain extent species-specific preferences to live at a depth characterized by an optimal temperature, salinity, light, and/or chlorophyll and nutrient regimes [*Hemleben et al.*, 1989; *Sautter and Thunell*, 1991; *Tedesco et al.*, 2007].

4.3. Carbonate System Calculations

[26] The [CO_3^{2-}] record for the upper 120 m over the course of the study period is shown in Figure 3b, along with the calcification depths determined for each sample population for both species. The [CO_3^{2-}] at the calcification depths for *G. ruber* ranged between 215 and 270 µmol/kg (mean = 240 µmol/kg) throughout the study period, coinciding with calcite saturation states (Ω_{calc}) ranging from 5.0 to 6.5 (mean = 5.7). [CO_3^{2-}] and Ω_{calc} for *G. sacculifer* were on average lower than those for *G. ruber* (165–240 µmol/kg, mean [CO_3^{2-}] = 200 µmol/kg, mean Ω_{calc} = 4.7), in agreement with *G. sacculifer*'s deeper depth habitat.

4.4. Carbonate, Temperature, and Phosphate Controls on Planktonic Foraminiferal ρ_A

4.4.1. Results from Simple and Multiple Linear Regression Analysis

[27] SLR revealed that the ρ_A for both species has a highly significant ($p < 0.001$) relationship with ambient [CO_3^{2-}] (Table 2 and Figure 2a). SLR performed using temperature as the predictor variable for ρ_A also revealed a significant positive linear relationship (Figures 4a and 4b). In comparison, SLR using [PO_4^{3-}] as the predictor variable revealed a less significant negative linear relationship with *G. ruber* ρ_A ($p < 0.05$), with no significant relationship between *G. sacculifer* ρ_A and [PO_4^{3-}] (Figures 4c and 4d). Additionally, SLR using [CO_3^{2-}] as the predictor variable and calcification temperature and [PO_4^{3-}] concentrations individually as the response variables yielded significant bivariate correlation amongst these variables, with the exception of *G. sacculifer* [PO_4^{3-}] and [CO_3^{2-}] (Table 2 and Figure 4). Table S2 shows

the results of the MLR using each predictor variable interchangeably as the dependent variable, with the other predictor variables serving as the independent variables. For both species, [CO_3^{2-}] and temperature are highly redundant with the other environmental parameters ($R^2 = 0.86$ and 0.82 and $R^2 = 0.98$ and 0.98 for *G. ruber* and *G. sacculifer*, respectively). MLR using [PO_4^{3-}] as the dependent variable and temperature and [CO_3^{2-}] as the independent variables reveal that [PO_4^{3-}] is moderately redundant with temperature and [CO_3^{2-}] for both *G. ruber* and *G. sacculifer* ($R^2 = 0.44$ and 0.26, respectively). By substituting in a variable we know does not share a statistically significant relationship with the predictor variables (i.e., mean area, $R^2 = 0.00$, 0.01, and 0.04 and $R^2 = 0.01$, 0.01, and 0.05 for *G. ruber* and *G. sacculifer* [CO_3^{2-}], temperature, and [PO_4^{3-}], respectively), we can quantify the specific redundancy each predictor variable shares with another (Table S2). This test revealed that *G. ruber* temperature and [PO_4^{3-}] are 81 and 42% redundant with [CO_3^{2-}] and that *G. sacculifer* temperature and [PO_4^{3-}] are 98 and 30% redundant with [CO_3^{2-}].

[28] The tolerance and VIF statistics were less than 0.2 and greater than 5, respectively, for both [CO_3^{2-}] and temperature for both species, revealing a strong case for collinearity for these variables (Table S3). Substituting in the residuals of temperature (T_{Cres}, [CO_3^{2-}]) and [PO_4^{3-}] ([PO_4^{3-}]$_{res}$, [CO_3^{2-}]) revealed no collinearity with [CO_3^{2-}]. For both species, the tolerance and VIF diagnostics for [PO_4^{3-}] did not indicate a strong case for collinearity with the other predictor variables. However, due its redundancy with the other predictor variables (Table S2), [PO_4^{3-}] is treated for possible collinearity with [CO_3^{2-}] or temperature in the subsequent HMR analyses. These results suggest that [CO_3^{2-}] and temperature, particularly with the *G. sacculifer* data, are nearly indistinguishable from one another in regression analyses.

[29] Based on the results of these statistical analyses, we hypothesize that the relationships exhibited between one predictor variable and ρ_A could be due to its strong collinearity with another predictor variable that serves as the dominant predictor for ρ_A. This hypothesis is graphically represented in Figure 4. Figures 4a and 4b show the relationships between temperature and ρ_A and temperature and [CO_3^{2-}] for *G. ruber* (left) and *G. sacculifer* (right), while Figures 4c and 4d illustrate the same relationships for [PO_4^{3-}]. The slopes of the best fit lines illustrated in each graph cannot be directly compared as they are on different scales. However, the correlation coefficients (R) for both species are similar in all cases, suggesting that the relationship between ρ_A and temperature or [PO_4^{3-}] could be due the collinearity of ρ_A with [CO_3^{2-}].

4.4.2. Results from Hierarchical Multiple Regression Analyses

[30] Four HMR models were run in order to determine the relative contributions of each predictor variable to ρ_A. The means, standard deviations, and number of data points (n) for each variable used in the HMR models are included in Table S4. The R^2, the R^2 change (ΔR^2), the significance of the ΔR^2 ($p\ \Delta R^2$), and the standardized coefficient (β) for each model are listed in Table 3. The first model uses results from prior studies examining the dominant control variable on foraminiferal calcification [*Barker and Elderfield*, 2002; *Naik et al*., 2010; *Manno et al*., 2012] to determine the ordering of predictor variables for HMR, with [CO_3^{2-}], and the residuals of calcification temperature and [PO_4^{3-}] based on their relationship with [CO_3^{2-}] (T_{Cres}, [CO_3^{2-}] and [PO_4^{3-}]$_{res}$, [CO_3^{2-}]) serving as X_1, X_2, and X_3, respectively. The R^2 values from model 1 indicate that [CO_3^{2-}] accounts for 89 and 86% of the variability seen in ρ_A for *G. ruber* and *G. sacculifer*, respectively. For both *G. ruber* and *G. sacculifer*, ΔR^2 for the additions of T_{Cres}, [CO_3^{2-}] and [PO_4^{3-}]$_{res}$, [CO_3^{2-}] were insignificant, with each accounting for ~0–2% of the variability in ρ_A once [CO_3^{2-}] was controlled for in the model. Significantly larger β values for [CO_3^{2-}] relative to those for T_{Cres}, [CO_3^{2-}] and [PO_4^{3-}]$_{res}$, [CO_3^{2-}] indicate a strong dominance of [CO_3^{2-}] for predicting variability in ρ_A.

[31] The other three models were performed on both species to test if [CO_3^{2-}] still played a significant role in predicting ρ_A when placed second or third in the ordering of predictor variables. For the *G. ruber* data, the addition of [CO_3^{2-}] as X_2 and X_3 in models 2 and 4 following the addition of temperature generated a significant contribution to the R^2 of the model, while the addition of temperature as X_2 and X_3 following the addition of [CO_3^{2-}] in models 1 and 3 did not contribute significantly to the R^2 of the model. However, the ordering of temperature and [CO_3^{2-}] in models 1–4 for *G. sacculifer* did not make a significant difference in the model output. This is likely a result of the strong—nearly perfect—collinearity that exists between *G. sacculifer* [CO_3^{2-}] and temperature (Tables 2 and 3), thus making them indistinguishable during HMR. The predictor variables for *G. ruber* are slightly less collinear and thus provide us with better estimates of the relative contributions of [CO_3^{2-}] and temperature to the variability in ρ_A. Taken together with the knowledge that *G. ruber* temperature and [CO_3^{2-}] are 81% redundant, these results indicate that [CO_3^{2-}] is the dominant factor controlling ρ_A and that model 1 most accurately reflects the relative contributions of each predictor variable. Based on this model, we cannot say with any confidence that either calcification temperature or [PO_4^{3-}] has an impact on the variability in *G. ruber* or *G. sacculifer* ρ_A, or by extension calcification efficiency. We conclude that [CO_3^{2-}] alone acts as an excellent predictor for both *G. ruber* and *G. sacculifer* ρ_A and the SLR equations reported in Table 2 (equations (7), (8), (13), and (14)) serve as reliable calibration equations.

4.4.3. *Globigerinoides ruber* and *Globigerinoides sacculifer* Area Density as a Proxy for [CO_3^{2-}]

[32] The ρ_A of *G. ruber* (pink; 355–650 μm) ranged from 1.04 to 1.31 × 10^{-4} μg/μm^2 over the 3 year study period with an average of 1.18 × 10^{-4} μg/μm^2, yielding a strong positive linear relationship with [CO_3^{2-}] ($R^2 = 0.89$, $p < 0.001$, Figure 2a). *Globigerinoides sacculifer* (425–850 μm) ρ_A ranged from 1.45 to 1.81 × 10^{-4} μg/μm^2 with an average of 1.62 × 10^{-4} μg/μm^2 and also correlated strongly with ambient [CO_3^{2-}] ($R^2 = 0.86$, $p < 0.001$, Figure 2a). The relationships between foraminiferal ρ_A and [CO_3^{2-}] reported in Table 2 are in line with the results of prior studies reporting an adverse effect of reduced [CO_3^{2-}] associated with ocean acidification on the calcification of planktonic foraminifera [*Spero et al*., 1997; *Bijma et al*., 1999; *Barker and Elderfield*, 2002; *Russell et al*., 2004; *Mekik and Raterink*, 2008; *Moy et al*. 2009; *Lombard et al*., 2010; *Manno et al*., 2012].

[33] The slopes and *y* intercepts for *G. ruber* reported for this study (Table 2) reveal a more sensitive relationship with [CO_3^{2-}] than those for *G. sacculifer*, with a 200 to 300 µm/kg change in [CO_3^{2-}] (%$\Delta[CO_3^{2-}]_{200–300}$) resulting in a change in ρ_A of 44% for *G. ruber* and 27% for *G. sacculifer* (Table 1). It has been well documented that different species of planktonic foraminifera undergo varying degrees of isotopic fractionation and elemental incorporation during the calcification process due to various vital effects associated with calcification [*Erez*, 1978; *Spero*, 1992; *Wolf-Gladrow et al*., 1999; *Zeebe et al*., 2008; *Henehan et al*., 2013]. Though the ρ_A for *G. ruber* and *G. sacculifer* reflects changes in ambient seawater [CO_3^{2-}], the [CO_3^{2-}] at the site of calcification could vary amongst species due to differences in both foraminiferal and symbiont vital effects (calcification, photosynthesis, respiration) [*Jorgensen et al*., 1985; *Rink et al*., 1998; *Wolf-Gladrow et al*., 1999; *Bentov et al*., 2009]. Thus, when using ρ_A or any other measure of shell weight as a proxy for past surface-ocean [CO_3^{2-}], it is necessary to use species-specific equations like those provided in this study.

[34] An additional consideration for the use of foraminiferal ρ_A as a proxy for [CO_3^{2-}] is the extent to which foraminifera are preserved in marine sediment samples [*Barker*, 2004; *Gibbs et al*., 2010]. The dissolution of planktonic foraminiferal calcite due to a low [CO_3^{2-}] at depth would result in lower foraminiferal ρ_A and complicate the use of ρ_A as a proxy for surface-ocean [CO_3^{2-}]. Conversely, the addition of secondary calcite would increase the shell thickness and hence the ρ_A of foraminifera. Thus, foraminiferal specimens should be collected from well above the lysocline for the study region and thoroughly examined for signs of dissolution and/or the precipitation of secondary calcite prior to being used for ρ_A-[CO_3^{2-}] reconstructions.

4.5. Comparison to Previous Studies

[35] Foraminiferal ρ_A cannot be directly compared to previous studies that investigated the relationship between foraminiferal calcification efficiency using SNW, shell thickness measurements or calculations, or calcification rates as the units are not the same (Table 1). Additionally, this study differs from most other field studies in that we use [CO_3^{2-}] at the predicted depth of calcification rather than surface water [CO_3^{2-}] to generate our calibration equations. We can compare the various shell weight proxies more directly by examining the change in each proxy resulting from a 200 to 300 µm/kg change in [CO_3^{2-}]. These changes in calcification were determined using regression equations reported in the respective studies or regression equations derived from digitized figures (Table 1). For studies that did not include [CO_3^{2-}] values, the %Δ reported in Table 1 represent either a reported %Δ in the study [*Spero et al*., 1997] or a change in SBW observed over the course of a geologic period characterized by significant changes in surface water [CO_3^{2-}] [*Moy et al*., 2009; *de Moel et al*., 2009; *Naik et al*., 2010]. The %$\Delta[CO_3^{2-}]_{200–300}$ varies widely depending on the species studied and the proxies used. The average %$\Delta[CO_3^{2-}]_{200–300}$ reported for *G. sacculifer* is 32% (Table 1), which is close to the %$\Delta[CO_3^{2-}]_{200–300}$ reported for this species in this study (27%), though this percentage was derived from both culture and core studies that vary widely in the range in [CO_3^{2-}] and methods for determining calcification. The %$\Delta[CO_3^{2-}]_{200–300}$ for G. *sacculifer* reported in this study is most similar to the percent change in *G. sacculifer* SBW reported in a core study spanning 25,000 years B.P. to 1000 years B.P. [*Naik et al*., 2010].

[36] The results from *Beer et al*. [2010a] are highly inconsistent with the results for *G. ruber* (pink) presented here, with *Beer et al*. [2010a] reporting a negative correlation between *G. ruber* (white) MBW and [CO_3^{2-}] collected from the Arabian Sea. Recent studies have distinguished between five different genetic types for the white variety of *G. ruber* [*Aurahs et al*., 2011], characterized broadly by two distinct morphotypes: sensu stricto (s.s.) and sensu lato (s.l.) [*Wang*, 2000]. These morphotypes have different depth habitats and temperature preferences, and thus paleoceanographic and paleoclimatic studies should distinguish between them [*Hecht and Savin*, 1972; *Wang*, 2000; *Kuroyanagi et al*., 2008; *Numberger et al*., 2009; *Aurahs et al*., 2011]. This difference in calcification habitat, as well as the evident difference in shell geometry (s.l. is more heavily calcified than s.s. (J. Durrant and M. Henehan, 2013, unpublished data)), would likely result in a significant differences in the MBW for the two *G. ruber* (white) morphotypes. The differences between the results from *Beer et al*. [2010a] and the results from other SNW studies also using *G. ruber* (white) collected from the Arabian Sea [*de Moel et al*., 2009; *Naik et al*., 2010] may be due to *Beer et al*. [2010a] not distinguishing between the two morphotypes which we know to be present in this region [*de Moel et al*., 2009; *Aurahs et al*., 2011] and whose relative abundances may have changed as sampling traversed upwelling and nonupwelling waters. The use of *G. ruber* (pink) in the current study and *G. ruber* (white) of an undetermined morphotype by *Beer et al*. [2010a] makes comparisons difficult between the two studies. Our results are closest to those reported in *de Moel et al*. [2009], who used the SBW of *G. ruber* (white; both morphotypes in equal distributions amongst samples), but had a much narrower range in [CO_3^{2-}] compared to the current study. As this is the first study reporting on the effect of [CO_3^{2-}] on the calcification in the pink variety of *G. ruber*, we can only state that the %$\Delta[CO_3^{2-}]_{200–300}$ reported here (44%) falls within the range of most percent changes reported in studies using other species (5 to 155%, with the majority between 5 and 50%). Thus, our results for the magnitude of change in ρ_A per unit change in [CO_3^{2-}] for both *G. ruber* and *G. sacculifer* are comparable to those changes previously reported in foraminiferal calcification-[CO_3^{2-}] studies.

5. Conclusions

[37] The results of this study suggest that surface [CO_3^{2-}] is responsible for 89 and 86% of the variability in ρ_A for both *G. ruber* (pink) and *G. sacculifer*, respectively, and by extension calcification efficiency, with no significant evidence that temperature or [PO_4^{3-}] contributes to ρ_A in these species. Thus, the ρ_A of *G. ruber* and *G. sacculifer* should serve as a reliable proxy for past [CO_3^{2-}] using the species-specific equations reported in Table 2. It is recommended that only well-preserved foraminiferal shells with an absence of

secondary calcite be used in down-core ρ_A reconstructions of past [CO_3^{2-}]. The ρ_A technique described in this study should be particularly useful for down-core studies where foraminiferal shell numbers are limited and the use of a broad size range is required.

[38] **Acknowledgments.** We would like to thank Eric Tappa for his extensive analytical contributions, including the processing of samples for stable isotopes and the overseeing of the collection of the sediment trap samples used in this study. This research was supported by NSF awards 1039503 and 0752037.

References

Aldridge, D., C. J. Beer, and D. A. Purdie (2012), Calcification in the planktonic foraminifera *Globigerina bulloides* linked to phosphate concentrations in surface waters of the North Atlantic Ocean, *Biogeosciences*, *9*(5), 1725–1739, doi:10.5194/bg-9-1725-2012.

Armstrong, R. A., C. Lee, J. I. Hedges, S. Honjo, and S. G. Wakeham (2001), A new, mechanistic model for organic carbon fluxes in the ocean based on the quantitative association of POC with ballast minerals, *Deep Sea Res. Part II*, *49*(1), 219–236, doi:10.1016/S0967-0645(01)00101-1.

Astor, Y. M., M. I. Scranton, F. Muller-Karger, R. Bohrer, and J. García (2005), fCO_2 variability at the CARIACO tropical coastal upwelling time series station, *Mar. Chem.*, *97*(3–4), 245–261, doi:10.1016/j.marchem.2005.04.001.

Aurahs, R., Y. Treis, K. Darling, and M. Kucera (2011), A revised taxonomic and phylogenetic concept for the planktonic foraminifer species *Globigerinoides ruber* based on molecular and morphometric evidence, *Mar. Micropaleontol.*, *79*(1–2), 1–14, doi:10.1016/j.marmicro.2010.12.001.

Barker, S. (2004), Temporal changes in North Atlantic circulation constrained by planktonic foraminiferal shell weights, *Paleoceanography*, *19*, PA3008, doi:10.1029/2004PA001004.

Barker, S., and Elderfield, H. (2002), Foraminiferal calcification response to glacial-interglacial changes in atmospheric CO_2, *Science*, *297*(5582), 833–836, doi:10.1126/science.1072815.

Bé, A. W. H. (1959), A method for rapid sorting of foraminifera from marine plankton samples, *J. Paleontol.*, *33*(5), 846–848.

Bé, A. W. H. (1980), Gametogenic calcification in a spinose planktonic foraminifer, *Globigerinoides sacculifer* (Brady), *Mar. Micropaleontol.*, *5*(3), 283–310, doi:10.1016/0377-8398(80)90014-6.

Bé, A. W. H., S. M. Harrison, and L. Lott (1973), Orbulina universa d'Orbigny in the Indian Ocean, *Mar. Micropaleontol.*, *19*(2), 150–192.

Beer, C. J., R. Schiebel, and P. A. Wilson (2010a), Technical note: On methodologies for determining the size-normalised weight of planktic foraminifera, *Biogeosciences*, *7*(7), 2193–2198, doi:10.5194/bg-7-2193-2010.

Beer, C. J., R. Schiebel, and P. A. Wilson (2010b), Testing planktic foraminiferal shell weight as a surface water [CO_3^{2-}] proxy using plankton net samples, *Geology*, *38*(2), 103–106. doi:10.1130/G30150.1

Bemis, B. E., H. J. Spero, J. Bijma, and D. W. Lea (1998), Reevaluation of the oxygen isotopic composition of planktonic foraminifera: Experimental results and revised paleotemperature equations, *Paleoceanography*, *13*(2), 150–160, doi:10.1029/98PA00070.

Bentov, S., C. Brownlee, and J. Erez (2009), The role of seawater endocytosis in the biomineralization process in calcareous foraminifera, *Proc. Natl. Acad. Sci. U. S. A.*, *106*(51), 21,500–21,504.

Bijma, J., J. Erez, and C. Hemleben (1990), Lunar and semi-lunar reproductive cycles in some spinose planktonic foraminifers, *J. Foraminiferal Res.*, *20*(2), 117–127, doi:10.2113/gsjfr.20.2.117.

Bijma, J., C. Hemleben, H. Oberhaensli, and M. Spindler (1992), The effects of increased water fertility on tropical spinose planktonic foraminifers in laboratory cultures, *J. Foraminiferal Res.*, *22*(3), 242–256, doi:10.2113/gsjfr.22.3.242.

Bijma, J., H. J. Spero, and D. W. Lea (1999). Reassessing foraminiferal stable isotope geochemistry: Impact of the oceanic carbonate system (experimental results), in *Uses of Proxies in Paleoceanography: Examples From the South Atlantic*, edited by G. Fischer and G. Wefer, pp. 489– 512, Springer, Berlin, doi: 10.1007/978-3-642-58646-0_20.

Bijma, J., B. Honisch, and R. E. Zeebe (2002), Impact of the ocean carbonate chemistry on living foraminiferal shell weight: Comment on "Carbonate ion concentration in glacial-age deep waters of the Caribbean Sea" by W. S. Broecker and E. Clark, *Geochem. Geophys. Geosyst.*, *3*(11), 1064, doi:10.1029/2002GC000388.

Broecker, W., and E. Clark (2001), A dramatic Atlantic dissolution event at the onset of the last glaciation, *Geochem. Geophys. Geosyst.*, *2*(11), 1065, doi:10.1029/2001GC000185.

Caldiera, K., and M. E. Wickett (2003), Anthropogenic carbon and ocean pH, *Nature*, *425*(6956), 365–365. doi:10.1038/425365a.

Caron, D. A., O. R. Anderson, J. L. Lindsey, W. W. Faber, and E. L. Lim (1990), Effects of gametogenesis on test structure and dissolution of some spinose planktonic foraminfera and implications for test preservation, *Mar. Micropaleontol.*, *16*(1–2), 93–116, doi:10.1016/0377-8398(90)90031-G.

De Moel, H., G. M. Ganssen, F. J. C. Peeters, S. J. A. Jung, D. Kroon, G. J. A. Brummer, and R. E. Zeebe (2009), Planktic foraminiferal shell thinning in the Arabian Sea due to anthropogenic ocean acidification?, *Biogeosciences*, *6*(9), 1917–1925, doi:10.5194/bg-6-1917-2009.

De Villiers, S. (2004), Optimum growth conditions as opposed to calcite saturation as a control on the calcification rate and shell-weight of marine foraminifera, *Mar. Biol.*, *144*(1), 45–49, doi:10.1007/s00227-003-1183-8.

Dickson, A. G. (1990), Thermodynamics of the dissociation of boric acid in synthetic seawater from 273.15 K to 318.15 K, *Deep Sea Res. Part A*, *37*(5), 755–766, doi:10.1016/0198-0149(90)90004-F.

Erez, J. (1978), Vital effect on stable-isotope composition seen in foraminifera and coral skeletons, *Nature*, *273*(5659), 199–202, doi:10.1038/273199a0.

Farmer, E. C., A. Kaplan, P. B. de Menocal, and J. Lynch-Stieglitz (2007), Corroborating ecological depth preferences of planktonic foraminifera in the tropical Atlantic with the stable oxygen isotope ratios of core top specimens, *Paleoceanography*, *22*, PA3205, doi:10.1029/2006PA001361.

Feely, R. A., Sabine, C.L., Lee, K., Berelson, W., J. A. Kleypas, V. J. Fabry, and Millero, F.J. (2004), Impact of anthropogenic CO_2 on the $CaCO_3$ system in the oceans, *Science*, *305*(5682), 362–366, doi:10.1126/science.1097329.

Gibbs, S. J., H. M. Stoll, P. R. Bown, and T. J. Bralower (2010), Ocean acidification and surface water carbonate production across the Paleocene–Eocene thermal maximum, *Earth Planet. Sci. Lett.*, *295*(3–4), 583–592, doi:10.1016/j.epsl.2010.04.044.

Goñi, M. A., H. L. Aceves, R. C. Thunell, E. Tappa, D. Black, Y. Astor, R. Varela, and F. Muller-Karger (2003), Biogenic fluxes in the Cariaco Basin: A combined study of sinking particulates and underlying sediments, *Deep Sea Res. Part I*, *50*(6), 781–807, doi:10.1016/S0967-0637(03)00060-8.

Gonzalez-Mora, B., F. J. Sierro, and J. A. Flores (2008), Controls of shell calcification in planktonic foraminifers, *Quat. Sci. Rev.*, *27*(9–10), 956–961, doi:10.1016/j.quascirev.2008.01.008.

Hecht, A. D. (1976), An ecologic model for test size variation in recent planktonic foraminifera: Applications to the fossil record, *J. Foraminiferal Res.*, *6*(4), 295–311, doi:10.2113/gsjfr.6.4.295.

Hecht, A. D., and S. M. Savin (1972), Phenotypic variation and oxygen isotope ratios in recent planktonic foraminifera, *J. Foraminiferal Res.*, *2*(2), 55–67, doi:10.2113/gsjfr.2.2.55.

Hemleben, C., M. Spindler, and O. R. Anderson (1989), *Modern Planktonic Foraminifera*, 363 pp., Springer, New York, doi:10.1007/978-1-4612-3544-6.

Henehan, M. J., et al. (2013), Calibration of the boron isotope proxy in the planktonic foraminifera *Globigerinoides ruber* for use in palaeo-CO_2 reconstruction, *Earth Planet. Sci. Lett.*, *364*, 111–122, doi:10.1016/j.epsl.2012.12.029.

Hoegh-Guldberg, O., et al. (2007), Coral reefs under rapid climate change and ocean acidification, *Science*, *318*(5857), 1737–1742, doi:10.1126/science.1152509.

Honisch, B., et al. (2012), The geological record of ocean acidification, *Science*, *335*(6072), 1058–1063, doi:10.1126/science.1208277.

Iglesias-Rodriguez, M. D., et al. (2008), Phytoplankton calcification in a high-CO_2 world, *Science*, *320*(5874), 336–340, doi:10.1126/science.1154122.

Jorgensen, B. B., J. Erez, N. P. Revsbech, and Y. Cohen (1985), Symbiotic photosynthesis in a planktonic foraminiferan, *Globigerinoides sacculifer* (Brady), studied with microelectrodes 1, *Limnol. Oceanogr.*, *30*(6), 1253–1267.

King, A., and W. Howard (2005), delta O-18 seasonality of planktonic foraminifera from Southern Ocean sediment traps: Latitudinal gradients and implications for paleoclimate reconstructions, *Mar. Micropaleontol.*, *56*(1–2), 1–24, doi:10.1016/j.marmicro.2005.02.008.

Klaas, C., and D. E. Archer (2002), Association of sinking organic matter with various types of mineral ballast in the deep sea: Implications for the rain ratio, *Global Biogeochem. Cycles*, *16*(4), 1116, doi:10.1029/2001GB001765.

Kuroyanagi, A., M. Tsuchiya, H. Kawahata, and H. Kitazato (2008), The occurrence of two genotypes of the planktonic foraminifer *Globigerinoides ruber* (white) and paleo-environmental implications, *Mar. Micropaleontol.*, *68*(3–4), 236–243, doi:10.1016/j.marmicro.2008.04.004.

Lombard, F., L. Labeyrie, E. Michel, H. J. Spero, and D. W. Lea (2009), Modelling the temperature dependent growth rates of planktic foraminifera, *Mar. Micropaleontol.*, *70*(1–2), 1–7, doi:10.1016/j.marmicro.2008.09.004.

]Lombard, F., R. E. da Rocha, J. Bijma, and J. P. Gattuso (2010), Effect of carbonate ion concentration and irradiance on calcification in planktonic foraminifera, *Biogeosciences*, *7*(1), 247–255, doi:10.5194/bg-7-247-2010.

Lueker, T. J., A. G. Dickson, and C. D. Keeling (2000), Ocean pCO_2 calculated from dissolved inorganic carbon, alkalinity, and equations for K1 and K2: Validation based on laboratory measurements of CO_2 in gas and seawater at equilibrium, *Mar. Chem.*, *70*(1–3), 105–119, doi:10.1016/S0304-4203(00)00022-0.

Manno, C., N. Morata, and R. Bellerby (2012), Effect of ocean acidification and temperature increase on the planktonic foraminifer *Neogloboquadrina pachyderma* (sinistral), *Polar Biol.*, *35*(9), 1311–1319, doi:10.1007/s00300-012-1174-7.

McConnell, M. C., R. C. Thunell, L. Lorenzoni, Y. Astor, J. D. Wright, and R. Fairbanks (2009), Seasonal variability in the salinity and oxygen isotopic composition of seawater from the Cariaco Basin, Venezuela: Implications for paleosalinity reconstructions, *Geochem. Geophys. Geosyst.*, *10*, Q06019, doi:10.1029/2008GC002035.

Mekik, F., and L. Raterink (2008), Effects of surface ocean conditions on deep-sea calcite dissolution proxies in the tropical Pacific, *Paleoceanography*, *23*, PA1216, doi:10.1029/2007PA001433.

Miles, J., and M. Shevlin (2001). *Applying Regression and Correlation: A Guide for Student Researchers*, Sage, London.

Miro, M. D. (1971), Los foraminiferous planctonicos vivos y sedimentados del margen continental de Venezuela, *Acta Geologica Hispanica VI*, 102–108.

Moy, A. D., W. R. Howard, S. G. Bray, and T. W. Trull (2009), Reduced calcification in modern Southern Ocean planktonic foraminifera, *Nat. Geosci.*, *2*(4), 276–280, doi:10.1038/ngeo460.

Mulitza, S., T. Wolff, J. Pätzold, W. Hale, and G. Wefer (1998), Temperature sensitivity of planktic foraminifera and its influence on the oxygen isotope record, *Mar. Micropaleontol.*, *33*(3–4), 223–240, doi:10.1016/S0377-8398(97)00040-6.

Mulitza, S., D. Boltovskoy, B. Donner, H. Meggers, A. Paul, and G. Wefer (2003), Temperature:δ^{18}O relationships of planktonic foraminifera collected from surface waters. *Palaeogeogr. Palaeoclimatol. Palaeoecol.*, *202*, 143–152, doi:10.1016/S0031-0182(03)00633-3.

Muller-Karger, F., et al. (2000), Sediment record linked to surface processes in the Cariaco Basin, *Eos Trans. AGU*, *81*(45), 529–535, doi:10.1029/EO081i045p00529-01.

Muller-Karger, F., et al. (2001), Annual cycle of primary production in the Cariaco Basin: Response to upwelling and implications for vertical export, *J. Geophys. Res.*, *106*(C3), 4527–4542, doi:10.1029/1999JC000291.

Naik, S. S., and P. D. Naidu (2007), Calcite dissolution along a transect in the western tropical Indian Ocean: A multiproxy approach, *Geochem. Geophys. Geosyst.*, *8*, Q08009, doi:10.1029/2007GC001615.

Naik, S. S., P. D. Naidu, P. Govil, and S. Godad (2010), Relationship between weights of planktonic foraminifer shell and surface water CO_3 = concentration during the Holocene and Last Glacial Period, *Mar. Geol.*, *275*(1–4), 278–282, doi:10.1016/j.margeo.2010.05.004.

Numberger, L., C. Hemleben, R. Hoffmann, A. Mackensen, H. Schulz, J.-M. Wunderlich, and M. Kucera (2009), Habitats, abundance patterns and isotopic signals of morphotypes of the planktonic foraminifer *Globigerinoides ruber* (d'Orbigny) in the eastern Mediterranean Sea since the Marine Isotopic Stage 12, *Mar. Micropaleontol.*, *73*(1–2), 90–104, doi:10.1016/j.marmicro.2009.07.004.

Orr, J. C., et al. (2005), Anthropogenic ocean acidification over the twenty-first century and its impact on calcifying organisms, *Nature*, *437*(7059), 681–686, doi:10.1038/nature04095.

Pelletier, G., E. Lewis, and D. Wallace (2007) CO2sys_ver16.xls: A calculator for the CO_2 system in seawater for Microsoft Excel/VBA, Wash. State Dep. of Ecol., Olympia.

Ridgwell, A., and R. Zeebe (2005), The role of the global carbonate cycle in the regulation and evolution of the Earth system, *Earth Planet. Sci. Lett.*, *234*(3–4), 299–315, doi:10.1016/j.epsl.2005.03.006.

Riebesell, U., I. Zondervan, B. Rost, P. Tortell, R. Zeebe, and F. Morel (2000), Reduced calcification of marine plankton in response to increased atmospheric CO_2, *Nature*, *407*(6802), 364–367, doi:10.1038/35030078.

Ries, J. B., A. L. Cohen, and D. C. McCorkle (2009), Marine calcifiers exhibit mixed responses to CO_2-induced ocean acidification, *Geology*, *37*(12), 1131–1134, doi:10.1130/G30210A.1.

Rink, S., M. Kühl, J. Bijma, and H. J. Spero (1998), Microsensor studies of photosynthesis and respiration in the symbiotic foraminifer *Orbulina universa*, *Mar. Biol.*, *131*(4), 583–595.

Russell, A. D., B. Hönisch, H. J. Spero, and D. W. Lea (2004), Effects of seawater carbonate ion concentration and temperature on shell U, Mg, and Sr in cultured planktonic foraminifera, *Geochim. Cosmochim. Acta*, *68*(21), 4347–4361, doi:10.1016/j.gca.2004.03.013.

Sabine, C. L. et al. (2004), The oceanic sink for anthropogenic CO_2, *Science*, *305*(5682), 367–371, doi:10.1126/science.1097403.

Sautter, L. R., and R. C. Thunell (1991), Seasonal variability in the δ^{18}O and δ^{13}C of planktonic foraminifera from an upwelling environment: Sediment trap results from the San Pedro Basin, Southern California Bight, *Paleoceanography*, *6*(3), 307–334, doi:10.1029/91PA00385.

Schiebel, R. (2002), Planktic foraminiferal sedimentation and the marine calcite budget, *Global Biogeochem. Cycles*, *16*(4), 1065, doi:10.1029/2001GB001459.

Schmidt, D. N., S. Renaud, J. Bollmann, R. Schiebel, and H. R. Thierstein (2004), Size distribution of Holocene planktic foraminifer assemblages: Biogeography, ecology and adaptation, *Mar. Micropaleontol.*, *50*(3–4), 319–338, doi:10.1016/S0377-8398(03)00098-7.

Spero, H. J. (1992), Do planktic foraminifera accurately record shifts in the carbon isotopic composition of seawater ΣCO_2?, *Mar. Micropaleontol.*, *19*(4), 275–285, doi:10.1016/0377-8398(92)90033-G.

Spero, H. J., J. Bijma, D. W. Lea, and B. E. Bemis (1997), Effect of seawater carbonate concentration on foraminiferal carbon and oxygen isotopes, *Nature*, *390*, 497–500, doi:10.1038/37333.

Takahashi, K., and A. W. H. Bé (1984), Planktonic foraminifera—Factors controlling sinking speeds, *Deep Sea Res. Part A*, *31*(12), 1477–1500, doi:10.1016/0198-0149(84)90083-9.

Tedesco, K., R. Thunell, Y. Astor, and F. Muller-Karger (2007), The oxygen isotope composition of planktonic foraminifera from the Cariaco Basin, Venezuela: Seasonal and interannual variations, *Mar. Micropaleontol.*, *62*(3), 180–193, doi:10.1016/j.marmicro.2006.08.002.

Thunell, R. C., R. Varela, M. Llano, J. Collister, F. Muller-Karger, and R. Bohrer (2000), Organic carbon fluxes, degradation, and accumulation in an anoxic basin: Sediment trap results from the Cariaco Basin, *Limnol. Oceanogr.*, *45*, 300–308.

Wang, L. (2000), Isotopic signals in two morphotypes of *Globigerinoides ruber* (white) from the South China Sea: Implications for monsoon climate change during the last glacial cycle, *Palaeogeogr. Palaeoclimatol. Palaeoecol.*, *161*(3), 381–394.

Wejnert, K. E. (2011), Seasonal and annual variability in elemental and isotopic proxies of past ocean conditions: Results from the Guaymas and Cariaco Basins, PhD dissertation, 236 pp., Mar. Sci. Program, Univ. of S. C., Columbia.

Wolf-Gladrow, D. A., J. Bijma, and R. E. Zeebe (1999), Model simulation of the carbonate chemistry in the microenvironment of symbiont bearing foraminifera, *Mar. Chem.*, *64*(3), 181–198, doi:10.1016/S0304-4203(98)00074-7.

Zeebe, R. E. (2012), History of seawater carbonate chemistry, atmospheric CO_2, and ocean acidification, *Annu. Rev. Earth Planet. Sci.*, *40*(1), 141–165, doi:10.1146/annurev-earth-042711-105521.

Zeebe, R. E., and D. A. Wolf-Gladrow (2001), *CO_2 in Seawater: Equilibrium, Kinetics, Isotopes*, Elsevier Oceanogr. Ser., vol. *65*, 346 pp., Elsevier, Amsterdam.

Zeebe, R. E., J. C. Zachos, K. Caldeira, and T. Tyrrell (2008), Carbon emissions and acidification, *Science*, *321*(5885), 51–52, doi:10.1126/science.1159124.

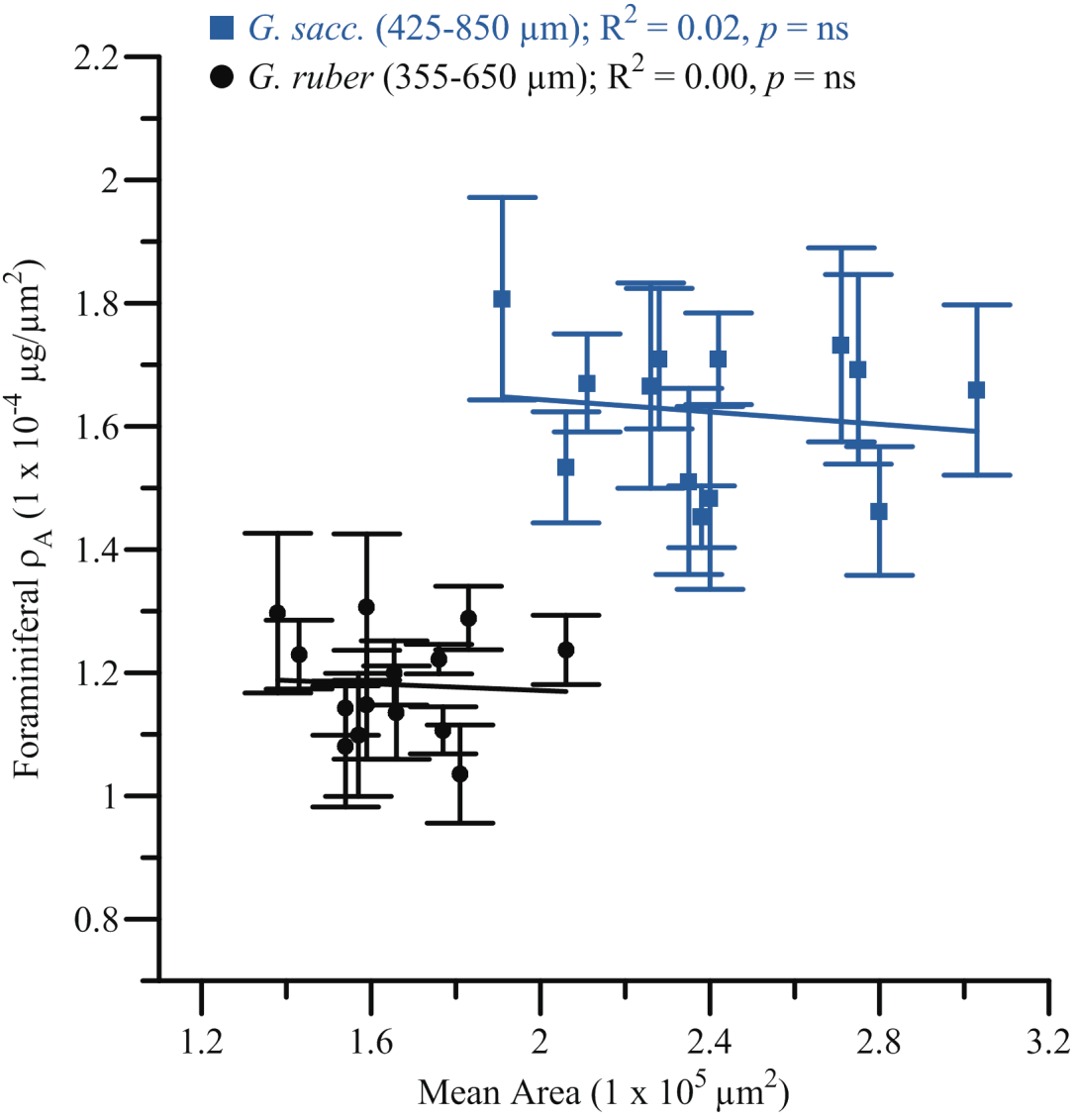

FIGURE E.1: Supplementary Figure 1

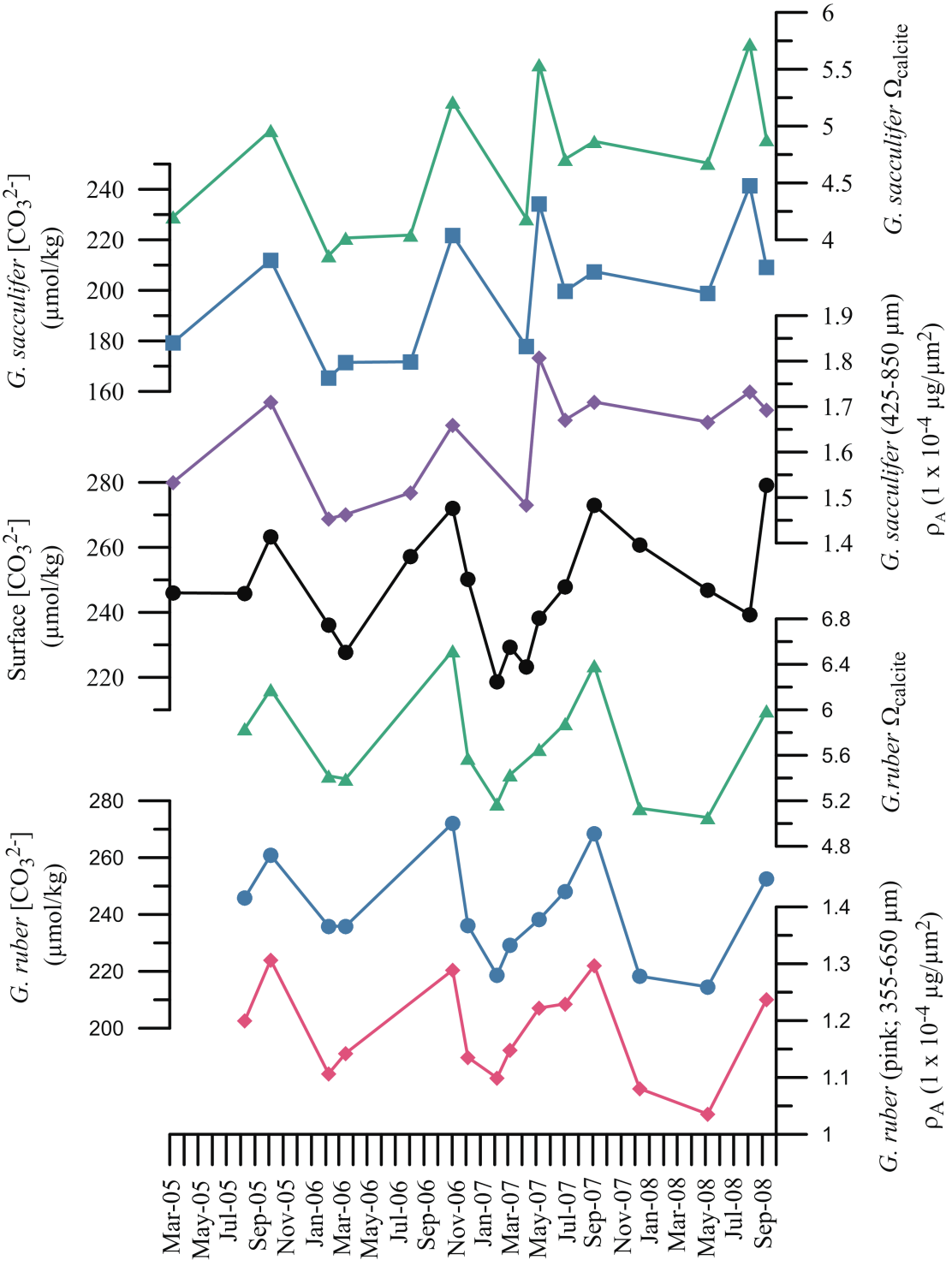

FIGURE E.2: Supplementary Figure 2

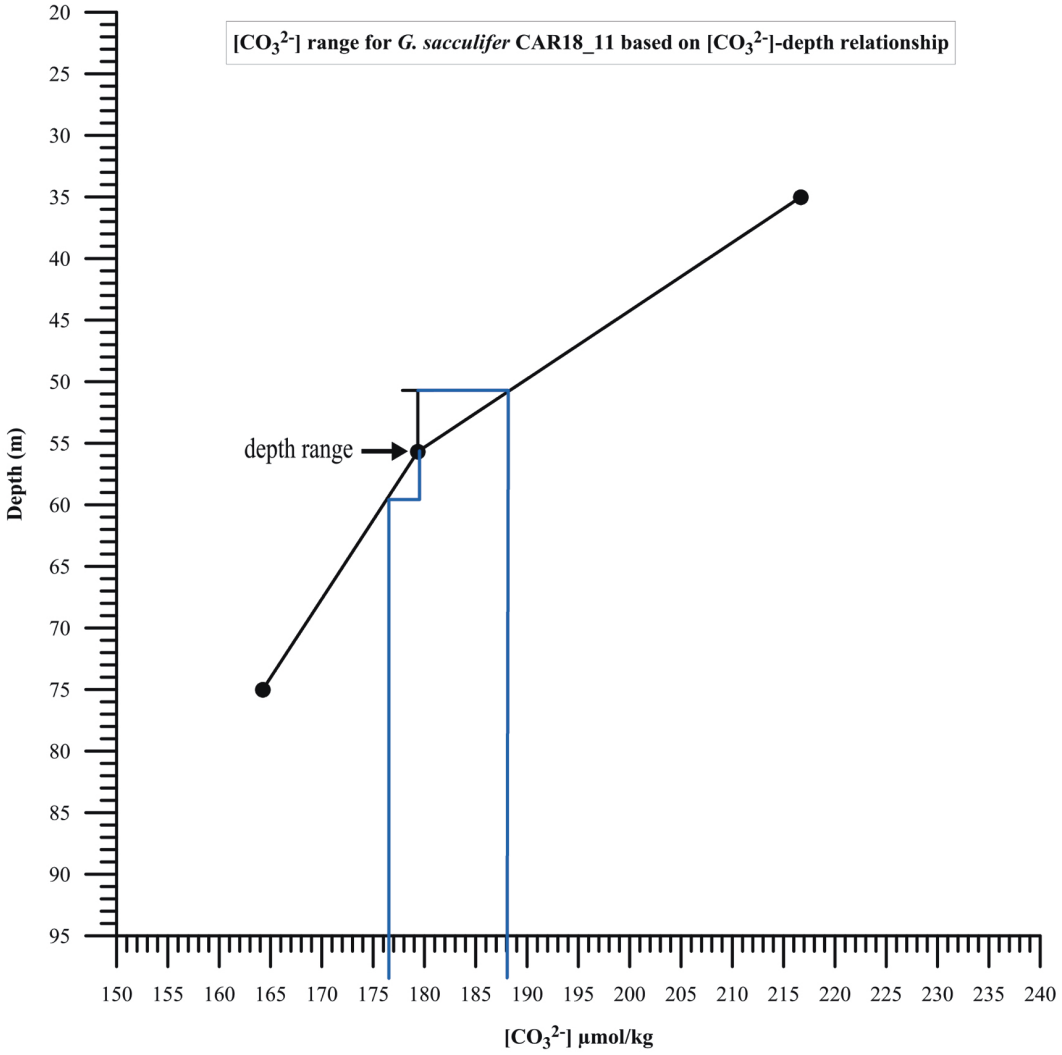

FIGURE E.3: Supplementary Figure 3

Bibliography

Jugdeep Aggarwal, Florian Böhm, Gavin L. Foster, Stanislaw Halas, Bärbel Hönisch, Shao-Yong Jiang, Jan Kosler, Amir Liba, Illia Rodushkin, Ted Sheehan, Jason Jiun-San Shen, Sonia Tonarini, Qianli Xie, Chen-Feng You, Zhi-Qi Zhao, and Evelyn Zuleger. How well do non-traditional stable isotope results compare between different laboratories: results from the interlaboratory comparison of boron isotope measurements. *Journal of Analytical Atomic Spectrometry*, 24(6):825–831, March 2009. doi: 10.1039/B815240C. URL http://pubs.rsc.org/en/Content/ArticleLanding/2009/JA/b815240c.

Jugdeep K. Aggarwal and Martin R. Palmer. Boron isotope analysis: A review. *Analyst*, 120:1301–1308, May 1995.

Emmanuel Kenneth Agyei. Isotopic and Elemental Composition of Boron in Meteorites, Tektites and Terrestrial Materials. *Ph.D. Thesis*, page 5, 1968. URL http://adsabs.harvard.edu/abs/1968PhDT.....5A.

Jinho Ahn, Edward J. Brook, Logan Mitchell, Julia Rosen, Joseph R. McConnell, Kendrick Taylor, David Etheridge, and Mauro Rubino. Atmospheric CO2 over the last 1000 years: A high-resolution record from the west antarctic ice sheet (WAIS) divide ice core. *Global Biogeochemical Cycles*, 26:11 PP., May 2012. doi: 201210.1029/2011GB004247. URL http://www.agu.org/pubs/crossref/2012/2011GB004247.shtml.

H. Akaike. A new look at the statistical model identification. *IEEE Transactions on Automatic Control*, 19(6):716–723, 1974. ISSN 0018-9286. doi: 10.1109/TAC.1974.1100705.

Assad S. Al-Ammar, Rajesh K. Gupta, and Ramon M. Barnes. Elimination of boron memory effect in inductively coupled plasma-mass spectrometry by ammonia gas

injection into the spray chamber during analysis. *Spectrochimica Acta Part B: Atomic Spectroscopy*, 55(6):629–635, June 2000. ISSN 0584-8547. doi: 10.1016/S0584-8547(00)00197-X. URL http://www.sciencedirect.com/science/article/pii/S058485470000197X.

D. Aldridge, C. J. Beer, and D. A. Purdie. Calcification in the planktonic foraminifera *Globigerina bulloides* linked to phosphate concentrations in surface waters of the North Atlantic Ocean. *Biogeosciences*, 9:1725–1739, May 2012. doi: 10.5194/bg-9-1725-2012. URL http://adsabs.harvard.edu/abs/2012BGeo....9.1725A.

Katherine A. Allen and Bärbel Hönisch. The planktic foraminiferal B/Ca proxy for seawater carbonate chemistry: A critical evaluation. *Earth and Planetary Science Letters*, 345–348:203–211, September 2012. ISSN 0012-821X. doi: 10.1016/j.epsl.2012.06.012. URL http://www.sciencedirect.com/science/article/pii/S0012821X12002968.

Katherine A. Allen, Bärbel Hönisch, Stephen M. Eggins, Jimin Yu, Howard J. Spero, and Henry Elderfield. Controls on boron incorporation in cultured tests of the planktic foraminifer *Orbulina universa*. *Earth and Planetary Science Letters*, 309 (3–4):291–301, September 2011. ISSN 0012-821X. doi: 10.1016/j.epsl.2011.07.010. URL http://www.sciencedirect.com/science/article/pii/S0012821X11004250.

Katherine A. Allen, Bärbel Hönisch, Stephen M. Eggins, and Yair Rosenthal. Environmental controls on B/Ca in calcite tests of the tropical planktic foraminifer species *Globigerinoides ruber* and *Globigerinoides sacculifer*. *Earth and Planetary Science Letters*, 351–352:270–280, October 2012. ISSN 0012-821X. doi: 10.1016/j.epsl.2012.07.004. URL http://www.sciencedirect.com/science/article/pii/S0012821X12003639.

Eleni Anagnostou, K.-F. Huang, C.-F. You, E.L. Sikes, and R.M. Sherrell. Evaluation of boron isotope ratio as a pH proxy in the deep sea coral *Desmophyllum dianthus*: Evidence of physiological pH adjustment. *Earth and Planetary Science Letters*, 349–350(0):251–260, October 2012. ISSN 0012-821X. doi: 10.1016/j.epsl.2012.07.006. URL http://www.sciencedirect.com/science/article/pii/S0012821X12003652.

Pallavi Anand and Henry Elderfield. Variability of Mg/Ca and Sr/Ca between and within the planktonic foraminifers *Globigerina bulloides* and *Globorotalia truncatulinoides*. *Geochemistry, Geophysics, Geosystems*, 6(11):n/a–n/a, 2005. ISSN 1525-2027. doi: 10.1029/2004GC000811. URL http://onlinelibrary.wiley.com/doi/10.1029/2004GC000811/abstract.

Pallavi Anand, Henry Elderfield, and Maureen H. Conte. Calibration of Mg/Ca thermometry in planktonic foraminifera from a sediment trap time series. *Paleoceanography*, 18(2):1050–1064, 2003. URL http://www.geo.vu.nl/~palmorph/staff/pallavi/Anand%202003%20Paleo.pdf.

O Roger Anderson and W W. Jr. Faber. An estimation of calcium carbonate deposition rate in a planktonic foraminifer *Globigerinoides sacculifer* using Ca-45 as a tracer- a recommended procedure for improved accuracy. *Journal of Foraminiferal Research*, 14(4):303–308, 1984.

T. Anning, N. Nimer, M.J. Merrett, and C. Brownlee. Costs and benefits of calcification in coccolithophorids. *Journal of Marine Systems*, 9(1–2):45–56, October 1996. ISSN 0924-7963. doi: 10.1016/0924-7963(96)00015-2. URL http://www.sciencedirect.com/science/article/pii/0924796396000152.

Svante Arrhenius. On the influence of carbonic acid in the air upon the temperature of the ground. *Philosophical Magazine and Journal of Science, Series 5*, 41:237–276, April 1896.

Elliot Leonard Atlas. *Phosphate equilibria in seawater and interstitial waters*. PhD thesis, Oregon State University, Corvallis, OR, June 1975. URL http://ir.library.oregonstate.edu/xmlui/handle/1957/28556. Graduation date: 1976.

Ralf Aurahs, Guido W. Grimm, Vera Hemleben, Christoph Hemleben, and Michal Kucera. Geographical distribution of cryptic genetic types in the planktonic foraminifer *Globigerinoides ruber*. *Molecular Ecology*, 18:1692–1706, 2009.

Ralf Aurahs, Yvonne Treis, Kate Darling, and Michal Kucera. A revised taxonomic and phylogenetic concept for the planktonic foraminifer species *Globigerinoides ruber* based on molecular and morphometric evidence. *Marine Micropaleontology*, 79:1–14, 2011. doi: doi:10.1016/j.marmicro.2010.12.001.

O. L. Bandy. Variations in *Globigerina bulloides* (d'Orbigny) as indices of water masses. *Antarcic Journal of the US*, 7:194–195, 1972.

Stephen Barker, Mervyn Greaves, and Henry Elderfield. A study of cleaning procedures used for foraminiferal Mg/Ca paleothermometry. *Geochemistry, Geophysics and Geosystems*, 4(9):8407–8426, September 2003.

G. A. Bartholomew and P. J. Campion. Neutron Capture Gamma Rays from Lithium, Boron, and Nitrogen. *Canadian Journal of Physics*, 35(12):1347–1360, December 1957. ISSN 0008-4204. doi: 10.1139/p57-147. URL http://www.nrcresearchpress.com/doi/abs/10.1139/p57-147.

F. A. Bazzaz and William E. Williams. Atmospheric CO2 concentrations within a mixed forest: Implications for seedling growth. *Ecology*, 72(1):12–16, February 1991. ISSN 0012-9658. doi: 10.2307/1938896. URL http://www.jstor.org/stable/1938896.

Allan W. H. Bé. A method for rapid sorting of foraminifera from marine plankton samples. *Journal of Paleontology*, 33(5):846–848, 1959.

A.W.H. Bé. Gametogenic calcification in a spinose planktonic foraminifer, *Globigerinoides sacculifer* (Brady). *Marine Micropaleontology*, 5:283–310, 1980. ISSN 0377-8398. doi: 10.1016/0377-8398(80)90014-6. URL http://www.sciencedirect.com/science/article/pii/0377839880900146.

Bryan E. Bemis, Howard J. Spero, Jelle Bijma, and David W. Lea. Reevaluation of the oxygen isotopic composition of planktonic foraminifera: Experimental results and revised paleotemperature equations. *Paleoceanography*, 13(2):150–160, 1998. ISSN 1944-9186. doi: 10.1029/98PA00070. URL http://onlinelibrary.wiley.com/doi/10.1029/98PA00070/abstract.

Shmuel Bentov and Jonathan Erez. Novel observations on biomineralization processes in foraminifera and implications for Mg/Ca ratio in the shells. *Geology*, 33(11): 841–844, November 2005. ISSN 0091-7613, 1943-2682. doi: 10.1130/G21800.1. URL http://geology.geoscienceworld.org/content/33/11/841.

Shmuel Bentov and Jonathan Erez. Impact of biomineralization processes on the Mg content of foraminiferal shells: A biological perspective. *Geochemistry, Geophysics,*

Geosystems, 7(1):n/a–n/a, 2006. ISSN 1525-2027. doi: 10.1029/2005GC001015. URL http://onlinelibrary.wiley.com/doi/10.1029/2005GC001015/abstract.

Shmuel Bentov, Colin Brownlee, and Jonathan Erez. The role of seawater endocytosis in the biomineralization process in calcareous foraminifera. *Proceedings of the National Academy of Sciences*, 106(51):21500 –21504, December 2009. doi: 10.1073/pnas.0906636106. URL http://www.pnas.org/content/106/51/21500.abstract.

Shmuel Bentov, Simy Weil, Lilah Glazer, Amir Sagi, and Amir Berman. Stabilization of amorphous calcium carbonate by phosphate rich organic matrix proteins and by single phosphoamino acids. *Journal of Structural Biology*, 171(2):207–215, August 2010. ISSN 1047-8477. doi: 10.1016/j.jsb.2010.04.007. URL http://www.sciencedirect.com/science/article/pii/S1047847710001206.

J. Bermin, D. Vance, C. Archer, and P.J. Statham. The determination of the isotopic composition of Cu and Zn in seawater. *Chemical Geology*, 226(3–4):280–297, February 2006. ISSN 0009-2541. doi: 10.1016/j.chemgeo.2005.09.025. URL http://www.sciencedirect.com/science/article/pii/S0009254105004456.

R. A. Berner, J. T. Westrich, R. Graber, J. Smith, and C. S. Martens. Inhibition of aragonite precipitation from supersaturated seawater; a laboratory and field study. *American Journal of Science*, 278(6):816–837, June 1978. ISSN 0002-9599, 1945-452X. doi: 10.2475/ajs.278.6.816. URL http://www.ajsonline.org/content/278/6/816.

Robert A. Berner and John W. Morse. Dissolution kinetics of calcium carbonate in sea water; IV, Theory of calcite dissolution. *American Journal of Science*, 274(2): 108–134, February 1974. ISSN 0002-9599, 1945-452X. doi: 10.2475/ajs.274.2.108. URL http://www.ajsonline.org/content/274/2/108.

Robert R. Bidigare, Arnim Fluegge, Katherine H. Freeman, Kristi L. Hanson, John M. Hayes, David Hollander, John P. Jasper, Linda L. King, Edward A. Laws, Jeffrey Milder, Frank J. Millero, Richard Pancost, Brian N. Popp, Paul A. Steinberg, and Stuart G. Wakeham. Consistent fractionation of 13C in nature and in the laboratory: Growth-rate effects in some haptophyte algae. *Global Biogeochemical*

Cycles, 11(2):279–292, 1997. ISSN 1944-9224. doi: 10.1029/96GB03939. URL http://onlinelibrary.wiley.com/doi/10.1029/96GB03939/abstract.

Jelle Bijma, Jonathan Erez, and Christoph Hemleben. Lunar and semi-lunar reproductive cycles in some spinose planktonic foraminifers. *The Journal of Foraminiferal Research*, 20(2):117–127, April 1990. doi: 10.2113/gsjfr.20.2.117. URL http://jfr.geoscienceworld.org/cgi/content/abstract/20/2/117.

Jelle Bijma, Christoph Hemleben, Hedi Oberhaensli, and Michael Spindler. The effects of increased water fertility on tropical spinose planktonic foraminifers in laboratory cultures. *The Journal of Foraminiferal Research*, 22(3):242–256, July 1992. ISSN 0096-1191,. doi: 10.2113/gsjfr.22.3.242. URL http://jfr.geoscienceworld.org/content/22/3/242.

Katharina Billups and Howard J. Spero. Relationship between shell size, thickness and stable isotopes in individual planktonic foraminifera from two Equatorial Atlantic cores. *The Journal of Foraminiferal Research*, 25(1):24–37, January 1995. ISSN 0096-1191,. doi: 10.2113/gsjfr.25.1.24. URL http://jfr.geoscienceworld.org/content/25/1/24.

Jon Blundy and Bernard Wood. Prediction of crystalmelt partition coefficients from elastic moduli. *Nature*, 372(6505):452–454, December 1994. doi: 10.1038/372452a0. URL http://www.nature.com/nature/journal/v372/n6505/abs/372452a0.html.

Annette Bolton, Joel A. Baker, Gavin B. Dunbar, Lionel Carter, Euan G. C. Smith, and Helen L. Neil. Environmental versus biological controls on Mg/Ca variability in *Globigerinoides ruber* (white) from core top and plankton tow samples in the southwest Pacific Ocean. *Paleoceanography*, 26:14 PP., June 2011. doi: 201110.1029/2010PA001924. URL http://www.agu.org/pubs/crossref/2011/2010PA001924.shtml.

Gabriel J. Bowen and David J. Beerling. An integrated model for soil organic carbon and CO2: Implications for paleosol carbonate pCO2 paleobarometry. *Global Biogeochemical Cycles*, 18(1):n/a–n/a, 2004. ISSN 1944-9224. doi: 10.1029/2003GB002117. URL http://onlinelibrary.wiley.com/doi/10.1029/2003GB002117/abstract.

Patrick Brading, Mark E. Warner, Phillip Davey, David J. Smith, Eric P. Achterberg, and David J. Suggett. Differential effects of ocean acidification on growth and photosynthesis among phylotypes of *Symbiodinium* (Dinophyceae). *Limnology and Oceanography*, 56(3):927–938, 2011. ISSN 0024-3590. URL http://cat.inist.fr/?aModele=afficheN&cpsidt=24185981.

D. O. Breecker, Z. D. Sharp, and L. D. McFadden. Atmospheric CO2 concentrations during ancient greenhouse climates were similar to those predicted for A.D. 2100. *Proceedings of the National Academy of Sciences*, 107(2):576–580, January 2010. ISSN 0027-8424, 1091-6490. doi: 10.1073/pnas.0902323106. URL http://www.pnas.org/content/107/2/576. PMID: 20080721.

Rachel E. Brown, Linda D. Anderson, Ellen Thomas, and James C. Zachos. A core-top calibration of B/Ca in the benthic foraminifers *Nuttallides umbonifera* and *Oridorsalis umbonatus*: A proxy for Cenozoic bottom water carbonate saturation. *Earth and Planetary Science Letters*, 310(3–4):360–368, October 2011. ISSN 0012-821X. doi: 10.1016/j.epsl.2011.08.023. URL http://www.sciencedirect.com/science/article/pii/S0012821X11004870.

Elizabeth A Burton and Lynn M Walter. The role of pH in phosphate inhibition of calcite and aragonite precipitation rates in seawater. *Geochimica et Cosmochimica Acta*, 54(3):797–808, March 1990. ISSN 0016-7037. doi: 10.1016/0016-7037(90)90374-T. URL http://www.sciencedirect.com/science/article/pii/001670379090374T.

Ken Caldeira and Michael E. Wickett. Oceanography: Anthropogenic carbon and ocean pH. *Nature*, 425(6956):365–365, September 2003. ISSN 0028-0836. doi: 10.1038/425365a. URL http://www.nature.com/nature/journal/v425/n6956/full/425365a.html.

David A. Caron, Allan W. H. Bé, and O. Roger Anderson. Effects of variations in light intensity on life processes of the planktonic foraminifer globigerinoides sacculifer in laboratory culture. *Journal of the Marine Biological Association of the United Kingdom*, 62(02):435–451, 1982. doi: 10.1017/S0025315400057374.

David A. Caron, O. Roger Anderson, Judith L. Lindsey, Walter W. Faber Jr., and E.E. Lin Lim. Effects of gametogenesis on test structure and dissolution of some spinose

planktonic foraminifera and implications for test preservation. *Marine Micropaleontology*, 16(1–2):93–116, August 1990. ISSN 0377-8398. doi: 10.1016/0377-8398(90)90031-G. URL http://www.sciencedirect.com/science/article/pii/037783989090031G.

Edward John Catanzaro, C. Champion, E. Garner, G. Marinenko, K. Sappenfield, and W. Shields. *Boric acid: isotopic and assay standard reference materials*. Number 260-17 in NBS (US) Special Publications. National Bureau of Standards, Institute for Materials Research, Washington D.C., 1970.

Thure E. Cerling. The stable isotopic composition of modern soil carbonate and its relationship to climate. *Earth and Planetary Science Letters*, 71(2):229–240, December 1984. ISSN 0012-821X. doi: 10.1016/0012-821X(84)90089-X. URL http://www.sciencedirect.com/science/article/pii/0012821X8490089X.

Thure E. Cerling. Carbon dioxide in the atmosphere; evidence from Cenozoic and Mesozoic Paleosols. *American Journal of Science*, 291(4):377–400, April 1991. ISSN 0002-9599, 1945-452X. doi: 10.2475/ajs.291.4.377. URL http://www.ajsonline.org/content/291/4/377.

Likwan Cheng. *Atomic-scale study of ion incorporation at calcite surface using synchrotron X-ray methods*. PhD thesis, Northwestern University, Evanston, Illinois, December 1998.

R. Coadic, Franck Bassinot, E. Douville, E. Michel, D. Dissard, and Mervyn Greaves. A core-top study of dissolution effect on B/Ca in *Globigerinoides sacculifer* from the tropical Atlantic: Potential bias for paleo-reconstruction of seawater carbonate chemistry. *Geochemistry, Geophysics and Geosystems*, 14:1053–1068, 2013. doi: doi:10.1029/2012GC004296.

Brian Colman, I. Emma Huertas, Shabana Bhatti, and Jeffrey S. Dason. The diversity of inorganic carbon acquisition mechanisms in eukaryotic microalgae. *Functional Plant Biology*, 29(3):261–270, January 2002. URL http://www.publish.csiro.au/paper/PP01184.

Dennis R. Cook and Sanford Weisberg. *Residuals and Influence in Regression*. Monographs on Statistics and Applied Probability. Chapman and Hall, New York, 1982.

Maggie Cusack and A. Freer. Biomineralization: Elemental and Organic Influence in Carbonate Systems. *Chemical Reviews*, 108:4433–4454, 2008.

D. Darbouret and I. Kano. Ultrapure water for boron and silica sensitive laboratory applications. *American Laboratory News*, January:12–16, January 2000.

Kate F. Darling and Christopher M. Wade. The genetic diversity of planktic foraminifera and the global distribution of ribosomal RNA genotypes. *Marine Micropaleontology*, 67(3–4):216–238, May 2008. ISSN 0377-8398. doi: 10.1016/j.marmicro.2008.01.009. URL http://www.sciencedirect.com/science/article/pii/S0377839808000212.

Jeffrey S. Dason, I. Emma Huertas, and Brian Colman. Source of Inorganic Carbon for Photosynthesis in Two Marine Dinoflagellates. *Journal of Phycology*, 40(2):285–292, 2004. ISSN 1529-8817. doi: 10.1111/j.1529-8817.2004.03123.x. URL http://onlinelibrary.wiley.com/doi/10.1111/j.1529-8817.2004.03123.x/abstract.

L. J. de Nooijer, T. Toyofuku, K. Oguri, H. Nomaki, and H. Kitazato. Intracellular pH distribution in foraminifera determined by the fluorescent probe HPTS. *Limnology and Oceanography: Methods*, 6:610–618, 2008. ISSN 15415856. doi: 10.4319/lom.2008.6.610. URL http://www.wwww.aslo.org/lomethods/free/2008/0610.html.

L. J. de Nooijer, G. Langer, G. Nehrke, and J. Bijma. Physiological controls on seawater uptake and calcification in the benthic foraminifer *Ammonia tepida*. *Biogeosciences*, 6(11):2669–2675, November 2009a. ISSN 1726-4170. URL http://www.biogeosciences.net/6/2669/2009/.

Lennart Jan de Nooijer, Takashi Toyofuku, and Hiroshi Kitazato. Foraminifera promote calcification by elevating their intracellular pH. *Proceedings of the National Academy of Sciences*, 106(36):15374–15378, 2009b. doi: 10.1073/pnas.0904306106. URL http://www.pnas.org/content/106/36/15374.abstract.

E.T. Degens, R.R.L. Guillard, W.M. Sackett, and J.A. Hellebust. Metabolic fractionation of carbon isotopes in marine plankton—I. Temperature and respiration experiments. *Deep Sea Research and Oceanographic Abstracts*, 15(1):1–9, February 1968. ISSN 0011-7471. doi: 10.1016/0011-7471(68)90024-7. URL http://www.sciencedirect.com/science/article/pii/0011747168900247.

Petra S. Dekens, David W. Lea, Dorothy K. Pak, and Howard J. Spero. Core top calibration of Mg/Ca in tropical foraminifera: Refining paleotemperature estimation. *Geochemistry, Geophysics, Geosystems*, 3(4):1–29, 2002. ISSN 1525-2027. doi: 10.1029/2001GC000200. URL http://onlinelibrary.wiley.com/doi/10.1029/2001GC000200/abstract.

W.G. Deuser, E.H. Ross, C. Hemleben, and M. Spindler. Seasonal changes in species composition, numbers, mass, size, and isotopic composition of planktonic foraminifera settling into the deep sargasso sea. *Palaeogeography, Palaeoclimatology, Palaeoecology*, 33(1–3):103–127, March 1981. ISSN 0031-0182. doi: 10.1016/0031-0182(81)90034-1. URL http://www.sciencedirect.com/science/article/pii/0031018281900341.

Annette Deyhle. Improvements of boron isotope analysis by positive thermal ionization mass spectrometry using static multicollection of Cs2BO2+ ions. *International Journal of Mass Spectrometry*, 206(1–2):79–89, February 2001. ISSN 1387-3806. doi: 10.1016/S1387-3806(00)00387-0. URL http://www.sciencedirect.com/science/article/pii/S1387380600003870.

Annette Deyhle and Achim Kopf. Possible influence of clay contamination on B isotope geochemistry of carbonaceous samples. *Applied Geochemistry*, 19(5):737–745, May 2004. ISSN 0883-2927. doi: 10.1016/j.apgeochem.2003.10.008. URL http://www.sciencedirect.com/science/article/pii/S0883292703002130.

Andrew G. Dickson. Thermodynamics of the dissociation of boric acid in synthetic seawater from 273.15 to 318.15 k. *Deep Sea Research Part A. Oceanographic Research Papers*, 37(5):755–766, May 1990. ISSN 0198-0149. doi: 10.1016/0198-0149(90)90004-F. URL http://www.sciencedirect.com/science/article/pii/019801499090004F.

Alcide Desallines d'Orbigny. Tableau méthodique de la classe de céphalopodes. *Annales des Sciences Naturelles*, 14:1–277, 1826.

Alcide Desallines d'Orbigny. *Voyage dans l'Amerique Meriodionale*. Strasbourg, France, 1839.

C. Dordas and P. H. Brown. Permeability of boric acid across lipid bilayers and factors affecting it. *The Journal of Membrane Biology*, 175(2):95–105, May 2000. ISSN

0022-2631, 1432-1424. doi: 10.1007/s002320001058. URL http://link.springer.com/article/10.1007/s002320001058.

Christos Dordas and Patrick H. Brown. Evidence for channel mediated transport of boric acid in squash (*Cucurbita pepo*). *Plant and Soil*, 235(1):95–103, August 2001. ISSN 0032-079X, 1573-5036. doi: 10.1023/A:1011837903688. URL http://link.springer.com/article/10.1023/A%3A1011837903688.

E. Douville, M. Paterne, G. Cabioch, P. Louvat, J. Gaillardet, A. Juillet-Leclerc, and L. Ayliffe. Abrupt sea surface pH change at the end of the Younger Dryas in the central sub-equatorial Pacific inferred from boron isotope abundance in corals (*Porites*). *Biogeosciences Discussions*, 7:1959–1993, March 2010. URL http://adsabs.harvard.edu/abs/2010BGD.....7.1959D.

Patricia M Dove and Michael F Hochella Jr. Calcite precipitation mechanisms and inhibition by orthophosphate: In situ observations by Scanning Force Microscopy. *Geochimica et Cosmochimica Acta*, 57(3):705–714, February 1993. ISSN 0016-7037. doi: 10.1016/0016-7037(93)90381-6. URL http://www.sciencedirect.com/science/article/pii/0016703793903816.

H. Effenberger, K. Mereiter, and J. Zemann. Crystal structure refinements of magnesite, calcite, rhodochrosite, siderite, smithonite, and dolomite, with discussion of some aspects of the stereochemistry of calcite type carbonates. *Zeitschrift fur Kristallographie*, 156:233–243, January 1981. doi: 10.1524/zkri.1981.156.3-4.233. URL http://adsabs.harvard.edu/abs/1981ZK....156..233E.

Stephen M. Eggins, Aleksey Sadekov, and Patrick De Deckker. Modulation and daily banding of Mg/Ca in *Orbulina universa* tests by symbiont photosynthesis and respiration: a complication for seawater thermometry? *Earth and Planetary Science Letters*, 225(3–4):411–419, September 2004. ISSN 0012-821X. doi: 10.1016/j.epsl.2004.06.019. URL http://www.sciencedirect.com/science/article/pii/S0012821X0400408X.

Douglas D. Ekart, Thure E. Cerling, Isabel P. Montanez, and Neil J. Tabor. A 400 million year carbon isotope record of pedogenic carbonate; implications for paleoatomospheric carbon dioxide. *American Journal of Science*, 299(10):805–827,

December 1999. ISSN 0002-9599, 1945-452X. doi: 10.2475/ajs.299.10.805. URL http://www.ajsonline.org/content/299/10/805.

Jonathan Erez. Calcification rates, photosynthesis and light in planktonic foraminifera. In P. Westbroek, editor, *Biomineralization and biological metal accumulation*, pages 307–312. D. Reidel Publishing Company, Dordrecht, Holland, 1983. ISBN 90-277-1515-7.

Jonathan Erez and Susumu Honjo. Comparison of isotopic composition of planktonic foraminifera in plankton tows, sediment traps and sediments. *Palaeogeography, Palaeoclimatology, Palaeoecology*, 33:129–156, March 1981. ISSN 00310182. doi: 10.1016/0031-0182(81)90035-3. URL http://elsevier-apps.sciverse.com/GoogleMaps/index.jsp?doi=10.1016/0031-0182%2881%2990035-3.

Richard G. Fairbanks, Marc Sverdlove, Rosemary Free, Peter H. Wiebe, and Allan W. H. Bé. Vertical distribution and isotopic fractionation of living planktonic foraminifera from the Panama Basin. *Nature*, 298(5877):841–844, August 1982. doi: 10.1038/298841a0. URL http://www.nature.com/nature/journal/v298/n5877/abs/298841a0.html.

Gavin L. Foster. Seawater pH, pCO_2 and $[CO_3^{2-}]$ variations in the Caribbean Sea over the last 130kyr: A boron isotope and B/Ca study of planktic foraminifera. *Earth and Planetary Science Letters*, 271(1-4):254–266, July 2008. ISSN 0012-821X. doi: 10.1016/j.epsl.2008.04.015. URL http://www.sciencedirect.com/science/article/B6V61-4SBY4X4-1/2/e2b661ff6b0ec87117d406cab237ee92.

Gavin L. Foster, Yunyan Ni, Brian Haley, and Tim R. Elliott. Accurate and precise isotopic measurement of sub-nanogram sized samples of foraminiferal hosted boron by total evaporation NTIMS. *Chemical Geology*, 230(1-2):161–174, June 2006. ISSN 0009-2541. doi: 10.1016/j.chemgeo.2005.12.006. URL http://www.sciencedirect.com/science/article/B6V5Y-4J7304C-1/2/9f36e06e3ed15aac8faa014249947f0d.

Gavin L. Foster, James W. B. Rae, and Tim R. Elliott. Boron isotope measurements of marine carbonate using MC-ICPMS. *Geochimica et Cosmochimica Acta*, 72(12, Supplement 1):A279, 2008. doi: doi:10.1016/j.gca.2008.05.009.

Gavin L. Foster, P. A. E. Pogge von Strandmann, and James W. B. Rae. Boron and magnesium isotopic composition of seawater. *Geochemistry Geophysics Geosystems*,

11:10 PP., August 2010. doi: 201010.1029/2010GC003201. URL http://www.agu.org/pubs/crossref/2010/2010GC003201.shtml.

Gavin L. Foster, Caroline H. Lear, and James W.B. Rae. The evolution of pCO2, ice volume and climate during the middle Miocene. *Earth and Planetary Science Letters*, 341–344(0):243–254, August 2012. ISSN 0012-821X. doi: 10.1016/j.epsl.2012.06.007. URL http://www.sciencedirect.com/science/article/pii/S0012821X12002919.

Gavin L. Foster, Bärbel Hönisch, Guillaume Paris, Gary S. Dwyer, James W.B. Rae, Tim Elliott, Jérôme Gaillardet, N. Gary Hemming, Pascale Louvat, and Avner Vengosh. Interlaboratory comparison of boron isotope analyses of boric acid, seawater and marine CaCO3 by MC-ICPMS and NTIMS. *Chemical Geology*, in review, 2013. ISSN 0009-2541. doi: 10.1016/j.chemgeo.2013.08.027. URL http://www.sciencedirect.com/science/article/pii/S0009254113003744.

I. Fraile, S. Mulitza, and M. Schulz. Modeling planktonic foraminiferal seasonality: Implications for sea-surface temperature reconstructions. *Marine Micropaleontology*, 72(1–2):1–9, June 2009. ISSN 0377-8398. doi: 10.1016/j.marmicro.2009.01.003. URL http://www.sciencedirect.com/science/article/pii/S037783980900005X.

Katherine H. Freeman and J. M. Hayes. Fractionation of carbon isotopes by phytoplankton and estimates of ancient CO2 levels. *Global Biogeochemical Cycles*, 6 (2):185–198, 1992. ISSN 1944-9224. doi: 10.1029/92GB00190. URL http://onlinelibrary.wiley.com/doi/10.1029/92GB00190/abstract.

Oliver Friedrich, Ralf Schiebel, Paul A. Wilson, Syee Weldeab, Christopher J. Beer, Matthew J. Cooper, and Jens Fiebig. Influence of test size, water depth, and ecology on Mg/Ca, Sr/Ca, 18O and 13C in nine modern species of planktic foraminifers. *Earth and Planetary Science Letters*, 319–320(0):133–145, February 2012. ISSN 0012-821X. doi: 10.1016/j.epsl.2011.12.002. URL http://www.sciencedirect.com/science/article/pii/S0012821X11007163.

P.N. Froelich, G.P. Klinkhammer, M.L. Bender, N.A. Luedtke, G.R. Heath, Doug Cullen, Paul Dauphin, Doug Hammond, Blayne Hartman, and Val Maynard. Early oxidation of organic matter in pelagic sediments of the eastern equatorial Atlantic: suboxic diagenesis. *Geochimica et Cosmochimica Acta*, 43(7):1075–1090, July 1979.

ISSN 0016-7037. doi: 10.1016/0016-7037(79)90095-4. URL http://www.sciencedirect.com/science/article/pii/0016703779900954.

Jérôme Gaillardet and Claude-Jean Allègre. Boron isotopic compositions of corals: Seawater or diagenesis record? *Earth and Planetary Science Letters*, 136(3–4): 665–676, December 1995. ISSN 0012-821X. doi: 10.1016/0012-821X(95)00180-K. URL http://www.sciencedirect.com/science/article/pii/0012821X9500180K.

H. E. Garcia, R. A. Locarnini, T. P. Boyer, J. I. Antonov, M. M. Zweng, O. K. Baranova, and D. R. Johnson. World ocean atlas 2009, volume 4: Nutrients (phosphate, nitrate, silicate). In S. Levitus, editor, *NOAA Atlas NESDIS 71*, page 398. U.S. Government Printing Office, 2010.

Franz Gingele, Sabine Kasten, Stefan Mulitza, and Carsten Rühlemann. Age model and isotopes of sediment core GeoB1523-1., 2000. URL www.pangaea.de.

Martin S. Glas, Katharina E. Fabricius, Dirk de Beer, and Sven Uthicke. The O2, pH and Ca2+ Microenvironment of Benthic Foraminifera in a High CO2 World. *PLoS ONE*, 7(11):e50010, November 2012a. doi: 10.1371/journal.pone.0050010. URL http://dx.doi.org/10.1371/journal.pone.0050010.

Martin S. Glas, Gerald Langer, and Nina Keul. Calcification acidifies the microenvironment of a benthic foraminifer (*Ammonia* sp.). *Journal of Experimental Marine Biology and Ecology*, 424–425(0):53–58, August 2012b. ISSN 0022-0981. doi: 10.1016/j.jembe.2012.05.006. URL http://www.sciencedirect.com/science/article/pii/S0022098112001712.

M. Gloor, N. Gruber, J. Sarmiento, C. L. Sabine, R. A. Feely, and C. Rödenbeck. A first estimate of present and preindustrial air-sea CO2 flux patterns based on ocean interior carbon measurements and models. *Geophysical Research Letters*, 30(1):1010, January 2003. doi: 10.1029/2002GL015594. URL http://adsabs.harvard.edu/abs/2003GeoRL..30a..10G.

Roberto Gonfiantini, Sonia Tonarini, Manfred Gröning, Alessandra Adorni-Braccesi, Assad S. Al-Ammar, Marcus Astner, Sebastien Bächler, Ramon M. Barnes, Randy L. Bassett, Alain Cocherie, Annette Deyhle, Andrea Dini, Giorgio Ferrara, Jérôme Gaillardet, Judith Grimm, Catherine Guerrot, Urs Krähenbühl, Graham Layne, Damien Lemarchand, Anette Meixner, D. Jack Northington, Maddalena

Pennisi, Eva Reitznerová, Ilia Rodushkin, Naoji Sugiura, Regina Surberg, Sabine Tonn, Michael Wiedenbeck, Samuel Wunderli, Yingkai Xiao, and Thomas Zack. Intercomparison of boron isotope and concentration measurements. part II: evaluation of results. *Geostandards Newsletter*, 27(1):41–57, 2003. ISSN 1751-908X. doi: 10.1111/j.1751-908X.2003.tb00711.x. URL http://onlinelibrary.wiley.com/doi/10.1111/j.1751-908X.2003.tb00711.x/abstract.

M. Grinstein, S. Bentov, S. Koller-Rink, D. de-Beer, and Jonathan Erez. Direct microelectrodes measurements at the calcification site of foraminifera. *AGU Fall Meeting Abstracts*, -1:0864, December 2004. URL http://adsabs.harvard.edu/abs/2004AGUFM.B21B0864G.

Ulrike Groemping. Relative importance for linear regression in r: The package relaimpo. *Journal of Statistical Software*, 17(1), September 2006.

Maoyong He, Yingkai Xiao, Zhangdong Jin, Weiguo Liu, Yunqi Ma, Yanling Zhang, and Chongguang Luo. Quantification of boron incorporation into synthetic calcite under controlled pH and temperature conditions using a differential solubility technique. *Chemical Geology*, 337–338:67–74, January 2013. ISSN 0009-2541. doi: 10.1016/j.chemgeo.2012.11.013. URL http://www.sciencedirect.com/science/article/pii/S0009254112005876.

C. Hemleben and Jelle Bijma. *Carbon cycling in the glacial ocean Constraints on the ocean's role in global change*, volume 1 of *NATO ASI Series*, chapter Foraminiferal population dynamics, stable isotopes and paleo-environment in the Red Sea and the North Atlantic, pages 145–166. Springer-Verlag, 1994. URL http://epic.awi.de/1274/.

Christoph Hemleben, Michael Spindler, Ingrid Breitinger, and Rolf Ott. Morphological and physiological responses of *Globigerinoides sacculifer* (Brady) under varying laboratory conditions. *Marine Micropaleontology*, 12:305–324, 1987.

Christoph Hemleben, Michael Spindler, and O. R Erson. *Modern planktonic foraminifera*. Springer, Berlin, 1989.

N. Gary Hemming and Gilbert N. Hanson. Boron isotopic composition and concentration in modern marine carbonates. *Geochimica et Cosmochimica Acta*, 56 (1):537–543, January 1992. ISSN 0016-7037. doi: 10.1016/0016-7037(92)90151-8.

URL http://www.sciencedirect.com/science/article/B6V66-48C8N0F-1VK/2/3a7f0d55ea9c772ce26a1be9d471c2a0.

N. Gary Hemming and Gilbert N. Hanson. A procedure for the isotopic analysis of boron by negative thermal ionization mass spectrometry. *Chemical Geology*, 114 (1-2):147–156, May 1994. ISSN 0009-2541. doi: 10.1016/0009-2541(94)90048-5. URL http://www.sciencedirect.com/science/article/pii/0009254194900485.

N. Gary Hemming and Bärbel Hönisch. Boron isotopes in marine carbonate sediments and the pH of the ocean. In Claude Hillaire-Marcel, Anne de Vernal, and H. Chamley, editors, *Proxies in Late Cenozoic Paleoceanography, 1*, volume 1 of *Developments in Marine Geology*, pages 717–734. Elsevier, Oxford, 2007. ISBN 978-0-444-52755-4.

N. Gary Hemming, Richard J. Reeder, and Gilbert N. Hanson. Mineral-fluid partitioning and isotopic fractionation of boron in synthetic calcium carbonate. *Geochimica et Cosmochimica Acta*, 59(2):371–379, January 1995. ISSN 0016-7037. doi: 10.1016/0016-7037(95)00288-B. URL http://www.sciencedirect.com/science/article/B6V66-3YYTKJS-C9/2/656510b604eaac3642d047211d93843b.

N.Gary Hemming, Richard J Reeder, and Stanley R Hart. Growth-step-selective incorporation of boron on the calcite surface. *Geochimica et Cosmochimica Acta*, 62 (17):2915–2922, September 1998. ISSN 0016-7037. doi: 10.1016/S0016-7037(98)00214-2. URL http://www.sciencedirect.com/science/article/pii/S0016703798002142.

Jorijntje Henderiks and Mark Pagani. Refining ancient carbon dioxide estimates: Significance of coccolithophore cell size for alkenone-based pCO2 records. *Paleoceanography*, 22(3):n/a–n/a, 2007. ISSN 1944-9186. doi: 10.1029/2006PA001399. URL http://onlinelibrary.wiley.com/doi/10.1029/2006PA001399/abstract.

Katharine R. Hendry, Rosalind E.M. Rickaby, Michael P. Meredith, and Henry Elderfield. Controls on stable isotope and trace metal uptake in *Neogloboquadrina pachyderma* (sinistral) from an Antarctic sea-ice environment. *Earth and Planetary Science Letters*, 278(1–2):67–77, February 2009. ISSN 0012-821X. doi:

10.1016/j.epsl.2008.11.026. URL http://www.sciencedirect.com/science/article/pii/S0012821X08007401.

Michael J. Henehan, James W.B. Rae, Gavin L. Foster, Jonathan Erez, Katherine C. Prentice, Michal Kucera, Helen C. Bostock, Miguel A. Martínez-Botí, J. Andy Milton, Paul A. Wilson, Brittney J. Marshall, and Tim Elliott. Calibration of the boron isotope proxy in the planktonic foraminifera *Globigerinoides ruber* for use in palaeo-CO2 reconstruction. *Earth and Planetary Science Letters*, 364:111–122, February 2013. ISSN 0012-821X. doi: 10.1016/j.epsl.2012.12.029. URL http://www.sciencedirect.com/science/article/pii/S0012821X12007157.

M. T. Hernandez-Sanchez, Rachel A. Mills, Helene Planquette, Richard D. Pancost, Laura Hepburn, Ian Salter, and Tania FitzGeorge-Balfour. Quantifying export production in the southern ocean: Implications for the baxs proxy. *Paleoceanography*, 26:PA4222, 2011.

J.Peter Hershey, Marino Fernandez, Peter J. Milne, and Frank J. Millero. The ionization of boric acid in NaCl, Na-Ca-Cl and Na-Mg-Cl solutions at 25 °C. *Geochimica et Cosmochimica Acta*, 50(1):143–148, January 1986. ISSN 0016-7037. doi: 10.1016/0016-7037(86)90059-1. URL http://www.sciencedirect.com/science/article/pii/0016703786900591.

Tim Hesterberg, David S. Moore, Shaun Monagahan, Ashley Clipson, and Rachel Epstein. Bootstrap methods and permutation tests. In D. S. Moore and G. P. McCabe, editors, *The Practice of Business Statistics*, chapter 18. Freeman, New York, 2005.

Sabine Hild, Othmar Marti, and Andreas Ziegler. Spatial distribution of calcite and amorphous calcium carbonate in the cuticle of the terrestrial crustaceans *Porcellio scaber* and *Armadillidium vulgare*. *Journal of Structural Biology*, 163(1):100–108, July 2008. ISSN 1047-8477. doi: 10.1016/j.jsb.2008.04.010. URL http://www.sciencedirect.com/science/article/pii/S1047847708001214.

M.Y. Hobbs and E.J. Reardon. Effect of pH on boron coprecipitation by calcite: further evidence for nonequilibrium partitioning of trace elements. *Geochimica et Cosmochimica Acta*, 63(7–8):1013–1021, April 1999. ISSN 0016-7037. doi:

10.1016/S0016-7037(98)00311-1. URL http://www.sciencedirect.com/science/article/pii/S0016703798003111.

Bärbel Hönisch and N. Gary Hemming. Ground-truthing the boron isotope-paleo-pH proxy in planktonic foraminifera shells: Partial dissolution and shell size effects. *Paleoceanography*, 19(4):PA4010, November 2004. doi: 200410.1029/2004PA001026. URL http://www.agu.org/pubs/crossref/2004/2004PA001026.shtml.

Bärbel Hönisch and N. Gary Hemming. Surface ocean pH response to variations in pCO2 through two full glacial cycles. *Earth and Planetary Science Letters*, 236(1-2): 305–314, July 2005a. ISSN 0012-821X. doi: 10.1016/j.epsl.2005.04.027. URL http://www.sciencedirect.com/science/article/B6V61-4GFV5V1-3/2/effd86ea0980a7a88beff93c762ca9b6.

Bärbel Hönisch and N. Gary Hemming. Surface ocean pH response to variations in pCO2 through two full glacial cycles. *Earth and Planetary Science Letters*, 236(1–2): 305–314, July 2005b. ISSN 0012-821X. doi: 10.1016/j.epsl.2005.04.027. URL http://www.sciencedirect.com/science/article/pii/S0012821X05002803.

Bärbel Hönisch, Jelle Bijma, Ann D. Russell, Howard J. Spero, Martin R. Palmer, Richard E. Zeebe, and Anton Eisenhauer. The influence of symbiont photosynthesis on the boron isotopic composition of foraminifera shells. *Marine Micropaleontology*, 49(1-2):87–96, September 2003. ISSN 0377-8398. doi: 10.1016/S0377-8398(03)00030-6. URL http://www.sciencedirect.com/science/article/pii/S0377839803000306.

Bärbel Hönisch, N. Gary Hemming, A.G. Grottoli, A. Amat, G.N. Hanson, and Jelle Bijma. Assessing scleractinian corals as recorders for paleo-pH: empirical calibration and vital effects. *Geochimica et Cosmochimica Acta*, 68(18):3675–3685, September 2004. ISSN 0016-7037. doi: 10.1016/j.gca.2004.03.002. URL http://www.sciencedirect.com/science/article/pii/S0016703704001905.

Bärbel Hönisch, N. Gary Hemming, and Brice Loose. Comment on "A critical evaluation of the boron isotope-pH proxy: The accuracy of ancient ocean pH estimates" by M. Pagani, D. Lemarchand, A. Spivack and J. Gaillardet. *Geochimica et Cosmochimica Acta*, 71(6):1636–1641, March 2007. ISSN 0016-7037. doi:

10.1016/j.gca.2006.07.045. URL http://www.sciencedirect.com/science/article/B6V66-4MVF50H-1/2/1c31f42d6329983ed7bb4d2d153398d4.

Bärbel Hönisch, Torsten Bickert, and N. Gary Hemming. Modern and Pleistocene boron isotope composition of the benthic foraminifer Cibicidoides wuellerstorfi. *Earth and Planetary Science Letters*, 272(1–2):309–318, July 2008. ISSN 0012-821X. doi: 10.1016/j.epsl.2008.04.047. URL http://www.sciencedirect.com/science/article/pii/S0012821X08003142.

Bärbel Hönisch, N. Gary Hemming, David Archer, Mark Siddall, and Jerry F. McManus. Atmospheric carbon dioxide concentration across the Mid-Pleistocene transition. *Science*, 324(5934):1551–1554, June 2009. doi: 10.1126/science.1171477. URL http://www.sciencemag.org/cgi/content/abstract/324/5934/1551.

Clive Howard-Williams, Rob DaviesColley, and Warwick F. Vincent. Optical properties of the coastal and oceanic waters off South Island, New Zealand: Regional variation. *New Zealand Journal of Marine and Freshwater Research*, 29(4):589–602, 1995. ISSN 0028-8330. doi: 10.1080/00288330.1995.9516690. URL http://www.tandfonline.com/doi/abs/10.1080/00288330.1995.9516690.

Mayuri Inoue, Masato Nohara, Takashi Okai, Atsushi Suzuki, and Hodaka Kawahata. Concentrations of trace elements in carbonate reference materials coral JCp-1 and giant clam JCt-1 by inductively coupled Plasma-Mass spectrometry. *Geostandards and Geoanalytical Research*, 28(3):411–416, 2004. ISSN 1751-908X. doi: 10.1111/j.1751-908X.2004.tb00759.x. URL http://onlinelibrary.wiley.com/doi/10.1111/j.1751-908X.2004.tb00759.x/abstract.

IPCC. Climate change 2007: The physical science basis. contribution of working group i to the fourth assessment report of the intergovernmental panel on climate change. Technical report, Cambridge University Press, Cambridge, UK, 2007.

Masamichi Ishikawa and Masami Ichikuni. Coprecipitation of phosphate with calcite. *Geochemical Journal*, 15:283–288, 1981.

Tsuyoshi Ishikawa and Kazuya Nagaishi. High-precision isotopic analysis of boron by positive thermal ionization mass spectrometry with sample preheating. *Journal of Analytical Atomic Spectrometry*, 26(2):359, 2011. ISSN 0267-9477, 1364-5544. doi:

10.1039/c0ja00060d. URL http://pubs.rsc.org/en/Content/ArticleLanding/2011/JA/c0ja00060d.

Mark Z. Jacobson. Studying ocean acidification with conservative, stable numerical schemes for nonequilibrium air-ocean exchange and ocean equilibrium chemistry. *Journal of Geophysical Research: Atmospheres*, 110(D7):n/a–n/a, 2005. ISSN 2156-2202. doi: 10.1029/2004JD005220. URL http://onlinelibrary.wiley.com/doi/10.1029/2004JD005220/abstract.

John P. Jasper and J. M. Hayes. A carbon isotope record of CO2 levels during the late Quaternary. *Nature*, 347(6292):462–464, October 1990. doi: 10.1038/347462a0. URL http://www.nature.com/nature/journal/v347/n6292/abs/347462a0.html.

Alistair B. Jeffcoate, Tim Elliott, Alex Thomas, and Claudia Bouman. Precise/ Small Sample Size Determinations of Lithium Isotopic Compositions of Geological Reference Materials and Modern Seawater by MC-ICP-MS. *Geostandards and Geoanalytical Research*, 28(1):161–172, 2004. ISSN 1751-908X. doi: 10.1111/j.1751-908X.2004.tb01053.x. URL http://onlinelibrary.wiley.com/doi/10.1111/j.1751-908X.2004.tb01053.x/abstract.

Seth G. John and Jess F. Adkins. Analysis of dissolved iron isotopes in seawater. *Marine Chemistry*, 119(1–4):65–76, April 2010. ISSN 0304-4203. doi: 10.1016/j.marchem.2010.01.001. URL http://www.sciencedirect.com/science/article/pii/S0304420310000022.

Lukas Jonkers, Steven van Heuven, Rainer Zahn, and Frank J.C. Peeters. Seasonal patterns of shell flux, 18O and 13C of small and large *N. pachyderma* (s) and *G. bulloides* in the subpolar North Atlantic. *Paleoceanography*, 28(1):164–174, 2013. ISSN 1944-9186. doi: 10.1002/palo.20018. URL http://onlinelibrary.wiley.com/doi/10.1002/palo.20018/abstract.

Bo Barker Jørgensen, Jonathan Erez, Niels Peter Revsbech, and Yehuda Cohen. Symbiotic photosynthesis in a planktonic foraminiferan, *Globigerinoides sacculifer* (Brady), studied with microelectrodes. *Limnology and Oceanography*, 30(6): 1253–1267, November 1985. ISSN 0024-3590. URL http://www.jstor.org/stable/2836480.

M. I. Kahn. Ecological and paleoecological implications of the phenotypic variation in three species of living planktonic foraminifera from the northeastern Pacific Ocean (50 degrees N, 145 degrees W). *The Journal of Foraminiferal Research*, 11(3): 203–211, July 1981. ISSN 0096-1191. doi: 10.2113/gsjfr.11.3.203. URL http://jfr.geoscienceworld.org/content/11/3/203.full.pdf+html.

H Kakihana, M Kotaka, and S Satoh. Fundamental studies on the ion-exchange separation of boron isotopics. *Bulletin of the Chemical Society of Japan*, 50(1):1, 1977.

Miriam E. Katz, Benjamin S. Cramer, Allison Franzese, Bärbel Hönisch, Kenneth G. Miller, Yair Rosenthal, and James D. Wright. Traditional and Emerging Geochemical Proxies in Foraminifera. *The Journal of Foraminiferal Research*, 40(2): 165–192, April 2010. ISSN 0096-1191,. doi: 10.2113/gsjfr.40.2.165. URL http://jfr.geoscienceworld.org/content/40/2/165.

Hodaka Kawahata. Stable isotopic composition of two morphotypes of *Globigerinoides ruber* (white) in the subtropical gyre in the north pacific. *Paleontological Research*, 9:27–35, April 2005. ISSN 1342-8144. doi: 10.2517/prpsj.9.27. URL http://www.bioone.org/doi/abs/10.2517/prpsj.9.27.

Klaus Keller and Franois M. M. Morel. A model of carbon isotopic fractionation and active carbon uptake in phytoplankton. *Marine Ecology Progress Series*, 182: 295–298, June 1999. doi: 10.3354/meps182295. URL http://www.int-res.com/abstracts/meps/v182/p295-298/.

R. M. Key, A. Kozyr, C. L. Sabine, K. Lee, R. Wanninkhof, J. L. Bullister, R. A. Feely, F. J. Millero, C. Mordy, and T.-H. Peng. A global ocean carbon climatology: Results from global data analysis project (GLODAP). *Global Biogeochemical Cycles*, 18(4):GB4031, December 2004. doi: 200410.1029/2004GB002247. URL http://www.agu.org/journals/ABS/2004/2004GB002247.shtml.

R. M. Key, T. Tanhua, A. Olsen, M. Hoppema, S. Jutterström, C. Schirnick, S. van Heuven, A. Kozyr, X. Lin, A. Velo, D. W. R. Wallace, and L. Mintrop. The CARINA data synthesis project: introduction and overview. *Earth System Science Data*, 2:105–121, March 2010. URL http://adsabs.harvard.edu/abs/2010ESSD....2..105K.

Sang-Tae Kim, Claude Hillaire-Marcel, and Alfonso Mucci. Mechanisms of equilibrium and kinetic oxygen isotope effects in synthetic aragonite at 25 °C. *Geochimica et Cosmochimica Acta*, 70:5790–5801, 2006.

Sang-Tae Kim, James R. O'Neil, Claude Hillaire-Marcel, and Alfonso Mucci. Oxygen isotope fractionation between synthetic aragonite and water: Influence of temperature and Mg2+ concentration. *Geochimica et Cosmochimica Acta*, 71(19): 4704–4715, October 2007. ISSN 0016-7037. doi: 10.1016/j.gca.2007.04.019. URL http://www.sciencedirect.com/science/article/pii/S0016703707002165.

Basak Kisakürek, A. Eisenhauer, F. Böhm, D. Garbe-Schönberg, and J. Erez. Controls on shell Mg/Ca and Sr/Ca in cultured planktonic foraminiferan, *Globigerinoides ruber* (white). *Earth and Planetary Science Letters*, 273(3–4):260–269, September 2008. ISSN 0012-821X. doi: 10.1016/j.epsl.2008.06.026. URL http://www.sciencedirect.com/science/article/pii/S0012821X08004007.

Basak Kisakürek, Anton Eisenhauer, Florian Böhm, Ed. C. Hathorne, and Jonathan Erez. Controls on calcium isotope fractionation in cultured planktic foraminifera, *Globigerinoides ruber* and *Globigerinella siphonifera*. *Geochimica et Cosmochimica Acta*, 75(2):427–443, January 2011. ISSN 0016-7037. doi: 10.1016/j.gca.2010.10.015. URL http://www.sciencedirect.com/science/article/pii/S0016703710005946.

E. Kiss. Ion-exchange separation and spectrophotometric determination of boron in geological materials. *Analytica Chimica Acta*, 211:243–256, 1988. ISSN 0003-2670. doi: 10.1016/S0003-2670(00)83684-3. URL http://www.sciencedirect.com/science/article/pii/S0003267000836843.

Yasushi Kitano, Minoru Okumura, and Masatoshi Idogaki. Co-precipitation of borate-boron with calcium carbonate. *Geochemical Journal*, 12(3):183–189, 1978a.

Yasushi Kitano, Minoru Okumura, and Masatoshi Idogaki. Uptake of phosphate ions by calcium carbonate. *Geochemical Journal*, 12(1):29–37, 1978b.

Kateryna Klochko, Alan J. Kaufman, Wengsheng Yao, Robert H. Byrne, and John A. Tossell. Experimental measurement of boron isotope fractionation in seawater. *Earth and Planetary Science Letters*, 248(1-2):276–285, August 2006. ISSN

0012-821X. doi: 10.1016/j.epsl.2006.05.034. URL http://www.sciencedirect.com/science/article/B6V61-4KBVWX6-7/2/0977914968e89682c428c8287413063b.

Kateryna Klochko, George D. Cody, John A. Tossell, Przemyslaw Dera, and Alan J. Kaufman. Re-evaluating boron speciation in biogenic calcite and aragonite using 11B MAS NMR. *Geochimica et Cosmochimica Acta*, 73(7):1890–1900, April 2009. ISSN 0016-7037. doi: 10.1016/j.gca.2009.01.002. URL http://www.sciencedirect.com/science/article/B6V66-4VF56YJ-2/2/27630cc27f7208f1b419ad7e75bf8d0b.

Stephanie Köhler-Rink and Michael Kühl. Microsensor studies of photosynthesis and respiration in larger symbiotic foraminifera. i the physico-chemical microenvironment of *Marginopora vertebralis*, *Amphistegina lobifera* and *Amphisorus hemprichii*. *Marine Biology*, 137:473–486, 2000.

Stephanie Köhler-Rink and Michael Kühl. The chemical microenvironment of the symbiotic planktonic foraminifer *Orbulina universa*. *Marine Biology Research*, 1(1): 68–78, 2005. doi: 10.1080/17451000510019015. URL http://www.informaworld.com/smpp/content~content=a713950223~db=all.

A. N. Kolmogorov. Dissipation of Energy in the Locally Isotropic Turbulence. *Proceedings of the Royal Society of London. Series A: Mathematical and Physical Sciences*, 434(1890):15–17, July 1991. ISSN 1364-5021, 1471-2946. doi: 10.1098/rspa.1991.0076. URL http://rspa.royalsocietypublishing.org/content/434/1890/15.

Ch Körner, P. Bannister, and A. F. Mark. Altitudinal variation in stomatal conductance, nitrogen content and leaf anatomy in different plant life forms in New Zealand. *Oecologia*, 69(4):577–588, July 1986. ISSN 0029-8549, 1432-1939. doi: 10.1007/BF00410366. URL http://link.springer.com/article/10.1007/BF00410366.

Shani Krief, Erica J. Hendy, Maoz Fine, Ruth Yam, Anders Meibom, Gavin L. Foster, and Aldo Shemesh. Physiological and isotopic responses of scleractinian corals to ocean acidification. *Geochimica et Cosmochimica Acta*, 74(17):4988–5001, September 2010. ISSN 0016-7037. doi: 10.1016/j.gca.2010.05.023. URL http://www.sciencedirect.com/science/article/pii/S0016703710003017.

Dick Kroon and Kate Darling. Size and upwelling control of the stable isotope composition of *Neogloboquadrina dutertrei* (d'Orbigny), *Globigerinoides ruber* (d'Orbigny) and *Globigerina bulloides* d'Orbigny; examples from the Panama Basin and Arabian Sea. *The Journal of Foraminiferal Research*, 25(1):39–52, January 1995. ISSN 0096-1191,. doi: 10.2113/gsjfr.25.1.39. URL http://jfr.geoscienceworld.org/content/25/1/39.full.pdf+html?frame=sidebar.

Michal Kucera. Planktonic foraminifera as tracers of past oceanic environments. In Claude Hillaire–Marcel and Anne de Vernal, editors, *Proxies in Late Cenozoic Paleoceanography*, volume Volume 1 of *Developments in Marine Geology*, pages 213–262. Elsevier, Amsterdam, 2007. ISBN 1572-5480. URL http://www.sciencedirect.com/science/article/pii/S1572548007010111.

Azumi Kuroyanagi and Hodaka Kawahata. Vertical distribution of living planktonic foraminifera in the seas around Japan. *Marine Micropaleontology*, 53(1–2):173–196, October 2004. ISSN 0377-8398. doi: 10.1016/j.marmicro.2004.06.001. URL http://www.sciencedirect.com/science/article/pii/S0377839804000659.

J.R.N. Lazier and K.H. Mann. Turbulence and the diffusive layers around small organisms. *Deep Sea Research Part A. Oceanographic Research Papers*, 36(11): 1721–1733, November 1989. ISSN 0198-0149. doi: 10.1016/0198-0149(89)90068-X. URL http://www.sciencedirect.com/science/article/pii/019801498990068X.

D. W. Lea, P. A. Martin, D. A. Chan, and H. J. Spero. Calcium uptake and calcification rate in the planktonic foraminifer *Orbulina universa*. *The Journal of Foraminiferal Research*, 25(1):14–23, January 1995. ISSN 0096-1191. doi: 10.2113/gsjfr.25.1.14. URL http://jfr.geoscienceworld.org/content/25/1/14.full.pdf+html.

John J. Lee, Hugo D. Freudenthal, Victor Kossoy, and Allan Bé. Cytological observations on two planktonic foraminifera, *Globigerina bulloides* d'Orbigny, 1826, and *Globigerinoides ruber* (d'Orbigny, 1839, Cushman, 1927). *Journal of Eukaryotic Microbiology*, 12(4):531–542, 1965. ISSN 1550-7408. doi: 10.1111/j.1550-7408.1965.tb03253.x. URL http://onlinelibrary.wiley.com/doi/10.1111/j.1550-7408.1965.tb03253.x/abstract.

Kitack Lee, Lan T. Tong, Frank J. Millero, Christopher L. Sabine, Andrew G. Dickson, Catherine Goyet, Geun-Ha Park, Rik Wanninkhof, Richard A. Feely, and Robert M. Key. Global relationships of total alkalinity with salinity and temperature in surface waters of the world's oceans. *Geophysical Research Letters*, 33(19):L19605, 2006. ISSN 1944-8007. doi: 10.1029/2006GL027207. URL http://onlinelibrary.wiley.com/doi/10.1029/2006GL027207/abstract.

Kitack Lee, Tae-Wook Kim, Robert H. Byrne, Frank J. Millero, Richard A. Feely, and Yong-Ming Liu. The universal ratio of boron to chlorinity for the North Pacific and North Atlantic oceans. *Geochimica et Cosmochimica Acta*, 74(6):1801–1811, March 2010. ISSN 0016-7037. doi: 10.1016/j.gca.2009.12.027. URL http://www.sciencedirect.com/science/article/pii/S0016703709007789.

D Lemarchand, J Gaillardet, C Göpel, and G Manhès. An optimized procedure for boron separation and mass spectrometry analysis for river samples. *Chemical Geology*, 182:323–334, February 2002a. ISSN 00092541. doi: 10.1016/S0009-2541(01)00329-1. URL http://elsevier-apps.sciverse.com/GoogleMaps/index.jsp?doi=10.1016/S0009-2541%2801%2900329-1.

Damien Lemarchand, Jérôme Gaillardet, Éric Lewin, and Claude J. Allègre. Boron isotope systematics in large rivers: implications for the marine boron budget and paleo-pH reconstruction over the cenozoic. *Chemical Geology*, 190(1-4):123–140, October 2002b. ISSN 0009-2541. doi: 10.1016/S0009-2541(02)00114-6. URL http://www.sciencedirect.com/science/article/B6V5Y-46FG82S-2/2/c4d1ace0954e9c53d3cc958989329222.

Bénédicte Lemieux-Dudon, Eric Blayo, Jean-Robert Petit, Claire Waelbroeck, Anders Svensson, Catherine Ritz, Jean-Marc Barnola, Bianca Maria Narcisi, and Frédéric Parrenin. Consistent dating for antarctic and greenland ice cores. *Quaternary Science Reviews*, 29(1–2):8–20, January 2010. ISSN 0277-3791. doi: 10.1016/j.quascirev.2009.11.010. URL http://www.sciencedirect.com/science/article/pii/S0277379109003734.

Ilana Levanon-Spanier, Etana Padan, and Zeev Reiss. Primary production in a desert-enclosed sea- the Gulf of Eilat (Aqaba), Red Sea. *Deep Sea Research Part A. Oceanographic Research Papers*, 26(6):673–685, June 1979. ISSN 0198-0149. doi:

10.1016/0198-0149(79)90040-2. URL http://www.sciencedirect.com/science/article/pii/0198014979900402.

Ernie Lewis and Douglas W. R. Wallace. Program developed for CO2 systems calculations. ORNL/CDIAC-105., 1998.

Hui-Ling Lin, Wei-Chiao Wang, and Gwo-Wei Hung. Seasonal variation of planktonic foraminiferal isotopic composition from sediment traps in the South China Sea. *Marine Micropaleontology*, 53(3–4):447–460, November 2004. ISSN 0377-8398. doi: 10.1016/j.marmicro.2004.08.004. URL http://www.sciencedirect.com/science/article/pii/S0377839804001033.

Yi-Pin Lin and Philip C. Singer. Inhibition of calcite precipitation by orthophosphate: Speciation and thermodynamic considerations. *Geochimica et Cosmochimica Acta*, 70(10):2530–2539, May 2006. ISSN 0016-7037. doi: 10.1016/j.gca.2006.03.002. URL http://www.sciencedirect.com/science/article/pii/S0016703706001165.

Richard H. Lindemann, Peter F. Merenda, and Ruth Z. Gold. *Introduction to Bivariate and Multivariate Analysis*. Scott Foresman and Co., Glenview, Illinois, 1980.

Yun Liu and John A. Tossell. Ab initio molecular orbital calculations for boron isotope fractionations on boric acids and borates. *Geochimica et Cosmochimica Acta*, 69 (16):3995–4006, August 2005. ISSN 0016-7037. doi: 10.1016/j.gca.2005.04.009. URL http://www.sciencedirect.com/science/article/pii/S0016703705003595.

G. P. Lohmann. A model for variation in the chemistry of planktonic foraminifera due to secondary calcification and selective dissolution. *Paleoceanography*, 10(3):445–457, 1995. doi: 199510.1029/95PA00059. URL http://www.agu.org/journals/pa/v010/i003/95PA00059/.

F. Lombard, Jonathan Erez, E. Michel, and L. Labeyrie. Temperature effect on respiration and photosynthesis of the symbiont-bearing planktonic foraminifera *Globigerinoides ruber*, *Orbulina universa*, and *Globigerinella siphonifera*. *Limnology and Oceanography*, 54(1):210–218, 2009. ISSN 00243590. doi: 10.4319/lo.2009.54.1.0210. URL http://www.www.aslo.org/lo/toc/vol_54/issue_1/0210.html.

Anna Lourantou, Jošt V. Lavrič, Peter Köhler, Jean-Marc Barnola, Didier Paillard, Elisabeth Michel, Dominique Raynaud, and Jérôme Chappellaz. Constraint of the

CO2 rise by new atmospheric carbon isotopic measurements during the last deglaciation. *Global Biogeochemical Cycles*, 24:15 PP., June 2010. doi: 201010.1029/2009GB003545. URL http://www.agu.org/pubs/crossref/2010/2009GB003545.shtml.

Ludvig Löwemark, Wei-Li Hong, Tzen-Fu Yui, and Gwo-Wei Hung. A test of different factors influencing the isotopic signal of planktonic foraminifera in surface sediments from the northern South China Sea. *Marine Micropaleontology*, 55(1–2):49–62, April 2005. ISSN 0377-8398. doi: 10.1016/j.marmicro.2005.02.004. URL http://www.sciencedirect.com/science/article/pii/S0377839805000162.

K. R. Ludwig. Isoplot, 2003. URL http://www.bgc.org/isoplot_etc/software.html.

Timothy J Lueker, Andrew G Dickson, and Charles D Keeling. Ocean pCO2 calculated from dissolved inorganic carbon, alkalinity, and equations for K1 and K2: validation based on laboratory measurements of CO2 in gas and seawater at equilibrium. *Marine Chemistry*, 70(1–3):105–119, May 2000. ISSN 0304-4203. doi: 10.1016/S0304-4203(00)00022-0. URL http://www.sciencedirect.com/science/article/pii/S0304420300000220.

Dieter Lüthi, Martine Le Floch, Bernhard Bereiter, Thomas Blunier, Jean-Marc Barnola, Urs Siegenthaler, Dominique Raynaud, Jean Jouzel, Hubertus Fischer, Kenji Kawamura, and Thomas F. Stocker. High-resolution carbon dioxide concentration record 650,000–800,000years before present. *Nature*, 453(7193): 379–382, May 2008. ISSN 0028-0836, 1476-4687. doi: 10.1038/nature06949. URL http://www.nature.com/nature/journal/v453/n7193/suppinfo/nature06949.html.

Julene Marr. Ecological, oceanographic and temperature controls on the incorporation of trace elements into *Globigerina bulloides* and *Globoconella inflata* in the southwest Pacific Ocean. Master's thesis, Victoria University, Wellington, 2009.

Julene P. Marr, Joel A. Baker, Lionel Carter, Aidan S. R. Allan, Gavin B. Dunbar, and Helen C. Bostock. Ecological and temperature controls on Mg/Ca ratios of *Globigerina bulloides* from the southwest Pacific Ocean. *Paleoceanography*, 26(2):

n/a–n/a, 2011. ISSN 1944-9186. doi: 10.1029/2010PA002059. URL http://onlinelibrary.wiley.com/doi/10.1029/2010PA002059/abstract.

Brittney J. Marshall, Robert C. Thunell, Michael J. Henehan, Yrene Astor, and Katherine E. Wejnert. Planktonic foraminiferal area density as a proxy for carbonate ion concentration: A calibration study using the Cariaco Basin Ocean Time Series. *Paleoceanography*, 28:1–14, 2013. ISSN 1944-9186. doi: 10.1002/palo.20034. URL http://onlinelibrary.wiley.com/doi/10.1002/palo.20034/abstract.

G. M. Martin. *Globigerina bulloides*: Preservation state and stable isotope variation. Master's thesis, University of Canterbury, Christchurch, NZ, November 2001.

Richard I. Masel. *Principles of adsorption and reaction on solid surfaces*. Wiley, New York, 1996. URL http://cds.cern.ch/record/643993.

Malcolm McCulloch, Julie Trotter, Paolo Montagna, Jim Falter, Robert Dunbar, André Freiwald, Günter Försterra, Matthias López Correa, Cornelia Maier, Andres Rüggeberg, and Marco Taviani. Resilience of cold-water scleractinian corals to ocean acidification: Boron isotopic systematics of pH and saturation state up-regulation. *Geochimica et Cosmochimica Acta*, 87(0):21–34, June 2012. ISSN 0016-7037. doi: 10.1016/j.gca.2012.03.027. URL http://www.sciencedirect.com/science/article/pii/S001670371200169X.

Fabrice Minoletti, Michaël Hermoso, and Vincent Gressier. Separation of sedimentary micron-sized particles for palaeoceanography and calcareous nannoplankton biogeochemistry. *Nature Protocols*, 4(1):14–24, 2009. ISSN 1754-2189. doi: 10.1038/nprot.2008.200. URL http://www.nature.com/nprot/journal/v4/n1/abs/nprot.2008.200.html.

Mahyar Mohtadi, Delia W. Oppo, Andreas Lückge, Ricardo DePol-Holz, Stephan Steinke, Jeroen Groeneveld, Nils Hemme, and Dierk Hebbeln. Reconstructing the thermal structure of the upper ocean: Insights from planktic foraminifera shell chemistry and alkenones in modern sediments of the tropical eastern Indian Ocean. *Paleoceanography*, 26(3):n/a–n/a, 2011. ISSN 1944-9186. doi: 10.1029/2011PA002132. URL http://onlinelibrary.wiley.com/doi/10.1029/2011PA002132/abstract.

Claudia I. Mora, Steven G. Driese, and Paula G. Seager. Carbon dioxide in the Paleozoic atmosphere: Evidence from carbon-isotope compositions of pedogenic carbonate. *Geology*, 19(10):1017–1020, October 1991. ISSN 0091-7613, 1943-2682. doi: 10.1130/0091-7613(1991)019⟨1017:CDITPA⟩2.3.CO;2. URL http://geology.gsapubs.org/content/19/10/1017.

Raphaël Morard, Frédéric Quillévéré, Gilles Escarguel, Yurika Ujiie, Thibault de Garidel-Thoron, Richard D. Norris, and Colomban de Vargas. Morphological recognition of cryptic species in the planktonic foraminifer *Orbulina universa*. *Marine Micropaleontology*, 71(3–4):148–165, May 2009. ISSN 0377-8398. doi: 10.1016/j.marmicro.2009.03.001. URL http://www.sciencedirect.com/science/article/pii/S0377839809000243.

Alfonso Mucci. Growth kinetics and composition of magnesian calcite overgrowths precipitated from seawater: Quantitative influence of orthophosphate ions. *Geochimica et Cosmochimica Acta*, 50(10):2255–2265, October 1986. ISSN 0016-7037. doi: 10.1016/0016-7037(86)90080-3. URL http://www.sciencedirect.com/science/article/pii/0016703786900803.

YunYan Ni. A comparative study of boron isotopes and trace elements of the marine foraminifers during the last glacial maximum and holocene. *SCIENCE CHINA Earth Sciences*, 53(1):91–100, 2010. ISSN 1674-7313. doi: 10.1007/s11430-009-0179-8. URL http://www.springerlink.com/content/3kq35m96w513560r/abstract/.

Yunyan Ni, Gavin L. Foster, Trevor Bailey, Tim R. Elliott, Daniela N. Schmidt, Paul Pearson, Brian Haley, and Chris Coath. A core top assessment of proxies for the ocean carbonate system in surface-dwelling foraminifers. *Paleoceanography*, 22: 3212–3226, August 2007. doi: 10.1029/2006PA001337. URL http://www.agu.org/pubs/crossref/2007/2006PA001337.shtml.

Yunyan Ni, Gavin L. Foster, and Tim Elliott. The accuracy of δ 11B measurements of foraminifers. *Chemical Geology*, 274(3-4):187–195, July 2010. ISSN 0009-2541. doi: 10.1016/j.chemgeo.2010.04.008. URL http://www.sciencedirect.com/science/article/pii/S0009254110001439.

Masao Nomura, Tadao Kanzaki, Takejiro Ozawa, Makoto Okamoto, and Hidetake Kakihana. Boron isotopic composition of fumarolic condensates from some volcanoes

in Japanese island arcs. *Geochimica et Cosmochimica Acta*, 46(11):2403–2406, November 1982. ISSN 0016-7037. doi: 10.1016/0016-7037(82)90212-5. URL http://www.sciencedirect.com/science/article/pii/0016703782902125.

Lee Nordt, Stacy Atchley, and Steve I. Dworkin. Paleosol barometer indicates extreme fluctuations in atmospheric CO2 across the Cretaceous-Tertiary boundary. *Geology*, 30(8):703–706, August 2002. doi: 10.1130/0091-7613(2002)030⟨0703:PBIEFI⟩2.0.CO;2. URL http://geology.gsapubs.org/cgi/content/abstract/30/8/703.

Lee Nordt, Stacy Atchley, and Steve I. Dworkin. Terrestrial evidence for two greenhouse events in the latest Cretaceous. *GSA Today*, 13(12):4–9, December 2003. doi: 10.1130/1052-5173(2003)013⟨4:TEFTGE⟩2.0.CO;2. URL http://www.gsajournals.org/perlserv/?request=cite-builder&doi=10.1130%2F1052-5173(2003)013%3C4:TEFTGE%3E2.0.CO%3B2.

Richard D. Norris. Symbiosis as an evolutionary innovation in the radiation of Paleocene planktonic foraminifera. *Paleobiology*, 22:461–480, 1996.

Lea Numberger, Christoph Hemleben, Ramona Hoffmann, Andreas Mackensen, Hartmut Schulz, Joern-Michael Wunderlich, and Michal Kucera. Habitats, abundance patterns and isotopic signals of morphotypes of the planktonic foraminifer *Globigerinoides ruber* (d'Orbigny) in the eastern Mediterranean sea since the Marine Isotopic Stage 12. *Marine Micropaleontology*, 73:90–104, 2009. doi: doi:10.1016/j.marmicro.2009.07.004.

Takao Oi. Ab initio molecular orbital calculations of reduced partition function ratios of polyboric acids and polyborate anions. *Zeitschrift für Naturforschung*, 55(a): 623–628, 2000. URL http://ci.nii.ac.jp/naid/10008227475/.

Takashi Okai, Atsushi Suzuki, Hodaka Kawahata, Shigeru Terashima, and Noboru Imai. Preparation of a new geological survey of japan geochemical reference material: Coral JCp-1. *Geostandards Newsletter*, 26(1):95–99, 2002. ISSN 1751-908X. doi: 10.1111/j.1751-908X.2002.tb00627.x. URL http://onlinelibrary.wiley.com/doi/10.1111/j.1751-908X.2002.tb00627.x/abstract.

Delia W. Oppo and Richard G. Fairbanks. Carbon isotope composition of tropical surface water during the past 22,000 years. *Paleoceanography*, 4(4):333–351, 1989.

ISSN 1944-9186. doi: 10.1029/PA004i004p00333. URL http://onlinelibrary.wiley.com/doi/10.1029/PA004i004p00333/abstract.

Delia W. Oppo, Yair Rosenthal, and Braddock K. Linsley. 2,000-year-long temperature and hydrology reconstructions from the Indo-Pacific warm pool. *Nature*, 460(7259): 1113–1116, August 2009. ISSN 0028-0836. doi: 10.1038/nature08233. URL http://www.nature.com/nature/journal/v460/n7259/full/nature08233.html.

M. Pagani and A. Spivack. Response to the Comment by B. Hönisch, N.G. Hemming, B. Loose on "A critical evaluation of the boron isotope-pH proxy: The accuracy of ancient ocean pH estimates". *Geochimica et Cosmochimica Acta*, 71(6):1642, March 2007. ISSN 0016-7037. doi: 10.1016/j.gca.2006.11.035. URL http://www.sciencedirect.com/science/article/pii/S0016703707000300.

Mark Pagani, Michael A. Arthur, and Katherine H. Freeman. Miocene evolution of atmospheric carbon dioxide. *Paleoceanography*, 14(3):273–292, 1999. ISSN 1944-9186. doi: 10.1029/1999PA900006. URL http://onlinelibrary.wiley.com/doi/10.1029/1999PA900006/abstract.

Mark Pagani, Katherine H. Freeman, Nao Ohkouchi, and Ken Caldeira. Comparison of water column [CO2aq] with sedimentary alkenone-based estimates: A test of the alkenone-CO2 proxy. *Paleoceanography*, 17(4):21–1–21–12, 2002. ISSN 1944-9186. doi: 10.1029/2002PA000756. URL http://onlinelibrary.wiley.com/doi/10.1029/2002PA000756/abstract.

Mark Pagani, Damien Lemarchand, Arthur Spivack, and Jérome Gaillardet. A critical evaluation of the boron isotope-pH proxy: The accuracy of ancient ocean pH estimates. *Geochimica et Cosmochimica Acta*, 69(4):953–961, February 2005a. ISSN 0016-7037. doi: 10.1016/j.gca.2004.07.029. URL http://www.sciencedirect.com/science/article/B6V66-4FHJ6TV-C/2/7e317375d57f462f0bd8551cf2f096e7.

Mark Pagani, James C. Zachos, Katherine H. Freeman, Brett Tipple, and Stephen Bohaty. Marked decline in atmospheric carbon dioxide concentrations during the paleogene. *Science*, 309(5734):600–603, 2005b. doi: 10.1126/science.1110063.

Mark Pagani, Matthew Huber, Zhonghui Liu, Steven M. Bohaty, Jorijntje Henderiks, Willem Sijp, Srinath Krishnan, and Robert M. DeConto. The role of carbon dioxide during the onset of Antarctic glaciation. *Science*, 334(6060):1261–1264, December

2011. ISSN 0036-8075, 1095-9203. doi: 10.1126/science.1203909. URL http://www.sciencemag.org/content/334/6060/1261. PMID: 22144622.

Didier Paillard, L. Labeyrie, and P Yiou. Analyseries 1.0: Macintosh software for the analysis of geographical time-series. *EOS*, 77(15), 1996. doi: 10.1029/96EO00259. URL http://d.wanfangdata.com.cn/NSTLQK_10.1029-96EO00259.aspx.

M. R Palmer and P. N Pearson. A 23,000-year record of surface water pH and PCO2 in the western equatorial Pacific Ocean. *Science*, 300(5618):480–482, April 2003. ISSN 0036-8075, 1095-9203. doi: 10.1126/science.1080796. URL http://www.sciencemag.org/content/300/5618/480.

M. R. Palmer, P. N. Pearson, and S. J. Cobb. Reconstructing past ocean pH-Depth profiles. *Science*, 282(5393):1468–1471, November 1998. ISSN 0036-8075, 1095-9203. doi: 10.1126/science.282.5393.1468. URL http://www.sciencemag.org/content/282/5393/1468.

Martin R. Palmer, G.J. Brummer, Matt J. Cooper, Henry Elderfield, M.J. Greaves, G.J. Reichart, Stefan Schouten, and Jimin M. Yu. Multi-proxy reconstruction of surface water pCO2 in the northern Arabian Sea since 29 ka. *Earth and Planetary Science Letters*, 295(1-2):49–57, June 2010. ISSN 0012-821X. doi: 10.1016/j.epsl.2010.03.023. URL http://www.sciencedirect.com/science/article/pii/S0012821X10002049.

M.R. Palmer, A.J. Spivack, and J.M. Edmond. Temperature and pH controls over isotopic fractionation during adsorption of boron on marine clay. *Geochimica et Cosmochimica Acta*, 51(9):2319–2323, September 1987. ISSN 0016-7037. doi: 10.1016/0016-7037(87)90285-7. URL http://www.sciencedirect.com/science/article/pii/0016703787902857.

F. L. Parker. Planktonic foraminiferal species in Pacific sediments. *Micropaleontology*, 8:219–254, 1962.

A. Parwel, H. v. Ubisch, and F. E. Wickman. On the variations in the relative abundance of boron isotopes in nature. *Geochimica et Cosmochimica Acta*, 10: 185–190, 1956.

Paul N. Pearson and Martin R. Palmer. Middle Eocene Seawater pH and Atmospheric Carbon Dioxide Concentrations. *Science*, 284(5421):1824–1826, June 1999. ISSN

0036-8075, 1095-9203. doi: 10.1126/science.284.5421.1824. URL http://www.sciencemag.org/content/284/5421/1824.

Paul N. Pearson and Martin R. Palmer. Atmospheric carbon dioxide concentrations over the past 60 million years. *Nature*, 406(6797):695–699, August 2000. ISSN 0028-0836. doi: 10.1038/35021000. URL http://www.ncbi.nlm.nih.gov/pubmed/10963587. PMID: 10963587.

Paul N. Pearson, Gavin L. Foster, and Bridget S. Wade. Atmospheric carbon dioxide through the Eocene–Oligocene climate transition. *Nature*, 461(7267):1110–1113, September 2009. ISSN 0028-0836. doi: 10.1038/nature08447. URL http://www.nature.com/nature/journal/v461/n7267/abs/nature08447.html.

Frank J.C Peeters, Geert-Jan A Brummer, and Gerald Ganssen. The effect of upwelling on the distribution and stable isotope composition of *Globigerina bulloides* and *Globigerinoides ruber* (planktic foraminifera) in modern surface waters of the NW Arabian Sea. *Global and Planetary Change*, 34(3–4):269–291, November 2002. ISSN 0921-8181. doi: 10.1016/S0921-8181(02)00120-0. URL http://www.sciencedirect.com/science/article/pii/S0921818102001200.

L.C. Peterson and W.L. Prell. Carbonate dissolution in Recent sediments of the eastern equatorial Indian Ocean: Preservation patterns and carbonate loss above the lysocline. *Marine Geology*, 64(3–4):259–290, April 1985. ISSN 0025-3227. doi: 10.1016/0025-3227(85)90108-2. URL http://www.sciencedirect.com/science/article/pii/0025322785901082.

F. Pinon, J. Deson, and R. Rosset. Propriétés de la résine échangeuse d'ions spécifique du bore Amberlite XE-243. *Bulletin de la Societé Chimique de France*, 8(535): 3454–3461, 1968.

I. Poole, J. D. B. Weyers, T. Lawson, and J. A. Raven. Variations in stomatal density and index: implications for palaeoclimatic reconstructions. *Plant, Cell & Environment*, 19(6):705–712, 1996. ISSN 1365-3040. doi: 10.1111/j.1365-3040.1996.tb00405.x. URL http://onlinelibrary.wiley.com/doi/10.1111/j.1365-3040.1996.tb00405.x/abstract.

Brian N. Popp, Ray Takigiku, J. M. Hayes, J. W. Louda, and Earl W. Baker. The post-Paleozoic chronology and mechanism of 13 C depletion in primary marine

organic matter. *American Journal of Science*, 289(4):436–454, April 1989. ISSN 0002-9599, 1945-452X. doi: 10.2475/ajs.289.4.436. URL http://www.ajsonline.org/content/289/4/436.

Brian N. Popp, Edward A. Laws, Robert R. Bidigare, John E. Dore, Kristi L. Hanson, and Stuart G. Wakeham. Effect of Phytoplankton Cell Geometry on Carbon Isotopic Fractionation. *Geochimica et Cosmochimica Acta*, 62(1):69–77, January 1998. ISSN 0016-7037. doi: 10.1016/S0016-7037(97)00333-5. URL http://www.sciencedirect.com/science/article/pii/S0016703797003335.

J.G. Prebble, E.M. Crouch, L. Carter, G. Cortese, H. Bostock, and H. Neil. An expanded modern dinoflagellate cyst dataset for the Southwest Pacific and Southern Hemisphere with environmental associations. *Marine Micropaleontology*, 101:33–48, May 2013. ISSN 0377-8398. doi: 10.1016/j.marmicro.2013.04.004. URL http://www.sciencedirect.com/science/article/pii/S0377839813000340.

R. M. Pytkowicz. Calcium carbonate retention in supersaturated seawater. *American Journal of Science*, 273(6):515–522, June 1973. ISSN 0002-9599, 1945-452X. doi: 10.2475/ajs.273.6.515. URL http://www.ajsonline.org/content/273/6/515.

James W. B. Rae. *Boron isotopes in benthic foraminifera: measurement, calibration and glacial CO2*. PhD thesis, University of Bristol, 2011.

James W.B. Rae, Gavin L. Foster, Daniela N. Schmidt, and Tim Elliott. Boron isotopes and B/Ca in benthic foraminifera: Proxies for the deep ocean carbonate system. *Earth and Planetary Science Letters*, 302(3-4):403–413, February 2011. ISSN 0012-821X. doi: 10.1016/j.epsl.2010.12.034. URL http://www.sciencedirect.com/science/article/pii/S0012821X1000796X.

Markus Raitzsch and Bärbel Hönisch. Cenozoic boron isotope variations in benthic foraminifers. *Geology*, March 2013. ISSN 0091-7613, 1943-2682. doi: 10.1130/G34031.1. URL http://geology.gsapubs.org/content/early/2013/03/26/G34031.1.

G. H. Rau, Ulf Riebesell, and Dieter A. Wolf-Gladrow. A model of photosynthetic 13C fractionation by marine phytoplankton based on diffusive molecular CO2 uptake. *Marine Ecology Progress Series*, 133:275–285, March 1996. doi: 10.3354/meps133275. URL http://www.int-res.com/abstracts/meps/v133/p275-285/.

M. E. Raymo, D. W. Oppo, and W. Curry. The Mid-Pleistocene climate transition: A deep sea carbon isotopic perspective. *Paleoceanography*, 12(4):546–559, August 1997. ISSN 0883-8305. doi: 10.1029/97PA01019. URL http://www.agu.org/pubs/crossref/1997/97PA01019.shtml.

Michael M. Reddy. Crystallization of calcium carbonate in the presence of trace concentrations of phosphorus-containing anions: I. Inhibition by phosphate and glycerophosphate ions at pH 8.8 and 25 °C. *Journal of Crystal Growth*, 41(2): 287–295, December 1977. ISSN 0022-0248. doi: 10.1016/0022-0248(77)90057-4. URL http://www.sciencedirect.com/science/article/pii/0022024877900574.

A Reitz, K. Pfeifer, GJ De Lange, and J Klump. Biogenic barium and the detrital Ba/Al ratio: a comparison of their direct and indirect determination. *Marine Geology*, 204(3-4):299–300, February 2004.

Stéphanie Reynaud, N. Gary Hemming, Anne Juillet-Leclerc, and Jean-Pierre Gattuso. Effect of pCO2 and temperature on the boron isotopic composition of the zooxanthellate coral *Acropora* sp. *Coral Reefs*, 23(4):539–546, December 2004. ISSN 0722-4028, 1432-0975. doi: 10.1007/s00338-004-0399-5. URL http://link.springer.com/article/10.1007/s00338-004-0399-5.

J.Donald Rimstidt, Anna Balog, and John Webb. Distribution of trace elements between carbonate minerals and aqueous solutions. *Geochimica et Cosmochimica Acta*, 62(11):1851–1863, June 1998. ISSN 0016-7037. doi: 10.1016/S0016-7037(98)00125-2. URL http://www.sciencedirect.com/science/article/pii/S0016703798001252.

S. Rink, Michael Kühl, Jelle Bijma, and Howard J. Spero. Microsensor studies of photosynthesis and respiration in the symbiotic foraminifer *Orbulina universa*. *Marine Biology*, 131:583–595, 1998.

L. L. Robbins, Mark E. Hansen, Joan A. Kleypas, and S. C. Meylan. CO2calc—A user-friendly seawater carbon calculator for windows, max OS x, and iOS (iPhone), 2010. URL http://pubs.usgs.gov/of/2010/1280/.

Stuart A. Robinson, Julian E. Andrews, Stephen P. Hesselbo, Jonathan D. Radley, Paul F. Dennis, Ian C. Harding, and Perce Allen. Atmospheric pCO2 and depositional environment from stable-isotope geochemistry of calcrete nodules

(Barremian, Lower Cretaceous, Wealden Beds, England). *Journal of the Geological Society*, 159(2):215–224, March 2002. ISSN 0016-7649, 2041-479X. doi: 10.1144/0016-764901-015. URL http://jgs.lyellcollection.org/content/159/2/215.

C. Rollion-Bard and Jonathan Erez. Intra-shell boron isotope ratios in the symbiont-bearing benthic foraminiferan *Amphistegina lobifera*: Implications for δ11b vital effects and paleo-pH reconstructions. *Geochimica et Cosmochimica Acta*, 74(5): 1530–1536, March 2010. ISSN 0016-7037. doi: 10.1016/j.gca.2009.11.017. URL http://www.sciencedirect.com/science/article/pii/S0016703709007169.

Björn Rost, Ingrid Zondervan, and Ulf Riebesell. Light-dependent carbon isotope fractionation in the coccolithophorid *Emiliania huxleyi*. *Limnology and oceanography*, 47(1):120–128, 2002. ISSN 0024-3590. URL http://cat.inist.fr/?aModele=afficheN&cpsidt=13438013.

Dana L. Royer, Robert A. Berner, and David J. Beerling. Phanerozoic atmospheric CO2 change: evaluating geochemical and paleobiological approaches. *Earth-Science Reviews*, 54(4):349–392, August 2001. ISSN 0012-8252. doi: 10.1016/S0012-8252(00)00042-8. URL http://www.sciencedirect.com/science/article/pii/S0012825200000428.

D.L. Royer. Stomatal density and stomatal index as indicators of paleoatmospheric CO2 concentration. *Review of Palaeobotany and Palynology*, 114(1–2):1–28, March 2001. ISSN 0034-6667. doi: 10.1016/S0034-6667(00)00074-9. URL http://www.sciencedirect.com/science/article/pii/S0034666700000749.

Carsten Rühlemann, Stefan Mulitza, Peter J. Müller, Gerold Wefer, and Rainer Zahn. Warming of the tropical Atlantic Ocean and slowdown of thermohaline circulation during the last deglaciation. *Nature*, 402:511–514, December 1999.

E. Ruiz-Agudo, C.V. Putnis, M. Kowacz, M. Ortega-Huertas, and A. Putnis. Boron incorporation into calcite during growth: Implications for the use of boron in carbonates as a pH proxy. *Earth and Planetary Science Letters*, 345–348:9–17, September 2012. ISSN 0012-821X. doi: 10.1016/j.epsl.2012.06.032. URL http://www.sciencedirect.com/science/article/pii/S0012821X12003160.

Encarnacion Ruiz-Agudo, Christine V. Putnis, and Andrew Putnis. Specific effects of background ions on magnesium incorporation into calcite. *Macla*, 13:187–188, September 2010.

Mats Rundgren and David Beerling. A Holocene CO2 record from the stomatal index of subfossil *Salix herbacea* leaves from northern Sweden. *The Holocene*, 9(5):509–513, July 1999. ISSN 0959-6836, 1477-0911. doi: 10.1191/095968399677717287. URL http://hol.sagepub.com/content/9/5/509.

Ann D. Russell, Bärbel Hönisch, Howard J. Spero, and David W. Lea. Effects of seawater carbonate ion concentration and temperature on shell U, Mg, and Sr in cultured planktonic foraminifera. *Geochimica et Cosmochimica Acta*, 68(21): 4347–4361, November 2004. ISSN 0016-7037. doi: 10.1016/j.gca.2004.03.013. URL http://www.sciencedirect.com/science/article/B6V66-4DKJCJ3-6/2/67be2e25cd29a18c3806626b687539b9.

James R. Rustad and Eric J. Bylaska. Ab initio calculation of isotopic fractionation in B(OH)3(aq) and BOH4-(aq). *Journal of the American Chemistry Society*, 129(8): 2222–2223, 2007. ISSN 0002-7863. doi: 10.1021/ja0683335. URL http://dx.doi.org/10.1021/ja0683335.

James R. Rustad, Eric J. Bylaska, Virgil E. Jackson, and David A. Dixon. Calculation of boron-isotope fractionation between B(OH)3(aq) and. *Geochimica et Cosmochimica Acta*, 74(10):2843–2850, May 2010. ISSN 0016-7037. doi: 10.1016/j.gca.2010.02.032. URL http://www.sciencedirect.com/science/article/pii/S001670371000102X.

C. Sanchez-Valle, B. Reynard, I. Daniel, C. Lecuyer, I. Martinez, and J. C. Chervin. Boron isotopic fractionation between minerals and fluids: New insights from *in situ* high pressure-high temperature vibrational spectroscopic data. *Geochimica et Cosmochimica Acta*, 69:4301–4313, 2005.

Abhijit Sanyal, N. Gary Hemming, Gilbert N. Hanson, and Wallace S. Broecker. Evidence for a higher pH in the glacial ocean from boron isotopes in foraminifera. *Nature*, 373(6511):234–236, January 1995. doi: 10.1038/373234a0. URL http://dx.doi.org/10.1038/373234a0.

Abhijit Sanyal, N. Gary Hemming, Wallace S. Broecker, David W. Lea, Howard J. Spero, and Gilbert N. Hanson. Oceanic pH control on the boron isotopic composition of foraminifera: Evidence from culture experiments. *Paleoceanography*, 11(5): 513–517, 1996. URL http://www.agu.org/journals/pa/v011/i005/96PA01858/.

Abhijit Sanyal, N. Gary Hemming, Wallace S. Broecker, and Gilbert N. Hanson. Changes in pH in the eastern equatorial Pacific across stage 5-6 boundary based on boron isotopes in foraminifera. *Global Biogeochemical Cycles*, 11(1):125–133, 1997. doi: 199710.1029/97GB00223. URL http://www.agu.org/pubs/crossref/1997/97GB00223.shtml.

Abhijit Sanyal, M. Nugent, R.J. Reeder, and Jelle Bijma. Seawater pH control on the boron isotopic composition of calcite: evidence from inorganic calcite precipitation experiments. *Geochimica et Cosmochimica Acta*, 64(9):1551–1555, May 2000. ISSN 0016-7037. doi: 10.1016/S0016-7037(99)00437-8. URL http://www.sciencedirect.com/science/article/pii/S0016703799004378.

Abhijit Sanyal, Jelle Bijma, Howie Spero, and David W. Lea. Empirical relationship between pH and the boron isotopic composition of *Globigerinoides sacculifer*: Implications for the boron isotope paleo-pH proxy. *Paleoceanography*, 16(5):515–519, 2001. URL http://adsabs.harvard.edu/abs/2001PalOc..16..515S.

Leslie Reynolds Sautter and Robert C. Thunell. Seasonal variability in the δ18O and δ13C of planktonic foraminifera from an upwelling environment: Sediment trap results from the San Pedro basin, southern California Bight. *Paleoceanography*, 6(3): 307–334, 1991. ISSN 1944-9186. doi: 10.1029/91PA00385. URL http://onlinelibrary.wiley.com/doi/10.1029/91PA00385/abstract.

Ralf Schiebel, Jelle Bijma, and Christoph Hemleben. Population dynamics of the planktic foraminifer *Globigerina bulloides* from the eastern North Atlantic. *Deep Sea Research Part I: Oceanographic Research Papers*, 44(9–10):1701–1713, September 1997. ISSN 0967-0637. doi: 10.1016/S0967-0637(97)00036-8. URL http://www.sciencedirect.com/science/article/pii/S0967063797000368.

Daniela N. Schmidt, Tim Elliott, and Simone A. Kasemann. The influences of growth rates on planktic foraminifers as proxies for palaeostudies: a review. In William E. N. Austin and Rachael H. James, editors, *Biogeochemical Controls on*

Palaeoceanographic Environmental Proxies., volume 303 of *Special Publications*, pages 73–85. Geological Society, London, 2008.

Matthew W. Schmidt, Howard J. Spero, and David W. Lea. Links between salinity variation in the Caribbean and North Atlantic thermohaline circulation. *Nature*, 428 (6979):160–163, March 2004. ISSN 0028-0836. doi: 10.1038/nature02346. URL http://www.nature.com/nature/journal/v428/n6979/full/nature02346.html.

Sonja Schulte and Edouard Bard. Past changes in biologically mediated dissolution of calcite above the chemical lysocline recorded in Indian Ocean sediments. *Quaternary Science Reviews*, 22(15–17):1757–1770, July 2003. ISSN 0277-3791. doi: 10.1016/S0277-3791(03)00172-0. URL http://www.sciencedirect.com/science/article/pii/S0277379103001720.

Osamu Seki, Gavin L. Foster, Daniela N. Schmidt, Andreas Mackensen, Kimitaka Kawamura, and Richard D. Pancost. Alkenone and boron-based pliocene pCO2 records. *Earth and Planetary Science Letters*, 292(1–2):201–211, March 2010. ISSN 0012-821X. doi: 10.1016/j.epsl.2010.01.037. URL http://www.sciencedirect.com/science/article/pii/S0012821X10000816.

S. Sen, J. F. Stebbins, N. G. Hemming, and B. Ghosh. Coordination environments of B impurities in calcite and aragonite polymorphs; A 11 B MAS NMR study. *American Mineralogist*, 79(9-10):819–825, October 1994. ISSN 0003-004X,. URL http://ammin.geoscienceworld.org/content/79/9-10/819.

Y. Shaked and A. Genin. The Israel National Monitoring Program at the Gulf of Eilat (NMP). Scientific report, Interuniversity Institute, Eilat, 2006.

Yonathan Shaked and Colomban de Vargas. Pelagic photosymbiosis: rDNA assessment of diversity and evolution of dinoflagellate symbionts and planktonic foraminiferal hosts. *Marine Ecology Progress Series*, 325:59–71, November 2006. doi: 10.3354/meps325059. URL http://www.int-res.com/abstracts/meps/v325/p59-71/.

Makoto Shima. Geochemical study of boron isotopes. *Geochimica et Cosmochimica Acta*, 27(8):911–913, August 1963. ISSN 0016-7037. doi: 10.1016/0016-7037(63)90114-5. URL http://www.sciencedirect.com/science/article/pii/0016703763901145.

K. Simkiss. The inhibitory effects of some metabolites on the precipitation of calcium carbonate from artificial and natural sea water. *Journal du Conseil*, 29(1):6–18, June 1964. ISSN 1054-3139, 1095-9289. doi: 10.1093/icesjms/29.1.6. URL http://icesjms.oxfordjournals.org/content/29/1/6.

Laurent Simon, Christophe Lécuyer, Chloé Maréchal, and Nicolas Coltice. Modelling the geochemical cycle of boron: Implications for the long-term δ11B evolution of seawater and oceanic crust. *Chemical Geology*, 225:61–76, 2006.

H. J. Spero and D. F. Williams. Opening the carbon isotope "vital effect" black box 1. Seasonal temperatures in the euphotic zone. *Paleoceanography*, 4(6):593–601, 1989. ISSN 1944-9186. doi: 10.1029/PA004i006p00593. URL http://onlinelibrary.wiley.com/doi/10.1029/PA004i006p00593/abstract.

Howard J Spero. Symbiosis in the planktonic foraminifer, *Orbulina universa*, and the isolation of its symbiotic dinoflagellate, *Gymnodinium béii* sp. nov. *Journal of Phycology*, 23:307–317, June 1987. ISSN 1529-8817. doi: 10.1111/j.1529-8817.1987.tb04139.x. URL http://onlinelibrary.wiley.com/doi/10.1111/j.1529-8817.1987.tb04139.x/abstract.

Howard J. Spero. Do planktic foraminifera accurately record shifts in the carbon isotopic composition of seawater ϵCO2? *Marine Micropaleontology*, 19(4):275–285, August 1992. ISSN 0377-8398. doi: 10.1016/0377-8398(92)90033-G. URL http://www.sciencedirect.com/science/article/pii/037783989290033G.

Howard J. Spero. Life history and stable isotope geochemistry of planktonic foraminifera. In Richard D. Norris and R. M. Corfield, editors, *Isotope Paleobiology and Paleoecology*, volume Special Publication of *Paleontological Society Papers*. Paleontological Society, 1998.

Howard J. Spero and David W. Lea. Intraspecific stable isotope variability in the planktic foraminifera *Globigerinoides sacculifer*: Results from laboratory experiments. *Marine Micropaleontology*, 22(3):221–234, October 1993. ISSN 0377-8398. doi: 10.1016/0377-8398(93)90045-Y. URL http://www.sciencedirect.com/science/article/pii/037783989390045Y.

Howard J. Spero and David W. Lea. Experimental determination of stable isotope variability in *Globigerina bulloides*: implications for paleoceanographic

reconstructions. *Marine Micropaleontology*, 28(3–4):231–246, September 1996. ISSN 0377-8398. doi: 10.1016/0377-8398(96)00003-5. URL http://www.sciencedirect.com/science/article/pii/0377839896000035.

Howard J Spero and Steven L Parker. Photosynthesis in the symbiotic planktonic foraminifer *Orbulina universa*, and its potential contribution to oceanic primary productivity. *The Journal of Foraminiferal Research*, 15(4):273–281, October 1985. ISSN 0096-1191,. doi: 10.2113/gsjfr.15.4.273. URL http://jfr.geoscienceworld.org/content/15/4/273.full.pdf+html?frame=sidebar.

Howard J. Spero and Douglas F. Williams. Extracting environmental information from planktonic foraminiferal δ13C data. *Nature*, 335(6192):717–719, October 1988. doi: 10.1038/335717a0. URL http://www.nature.com/nature/journal/v335/n6192/abs/335717a0.html.

Howard J. Spero, Jelle Bijma, David W. Lea, and Bryan E. Bemis. Effect of seawater carbonate concentration on foraminiferal carbon and oxygen isotopes. *Nature*, 390: 497–500, December 1997. URL http://adsabs.harvard.edu/abs/1997Natur.390..497S.

Michael Spindler, C. Hemleben, J. B Salomons, and L. P Smit. Feeding behavior of some planktonic foraminifers in laboratory cultures. *The Journal of Foraminiferal Research*, 14(4):237–249, October 1984. ISSN 0096-1191,. doi: 10.2113/gsjfr.14.4.237. URL http://jfr.geoscienceworld.org/content/14/4/237.full.pdf+html?frame=sidebar.

Arthur J. Spivack and John M. Edmond. Boron isotope exchange between seawater and the oceanic crust. *Geochimica et Cosmochimica Acta*, 51(5):1033–1043, May 1987. ISSN 0016-7037. doi: 10.1016/0016-7037(87)90198-0. URL http://www.sciencedirect.com/science/article/B6V66-488Y3JM-11N/2/0d4a01a01833d5f56a15b2fe4cc9146a.

D. A. Stainforth, T. Aina, C. Christensen, M. Collins, N. Faull, D. J. Frame, J. A. Kettleborough, S. Knight, A. Martin, J. M. Murphy, C. Piani, D. Sexton, L. A. Smith, R. A. Spicer, A. J. Thorpe, and M. R. Allen. Uncertainty in predictions of the climate response to rising levels of greenhouse gases. *Nature*, 433(7024):403–406,

January 2005. ISSN 0028-0836. doi: 10.1038/nature03301. URL http://www.nature.com/nature/journal/v433/n7024/abs/nature03301.html.

Noga Stambler. Light and picophytoplankton in the Gulf of Eilat (Aqaba). *Journal of Geophysical Research: Oceans*, 111(C11):n/a–n/a, 2006. ISSN 2156-2202. doi: 10.1029/2005JC003373. URL http://onlinelibrary.wiley.com/doi/10.1029/2005JC003373/abstract.

Stephan Steinke, Han-Yi Chiu, Pai-Sen Yu, Chuan-Chou Shen, Ludvig Löwemark, Horng-Sheng Mii, and Min-Te Chen. Mg/Ca ratios of two *Globigerinoides ruber* (white) morphotypes: Implications for reconstructing past tropical/subtropical surface water conditions. *Geochemistry Geophysics Geosystems*, 6:Q11005, November 2005. doi: 10.1029/2005GC000926. URL http://www.agu.org/pubs/crossref/2005/2005GC000926.shtml.

Stephan Steinke, Markus Kienast, Jeroen Groeneveld, Li-Chuan Lin, Min-Te Chen, and Rebecca Rendle-Bühring. Proxy dependence of the temporal pattern of deglacial warming in the tropical south china sea: toward resolving seasonality. *Quaternary Science Reviews*, 27(7-8):688–700, April 2008. ISSN 0277-3791. doi: 10.1016/j.quascirev.2007.12.003. URL http://www.sciencedirect.com/science/article/pii/S0277379107003630.

Heather Stoll, Gerald Langer, Nobumichi Shimizu, and Kinuyo Kanamaru. B/Ca in coccoliths and relationship to calcification vesicle pH and dissolved inorganic carbon concentrations. *Geochimica et Cosmochimica Acta*, 80:143–157, 2012.

Chunming Su and Donald L. Suarez. Coordination of adsorbed boron: A FTIR spectroscopic study. *Environmental Science and Technology*, 29(2):302–311, 1995. ISSN 0013-936X. doi: 10.1021/es00002a005. URL http://dx.doi.org/10.1021/es00002a005.

Taro Takahashi, Stewart C. Sutherland, Rik Wanninkhof, Colm Sweeney, Richard A. Feely, David W. Chipman, Burke Hales, Gernot Friederich, Francisco Chavez, Christopher Sabine, Andrew Watson, Dorothee C.E. Bakker, Ute Schuster, Nicolas Metzl, Hisayuki Yoshikawa-Inoue, Masao Ishii, Takashi Midorikawa, Yukihiro Nojiri, Arne Körtzinger, Tobias Steinhoff, Mario Hoppema, Jon Olafsson, Thorarinn S. Arnarson, Bronte Tilbrook, Truls Johannessen, Are Olsen, Richard Bellerby, C.S.

Wong, Bruno Delille, N.R. Bates, and Hein J.W. de Baar. Climatological mean and decadal change in surface ocean pCO2, and net sea–air CO2 flux over the global oceans. *Deep Sea Research Part II: Topical Studies in Oceanography*, 56(8-10): 554–577, April 2009. ISSN 0967-0645. doi: 10.1016/j.dsr2.2008.12.009. URL http://www.sciencedirect.com/science/article/pii/S0967064508004311.

Mayuki Tanaka and Toru Fujiwara. Physiological roles and transport mechanisms of boron: perspectives from plants. *Pflügers Archiv - European Journal of Physiology*, 456(4):671–677, July 2008. ISSN 0031-6768, 1432-2013. doi: 10.1007/s00424-007-0370-8. URL http://link.springer.com/article/10.1007/s00424-007-0370-8.

S. R. Taylor and S. M. McLennan. *The continental crust: Its composition and evolution*. Blackwell Scientific, Palo Alto, CA, January 1985.

P. R. Thompson, Allan W. H. Be, J. -C. Duplessy, and Nicholas J. Shackleton. Disappearance of pink-pigmented *Globigerinoides ruber* at 120,000 yr B.P. in the indian pacific ocean. *Nature*, 280:554–558, 1979.

Franck Touratier and Catherine Goyet. Impact of the Eastern Mediterranean Transient on the distribution of anthropogenic CO2 and first estimate of acidification for the Mediterranean Sea. *Deep Sea Research Part I: Oceanographic Research Papers*, 58 (1):1–15, January 2011. ISSN 0967-0637. doi: 10.1016/j.dsr.2010.10.002. URL http://www.sciencedirect.com/science/article/pii/S0967063710002098.

Aradhna K. Tripati, Christopher D. Roberts, and Robert A. Eagle. Coupling of CO2 and ice sheet stability over major climate transitions of the last 20 million years. *Science*, 326(5958):1394–1397, December 2009. doi: 10.1126/science.1178296. URL http://www.sciencemag.org/cgi/content/abstract/326/5958/1394.

Aradhna K. Tripati, Christopher D. Roberts, Robert A. Eagle, and Gaojun Li. A 20 million year record of planktic foraminiferal B/Ca ratios: Systematics and uncertainties in pCO2 reconstructions. *Geochimica et Cosmochimica Acta*, 75(10): 2582–2610, May 2011. ISSN 0016-7037. doi: 10.1016/j.gca.2011.01.018. URL http://www.sciencedirect.com/science/article/pii/S0016703711000263.

Julie Trotter, Paolo Montagna, Malcolm McCulloch, Sergio Silenzi, Stéphanie Reynaud, Graham Mortimer, Sophie Martin, Christine Ferrier-Pagès, Jean-Pierre

Gattuso, and Riccardo Rodolfo-Metalpa. Quantifying the pH 'vital effect' in the temperate zooxanthellate coral *Cladocora caespitosa*: Validation of the boron seawater pH proxy. *Earth and Planetary Science Letters*, 303(3–4):163–173, March 2011. ISSN 0012-821X. doi: 10.1016/j.epsl.2011.01.030. URL http://www.sciencedirect.com/science/article/pii/S0012821X11000549.

Jeffrey V. Turner. Kinetic fractionation of carbon-13 during calcium carbonate precipitation. *Geochimica et Cosmochimica Acta*, 46(7):1183–1191, July 1982. ISSN 0016-7037. doi: 10.1016/0016-7037(82)90004-7. URL http://www.sciencedirect.com/science/article/pii/0016703782900047.

John E. Tyler. The in situ quantum efficiency of natural phytoplankton populations. *Limnology and Oceanography*, 20(6):976–980, 1975. ISSN 00243590. doi: 10.4319/lo.1975.20.6.0976. URL http://www.aslo.org/lo/toc/vol_20/issue_6/0976.html.

John Tyndall. On the absorption and radiation of heat by gaseous matter; second memoir. *Philosophical Transactions of the Royal Society of London*, 152:59–98, January 1862. ISSN 0261-0523,. doi: 10.1098/rstl.1862.0008. URL http://rstl.royalsocietypublishing.org/content/152/59.

Harold C. Urey. The thermodynamic properties of isotopic substances. *Journal of the Chemical Society*, pages 562–581, January 1947. doi: 10.1039/JR9470000562. URL http://pubs.rsc.org/en/content/articlelanding/1947/jr/jr9470000562.

E. van den Broeck. Etude sur les foraminifères de la Barbade (Antilles). *Annales de la Société Belge de Microscopie*, 1(55-152), 1876.

S. van Heuven, D. Pierrot, James W. B. Rae, Ernie Lewis, and Douglas W. R. Wallace. MATLAB program developed for CO2 system calculations., 2011. URL http://cdiac.ornl.gov/ftp/co2sys/CO2SYS_calc_MATLAB/.

Colomban de Vargas, Richard Norris, Louisette Zaninetti, Stuart W. Gibb, and Jan Pawlowski. Molecular evidence of cryptic speciation in planktonic foraminifers and their relation to oceanic provinces. *Proceedings of the National Academy of Sciences*, 96(6):2864–2868, March 1999. ISSN 0027-8424, 1091-6490. doi: 10.1073/pnas.96.6.2864. URL http://www.pnas.org/content/96/6/2864.

Colomban de Vargas, Alberto G. Sáez, Linda K. Medlin, and Hans R. Thierstein. Super-Species in the calcareous plankton. In Hans R. Thierstein and Jeremy R. Young, editors, *Coccolithophores*, pages 271–298. Springer Berlin Heidelberg, January 2004. ISBN 978-3-642-06016-8, 978-3-662-06278-4. URL http://link.springer.com/chapter/10.1007/978-3-662-06278-4_11.

Avner Vengosh, Yehoshua Kolodny, Abraham Starinsky, Allan R. Chivas, and Malcolm T McCulloch. Coprecipitation and isotopic fractionation of boron in modern biogenic carbonates. *Geochimica et Cosmochimica Acta*, 55(10):2901–2910, October 1991. ISSN 0016-7037. doi: 10.1016/0016-7037(91)90455-E. URL http://www.sciencedirect.com/science/article/B6V66-489SJ22-3R/2/cf6051afc93d467ff609323700d8dc07.

Alexander A. Venn, Eric Tambutté, Michael Holcomb, Julien Laurent, Denis Allemand, and Sylvie Tambutté. Impact of seawater acidification on pH at the tissue–skeleton interface and calcification in reef corals. *Proceedings of the National Academy of Sciences*, 110(5):1634–1639, January 2013. ISSN 0027-8424, 1091-6490. doi: 10.1073/pnas.1216153110. URL http://www.pnas.org/content/110/5/1634.

Lael Vetter, Reinhard Kozdon, Claudia I. Mora, Stephen M. Eggins, John W. Valley, Bärbel Hönisch, and Howard J. Spero. Micron-scale intrashell oxygen isotope variation in cultured planktic foraminifers. *Geochimica et Cosmochimica Acta*, 107: 267–278, April 2013. ISSN 0016-7037. doi: 10.1016/j.gca.2012.12.046. URL http://www.sciencedirect.com/science/article/pii/S0016703713000197.

Annemiek Vink, Carsten R uhlemann, Karin A. F. Zonneveld, Stefan Mulitza, Matthias Hüls, and Helmut Willems. Shifts in the position of the North Equatorial Current and rapid productivity changes in the western tropical Atlantic during the last glacial. *Paleoceanography*, 16(0):1–12, 2001.

David S. Vinson, Haylee G. Schwartz, Gary S. Dwyer, and Avner Vengosh. Evaluating salinity sources of groundwater and implications for sustainable reverse osmosis desalination in coastal North Carolina, USA. *Hydrogeology Journal*, 19(5):981–994, August 2011. ISSN 1431-2174, 1435-0157. doi: 10.1007/s10040-011-0738-x. URL http://link.springer.com/article/10.1007/s10040-011-0738-x.

Jochen Vogl and Martin Rosner. Production and Certification of a Unique Set of Isotope and Delta Reference Materials for Boron Isotope Determination in Geochemical, Environmental and Industrial Materials. *Geostandards and Geoanalytical Research*, 36(2):161–175, 2012. ISSN 1751-908X. doi: 10.1111/j.1751-908X.2011.00136.x. URL http://onlinelibrary.wiley.com/doi/10.1111/j.1751-908X.2011.00136.x/abstract.

Bridget S. Wade. Planktonic foraminiferal biostratigraphy and mechanisms in the extinction of *Morozovella* in the late middle Eocene. *Marine Micropaleontology*, 51: 23–38, 2004.

Bo-Shian Wang, Chen-Feng You, Kuo-Fang Huang, Shein-Fu Wu, Suresh Kumar Aggarwal, Chuan-Hsiung Chung, and Pei-Ying Lin. Direct separation of boron from Na- and Ca-rich matrices by sublimation for stable isotope measurement by MC-ICP-MS. *Talanta*, 82(4):1378–1384, September 2010. ISSN 0039-9140. doi: 10.1016/j.talanta.2010.07.010. URL http://www.sciencedirect.com/science/article/pii/S0039914010005242.

Luejiang Wang. Isotopic signals in two morphotypes of *Globigerinoides ruber* (white) from the south china sea: implications for monsoon climate change during the last glacial cycle. *Palaeogeography, Palaeoclimatology, Palaeoecology*, 161(3–4):381–394, September 2000. ISSN 0031-0182. doi: 10.1016/S0031-0182(00)00094-8. URL http://www.sciencedirect.com/science/article/pii/S0031018200000948.

M. W. Wara, M. L. Delaney, T. D. Bullen, and A. C. Ravelo. Possible roles of pH, temperature, and partial dissolution in determining boron concentration and isotopic composition in planktonic foraminifera. *Paleoceanography*, 18(4):n/a–n/a, 2003. ISSN 1944-9186. doi: 10.1029/2002PA000797. URL http://onlinelibrary.wiley.com/doi/10.1029/2002PA000797/abstract.

M. Wedborg, D. R. Turner, L. G. Anderson, and D. Dyrssen. Determination of pH. In Klaus Grasshoff, Klaus Kremling, and Manfred Ehrhardt, editors, *Methods of Seawater Analysis*, chapter 7, pages 109–125. Wiley-VCH Verlag, Weinheim, 3rd edition, 1999. ISBN 9783527613984. URL http://onlinelibrary.wiley.com/doi/10.1002/9783527613984.ch7/summary.

P. H. Wiebe, A. W. Morton, A. M. Bradley, R. H. Backus, J. E. Craddock, V. Barber, T. J. Cowles, and G. R. Flierl. New developments in the MOCNESS, an apparatus for sampling zooplankton and micronekton. *Marine Biologyiology*, 87(3):313–323, 1985. ISSN 0025-3162. URL http://cat.inist.fr/?aModele=afficheN&cpsidt=8413126.

Dieter A Wolf-Gladrow, Jelle Bijma, and Richard E. Zeebe. Model simulation of the carbonate system in the microenvironment of symbiont bearing foraminifera. *Marine Chemistry*, 64:181–198, 1999. URL http://epic.awi.de/3413/.

F. I. Woodward and F. A. Bazzaz. The responses of stomatal density to CO2 partial pressure. *Journal of Experimental Botany*, 39(12):1771–1781, December 1988. ISSN 0022-0957, 1460-2431. doi: 10.1093/jxb/39.12.1771. URL http://jxb.oxfordjournals.org/content/39/12/1771.

F. I. Woodward and C. K. Kelly. The influence of CO2 concentration on stomatal density. *New Phytologist*, 131(3):311–327, 1995. ISSN 1469-8137. doi: 10.1111/j.1469-8137.1995.tb03067.x. URL http://onlinelibrary.wiley.com/doi/10.1111/j.1469-8137.1995.tb03067.x/abstract.

J. Xiao, Z. D. Jin, Y. K. Xiao, and M. Y. He. Controlling factors of the δ11B-pH proxy and its research direction. *Environmental Earth Sciences*, pages 1–10, June 2013. ISSN 1866-6280, 1866-6299. doi: 10.1007/s12665-013-2568-8. URL http://link.springer.com/article/10.1007/s12665-013-2568-8.

Derek York. Least squares fitting of a straight line with correlated errors. *Earth and Planetary Science Letters*, 5:320–324, January 1968. ISSN 0012821X. doi: 10.1016/S0012-821X(68)80059-7. URL http://elsevier-apps.sciverse.com/GoogleMaps/index.jsp?doi=10.1016/S0012-821X%2868%2980059-7.

Jeremy R. Young, Sean A. Davis, Paul R. Bown, and Stephen Mann. Coccolith ultrastructure and biomineralisation. *Journal of Structural Biology*, 126(3):195–215, June 1999. ISSN 1047-8477. doi: 10.1006/jsbi.1999.4132. URL http://www.sciencedirect.com/science/article/pii/S1047847799941321.

Jimin Yu and Henry Elderfield. Benthic foraminiferal B/Ca ratios reflect deep water carbonate saturation state. *Earth and Planetary Science Letters*, 258(1-2):73–86, June 2007. ISSN 0012-821X. doi: 10.1016/j.epsl.2007.03.025. URL

http://www.sciencedirect.com/science/article/B6V61-4N9P4RR-3/2/7c6aedb3d50cdfdcf464e67081feff3a.

Jimin Yu, Henry Elderfield, Mervyn Greaves, and Jason Day. Preferential dissolution of benthic foraminiferal calcite during laboratory reductive cleaning. *Geochemistry, Geophysics, Geosystems*, 8(6):n/a–n/a, 2007a. ISSN 1525-2027. doi: 10.1029/2006GC001571. URL http://onlinelibrary.wiley.com/doi/10.1029/2006GC001571/abstract.

Jimin Yu, Henry Elderfield, and Bärbel Hönisch. B/Ca in planktonic foraminifera as a proxy for surface seawater pH. *Paleoceanography*, 22:PA2202, April 2007b. doi: 10.1029/2006PA001347. URL http://www.agu.org/journals/pa/pa0702/2006PA001347/body.shtml.

Jimin Yu, Gavin L. Foster, Henry Elderfield, Wallace S. Broecker, and Elizabeth Clark. An evaluation of benthic foraminiferal B/Ca and 11B for deep ocean carbonate ion and pH reconstructions. *Earth and Planetary Science Letters*, 293 (1–2):114–120, April 2010. ISSN 0012-821X. doi: 10.1016/j.epsl.2010.02.029. URL http://www.sciencedirect.com/science/article/pii/S0012821X10001317.

Jimin Yu, David J.R. Thornalley, James W.B. Rae, and I. Nick McCave. Calibration and application of B/Ca, Cd/Ca and δ11B in *Neogloboquadrina pachyderma* (sinistral) to constrain CO2 uptake in the subpolar North Atlantic during the last deglaciation. *Paleoceanography*, 28(2):237–252, 2013. ISSN 1944-9186. doi: 10.1002/palo.20024. URL http://onlinelibrary.wiley.com/doi/10.1002/palo.20024/abstract.

Jimin M. Yu, Jason Day, Mervyn J. Greaves, and Henry Elderfield. Determination of multiple element/calcium ratios in foraminiferal calcite by quadropole ICP-MS. *Geochemistry, Geophysics and Geosystems*, 6(8):Q08P01, August 2005.

James C. Zachos, Gerald R. Dickens, and Richard E. Zeebe. An early Cenozoic perspective on greenhouse warming and carbon-cycle dynamics. *Nature*, 451(7176): 279–283, January 2008. ISSN 0028-0836. doi: 10.1038/nature06588. URL http://www.nature.com/nature/journal/v451/n7176/full/nature06588.html.

Richard E. Zeebe. Stable boron isotope fractionation between dissolved $B(OH)_3$ and $B(OH)_4^-$. *Geochimica et Cosmochimica Acta*, 69(11):2753–2766, June 2005. ISSN

0016-7037. doi: 10.1016/j.gca.2004.12.011. URL http://www.sciencedirect.com/science/article/B6V66-4GB0B9G-5/2/716c4b2639d8166f9b15e4e9de3bdfe6.

Richard E. Zeebe and Dieter A Wolf-Gladrow. *CO_2 in seawater: Equilibrium, Kinetics, Isotopes.* Number 65 in Elsevier Oceanography Series. Elsevier, Amsterdam, 2001. ISBN 0-444-50946.

Richard E. Zeebe, Jelle Bijma, and Dieter A Wolf-Gladrow. A diffusion-reaction model of carbon isotope fractionation in foraminifera. *Marine Chemistry*, 64(3):199–227, March 1999a. ISSN 0304-4203. doi: 10.1016/S0304-4203(98)00075-9. URL http://www.sciencedirect.com/science/article/pii/S0304420398000759.

Richard E. Zeebe, Dieter A. Wolf-Gladrow, and H. Jansen. On the time required to establish chemical and isotopic equilibrium in the carbon dioxide system in seawater. *Marine Chemistry*, 65:135–153, 1999b.

Richard E Zeebe, Abhijit Sanyal, Joseph D Ortiz, and Dieter A Wolf-Gladrow. A theoretical study of the kinetics of the boric acid–borate equilibrium in seawater. *Marine Chemistry*, 73(2):113–124, February 2001. ISSN 0304-4203. doi: 10.1016/S0304-4203(00)00100-6. URL http://www.sciencedirect.com/science/article/pii/S0304420300001006.

Richard E. Zeebe, Dieter A Wolf-Gladrow, Jelle Bijma, and Bärbel Hönisch. Vital effects in foraminifera do not compromise the use of δ11B as a paleo-pH indicator: Evidence from modeling. *Paleoceanography*, 18:9 PP., May 2003. doi: 200310.1029/2003PA000881. URL http://www.agu.org/journals/ABS/2003/2003PA000881.shtml.

H. Zeininger and K.G. Heumann. Boron isotope ratio measurement by negative thermal ionization mass spectrometry. *International Journal of Mass Spectrometry and Ion Physics*, 48:377–380, January 1983. ISSN 0020-7381. doi: 10.1016/0020-7381(83)87106-X. URL http://www.sciencedirect.com/science/article/pii/002073818387106X.

Erik Zeuthen. Oxygen uptake as related to body size in organisms. *The Quarterly Review of Biology*, 28(1):1–12, March 1953.